



Electrospinning and electrospun nanofibers: From academic research to industrial production

Ce Wang^{a,*}, Wei Wang^b, Hongxu Qi^c, Yunqian Dai^d, Shaohua Jiang^e, Bin Ding^f, Xianfeng Wang^f, Congju Li^f, Jinfeng Zeng^f, Tong Wu^g, Haoyi Li^h, Yuanfei Wangⁱ, Yong Zhao^j, Wenli Wang^k, Zhenyu Li^l, Xiumei Mo^f, Haoqing Hou^m, Lijie Dongⁿ, Hongyang Ma^h, Yong Liu^h, Chunlei Su^o, Jie Bai^p, Weiwei Wu^q, Gang Guo^r, Guangdi Nie^g, Nü Wang^s, Han Zhu^t, Jing Bai^d, Jian Fang^k, Daxin Liang^u, Zhichen Ba^u, Guangping Han^u, Xiaofeng Lu^v, Kaizhong Wang^w, Xiaoyong Zhang^x, Weimin Kang^y, Nanping Deng^y, Wei Hu^z, Weihua Chen^{aa}, Xiuling Zhang^h, Dongzhi Yang^h, Fengyun Wang^g, Ye Bian^d, Zi'ang Liuⁿ, Liang Zhang^{ab}, Xiang Li^v, Lei Li^y, Yongxin Li^v, Hui Huang^v, Xiaoteng Jia^v, Xiaofeng Li^h, Daxiang Yang^{ac}, Xianchang Jin^{ad}, Shiyang Li^{ae}, Xindan Zhang^h, Nan Tang^h, Ruinan Hao^{af}, Feng Tian^{h,**}, Liqiang Mai^{ag,***}, Yen Wei^{ah,****}, Jiajia Xue^{h,*****}

^a Alan G. MacDiarmid Institute, Jilin University, Changchun 130012, China

^b Harbin Institute of Technology, Harbin 150001, China

^c Tsinghua University, Beijing 100084, China

^d Southeast University, Nanjing 211189, China

^e Nanjing Forestry University, Nanjing 210037, China

^f Donghua University, Shanghai 201620, China

^g Qingdao University, Qingdao 266071, China

^h State Key Laboratory of Organic-Inorganic Composites, Beijing University of Chemical Technology, Beijing 100029, China

ⁱ Qingdao Stomatological Hospital Affiliated to Qingdao University, Qingdao 260001, China

^j School of Chemistry, Beihang University, Beijing 100191, China

Abbreviations: 1D, One-dimensional; 2D, Two-dimensional; 3D, Three-dimensional; ADSC, Adipose-derived stem cells; AFM, Atomic force microscopy; AI, artificial intelligence; Bi/BTO, Bi deposition modified BTO; BMP2, Bone morphogenetic protein-2; bPEI, Branched polyethyleneimine; BT, Barium titanate; BTO, Barium t*itanate; CaCO₃, Calcium carbonate; CNF, Carbon nanofibers; CO₂RR, Carbon dioxide reduction reaction; CSCs, Cardiac-derived stem cells; dB, Decibel; DCM, Dichloromethane; DMac, Dimethylacetamide; DMF, N,N-dimethylformamide; DMSO, Dimethylsulfoxide; DSSCs, Dye-sensitized solar cells; DWE, Direct-writing electrospinning; ECM, Extracellular matrix; EDS, Energy-dispersive X-ray spectroscopy; EELS, Electron energy loss spectroscopy; EMI, Electromagnetic interference; EpCAM, Epithelial cell adhesion molecule; ESCs, Embryonic stem cells; Fe₃O₄, Magnetite; FETs, Field-effect transistors; FO, Forward osmosis; FTIR, Fourier transform infrared spectroscopy; G/CNF, Graphene/carbon nanofibers; GBR, Guided bone regeneration; GCIB-XPS, Gas cluster ion beam XPS; GelMA, Methacrylated gelatin; GHz, Gigahertz; GO, Graphene oxide; GTR, Guided tissue regeneration; HA, Hyaluronic acid; HAP, Hydroxyapatite; HER, Hydrogen evolution reaction; HFIP, Hexafluoroisopropanol; HNTs, Halloysite nanotubes; HUVEC, Human umbilical vein endothelial cell; iPP, Isotactic polypropylene; iPSCs, Induced pluripotent stem cells; KNN, Potassium sodium niobate.

* Corresponding author.

** Corresponding author.

*** Corresponding author.

**** Corresponding author.

***** Corresponding author.

E-mail addresses: cwang@jlu.edu.cn (C. Wang), fengtian@buct.edu.cn (F. Tian), mlq518@whut.edu.cn (L. Mai), weiyen@tsinghua.edu.cn (Y. Wei), jiajiaxue@mail.buct.edu.cn (J. Xue).

<https://doi.org/10.1016/j.pmatsci.2025.101494>

Received 14 September 2024; Received in revised form 3 February 2025; Accepted 15 April 2025

Available online 24 April 2025

0079-6425/© 2025 Elsevier Ltd. All rights are reserved, including those for text and data mining, AI training, and similar technologies.

^k College of Textile and Clothing Engineering, Jiangsu Engineering Research Center of Textile Dyeing and Finishing for Energy Conservation, Discharge Reduction and Cleaner Production, National Engineering Laboratory for Morden Silk, Soochow University, Suzhou 215123, China

^l Southwest Petroleum University, Chengdu 610500, China

^m Jiangxi Normal University, Nanchang 330022, China

ⁿ Wuhan University of Technology, Wuhan 430070, China

^o Institute of Process Engineering, Chinese Academy of Sciences, Beijing 100190, China

^p Inner Mongolia University of Technology, Hohhot 010051, China

^q Xidian University, Xian 710071, China

^r Sichuan University, Chengdu 610065, China

^s Beihang University, Beijing 100191, China

^t Jiangnan University, Wuxi 214122, China

^u Northeast Forestry University, Harbin 150040, China

^v Jilin University, Changchun 130012, China

^w First Hospital of Jilin University, Changchun 130031, China

^x Nanchang University, Nanchang 330031, China

^y Tiangong University, Tianjin 300387, China

^z Northeast Normal University, Changchun 130024, China

^{aa} Zhengzhou University, Zhengzhou 450001, China

^{ab} University of Science and Technology Beijing, Beijing 100083, China

^{ac} CHinano Technology (Chongqing) Co., Ltd., Chongqing 404617, China

^{ad} Beijing Guo Wei Na Research Center for Fiber Materials, Beijing, China

^{ae} Shanghai University, Shanghai 200444, China

^{af} South China University of Technology, Guangzhou 510006, China

^{ag} State Key Laboratory of Advanced Technology for Materials Synthesis and Processing, Wuhan University of Technology, Wuhan 430070, China

^{ah} Department of Chemistry and the Tsinghua Center for Frontier Polymer Research, Tsinghua University, Beijing 100084, China

ARTICLE INFO

Keywords:

Electrospinning
Electrospun nanofibers
Applications
Characterization
Industrialization
Future perspectives

ABSTRACT

Electrospinning is a versatile and rapidly evolving technique that has gained significant attention for its ability to produce nanofibers with unique structures and properties. Over the past few decades, the scope of electrospun nanofibers has expanded from simple polymer fibers to more complex composites and ceramics, enabling a wide range of applications across fields such as environmental protection, biomedical engineering, energy storage, and smart materials. This review provides a comprehensive overview of recent advancements, covering material selection, process optimization, and innovative applications. We discuss the unique structural features of electrospun nanofibers, including their tunable diameters, porous architectures, and diverse compositions, which underpin their multifunctionality. Key applications are highlighted in areas including environmental protection and safety, biomedical engineering, energy storage and conversion, and catalysis, as well as emerging uses in flexible electronics, advanced engineering materials, and textiles. Additionally, we review state-of-the-art characterization techniques and discuss the challenges and opportunities involved in scaling up industrial production. Finally, we

LBL, Layer-by-layer; LIBs, Lithium-ion batteries; Li-O₂, Lithium-oxygen; LLDPE, Linear low-density polyethylene; LLTO, Li_{0.33}La_{0.557}TiO₃; LLZO, Li_{6.4}La₃Zr₂Al_{0.2}O₁₂; MEW, Melt electrowriting; MF, Microfiltration; MFCs, Microbial fuel cells; Mo₂C, Molybdenum carbide; MOFs, Metal-organic frameworks; MRI, Magnetic resonance imaging; MSCs, Mesenchymal stem cell; MXene, Transition metal carbides/nitrides; NC NTs, N-doped carbon nanotubes; NCNF, Nitrogen-doped carbon nanofibers; NF, Nanofiltration; NFES, Near-field electrospinning; NGC, Nerve guidance conduit; NIR, Near-infrared; NRR, Nitrogen reduction reaction; OER, Oxygen evolution reaction; OLEDs, Organic light-emitting diodes; ORR, Oxygen reduction reaction; OVs, Oxygen vacancies; P(VDF-HFP), Poly(vinylidene fluoride-co-hexafluoropropylene); PA, Polyamide; PA6, Polyamide 6; PAA, Polyacrylic acid; PAN, Polyacrylonitrile; PC, Polycarbonate; PCE, Porous cationic electrospun; PCL, Polycaprolactone; PDA, Polydopamine; PDGF, Platelet-derived growth factor; PDMS, Polydimethylsiloxane; PEDOT, Poly(3,4-ethylenedioxythiophene); PEG, Polyethylene glycol; PEO, Polyethylene oxide; PES, Polyethersulfone; PET, Polyethylene terephthalate; PGA, Polyglycolic acid; PHA, Polyhydroxyalkanoates; PHBV, Poly(3-hydroxybutyrate-co-3-hydroxyvalerate); PI, Polyimide; PLA, Polylactic acid; PLCL, Poly (L-lactide-co-ε-caprolactone); PLGA, Poly (lactic-co-glycolic acid); PLLA, Poly (L-lactic acid); PM, Particulate Matter; PMDES, Polymer melt differential electrospinning; PMIA, Poly (isophthaloyl meta-phenylene diamine); PMMA, Poly (methylmethacrylate); PMN-PT, Lead magnesium niobate-lead titanate; PNS, Peripheral nervous system; PPy, Polypyrrole; PS, Polystyrene; PSA, Polysulfonamide; PSS, Polystyrene sulfonic acid; PSU, Polysulphone; PTFE, Polytetrafluoroethylene; PU, polyurethane; PVA, Polyvinyl alcohol; PVAc, Poly(vinyl acetate); PVDF, Poly(vinylidene fluoride); PVDF-HFP, Poly(vinylidene fluoride-co-hexafluoropropylene); PVP, Polyvinylpyrrolidone; PZT, Lead zirconate titanate; RHE, Reversible hydrogen electrode; RO, Reverse osmosis; ROS, Reactive oxygen species; SAED, Selected area electron diffraction; SCI, Spinal cord injury; SEBS, Styrene-Ethylene-Butylene-Styrene; SEM, Scanning electron microscopy; SIBs, Sodium-ion batteries; SiO₂, Silicon dioxide; SMCs, Smooth muscle cells; TEM, Transmission electron microscopy; TENG, Triboelectric nanogenerator; TEOS, Tetraethyl silicate; TFE, Trifluoroethanol; THF, Tetrahydrofuran; TiO₂, Titanium dioxide; TPU, Thermoplastic polyurethanes; TRP2, Tyrosinase-related protein-2; UF, Ultrafiltration; UV, Ultraviolet; VEGF, Vascular endothelial growth factor; XAFS, X-ray absorption fine structure; XANES, X-ray absorption near edge structure; XAS, X-ray absorption spectroscopy; XPS, X-ray photoelectron spectroscopy; XRD, X-ray diffraction; ZnO, Zinc oxide; ZrO₂, Zirconium oxide.

offer a forward-looking perspective on the future of electrospun nanofibers, emphasizing the need for continued innovation in both academic research and commercial applications.

1. History and development of electrospinning

Nowadays, nanofibers are believed to be the vanguard of essential fibrous materials [1]. They have gained massive attention from material scientists around the globe because of their ability to tailor the behavior of materials targeting a vast range of applications which signifies the extent of their potential [2]. Additionally, their fundamental features (*i.e.*, high volume, tailored fiber and membrane porosity and surface structures) and unique shape lead to the production of extremely light weight and highly porous materials with tuned average pore size and regulated fiber structure along with certain mechanical, chemical, and thermal characteristics to meet needs of targeted of applications [3,4]. Nanofibers can be fabricated by several manufacturing techniques [5–9]. Among these techniques, electrospinning is one of the most versatile, easy, and relatively economical production processes. Introduced by William Gilbert, the concept of the process dates to sixteenth century, but there was not much progress reported until the 20th century [10]. One of the most important discoveries and breakthroughs of the 20th century in electrospinning field was made by Sir. G. I. Taylor. He established the theoretical underpinning of electrospinning and designed mathematical modeling of conical shape of the fluid droplet formed in an electric field, which is now known as Taylor's cone [11]. Lately, it was Reneker's group and Wendorff's group whose work gave high recognition to the electrospinning process and made it a famous process [2,10]. Since then, a huge number of researchers have joined/pursued this field which has resulted in an exponential rise in the number of research articles (*i.e.*, from few articles per annum in the early 2000 s to over 3600 articles in 2023) featuring studies on various characteristics of electrospinning process and the resultant nanofibers, which provide new insights into the prominent aspects of the process.

Typically, a standard electrospinning set up is simple in terms of apparatus, whereas the behavior of the process is quite sophisticated. Simply, electric force is applied to form liquid jet by distorting a hemispherical liquid drop into a Taylor cone, which is readily drawn and solidified [12]. The liquid jet moves in a straight line at first for a short distance, suffers devastating bending instability, and takes a spiraling and loop path with evolving circumference [13]. Production of nanofibers is influenced by several factors from material characteristics including conductivity, concentration, and molecular weight of the material, to process parameters such as applied voltage, flow rate, tip-to-collector distance, *etc.* Furthermore, bending instability in the presence of electric force is observed during electrospinning process because of the competition between lateral bending and axial compression near collector surface. Fluid jets may offer intricate whipping dynamics with multi-level bending instabilities [14]. This buckling frequency of the unstable fluid jets is determined by various factors such as solution viscosity and jet velocity, *etc* [15].

The development of electrospinning is mainly categorized into four stages, *i.e.*, conventional electrospinning, electrode-assisted

Table 1
The development and evolution of different electrospinning techniques over time.

Stage	Year	Typical event
Exploratory	1878	Rayleigh pointed out that when the electrostatic repulsion on the surface of a droplet exceeds the surface tension, small jets will form on its surface [29].
Foundation	1934	Formalas invented an experimental device for the preparation of polymer fibers using electrostatic forces and applied for a patent [30].
	1936	Norton applied for the patent of melt electrospinning [31].
	1964	Taylor revealed that droplets can form cone shape and subsequently eject when subjected to high pressure, known as the "Taylor cone". The cone shape can maintain equilibrium at 49.3° of cone angle [11].
Renaissance	1990 s	Reneker group conducted extensive in-depth studies on electrospinning process and application. They investigated the spinnability and processing parameters of various polymers [32,33].
Development	2001	Wendorff et al. leveraged the rapid evaporation of solvent to produce PLLA fiber with porous structure [34].
	2003	Ko et al. constructed continuous nanofiber yarn [35].
	2003	Greiner et al. used coaxial electrospinning to produce core-sheath nanofibers [36].
		Xia et al. proposed a strategy using coaxial electrospinning to fabricate inorganic hollow fiber [37].
	2004	
	2004	Yarin et al. were the first to propose needleless electrospinning [38].
	2003	Xia et al. utilized parallel electrodes to collect oriented polymeric and ceramic nanofiber [39].
		Xu et al. used disk collector to prepare aligned nanofibers [40].
	2004	Chase et al. collected aligned nanofibers using rotary copper wire drum [41].
		Jiang et al. fabricated an aligned nanofiber array by magnetic electrospinning [42].
	2007	
	2005	Lin et al. prepared bicomponent nanofibers based on side-by-side electrospinning [43,44].
	2006	Lin et al. reported near-field electrospinning [45].
	2006	Ding et al. obtained 2D polymer nanowebs via electrospinning/netting [46].
	2007	Zhao et al. used multi-fluid electrospinning to produce fiber with multi-channel structure [47].
	2014	Ding et al. reconstituted fragmented electrospinning nanofibers into three-dimensional aerogel with superelasticity and multifunctionality [48].
	2015	Mai et al. proposed a general synthesis strategy for complex nanotubes by gradient electrospinning and controlled pyrolysis [49].

electrospinning, near-field electrospinning (NFES), and mechano-electrospinning. All these electrospinning setups produce different structures of nanofibers. Conventional electrospinning is used to produce traditional randomly oriented nanofiber nonwovens which limits its application in single fiber devices. Electrode-assisted electrospinning is used to fabricate fiber assembly (aligned nanofibers). However, the process cannot control the position of an individual fiber. NFES can regulate the position of an individual nanofiber which is essential for devising nano-scaled structures and equipment [16]. Mechano-electrospinning enables the fabrication of controlled position and morphology of nanofibers which is vital for designing equipment that requires precisely controlled patterns with customized fiber morphology [17].

Different innovations in both fiber generation as well as collecting systems have also been introduced. For instance, the use of multi-nozzles and multi-component nozzles along with stationary and dynamic needleless nozzles have been reported to manufacture different types of nanofiber structures targeting a variety of applications [11]. Furthermore, different collectors with customized designs (*i.e.*, plates, cylindrical drums, discs, *etc.*) and dynamics have been introduced in conventional electrospinning setups to ensure selective deposition of nanofibers [13]. Additionally, different materials, *i.e.*, glossy paper, conventional nonwovens and metal meshes wrapped over cylindrical drums, have been reported as the collectors to generate tailored nanofiber designs. The use of these collectors can also produce aligned nanofibers as well as nanofiber yarns. Lately, portable electrospinning devices have also been reported to instantly produce wound care dressings [18–20]. These developments have resulted in enhanced controllability of electrospinning process to produce a variety of nanofiber structures from disordered nanofiber mats to highly customized nanofiber structures. By now, it has been established that the electrospinning process is versatile enough to produce nanofibers from almost all kinds of materials such as natural and synthetic polymers, metals, alloys, ceramics, and composites. In recent years, using different tools and techniques for fiber generation and collection setup, a wide variety of fibrous morphology and architectures have been produced including bioinspired fibers [21], bonded fibers [22], porous fibers [23], core-sheath fibers [24], hollow fibers [25], spider-web-like fibers [26], and ribbon and necklace-like fibers, *etc* [27].

Electrospun nanofibers fabricated by these processes have been employed for numerous applications ranging from the hottest fields of defense, energy, and personal protection to complicated fields like healthcare and environmental engineering, *etc.* [28]. Furthermore, extensive research and development in the past two decades have concluded that electrospun nanofibers offer enormous potential for various fields. Efforts have been made to commercialize the use of electrospun nanofibers to transfer their amazing benefits to the public. In this regard, rising interest and active engagement of commercial companies such as eSpin Technologies, Nano Technics, KATO Tech, and Elmarco Ltd., implies significance and impact of electrospinning in the field of material science [10]. Some companies such as Freudenberg and Donaldson Company have even been earning significant capital by reaping the benefits of electrospun nanofibers for the last couple of decades. Moreover, the COVID-19 pandemic has further pressed the need for designing ultrafine filtration materials for efficient personal protection. Therefore, scientists are now highly interested in improving the productivity of the electrospinning process while retaining small diameters and precisely controlled fiber morphology to meet the growing demand for nanofibers for commercial applications. The development and evolution of the different electrospinning technologies are summarized in Table 1.

2. The Structure, Composition, and properties of electrospun nanofibers

The electrospinning technique stands out for its remarkable versatility in fabricating one-dimensional (1D) nanomaterials with versatile structures from a broad range of materials, variable microscopic structures, various properties and applications. Regarding structures, the nanofibers with controllable diameter, shape, secondary microscopic outer and inner structures can be facily created.

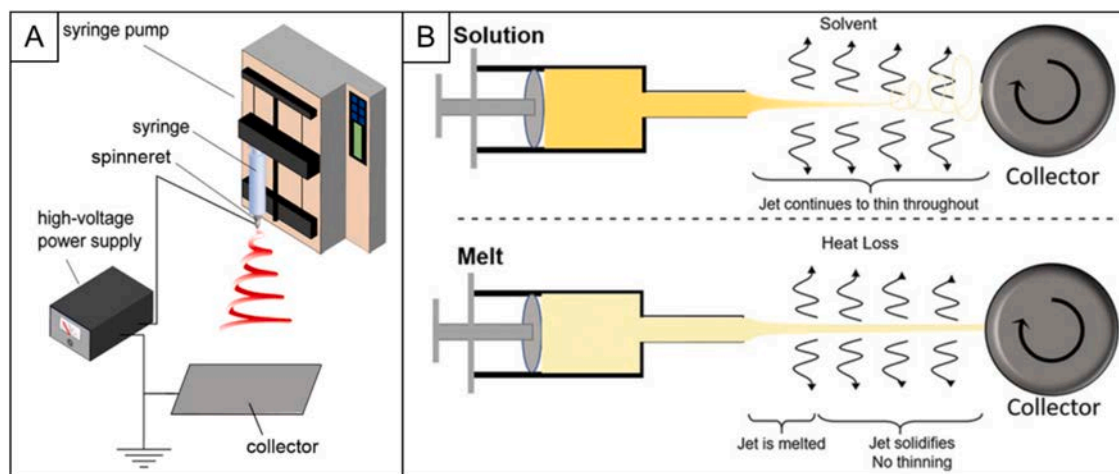


Fig. 1. (A) Schematic illustration of a typical setup for electrospinning. Reproduced from ref. [50] with permission from the American Chemical Society, copyright 2017. (B) Schematic demonstrating fundamental differences between solution and melt electrospinning. Reproduced from ref. [52] with permission from the Wiley-VCH, copyright 2018.

It enables the fabrication of nanofibers from different materials, including polymers, small organic molecules, metals, metal oxides, and organic/inorganic hybrids. Through direct electrospinning, indirect doping, or chemical conversion methods, nanofibers composed of polymer, assembled small molecules, metals, metal oxides, carbon, and organic/inorganic composites have been generated. By virtue of the diverse composition and structures, it is imaginable that the properties of electrospun nanofibers are diversified, and the derivative functions and applications are widespread in many domains.

2.1. Adjustable diameters of the electrospun nanofibers

The successful construction of various electrospun nanofiber products with various properties and functions is based on the electrospinning of nanofibers to a controllable diameter on a 1D level. The principles and key factors for electrospinning the raw materials into nanofibers are different depending on the electrospinning technologies [10,50–52]. In general, solution and melt electrospinning are the two most commonly used methods (Fig. 1) [50,52].

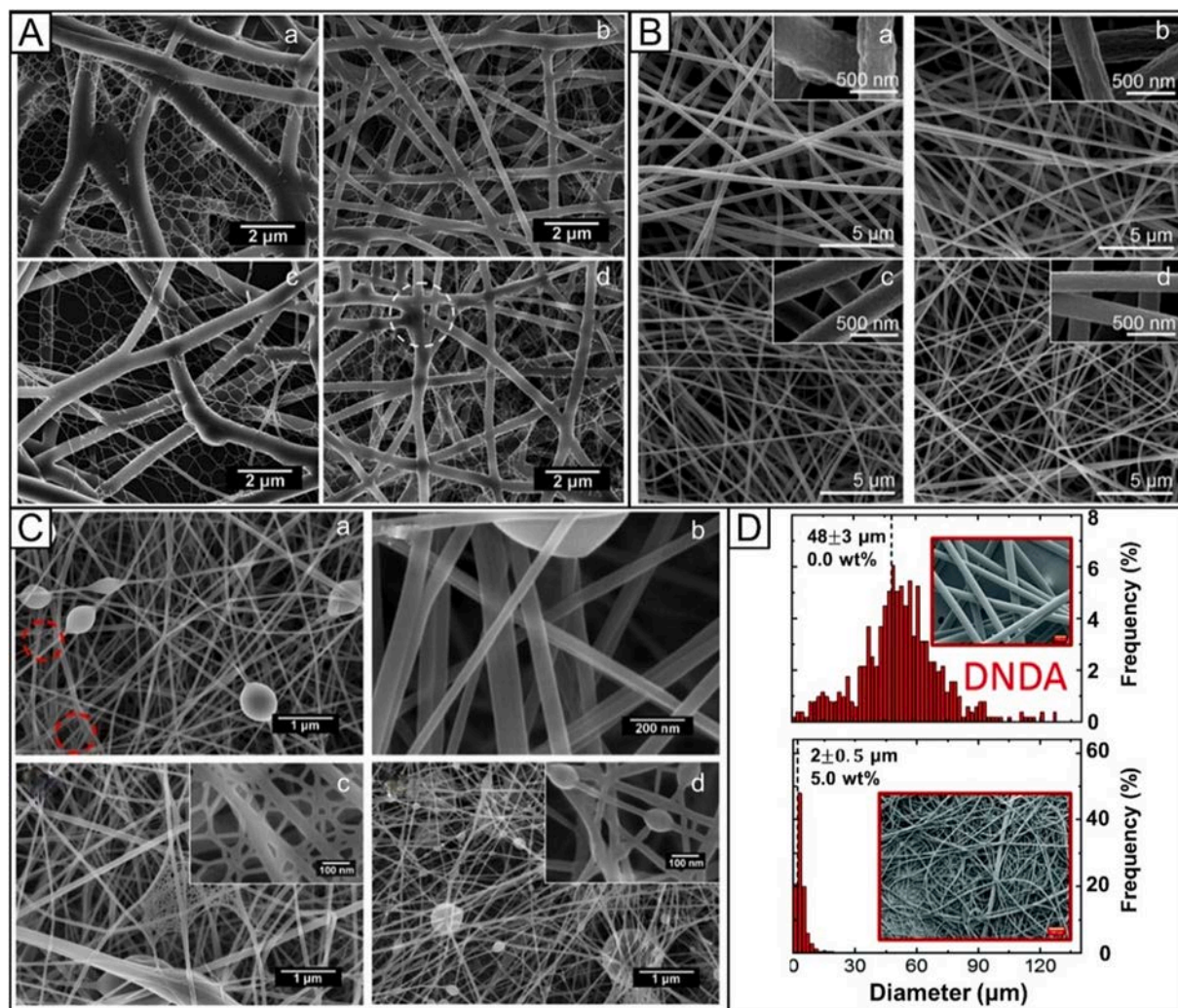


Fig. 2. Different methods to control electrospun fiber diameter. (A) Voltage: SEM images of PU/NaCl (0.1 wt%) nanofiber membranes obtained at different voltages, distances and relative humidity: (a) 20 kV, 15 cm, 25 %; (b) 40 kV, 15 cm, 25 %; (c) 30 kV, 25 cm, 25 %; (d) 30 kV, 15 cm, 55 %. Reproduced from ref. [54] with permission from Wiley-VCH, copyright 2011. (B) Temperature: SEM images of PAN nanofibers prepared under different working temperatures, (a) ambient temperature (20 $^{\circ}\text{C}$), (b), 40 $^{\circ}\text{C}$, (c) 60 $^{\circ}\text{C}$, and (d) 80 $^{\circ}\text{C}$. The upper-right insets show enlarged images of the corresponding PAN fibers. Reproduced from ref. [59] with permission from Springer, copyright 2017. (C) Humidity: SEM images of fibers electrospun from 10 wt% gelatin/FA solution containing NaCl (0.1 wt%) at temperature of 15 $^{\circ}\text{C}$ (a and b) (voltage of 30 kV, and RH of 25 %) and different RH: (c) 45 % and (d) 60 % (voltage of 30 kV, temperature of 24 $^{\circ}\text{C}$). The insets are the corresponding higher-magnification images. Reproduced from ref. [60] with permission from Elsevier, copyright 2011. (D) Electrical conductivity of the melt: SEM images (scale bars = 200 μm) of the electrospun fibers and the corresponding histogram graphs of the fiber diameter before and after adding additive in the melt (top to lower row). Reproduced from ref. [61] with permission from Royal Society of Chemistry, copyright 2021.

Solution electrospinning. For solution electrospinning, the raw material or precursor (usually a polymer) is first dissolved in a suitable solvent (usually a volatile organic solvent) to form the electrospinning solution with suitable concentration, volatility, and polarity [50]. A large number of solvents have been used in electrospinning, including alcohol, methylene chloride, trichloromethane, dimethylformamide (DMF), tetrahydrofuran (THF), acetone, dimethylsulfoxide (DMSO), hexafluoroisopropanol (HFIP), and trifluoroethanol (TFE) *etc.* The electrospinning solution is then stretched into filaments under the action of an external electric field, so that it gradually solidifies into nanofibers with the evaporation of solvent. This process involves the formation of a Taylor cone, the jet extension, stretching and volatilization of the solution, and the solidification phase [10,50]. The jet will eventually deposit on the collector and form stacked electrospun fibers. The diameter of the final dried fibers can be about 1.3×10^{-3} times that of the initial jet, and this size difference is huge [51].

The radius of the jet during the electrospinning process has a decisive influence on the size of the final nanofibers. Specifically, the terminal jet radius can be described as [53]:

$$d_t = \left(\gamma^\varepsilon \frac{Q^2}{I^2} \frac{2}{\pi(2\ln\chi - 3)} \right)^{1/3}$$

where d_t is the radius of the terminal jet, γ is the surface tension, ε is the dielectric constant of the medium, Q is the flow velocity, I is the current through the jet, and $\chi \sim R/h$ (h is the diameter of the jet, and R is the radius of curvature) is the dimensionless wavelength that causes the instability of the normal displacement. The flow velocity, current, and surface tension have a strong influence on the jet radius. The flow velocity and the magnitude of the surface tension are positively correlated with the fiber radius, while the magnitude of the current is negatively correlated, and together they determine the final received jet radius. These parameters, in turn, are determined by a combination of operating parameters, including applied voltage (V), flow velocity, nozzle diameter, and tip-to-collector distance, as well as material properties, including conductivity (K), dielectric constant (ε), dynamic viscosity (μ), surface tension (γ), and density.

During the electrospinning process, the operating parameters, including applied voltage, flow velocity, nozzle diameter, and tip-to-collector distance are often tailored to adjust the diameter of the obtained fibers. The applied voltage is an important influencing parameter that determines the current of the jet, the magnitude of the electrostatic repulsion between the carried charges, and the interaction between the jet and the external electric field. In general, a higher voltage results in the formation of finer electrospun fibers. As the current (I) rises during the jetting process, it leads to greater solution stretching, resulting in thinner fibers, which has been confirmed in many studies (Fig. 2A) [54–57]. However, it is important to note that a higher voltage may also lead to an increase in the ejection of the liquid from the nozzle, which means that the flow rate (Q) will increase. This will cause an increase in the size of the electrospun fibers. Such a paradox has now likewise been demonstrated in a number of studies. For example, one study showed that the fiber diameter initially increased with increasing voltage, but beyond a certain voltage, the fiber diameter started to decrease [58].

The tip-to-collector distance synergistically affects the diameter of the end product along with the voltage. A sufficiently long distance ensures that the jet extends and solidifies sufficiently to form the theoretical minimum fiber diameter. However, when the voltage is increased, the accelerated flow rate results in less flying time for the jet to stretch prior to deposition, potentially resulting in incomplete stretching and thus increased fiber diameter. To address this issue, an attempt may be made to increase the distance from the tip to the collector [62]. Of course, when this distance is long enough, the diameter of the fibers does not continue to decrease because the solution has completely evaporated, and the polymer has solidified into fibers [10]. Even beyond a certain distance, the fiber diameter may increase due to a significant weakening of the field strength [57,63].

The nozzle is the starting point for the formation of the jet. It is important to achieve a balance between the feed rate of the solution, the applied electric field, and the diameter of the nozzle to have the narrowest distribution of fiber diameters. Too fast feed rate will coarsen the fibers, even forming periodic drops of solution from the nozzle, while too slow feed rate results in spinning interruptions and the continuous formation and disappearance of Taylor cones in the nozzle, leading to large deviations in fiber diameter. Whenever possible, special attention needs to be paid to the possibility of a clogged hollow needle nozzle.

In addition to the operating parameters, the nature of the polymer solution itself can have a tremendous effect on the diameter of electrospun fibers. The first is the dielectric constant of the solution, which reflects the intermolecular charge distribution and polarity. In general, a lower dielectric constant means that the electric field propagates better in the solution and the charges are more likely to collect on the surface of the jet, which promotes fiber formation [64]. As a result, a lower dielectric constant usually results in smaller diameter fibers. This reveals the reason why water is usually not used as a solvent for electrospinning, as it has a higher dielectric constant.

The conductivity of a solution indicates the ability of an electric charge to conduct through the solution and is determined by the conductivity of the solvent itself. A higher conductivity means that the charge can move more easily through the solution, and therefore during electrospinning, the charge will be distributed more uniformly in the jet, leading to a bending instability of the solution jet, allowing for an increased stretching path, which reduces the diameter distribution of the fibers [65,66]. Therefore, smaller electrospun fibers are sometimes obtained by adding organic/inorganic salts to the solvent, or by mixing highly conductive solvents to increase conductivity [10,67,68].

Surface tension is an important property of the solution in the electrospinning process. A critical value of voltage is required to generate a sufficiently strong electrostatic repulsion to overcome the surface tension of the solution, thus ejecting the jet to form the spinning fiber [10,11,69]. Surface tension is thus a hindering factor for electrospinning, and the higher it is the more difficult to spin and the larger the diameter of the electrospun fibers. This is another reason why water as a solvent is difficult to electrospin because of its high surface tension. The surface tension can be reduced by using surfactants, and the introduction of cationic/anionic surfactants

can also increase the conductivity at the same time, further reducing the diameter of electrospun fibers. For example, one study was able to produce electrospun poly(vinylidene fluoride) (PVDF) fibers with an average diameter of less than 65 nm by adding hexadecyl trimethyl ammonium bromide [70]. It is important to note that the introduction of surfactants can also introduce impurities to the electrospun fiber product, which should be considered in advance during design.

Viscosity is also an important property of the solution and depends on the interaction forces among the polymer molecules, *i.e.* their chain entanglement [10]. This is determined by both the molecular weight and the concentration of the polymer. In general, a sufficiently large molecular weight and a sufficient concentration are necessary for electrospinning into fibers to ensure sufficient chain entanglement [71]. However, the resulting viscosity hinders the ejection of the solution from the nozzle on the one hand and increases the diameter of the ejected jet on the other hand [72]. Thus, lowering the viscosity of the solution facilitates the formation of finer fibers. However, too low a viscosity may prevent the formation of fibers. For example, by lowering the molecular weight of the polymer, beads rather than fibers tend to be produced. Besides, the selection of a suitably volatile solvent is critical throughout the electrospinning process. If the solvent evaporates too quickly, the polymer will solidify at the nozzle and cause blockage. If the solvent evaporates too slowly, a large amount of solution remains when it falls on the collector, causing the fibers to melt and form a film instead of fibers [73].

Some external factors also affect the final diameter of the electrospun fibers by influencing the parameters raised above, such as ambient temperature and humidity. At elevated temperatures, the solvent evaporates faster, preventing the extension of the jet and resulting in an increase in the fiber diameter. On the other hand, an increase in temperature itself causes a decrease in both the surface tension and viscosity of the solution, which reduces the size of the fibers. The optimal solution for fiber size can be achieved by choosing the appropriate temperature. In one study, the effect of ambient temperature on the diameter of electrospun fibers of two polymers, polyacrylonitrile (PAN) and polyvinylpyrrolidone (PVP), was separately investigated [59]. PAN was dissolved in dimethylacetamide (DMAc), and the optimum temperature was found to be 69 °C, with a minimum fiber diameter of 250 nm. For PVP in ethanol, the optimum temperature was found to be 39 °C, with a corresponding fiber diameter of 415 nm (Fig. 2B) [59].

The effect of humidity on fiber diameter depends on the interaction between the solution and the surrounding water vapor. Like temperature, the effect of humidity on the jet is multifaceted. On the one hand, at low relative humidity, the solvent evaporates faster, resulting in an increased rate of solidification and thus generating larger fiber diameters (Fig. 2C) [60]. On the other hand, when the relative humidity is too high, water condenses on the surface of the jet, causing the polymer to precipitate quickly, preventing polymer extension and leading to larger diameters. Therefore, the ambient humidity also needs to be optimized.

In a word, the diameter of electrospun fibers is determined by a combination of factors, and these parameters interact with each other to affect the behavior of the electrospinning jet, which in turn has an impact on the structures and properties of the resultant fibers. Comprehensively adjusting the solution composition and properties and regulating various operating parameters can regulate these parameters to a certain extent, thus realizing the control and optimization of the electrospinning process as well as the fiber diameter.

In recent years, by continuously optimizing the parameters, researchers have attempted to produce very fine nanofibers. For example, nanofibers with a diameter of about 20 nm have been constructed by introducing a cationic surfactant, dodecyl trimethylammonium bromide, and optimizing the ambient humidity, which has been applied in air filters [25]. In addition, borrowing some other external aids can also be used to construct ultrafine nanofibers, such as the aid of introducing an air stream. Airflow was initially used for melt-blown production of fibers with diameters of a few micrometers. By introducing this technique appropriately, the size of electro-discharged nanofibers can be drastically reduced. For example, poly(vinyl alcohol)/poly(3,4-ethylenedioxythiophene): polystyrene sulfonic acid (PVA/PEDOT:PSS) composite ultrafine fibers were successfully prepared using a high-pressure airflow-assisted electrospinning technique [74]. The average diameter of the nanofibers could be as low as 68 nm, which could be attributed to the high air-induced shear and elongation stresses that reduced the solution viscosity.

Melt electrospinning. Unlike solution electrospinning, melt electrospinning does not need solvent [52]. The polymers used in melt electrospinning typically have a melting temperature and do not decompose in the molten state, which is the fundamental requirement of melt electrospinning [75]. At high temperatures, the polymer is melted into a liquid state and then ejected into fibers by mechanical extrusion as well as by voltage. This makes thermoplastic polymers ideal candidates, such as polyurethane (PU), polycaprolactone (PCL), polylactic acid (PLA), and polymethylmethacrylate (PMMA). In addition, polymers such as polyethylene (PE) and polypropylene (PP) are difficult to dissolve in solvents suitable for solution electrospinning. In addition, polymers such as polyethylene and polypropylene are difficult to dissolve in solvents suitable for solution electrospinning. In such cases, this insoluble problem can be avoided by electrospinning directly from the melt. The heating device also plays a key role in the process of melt electrospinning, and by using electrically heated belts, circulating fluids, or even lasers, the proper temperature in the nozzle needs to be maintained to ensure that the polymer remains in a molten state [76,77].

Melt electrospinning is suitable for high molecular weight polymers, where meltability and flowability are key to a successful electrospinning process. Meanwhile, melt electrospinning allows the preparation of fibers with higher mechanical properties because the molecular chains of polymers in the molten state can be better aligned. In this process, the choice of polymer, the design of the heating device, the temperature control, and the adjustment of the processing parameters all affect the morphology, size, and properties of the final fibers to varying degrees. Typically, the fiber diameter depends mainly on the viscosity and the electrical conductivity of the melt fluid as well as the processing parameters.

The viscosity of the molten fluid depends on a number of factors, including the nature of the polymer itself, the processing temperature, and the applied voltage. The nature of the polymer, especially the molecular weight and chemical structure of the polymer, affects the viscosity. The interaction forces between polymer molecules and the arrangement of the molecular chains affect the mobility of the polymer molecules. Polymers with higher molecular weight typically have higher viscosities because longer molecular

chains increase the intermolecular interaction forces. In addition, the chemical structure of the molecular chains, such as the degree of branching and the location of the branches, also affects the mobility of the polymer and thus the viscosity of the fluid. It is also possible to reduce the viscosity and thus the diameter by adding additives into the polymer melt that can reduce the viscosity. For example, a PP fiber was successfully reduced in diameter from $35 \pm 8 \mu\text{m}$ to $840 \pm 190 \text{ nm}$ by the addition of viscosity-reducing Irgatec additives [78]. Temperature is another important factor that affects the viscosity of the molten fluid. Generally, as the temperature increases, the thermal mobility of molecules is enhanced, the intermolecular interaction forces are weakened, and thus the viscosity of the fluid is reduced. In melt electrospinning, the appropriate temperature can reduce the viscosity of the polymer and make it sufficiently stretched for fiber formation. Ambient temperature also has a significant effect on fiber diameter and properties. When a melt jet is ejected into a lower-temperature environment, the surface cools and solidifies rapidly, which can lead to faster fiber formation and thus coarser fiber diameters. Therefore, increasing the ambient temperature may also reduce the fiber diameter.

There exists a specific trade-off between diameter control and scalability in the electrospinning process, particularly when comparing solution electrospinning and melt electrospinning. While solution electrospinning offers superior diameter control, it is more challenging to scale up due to the reliance on solvents and drying processes. Conversely, melt electrospinning is more scalable and environmentally friendly, but it may sacrifice some degree of diameter precision, especially for certain high-viscosity or high-melting-point materials. Balancing these factors requires careful selection of materials and optimization of processing conditions, depending on the intended application and production scale.

The electrical conductivity of the polymer is another factor that affects the diameter of melt electrospinning. Similar to solution electrospinning, generally the higher conductivity makes the smaller fiber diameter. By adding additives with electrical conductivity, the fiber diameter can be effectively controlled. For example, the conductivity of linear low-density polyethylene (LLDPE) was increased by adding Hostatstat FA38, one commercial antistatic agent, resulting in the reduction of the fiber diameter from $48 \pm 3 \mu\text{m}$ to $2 \pm 0.5 \mu\text{m}$ by a factor of about 20 (Fig. 2D) [61]. In another study, the electrical conductivity of PP melt was increased by adding additives such as sodium oleate and sodium chloride, achieving an average fiber diameter of 310 nm [79].

The fiber diameter is also affected by the processing parameters, especially the temperature and the applied voltage. By analyzing these key factors in depth, the mechanism of melt electrospinning can be better understood to provide guidance for achieving desired fiber properties. These factors can be optimized in an integrated manner by combining various methods to obtain the smallest possible melt electrospinning fiber diameter. For example, sodium stearate and Irgastat® P16 were used as additives to increase the electrical conductivity of PP polymer melt, and at the same time, the process parameters could be optimized by optimizing the temperature of the climatic chamber, using different collector voltages, and varying the nozzle collector distance [80]. Increasing the ambient temperature to 100°C reduced the fiber size of the PP to about 210 nm.

Compared with solution electrospinning, melt electrospinning makes it somewhat easier to control fiber diameter and morphology due to the higher viscosity of the polymer itself in the molten state, reducing the effect of solvent volatilization from the solution. This is also a double-edged sword, as mentioned earlier, too high viscosity will naturally increase the diameter of the electrospun fibers, which is an important reason why it is difficult for melt electrospinning fibers to be as fine as solution electrospinning. In addition, another difference is that melt electrospinning does not have a polar solvent and therefore has a low electrical conductivity, and the jetting process also does not involve evaporation of the solvent, both of which can result in coarser fibers than those of solution electrospinning.

Although the size of the fibers generated by melt electrospinning is coarser compared to solution electrospinning, the absence of instability due to whipping makes the two-dimensional (2D), or even three-dimensional (3D) arrangement of 1D nanofibers more precisely controllable, allowing the formation of a variety of desired spatial structures and thus special performance. In addition, because of the absence of solvents, which are often polluting and require extensive post-treatment, melt electrospinning is naturally

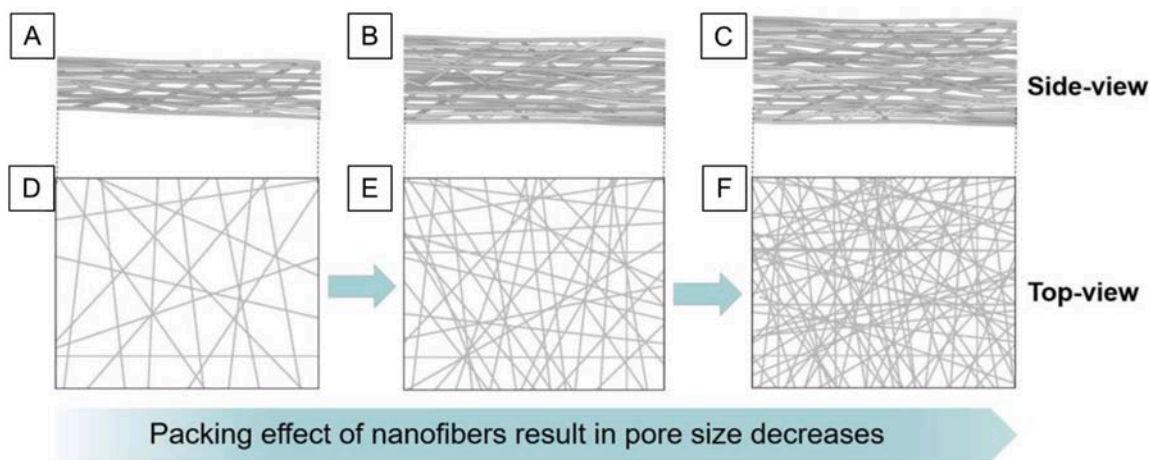


Fig. 3. The increase of the thickness of the nanofiber membrane results in a decrease in pore size owing to the packing effect. Reproduced from ref. [82] with permission from American Chemical Society, copyright 2019.

Table 2

Representative materials used for preparing electrospun nanofibers.

Types	Materials	Solvent	Parameter (voltage/flow rate/ distance)	Diameter	Ref.
Synthetic polymers	PCL	Chloroform and DMF	15–18 kV 0.5–1.5 mL h ⁻¹ 15 cm	412–1460 nm	[170]
		DCM and DMF	–4/16 kV	~100 nm	[171]
		Chloroform	20–22 kV 0.6–0.7 mL h ⁻¹ 20 cm	1215 µm	[172]
		Acetic acid	16 kV 0.5 cm h ⁻¹ 15 cm	~1 µm	[173]
		(TFE)	15 kV 2.5 mL h ⁻¹ 7.5 cm	980 ± 300 nm	[174]
		HFIP	22–23 kV 0.3–0.42 mL h ⁻¹ 15 cm	560 ± 28 nm	[175]
	PLA	HFIP	15 kV 1 mL min ⁻¹ 15 cm	1200 ± 230 nm	[176]
		Acetone and DMF	25–27 kV 0.5–1.2 mL h ⁻¹ 17 cm	200–500 nm	[177]
		Chloroform and DMF	50 kV 18 cm	830–1347 nm	[178]
		DCM and DMF	13 kV 1 mL h ⁻¹ 15 cm	550–730 nm	[179]
		PLLA	17 kV 0.5 mL h ⁻¹ 10 cm	30–500 nm	[180]
	PGA	DCM and DMF	10 kV 0.8 mL h ⁻¹ 22 cm	2469 ± 820 nm	[181]
		HFIP	15–20 kV 8 mL h ⁻¹	1 ± 0.37 µm	[182]
		PLGA	16 kV 1 mL h ⁻¹ 15 cm	705 nm	[183]
	PLCL	HFIP	11–13 kV 2.5 mL h ⁻¹ 18 cm	~1069 nm	[184]
		HFIP	12 kV 1.2 mL h ⁻¹ 10 cm	~1 µm	[185],
		HFIP	16 kV 0.2 mL h ⁻¹ 9 cm	908 ± 68 nm	[186]
		DCM	25 kV 1.5 mL h ⁻¹ 15 cm	373 ± 127 nm	[86]
		PU	10 kV 0.1 mL h ⁻¹ 10 cm	~1 µm	[187]
	PEO	Ethanol and H ₂ O	11 kV 0.1, 0.6, 0.9 mL h ⁻¹ 10 cm	0.6–1.2 µm	[188]
		H ₂ O	14 kV 1.0 mL h ⁻¹ 17 cm	450 ± 72 nm	[189]
		PGS	+15/–4 kV 1.2 mL h ⁻¹ 18.5 cm	468 ± 166 nm	[190]
	PVA	HFIP	18 kV 0.1–0.35 mL h ⁻¹ 10 cm	300–450 nm	[191]

(continued on next page)

Table 2 (continued)

Types	Materials	Solvent	Parameter (voltage/flow rate/ distance)	Diameter	Ref.
		DMF	55 kV 0.25 mL h ⁻¹ 25–28 cm	200–300 nm	[193]
	PET	Trifluoroacetic acid and DCM	20 kV 1 mL h ⁻¹ 14 cm	195 nm	[194]
	PAN		19 kV 0.6 mL h ⁻¹ 15 cm	~1 µm	[195]
		DMF	8.5–11 kV 0.6 mL h ⁻¹ 5 cm	800 nm	[196]
	PVDF	DMSO and acetone	10 kV 0.7 mL h ⁻¹ 10 cm	1400–2000 nm	[197]
		DMAc and acetone	1.8 kV 1.5 mL h ⁻¹ 2 mm	~10 µm	[198]
		DMF and acetone	–1.5 kV–18 kV 0.3 mL h ⁻¹ 0.5 mL h ⁻¹	0.5–1 µm	[199]
			22 kV	0.5–1.4 µm	[200]
	PVDF-HFP	DMF	0.5 mL h ⁻¹ 15 cm –2–13 kV	225.16 nm	[201]
		DMF and acetone	0.1 mm s ⁻¹ 15 cm 15 kV	300–400 nm	[202]
			1 mL h ⁻¹ 16 cm 16 kV	187.4 nm	[203]
	PS		0.6 mL h ⁻¹ 15 cm 10 kV 5 mL h ⁻¹	~100 nm	[204]
		DMF	15 cm 14 kV	9.54 ± 0.38 µm	[205]
		DMF and THF	1 mL h ⁻¹ 10 cm 12 kV 1.2 mL h ⁻¹ 20 cm	0.22–3.5 µm	[206]
	PES	DMF	21 kV 0.5 ~ 1 mL h ⁻¹ 15 cm	760–1360 nm	[207]
		DMAc and DMF	20 kV 0.8 mL h ⁻¹ 15 cm	1120 nm	[208]
	PA	Ethanol	35 kV 3 mL h ⁻¹ 20 cm	700 nm	[209]
		Formic acid	16 kV 0.5 mL h ⁻¹ 12 cm	155 nm	[210]
			30 kV 1 mL h ⁻¹ 20 cm	298–350 nm	[211]
		Formic acid and acetic acid	24 kV 0.15 mL h ⁻¹ 15 cm	81–297 nm	[212]

(continued on next page)

Table 2 (continued)

Types	Materials	Solvent	Parameter (voltage/flow rate/ distance)	Diameter	Ref.
	PMMA	DMF	16–20 kV 1.2 mL h ⁻¹ 12 cm	300 ± 50 nm	[213]
		DMAc and acetone	13.5 kV 0.8 mL h ⁻¹ 15 cm	180–300 nm	[214]
		DMAc	17 kV 0.8 mL h ⁻¹ 16 cm	200 nm	[215]
	PVP		18 kV		[216]
		Ethanol	0.2 mL h ⁻¹ 18 cm	200 nm	
		TFE	15 kV 1–1.5 mL h ⁻¹ 20 cm	239–341 nm	[217]
		DMF and THF	13 kV 30 µL h ⁻¹ 15 cm	0.2–1.3 µm	[218]
		DMF	21 kV 0.008 mm s ⁻¹ 20 cm	2–5 µm	[219]
	PEG		21.5–22.5 kV		[220]
		H ₂ O	0.6 mL h ⁻¹ 17 cm	1–2 µm	
	PC	Chloroform	18 kV 1 mL h ⁻¹ 15 cm	5–10 µm	[103]
		Chloroform camphor sulfonic acid PEO	25 kV 1–1.5 mL h ⁻¹ 20–26 cm	3.5–8 µm	[221]
	PANI	HFIP/PES	25 kV 0.5 mL h ⁻¹ 16 cm	213–901 nm	[222]
	PAA		23 kV	221–340 nm	[223]
		H ₂ O	0.8 mL h ⁻¹ 23 cm		
	PHEMA	Trifluoroacetic acid	26 kV 1 mL h ⁻¹ 13 cm	298–977 nm	[224]
		Ethanol	25 kV 3.8–80 µL min ⁻¹ 15 cm	269.7–1025 nm	[225]
Types	Materials	Solvent	Parameter	Diameter	Ref.
Natural materials	HA	PEO/DMEM	45 kV 0.8 mL h ⁻¹ 12 cm	120–348 nm	[226]
		H ₂ O	15 kV		[227]
	MeHA		0.02 mL h ⁻¹ 10 cm	74 nm	
		PEO/Photoinitiator/H ₂ O	18 kV 0.4 mL h ⁻¹ 26–27 kV	190 nm	[228]
		PS80/PEO/H ₂ O	17.5 kV 2 mL h ⁻¹ 17 cm	830 nm 125–305 nm	[229] [93]
	Sodium alginate	H ₂ O, DMSO/H ₂ O DMSO/ DMF	20 kV 10 µL min ⁻¹ 15 cm	100–150 nm	[230]
	Dextran		20 kV	0.28–0.88 µm	[231]
		Acetic acid	1 mL h ⁻¹ 20 cm		
	Chitin		12–17 kV 8–10 cm	~200 nm	[232]
		HFIP	0.1–1 mL h ⁻¹ 25 kV	30–700 nm	[233]
		Acetic acid/SDS	5 cm		

(continued on next page)

Table 2 (continued)

Types	Materials	Solvent	Parameter (voltage/flow rate/ distance)	Diameter	Ref.
			mL h ⁻¹		
			30 kV	247.2 nm	[234]
			15 cm		
	Chitosan		3/25 kV	73–95 nm	[235]
			0.60 mL h ⁻¹		
		Formic acid	20 cm		
			18 kV	320–350 nm	[236]
			0.5 mL h ⁻¹		
	Starch		10 cm		
			20 kV	635 ± 198 nm	[92]
		DMSO	1 mL h ⁻¹		
			15 cm		
			15–18 kV	70–264 nm	[237]
		Formic acid	0.6–0.8 mL h ⁻¹		
			15 cm		
	Gelatin	Acetic acid/H ₂ O/sodium dodecyl sulfate			[238]
			17–21 kV	297.6–565 nm	
			0.3 mL h ⁻¹		
			12 cm		
	Collagen		10–25 kV	200–500 nm	[239]
			30–69 μL min ⁻¹		
		HCL	12 cm		
			22 kV	208 ± 18 nm	[240]
			1.9 mL h ⁻¹		
		HFPmin–limal essential medium	12.5 cm		
			22 kV	~500 nm	[241]
			1.8 mL h ⁻¹		
			10 cm		
	Elastin		10–25 kV	200–500 nm	[239]
		HCL	30–69 μL min ⁻¹		
			12 cm		
	Silk fibroin		14 kV	0.1–0.7 μm	[242]
		Formic acid	20 cm		
			0.2–1.5 mL h ⁻¹		
		Aqueous solution	20 kV		[243]
			18 cm	370 ± 3 nm	
			1 mL h ⁻¹		
	Poly(γ-glutamic acid)	Trifluoroacetic acid	15 kV	255 ± 53 nm	[244]
			1 mL h ⁻¹		
			15 cm		
	PHBV	Chloroform/butanol	10 kV	2.2 ± 0.2 μm	[245]
			4 mL h ⁻¹		
			15 cm		
			15–16 kV	551 ± 122 nm	[246]
		Chloroform	0.5–1 mL h ⁻¹		
			10–18 cm		
			15–25 kV		[247]
		Chloroform	0.12–1.15 mL h ⁻¹	814 ± 91 nm	
			15 cm		
		Trifluoroacetyl	20 kV	1.2 ± 0.2 μm	[248]
			2 mL min ⁻¹		
			10 cm		
	PHB	Chloroform/DMF	15 kV	1.28 ± 0.22 μm	[249]
			0.7 mL h ⁻¹		
			9 cm		
Types	Materials	Solvent	Parameter	Diameter	Ref.
Inorganic materials	HAuCl ₄		15 kV		[250]
		Acetic acid	0.4 mm min ⁻¹		
		H ₂ O	15 cm	~250 nm	
	TiO ₂	Ethanol, Acetic acid	15 kV		[145]
			2.5 mL h ⁻¹	367 nm	
			15 cm		
	Al ₂ O ₃	H ₂ O, Ethanol, Acetic acid	22 kV	2720–1180 nm	[147]
			6 mL h ⁻¹		
			30 cm		

(continued on next page)

Table 2 (continued)

Types	Materials	Solvent	Parameter (voltage/flow rate/ distance)	Diameter	Ref.
	ZrO ₂	H ₂ O, Ethanol, Oxalic Acid	30 kV 2 mL h ⁻¹ 25 cm	500 nm	[148]
	SiO ₂	H ₂ O, Phosphoric acid	20 kV 1 mL h ⁻¹ 10 cm	642.3 ± 185.4 nm	[149]
Types Supramolecular materials	Materials Hydrocortisone:HP-β-CYD = 0.5:1, 1:1, 2:1 (the molar ratios)	Solvent DMF THF	Parameter 11 kV 0.3 mm min ⁻¹ 15 cm	Diameter 462 ± 94 nm	Ref. [251]
	Curcumin:CYD = 1:4 (the molar ratios)	H ₂ O	15 kV 0.5 mL h ⁻¹ 15 cm	165–940 nm	[252]
	HP-β-CYD	Distilled water	15 kV	505 ± 160 nm	[253]
	HP-γ-CYD	Tap water	0.5 mL h ⁻¹	1660 ± 275 nm	
Types Small molecules	Materials Phospholipid	Solvent	Parameter 16 kV 1 mL h ⁻¹ 15 cm	Diameter 976 ± 206 nm	Ref. [254]
	Ibuprofen, HP-β-CYD	H ₂ O	15 kV 0.5 mL h ⁻¹ 15 cm	210 ± 55 nm	[142]
	Ferulic acid, CD	H ₂ O	15 kV 0.5 mL h ⁻¹ 15 cm	220–1355 nm	[253]
Types Organic-Inorganic	Materials Ferric nitrate PAN	Solvent Acetic acid H ₂ O	Parameter 15 kV 0.3 mL h ⁻¹ 15 cm	Diameter 300–400 nm	Ref. [165]
	PAN		17 kV		[255]
	Fe ₂ O ₃	DMF	1 mL h ⁻¹	~650 nm	
	carbon nano-necklaces	HCl	12 cm		[256]
	Chitosan				
	Cobalt ferrite nanoparticles	TFA/DCM	15 kV		
	Titanium oxide nanoparticles	H ₂ O	0.5 mL h ⁻¹ 12 cm	110 nm	
	PAN	Ethanol	24 kV 1 mL h ⁻¹	600 nm	[257]
	TeNWs				
	PAN	DC, Dichloroethane, Trichloromethane	15 kV 1 mL h ⁻¹ 15 cm	~0.5 μm	[258]
	Bismuth nitrate pentahydrate KCl		25 kV 2 mL h ⁻¹ 15 cm		[166]
	PVP		12 kV		[259]
	Ni(NO ₃) ₂	H ₂ O	1.6 mL h ⁻¹ 12 cm	800 nm	
	Co(NO ₃) ₂		15 kV 0.5 mL h ⁻¹	279.34– 891.72 nm	[260]
	TBT, PVP	DMF	7 cm		
	Branched TiO ₂		16 kV 15 μL min ⁻¹ 13 cm	270–290 nm	[261]
	CS		40 kV		[262]
	PVA	DMF	1 mL h ⁻¹ 10 cm	250–300 nm	
	ZnO NPs		20 kV	290–400 nm	[263]
	PVP		0.5 mL h ⁻¹ 10 cm		
	SnCl ₂	DMF	18 kV		[264]
	PVA		0.6 mL h ⁻¹ 16 cm	200–400 nm	
	Zirconium-based MOF (UiO-66-NH ₂) particles	DMF			
	PVA				
	Lithium nitride	DMF			
	PVP				
	La(NO ₃) ₃ ·6H ₂ O, Fe(NO ₃) ₃ ·6H ₂ O, Ni(NO ₃) ₃ ·9H ₂ O	DMF			

(continued on next page)

Table 2 (continued)

Types	Materials	Solvent	Parameter (voltage/flow rate/ distance)	Diameter	Ref.
	PVA	H ₂ O	18 kV	439 ± 103 nm	[265]
	Sodium lignosulfonate		0.6 mL h ⁻¹		
			15 cm		
	Polyvinylidene difluorideethylene, glycol	DMF	22 kV	150 nm	[266]
			0.5 mL h ⁻¹		
			13 cm		
	TBT	DMF	18 kV	1.13–1.39 µm	[267]
	TEOS		4.5/0.6 mL h ⁻¹		
	PVP		15 cm		
	LiNO ₃	DMF		500 nm	[96]
	La (NO ₃) ₃ ·6H ₂ O		15 kV		
	Tributyltin		2 mL h ⁻¹		
	PVP/AlCl ₃ ·6H ₂ O	DMF	20 cm		
	Al ₂ O ₃				
	Acetic acid				
	PVP	DMF		200 nm	[268]
	Mn(CH ₃ COO) ₂ ·4H ₂ O		17 kV		
	NaNO ₃		15 µL min ⁻¹		
	Cu(NO ₃) ₂ ·3H ₂ O	DMF/Ethanol (ethanol:water = 1:1)	15 cm	400 nm	[168]
	Fe(NO ₃) ₃ ·9H ₂ O		15 kV		
	C ₄ H ₆ MnO ₄ ·4H ₂ O		0.5 mL h ⁻¹		
	C ₁₀ H ₁₄ O ₅ V	H ₂ O/PVP solution	15 cm	800–1000 nm	[169]
	PVP		17 kV		
	PS		1 mL h ⁻¹		
	PAN	Acetone and DMAc	15 cm	0.41–1.05 µm	[269]
	Co(Ac) ₂ ·4H ₂ O		16.5 kV		
	Ni(Ac) ₂ ·4H ₂ O		0.62 mL h ⁻¹		
	PAN	HFIP/Formic acid	17 cm	0.7 µm	[270]
	SnO ₂		25 kV		
	PLLA		0.8–1.2 mL h ⁻¹		
	MWCNTs		20 cm		
Types Organic-Organic	Materials	Solvent	Parameter	Diameter	Ref.
	CAB	DMF	11 kV	468.88 ±	[271,272]
	PEG	Acetone	1.5 mL h ⁻¹	154.08 nm	
			12 cm		
	PVDF	DMF	–2/20 kV	0.9 µm	[273]
	PDMS		1.1/0.44 mL h ⁻¹		
			18 cm		
	PMMA	DMF	18 kV	~800 nm	[274]
	PAN		2 mL h ⁻¹		
			12 cm		
	PCL	Chloroform, Methyl alcohol/ Chloroform	30 kV	8 µm	[275]
	PEG		3 mL h ⁻¹		
			20 cm		
	PCL	DCM and DMF	14–18 kV	500 nm	[276]
			1 mL h ⁻¹		
			13 cm		
	nHA	TFE	12 kV	0.38 ± 0.08 µm	[118]
			0.3 mL h ⁻¹		
			18 cm		
	PCL	Acetic acid	20 kV	95 ± 105 nm	[277]
	CS		0.3 mL h ⁻¹		
			12.5 cm		
		Acetic acid, H ₂ O	15 kV	0.1–0.2 µm	[278]
			10 µL min ⁻¹		
			22 kV		
	PCL	TFE and acetic acid	7.5 mL h ⁻¹	228 ± 95 nm	[279]
	β-cyclodextrin		15 cm		
			15 kV		
	PLLA	HFIP	15 kV	0.15–3 µm	[280]
	Lecithin		2 mL h ⁻¹		
			15 cm		
	PCL	HFIP	10 kV	441.6 ± 118.0 nm	[281]
	Gelatin		2 mL h ⁻¹		
			13 cm		

(continued on next page)

Table 2 (continued)

Types	Materials	Solvent	Parameter (voltage/flow rate/ distance)	Diameter	Ref.
		DMF and Chloroform	14 kV 0.4 mL h ⁻¹ 14 cm	372 nm	[160]
		DMF and THF	17 kV 1.2 mL h ⁻¹ 8 cm	1.42 ± 0.06 μm	[282]
	PVP Lecithin	THF/DMF	20 kV 2 mL h ⁻¹ 30 cm	100 nm	[283]
Types	Materials	Solvent	Parameter	Diameter	Ref.
Inorganic-Inorganic	SiO ₂ Ag	DMF	18 kV 0.05 mL min ⁻¹ 33 cm	~250 nm	[284]

more environmentally friendly. Also, solution electrospinning typically uses about 5–30 % polymer, so the productivity is also naturally lower than melt electrospinning. Currently, the bottleneck in the development of melt electrospinning, in addition to the inability to produce very fine nanofibers, another limitation is high temperature. The polymers themselves can withstand high temperatures without decomposition, but the functionalized small or large molecules expected to be loaded are often thermally unstable, especially for biomedical applications, which severely limits further expansion of functionality. Therefore, solution and melt electrospinning are complementary and indispensable, and the user has to consider all issues when choosing between them.

After continuous theoretical research and technological updates, the diameter of electrospun nanofibers can be controlled from a few nanometers to several micrometers, but most of them are still a few hundred nanometers. Achieving finer fibers is still a major challenge in the field of electrospinning. Already, some researchers have reported that the finest nanofibers can be as small as a few nanometers. Although very fine nanofiber products have been obtained, controllability and scalability are still poor, and there may be problems with overly complex electrospinning equipment and processes. Therefore, there is still a long way to go to achieve true “nano” fibers. It is believed that through the tireless efforts of researchers, the precise and easy availability of ultrafine electrospun nanofibers as well as their preparation in large quantities will soon be achieved.

2.2. Adjustable pore sizes of the non-woven network of electrospun nanofibers

The fundamental mechanism of electrospinning technique determines that the nanofibers are naturally deposited in a non-woven network structure because of the randomly whipping instability. Consequently, the nanofibers normally interweave to form a highly porous membrane. The pore size of the interweaved network mainly depends on the diameter of nanofibers and the thickness of the membrane [81]. In general, the finer fibers and thicker membranes result in smaller pore sizes (Fig. 3) [82]. However, smaller fiber diameters often correspond to weaker strengths. To achieve an electrospun fiber membrane with small pore size and sufficient strength, researchers have proposed a dual-scale fiber strategy that combines two kinds of fibers with quite different diameters. In this strategy, larger diameter fibers serve as the reinforcing framework, while smaller diameter fibers contribute to pore size reduction [69]. In addition to the 2D porous membrane composed of nanofibers, these nanofibers can also be assembled into 3D porous blocks through direct accumulating or indirect remodeling such as freeze-drying.

The 2D/3D porous structures endow nanofibers with numerous functional possibilities for various applications, including air filtration, liquid separation, pollution adsorption, waterproof breathable textiles, electromagnetic wave absorbing or shielding, sound absorption, battery separator, catalysis, tissue engineering, etc [83,84]. These applications are closely related to the pore size of the nanofibers. One significant application that relies on pore size is filtration, where porous media with appropriate pore sizes separate objects of different sizes. For instance, porous nanofiber membranes are crucial in air filtration, finding applications in masks, protective suits, air cleaners, air conditioners, and screen windows [81,85,86]. Owing to the small diameter, the nanofiber-based air filtration products can achieve a better filtration effect with reduced material consumption, which is much superior to common melt-blown fabrics. This advantage is particularly important in the background of COVID-19 pandemic [87]. Besides air filtration, the porous electrospun nanofiber membranes are also competent in liquid separation for particulate filtration, oil/water separation, and emulsion separation [71,88,89]. Except for these explicit filtration scenarios, some other applications of porous nanofiber membranes can be regarded as implicit “filtration”. For example, electrospun nanofibers can be fabricated as waterproof breathable textiles, which prohibit the penetration of continuous-phase bulk water while allowing the transport of water vapor (i.e., water molecules) [71,90]. The electrospun nanofiber membrane can also be used as battery separator, which prevents the electric conduction between anode and cathode while allowing reverse ion transfer.

In addition to tangible substances, the porous feature of electrospun nanofibers membrane combined with specific functional materials can be used for wave absorption such as electromagnetic wave absorbing/shielding or sound absorption. For example, magnetic conductive nanofibers are good candidates for light weight electromagnetic wave absorbing/shielding due to their suitable porous structure as well as tunable electromagnetic parameters, which is in favor of energy dissipation [91,92]. Furthermore, electrospun nanofiber porous membranes or 3D foam/aerogel blocks are also well-suited for sound absorption because of their flexible

Table 3

Preparation of nanofibers with different structures and their properties.

Structure	Composition	Preparation method	Property	Reference
Core-sheath nanofibers	Gelatin and PLLCL/EGF	coaxial electrospinning	drug release	[285]
	PEO/Silk and collagen/Flurbiprofe		antimicrobial	[286]
	PANi well blended P(LLA-CL)/PS/NGF		support neurite outgrowth	[287]
	PCL/Gelatin/G. sylvestre extracts		antimicrobial and antibiofilm	[84]
Hollow nanofibers	PVDF/CNT	coaxial electrospinning surface polymerization <i>in-situ</i> magnesiothermic reduction reaction	monitoring respiratory	[288]
	Carbon/Si		Li-ion battery anodes	[289]
			with high structural stability	
	Titanium alkoxide/PVP/PEO		photocatalysis	[290]
	Sn/SnO ₂ /Carbon		high-rate and long-life lithium-ion batteries	[261]
Porous nanofibers	ZnO	electrospinning and calcination method	operating temperature and sensitivity	[291]
	PVP/PSN	electrospinning	high-performance electrode materials	[292]
	PCL/PAN/PVDF	electrospinning	high porous and surface areas	[293]
	biomass tar/PAN/silver nanoparticles		antimicrobial	[294]
	PLA		typical nonsolvent performance	[295]
	SA/PEG/PLA	coaxial electrospinning	drug release	[296]
Fibers decorated with grooves or protrusions	PCL	gas-foaming technology and electrospinning	mimic the ECM	[297]
	PLA/Chitosan PLA/Chitosan/NFM	electrospinning	enhanced mineralization ability	[178]
	Carbon/SiO ₂ /Sb		antibacterial and biocompatible	
			excellent cycling stability and rate capability	[298]
	PCL/PVP	coaxial electrospinning	promoting migration and growth of cells and neurons	[217]
Bead-on-string nanofiber	TiO ₂ /α-Fe ₂ O ₃	electrospinning/hydrothermal	gas sensor	[299]
	PLLA	electrospinning and femtosecond laser	directing myoblasts behavior	[300]
	PLGA/Aspirin	electrospinning	drug release	[301]
	PLA/BSA		drug release	[302]
	PLGA/β-carotene	electrospinning	induced the early phase of osteogenesis	[303]
	PCL-b-PAA		promoting bone growth	[304]
	PLA/PCL		resembling ECM	[305]
	PCL/Chitosan		optimizing cell attachment, cell viability, metabolic activity	[306]
	PLA		air filtration	[307]
			filtration	[308]
	PCL		rapid tissue endothelialization	[156]
	PCL	electrospinning	promoting cells migration	[156]
Ribbon-like fibers			promoting bone growth	[309]
			super-hydrophobicity improved	[310]
			mechanical properties and osteogenic potential	
	Macro-hydroxyapatite/polyacrylate	wet-spinning	superior mechanical properties	[311]
Nanofiber yarns	PAN	needleless electrospinning	good photodegradation performance and mechanical property	[196]
	Gelatin	electrospinning	tunable fiber shape	[312]
	PLGA, PU, PVDF-HFP, cellulose	electrospinning	highly stretchable engineered microtissue	[313]
	PS		controlling the solvent and relative humidity	[100]
	PVB, CuO, V ₂ O ₅		wastewater cleaning	[314]
3D bulk nanofibrous scaffold	PLLA	dual-nozzle electrospinning	strengthened mechanical properties	[315]
	Cotton yarn, GO, PEI, AgNPs, PAN	multi-needle conjugated electrospinning device	antibacterial	[316]
		electrospinning, freeze-drying	excellent cytocompatibility and elastic properties in the wet state	[317]
	Gelatin, PLA		enhancing cathelicidin production	[318]
	PCL	gas-foaming technology and electrospinning		
Nanofibrous microspheres and aerogels	PCL/PCS	electrospinning and gas foaming	excellent antibacterial ability, hemocompatibility and biocompatibility	[319]
			higher cell carrier efficiency	
	PCL, gelatin, PLGA	electrospinning and electrospaying		[183]

(continued on next page)

Table 3 (continued)

Structure	Composition	Preparation method	Property	Reference
Nanofiber-elastomer composites	PCL/PLGA/gelatin/methacrylated gelatin/bioglass/magneto-responsive polymer composite	electrospinning	faster cell infiltration and host tissue integration	[320]
	PAN/BIP/CNC	electrospinning and homogenization	low-frequency sound absorption	[321]
	Cellulose acetate and PAN	electrospinning	flexible luminescence	[322]
	PUU/EDS/POSS	electrospinning	guiding myotube orientation	[323]
	SBS	electrospinning	high signal linearity and good reproducibility	[324]
	ZE/EGDE	melt electrowriting fused deposition modeling techniques	wound monitoring	[325]
	PCEC/GelMA/PLGA		increasing mechanical strength	[326]
Nanofiber-microcapsule composite	Chitosan/hydrogel	electrospinning	enhancing nerve regeneration	[327]
	PU/ scaffold-reinforced sulfobetaine methacrylate hydrogels		promoting vascular penetration	[328]
			higher resistance to tensile fracture and original non-fouling properties	
			ideal blood compatibility	[329]
			anticoagulation properties	
	PCL/gelatin/GelMA	electrospray	injectable	[329]
	TiO ₂	hydrothermal reaction	hybrid solar cell	[330]
Bio-printed nanofibrous scaffolds	PDVF/PVA/MOF	electrospinning	selective recognition and separation of atrazine	[316]
	PCL	electrospinning and 3D printing	promoting chondrocyte adhesion and infiltration	[331]
	PLLA	stable jet electrospinning	promoting nerve tissue regeneration	[332]
	Gelatin/GelMA/alginate/pHA	coaxial electrospinning and 3D bioprinting method	promoting bone vascularization and regeneration	[333]
	PCL/collagen/rGO	melt electrowriting technology	enhancing peripheral nerve regeneration	[334]

PLLCL, poly (*L*-lactic acid)-*co*-poly-(*ε*-caprolactone); EGF, epidermal growth factor; PEO, polyethylene oxide; PANi, polyaniline; NGF, nerve growth factor; P(LLA-CL), poly(*L*-lactic acid-*co*-*ε*-caprolactone); PS, polystyrene; PCL, Poly-*ε*-caprolactone; PVP, polyvinylpyrrolidone; PSN, polyureasilazane; PBT, poly(butylene terephthalate); PLLA, poly(*L*-lactic acid); PLCL, poly(*L*-lactide-*co*-*ε*-caprolactone); PAN, polyacrylonitrile; SA, salicylic acid; PEG, poly (ethylene glycol); PLA, poly (lactic acid); PVDF, poly(vinylidene fluoride); PVA, poly(vinyl alcohol); PLGA, poly (lactic-*co*-glycolic acid); PHBV, poly(3-hydroxybutyrate-*co*-3-hydroxyvalerate); PCL-*b*-PAA, polycaprolactone-polyacrylic acid.

fiber components and appropriate pore sizes relative to the wavelength of sound.

2.3. Large specific-surface-area of electrospun nanofibers

Electrospun nanofibers normally exhibit large specific-surface-area. Reducing the diameter of fibers is an effective method to improve the specific surface area, but it is challenging to reduce fiber diameter to less than 100 nm, say nothing of less than 10 nm. It means that it is quite limited to increase the specific surface area by simply making the fibers finer. Designing multi-structured fibers with features such as porous or hollow structures is another strategy to increase specific surface area and related properties [93-96]. Using electrospinning and template method, grape-cluster-like titanium monoxide@carbon hollow fiber with a larger specific surface area of 140.5 m² g⁻¹ was designed [97]. A facile single-nozzle electrospinning technique was applied to fabricate tube-in-tube composite oxides (including CoMn₂O₄, NiCo₂O₄, CoFe₂O₄, NiMn₂O₄ and ZnMn₂O₄) [98]. Among them, the NiCo₂O₄ tube-in-tube fibers achieved an impressive specific surface area of 47.3 m² g⁻¹, compared to 28.0 and 12.9 m² g⁻¹ for the NiCo₂O₄ nanotubes and solid 1D structures, respectively. To further increase the specific surface area, electrospun nanofibers can be combined with mesoporous or microporous zeolites, metal-organic frameworks (MOFs), porous carbon, etc. For example, an electrode structure was designed in atomically dispersed Co-N-C catalysts using electrospinning [99]. The Co-N-C electrospun nanofibers exhibited hierarchically microporous and a specific surface area of 825 m² g⁻¹, exposing more effectivity active sites and accelerating the mass/proton/electron transport of the reactant. A cross-scale pore-forming strategy was applied to create intriguing sponge fiber molecular sieves with hierarchical, tailorable, and molecularly defined nano-porosity by nanospace-confined chain-packing modulation at the molecular level [100]. The resultant polymeric fiber molecular sieves exhibited the integrated properties of ultrahigh surface area (860 m² g⁻¹), large pore volume (0.6 cm³ g⁻¹), and excellent molecular sieving performance, which could be applied in acetophenone/phenyl ethanol separation, hydrogen peroxide purification, ethyl acetate separation, and CO₂ adsorption fields.

2.4. Wide range of material resources for electrospinning

Electrospinning has been successfully applied to a wide variety of materials, including single-component materials (*i.e.*, synthetic polymers, natural materials, small molecules, supramolecules, inorganic materials, and carbon materials) and composite/hybrid materials (*i.e.*, organic/organic blend, organic/inorganic hybrid, and inorganic/inorganic blend). By selecting different categories of electrospinning raw materials, nanofibers' structure, properties, and functionality can be tuned to target specific applications. In this

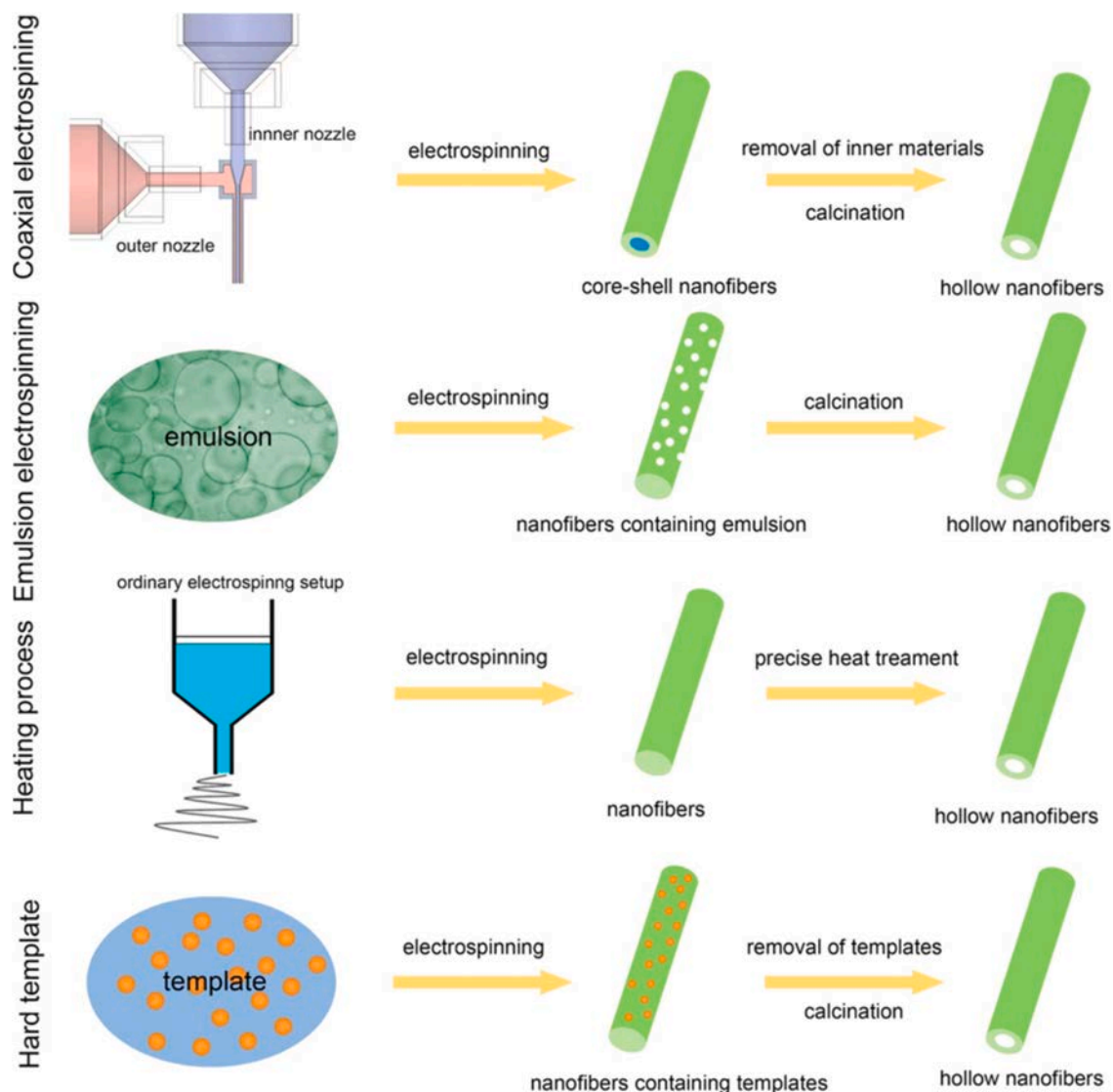


Fig. 4. Scheme Schematic of four main methods to prepare hollow nanofibers [342]. Reproduced from ref. [342] with permission from Elsevier, copyright 2017.

section, we provide a comprehensive overview of materials suitable for electrospinning, including various monomer and composite compositions, as well as their characteristics and application scenarios.

2.4.1. Single-component materials

A variety of single-component materials can be used to fabricate electrospun nanofibers, including synthetic polymers, natural materials, small molecules, supramolecules, inorganic materials, and carbon materials. Among them, synthetic polymers, natural materials, inorganic materials and carbon materials are the most commonly used materials in electrospinning. In contrast, small molecules and supramolecules have limited utilization.

Synthetic polymers. Hundreds of synthetic polymers with distinct mechanical, optical, and biological properties have been applied for generating nanofibers by electrospinning, which have been applied in various fields. Based on the specific requirements, selecting suitable synthetic polymers is the primary concern when constructing electrospun fibers. For example, PMMA is a promising building block for photonic circuits and integration as a polymer waveguide in optical nanofibers. This material can suppress the light effect and has excellent optical cavity function. This material can suppress the light effect and has excellent optical cavity function. The PMMA/PVDF fiber is produced by coaxial electrospinning, and the smooth surface of the PMMA material is conducive to the smooth transmission of light [101]. Polycarbonate (PC) offers excellent mechanical stability, hydrophobicity, and laser sensitivity. The surface properties of PC fibers can be changed by controlling voltage and ambient humidity during electrospinning, which can enhance water collection efficiency from fog [102]. In addition, laser irradiation technology can treat laser-sensitive PC fibers to form porous fibers for

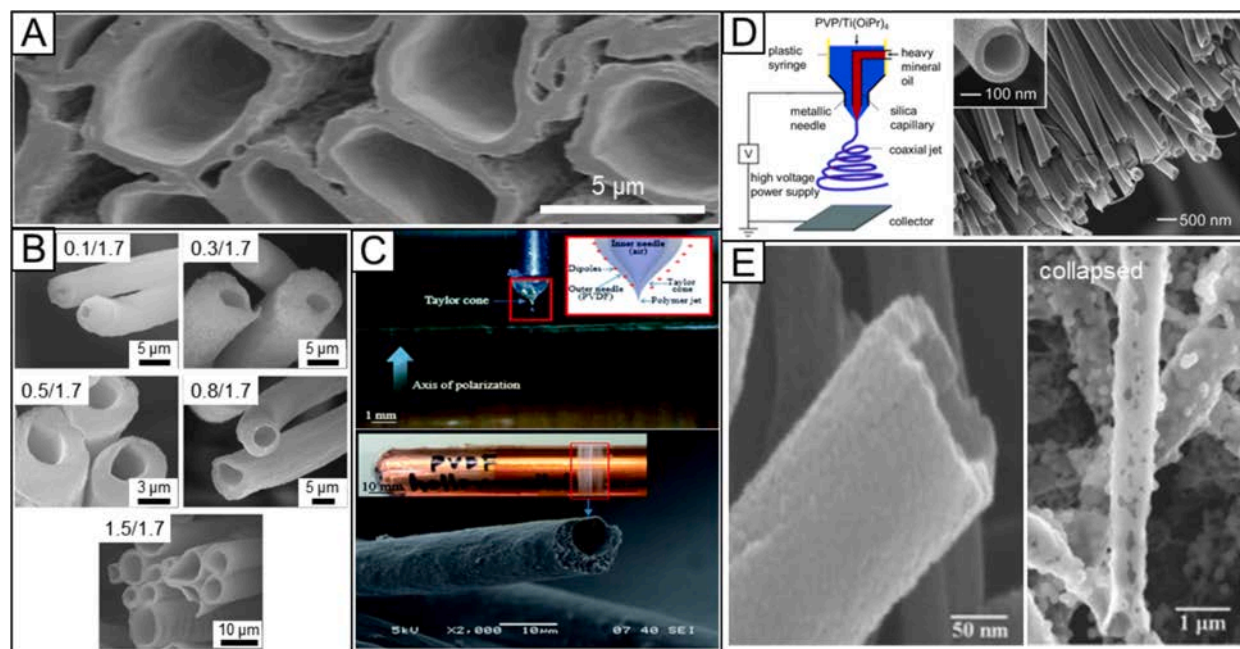


Fig. 5. (A) SEM image of PCL hollow fibers by co-electrospun PCL shell-PEO core fibers followed by removing the PEO core. Reproduced from ref. [344] with permission from Wiley-VCH, copyright 2007. (B) SEM micrographs of the PVDF/PVA microtubules prepared at different core/shell feed rates, 0.1/1.7, 0.3/1.7, 0.5/1.7, 0.8/1.7, and 1.5/1.7, respectively. Reproduced from ref. [345] with permission from Elsevier, copyright 2012. (C) The photograph of the Taylor cone during co-axial electrospinning when the inner needle was directly injected with air and the SEM micrograph of the formed electrospun hollow fibers. Reproduced from ref. [346] with permission from Royal Society of Chemistry, copyright 2015. (D) Schematic illustration of the co-axial electrospinning setup and the SEM micrograph of the formed electrospun nanofibers with a core/sheath structure. Reproduced from ref. [37] with permission from American Chemical Society, copyright 2004. (E) SEM micrographs of the calcined TiO_2 nanofibers and the fiber structure collapsed partly. Reproduced from ref. [347] with permission from Elsevier, copyright 2013.

the adsorption of volatile organic compound gases in the air [103].

A large class of synthetic polymers with biocompatibility have been electrospun into nanofibers for biomedical applications, such as PCL [104–107], PLA [108–111], polyglycolic acid (PGA) [112], poly(lactic-co-glycolic acid) (PLGA) [112–114], polyethylene oxide (PEO) [115], and polyvinyl alcohol (PVA) [116,117]. PVP, soluble in water and most organic solvents, has excellent solubility and physiological compatibility. Electrospun drug-loaded PVP nanofibers, owing to their hydrophilic properties, could facilitate the rapid wetting of the drug, promoting rapid release [118]. These nanofibers possess the suitable mechanical strength to withstand physiological loads while maintaining structural integrity. Furthermore, the nanofibers can mimic the components and structure of natural tissue extracellular matrix (ECM) due to their appropriate porosity and pore size, providing a suitable microenvironment for cell adhesion, migration, and proliferation. Notably, the degradation rate can be controlled, allowing for gradual absorption and replacement by newly formed tissue. Therefore, these polymers are extensively investigated as potential candidates for biomedical scaffold applications.

There are also polymers with multiple functions and properties that can be used in different applications. Polystyrene (PS) has good biocompatibility and hydrophobicity. The electrospun PS nanofibrous matrix could provide cells with a fibrous, topographically altered microenvironment, which activated internal related biochemical signals [119]. In addition, when the pore size of the electrospun PS membrane was adjusted to the correct size, vacuum aspiration could filter all the cells in the blood in a few seconds without causing mechanical damage [90]. Polyethersulfone (PES) has excellent heat resistance, corrosion resistance, physical and mechanical properties, insulation properties, etc. Therefore, it has been applied to adsorb free bilirubin from blood for the treatment of hypercholinemia [120] and as an efficient adsorbent for water pollution control [121]. Polyamide (PA) encompasses various materials, with PA-6 being the most commonly used for electrospinning. PA-6 exhibits a unique structure that enhances its solubility in common solvents. Electrospun PA nanofibers possess surface hydrophilicity, excellent mechanical strength, toughness, and remarkable biocompatibility [122]. Piezoelectric polymer nanofibers are commonly made into flexible sensors and are widely used in fields such as biomedical engineering [123], electronic skin [124], environmental monitoring [125], and sports equipment [126]. PVDF is a well-known piezoelectric polymer with excellent pyroelectricity, piezoelectricity, and high dielectric constants. Electrospun PVDF nanofiber membranes have higher piezoelectric outputs and mechanical properties by hot stretching [127].

Natural materials. Without chemical modification, natural materials are usually derived from plants, animals, and microorganisms. The most commonly used natural materials for generating electrospun nanofibers mainly include hyaluronic acid (HA), alginate, β -chitin [128], starch [129], silk fibroin [130], chitosan [131], collagen [132], gelatin [133] and so on. The rigidity, viscosity, surface tension, and conductivity of natural material solutions often result in poor spinnability, so special treatment processes or the addition

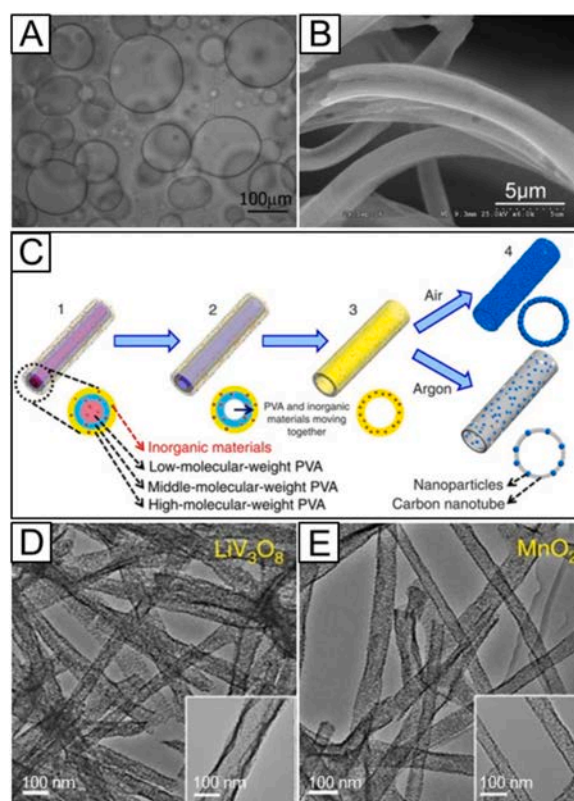


Fig. 6. (A) Optical image of a PMMA/PAN emulsion in DMF. (B) SEM image of core-sheath PMMA/PAN fibers after heat treatment. Reproduced from ref. [350] with permission from American Chemical Society, copyright 2007. (C) Schematic of gradient electrospinning and controlled pyrolysis method for the preparation of hollow nanofiber. TEM images of (D) LiV_3O_8 and (E) MnO_2 hollow nanofibers fabricated by the gradient electrospinning method. Reproduced from ref. [49] with permission from Springer Nature, copyright 2015.

of carrier polymers, as well as salt ions, etc., are usually required during electrospinning. A typical example is that the modification of HA is conducive to electrospinning due to its high viscosity properties, which allows for smooth processing. This modification has been widely applied in various fields of tissue engineering, such as drug delivery and tissue engineering scaffolds, due to its unique rheological properties and biocompatibility [134,135]. Silk fibroin, a protein-based material derived from silkworm cocoons, garners attention for its natural accessibility, physicochemical properties, biocompatibility, and adaptability. It is regarded as a promising material for developing a more sustainable generation of devices. A study successfully demonstrated the electrospinning of conductive polymers in the form of blended polypyrrole (PPy) with natural biomaterials, and the prepared PPy-encapsulated silk fibroin fiber membrane was employed as an electroactive scaffold in myocardial tissue engineering, where it served to enhance the structural integrity and electrical conductivity of the myocardial tissues and to impart the desired viscoelastic properties [136].

Small molecules. Compared to synthetic polymers, small molecules have difficulty in generating sufficient chain entanglement, and therefore, fewer small molecule materials are available for electrospinning. Adequate interaction between small molecules is an essential factor [137], and supramolecular assembly occurs through strong noncovalent bonding interactions between molecules, which can guarantee the preparation of their highly concentrated solutions or pure melts for producing nanofibers.

The reported electrospun nanofibers based on small molecules mainly consist of amphiphilic compounds and cyclodextrins. Phospholipids are amphiphilic molecules with strong self-assembly ability. As the concentration of phospholipids increases, they will first be assembled into spherical micelles and then further assembled into cylindrical micelles. The cylindrical micelles can be directly intertwined with each other in a polymer-like chain entanglement, realizing the electrospinning of phospholipid small molecules. Due to the natural ability of micelles to encapsulate hydrophobic small-molecule drugs, electrospun phospholipid fibrous membranes have been used in drug-carrying and releasing systems [138]. Cyclodextrin is a series of cyclic oligosaccharides produced by amylose under the action of cyclodextrin glucose transferase, and supramolecular assembly can occur with strong hydrogen bonding between molecules. However, the low solubility of cyclodextrins limits their application in electrospinning. Increasing its hydrophilicity through chemical modification can create high-concentration aggregate solutions to prepare electrospun fibers. With the increase of solution concentration or viscosity, electrospinning will change the morphology from beaded to non-beaded fiber [139]. Furthermore, cyclodextrins can form molecular inclusion complexes with organic/inorganic substances, improving the solubility of certain substances that are not readily soluble in water, so cyclodextrins are commonly used in drug delivery and antibacterial activities, and the introduction of electrospinning technology can further control the release of drugs [140,141]. In one study, by utilizing the water

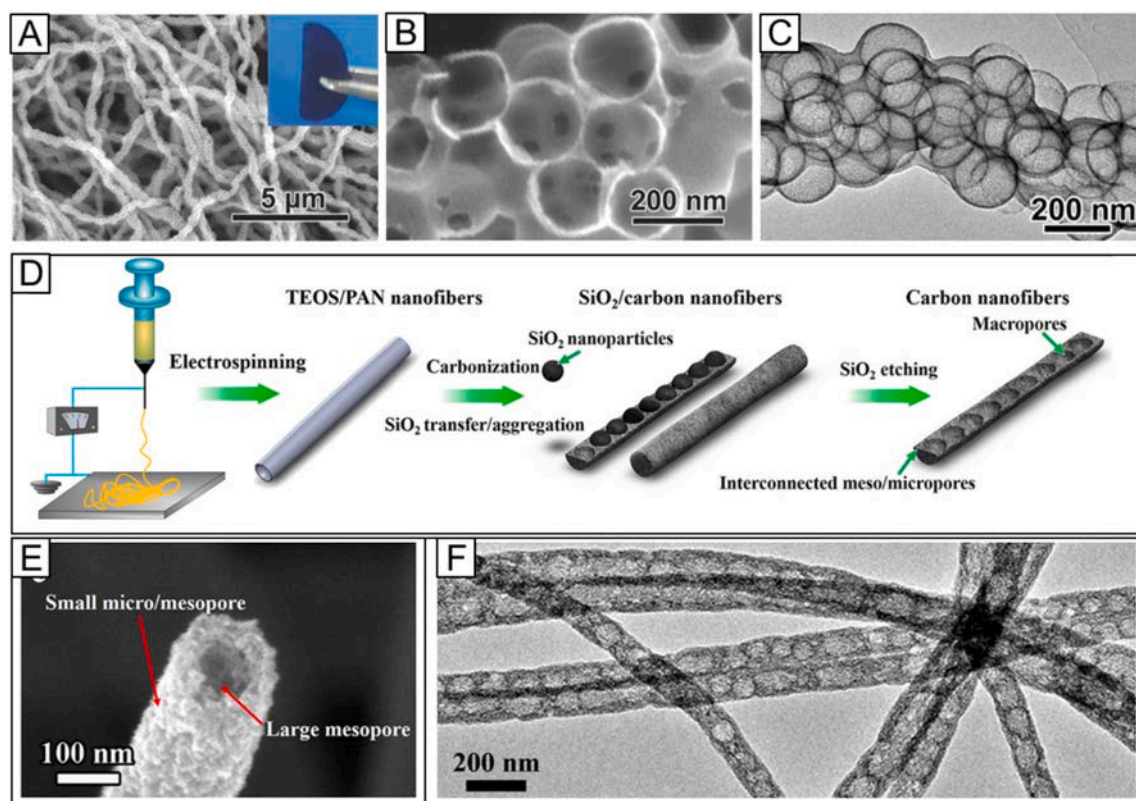


Fig. 7. (A, B) SEM and (C) TEM images of the macroporous active carbon fibers prepared by hard templates method. Reproduced from ref. [356] with permission from Wiley-VCH, copyright 2016. (D) Schematic diagram of the preparation process of bamboo-like carbon nanofibers. (E, F) SEM and TEM images of the bamboo-like carbon nanofibers. Reproduced from ref. [357] with permission from American Chemical Society, copyright 2015.

solubility and certain relative hygroscopicity of hydroxypropyl- β -cyclodextrin, cyclodextrin/ibuprofen inclusion nanofibers were prepared, which could significantly improve the water solubility of ibuprofen and achieve its controlled loading and release [142].

Inorganic materials. Inorganic materials for electrospinning include metals, oxides, and their derivatives, which can produce superior products in lighting, electronic displays, solar cells, and energy storage. Harnessing the fundamental properties of inorganic materials, these nanofibers are especially suitable for acid, alkali, corrosive, and other serious occasions. However, inorganic materials are difficult to dissolve in various solutions, so nanofibers composed of inorganic materials are often formed by electrospinning their precursors and then performing subsequent reactions.

For example, it is considered an effective method for solving the non-spinning of inorganic materials by electrospinning of colloids with a specific viscosity, obtained through the sol-gel method by hydrolyzing, condensing, and aging inorganic metal alkoxides or metal salts [143]. During electrospinning, the spinning nozzle emits a charged jet and undergoes hydrolysis so that precursor inorganic nanofibers can be deposited on the substrate [144]. A variety of inorganic nanofibers have been successfully prepared using this sol-gel method, including TiO₂ [145,146], Al₂O₃ [147], ZrO₂ [148], and SiO₂ [149–151]. However, fast hydrolysis rates tend to produce branched gel networks of monomers unsuitable for electrospinning. Meanwhile, too-slow condensation rates are not conducive to obtaining linear molecular chains with high degrees of polymerization, resulting in low entanglement between molecular chains and insufficient viscosity for electrospinning [152,153]. Therefore, the reactivity (hydrolysis rate) and degree of cross-linking (viscosity) between colloidal particles are critical factors in determining whether inorganic nanofibers can be produced. Fibers prepared by direct electrospinning of inorganic sols are usually hundreds of nanometers in diameter and poorly monodisperse. Additionally, it is difficult to accurately control the rheological properties of the sol, limiting the ability to control fiber size and uniformity. One method is to increase the viscosity of the precursor sol by introducing polymers with high molecular weight and significant degrees of chain entanglement as carriers in the sol-gel precursor [154]. After electrospinning a solution containing both the polymer and metal oxide precursor into a fine jet, the metal alcohol salt hydrolyzes and forms a continuous gel network within the polymer matrix. Subsequently, high-temperature calcination treatment evaporates the solvent and degrades the polymer, resulting in homogeneous, stable, smaller-diameter inorganic nanofibers [155].

2.4.2. Composite materials

Composite nanofibers are composed of at least two materials. Generally, composites can be categorized into three groups: organic-

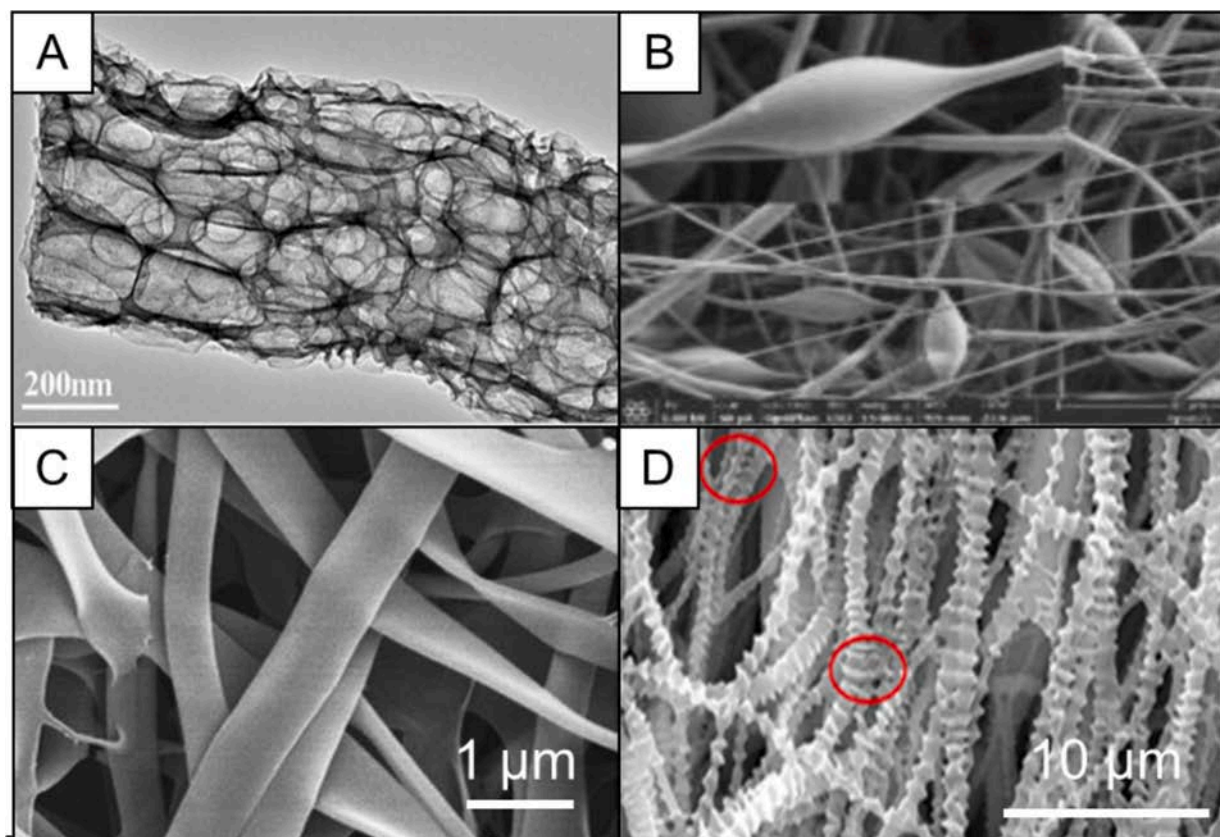


Fig. 8. (A) TEM images of the macroporous CNFs obtained by etching $\text{SiO}_2/\text{Sb@CNF}$ composites with an aqueous HF solution. Reproduced from ref. [298] with permission from American Chemical Society, copyright 2018. (B) SEM image of the porous bead-on-string PLA membrane. Reproduced from ref. [376] with permission from Elsevier, copyright 2023. (C) SEM image of nanoribbons obtained by electrospinning from aqueous solution of SELP47K [377]. Reproduced from ref. [377] with permission from Elsevier, copyright 2009. (D) SEM images of shish-kebab string structure on PCL fibers. Reproduced from ref. [156] with permission from American Chemical Society, copyright 2020.

organic, organic–inorganic, and inorganic–inorganic composites. Composite nanofibers can acquire new functions and enhance the original functions by utilizing the properties of different materials.

Organic–organic. Various organic materials incorporated into a composite nanofiber have been classified as mixing natural materials with synthetic polymers, mixing multiple natural materials, mixing various synthetic polymers, mixing polymers with organic small molecules, *etc* [156–158]. When different organic materials are used to construct composite electrospun nanofibers, the basic principle is to realize the complementary advantages of the respective components. In addition, organic–organic electrospun composite fibers can be obtained by introducing small organic molecules. The non-spinnable small molecules can be co-electrospun to provide additional functionality to the fibers or to improve the overall performance of the fibers. For example, distearoyl phosphatidylethanolamine-phospholipid layer-supported copolymerized PLGA electrospun fibers were tethered to CD11b/CD68 subpopulations screened in the immune milieu after tendon injury to counteract tissue damage [159]. Bioactive small molecules are also commonly used in electrospinning. Notably, some biotechnologies have also been introduced in combination with co-spinning systems, *e.g.*, electrospinning was combined with molecular blotting to produce different PCL/proteins (gelatin, collagen, and elastin) scaffolds [160].

Organic–inorganic. Organic and inorganic materials are two materials with vastly different properties. The rational composition of organic–inorganic materials can integrate the characteristics of the two materials and complement both advantages, providing new properties for developing and applying materials. Inorganic materials generally provide various functions, such as catalysis, piezoelectricity, *etc.*, while organic materials act as immobilization matrix, supporting and providing specific topologies [153]. Therefore, electrospinning organic polymers into nanofiber membranes followed by adsorption of inorganic nanoparticles on the membranes are reasonable methods of generating electrospun fibers made of organic–inorganic materials [161]. For example, CuO_2 , PVA, and PCL composite nanofiber membrane was fabricated by electrospinning to promote the healing of diabetic wounds [162].

Inorganic–inorganic. Inorganic–inorganic nanofibers integrate the advantages of two or more materials, significantly increasing their value for various applications. One way to prepare high-quality inorganic–inorganic nanocomposite structures is by combining the sol–gel method with electrospinning. In a typical procedure, $\text{In}_2\text{O}_3/\text{SnO}_2$ heterojunction nanostructures could be prepared using a simple sol–gel electrospinning approach [163]. The slight blue-shift of the absorption peak of $\text{In}_2\text{O}_3/\text{SnO}_2$ compared to In_2O_3

nanofibers increased the energy band gap value, effectively improving the photocatalytic performance for pollutant degradation applications. In another study, porous SnO_2 -CuO hollow nanofibers were fabricated using a two-step process involving single-needle electrospinning and heat treatment [164]. The SnO_2 -CuO nanotubes had 15 nm-thick walls, and CuO nanoparticles were uniformly distributed in the tubular SnO_2 structure through the heat treatment process at 600 °C because of the Kirkendall effect. The hollow structure of the nanofiber and the p - n junction between SnO_2 and CuO nanoparticles endowed the SnO_2 -CuO nanotube sensor with excellent sensing performance for H_2S gas. Another way to form inorganic-inorganic nanofibers is to post-treat the nanofibers, such as

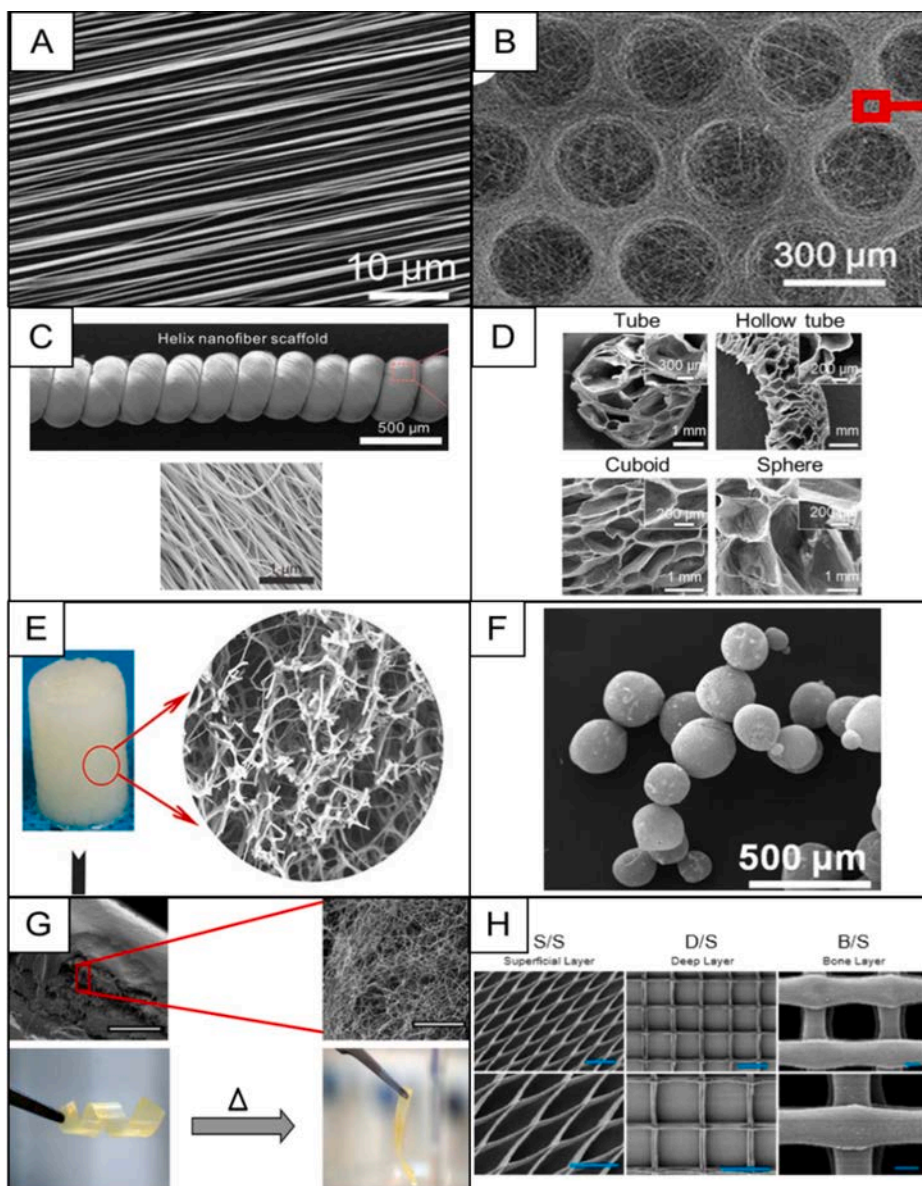


Fig. 9. (A) SEM image of the aligned PLGA nanofiber array. Reproduced from ref. [393] with permission from Springer, copyright 2019. (B) Morphology characterization of CS-PLA/PCL membranes. Reproduced from ref. [394] with permission from American Chemical Society, copyright 2017. (C) iSEM images of the hierarchical helix nanofiber yarn. Reproduced from ref. [313] with permission from National Academy of Sciences, copyright 2019. (D) SEM image showing the cross-section of cylinder-shaped nanofiber scaffolds with 0.25 mm thick. Reproduced from ref. [297] with permission from American Institute of Physics, copyright 2020. (E) SEM images of 3D scaffolds cross-linked with hyaluronic acid (HA). Reproduced from ref. [395] with permission from American Chemical Society, copyright 2016. (F) SEM images of NMs composed of PCL:gelatin:GelMA (1:0.5:0.5) nanofiber segments. Reproduced from ref. [329] with permission from Future Medicine, copyright 2019. (G) SEM images of the PEBA/PVA and PVA electrospun fiber mat, and the shape memory behavior of a PEBA/PVA composite film. Reproduced from ref. [396] with permission from American Chemical Society, copyright 2016. (H) SEM images of the fibrous networks prepared for the S (0°–30° orientation, 100 μm spacing), D (0°–90° orientation, 200 μm spacing) and B (0°–90° orientation, 600 μm spacing) layers. Reproduced from ref. [326] with permission from Elsevier, copyright 2021.

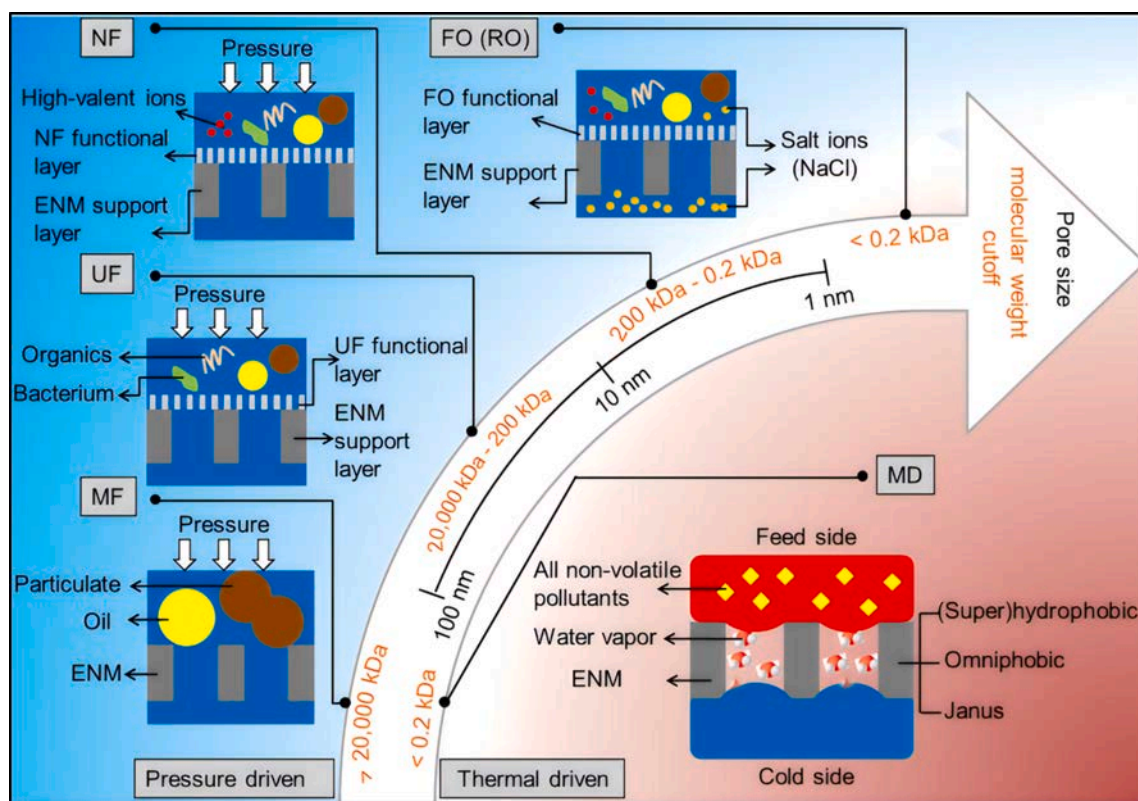


Fig. 10. Electrospun nanofibrous membranes for water filtration and desalination include pressure-driven filtration membranes based on micro-filtration (MF), ultrafiltration (UF), nanofiltration (NF), reverse osmosis (RO), and forward osmosis (FO), and thermal-driven filtration membranes.

calcination, where the organic material component is carbonized to form carbon fibers. This is the most common and simplest method widely used in batteries, water separation, catalysis, etc. For example, a flexible Fe_xO_y /nitrogen-doped carbon membrane was prepared by electrospinning and high-temperature carbonization using iron-based metal organogel as raw material [165].

Combining the two inorganic materials can lead to a unique topological structure, which can also provide new ideas for water separation [166]. A simple electrospinning-pyrolysis method was reported, which directly fixed uniform Ni_3Co nanoparticles into a hierarchical branched structure composed of nitrogen-doped carbon nanotubes grafted with carbon nanofibers (CNF) formed *in-situ* [167]. The elaborate construction of this hybrid hierarchical structure could effectively adjust the electronic structure and expand the exposure of the active center, promoting electron transfer and mass diffusion. In another study, through co-electrospinning and subsequent nitriding treatment, MnO nanoparticles with tailor-made structures were attached to the surface of vanadium nitride/CNF with good microwave absorption capacity [168]. Through electrospinning, phosphating, and carbonization steps, highly dispersed nickel cobalt oxide phosphorus nanoparticles were immobilized in multi-channel hollow carbon fibers [169].

To date, electrospun nanofibers have been derived from a wide range of materials. Table 2 lists representative materials used for electrospinning, along with their spinning parameters and the resulting fiber dimensions. The precise preparation of functional electrospun nanofibers tailored for specific applications is a key direction for future development.

2.5. Structure variation of electrospun nanofibers

2.5.1. Diverse structures of electrospun nanofibers

Electrospun nanofibers hold high surface area-to-volume ratio, porosity, and varied topological morphology. Due to the versatility of different electrospinning techniques, a wide range of secondary structures can be formed on individual fibers. These varieties can involve core-sheath fibers, hollow fibers, porous fibers, fibers decorated with grooves or protrusions, bead-on-string fibers, nanorod-on-nanofiber hierarchical structures, ribbon-like fibers, shish-kebab fibers, etc. The different structures of nanofibers and their properties are shown in Table 3.

Core-sheath nanofibers. Core-sheath nanofibers are mainly composed of an internal core and an external sheath component, and coaxial electrospinning technology is a versatile and effective strategy for preparing this structure [84]. The working mechanism and setup of coaxial electrospinning are consistent with conventional electrospinning [335], with only modification made to the nozzle, in which a smaller hollow needle is placed concentrically inside an outer hollow needle to obtain a coaxial setup. The outer needle is filled with sheath solution, while the inner needle is filled with core solution. Simultaneous pumping of the core and sheath solutions

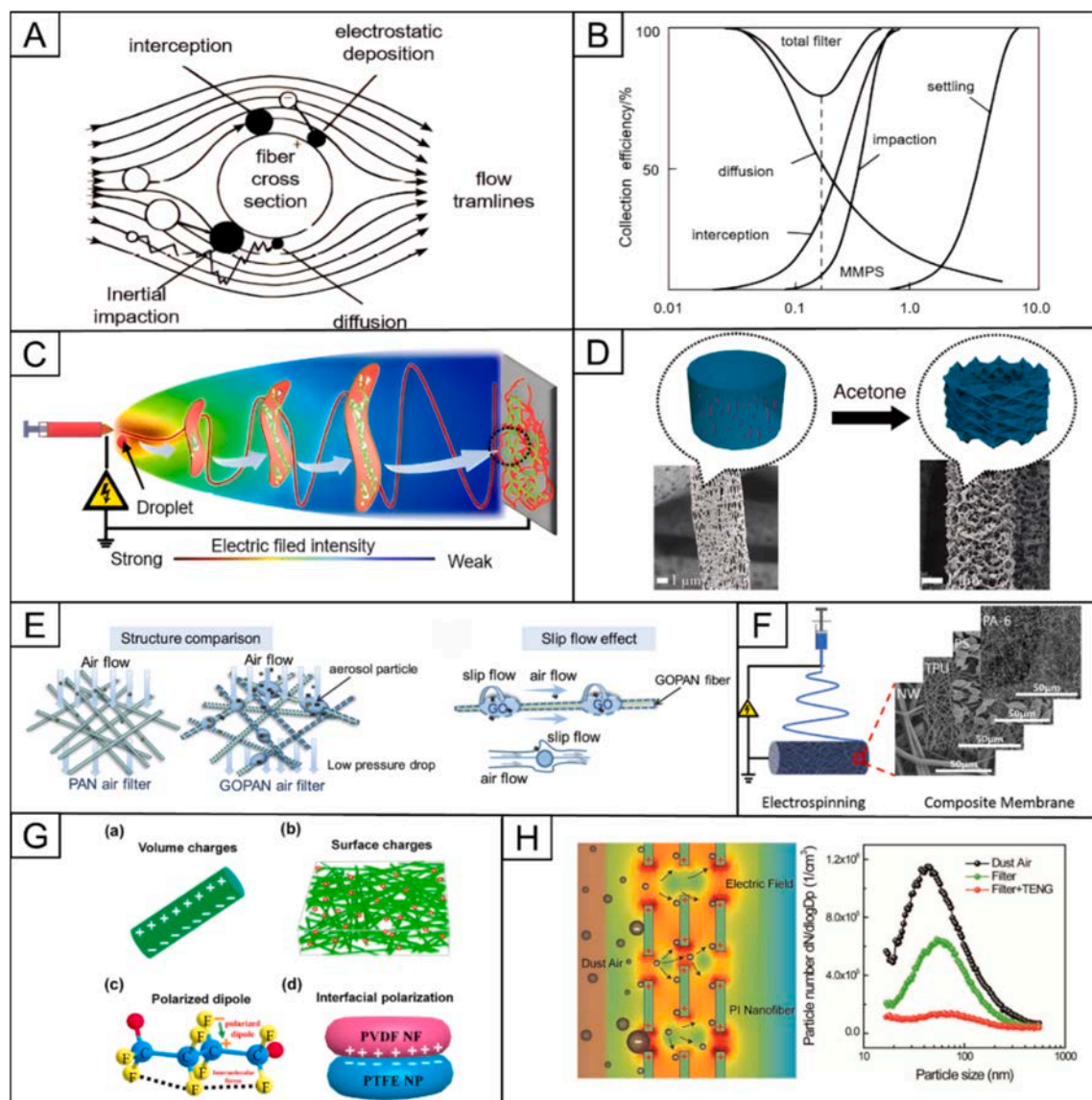


Fig. 11. The application of electrospun nanofibers for filtration of PM: (A) Mechanisms for particle filtration. (B) Dominate and total removal efficiency for particles with different sizes. Reproduced from ref. [482] with permission from Elsevier, copyright 2012. (C) Hypothetical simulation of electrospinning/netting process. Reproduced from ref. [483] with permission from Elsevier, copyright 2019. (D) Pore structure generated by using post-treatment with acetone. Reproduced from ref. [484] with permission from American Chemical Society, copyright 2019. (E) Structure comparison of PAN and GO/PAN nanofibrous membranes, and airflow slip-effect on beaded structure. Reproduced from ref. [485] with permission from Elsevier, copyright 2018. (F) The electrospun multilevel TPU/PS/PA-6 composite membrane on nonwoven substrate. Reproduced from ref. [204] with permission from Elsevier, copyright 2021. (G) The four types of electrified charges within PVDF/polytetrafluoroethylene (PTFE) membranes. Reproduced from ref. [486] with permission from American Chemical Society, copyright 2016. (H) Filtration mechanism and performance of the PI filter with rotating TENG. Reproduced from ref. [487] with permission from American Chemical Society, copyright 2017.

produces a core-sheath droplet at the nozzle. As with single-fluid electrospinning, the core-sheath droplet is elongated and stretched to form a Taylor cone under the action of the electric field. This is followed by the formation of a coaxial jet [336] and deposition on a substrate to form electrospun nanofibers with core-sheath structures [337]. The core component is surrounded by the sheath structure, allowing a different polymer to act as a protective sheath over the solid core of another polymer. This generates a variety of modified properties while maintaining the main fiber properties. For example, nanofiber membranes with lauric acid as the core layer and PS as the sheath layer were prepared to obtain a core-sheath structure with energy-dense and form-stable lauric acid PS core-sheath nanofibers, which have great potential for various thermal energy storage applications, such as building insulation, smart textiles, and electronic cooling systems, providing efficient temperature regulation and energy conservation [338]. Core-sheath nanofibers have also been identified as an effective strategy for achieving sustained drug release by encapsulating drugs, proteins, and cells within

a “core” layer for targeted or sustained release [337]. Coaxial electrospinning can also be combined with centrifugal spinning, which can prepare core-sheath nanofibers in large quantities at low cost and in a stable manner, solving problems such as nozzle clogging, high cost, and insufficient yield in traditional coaxial electrospinning [339]. It also enhances the possibility of processing dopants from high-viscosity spinning into composite nanofibers.

Hollow nanofibers. Hollow nanofibers are structurally removing the core from core-sheath fibers. Compared to ordinary fibers, the advantages of hollow nanofibers are mainly reflected in the following aspects: (i) the hollow structure endows the fibers with a larger specific surface area, increasing the possibility of subsequent engineering; (ii) the fibers have a large accessible active area, porosity, and sensitivity; (iii) the fibers possess a greater depth of space charge modulation, higher electron transport performance, and shorter ionic or electronic diffusion length. Nanostructures with hollow interiors are increasingly gaining attention due to their wide applications, including drug delivery, gas storage, sensing, energy conversion, and environmental protection [340,341]. As shown in Fig. 4, the construction of hollow nanofibers consists of four main methods: coaxial electrospinning, emulsion electrospinning, heating process, and hard templates [342,343].

As with core-sheath structures, coaxial electrospinning is one of the most common and simplest methods for preparing hollow nanofibers. After preparing the core-sheath fibers, hollow nanofibers can be easily obtained by removing the core layer. The different methods of removing the core layer structure can be categorized into one-step and two-step coaxial electrospinning methods. The one-step coaxial electrospinning method means that the desired hollow nanofibers can be obtained directly after co-axial electrospinning. In a typical example, PCL was used as the sheath layer and PEO as the core layer to obtain nanofibers with a hollow structure by coaxial electrospinning (Fig. 5A) [344]. The outer surface of the PCL shell experienced a dry spinning process due to exposure to the surrounding air, so diffusion and volatilization of solvent dominated the solidification and morphology of the outer surface. With strong infiltration of the sheath by PEO in core fluid, effective deposition of polymer resulted in the formation of nanofibers with hollow structures. Key factors in this process are the highly volatile nature of the core-sheath precursor solution and the sufficient wettability

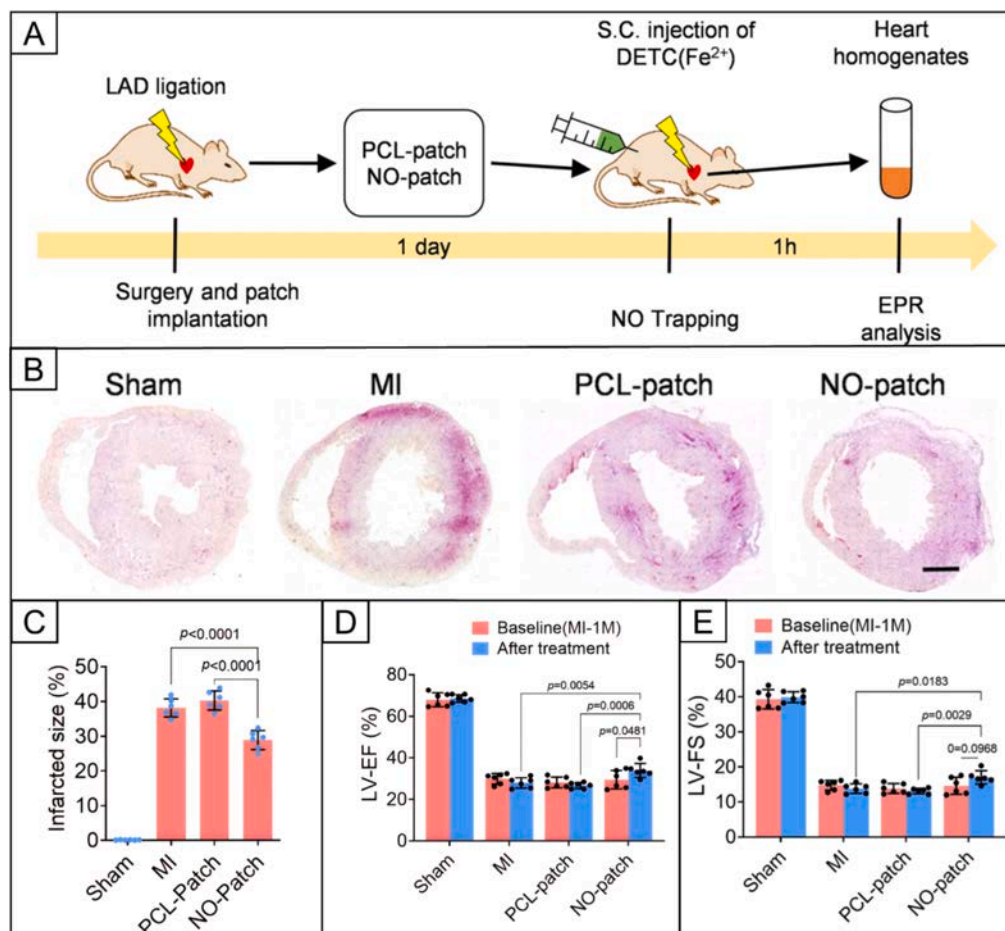


Fig. 12. Nitrate-functionalized patch used for cardiac repair. (A) The treatment of the NO-patch in a chronic mouse model. (B) Masson staining with different treatment after 4 weeks. (C) The infarcted size of different treatment. (D) The left ventricular (LV) ejection fraction (LV-EF) after different treatment. (E) The left ventricular fraction shortening (LV-FS) after different treatment. Reproduced from ref. [488] with permission from NATURE Publishing, copyright 2021.

of the core polymer. In another study, two incompatible polymer solutions (PVDF and PVA) were used as core and sheath fluids, respectively [345]. During the electrospinning process, the solvent of the PVDF solution evaporated to form a sheath, and subsequently, PVA was deposited on the inner surface of the sheath layer to obtain hollow nanofibers. The diameter and wall thickness of the hollow nanofibers can be controlled by adjusting the flow rate of the polymer solution. With the increase of core fluid feed rate, the outer diameter of the fiber significantly increased (Fig. 5B). In addition, the inner needle of coaxial electrospinning can be directly injected with air to realize the construction of a one-step hollow structure (Fig. 5C) [346]. As the gas flow rate of the inner needle increases, the inner diameter of prepared hollow fibers also increases accordingly. However, the gas flow rate cannot be increased indefinitely because the viscosity of the solution will not be able to withstand the air tension required to maintain the Taylor cone, resulting in an interruption of the electrospinning process.

The generation of hollow nanofibers by two-step coaxial electrospinning consists of (i) preparation of nanofibers with a core-sheath structure by the electrospinning process and (ii) removal of the core material by calcination, solvent extraction, or washing to obtain nanofibers with a hollow structure [343]. In an example, nanofibers with a core-sheath structure were prepared by injecting heavy mineral oil and an ethanol solution comprising PVP/Ti(OiPr)₄ into the inner and outer layers of a coaxial electrospinning needle, respectively. Uniform hollow tubular nanofibers could be obtained by octane extraction or high-temperature calcination (Fig. 5D) [37]. A similar method has been used to obtain two kinds of hollow TiO₂ nanofibers with different morphological characteristics after

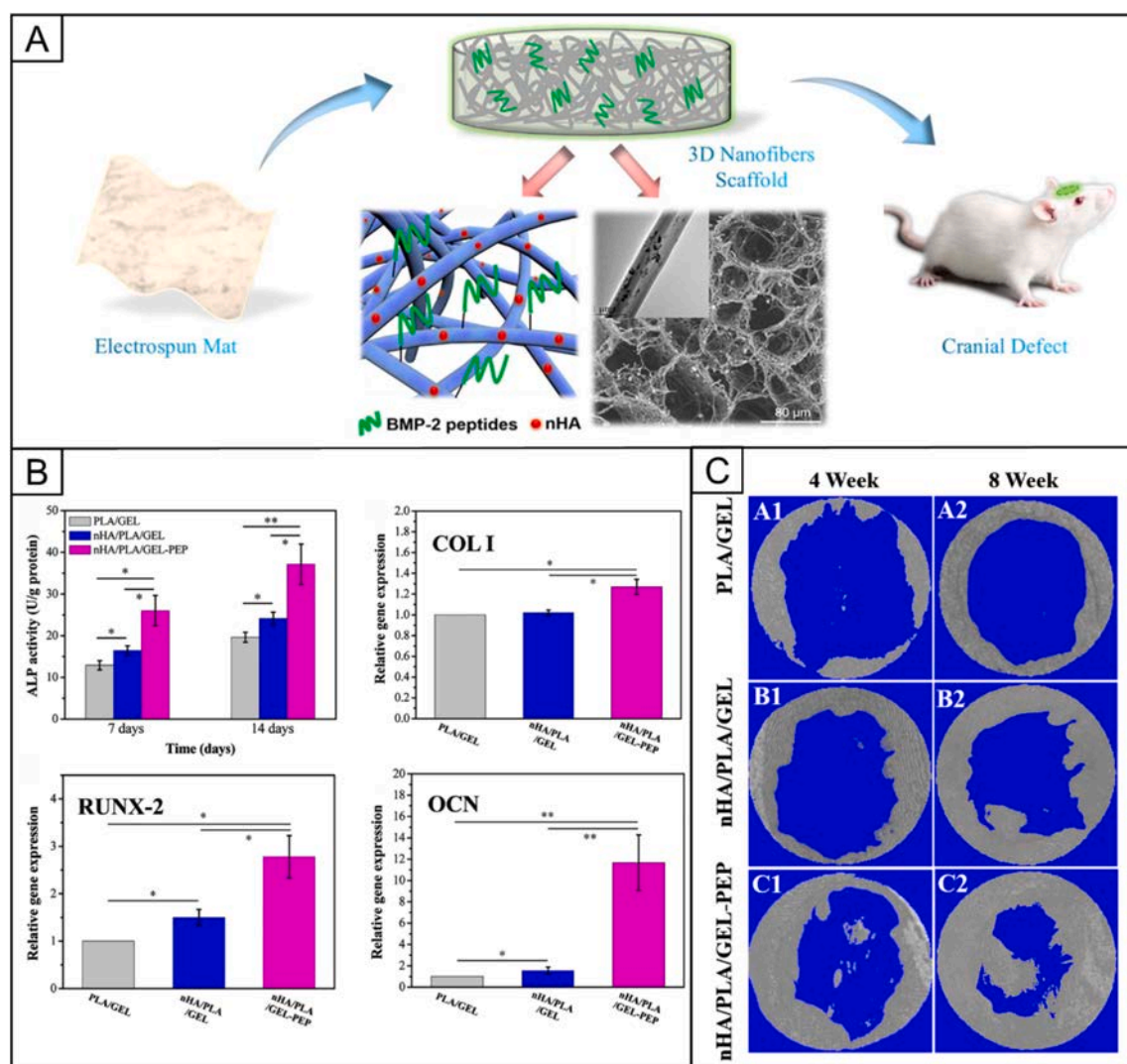


Fig. 13. Three-dimensional electrospun nanofibrous scaffolds displaying bone morphogenetic protein-2-derived peptides promote stem cell osteogenic differentiation and bone regeneration. (A) Schematic of 3D nanofibrous scaffold preparation and application. (B) ALP activities and relative gene expressions of COL I, RUNX-2, and OCN of BMSCs cultured on different scaffolds for 7 and 14 days. (C) Micro-CT images of rat cranial bone defects (diameter = 6 mm) repaired by different scaffolds 4 and 8 weeks after surgery. Reproduced from ref. [662] with permission from Elsevier, copyright 2019.

coaxial electrospinning and high-temperature calcination treatments using titanolsol and titanium precursor as shell materials, respectively [347]. The nanofibers would shrink along the fiber axis between the fiber junctions during the calcination process, resulting in cracks around the fiber junctions, which would manifest as local collapse of the hollow fiber walls (Fig. 5E). In addition, the diameter of the prepared hollow fibers can be up to several micrometers, and the thickness of the shell layer can be controlled from tens of nanometers to several micrometers [348]. Although coaxial electrospinning has been used as a promising technique to produce hollow nanofibers, there are still several limitations. The initial sheath layer must be strong enough to maintain the hollow structure, otherwise, the resulting hollow nanofibers will be prone to collapse. The core material in the core-sheath structured fibers needs to be removed quickly and efficiently. The miscibility of the solutions used, relative viscosity, and interfacial tension largely limit its versatility as a hollow nanofiber preparation process [349].

Hollow nanofibers can also be obtained by removing the core material of core-sheath nanofibers generated by emulsion

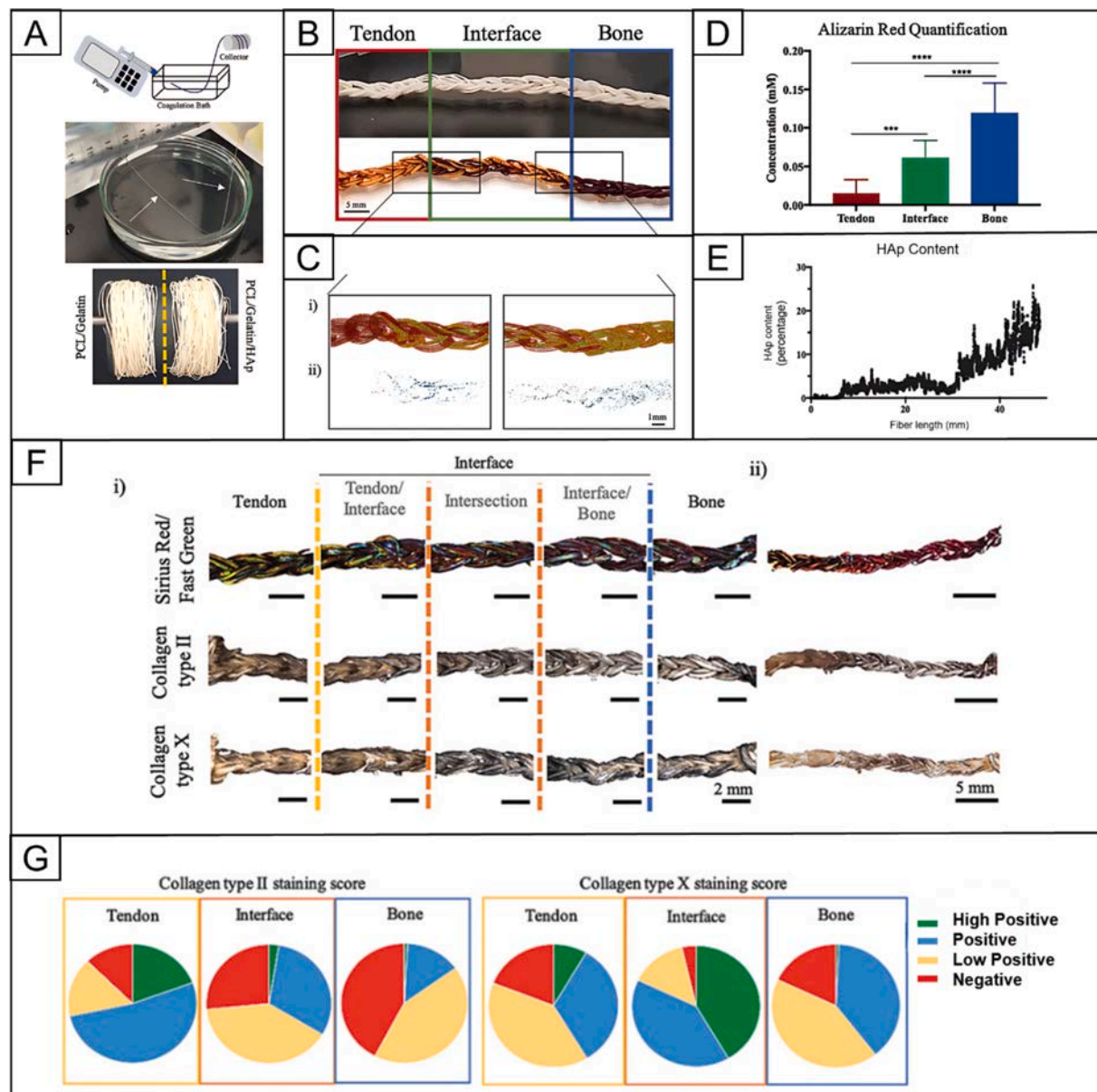


Fig. 14. Continuous aligned and textured composite microfiber gradient scaffolds for tendon-bone interface injury repair. (A) Schematic of fiber preparation by continuous wet spinning system. (B) Schematic of 3D scaffolds that simulate tendons, interfaces and bones. (C) Alizarin red staining of the Hap gradient. (D) Different parts of the scaffold and HAp particle content scanned by micro-CT. (E) Changes in HAp content along the stent. (F) Immunostaining of the gradients of type II and X collagen and non-collagen deposition along the fibrous scaffold. (G) DAB staining in several parts of the stent. Reproduced from ref. [677] with permission from Wiley-VCH, copyright 2019. (For interpretation of the references to color in this figure legend, the reader is referred to the web version of this article.)

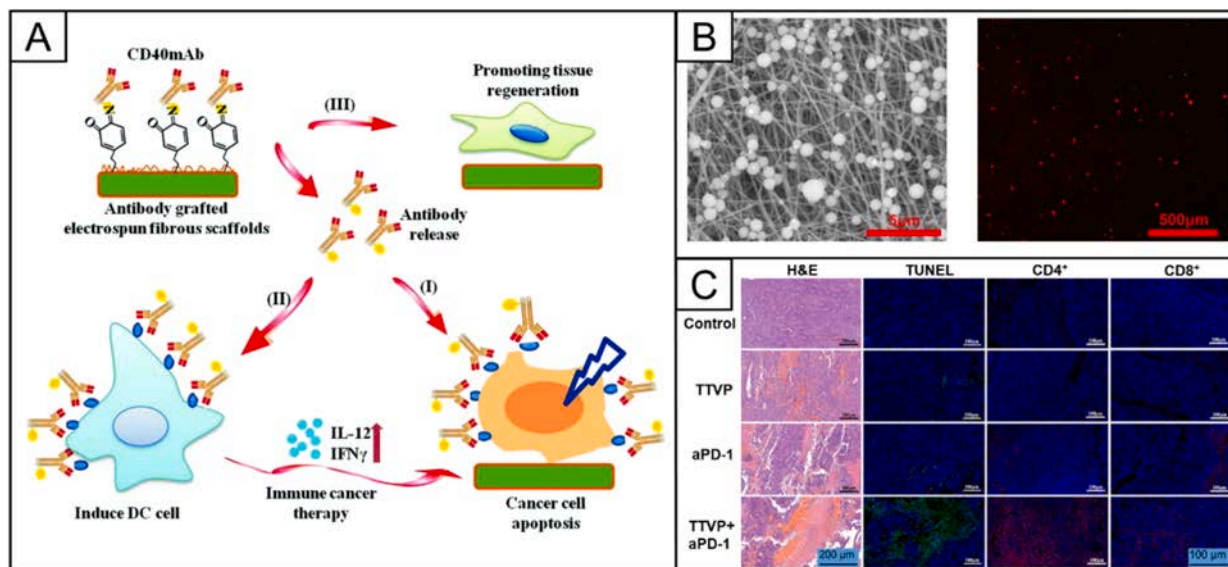


Fig. 15. Stem cell therapy and cellular immunotherapy combined with electrospinning technology for cancer treatment. (A) The pipeline of CD40mAb-grafted electrospun fibrous scaffold for anti-cancer therapy and tissue regeneration. Reproduced from ref. [716] with permission from Royal Society of Chemistry, copyright 2018. (B) Morphology of TTVP (a: SEM micrograph; b: fluorescent photograph). Reproduced from ref. [717] with permission from (2022) Elsevier. (C) Micrographs of tumor tissues stained by H&E, TUNEL and antibodies of CD4/CD8, showing the combined therapeutic effect for enhanced tumor apoptosis and infiltration of CD4 $^{+}$ and CD8 $^{+}$ T cells in the tumor site. Reproduced from ref. [717] with permission from Elsevier, copyright 2022.

electrospinning by inducing phase separation of two different polymer solutions. A typical example is the preparation of hollow nanofibers based on immiscible PAN and PMMA [350]. First, PMMA and PAN were dissolved in DMF to form a metastable emulsion consisting of PMMA/DMF solution with an emulsion size of 100–200 μm , which was encapsulated by PAN/DMF solution (Fig. 6A). The PAN/DMF solution had better stretchability compared to the PMMA/DMF solution and could be drawn into the PAN/DMF jet. Under

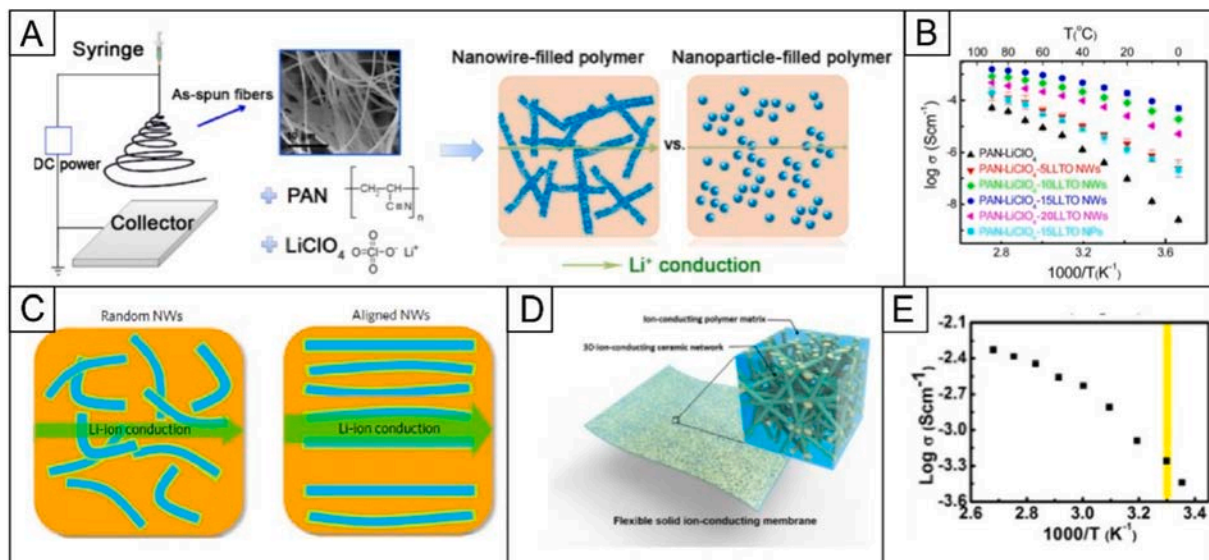


Fig. 16. Regulation of material properties by electrospun nanofibers. (A) Schematic illustration for the synthesis of ceramic nanowire-filled polymer-based composite electrolytes, and the possible Li-ion conduction pathway in nanowire-filled and nanoparticle-filled composite electrolytes, and (B) Arrhenius plots of the composite electrolytes with various LLTO nanowire concentrations. Reproduced from ref. [764] with permission from American Chemical Society, copyright 2015. (C) Schematic illustration of the Li-ion conduction pathways in composite polymer electrolytes with random nanowires and aligned nanowires, respectively. Reproduced from ref. [765] with permission from Springer Nature, copyright 2017. (D, E) Schematic of the hybrid solid-state composite electrolyte and its Arrhenius plot at elevated temperatures (from 20 $^{\circ}\text{C}$ to 90 $^{\circ}\text{C}$ and record every 10 $^{\circ}\text{C}$ increase). Reproduced from ref. [766] with permission from National Academy of Sciences, copyright 2016.

the action of the electric field, the emulsion formed a core-sheath jet and ejected out from the Taylor cone to form a core-sheath nanofiber with a diameter between 0.5–5 μm and a wall thickness between 200 nm and 1 μm (Fig. 6B). Therefore, the sheath of the electrospun fiber consisted of PAN. Subsequently, the PMMA core was removed by heat treatment at 750 $^{\circ}\text{C}$ under a nitrogen atmosphere to obtain hollow PAN nanofibers. Porous and multi-channel nanofibers can also be obtained by replacing the core polymer in the emulsion [351]. In addition, PAN/cellulose acetate [352], PAN/PEO, etc [352,353], can be prepared by this method to obtain hollow nanofibers. In another study, gradient electrospinning was applied to prepare hollow nanofibers [49]. The key to the method was the use of low/medium/high molecular weight PVA (Fig. 6C), which could be evenly distributed into three layers in a gradient form under the action of electrostatic force. During heat treatment, the internal low-molecular-weight PVA first underwent pyrolysis and shrinkage and moved to the boundary of low-molecular-weight/medium-molecular-weight PVA, resulting in expansion of the inner diameter of the nanotubes and initial formation of a hollow structure. As heat treatment deepens, PVA with medium molecular weight and high molecular weight also underwent pyrolysis and shrinkage in the same way. Finally, with the depletion of organic components, inorganic materials accumulated, resulting in inorganic nanofibers with hollow structures. At the same time, this approach has been extended to various inorganic multi-element oxides, binary metal oxides, and single metal oxides such as LiV_3O_8 (Fig. 6D) and MnO_2 (Fig. 6E) [49].

Another method to generate the hollow structures is heating polymer-based composite nanofibers containing inorganic precursors under different gas atmospheres. The principle of preparation is that as the temperature increases, the inorganic salts in the polymer migrate from the interior of the fiber to the surface due to the salt concentration gradient. The carrier polymer is carbonized and

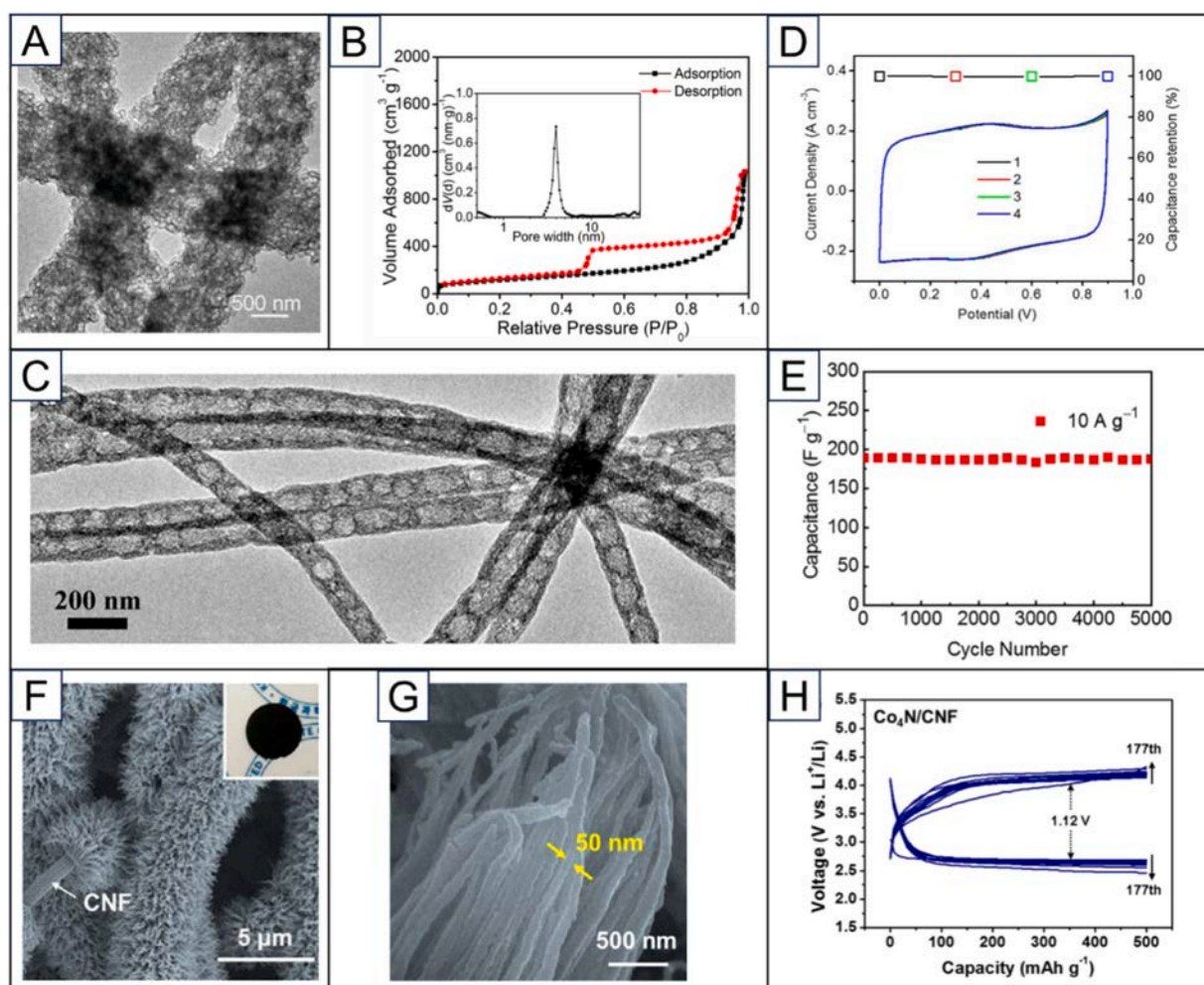


Fig. 17. Biomimetic structure design of electrospun nanofibers (A) TEM image of hollow particle-based nitrogen-doped carbon nanofibers sample. (B) N_2 adsorption/desorption isotherms and the corresponding pore-size-distribution curve of HPCNFs-N. Reproduced from ref. [770] with permission from Royal Society of Chemistry, copyright 2017. (C) TEM images of bamboo-like carbon nanofibers. (D) Cyclic stability of a carbon electrode at a current density of 10 A g^{-1} . (E) CV curves and capacitance retention of the all-solid-state supercapacitor tested at 100 mV s^{-1} under different mechanical deformation conditions: (1) 0°, (2) 90°, twisted by (3) 90° and (4) 180°. Reproduced from ref. [357] with permission from American Chemical Society, copyright 2015. (F, G) $\text{Co}_4\text{N/CNF}$ membrane with different magnifications. (H) Cycling performance of $\text{Co}_4\text{N/CNF}$ electrode, corresponding charge/discharge profiles. Reproduced from ref. [779] with permission from American Chemical Society, copyright 2017.

decomposed, and the inorganic salts on the surface are oxidized to form corresponding oxides and hybrids and finally nanofibers with a hollow structure are formed. In a typical example, Fe_2O_3 hollow nanofibers were prepared by simply calcining $\text{PVP}/\text{Fe}(\text{NO}_3)_3$ composite fibers under certain temperature conditions [354]. The key factors were the rigidity of the surface gel layer and the decomposition rate of PVP. The former could be adjusted by changing the addition amount of $\text{Fe}(\text{NO}_3)_3$ and PVP, while the latter could be adjusted by changing the heating rate. In another study, hollow TiO_2 nanofibers were prepared by coaxial electrospinning method and heat treatment [347]. In addition, nanofibers with a unique tube-in-tube structure can also be obtained by properly adjusting the heating rate during the heat treatment process. For example, a tube-in-tube structure was obtained by heating the composite fibers electrospun from the DMF solution containing PAN, PVP, and salts [355]. Multilayer tube-in-tube hollow nanofibers have also been prepared by adjusting parameters such as calcination atmosphere, temperature, and heating rate during the process [349].

The hard templates method is another method to prepare hollow nanofibers with high homogeneity by adding a hard template to the electrospinning solution or by applying electrospun nanofibers as hard templates followed by the removal of the rigid template.

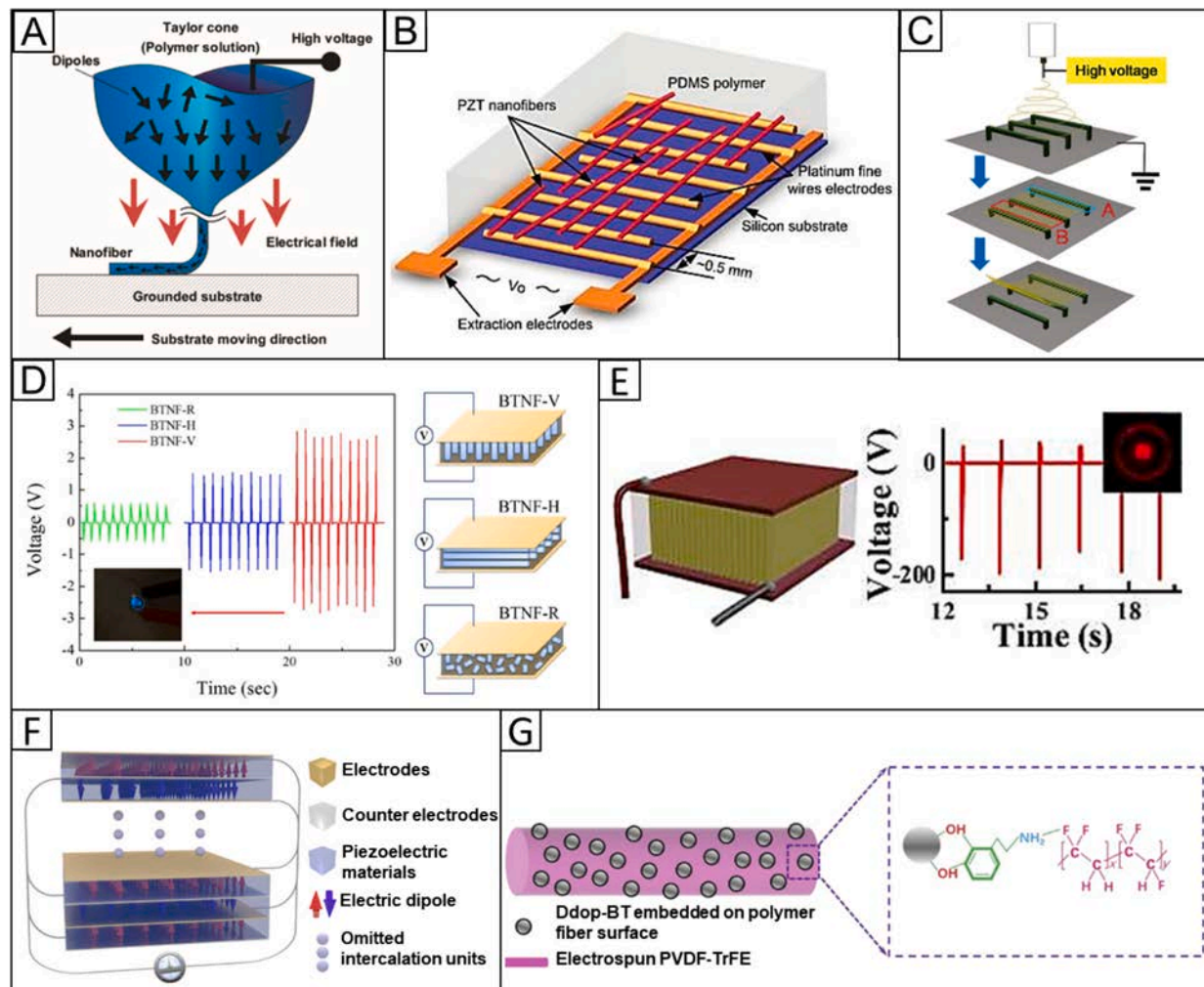


Fig. 18. The applications of electrospun nanofibers-based nanogenerator. (A) Schematic illustration indicating the fabrication of PVDF nanofibers by near-field electrospinning. Reproduced from ref. [859] with permission from American Chemical Society, copyright 2010. (B) Schematic illustration of PZT nanofibers nanogenerator based on rigid substrate. Reproduced from ref. [423] with permission from American Chemical Society, copyright 2010. (C) Schematic illustration of "aligned electrospun-film peeling off-free sintering" technology for fabricating piezoelectric ceramic nanofibers. Reproduced from ref. [428] with permission from American Chemical Society, copyright 2012. (D) The comparison of output voltage between different alignment states of BaTiO_3 nanofibers based nanogenerator. Reproduced from ref. [424] with permission from American Chemical Society, copyright 2016. (E) The schema and voltage output curve of vertical-aligned PZT nanofibers-based nanogenerator. Reproduced from ref. [429] with permission from American Chemical Society, copyright 2012. (F) (left) Schematic diagram of device design of laminated Sm-PMN-PT nanofibers based nanogenerator. (right) Output performance of the new design of PENG with a 3D intercalation electrode, a, b. The rectified current and voltage signals. Reproduced from ref. [425] with permission from Nature publisher, copyright 2020. (G) (left) Schematic diagram of electrospun BT/P(VDF-TrFE) composite nanofibers. (right) Dependence of output current and voltage on load resistance. Reproduced from ref. [865] with permission from Elsevier, copyright 2020.

SiO₂ nanoparticles are often added to the electrospinning solution to be used as hard templates. Hollow nanofibers are then obtained by removing the SiO₂ nanoparticles through a chemical etching process with NaOH, HF, or NH₄HF₂. In one typical example, SiO₂ nanoparticles were homogeneously mixed in a PAN/DMF electrospinning solution [356]. After going through the procedures of electrospinning, pre-oxidation, carbonization, and chemical etching with HF acid, free-standing, lightweight, and hierarchical macroporous activated carbon fibers were prepared (Fig. 7A). The fiber consisted of hollow carbon spheres with a diameter of 180 nm, containing many surface cavities and interconnected pores with diameters in the range of 20–50 nm (Fig. 7B, C). In another example, TEOS was used as the source of hard template SiO₂ [357]. Electrospun PAN/TEOS nanofibers were heated to produce SiO₂ particles (Fig. 7D), and then by chemical corrosion with HF acid, bamboo-like hollow graphitic CNF was obtained (Fig. 7E, F). These fibers showed uniformly discontinuous hollow interiors (macropores) as well as hierarchical nanopores (mesopores and micropores) through the nanofiber cross-section and exhibited well-balanced porosity at the micro-, meso-, and macro-scales. Another type of hard template method mainly relies on electrospinning nanofibers as templates. Through various physical and chemical effects, inorganic precursors were enriched on the surface of the fibers. After the templates were removed, nanofibers with hollow structures could be obtained. For example, electrospun PAN nanofibers were used as templates, and the surface of the fibers was covered with dense Co(OH)₂ nanosheets through coordination [358]. After heat treatment, the fiber templates were removed to obtain highly crystalline C-doped Co₃O₄ hollow nanofibers. Electrospun bioglass fibers have also been applied as a hard template to prepare uniformly graded porous nanofibers with a hollow structure by ion exchange [356]. The prepared electrospun glass fiber was dissolved in K₂HPO₄ solution and reacted with PO₄³⁻ in the solution to generate amorphous calcium phosphate. With time passing by, the glass fiber template in the core layer was completely removed, generating nanofibers with a hollow structure.

Porous nanofibers. Porous nanofibers have an abundant pore structure that provides a higher specific surface area, more active sites, and ease of modification through functionalization. Porous nanofibers show great potential in various fields, including adsorption and separation, water treatment, catalysis, energy storage, air filtration, drug delivery, tissue engineering, sensors, and food

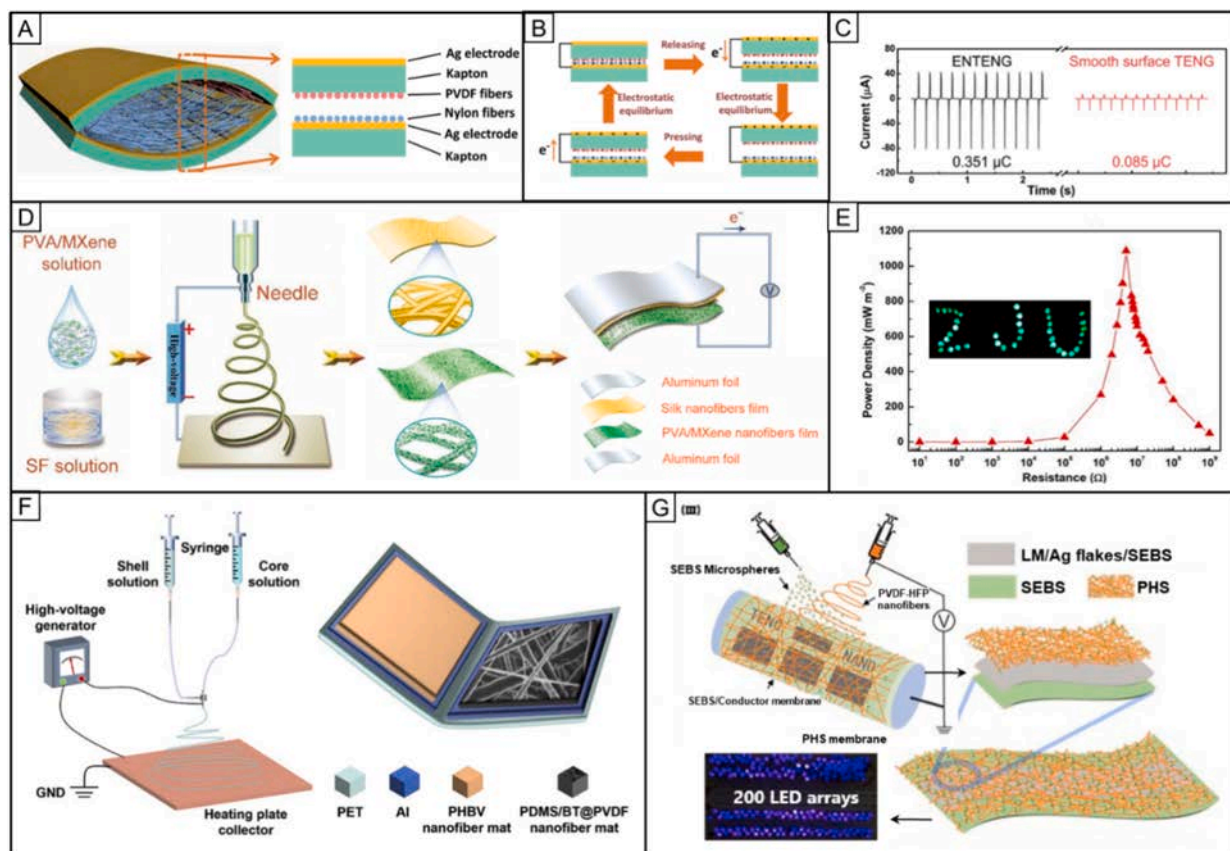


Fig. 19. The applications of electrospun nanofibers-based Triboelectric nanogenerator (TENG). (A–C) Schematic, working principle and electric output of the TENG based on single-spun Nylon nanofibers and single-spun PVDF nanofibers. Reproduced from ref. [873] with permission from Royal Society of Chemistry, copyright 2014. (D,E) Schematic of fabrication and instantaneous output power of single-spun PVA/MXene and single-spun silk nanofibers based TENG. Reproduced from ref. [877] with permission from Elsevier, copyright 2019. (F) Coaxial electrospinning apparatus and schematic illustration the TENG based on PDMS/BaTiO₃@PVDF nanofibers and PHBV nanofibers. Reproduced from ref. [880] with permission from Elsevier, copyright 2020. Schematic of the fabrication process of the TENG based on styrene-ethylene-butylene-styrene (SEBS) microspheres and PVDF nanofibers, prepared by electrospinning and electrostatic spray. Reproduced from ref. [881] with permission from Elsevier, copyright 2020.

packaging [359–361]. Electrospun porous nanofibers can be prepared mainly by the phase separation method and template sacrificial method.

Regarding the phase separation method, nanofibers with rich pore structures were prepared by dissolving PCL in the volatile solvent dichloromethane (DCM) followed by electrospinning [362]. The formation of the pores was caused by the phase separation between the polymer and the solvent due to the rapid evaporation of the solvent. Phase separation can be induced by vapor, heat, and non-solvent. Vapor-induced phase separation occurs when water vapor in the air interacts with the fiber surface and penetrates the interior of the fiber to mix with the solvent under high ambient humidity conditions. At this point, the hydrophobic polymer and solvent phases separate into a polymer-rich phase and a solvent-rich phase. The polymer-rich phase eventually solidifies into the entire skeleton of the nanofibers, while the solvent-rich phase forms the porous structure inside the fibers. Therefore, the volatility of the solvent plays a key role in the formation of pores in the fiber structure. Commonly used fast volatile solvents mainly include DCM

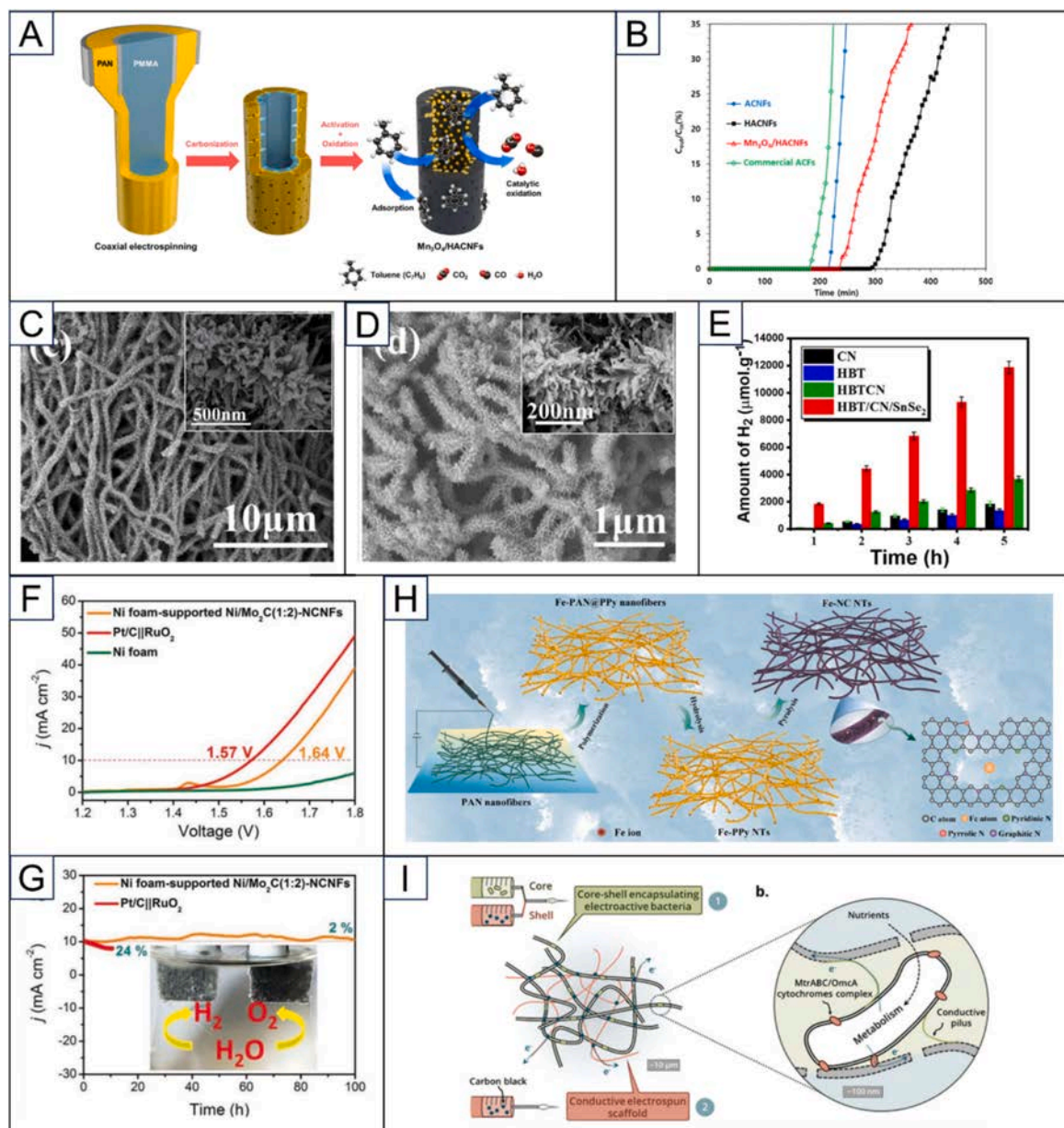


Fig. 20. Application of electrospun nanofibers for catalysis. (A) The schematic process involves electrospinning double-layer nanofibers with PMMA/manganese acetate as the core and PAN as the shell. These nanofibers are then carbonized and CO₂-activated to produce Mn₃O₄ nanoparticles embedded in hollow activated carbon NFs (Mn₃O₄/HACNFs). Mn₃O₄/HACNFs act as catalysts for the oxidation of toluene at high temperatures. (B) Breakthrough curves of toluene (10 ppm) for the activated CNFs (ACNFs), HACNFs, Mn₃O₄/HACNFs, and commercial ACFs, obtained

at 20 °C. Reproduced from ref. [900] with permission from Elsevier, copyright 2019. (C) FESEM images of branched TiO₂ fiber after decorating g-C₃N₄ QDs on it (HBT/CN), (D) FESEM images of the hairy structure of TiO₂ fiber loading with g-C₃N₄ QDs and SnSe₂ nanoflakes (HBT/CN/SnSe₂), inset is the magnified image of same sample in which nanoflakes can be seen on branches. (E) Photocatalytic Hydrogen performance of sample CN, HBT, HBT/CN, HBT/CN/SnSe₂, n = 3. Reproduced from ref. [901] with permission from Elsevier, copyright 2020. (F) LSV curves of overall water splitting in a two-electrode configuration. (G) Chronoamperometry curves of Ni/Mo₂C(1:2)-NCNFs and benchmark electrodes of Pt/C/RuO₂ at constant voltages of 1.64 and 1.57 V, respectively. Reproduced from ref. [902] with permission from Wiley-VCH, copyright 2019. (H) Schematic diagram for the synthetic process of Fe-N-doped carbon nanotubes (Fe-NC NTs) catalyst. Reproduced from ref. [903] with permission from Elsevier, copyright 2021. (I) left: Schematic diagram of dual electrospinning featuring (1) a coaxial nozzle producing core-sheath fibers that encapsulate bacteria within a porous, carbon black-containing shell, and (2) a simple nozzle producing conductive, carbon black-rich scaffold fibers. right: Schematic diagram of the intended bacterial environment inside a core-sheath fiber. Reproduced from ref. [904] with permission from the Royal Society of Chemistry, copyright 2021.

[363], chloroform [364], THF, etc [365]. With the rapid evaporation of the solvent, the temperature of the fiber surface drops sharply, causing condensation of water vapor. The condensed water droplets act as templates on the surface of the fiber and form holes after drying [336]. As a result, the formed porous structure tends to exist on the fiber surface. When a slow volatile solvent is selected, such as DMF [366,367], its slow evaporation provides enough time for water vapor to penetrate the interior of the fiber, inducing an internal porous structure [367]. Thermally-induced phase separation is another important mechanism. The temperature difference is the driving force for phase separation, which occurs during cooling between the polymer and the remaining low-volatility solvent in the fiber, leading to a highly porous structure formation. For example, electrospun fibers were placed in liquid nitrogen to create a temperature difference, inducing phase separation to construct porous nanofibers [368]. In addition, phase separation can also be induced by introducing a non-solvent into a polymer solution to form a ternary system of polymer/solvent/non-solvent [369]. It is worth noting that there needs to be a large difference in volatile properties between the introduced non-solvent and solvent. With high volatility of the solvent and low volatility of the non-solvent, the ratio of solvent to non-solvent content decreases continuously, followed by the formation of a polymer-rich phase and a polymer-poor phase. Finally, after all solvent evaporates, nanofibers with porous structures can be obtained. For example, the non-solvent, water and ethylene glycol, were added to a PAN/PS solution to prepare nanofibers with a porous structure [370]. In another study, a PAN/DMF solution was directly electrospun into a non-solvent pool to prepare porous PAN fibers [371].

The template sacrificial method involves adding porogens, including polymers, inorganic salts, nanoparticles, etc., to the electrospinning polymer solution. After electrospinning to form composite fibers, further post-treatments such as washing, organic dissolution, and ultraviolet (UV) radiation are required. This method removes relevant components in the fiber, thus leaving behind a porous structure. In one study, porous PVDF fibers were obtained by removing PVP from electrospun PVDF and PVP nanofiber membranes [372,373]. In another study, hydrochloric acid was applied to remove the CaCO₃ template from PAN/CaCO₃ nanofibers to prepare porous nanofibers [374]. NaHCO₃ was added to PVDF/PAN solution to prepare PVDF/PAN composite nanofibers, and then the as-prepared fibers were soaked in hydrochloric acid solution to remove NaHCO₃ for generating porous PVDF/PAN fibers [375]. In another study, the removal of SiO₂ and Sb from SiO₂/Sb@CNF using HF resulted in highly porous structures with a pore size up to hundreds of nanometers (Fig. 8A) [298].

Fibers decorated with grooves or protrusions. Electrospun nanofibers can be decorated with grooves or protrusions to change their secondary structures. Modifying the grooves on nanofibers can effectively increase the specific surface area [378]. The formation mechanisms of groove structures mainly include (i) void-based elongation, (ii) wrinkle-based elongation, and (iii) collapsing jet-based elongation [378]. For void-based elongation, when two solvents with significant differences in volatility are present in the electrospinning solution, phase separation occurs during the electrospinning process, resulting in pore generation. These pores can be stretched and solidified into a grooved structure through the void-based productivity mechanism. The volatility difference between solvents is a key factor in the formation of groove structures. For the wrinkle-based elongation mechanism, a glassy skin is formed in the early stage of electrospinning and then stretched into fluted fibers. The wrinkled surface is formed due to the buckling of the cylindrical polymer shell under compressive radial stress arising from the solvent removal from the jet's core. Under continuous jet stretching, internal porosity or transverse shrinkage effects are produced by axial tensile stress [379]. After glass-like skin fibers are formed, the evaporation rate of high-boiling point solvent is slow, and the viscosity is high, causing jet collapse and stretching into a smooth groove structure through the collapsing jet-based elongation mechanism. In a typical study, PLLA grooved fibers were fabricated using DCM/DMF (2/1, v/v) solvent [380]. By adjusting the solvent ratio and relative humidity during electrospinning, similar groove structures can be obtained. In another study, the surfaces of PCL microfibers were engraved with nanoscale grooves through phase separation of PCL and PVP during coaxial electrospinning [217]. In another example, PLA fibers were modified with chitosan islands on the surfaces owing to the phase separation and crystallization during electrospinning [381]. Nanofibers with different PLA/Chitosan ratios were analyzed for morphology, internal structure, surface composition, crystallinity and thermodynamics, and the core-sheath or island morphology structure was speculated for the rotation mechanism. The outer chitosan composition and the rough nanoscale topography of the nanofiber surface balanced the hydrophilicity and hydrophobicity of the fibers. Particles made of inorganic components can also be incorporated with fibers to form the protrusion structures through directly blended electrospinning or the post-treatment of the as-obtained electrospun fibers [382].

Bead-on-string nanofibers. Bead-on-string nanofibers are nanofibers that contain a certain number of bead-like particles within their long and thin fibers. Initially, the appearance of beaded fibers is often considered a defect in the electrospinning process. However, it has been discovered that the beaded structure in nanofibers can alter the packing density and pore structure of the nanofibers. The presence of these beads increases the distance between fibers, allowing more air to flow through the membrane,

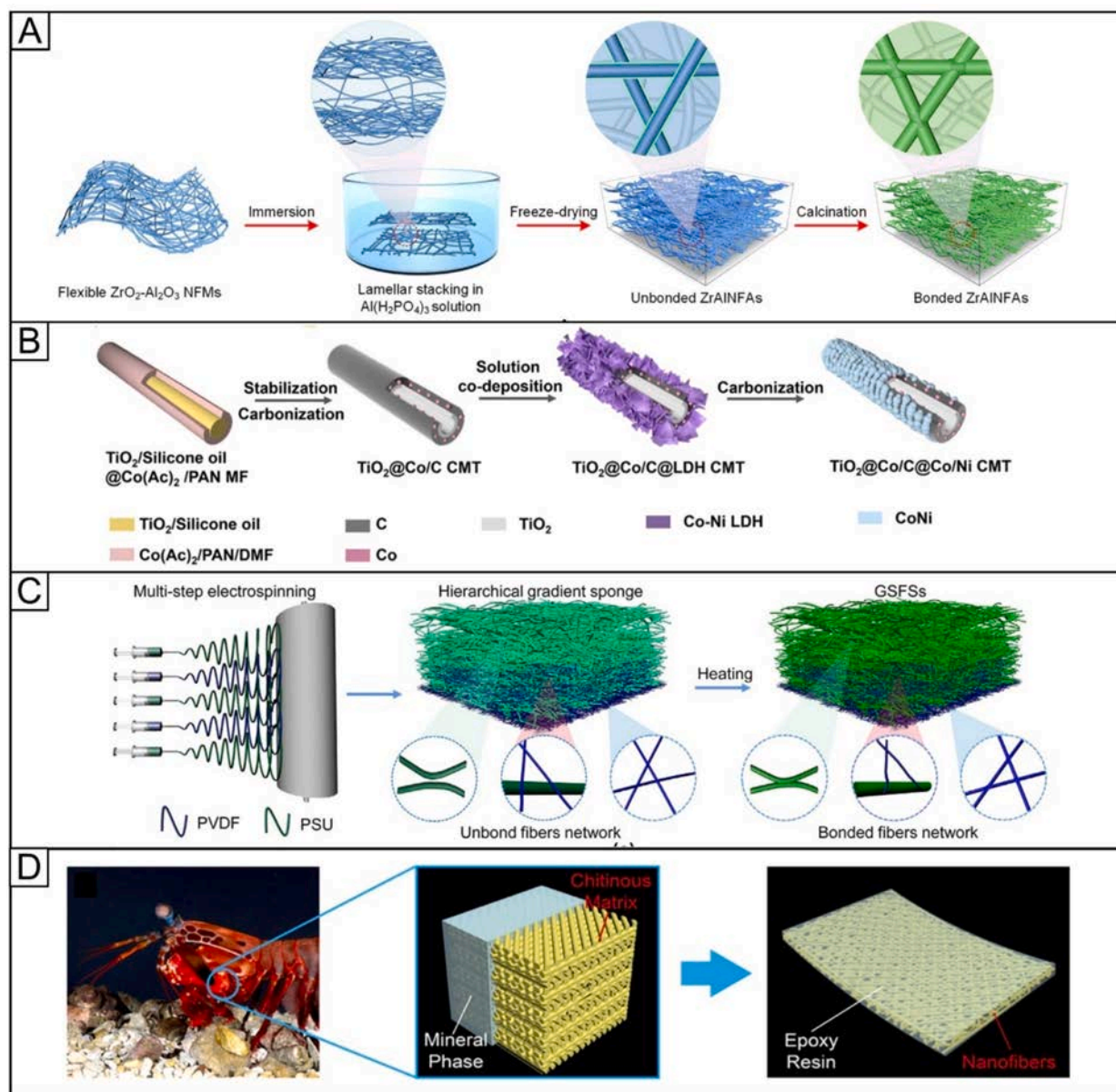


Fig. 21. Bioinspired design of electrospun nanofiber composite films. (A) Schematic illustration of the fabrication of $\text{ZrO}_2\text{-Al}_2\text{O}_3$ nanofibrous aerogels. Reproduced from ref. [1048] with permission from American Chemical Society, copyright 2020. (B) Schematic preparation process of 1D electromagnetic-gradient hierarchical $\text{TiO}_2@Co/C@Co/Ni$ carbon microtube composites. Reproduced from ref. [1051] with permission from American Chemical Society, copyright 2021. (C) Schematic illustration for the fabrication of gradient structured fibrous sponges. Reproduced from ref. [1052] with permission from Elsevier, copyright 2021. (D) A snapshot of a stomatopod with hammerlike smasher dactyl clubs. The hierarchical structure at multilength scales contributes to its excellent impact-resistant property and inspires the design of impact-resistant composite films reinforced with helicoidally aligned nanofibers. Reproduced from ref. [1053] with permission from American Chemical Society, copyright 2019.

resulting in a lower pressure drop without significantly affecting filtration efficiency. Additionally, the bead-like structure in the nanofiber provides a large “storage” space and a site for the fiber to wrap and store substances, which can be applied for drug delivery and release. The mechanism of Rayleigh instability is generally recognized in the study of beaded nanofibers. Specifically, when the jet is ejected from the nozzle, droplets tend to form smooth spheres under the influence of surface tension. Simultaneously, a portion of the jet tends to form elongated fibers under the influence of electric field force. Beads form within fibers when the electric field force does not stretch the droplet enough to resist surface tension. Another scenario occurs when the electric field force exceeds surface tension during spinning, causing the spinning solution to form smooth fibers while its viscoelastic force maintains the jet’s “status quo”. In this case, viscoelastic force and surface tension have a hindering and hysteresis effect on jet stretching, facilitating bead formation. Due to comprehensive effects of various forces and other conditions, beads formed within fibers exhibit different shapes, including spherical,

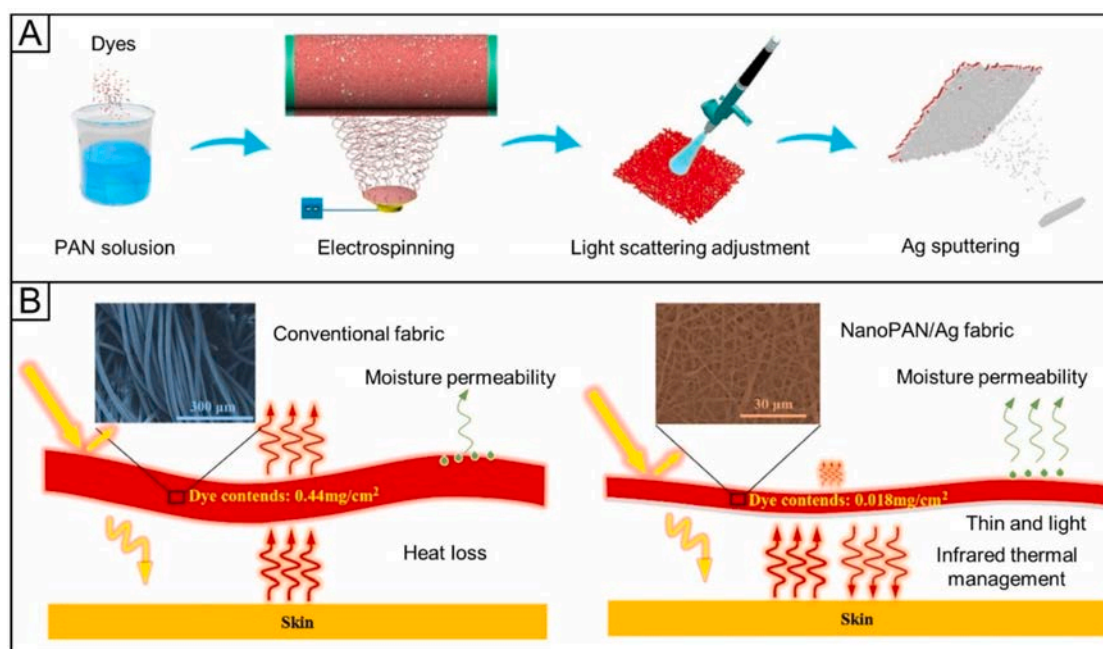


Fig. 22. Schematic diagram of NanoPAN/Ag textile preparation (A) Manufacturing process of a colored NanoPAN/Ag passive radiative heating textile. (B) Principles of infrared thermal management of NanoPAN/Ag textile. Reproduced from ref. [1074] with permission from Elsevier, copyright 2021.

spindle (shuttle) shaped, and jujube-shaped. In one study, a kind of polyethylene terephthalate (PET) based filter media with a bead-on-string structure and hydrophobic/oleophobic property was designed and fabricated by electrospinning (Fig. 8B). Compared with the commercial 3701CN filter media, the advantages of the regular breathing frequency and strong heart rate control ability indicated that this filter media had better wear comfortable performance with broad application prospects in the personal protection of dust in mines [376]. In another study, the morphology of beaded microfibers could be accurately controlled by a simple microfluidic device [302]. Electrospun multi-porosity beaded PLGA fibers were prepared from PLGA solutions with different concentrations, and the fibers with appropriate density were selected as drug reservoirs to further realize sustained release of β -carotene [303].

Ribbon-like fibers. Electrospinning can also form thin fibers with sheet cross sections, which can be called nanoribbons. Nanoribbons can be produced from polymer solutions with strong internal and/or interaction between polymer chains [383,384]. The solvent inside the jet dissolves, and the jet forms a tubular structure, which may collapse, and the cross-section of the jet becomes flat, similar to satin ribbon. When the solvent evaporated, atmospheric pressure often caused the soft liquid thread to collapse. The cross-section changed from circular to elliptical, then flat, similar to ribbon, and its cross-section perimeter was almost the same as that of the jet [385]. SELP47K, as an artificial protein material, has the characteristics of silk protein and elastin and supplies excellent conditions for electrospinning because of its solubility properties. SELP47K can form independent non-woven fiber webs (Fig. 8C) [377].

Shish-kebab nanofibers. The shish-kebab morphology consists of polymer row crystals (shish) that are often overgrown *in-situ* by plate-like folded lamellae (kebabs). Typically, semi-crystalline polymers crystallized under shear flow exhibit a distinct shish-kebab morphology. The shear flow elongates the polymer chains undergoing a helical-extension transition, eventually crystallizing into row crystals (shish, often also called row nuclei/crystals). The less stretched strands then overgrow on the shish, forming folded, sheet-like crystals that form the kebab [386]. Controlling the crystallization of polymer during electrospinning can produce nanofibers with shish-kebab structures [92,303,306,309,381,387,388]. For example, when subjected to shear flow, ultrahigh molecular weight PE can form a special shish-kebab structure that is composed of threadlike cores as shish encircled with disk-like lamellae as kebabs. This micro/nano hierarchical structure is supposed to be favorable for creating a superhydrophobic surface [389]. In another study, through self-induced crystallization, PCL formed self-induced nano-hybrid shish-kebab string structure on PCL fibers (Fig. 8D) [156]. Isotactic polypropylene (iPP) fibers [390] can also be prepared by high-temperature solution electrospinning to form shish-kebab fibers.

Complex Nanofiber Production. In industrial production of electrospun nanofibers, transitioning to more complex fiber morphologies, such as hollow and core-sheath structures, presents several technological challenges. Producing these intricate fibers demands more precise process control. Unlike conventional fibers, hollow and core-sheath fibers require multi-nozzle or dual-head electrospinning techniques. While these methods have shown success in laboratory settings, issues with reproducibility and precision still hinder large-scale production. Therefore, optimizing nozzle designs and equipment configurations is critical to improving production stability. Additionally, precise control over environmental parameters—such as automatic adjustment of temperature, humidity, and multi-channel systems—can enhance fiber uniformity and reduce fluctuations during production. Another key challenge is

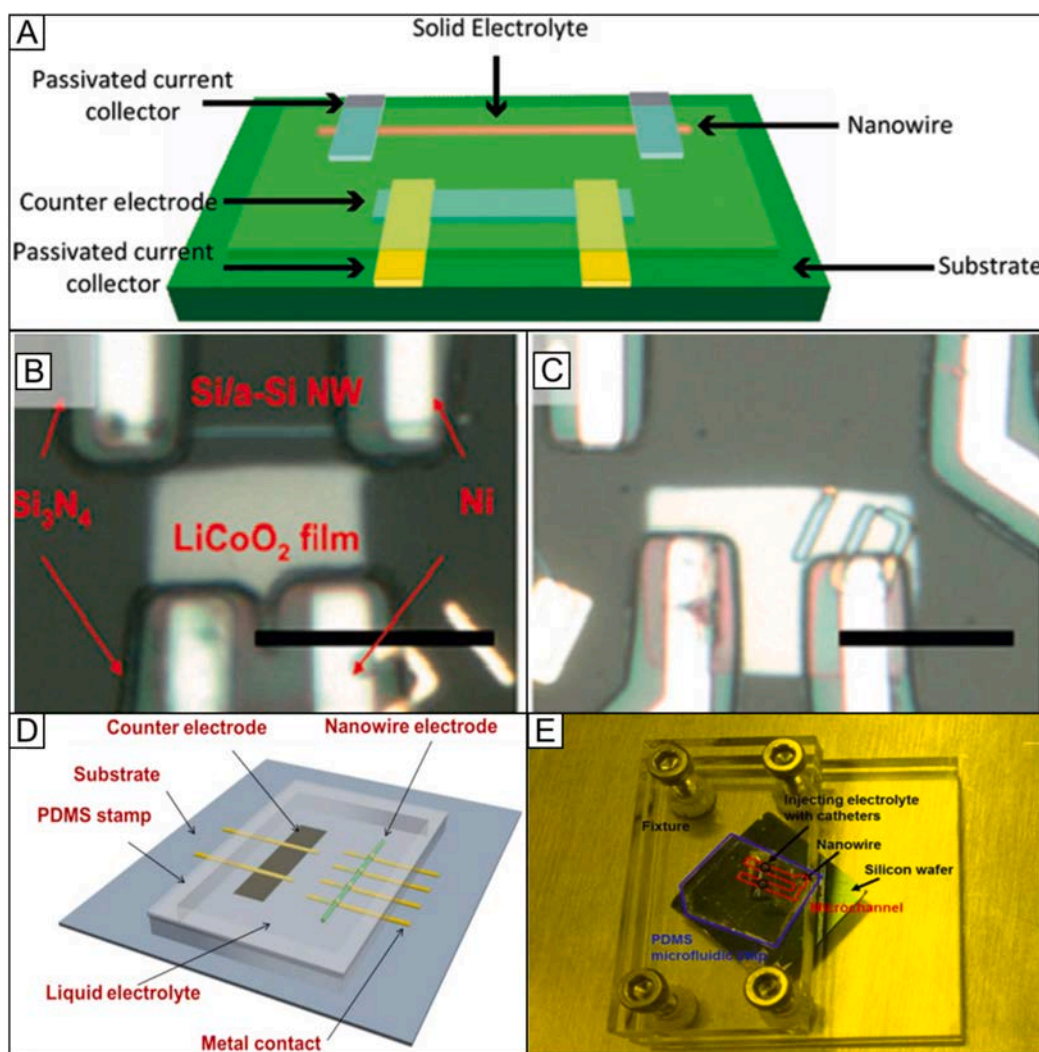


Fig. 23. Schematic diagram and electrochemistry of a single-nanowire electrode device. (A) the scheme indicates the design of a single nanowire electrode device containing a single vanadium oxide nanowire or Si nanowire as the working electrode and highly ordered pyrolytic graphite (HOPG) or LiCoO₂ nanofilm as the counter electrode. Optical images of (B) a typical Si/a-Si nanowire/LiCoO₂ electrode device and (C) The control device with the same electrode design but without Si/a-Si nanowires. Scale bar is 10 μm . Reproduced from ref. [1084] with permission from American Chemical Society, copyright 2010. (D) The overview of the device. Four metal contacts were integrated into one nanowire, and the liquid electrolyte was sealed into a PDMS stamp with microchannels. (E) The optical image of the device. The device was sealed by a PDMS stamp with microchannels, in which the liquid electrolyte was injected to fully immerse the electrodes in an argon-filled glovebox, to ensure no exposure to air. Reproduced from ref. [1085] with permission from American Chemical Society, copyright 2016.

increasing production speed and yield. The complexity of these fiber structures slows the process, and current electrospinning equipment struggles to balance high yield with maintaining precise fiber morphology. One potential solution is the adoption of multi-nozzle systems, which allow simultaneous electrospinning at multiple points, significantly increasing throughput. Moreover, improving collector designs, such as rotating or larger-area collectors, can accelerate fiber collection and boost production efficiency. In the post-processing stage, solvent removal and functionalization treatments are crucial. Techniques like supercritical fluid extraction, thermal treatment, and freeze-drying can efficiently remove solvents without damaging the fiber structure, while surface functionalization methods can endow the fibers with additional properties and stability. Lastly, while hollow and core-sheath fibers have shown promise in laboratory environments, scaling up their production remains costly. The high initial investment in equipment—especially multi-nozzle and multi-head systems—combined with the complexity of the process and the need for skilled operators, results in high production costs. To address this, adopting continuous production lines, modular equipment, and optimized process flows could help reduce capital investment and operational costs, making large-scale production more feasible. Through these technological advancements, the challenges of transitioning to complex fiber structures can be overcome, paving the way for broader industrial applications of electrospun nanofibers.

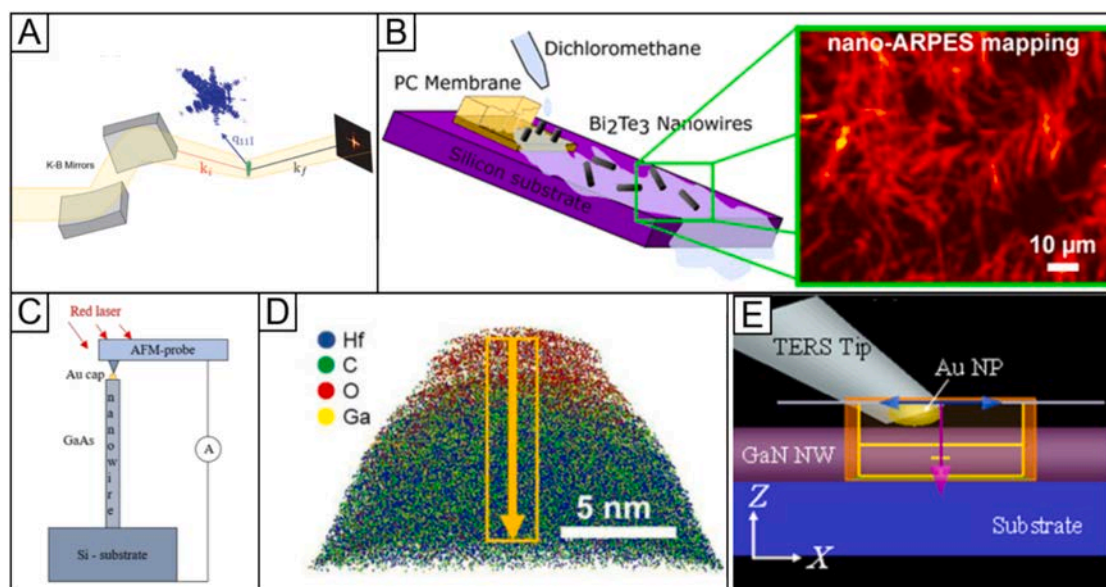


Fig. 24. Nanowire platform combination with characterization methods. Single-nanowire platform combined with (A) coherent X-ray diffractive imaging, (B) nano-angle-resolved photoemission spectroscopy, (C) conductive atomic force microscopy, (D) atom probe tomography, and (E) tip-enhanced Raman spectroscopy, respectively. (A) Reproduced from ref. [1087] with permission from American Chemical Society, copyright 2020. (B) Reproduced from ref. [1088] with permission from American Chemical Society, copyright 2016. (C). Reproduced from ref. [1093] with permission from IOP Publishing Ltd, copyright 2021. (D), Reproduced from ref. [1094] with permission from Royal Society of Chemistry, copyright 2020. (E) Reproduced from ref. [1095] with permission from American Institute of Physics, copyright 2020.

2.5.2. Stacking of nanofibers

The electrospun nanofibers can be stacked to create 2D or 3D materials with a high structural diversity. These materials include 2D nonwoven mats of nanofibers, 3D bulk scaffolds, aerogels, *etc.* With the development of these specific structured fiber materials, electrospun nanofibers can be endowed with different functions or capabilities to extend their applications.

2D nonwoven nanofibrous mats. Typically, by changing the collector, 2D nonwoven nanofibrous mats with different structures can be prepared, such as random, aligned, and even patterned nanofiber scaffolds. For solution electrospinning, the fibers deposited on the top of the collector tend to be stacked in a disordered manner because of the whipping effect of the jet. It is necessary to introduce mechanical displacements and specific electric or magnetic fields to achieve a specific arrangement of nanofibers. Mechanical displacement refers to the high-speed rotation of the collector during the electrospinning process, which causes the fibers to be oriented and stretched in the direction of rotation. A high degree of alignment of the nanofibers can be achieved when the linear velocity of the receptive sites on the collector coincides with the velocity of the jet deposition [391]. For example, directionally aligned PCL nanofibers were constructed by rotating an aluminum disk (rotational speed: 5,000 rpm, linear speed: 1,400 m/min) for directional induction of nerve cell migration [392]. In another study, highly aligned PLGA nanofiber arrays on glass slices were successfully fabricated (Fig. 9A) [393].

By editing the distribution and direction of the electric field, the directional arrangement of the fibers can also be achieved, even in a radial shape. For example, a collector consisting of a metal needle in the center with a metal ring on the outer can also be prepared with radially aligned nanofibers radiating from the center in all directions [397]. The electric and magnetic fields are dependent on each other, and the jets are self-charged, so electrospun fibers are generally aligned in a specific direction along the magnetic field.

In relative terms, melt electrospinning has a natural advantage in making fiber supports with specific patterns because the relative position between the extrusion nozzle and the collector can be easily varied. Therefore, various complex orientations and even specific patterns are possible in addition to aligned spun fibers. For example, in one study, highly ordered nanofiber structures with aligned alignments and different spacing (250 μm or 500 μm) were constructed by melt electrospinning for periodontal tissue regeneration [398]. The results showed that the aligned fibers were more supportive of ligament genesis, while the 500 μm fiber spacing was more supportive of osteogenesis. Micropatterned fiber scaffolds, such as honeycomb, map patterns, and other patterns, have been successfully fabricated. Fig. 9B shows the morphology of the chitosan-PLA/PCL membrane with honeycomb structure [394].

Nanofiber yarns. Converting nanofibers into twisted continuous bundles, *i.e.*, nanofiber yarns, can improve their strength and facilitate their subsequent processes. Nanofiber yarns also create opportunities to develop well-defined 3D nanofibrous architectures. The common methods used to prepare nanofiber yarns are a conjugate method, modified conjugate method, dynamic liquid method, water bath collection method, and modified conjugate method. Conjugate methods are generally sprayed with two conjugate electrode devices. For example, PLLA nanofiber yarns consisting of highly oriented nanofibers were prepared using a dual-nozzle electrospinning device [399]. Afterwards, a noosing technique was applied to fabricate multilayered scaffolds with three orthogonal sets of PLLA nanofiber yarns, without interlacing them. The conjugation method can also be modified by adding the number of nozzles to produce

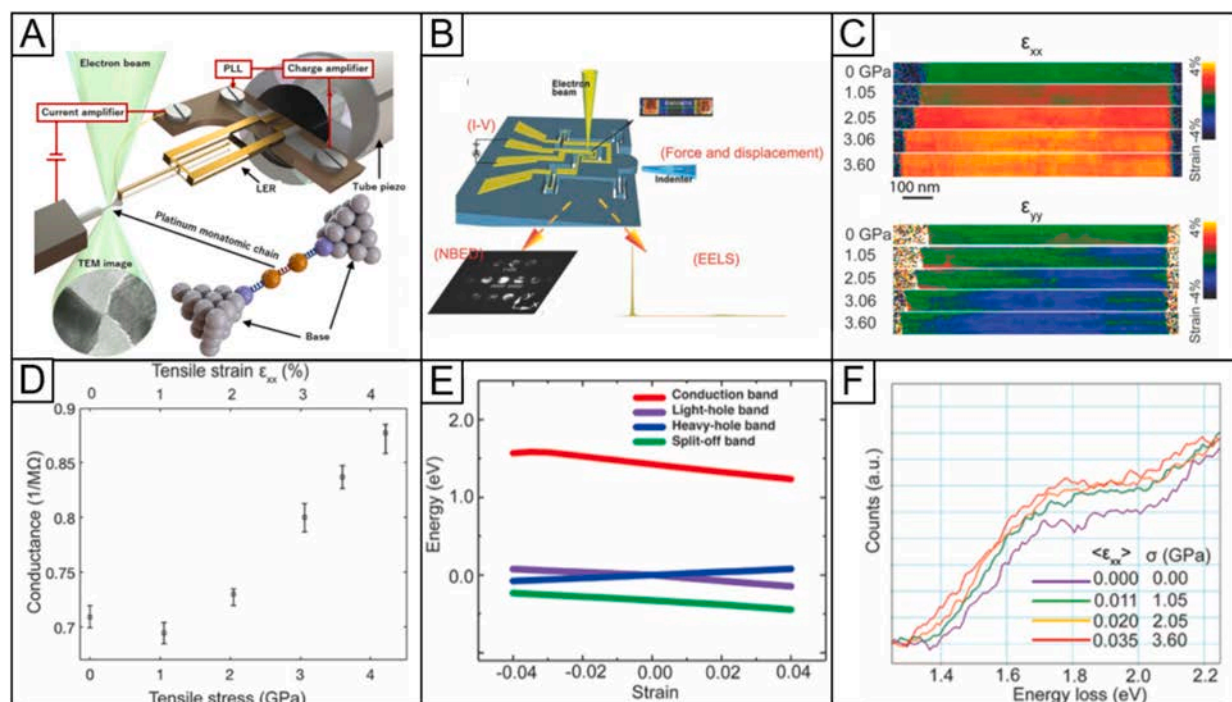


Fig. 25. Exploring the impact of tensile stress on the structural integration of nanofibers using *in-situ* TEM. (A) A schematic illustration of the experimental setup. Reproduced from ref. [1161] with permission from American Chemical Society, copyright 2021. (B) A schematic illustration of the electrical push-to-pull (EPTP) microelectromechanical system (MEMS) device and the *in-situ* TEM experimental setup. (C) Strain maps of the GaAs nanowires under tensile stress, with strain measured along the nanowire length (x) and perpendicular (y) direction. (D) The conductance of the nanowire as a function of applied tensile stress and strain. (E) Tight-binding simulation of band edges at the valence band top and conduction band bottom in GaAs and their shift as a function of strain along direction. (F) *In-situ* monochromated EELS spectra showing the redshift of the bandgap onset of the GaAs nanowire under stress and strain. Reproduced from ref. [1162] with permission from American Chemical Society, copyright 2021.

multi-needle conjugated electrospun nanofiber yarn [304]. The water bath collection method uses a grounded water bath as a collection device for electrospun nanofibers, and then the fiber film deposited on the water surface is wound into a yarn. Yarns prepared by this method have a high degree of neatness in fiber alignment, but a small number of disordered fibers and curved fiber loops are also present. In one study, yarns with high fiber orientation were obtained by tilting the coagulation bath so that water naturally flowed down to bind the nanofibers [400]. Fig. 9C shows the scanning electron microscopy (SEM) micrograph of a hierarchical helix nanofiber yarn [313].

3D bulk nanofibrous scaffolds. The transformation of 2D nanofiber mats into 3D nanofibrous scaffolds can expand their application. For solution electrospinning, it is impractical to change 2D nonwoven fiber mats into 3D nanofiber clumps with considerable height by increasing the electrospinning time due to the limitation of the electrospinning speed. Gas foaming technology is an effective strategy to transform 2D nanofiber mats into 3D nanofiber scaffolds. The technique involves combining prepared nanofiber scaffolds with feedstocks that can self-generate gases, such as NaBH_4 , which generates hydrogen gas, or dry ice, which generates CO_2 gas, to expand the nanofiber mats into a 3D bulk material. In a typical study, after 2D oriented PCL nanofiber scaffolds were prepared by conventional electrospinning, using a unique method of combining innovative gas-foaming and molding technologies, we report the rapid transformation of 2D nanofiber membranes into pre-designed 3D scaffolds with biomimetic and oriented porous structure [401]. To further increase the expansion rate, in another study, a surfactant, Pluronic F-127, was added to PCL nanofibers to obtain more stable bubbles in the foaming. When fixed in a closed mold, the 2D nanofiber mat could be quickly transformed into pre-designed 3D scaffolds of various shapes on demand, including cylindrical, hollow cylindrical, rectangular, spherical, and irregularly shaped 3D objects (Fig. 9D) [297].

In addition, 3D printing technology has also been widely used in the preparation of 3D nanofiber scaffolds, providing a new idea and method for the modification of nano-scaffolds. For example, Dilshan and colleagues prepared a novel meniscus tissue scaffold using a 3D-printed frame made of PLA and random or aligned PCL and collagen nanofibers embedded between two frames. MG-63 cells were used to characterize scaffolds *in vitro*. According to the results, MG-63 cells adhered to and proliferated on the hybrid scaffold, and topological/biophysical cues can be incorporated into a nanofiber matrix to influence cell growth [402]. Like 2D nanofiber mats, 3D nanofiber scaffolds are available in random, aligned, and pattern forms. In another study, wet electrospinning of PLA nanofibers was utilized with a target bath of ethanol saturated with CO_2 as the collector. The 2D PLA membranes collected were effectively foamed into a 3D structure by the escaping CO_2 to modulate cell behavior [403]. The 3D nanofiber scaffold cross-linked and modified with HA showed high water absorption, good cell compatibility, and elasticity in a wet state (Fig. 9E) [395].

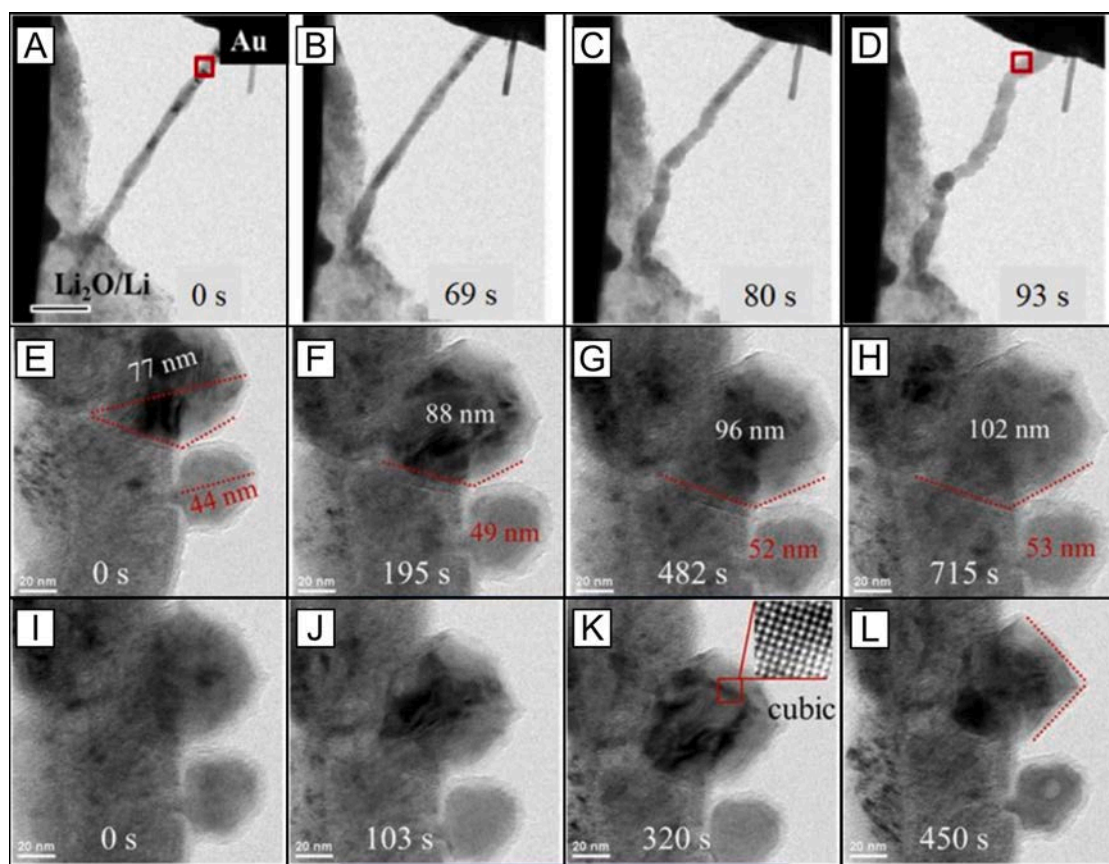


Fig. 26. In-situ cycling rate performance of vanadium oxide coated tin dioxide nanowire electrode. (A-D) in-situ lithiation process for V_2O_5 loaded SnO_2 nanowire when a constant current of 100 pA applied on the open cell. (E-H) Time-sequenced TEM images of in-situ lithiation process for the pre-cycled V_2O_5 coated SnO_2 nanowire. Two Sn nanoparticles on the surface expanded $\sim 30\%$ in diameter without any crack forming during the lithiation. (I-L) In-situ TEM images of the nanowire during the following delithiation process. Two Sn nanoparticles shrank to their original sizes and remain stable single-crystal structures. Reproduced from ref. [1166] with permission from Elsevier, copyright 2017.

Nanofibrous microspheres and aerogels. Nanofibrous microspheres and aerogels can also be prepared by different preparation strategies using nanofibers as the base material. Usually, nanofibers are first produced by homogenization methods to produce short nanofibers with smaller sizes, which are then subjected to different further processing methods. This is also an advanced and efficient strategy to improve the performance and function of nanofiber scaffolds. Nanofiber microspheres have stronger properties such as injectable and sustained release, prompting them to have broader application prospects in drug carriers, diagnostics, and other fields. In one study, by combining electrospinning, electrospaying and surface-coupling techniques, biomimetic injectable microspheres made of PCL:gelatin: methacrylated gelatin (GelMA) (1:0.5:0.5) nanofiber segments were prepared (Fig. 9F) [329]. The aerogel has higher porosity and specific surface area. In one study, 3D mesoporous graphene/CNF was prepared from electrospun PAN/poly(4-vinyl phenol) fibers [401]. Through hydrogen bonding interactions between PAN and poly(4-vinyl phenol) polymer chains, traditional soft CNF was converted to form hard nanofiber aerogels with excellent mechanical, electrical, and sorption properties. The specific interactions among PAN/ poly(4-vinyl phenol) led to the formation of porous features on carbonized nanofiber foams.

2.5.3. Composites made of electrospun nanofibers and other materials

Electrospun nanofibers can also be used as part of the composition in combination with other types of materials, such as elastomers and hydrogels, to significantly improve the overall properties of the material, such as mechanical strength, hydrophilicity, tensile strength adhesion, bioactivity, thermal and electrical conductivity [404].

Nanofiber-elastomer composites. Elastomers have good elastic properties, and the addition of filled nanofiber materials to an elastomer matrix can significantly improve their properties, such as thermal and electrical conductivity. In one study, functionalized graphene oxide (GO) was dispersed in composite elastomers and then loaded with silica nanofibers, improving the electrical and thermal conductivity of the composite elastomers [404]. Besides, when elastomers are combined with switching elements, the polymers are endowed with shape memory properties, i.e., shape memory polymers. In another study, semicrystalline PVA electrospun fibers were combined with thermoplastic polyether block amide elastomer through a melt compaction process to make shape memory composites (Fig. 9G) [396]. The mechanical properties of the polymer were enhanced, and the shape of the polymer could be changed

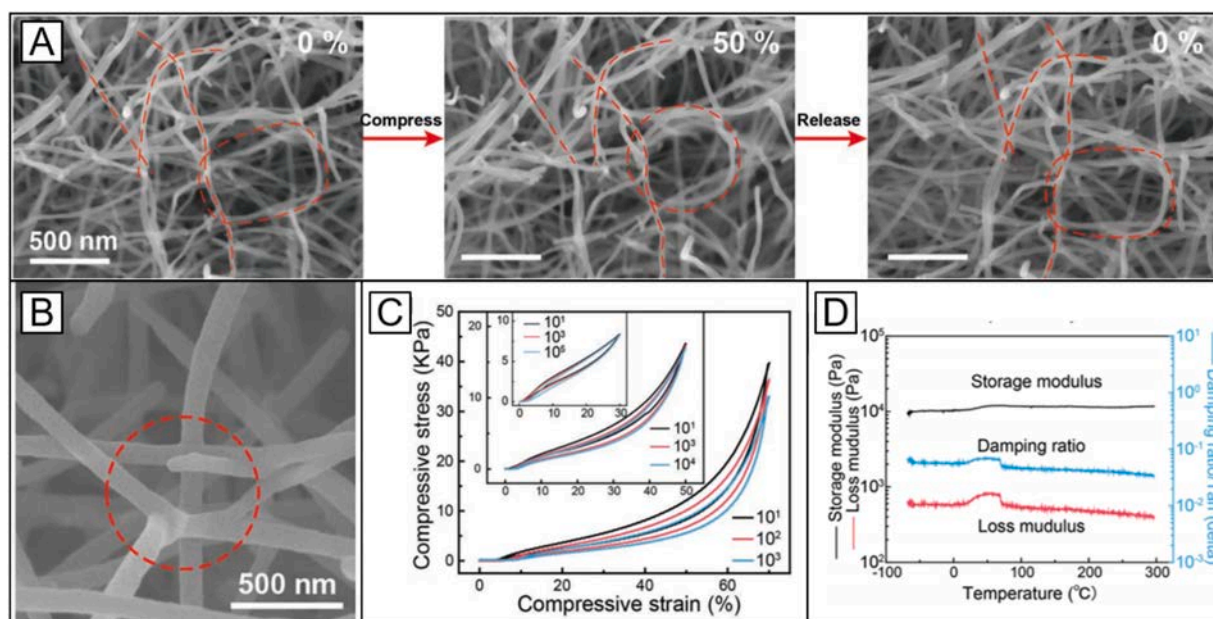


Fig. 27. The mechanical performances of the obtained carbon aerogels. (A) The in-situ SEM of the structural deformation of the BCNF@C aerogel at 50% compression and after release. The scale bar is 500 nm. (B) SEM images of the fiber–fiber joints (red circle). (C) Stress–strain curves of BCNF@C carbon aerogel at 30% strain for 10^5 cycles, 50% strain for 10^4 cycles, and 70% strain for 10^3 cycles. (D) Viscoelastic property of the carbon aerogel over the temperature from -70 to 300 °C at 1 Hz. Reproduced from ref. [1171] with permission from Wiley-VCH, copyright 2019. (For interpretation of the references to color in this figure legend, the reader is referred to the web version of this article.)

or restored by changing the temperature.

Nanofiber-hydrogel composites. Hydrogel has excellent biocompatibility and can be cured by UV light to form a 3D structure. By integrating electrospun nanofibers in hydrogel, its mechanical properties can be enhanced while maintaining the original properties. For example, PCL and Polyethylene glycol (PEG) nanofibers were embedded in GelMA hydrogel to mimic the three-layer structure of native osteochondral tissue (Fig. 9H) [326]. In addition, short electrospun fibers laminated within injectable hydrogels have received increasing attention. For example, an injectable antimicrobial hydrogel was obtained by cutting electrospun fibers into short nanofibers and wrapping them in GelMA to increase the modulus of the hydrogel [405].

Nanofiber-microcapsule composite. Electrospun nanofibers can be compounded with other materials to enhance the properties of nanomaterials. One common strategy is the deposition of polymeric microcapsules onto polymeric microfiber scaffolds. Thus, the nanomaterials have both the stable mechanical properties of fibrous scaffolds and the excellent properties of nanospheres, such as controlled and sustained release, in a stable tandem. In one study, developing silk microcapsules functionalized electrospun biocompatible PCL fibers with capacity to be used as a drug delivery platform in four approaches: (i) using electrospinning of PCL/DCM/MeOH solution containing dispersed silk microcapsules suspension to encapsulate capsules into PCL fibers; (ii) using electrospinning of PCL/DCM/methanol organic phase with silk fibroin microcapsules water phase emulsion to encapsulate capsules into PCL fibers with core-sheath structure; (iii) using covalent bonding to immobilize silk fibroin microcapsules onto electrospun PCL fibers by Cu (I)-catalyzed azide-alkyne cycloaddition click chemistry and silk layer-by-layer (LBL) coating; (iv) using cleavable disulfide-linkage to immobilize silk fibroin microcapsules onto electrospun PCL fibers by click chemistry and NHS ester reaction chemistry and these capsules can be triggered release by a reducing environment. These can be applied to various physicochemical characteristics of drugs and specific release behavior requirements, which have potential applications in tissue engineering and drug delivery [406].

Bio-printed nanofibrous scaffolds. 3D printing is a method of manufacturing objects by 3D printing ink layer by layer through digital control. It allows customizing the geometry of the desired object on demand with low material consumption [407–409]. Since hydrogels can hold and release large amounts of water or biofluids with tunable mechanical properties, porosity and biocompatibility [407], the preparation of hydrogel 3D scaffolds by 3D printing using hydrogels as bioinks is currently receiving increasing attention. In general, hydrogel bioinks can be crosslinked or stabilized during or immediately after printing to prepare hydrogels with 3D structures. However, since the printed hydrogel structures are prone to deform under gravity, this poses a great challenge for hydrogel 3D printing [410].

Electrospun nanofibers are promising printer-friendly materials due to their good biocompatibility and mechanical properties with shear thinning behavior, high zero-shear viscosity, high shape fidelity and structural stability during 3D printing [9,411]. For example, SF nanofibers were added to bioinks to thin the enhanced shear-thinning ink for preparing hydrogel scaffolds with higher fidelity [412]. In another study, cellulose nanofibers were added to bioink to prepare 3D-printed composite hydrogel scaffolds with filamentous structures, which improved the mechanical properties and shape fidelity of the scaffolds [413]. In addition, cellulose nanofibers-based inks were prepared to increase support for printing hydrogel structures, enabling the expansion of ink diversity

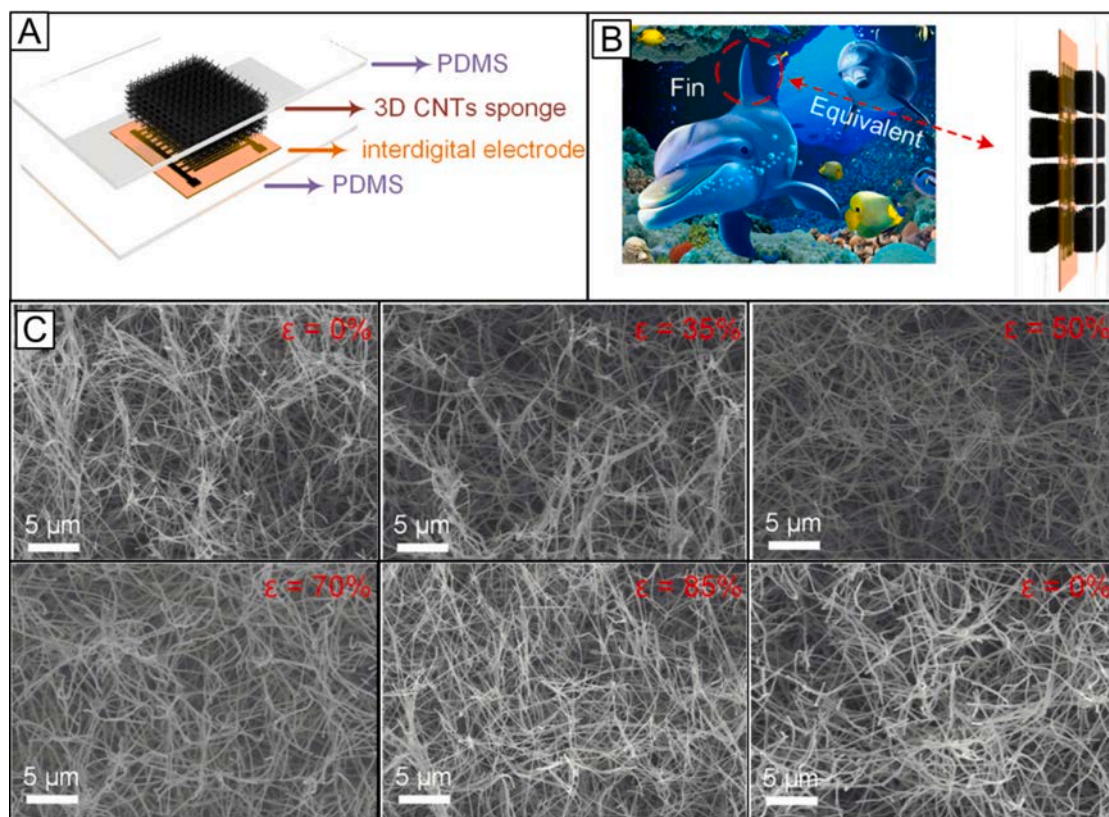


Fig. 28. The conductivity and sensing pathways of carbon nanotube fibers in the bionic flexible double-sided electronic skin. (A) Schematic diagram of the CNT sponge-based pressure sensor. (B) The working mechanism of fins is used to design the pressure sensor, realizing the function of force direction detection. (C) In-situ SEM images of the CNT sponge press-release dynamic process. The CNT sponge in the original state, pressed state of $\sim 35\%$, 50% , 70% , 85% , and after releasing completely. Reproduced from ref. [1172] with permission from American Chemical Society, copyright 2020.

[414].

2.6. Properties and functions of electrospun nanofibers

The diverse compositions, fabrication processes and structures of electrospun nanofibers allow for unlimited possibilities in terms of tunability of properties and customizability of functions. They exhibit attractive properties in electronic, magnetic, optical, acoustics, thermal, mechanics and combined properties, such as electromagnetic, photoelectric, piezoelectric, triboelectric, photothermal, *etc.* By virtue of one or more of these properties, various fantastic functions can be achieved to derive numerous important applications [415]. To achieve different properties, it is necessary to select specific materials with intrinsic physicochemical properties, including monomer materials or composites, and then further adjust the properties of the final nanofiber product through the modulation of morphology and diameter at the 1D level, as well as the layered structure of the fibers at the 2D and 3D levels, the different forms of fiber assemblies, and the combination with other types of materials and components.

Conductive nanofibers, for example, are widely used in flexible electronics, transparent electrodes, electromagnetic wave absorption, nanogenerators, *etc.* [416]. To construct a conductive nanofiber, a suitable material must be chosen. There are two approaches to achieving this goal. One is the direct method, which involves choosing and electrospinning conductive materials such as metal nanowires/nanoparticles, carbon nanotubes, graphene, transition metal carbides/nitrides (MXene), *etc.* with some polymer additives [163]. This method is straightforward in concept and preparation procedure but also faces some challenges. Appropriate conductive materials that are applicable for electrospinning are quite limited. In addition, if the conductivity of the electrospinning solution is too high, electrospinning is not possible due to charging effects or even short circuits. Therefore, conductive nanofibers are more often prepared with an alternative approach: the indirect material transformation method. For example, conductive metal nanofibers such as Au, Pt, Ag, Cu, *etc.* could be prepared by electrospinning a precursor metal salts/polymer composite solution into nanofibers and then reducing it to metal in a reducing atmosphere. It is also feasible to employ common electrospun nanofibers as a 1D template and then deposit a layer of metal on the surfaces of nanofibers by electroless deposition, chemical vapor deposition, physical vapor deposition, or atomic layer deposition. Besides metal, carbon materials are also good candidates for conductive nanofibers. These can be fabricated through pyrolysis of carbon precursor polymers such as PAN, PVA or many other polymers. These CNFs are

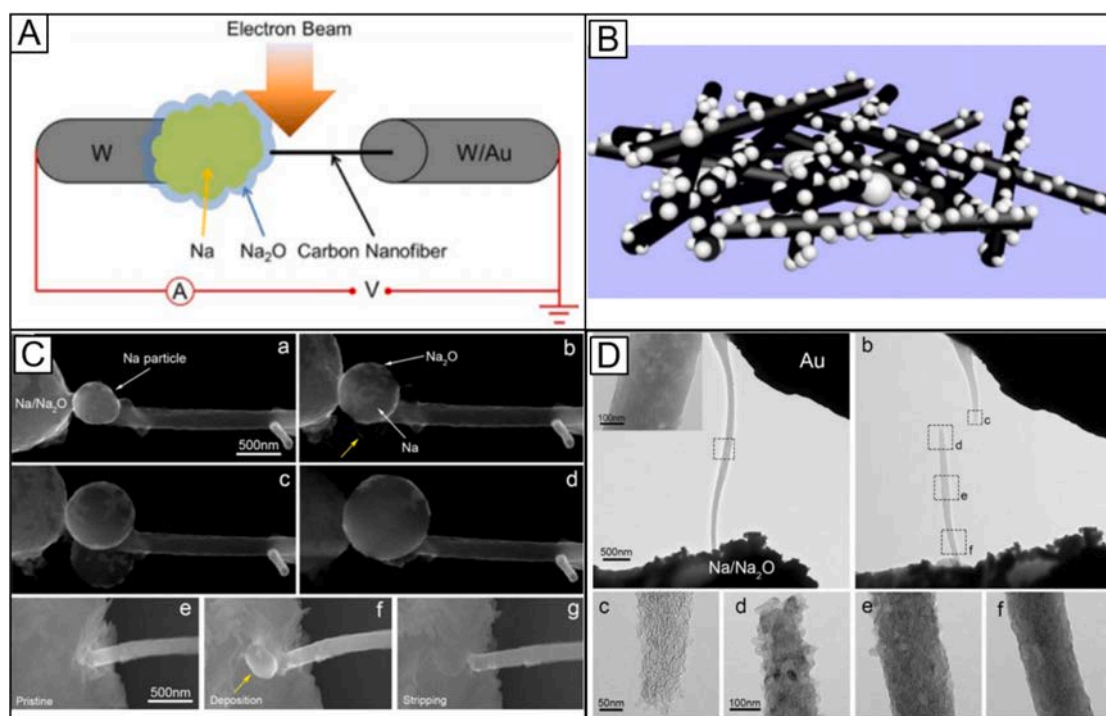


Fig. 29. The electrochemical deposition and dissolution behavior of sodium metal on CNF current collector. Schematic illustrations of (A) the in-situ Na battery experimental setup and (B) CNF-Na composite anode comprised of a CNF network and embedded Na depositions. (C) In-situ SEM observation of the structural evolution of the particles at the interface of CNF/Na₂O electrolyte. (a-d) The expansion and fusion of sphere-like Na particles during a plating process. The yellow arrow in b indicated a new particle that just appeared below the former one. (e-g) A typical case of particle deposition and dissolution at the CNF/electrolyte interface during a plating/stripping cycle. (D) In-situ TEM investigation of the sodiation response of a partially graphitized CNF. (a) A nanofiber bridging the upper Au wire and the lower Na/Na₂O electrode. The Insert showed the structural detail of the pristine CNF in the boxed area. (b) The broken nanofiber with its two segments attached to two electrodes after the current-induced breakdown of the fiber. (c-f) The enlarged images of the four indicated regions in (D). Reproduced from ref. [1173] with permission from Elsevier, copyright 2017. (For interpretation of the references to color in this figure legend, the reader is referred to the web version of this article.)

broadly utilized in electrochemistry, batteries, supercapacitors, electromagnetic wave absorbing, *etc* [93,417,418]. In addition, conductive polymers can be made into nanofibers by *in-situ* polymerization on a nanofibers template and used in sensors, biology, flexible electronics, *etc*.

Among several physical properties, electric, magnetic, and optical properties mainly rely on the starting materials with corresponding properties. Structural parameters play an auxiliary role in tuning these properties to some extent [91,92]. However, for acoustics, thermal and mechanical properties, structural configuration and materials are often equally important. For example, sound-absorbing materials mainly rely on porous structures and are not very sensitive to the composition of the materials. Structural parameters also play an important role in mechanical strength or elasticity even when based on the same material [163,359]. For instance, an aligned nanofiber bundle is much stronger than random nanofibers, while a twisted nanofiber yarn can be even stronger. An over-twisted helical yarn could exhibit unusual stretchability due to its multi-level structures [419]. For thermal insulation materials, intrinsically low heat conductivity materials must be combined with suitable porous structures to achieve better heat shielding performance [420,421].

A single function is not enough to satisfy real requirements, and multiple physical properties must be considered. For example, piezoelectric sensors or generators need to consider both electronic output and mechanical deformation simultaneously. The piezoelectricity of electrospun nanofibers is mainly exhibited in ferroelectric nanofibers, *e.g.*, polymer (PVDF) [422] and inorganic ceramics (PZT [423], BTO [424], PMN-PT [425], *etc.*), after polarization process. The concept of piezoelectricity is broader than that of ferroelectricity. However, non-ferroelectric piezoelectricity, which is ascribed to the spontaneous polarity in single-crystal 1D nanomaterials [426,427], is unable to be exhibited in electrospun nanofibers. This is because the electrospinning technology can only fabricate polycrystal nanofibers. The piezoelectricity of electrospun ferroelectric nanofibers is contributed by the aligned dipoles and/or domains inside the fibers. These can be parallel [425,428] or perpendicular [429] to the axis direction of the nanofibers. The piezoelectricity with aligned domains parallel to the axis direction of nanofibers is more preferable and stable due to the lower depolarization field [430], which usually takes advantage of piezoelectric nanofibers based nanogenerator [423,428,429,431]. In addition, these inorganic ceramics nanofibers become more flexible [432], a favorable factor in fabricating nanogenerators, after scaling down from their fragile bulks.

Different properties of electrospun nanofibers can be achieved through rational composition combinations and multiscale

Table 4

The advantages and disadvantages of the different advanced characterization techniques.

Techniques		Pros.	Cons.
<i>In-situ</i> spectroscopy	<i>In-situ</i> XRD	(1) monitors the structural evolution in high temperature (2) investigates the mechanism of LIBs materials	(1) cannot detect its morphology characteristics
	<i>In-situ</i> XPS	(1) analyzes the layered or core-sheath structure materials (2) monitors under different conditions (atmosphere, temperature, light, <i>etc.</i>) (3) explores the electrochemical changes of the solid/liquid interfaces	(1) limited depth of the top few atomic layers
	<i>In-situ</i> FTIR	(1) detects the chemical bonds and functional groups and constitution (2) monitors under different conditions (atmosphere, temperature, light, electricity, <i>etc.</i>)	(1) only detects the changes of the bonds
	<i>In-situ</i> Raman	(1) identifies the active site (2) establishes relationships between structure and performance (3) monitors under different conditions (atmosphere, temperature, light, electricity, <i>etc.</i>)	(1) without morphology characteristics
	<i>In-situ</i> XAFS	(1) provides atom-specific structural and elemental information (2) monitors under different conditions (atmosphere, temperature, light, electricity, <i>etc.</i>)	
<i>In-situ</i> Microscopy	<i>In-situ</i> TEM	(1) provides more superior and comprehensive characterization characteristics combined with spectroscopy (2) monitors under different conditions (atmosphere, temperature, light, electricity, <i>etc.</i>)	(1) damages the sample (2) requires environmental vacuum
	<i>In-situ</i> SEM	(1) has large sample space, low damage, and low requirement for environmental vacuum. (2) monitors under different conditions (atmosphere, temperature, light, electricity, <i>etc.</i>)	(1) poor resolution compared to TEM
	<i>In-situ</i> FM	(1) performs element tracking, morphology observation, and physical performance analysis (2) views fibers around any perspective without physical cutting (3) monitors under different conditions (atmosphere, temperature, light, electricity, <i>etc.</i>)	(1) limited to several specific excitation wavelengths

structural (1D, 2D, and 3D) design. The composition and structures play synergetic but not equivalent roles in different properties. Sometimes, the composition takes center stage and structure enhances performance, such as electronic and magnetic optical properties. In other cases, the suitable structures are dominant while the composition is relatively less sensitive, such as sound absorption and filtration. No matter what cases, comprehensive understanding of the roles played by both composition and structure and the rational design are necessary to achieve better performance for the electrospun nanofibers.

3. Applications of electrospun nanofibers

3.1. Electrospun nanofibers for environmental protection and safety guarantee

3.1.1. Water filtration and desalination

The shortage of fresh and clean water drives the development of separating materials and techniques with low energy costs and high efficiency. Water filtration and desalination are the major means of obtaining fresh and clean water, during which separation membrane is of great importance. The most commonly used membrane separation technologies include pressure-driven and thermal-driven such as membrane distillation. Owing to the advantages of interconnected porous structure, high porosity and excellent mass transfer properties, separation membranes made of electrospun nanofibers are competitive in water purification and remediation based on pressure-driven or thermal-driven mechanisms, as the details are shown in Fig. 10.

3.1.1.1. Pressure-driven filtration membranes. Pressure-driven separation technology mainly includes microfiltration (MF), ultrafiltration (UF), nanofiltration (NF), reverse osmosis (RO), and forward osmosis (FO). Owing to the high porosity (70 %~90 %), appropriate sub-micron levels of pore size, and interconnected porous structure with lower tortuosity, electrospun nanofibrous membranes are naturally outstanding contenders for MF with excellent mass transfer. For example, membrane made of electrospun PVDF nanofibers was used for liquid separation and particulate removal, which could successfully reject 90 % of PS particles with 1, 5, and 10 μm diameters [433]. Electrospun nanofibrous membranes made of different polymer materials, such as PAN, PSU, PES, and polyamide 6 (PA6), with varied parameters (nanofiber diameter and membrane thickness) and different modifications have been applied for separating microparticles or microbes (e.g., bacteria and activated sludge) from water [121,434,435]. Nanofibrous membranes tend to have a high rejection rate in the micro-particle retention test. However, due to the deeper pore and longer channel of nanofibrous membranes, membrane fouling is prone to occur, mainly due to the clogging of small particles (diameter < 2 μm) into a cake-like fouling layer, leading to a drastic decrease in liquid flux. Moreover, the mechanical failure of nanofibrous membranes is also a vital issue in the long-term application of MF. Therefore, in the above case, the pretreatment processes are necessary before application on an industry scale.

Electrospun nanofibrous membranes can be applied in liquid drops filtration towards oil/water separation. The key to improving





Table 5

Representative industrial multi-needle electrospinning equipment.

Company	Product model	Equipment size	Country	Website	Industrial Electrospinning Equipment
Nanoscience Instruments	Fluitnatek HT	Capable of simultaneous use of more than 5500 needles, 1.6 m wide roll substrate, up to 50 L of solution	America	https://www.nanoscience.com/	
NanoTechnology Solutions	NanoSpinner 416	Equipped with 110 electrospinning needles, it can produce 5,000 g of nanofibers a day with a width of one meter	Australia	https://nanotechnologiesolutions.com.au/	
Fanavar Nano-Meghyas	INFL6100	Depending on the number of electrospinning (units 4–8), the nanofiber coating rate will be about 50–800 square meters per hour.	Iran	https://en.fnm.ir/Gallery	
Shenzhen Tongli Weina	TL-20 M–1600	The array is arranged with 384 needles, the material width is 1.6 m, and the output is about 7500 m ² per hour	China	https://www.qdjunada.com/	
Qingdao Pan Silk Technology Co., LTD	—	Customize according to customer requirements	China	https://www.pansitech.com/gongsijianjie/	
Junada (Qingdao) Technology Co., LTD	NES-2	The maximum width of nanofibers is 1.6 m	China	https://www.qdjunada.com/	
Inovenso	PE-3550	Type Bottom-Up Spinning, up to 56 nozzles during full operation (Each Unit)	America	https://www.inovenso.com/	

(continued on next page)

Table 5 (continued)

Company	Product model	Equipment size	Country	Website	Industrial Electrospinning Equipment
Matregenix	—	—	America	https://matregenix.com/	
NANOFLUX	NF-Star	Nozzle or needle:135 pcs (adjustable)	Singapore	https://www.nanoflux.com.sg/en/	
Spectral Systems	—	Nanofiber-based nonwoven membranes/scaffolds/mats, massive functional nanoparticles or thin coatings homogeneously deposited onto flexible industrial nonwoven rolls (width up to 1.7 m) can be produced	Russia	https://spectralsystems.ru/	
Foshan Nanofiberlabs Co., Ltd	MF03-002	The width of nanofiber mat is 1.2 m	China	https://www.nanofiberlabs.com/	

the efficiency of oil–water separation is controlling the surface energy and increasing the contact area. Controlling the surface energy requires surface modification, and surface superhydrophobicity or superhydrophilicity modification of nanofibers can improve the selectivity between oil and water. The superhydrophobic membrane allows oil to pass through while blocking water. On the contrary, the superhydrophilic/underwater super-oleophobic membrane prevents oil while allowing water to penetrate [436–439]. For example, a liquid with a high polar component was infused into porous flexible TiO_2 - SiO_2 nanofiber membranes to regulate the wetting behavior [440]. Thus, a relatively stable liquid-infusion-interface was formed to repel the immiscible low polar component of liquid. By this facile and universal strategy, even immiscible liquids with a surface energy difference as small as 2 mJ m^{-2} , or emulsions could be effectively separated. The contact area can be increased by modulating the surface of the nanofibers to increase the roughness. By controlling the surface energy and porous structure, the separation of emulsions has been realized.

Membrane fouling by organics in water is another important issue that greatly impairs the practical application of electrospun nanofibrous membranes for MF. Even the underwater super-oleophobic membrane based on a superhydrophilic surface suffers from fouling by polar organics in water (e.g., humic acids, polyoses, proteins, and biofilms) during long-term operation, resulting in a gradual decrease in the flux and separation efficiency. Designing fiber membranes that are cleanable or even self-cleaning is an effective strategy. For example, a superhydrophilic calcinable polymer membrane was fabricated based on inter-bonding structured polysulfonamide (PSA)/ TiO_2 composite fibers, which could be easily reclaimed by calcination at 400°C even after being fouled by amphiphilic organics [441]. In addition, a hydraulic-pressure-responsive membrane (PiezoMem) could transform pressure pulses into electroactive responses for *in-situ* self-cleaning. A transient hydraulic pressure fluctuation across the membrane resulted in the generation of current pulses and rapid voltage oscillations (peak, $+5.0/-3.2 \text{ V}$), enabling broad-spectrum antifouling action towards a range of membrane foulants such as organic molecules, oil droplets, proteins, bacteria and inorganic colloids through reactive oxygen species (ROS) production and dielectrophoretic repulsion [442].

UF and NF often require membranes with smaller pore sizes and high-pressure resistance to sieve solute molecules and saline ions, which is far beyond the tolerance of electrospun nanofibrous membranes. In this case, the fiber membranes could be used as a flexible barrier, or as a mid or supporting layer for UF and NF composite membranes to reduce the working pressure, maintain high flux, and

Table 6
Needleless electrospinning nozzle in different characters.

Structure	Specific character	Single system efficiency/g·h ⁻¹
Linear	Linear laser [1221]	0.36 ~ 1.28
	Coated wire [1222]	288
	Flat roller [1223]	—
	Line electrode [1202,1206,1224,1225]	—
	Linear flume nozzle [1226]	3.91 ~ 4.85
	Linear array nozzle [1227–1230]	—
	Screw rod [1219]	1.5 ~ 6
Curvilinear style	Melt differential [1204]	20 ~ 75.6
	Circular curve [1231,1232]	4.2
	Disk curve [1233]	6.85
	Rotary cone [1208]	0.083 ~ 0.208
	Curve convex slot [56]	10 ~ 20
Surface type	String [38]	2.64
	Double magnetic fluid [1234]	0.12 ~ 1.2
	Rotating disk [1210,1235]	2.09 ~ 5.24
	Roller spinning [1214,1236,1237]	1.25 ~ 12.5
	Ball spinning [1215]	—
	Sputtering jet [1238]	0.44 ~ 6
Stereometrical structure	Bubble jet [1216,1217]	0.06 ~ 0.6
	Conical wire coil [1218]	0.86 ~ 2.75
	Spiral coil [1220,1239–1241]	2.94 ~ 9.42
	Bowl [1231,1242]	0.265 ~ 0.684
	Threaded rod [1219]	5 ~ 6

provide special hydrophobic and hydrophilic properties. In one study, chitosan-coated PAN nanofibrous composite UF membranes reached a 130 L m⁻¹h⁻¹ flux while maintaining a high oil and water separation rate (>99.9 %) [427]. PAN thin-film nanofibrous composite was applied for NF to filter 2000 ppm MgSO₄ with 2.4 times flux than commercial NF membrane [443]. The water resistance and surface properties can be further improved by crosslinking and loading functional particles, which were only applied on a lab scale [444–446].

For desalination, the widely accepted pressure-driven membrane technology is RO membranes. However, there are few reports on electrospun nanofibrous membranes for RO mainly due to the unsatisfactory mechanical properties of electrospun nanofibers under quite high working pressure. Several researchers pointed out that RO membranes composed of electrospun nanofibers could gain a range for 40–70 L m⁻²h⁻¹ flux and > 95 % salt rejection rate [440,447]. On the contrary, electrospun nanofibers-supported FO membranes draw more attention than RO membranes. Electrospun nanofibers supporting layers with FO membranes could help to increase the water flux by 2–5 times [448,449]. It is the special structure of these nanofiber substrates that ensures the direct diffusion path of salt and water, providing a promising choice for inhibiting the internal concentration polarization of FO. Although results on Electrospun Nanofibrous Membrane supported FO membranes have been widely reported, there are still some critical issues that need to be resolved. For example, additional research is needed to improve its mechanical characteristics, optimize the pore size of nanofiber substrates, and eliminate the PA layer delamination from the nanofiber substrates.

Thermal-driven filtration membranes

Membrane distillation, a thermal-driven membrane process, is regarded as a promising method for desalination of hypersaline water. The hydrophobic membrane, as the critical unit of membrane distillation, can allow the transmission of clean vapor driven by temperature gradient and resist the permeation of polluted liquid waters. Compared with other desalination technologies, membrane distillation excels in utilizing low-grade or waste heat to generate high-quality water with high recovery and high rejection of salts (100 % in theory) [450]. Recently, electrospun nanofibrous membranes have attracted increasing research attention in the field of membrane distillation because of their higher water flux compared to conventional phase-conversion membranes. However, they are also simultaneously threatened by more severe membrane wetting. To balance the trade-off between mass transfer and membrane wetting, surface chemical modification was applied to construct superhydrophobic membrane for reinforcing membrane distillation and resisting wetting [451,452]. Besides the threats of hot water, organic pollutants tend to result in more severe membrane wetting and fouling [453], which affects the efficiency and durability of the purification membrane. Facing amphiphilic contaminants, omniphobic nanofibrous membrane with re-entrant structure was developed to act as a local kinetic barrier for the replacement of the air layer by liquid water and then reduce wetting [454,455]. Facing hydrophobic pollutants (e.g., oil), superhydrophilic/superhydrophobic *Janus* membrane was developed to form a water-protecting layer on the superhydrophilic side to resist oil adhesion [456,457].

In addition to intrinsic surface wettability, the internal pore structure of the membrane is another crucial factor in determining its durability [458,459]. Since the electrospun nanofibrous membrane is formed by a stack of nanofibers with weak interactions, it is prone to large pore deformation during distillation, resulting in a decrease in the overall hydrophobicity of the membrane. Therefore, only relying on the hydrophobic surface of the fiber membrane is not enough. To resolve this problem, electrospun nanofibrous membranes with anti-deformable pores were obtained by welding fibers at their intersections via chemical or physical post-treatment methods [460,461]. Especially, a 3D welded electrospun nanofibrous membrane was fabricated by in-situ emulsion-electrospinning of

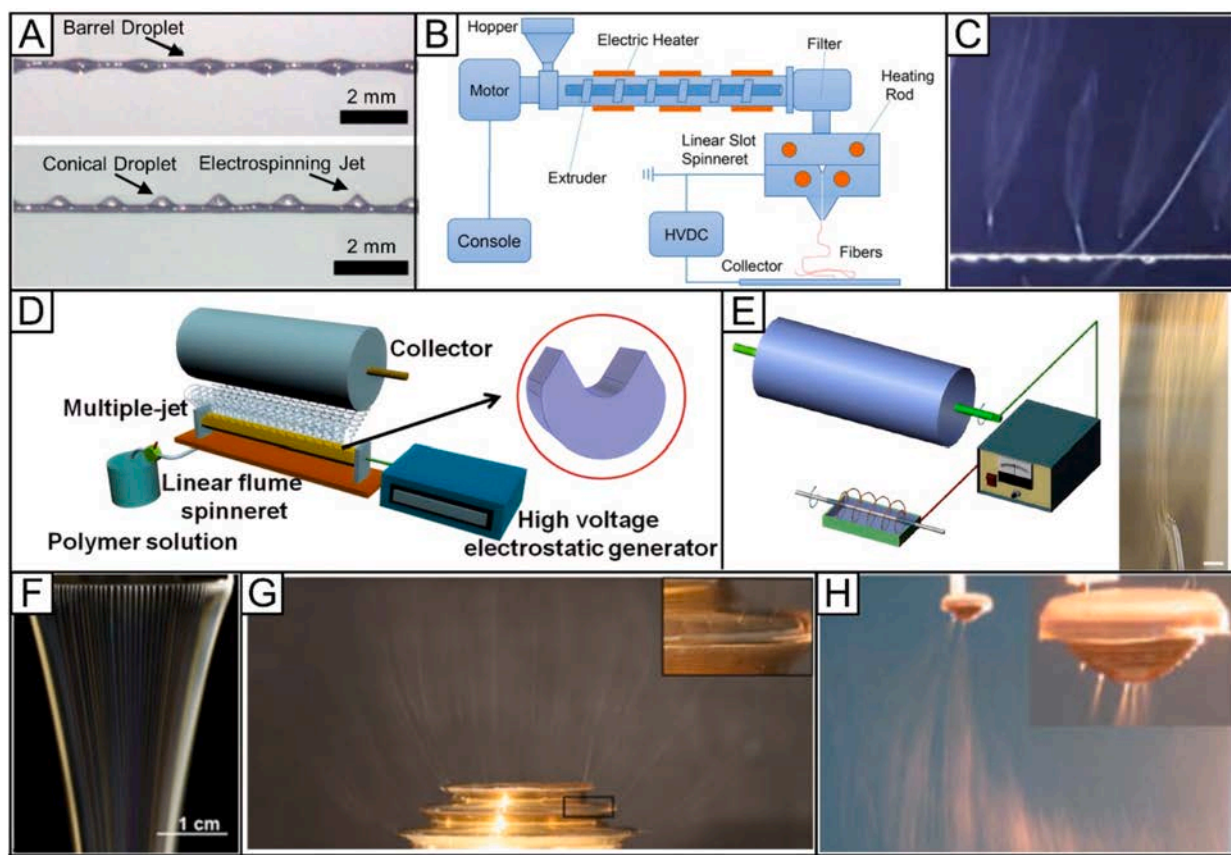


Fig. 30. Diagram of different nozzles of needleless electrospinning process. (A) Wire electrospinning. Reproduced from ref. [1202] with permission from Elsevier, copyright 2012. (B) Linear melt differential electrospinning. Reproduced from ref. [1204] with permission from Wiley-VCH, copyright 2020. (C) Moving conventional yarn. Reproduced from ref. [1205] with permission from Korean Fiber SOC, copyright 2018. (D) Linear flume nozzle. Reproduced from ref. [1206] with permission from MDPI, copyright 2019. (E) Spiral coil. Scale bar=1 cm. Reproduced from ref. [1207] with permission from Hindawi, copyright 2012. (F) Umbrella-like melt differential nozzle. Reproduced from ref. [1211] with permission from Elsevier, copyright 2019. (G) Pyramid. Reproduced from ref. [1217] with permission from Elsevier, copyright 2013. (H) Conical wire coil. Reproduced from ref. [1218] with permission from Wiley-VCH, copyright 2009.

poly (vinylidene fluoride-co-hexafluoropropene)/polydimethylsiloxane (PDMS) [462]. The welding of the nanofibrous membrane was uniform in the vertical direction of the 3D space, resulting in excellent 3D hydrophobic stability of the fiber membrane, reducing the wetting of the inner membrane layer. Thus, it showed robust anti-scaling when for long-term membrane distillation of practical concentrated seawater. By far, membrane distillation based on electrospun nanofibrous membranes has made great progress. In the future, it is expected to further simplify the preparation process and improve the uniformity of membrane pores. In addition, it is anticipated to develop scaled-up hollow nanofiber membranes with much larger desalination surface areas for membrane distillation.

3.1.2. Water pollutants treatment by adsorption

Due to the characteristics of high porosity, large specific surface area, easy functionalization, easy operation, reusability, and low cost, electrospun nanofibers have broad application prospects in the field of wastewater pollutant treatment [463,464]. The main pollutants in wastewater contain heavy metals, organic dyes, pesticides, antibiotics, endocrine, oil contamination, bacteria, viruses and so on [465,466]. Until now, various types of functional polymer nanofibers, organic/inorganic composite nanofibers and inorganic nanofibers have been prepared by electrospinning, which display satisfactory adsorption performance.

Functional polymer electrospun nanofibers can possess more adsorption sites *via* special grafting reactions. Modified PAN nanofibers have been investigated as adsorbents for metal ions [467,468]. The thioamide-group chelating nanofibers, phosphorylated PAN-based nanofibers and branched polyethyleneimine (bPEI) grafted PAN nanofibers exhibited excellent adsorption properties for a variety of metal ions [469,470]. For example, a bPEI grafted electrospun PAN nanofibers (bPEI-PAN) was prepared by a facile refluxing approach. Due to the electrostatic interaction and reduction mechanism, the bPEI-PAN exhibited excellent adsorption performance for Cr(VI) (637.46 mg/g) [471]. Moreover, for a real river water sample treating, the Cr(VI) concentration decreased below the WHO drinking water limit after adsorption and dynamic filtration by the bPEI-PAN membrane.

The introduction of novel nanomaterial adsorbents into polymer nanofibers (e.g., inorganic nanoparticles, MOFs and porous

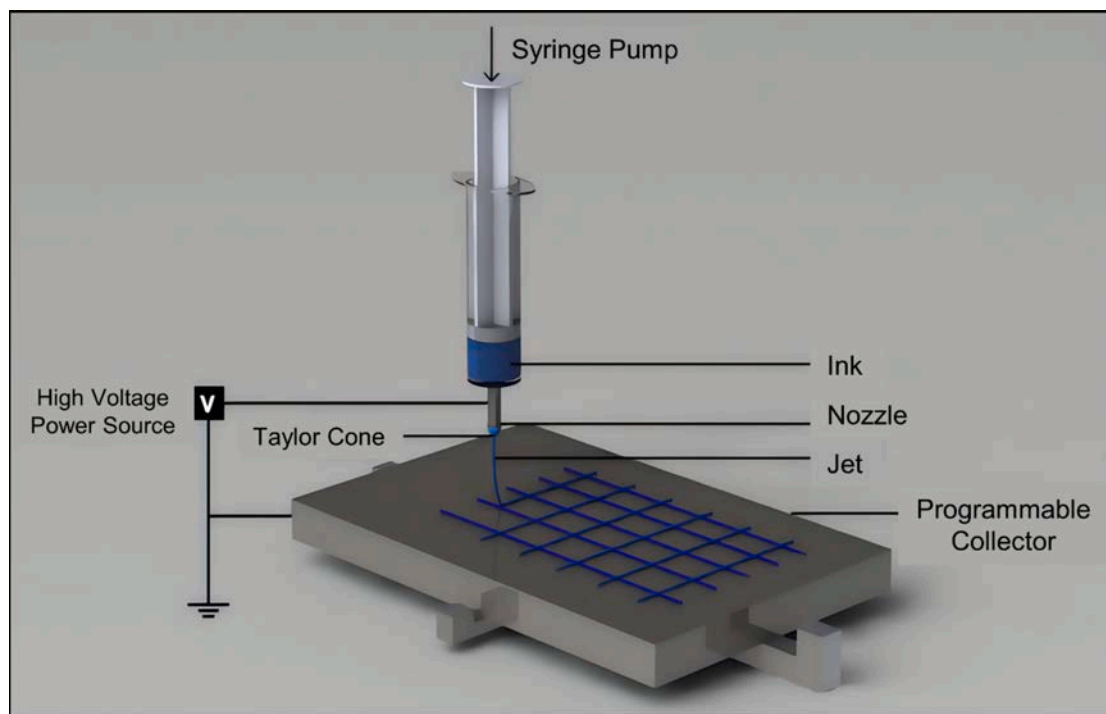


Fig. 31. Schematic representation of NFES. Reproduced from ref. [1248] with permission from American Chemical Society, copyright 2022.

aromatic frameworks) can increase the adsorption sites and enhance selective adsorption capacity. These organic/inorganic composite nanofibers can be fabricated by a combination of electrospinning process, chemical modification and hydrothermal reaction. For instance, MnO_2 nanosheets were in-situ grown onto electrospun PAN nanofibers with the assistance of polydopamine (PDA) coating [472]. The PDA coating facilitated the growth of MnO_2 onto PAN nanofibers, preventing the agglomeration of MnO_2 due to its special adhesive ability. The resulting MnO_2 /PDA/PAN nanofibers showed a high adsorption capacity for Pb^{2+} , with a maximum adsorption capacity of 185.19 mg/g. These hierarchical nanofibers could also effectively remove Pb^{2+} from real industrial effluent with a removal efficiency of above 95 %. Porous framework materials can be introduced to form composite nanofibers with hierarchical structures due to their fine-tunable and designable networks, higher surface area and pore volume, tunable pore size, and good compatibility with polymers [473]. For example, MOFs [e.g., MIL-100(Fe), ZIF-8 and UiO-67(Zr)] and porous aromatic frameworks can be loaded on nanofibers by electrospinning [474]. Among them, the maximum adsorption capacities of amaranth red, vanillic aldehyde, ibuprofen, chloroxylenol, and *N, N*-diethyl-*meta*-toluamide on the PAN@MIL-100(Fe) nanofibers were 615.40, 576.70, 613.50, 429.18, and 384.61 mg/g, respectively. Moreover, the ZIF-8/PDA/PAN nanofibers displayed excellent adsorption performance and reusability towards tetracycline, with an adsorption capacity of 478.18 mg/g [475]. UiO-67(Zr) modified cyclodextrin-based nanofiber membrane (UiO-67@ β -CD-NP) shows a high adsorption capacity of 226.24 mg/g for ibuprofen removal due to the synergetic adsorption effect of cyclodextrin and MOFs [476].

The use of organic polymers as nanofiber substrates may have problems with continuous purification and recyclability. In contrast, nanofibers based on inorganic materials can solve these problems by introducing such as high-temperature calcination due to their high stability. However, the low toughness of inorganic materials limits their further application in wastewater treatment. The emergence of flexible inorganic fibers combines the advantages of both, solving the problems of difficult recycling and secondary pollution. For example, flexible magnesium silicate fiber membrane was prepared via hydrothermal reaction using electrospun flexible SiO_2 fiber membrane as silicon template [477]. The fiber membrane exhibited not only high tensile strength and good mechanical stability but also a superior specific surface area of up to 463.4 m^2/g , similar to powdery MgSi adsorbents. The adsorption capacity for the cationic dye methylene blue was 609.75 mg/g. After five calcination cycles, the high stability ensured that it maintained its filtration performance. Compared to commercial nylon 6 MF membranes, it offered better recovery and filtration performance.

Owing to the acute shortage of energy, nuclear energy has been attracting much attention and is gradually being widely utilized. However, the possible leakage of nuclear fuel in the utilization of nuclear energy is particularly serious in the case of water pollution due to its serious hazards, posing a serious threat to human health and the environment. Recently, modified electrospun nanofibers have been applied to remove the radioactive metal ions (such as ^{235}U , ^{99}Tc , ^{137}Cs and ^{90}Sr) from aqueous solutions. Surface modification could enhance the adsorption ability of electrospun nanofibers for uranium ions. For instance, the nitrile groups on the surface of PAN fibers were modified to amidoxime groups. The amidoximated PAN fibers could chelate with U(VI), with 81 % adsorption. The binding mechanism of the amidoxime group to U(VI) ions was proposed to involve the deprotonation of amidoxime groups and the formation of bidentate ligands with U(VI) ions [478]. The porous cationic electrospun (PCE) fibers were fabricated through a pore-

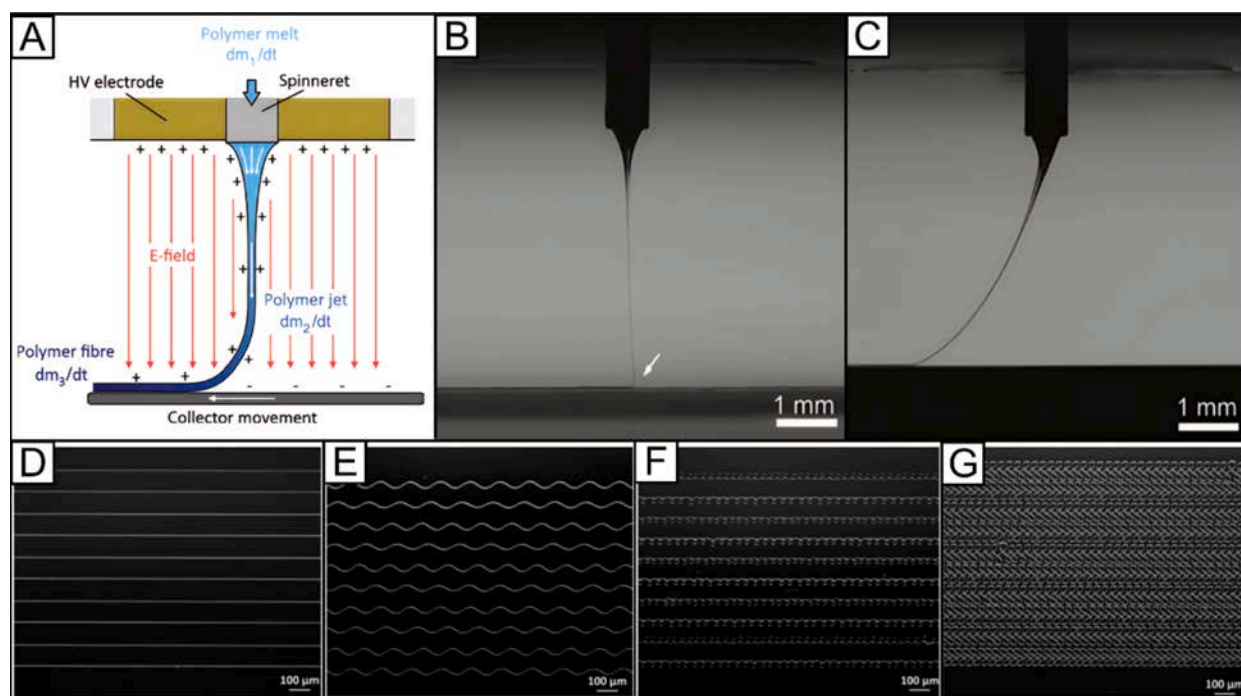


Fig. 32. Changes of obtained patterns with different relationships between jet speed and collector translation speed. (A) A schematic of MEW process in equilibrium. Images of a PCL MEW jet with collector translation speed: (B) at the CTS on a flat collector and (C) above the CTS on a cylindrical mandrel. A series of fiber patterns were collected with decreasing collector translation speed at (D) 1 ~ 1.1 times of CTS, (E) 0.75 ~ 0.8 times of CTS, (F) 0.3 ~ 0.35 times of CTS, and (G) 0.10 ~ 0.15 times of CTS. Reproduced from ref. [1245] with permission from American Chemical Society, copyright 2021.

forming inside electrospun fibers hyperbranched graft modification route, and have been used for ^{99}Tc removal, with the rapid 99 % removal of $^{99}\text{TcO}_4^-$ in 22 min [479]. The introduction of inorganic materials can further enhance the adsorption of radioactive metal ions. For example, Prussian blue/PAN composite nanofibers showed rapid and efficient removal of Cs, with 87 % removal efficiency in 10 s, owing to the increase of the surface area and pore volume with the incorporation of Prussian blue nanoparticles into PAN matrix [480]. Dicalcium phosphate dihydrate/PAN fibers exhibited a 94.0 % removal efficiency toward Sr ions with a Sr uptake capacity of 146 mg/g [481]. Overall, the combination of nanoparticles with electrospun nanofibers avoids the obstacle of separation and recycling after the practical application of nanoparticle adsorption.

3.1.3. Air filtration

Air pollution is also a serious threat to public health. Air pollutants mainly include respirable particulate matter (PM), as well as carbon monoxide, nitrous oxide, and sulfur dioxide. Fiber-based air filters are commonly used to remove PM to protect individuals. Compared with traditional fiber filters, filters made of electrospun nanofibers often show a better performance in terms of removal efficiency and air resistance because of their high porosity, micron-sized pore size, and large specific surface area. Since the filtration effect of an air filter depends on the size and composition of particles, it is very important to adjust the properties of filter media according to the removal mechanism of particles. Fig. 11A illustrates the mechanism of PM capture, with the dominant mechanism varying with particle size (Fig. 11B) [482]. According to these mechanisms, the strategy of constructing electrospun fiber membranes for air filtration is mainly by adjusting fiber diameter, changing fiber morphology, and regulating fiber charge. Eventually, the improvement of filtration efficiency and the reduction of pressure drop on the inlet and outlet sides were realized.

To optimize the structure of filter media, reducing the fiber diameter by adjusting the electrospinning parameters is a widely used approach [489,490]. In one study, a one-step electrospinning/netting technology evolving both jets and droplets was applied to construct a bimodal network structure consisting of ordinary electrospun fibers and ultrathin nanonets (Fig. 11C) [483,491,492]. The average diameter of ultrathin nanonets was decreased to ca. 20 nm and the size of formed pores was ca. 200 nm, which significantly improved filtration efficiency. Meanwhile, the decrease in fiber diameter also caused an airflow slippage effect, which effectively reduced the pressure drop of the filter medium [493].

The fiber morphology can be manipulated to increase the specific surface area and create an airflow sliding effect and thus the filtration performance. For example, porous PLLA nanofibers were fabricated by post-treatment with acetone (Fig. 11D) [484], and the membrane showed a filtration efficiency of 99.99 % for ultrafine NaCl particles of 30–100 nm with a pressure drop of 110–230 Pa. An electrospun GO/ PAN composite nanofibrous membrane with an olive-like bead-on-string structure was developed [485]. The high porosity of the beaded structure, combined with the airflow slip effect, resulted in a pressure drop of only 8 Pa, while achieving a

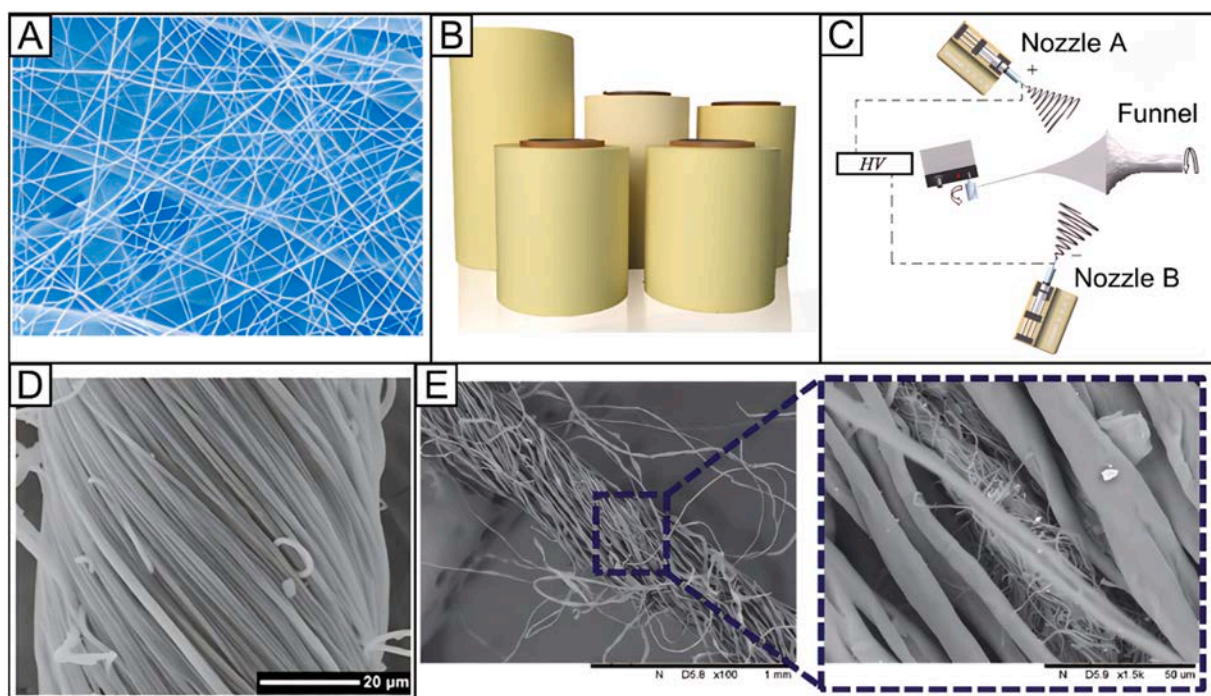


Fig. 33. Structure of different nanofibrous products. (A) SEM image of electrospun nanofibers and their supporting layer in a commercial air filter. Reproduced from ref. with permission from Donaldson website: www.donaldson.com. (B) Digital image of nanofibrous battery separators based on self-supported polyimide nanofibers. Reproduced from ref. [1265] with permission from Jiangxi Xiancai website: www.hinano fiber.com. (C) Schematic illustration of fabrication setup of nanofiber yarns based on rotating-funnel, and (D) SEM image of twisted polyacrylonitrile nanofiber yarn. Reproduced from ref. [1207] with permission from Taylor & Francis, copyright 2012. (E) SEM images of a nanofiber/cotton composite yarn. Reproduced from ref. [1266] with permission from Sage Journals, copyright 2021.

filtration efficiency of 99.97 % for PM_{2.5} (Fig. 11E). Additionally, through the use of tetrabutylammonium chloride, an organic salt, a PVDF nanofiber web with a tree-like branched structure was prepared [494]. At a base weight of 1 g m^{-2} , this filter demonstrated a filtration efficiency of 99.999 % for 260 nm NaCl particles, along with a pressure drop of 124.2 Pa.

Combining the adjustment of fiber diameter with fiber morphology to construct a multi-layered structure can further enhance the filtration effect. For example, a multilayer composite membrane, composed of thermoplastic polyurethanes (TPU) sub-micron fibrous layer (diameter of *ca.* 900 nm), PS bead-on-string nanofibrous layer, and the PA-6 ultrafine fibrous layer (diameter of *ca.* 60 nm) (Fig. 11F), showed a filtration efficiency of 99.99 % and a low-pressure drop of 54 Pa [204,495]. Furthermore, this hierarchical structure improved the mechanical strength (6.72 MPa) and the uniform spatial distribution of particles in the filter media, enhancing the particle capacity.

The storage of active charges in the filtration media also contributes to the filtration performance through the electrostatic effect (Fig. 11G) [486,496]. Building filter media using appropriate electret materials or nanoparticles can significantly enhance active charge storage [497,498]. For example, the surface chemistry of five types of electrospun nanofiber membranes made of different polymers was investigated [499]. Polymers with higher dipole moments such as PAN could better remove particles from smoke due to stronger dipole-dipole and induced dipole-molecular interaction. Thus, it is evident that the greater the polarity of the polymer, the higher the filtration efficiency. Nanoparticles could also be introduced in the nanofibers to capture the target contaminants mainly by electrostatic adsorption. MOFs loaded on electrospun nanofibers could provide positive charges to attract PM as a result of unbalanced metal ions caused by unsaturated metal sites and defects [500]. Electrospun polyimide (PI) nanofibrous air filters could also relate to triboelectric nanogenerators (TEG), leading to a significant enhancement in the removal efficiency from 27.1 % to 83.6 % for particles with a diameter of 76.4 nm (Fig. 11H) [487,501].

Beyond enhancing the filtration performance, with growing concerns about possible plastic contamination from electrospun fiber membranes, many studies have shifted focus to using biodegradable polymers. Therefore, natural and synthetic biodegradable polymers have been used to prepare environmentally friendly and recyclable filter materials [502,503]. Since a large number of solvents involved in electrospinning process may cause health and environmental problems, it is also necessary to develop electrospun fiber air filters with water-soluble polymers [504–506]. Chemical warfare agent degradation functions can be realized by loading various kinds of materials, such as metal oxides, polyoxometalates, MOF materials, fluorescent dyes, *etc.* In one study, mustard gas substitutes were detoxified by uniformly attaching magnesium oxide nanoparticles to the surface of poly (m-benzodicarbonamide) nanofibers [507].

To sum up, electrospinning is an ideal technology for fabricating air filters with high filtration efficiency and low air resistance.

Table 7

Global companies that provide electrospun nanofiber products.

Company	Country	Products
Biomimetic Electrospinning Technologies Inc.	USA	Biomedical scaffolds
BioSurfaces Inc.	USA	Drug delivery
Cella Energy	UK	Energy materials
Clarcor	USA	Filter
Donaldson	USA	Filter
Esfil Techno	Estonia	Filter
Finetex EnE, Inc.	Korea	Filter
Hirose Paper Mfg Co., Ltd	Japan	Filter
MANN + HUMMEL	Germany	Filter
Nanofiber Separations LLC	USA	Filter
Nanofiber Solutions	USA	Cell culture substrate
Neotherix	UK	Biomedical scaffolds
Nicast	Israel	Nanofiber implants
Pardam nanotechnology	Czech	Organic and inorganic nanofiber
PolyElements	USA	Cell culture materials
PolyNanoTec	Germany	Electrospun materials
PolyRemedy	USA	Wound care
Sigma Aldrich	USA	Cell culture materials
Sorbent	Russia	Filter
SPUR	Czech	Filter
The Electrospinning Company	UK	Tissue engineering scaffolds
Zeus	USA	Ultrasmall PTFE polymeric fibers
E-SPin NanoTech	India	Mask
Nicast	Israel	Vascular Graft
Biotronic	Germany	Stent, membrane
St. Theresa Medical Inc	USA	Dextran nanofibers; fibrin sealant
Nanofiber Solutions	USA	Veterinary product; ECM-like fiber structure
Ortho ReBirth	Japan	Bioabsorbable Polymer and SiV
PolyRemedy®, Inc	USA	Antimicrobial Dressings
NANOLAYR LTD	New Zealand	Filtration, Skincare and Acoustic

However, the current understanding of particle filtration mechanisms is based on ideal hypotheses, necessitating further exploration under realistic conditions to construct more effective filters. In addition, the filtration performance of biodegradable filter materials may not yet match that of high-performance filters. Therefore, the development of environmentally friendly electrospun air filters with better performance is necessary.

3.1.4. Electromagnetic interference shielding

With the rapid development of electronic information technology, electromagnetic wave radiation pollution is becoming increasingly serious. Therefore, there is an urgent need to develop high-performance electromagnetic interference (EMI) shielding materials against various electromagnetic waves, such as radio waves, microwaves, infrared light, visible light, UV light, X-rays, and γ -rays. Electromagnetic waves are commonly used in communications, and unwanted high-frequency electromagnetic waves not only interrupt the normal operation of electronic equipment and communication systems, but also disrupt the human bio-immune system and induce a variety of diseases [508].

Electrospun nanofibers have shown great potential due to their superior porosity, large specific surface area, ideal lightweight, corrosion resistance, and good flexibility [477]. The high porosity and interconnected structure of electrospun polymer nanofiber-based membranes are ideal for efficiently absorbing and reflecting incident electromagnetic waves within the material. Electrospun ceramic nanofibers with stable chemical properties, tunable dielectric properties, and good shielding performance at gigahertz frequencies have attracted attention. Lightweight and flexible SiCN ceramic nanowires prepared by electrospinning and high-temperature annealing demonstrated an optimal reflection loss of the nanowires as low as -53.1 dB (dB) and an absorption bandwidth of 5.6 GHz (GHz), effectively covering the entire Ku band (12 – 18 GHz) [508]. With optimal impedance matching, considerable conductive loss and interfacial polarization, composite fiber membranes exhibit excellent electromagnetic absorption performance. Lightweight conductive fillers such as carbon-based materials, 2D nanomaterials, and conductive polymers can be embedded in or coated on nanofibers. For instance, a flexible electrospun composite nanofiber with a sandwich structure, with a thickness of 0.26 mm, exhibited a higher EMI shielding performance (approximately 30 dB) in the X-band (8 – 12 GHz) [509]. In another work, MXenes [e.g., ($\text{Ti}_3\text{C}_2\text{T}_x$)] were introduced as EMI shielding materials, and the $\text{Ti}_3\text{C}_2\text{T}_x$ -sodium alginate composites indicated the highest EMI shielding value of 92 dB for a 45 - μm -thick film with the SSE/t value of 30830 dB $\text{cm}^2 \text{g}^{-1}$ [510].

X-rays are a type of high-energy electromagnetic radiation characterized by high penetrating power, which has important applications in medical diagnostics and industrial testing, but high doses of X-rays pose a serious threat to human health [511]. For X-ray inference shielding, metal elements with high density and high atomic number offer better shielding capabilities. However, the significant toxicity and ecotoxicity of these materials, such as Pb-based, have attracted concerns. As an alternative, Bi_2O_3 and WO_3 have been proposed as promising X-ray shielding materials due to their low toxicity, high density, and high adequate atomic number. In one study, electrospun PVA/ Bi_2O_3 composite fibers demonstrated the highest X-ray attenuation among various fillers tested [511].



Fig. 34. The challenges in the industrialization of electrospinning technology.

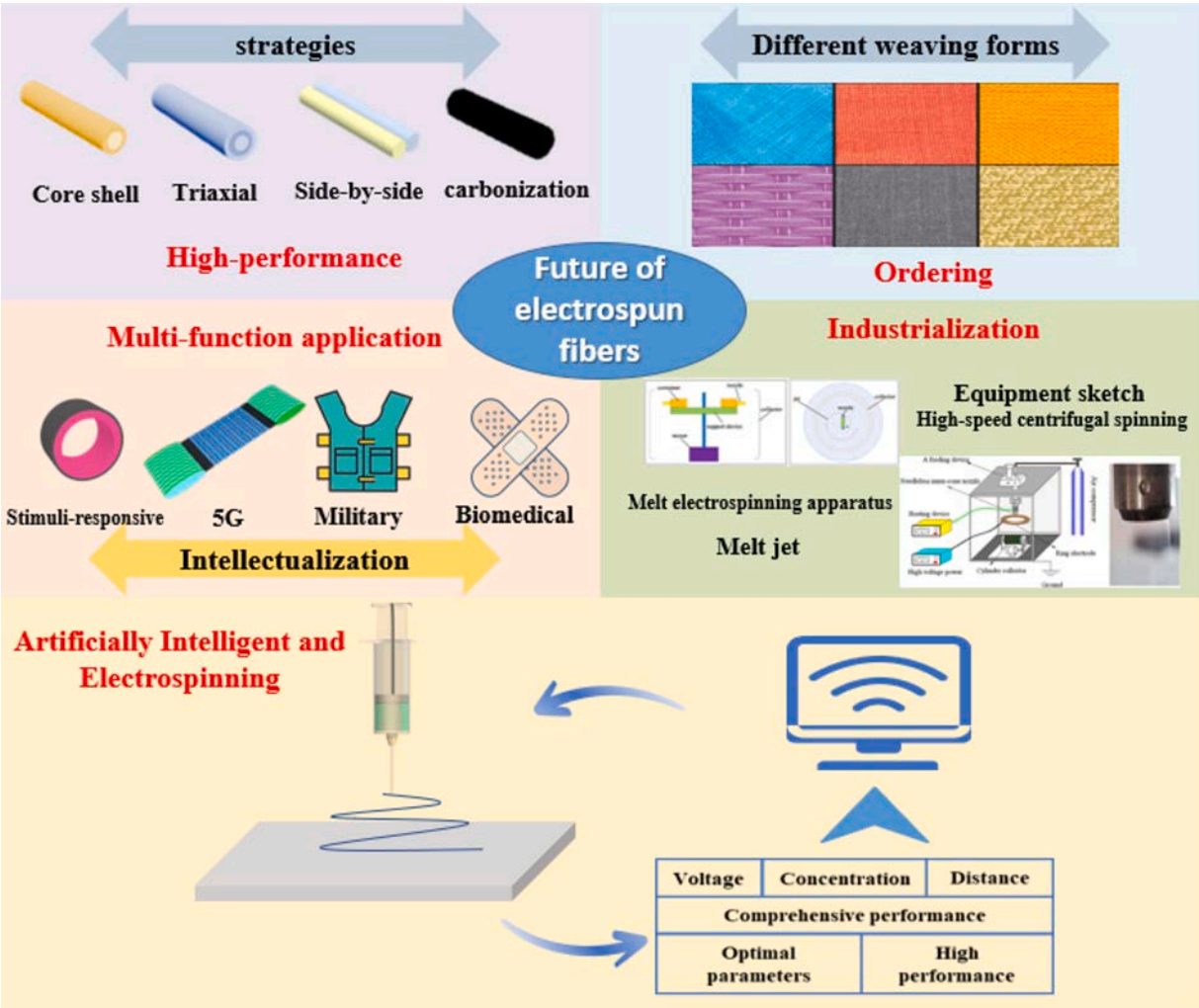


Fig. 35. Schematic indicating the future of electrospun nanofibers.

Table 8
GB19083-2010D mask production standards.

Project	Indicators												
Basic requirements for masks	The wearer's mouth and nose should be covered, with good facial tightness, no holes and stains on the surface, and no air valve.												
Nose bridge bar	Masks should have an adjustable nose bridge bar.												
Face mask belt	The breaking force between each mask belt and the mask body should not be less than 10 N.												
Filtration efficiency % (Filtration efficiency for non-oily particles at a gas flow rate of 85 L/min)	<table><tr><td>Class</td><td>Class 1</td><td>≥95</td></tr><tr><td></td><td>Class 2</td><td>≥99</td></tr><tr><td></td><td>Class 3</td><td>≥99.97</td></tr></table>	Class	Class 1	≥95		Class 2	≥99		Class 3	≥99.97			
Class	Class 1	≥95											
	Class 2	≥99											
	Class 3	≥99.97											
Resistance to airflow (Gas flow is 85 L/min)	≤343.2 Pa (35 mmH ₂ O)												
Synthetic blood penetration	2 mL of synthetic blood is sprayed into the mask at 10.7 KPa (80 mmHg). Infiltration should not occur on the inside of the mask.												
Surface moisture resistance	The moisture level on the surface of the mask should not be lower than the class 3 in GB/T 4745-1997												
Microbiological indicator (In accordance with GB15979-2002) (Respirators marked sterilized or sterile on the package should be sterile)	<table><tr><td>Total number of bacterial colonies CFU/g</td><td>≤200</td></tr><tr><td>Coliform</td><td>Not detectable</td></tr><tr><td>Pseudomonas aeruginosa</td><td></td></tr><tr><td>Staphylococcus aureus</td><td></td></tr><tr><td>Hemolytic streptococcus</td><td></td></tr><tr><td>Total number of fungal colonies CFU/g</td><td>≤100</td></tr></table>	Total number of bacterial colonies CFU/g	≤200	Coliform	Not detectable	Pseudomonas aeruginosa		Staphylococcus aureus		Hemolytic streptococcus		Total number of fungal colonies CFU/g	≤100
Total number of bacterial colonies CFU/g	≤200												
Coliform	Not detectable												
Pseudomonas aeruginosa													
Staphylococcus aureus													
Hemolytic streptococcus													
Total number of fungal colonies CFU/g	≤100												
Ethylene oxide residue (Ethylene oxide sterilized masks)	≤10 μ/g												
Flame retardancy	All materials shall not be inflammable, and the burning time shall not exceed 5 s.												
Skin stimulation	The score for primary irritation of mask materials should not exceed 5 s.												
Fitness	Mask design should provide a good fit with a total fit factor of not less than 100.												

Furthermore, Bi₂WO₆/WO₃/PAN composite nanofibrous membranes showed excellent X-ray shielding performance and photocatalytic degradation of cationic organic pollutants under simulated sunlight [512].

3.1.5. Food safety and protection

Food is susceptible to adverse effects from the external environment, such as microorganisms and oxygen, during transportation, storage, and sales, which can compromise its quality and safety. Active food packaging is an innovative and promising food packaging technique that inhibits the growth and reproduction of microorganisms as well as the occurrence of oxidative reactions, which can meet consumer demand for higher quality, safer, and fresher food. The effective encapsulation of active factors, such as antimicrobial agents and antioxidants, is critical to the preparation of active packaging materials.

Electrospinning has attracted increasing interest in the development of active packaging materials as a result of its structural and functional advantages. The large specific surface area of electrospun nanofibers enhances their response to the surrounding environment, facilitating the timely release of active factors to counteract factors that may adversely affect food quality. Moreover, electrospun fibers can be manufactured without thermal effects, which is conducive to high encapsulation efficiency (usually above 80 %) and maintaining their activity and specificity [513,514]. Therefore, the key to the application of electrospun nanofibers for food safety protection mainly includes the controllable encapsulation and release of active factors while maintaining the activity. Currently, co-blending, coaxial, and emulsion electrospinning techniques are mostly applied in the encapsulation of active factors. Co-blending electrospinning involves the direct electrospinning of polymer carrier solution containing the active factors. For example, active food packaging films were fabricated by electrospinning the carrier matrix gelatin/zein solution containing resveratrol, an active factor with antibacterial and antioxidant activity [515]. Resveratrol was effectively encapsulated in the fibers with an encapsulation efficiency of over 90 %, and the fiber mats exhibited superior antimicrobial activity against *E. coli* and *S. aureus*, extending the shelf life of pork for 3 days at 4 °C. Although co-blending electrospinning exhibited outstanding convenience and versatility, it still faces some challenges in embedding active factors into fibers, such as the burst release of active factors, low encapsulation efficiency due to the difference in hydrophilicity between active factors and carrier matrix, and inactivation of certain hydrophilic active factors when coexisting with organic solvents. In response to these challenges, coaxial and emulsion electrospinning have been rapidly developed to compensate for the shortcomings of blending electrospinning.

Coaxial electrospinning allows for the fabrication of nanofibers with a “core-sheath” structure, where the active factors are encapsulated inside the core. Emulsion electrospinning can embed micro/nanospheres containing active factors into the fibers. They have a wide range of applications in food packaging, both enabling a sustained release of the active factors and protecting the activity from organic solvents [516]. For instance, thymol, an antimicrobial agent, was encapsulated in the core of the nanofiber through coaxial electrospinning [517]. The slow release of thymol into the headspace between the strawberry and the nanofibrous film inhibited the growth of bacteria, fungi and yeast on the strawberry's surface, extending its shelf life without affecting the flavor. In another study, tangeretin was loaded into a nano-emulsion and then loaded in water-resistant PVA/PAA fibers through emulsion electrospinning [518]. The encapsulated tangeretin exhibited sustained release profiles and lower burst release rates compared to pure

Table 9

Production standards of adult woven fabric functional clothing processed by nanotechnology.

Project	Indicators		
Instructions	Instructions for the use of finished products shall be carried out in accordance with GB5296.4, GB18401 and 7.1, and shall indicate the date of production, date of use and specific functions		
Type specification (Model setting and specification of a main part of the finished product)	According to GB/T 1335.1、GB/T1 335.2、GB/T 1335.3		
Material requirements	Nanotechnology processes the nanomaterials used in clothing		Comply with relevant national safety standards
	Fabric		In line with the national textile fabric standard quality requirements
	Lining		Fabric properties and color suitable, except for special needs
	Ingredients	Interlining	The change rate of water size is suitable for the fabric
			Suture
Buttons, zippers and accessories	After washing, hot dyeing, no deformation, no color, no rust and in line with the relevant national standards		
Fillers	Choose all kinds of natural fiber, chemical fiber, animal nap (excluding eiderdown), animal fur and artificial fur according to the standard		
Appearance quality	Conform to the corresponding national or industrial standards of all kinds of clothing		
Functional indicators	In Table 4		
Physical and chemical properties index	In Table 5		
Security (Nanotechnology treats clothing)	1. The skin irritation, allergenicity and human patch test of the treated materials were negative		
	2. Dissolution index of antibacterial class: After washing once, the bacteriostatic band width ≤ 5 mm (Not applicable to disposable products)		
	3. Color fastness, formaldehyde content, pH value, odor and resolvable aromatic amine dyes should comply with GB18401		

tangeretin emulsion, solving the problems of thermodynamically unstable structure and poor sustained-release properties of emulsions. Moreover, the encapsulated tangeretin still maintained good antioxidant activity.

In addition to providing food preservation, nanofiber membranes with intelligent responses can be embedded as nano-sensors within food packaging to monitor changes in the food itself or external conditions, providing real-time insights into its freshness status. The large specific surface area and high porosity of electrospun nanofiber membranes provide favorable conditions for intelligent food packaging systems to achieve higher sensitivity and faster responsiveness [419]. pH-sensitive compounds, such as anthocyanins and curcumin, are commonly used as sensitive units in intelligent food packaging. For example, an electrospun fibrous membrane containing purple sweet potato extraction showed a rapid and sensitive color response to volatile ammonia [519]. When the color of the films changed from dark pink to blue, it indicated that the pork being monitored reached the standard for refusal of consumption. Meanwhile, materials with fluorescent responses to biogenic amines have also been utilized to develop smart tags for monitoring food freshness. Cellulose-based ratiometric fluorescent materials with sensitive ammonia response were processed into the form of nanofibrous membranes through electrospinning [520]. The fluorescence color changes of the membrane represented different freshness levels of shrimp and crab, red for freshness, yellow for slight deterioration, and green for deterioration, enabling real-time and visual monitoring of shrimp and crab freshness.

3.2. Electrospun nanofibers for biomedical applications

3.2.1. Drug delivery

An ideal drug delivery system should be able to deliver drugs directly to the site of injury, achieve sustained drug release and drug targeting, improve water drugs solubility and stability, control drug metabolism time, improve drug absorption, and effectively cross biological barriers, and thus finally achieve long-term therapeutic effects, improve therapeutic efficiency, and reduce drug loss. Current research focuses on the development of biomaterials with specific structures as drug delivery carriers, such as micelles, microspheres, liposomes, fibers, and various other drug delivery carriers have been studied [521–524]. Electrospun nanofibers have significant advantages as drug delivery carriers because of their high surface-to-volume ratio, allowing effective loading of drugs [50,525]. Moreover, the pore interconnectivity and high porosity of nanofibrous membranes facilitate drug-flexible diffusion. By adjusting the electrospinning process, nanofibers with different structures can be obtained, enabling the modulation of drug release modes and rates [526]. Blending electrospinning, coaxial electrospinning, emulsion electrospinning, and microfluidic electrospinning have been mainly applied in drug delivery.

Blending electrospinning is the simplest method for fabricating drug-loaded nanofibers, where the drug is dispersed in the nanofibers by mixing it with a polymer matrix material in the spinning solution. After implantation, the encapsulated drugs can be released at the specific site [527]. For example, metronidazole-loaded PCL nanofiber membranes were fabricated by blending electrospinning, indicating guided tissue regeneration/guided bone regeneration (GTR/GBR) and antimicrobial properties [528]. However, most biocompatible polymers need to be dissolved in organic matter during blending electrospinning, which can lead to

Table 10

Functional indexes of clothing treated by nanotechnology.

Project		superior quality	First-class	qualified product
Waterproof/grade	Before washing	5	5	≥4
	After 15 washes	≥4	≥4	≥4
Oil repellent/ grade	Before washing	≥7.0	≥6.0	≥5.0
	After 15 washes	≥6.0	≥5.0	≥4.0
UV protection	Before washing	UPF50+	UPF50+	UPF50+
	After 15 washes	UPF50+	UPF40+	UPF40+
Antibacterial properties	Before washing	Good		
	After 15 washes	Good	Well	Well
Easy decontamination/ grade	Before washing	Colored textiles	≥4	≥4
		Bleached textile	≥4	≥3
	Before washing	Colored textiles	≥3-4	≥3
		Bleached textile	≥3	≥2-3

Note 1: Assessment by express function

Note 2: Samples shall be taken at the indicated site only for products that are woven or patched with nanotechnology-treated fabric at a specific site.

challenges such as reduced drug bioactivity [529]. In addition, the release profile of the drug is often a non-homogeneous process, which is non-ideal to tissue repair therapy [530].

To achieve controlled release of drugs, preparation of drug-carrying core-sheath nanofibers using coaxial electrospinning technique is an optional way. The flow rates of the two electrospinning solutions can be adjusted to fabricate nanofibers with a sheath layer of polymer wrapped around a core layer of polymer containing drugs [343,531]. By adjusting the composition and physicochemical properties of the core and sheath layers, as well as the relevant settings during the electrospinning process, controlled, long-lasting, and sustained release can be achieved to effectively avoid drug burst release [515,517,532,533]. Meanwhile, the outer sheath structure can encapsulate the inner core structure under mild conditions to protect the bioactivity of the drug molecules [534]. For example, the core-sheath electrospun fibrous mats consist of a gelatin/PVA core containing lysozyme biomolecules, encapsulated by a gelatin sheath containing phenytoin sodium [535]. A sustained release profile was obtained, significantly extending the therapeutics' release time compared to directly loading the drug into the fiber matrix.

Inspired by coaxial electrospinning, triaxial electrospinning and quadriaxial electrospinning have been developed to prepare multilayer nanofibers, which provide more locations for drug loading and allow a wider variety of drugs to be loaded in different layers to achieve multi-level drug release [536]. For example, cellulose acetate-based trilayer core-sheath fibers were fabricated through triaxial electrospinning, and ketoprofen was loaded in different layers with varied contents [537]. The tri-layer nanofibers, which featured discrete drug distributions, demonstrated improved dual-stage release profiles, offering precise release during the initial stage and extended sustained release in the subsequent stage. This provides a simple method to create functional nanofibers with sophisticated structural features. Furthermore, PCL was used to construct both the outermost and second innermost layers, while gelatin was used for both the second outermost and innermost layers, creating quad-axial nanofibers through quadriaxial electrospinning [538]. Moxifloxacin, an antibacterial drug, was encapsulated in different layers of the nanofibers. The efficacy of drug delivery using quad-axial nanofibers was superior to that of core-sheath nanofibers. The triaxial or quad-axial electrospinning process is still too complex and can be easily limited by problems such as nozzle clogging.

Emulsion electrospinning is another approach to fabricating nanofibers for delivering bioactive molecules [539–541]. It is not formed by the structure of the nozzle used, but by a stable emulsion of two or more fluids. For example, nanofibers with hydrophobic 10-hydroxycamptothecin as the sheath and hydrophilic tea polyphenols as the core were prepared by emulsion electrospinning [539]. The two components were released successively to achieve programmed release.

Compared with conventional electrospinning, microfluidic electrospinning can utilize the laminar flow and diffusion properties of the fluid to dynamically regulate the composition and structure of the spinning fluid [542–544]. For example, an implantable hierarchical-structured ultrafine fiber scaffold was fabricated using this technology for localized codelivery of doxorubicin and apatinib to overcome cancer multidrug resistance [545]. The obtained nanofibers have smooth surfaces, relatively uniform diameters, and clear elliptical cavities. Encapsulating DOX-loaded micelles into nanofibers extended the release time of doxorubicin. The *in vivo* research showed that the dual drug-loaded hierarchical-structured nanofibrous scaffold was more effective in controlling tumor volume after 21 days.

In addition, the on-demand release of drugs from the electrospun fibers can be achieved by endogenous or exogenous stimuli, such as pH, enzyme expression, ROS levels, temperature, light, electric fields, magnetic fields, and ultrasound. For instance, ROS-responsive nanofibers patch utilizes high ROS levels in pathological environments to achieve controlled drug release [546]. Drug-loaded electrospun nanofiber scaffold combined with electric stimulation can also control drug release under real physiological conditions by manipulating the external environment. For example, electrical stimulation could modulate the delivery of curcumin through volume changes induced by the voltammetric response of PEDOT nanoparticles [547]. In conclusion, developing electrospun nanofiber scaffolds responsive to multiple endogenous and exogenous stimuli is essential for realizing precise drug delivery.

Although electrospun nanofibers demonstrate excellent performance as drug delivery carriers for tissue repair and cancer therapy, certain issues need to be addressed before clinical trials. First, an accurate study of *in vivo* release kinetics is required to clarify drug release behavior and further optimize the design of drug delivery systems. Moreover, the avoidance of inflammatory and immune

Table 11

Physical and chemical properties of clothing treated by nanotechnology.

Project		superior quality	First-class	qualified product
Tearing strength /N	Light-weight Thick-weight	≥ 7 ≥ 13	≥ 11	≥ 9
Breaking strength /N	Light-weight Thick-weight	≥ 160 ≥ 300	≥ 250	≥ 200
Stitch slipping /cm		≥ 0.5	≥ 0.6	
Strength of crotch seam /N		Fabric not less than 140 N, lining not less than 80 N		
Peel strength of fusible lining /N		≥ 6		
Ventilation rate / (mm/s)		≥ 180		
Fiber content %		According to FZ/T 01,053		
Nanotechnology identification		Total number of nano-structured units > Total number of non-nano-structured units		

Silk products and the quality of the products below 50 g/m² of the suture crack degree according to GB/T 18,132 regulations.

Note 1: Light and thin fabric – 150 g/m² and below; Medium thickness – fabric 150 g/m² and above.

responses that may be caused by material degradation, as well as the realization of safe, non-toxic, and side-effect-free are also essential. Introducing bioactive substances that enhance bioactivity and promote cell adhesion is one strategy to address the above challenges. Additionally, combining imaging agents-loaded fibers with imaging technology allows the real-time monitoring of drug release in the body, thus improving the efficiency of drug delivery and enabling precise and controlled therapy.

3.2.2. Bioimaging

The advancement of *in vivo* imaging is an important challenge for biomedical materials and an inevitable direction of development. *In vivo* imaging plays a vital role in targeted precision therapeutics, early diagnosis of tumors, real-time monitoring of tissues during treatment, and monitoring of processes like implant degradation *in vivo* [548]. Therefore, the realization of biological imaging is essential to expanding the applications of biomedical materials and advancing toward clinical use. Imaging probes serve as a fundamental and core technology for achieving effective imaging. Sensitive materials used to fabricate imaging probes have made significant advancements in precision theragnostic, including ultrasound imaging probes [74,549–551], photoacoustic imaging probes [549,552–556], nuclear magnetic resonance imaging (MRI) probes, near-infrared (NIR) imaging probes [557], fluorescent imaging probes [558–560] and others. These imaging probes have shown great potential in personalized medicine, facilitating the clinical diagnosis and treatment of various diseases.

Biocompatible nanomaterials loaded with imaging probes have been widely used as imaging scaffolds, providing a novel approach for creating a more stable and controllable imaging system [561–565]. Among various techniques, electrospinning has emerged as a promising strategy for fabricating nanofibers due to its outstanding properties. Electrospun nanofiber drug delivery approach can also be used for imaging probe delivery. For instance, one study fabricated a metal-enhanced fluorescence-based biosensor platform using photo-reduced silver nanoparticles and silica-decorated PCL nanofibers, resulting in silver-decorated PCL nanofibers with a silica layer (Ag@SiO₂-PCL) [566]. The Ag@SiO₂-PCL nanofibers demonstrated excellent properties in fluorescence-based biosensing.

Using electrospun nanofibers, it is also possible to encapsulate both imaging probes and drugs. On the one hand, diagnosis and monitoring of diseases can be realized by imaging probe combinations [567]. On the other hand, the therapeutic effects can be achieved at the injury site via controlled drug release [568]. For example, a core-sheath nanofiber was fabricated as an oral drug for the colon [569]. It consisted of a sheath layer that was non-degradable under acidic conditions wrapped around a core layer loaded with magnetic resonance contrast agent Gd (DTPA) and drug. This design allowed the drug to be released only in the colon bypassing the effects of gastric acid, while real-time imaging with Gd (DTPA) enabled precise treatment of the disease.

Currently, the utilization of electrospun nanofibers for delivering imaging probes is a less explored area and has untapped applications in many imaging modalities. Current challenges include finding suitable solvents to carry imaging probes through the high-voltage electrospinning process and stabilizing them within the nanofibers. Furthermore, it is essential to investigate how imaging probes encapsulated in electrospun nanofibers enable *in vivo* imaging and the imaging process itself. It is a huge challenge to monitor the disease progression and treatment processes in a form where the imaging signal itself has been quantified. Therefore, leveraging electrospun nanofibers as delivery carriers for the integration of diagnosis and treatment holds significant promise for clinical medicine and warrants further exploration.

3.2.3. Tissue engineering and regenerative medicine

Tissue engineering and regenerative medicine aim to restore or regenerate the function of lost or functionally damaged tissues and organs using cells, biomolecules, and scaffolds [570]. Tissue-engineered scaffolds provide the necessary microenvironment for the growth of cells damaged by disease, injury, or congenital defects [571]. For tissue repair and regeneration, a significant challenge lies in scaling biomaterials into constructs that can mimic the biological, chemical, and mechanical properties of the tissue microenvironment [572]. Electrospinning is a biomaterial fabrication tool using a variety of natural and synthetic polymers to create nanofibers that resemble the ECM network found in most tissues and organs [10]. Due to its relative simplicity, versatility, and control over fiber production, electrospinning is particularly attractive for tissue engineering applications to manipulate cell adhesion, migration, differentiation, and proliferation [9].

Skin tissue wound healing. As the largest organ of human body, skin tissue integrity is critical for protecting the body from trauma and bacterial infection [573]. Under normal conditions, the skin possesses self-healing capabilities after acute injuries. The healing process consists of four overlapping phases, inflammation, granulation, matrix remodeling, and re-epithelialization [574]. However, chronic wounds caused by burns, infections, diabetes, and other factors associated with skin injuries can impede the development of mature granular tissue, resulting in prolonged inflammation, thus slowing down the healing process of the wound. Proper therapeutic management is crucial due to the potential for systemic infection [575]. While autografts are the gold standard of treatment, extensive skin defects may exceed the capacity of autografts, necessitating the rapid production of functional skin substitutes *in vitro* for wound regeneration [576]. Skin repair scaffolds are expected to play active roles, such as maintaining the moisture at the defect area, absorbing secretions, and inhibiting bacterial growth. A variety of scaffolds composed of electrospun nanofibers have been utilized to restore skin function.

Bacterial infection is a major impediment to skin repair. To address this issue, materials or small molecules with antimicrobial capacity have been integrated into electrospun fiber scaffolds for skin repair. For example, chitosan, proving high versatility and suitability for many types of wounds, exhibits several biological properties such as antimicrobial and wound acceleration [577]. Electrospun chitosan/collagen or silk fibroin nanofiber scaffolds showed good biocompatibility and antimicrobial properties and accelerated wound healing [578]. Similarly, a composite electrospun silk fibroin nanofibrous scaffold containing antimicrobial peptides exhibited significant antibacterial activity against both gram-positive and gram-negative bacteria, promoting wound healing [579]. In addition, the incorporation of inorganic metal oxides as antimicrobial agents could accelerate wound healing [580].

Modulating the inflammation phase is crucial for skin repair. Introducing anti-inflammatory effects to electrospun fibrous scaffolds that promote tissue repair can further enhance the repair effect. Electrospun nanofiber scaffolds were fabricated by introducing type I collagen from tilapia skin, which showed good biocompatibility and low immunogenicity [581]. In another study, electrospun composite nanofibers composed of collagen and bioactive glass showed an enhanced tensile strength in comparison with pristine collagen nanofibers, which could accelerate the healing of rat skin wounds by promoting keratinocyte adhesion and proliferation, anti-inflammation, and pro-early re-epithelialization [582]. Anti-inflammatory components can also be integrated into the scaffolds. For example, ligustrazine was blended in silk fibroin nanofibers, indicating anti-inflammatory capability and promoting wound hemostasis [583].

Other approaches aiming to build 3D environments to promote cellular infiltration and tissue regeneration have also been reported. By combining gas foaming technology and electrospinning, 3D porous multi-layered nanofibrous scaffolds were created, promoting macrophage polarization, vascularization, and wound regeneration [584]. The surface morphology of electrospun nanofibers plays a crucial role in skin tissue repair. The adhesion, proliferation and differentiation of cells can be affected by adjusting the diameter, pore size, surface roughness and topography of the fibers. For example, an aligned PLGA/fish collagen nanofiber membrane with a diameter of 300 nm promoted fibroblast proliferation, keratinocyte spreading and macrophage polarization to reparative phenotypes [585]. Electrospinning technology can also be used to construct drug delivery systems by incorporating drugs into the nanofibers or the surface of nanofiber, achieving controlled release to promote skin tissue repair. By leveraging electrospinning techniques to create core-sheath structures, multi-layered fibers, and stimuli-responsive materials, it is possible to deliver multiple drugs in a controlled and timely manner. Loading cells directly into electrospun fiber scaffolds is another effective method to promote skin tissue repair. These cell-fiber composite scaffolds can provide a good environment for cell adhesion and growth, mimicking the ECM, and promoting cell migration, proliferation, and differentiation. For example, an *in-situ* electrospun scaffold loaded with mesenchymal stem cells (MSCs) promoted angiogenesis and epidermal regeneration and reduced the expression of interleukin-6 to accelerate cutaneous wound healing [586]. In summary, these examples provided scientific bases for the potential use of electrospinning for skin tissue engineering.

3.2.3.1. Nerve tissue. Severe damage to the peripheral nervous system (PNS) is a common global problem, which usually leads to loss of sensory and motor functions [587–589]. The most widely used treatment for restoring peripheral nerves is the autologous nerve graft, but its application is limited by the availability of the donor nerves and immune rejection [590,591]. Recent progress in bioengineering strategies provides an alternative approach using a nerve guidance conduit (NGC) to facilitate nerve growth [591,592]. Synthetic NGCs composed of electrospun nanofibers have gained increasing popularity for nerve regeneration over the past few years [334,593–595]. A hollow NGC provides a canal lumen and serves as a bridge for nerve growth. For example, a self-forming multi-channel NGC with topographical cues based on a degradable shape memory PLA polymer could be temporarily formed into a planar shape for cell loading to realize the uniform distribution of cells [596]. Triggered by a physical temperature around 37 °C, it could automatically restore its permanent tubular shape to form the multichannel conduit and exhibited excellent performance in terms of cell growth and nerve regeneration *in vivo*. The topological structure of the fibers in the conduit affects nerve regeneration. Longitudinal grooves can be formed on the surface of nanofibers to increase the specific surface area for improving nerve regeneration [597]. In the inner wall of NGC, 5 mm arranged grooves were formed and 4–5 mm arranged fibers were filled, and the effect of forming bundles was better than flat NGCs filled with random or aligned fiber and patterned NGCs filled with random fibers [598]. In general, the grooved structure can better simulate the primary neural structure, thus promoting regeneration.

Electrospun nanofibrous scaffolds are ideal matrices for loading various bioactive growth factors to promote nerve growth. In one study, a multi-functional NGC was constructed to promote nerve regeneration by combining ordered topological structure, density gradient of biomacromolecular nanoparticles, and controlled delivery of biological effectors to provide the topographical, haptotactic, and biological cues, respectively [593]. On the surface of aligned PCL nanofibers, a density gradient of bioactive nanoparticles capable of delivering recombinant human acidic fibroblast growth factor was deposited. On the graded scaffold, the proliferation of Schwann cells was promoted, and the directional extension of neurites from both PC12 cells and dorsal root ganglions was improved in the

direction of increasing particle density.

Since the nerve signal is actually an electrical signal, PPy and graphene have been utilized to coat electrospun nanofiber-based NGC to guide Schwann cell migration and promote nerve regeneration *in vivo* [581,595]. To provide more space for guiding the migration and proliferation of nerve cells, filaments or sponges were integrated into the hollow NGCs, which were more conducive to cell migration and performed better in nerve function recovery than hollow NGC group [594,599,600]. Electrical stimulation can promote nerve regeneration after sciatic nerve injury [601]. Electrospun fiber membrane with conductive coating can significantly improve the regeneration effect of peripheral nerves under electrical stimulation [602]. In addition, electrical stimulation has a synergistic effect with oriented fibers. It can significantly enhance myelin and axon regeneration, thus promoting peripheral nerve regeneration [603].

Similar challenges also exist in spinal cord injury (SCI). An injectable nanofiber-hydrogel composite was prepared by combining thiol-modified HA hydrogel and PCL fibrous membrane [604]. The composite supported pro-regenerative macrophage polarization, angiogenesis, axon growth, and neurogenesis in the injured site. The repair effect may be further promoted by loading functional substances. For example, neurotrophin-3, a protein that promotes neuronal survival and axonal sprouting, was dispersed in poly (ϵ -caprolactone-co-ethyl ethylene phosphate) nanofibers to induce nerve regeneration [605]. In another study, polysialic acid was adopted to control central nervous system development by regulating cell adhesive properties and promoting axonal growth [606]. Besides, CeO₂ nanoparticles were extensively studied and could be combined with electrospun fibers for potential use in nerve regeneration [607].

3.2.3.2. Blood vessel tissue. It is estimated that approximately 1.4 million patients require arterial prostheses each year in the USA [608]. However, up to 30 % of patients requiring lower limb revascularization and up to 50 % of patients who require secondary bypass surgery, lack an autologous saphenous vein and mammary artery suitable for grafting, despite this being the current gold standard [609]. There is considerable importance in replacing autologous veins with engineered grafts to restore vascular regeneration and function. Large-diameter (≥ 6 mm) vascular grafts made by polymers (such as Dacron, polytetrafluoroethylene (PTFE), etc.) have been successfully applied since 1957 [610]. However, the efficacy of synthetic materials has not been comparable to that of transplanted natural tissue, and small-diameter (< 6 mm) grafts are rarely used in the clinic because of their susceptibility to acute thrombosis or graft occlusion. As a result, significant efforts have been devoted to developing resorbable small-diameter vascular grafts. To promote antithrombotic properties, a combination of surface modification and manufacturing methods has been explored. In addition to biocompatibility, biodegradability and mechanical compatibility are important factors that need to be considered when selecting graft materials.

Electrospun nanofibrous scaffolds are widely used in studies to develop vascular grafts due to their excellent maneuverability. For example, tubular HA/collagen nanofibrous composite scaffolds were obtained by sequential electrospinning and cross-linking, providing a good matrix for the adhesion and proliferation of vascular endothelial cells [611]. Heparin, as a commonly used anticoagulant in clinical practice, functions early after implantation, while long-term patency is largely dependent on rapid endothelialization of the lumen. Heparin/silk-PLCL composite nanofibers were fabricated via conjugate electrospinning technology for the inhibition of intimal hyperplasia [612]. From the results of a canine femoral artery model, the mixed grafts exhibited higher patency, better smooth muscle cells (SMCs) growth, and higher expression of angiogenesis-related genes compared to PLCL grafts. The most intensively studied strategies for promoting vascular graft success are heparin-loaded antithrombotic and active substance-promoting endothelialization. Several research groups have also further explored the use of heparin to reduce thrombosis. By introducing heparin-VEGF into the PCL nanofibers via coaxial electrospinning, the vascular patency in a rat aorta model was improved [613]. In another study, vascular grafts were prepared by coaxial electrospinning, with the core containing heparin and the shell consisting of salivianolic acid B-loaded mesoporous silica nanoparticles, synergistically promoting human umbilical vein endothelial cell (HUVEC) growth [614]. Salivianolic acid B, extracted and purified from saliva, could offer anti-inflammatory, antioxidant, anti-hypoxic, and anti-arteriosclerotic properties [615].

From a bionic perspective, the intima and media are considered to be functionally important layers in native blood vessels, consisting of a continuous monolayer of endothelial cells and SMCs arranged along the circumference, respectively [616]. Replicating this multilayered structure of native vessels in a man-made scaffold is believed to be more conducive to the regeneration of vascular tissue. To this end, multilayered electrospun vascular grafts have been developed to mimic both the nascent endothelium, which is important for anticoagulation, and the mesentery, which is important for mechanical integrity. The main design concept is that the compact inner layer promotes endothelialization, and the loose middle layer promotes SMCs infiltration. *In vivo* evaluation showed that endothelial cells, as well as infiltrated smooth muscle tissue, regenerated in the inner and outer layers of the prefabricated scaffold, respectively, demonstrating the feasibility of biomimetic bilayer scaffold in vascular tissue regeneration [617,618]. Furthermore, electrospun nanofibers encapsulated with growth factors, such as vascular endothelial growth factor (VEGF), show excellent hemocompatibility and biocompatibility properties to promote vascular regeneration *in vivo* [619]. These studies demonstrate that electrospun fiber-based vascular grafts with elaborate designs will be beneficial for small-diameter vascular reconstruction.

3.2.3.3. Myocardium tissue. Cardiovascular diseases are one of the most morbid and deadly diseases in the world [620]. Among them, myocardial infarction can lead to severe damage to myocardial tissue [621]. Due to the extremely limited regenerative capacity of the adult heart, large numbers of cardiomyocytes are lost and replaced by non-contractile scar tissue, resulting in pathological cardiac remodeling and heart failure [622,623]. The central reason is that mature cardiomyocytes are terminally differentiated cells, and they do not have self-regeneration ability [624], making it challenging to repair necrotic myocardium after myocardial injury. At present, the clinical treatment methods mainly include drug therapy, angioplasty, and coronary artery bypass operation. However, it is difficult

to use these traditional treatments to repair damaged myocardial tissue and normalize dead and fibrotic myocardium to normal. Therefore, improving the curative effect of traditional treatment and looking for new treatment strategies are imperative [625]. The rise and rapid development of cardiac tissue engineering has become a focus of research on myocardial infarction repair, aiming to construct tissue-engineered cardiac tissue to repair or replace damaged myocardium. At present, methods for producing tissue engineering scaffolds include acellular technique [626,627], electrospinning [626,627], molecular self-assembly [628], bioprinting [628], etc.

Electrospinning has been applied to fabricate various scaffolds with different forms and functions according to different needs [9]. Cardiac patches composed of brown adipose-derived stem cell sheets and conductive electrospun nanofibers restored infarcted hearts for ischemic myocardial infarction [372]. Another study showed that co-axial fibrous scaffolds integrating with carbon fiber promoted cardiac tissue regeneration post-myocardial infarction [629]. Focused rotary jet spinning was applied to manufacture biodegradable polymer poly(*L*-lactide-co- ϵ -caprolactone) fibers in minutes and assembled to produce nanofibrous heart valve scaffolds (FibraValves), a heart valve replacement [630]. The fibers allowed for the cells from patients to attach and remodel in the implanted scaffold, eventually building a native valve that could grow and live with the child throughout their life. Furthermore, a scaffold with a 3D highly ordered microstructure with a fiber diameter of 10–20 μm and spacing of 60–80 μm was fabricated by maintaining a vertical jet during electrospinning [631]. The induced pluripotent stem cells (iPSCs)-derived cardiomyocytes formed ordered engineered cardiac tissues with their sarcomere growth along the fiber, and synchronous functional engineered cardiac tissues were developed inside the scaffold with matured calcium handling compared to that on a 2D coverslip.

Loading of active substances is an effective means of applying electrospun fiber patches for repairing myocardial infarction. For example, a ROS-responsive biodegradable elastomeric PU with thioketal linkages was synthesized from PCL-diol, 1,6-hexamethylene diisocyanate, and ROS-cleavable chain extenders, and then electrospun into a nanofibrous patch loaded with glucocorticoid methylprednisolone [546]. The patch exhibited good antioxidant activity, reduced infarct size, and restored blood transport capacity in the infarcted myocardium. Core-sheath nanofibrous patches with a sustained release of rhACE2 could reduce myocardial apoptosis and cell fibrosis, preventing poor ventricular remodeling under hypoxia stress [632]. The controlled release of specific gases is another efficient way. For example, nitric oxide plays a critical role in the treatment of myocardial infarction because it can increase cardiac protection through cardiovascular homeostasis regulation. Therefore, local nitric oxide release needs to be carefully managed. In one study, an electrospun PCL nanofibrous mat covalently combined with nitrate was implanted into the heart muscle to localized release nitric oxide in a chronic model with 4 weeks of myocardial infarction (Fig. 12A) [488]. Masson staining (Fig. 12, B, C) and functional measurements (Fig. 12D, E) demonstrated that implantation of the patch effectively improved cardiac function and suppressed cardiac dilation.

A variety of cell types are beneficial in cardiac repair [633], such as MSCs [634], embryonic stem cells (ESCs), iPSCs, cardiac-derived stem cells (CSCs), etc [631,635,636]. However, the cell therapy of myocardial injury still faces many challenges such as limited cell survival rate and low cell maturity due to local microenvironmental limitations. Myocardial patches based on electrospun nanofibers can provide good mechanical support and microenvironment for cells and improve the survival rate of cell transplantation. Electrospun cellulose nanofibrous mat was modified with multilayers of chitosan/silk fibroin via LBL coating and then loaded with adipose tissue MSCs to generate a cell nano-patch [637]. After adhering to the epicardium in the infarcted area of the rat heart, the patch promoted the functional survival of engrafted cells and restrained ventricular remodeling through attenuating myocardial fibrosis. In another study, uniaxially aligned electrospun PCL nanofibers loaded with child progenitor cells were applied to treat right ventricular heart failure caused by congenital heart disease [638]. The uniaxially aligned structure of the patch induced CPCs growth, and coating fibronectin on the nanofibers enhanced the metabolism of both neonatal and child CPCs. It is also crucial to ensure that the cardiac patches can grow with the growth of human heart, especially for the child. The lack of growth of the implanted material remains a particularly problematic issue, especially for pediatric patients with precordial defects. Additionally, preventing infection and aneurysm formation during tissue reconstruction is also important. Therefore, more experimental exploration is needed for the development of tissue-engineered patches.

3.2.3.4. Tendon/ligament tissue. Tendons and ligaments are prone to rupture and laceration because of their load-bearing nature, leading to injury and a significant loss of flexibility and mobility in patients [639]. Due to their poor intrinsic healing capacity, it remains a clinical challenge to restore injured tendons and ligaments [640]. Various clinical approaches, including autografts, allografts, and artificial prostheses, are employed to repair or replace damaged tendons, but they are limited by the morbidity of the donor site, immune rejection, a high rate of injury recurrence, and limited long-term function restoration [640,641]. Consequently, tissue engineering offers a promising alternative treatment to facilitate tendon and ligament healing and the development of new reparative tissue constructs [642].

In recent years, electrospun-aligned nanofibers, resembling the ultrastructure of tendons, offer a possible option for the treatment and regeneration of damaged tendons and ligaments. In one study, a scaffold was fabricated by melt electrospinning, in which fiber-guiding features comprising 100 μm spaced channels were constructed to facilitate periodontal ligament attachment and a pore size gradient was generated in the bone component, while a highly porous and fully interconnected interface was maintained between the compartments [643]. The scaffold induced a systematic tissue orientation at the dentin-ligament interface, resembling the native periodontium and resulting in enhanced alignment mimicking the periodontal ligament regeneration in an ectopic periodontal attachment model in immunocompromised rats.

A variety of scaffolds with hierarchical structure and function have been developed to promote healing of tendon injuries [644]. For example, a multi-layered electrospun tubular construct was fabricated to exhibit three layers: an inner layer containing an anti-

inflammatory component (Naproxen), a middle layer of braided monofilament as reinforcement, and an outer layer containing HA, an anti-adhesion component [20]. *In vitro* assays using human fibroblasts showed that the incorporation of the bioactive components was successful and noncytotoxic. Moreover, tensile testing using *ex vivo* sheep tendons proved that the developed multi-layered constructs could fulfill the required strength for tendon repair (*i.e.*, 2.79–3.98 MPa), with an ultimate strength of 8.56 ± 1.92 MPa and 8.36 ± 0.57 MPa for PCL and acrylate endcapped urethane-based precursor/PCL constructs, respectively [645]. Electrospun nanofibrous scaffold with crimped nanofibers and welded joints was fabricated to mimic the intricate natural microstructure of tendon-to-bone interface [646]. The crimped nanofiber scaffold featured bionic tensile stress and induced chondrogenic differentiation, laying credible basis for *in vivo* experimentation.

Adhesion formation during tendon healing remains a severe problem in clinical practice [647]. Electrospun nanofibers with a porous structure can be loaded with different drugs to prevent tendon adhesion and promote tendon healing. For example, miR-29a was loaded in lipid nanoparticles and then integrated into core-sheath nanofibers [648]. PLA-PEG copolymer was used as the shell layer for anti-adhesion, and miR-29a was used to regulate collagen synthesis and NF- κ B activation in tenocytes while promoting macrophage polarization by inhibiting the inflammation pathway. From the *in vivo* studies of the Achilles tendon-rupture model, the scaffold promoted collagen composition and alignment with higher mechanical strength and better functional recovery. Loading growth factors, such as VEGF, insulin-like growth factor, and mechano-growth factor, through electrospinning to promote tissue healing is one of the commonly used strategies [649,650]. In one study, Ex-4, a peptide growth factor favoring tenogenic differentiation, was encapsulated in the open lumen of halloysite nanotubes (HNTs), and then the HNT tube endings were sealed with a polymer blend [651]. Afterward, Ex-4-loaded HNTs were integrated into the electrospun nanofibrous mats composed of a blend of PCL and cellulose acetate. The nanofiber scaffold containing Ex-4 accelerated the hMSCs proliferation and improved the expression levels of sulfated glycosaminoglycan, tendon-related genes (Scx, Mxk, and Tnmd), and ECM-related genes (Col-I, Col-III, and Dcn). Moreover, the nanofiber scaffold containing Ex-4 enhanced tendon healing and reduced fibrocartilage formation in comparison to the pristine nanofiber scaffold in the full-thickness rat Achilles tendon defect. In another study, the mechano-growth factor, which could regulate the macrophage polarization to an anti-inflammatory M2 phenotype, was modified on the surface of an electrospun PCL nanofibrous scaffold through LBL self-assembly with silk and click chemistry [652]. The modified scaffold not only mitigated the foreign-body reaction *in vivo* but also exhibited excellent anti-tissue adhesion effects, promoting the repair of tendon injuries.

3.2.3.5. Bone/cartilage tissue. Bone damage and defects are common clinical orthopedic disorders, with a high incidence of bone defects, mainly caused by trauma, tumors, osteoporosis, and infections [653]. Currently, bone grafting is considered the “gold standard” for clinical repair of severe bone defects, but autologous bone grafting is constrained by supply shortages, secondary injuries, and complications, and allogeneic bone grafting also suffers from immune rejection and infection risk [654,655]. As a result, tissue engineering approaches hold promise for restoring bone defects, and various elaborate scaffolds have been developed as alternatives for clinical treatment [656,657].

Electrospun nanofibers can mimic the predominantly hierarchically organized collagen fibrils of the ECM in natural bone and can create a 3D environment for cell adhesion, proliferation, and differentiation through a variety of techniques and the introduction of active ingredients [658,659]. For example, the incorporation of inorganic particles in the scaffolds can promote bone regeneration. In one study, composite electrospun PCL/gelatin nanofibrous scaffolds containing hydroxyapatite (HAp) and niobium pentoxide particles could improve osteoblast cell proliferation and differentiation [660]. Electrospun silk fibroin nanofibrous scaffolds containing HAp particles could enhance the osteogenic differentiation of human adipose-derived MSCs *in vitro* and repair bone defects *in vivo* [661]. Besides, nanofibrous scaffolds loaded with functional factors and bioactive molecules can provide the possibility of mimicking natural ECM to direct cellular growth. For example, 3D nanofibrous scaffold containing homogenized nano-HAp/PLLA/gelatin short electrospun fibers was fabricated by combining freeze-drying and thermal crosslinking [662]. Then, synthetic bone morphogenetic protein-2 (BMP2)-derived peptide was immobilized on the surface of the scaffold by PDA-assisted coating strategy (Fig. 13A). The scaffold could increase the expressions of genes associated with osteogenic differentiation both *in vitro* and *in vivo* (Fig. 13B, C). In another study, alendronate sodium, which can inhibit bone resorption, was loaded into mesoporous silicate nanoparticles and then incorporated in PCL/gelatin nanofibers by electrospinning [663]. The delivery of alendronate sodium from the nanofibrous scaffold could modulate the bone remodeling process. The above studies illustrate the promising potential of electrospun nanofibrous scaffolds for bone tissue engineering applications.

Cartilage tissue damage from sports-related injuries can contribute directly to developing joint osteoarthritis, and in severe cases, total joint replacement is required [664]. Current treatments for cartilage defect include microfracture surgery, implantation of autografts, and transplantation of autologous chondrocytes, while these modalities are often ineffective due to shortcomings such as complex processing, lack of appropriate donors, and adverse immune response [665]. Tissue engineering treatment using electrospun nanofibrous scaffolds is a promising strategy for cartilage regeneration, and current research focuses on the development of 3D structures with porous architecture for cartilage repair. For example, electrospun nanofibrous membranes were homogenized to produce short fibers [395]. Followed by thermal cross-linking and modification with HA to the short fibers, a 3D nanofibrous scaffold was prepared via a freeze-drying method. The scaffold showed good elasticity, promoted chondrocyte adhesion and proliferation, and promoted repair efficacy in the rabbit articular cartilage model. Furthermore, electrospun nanofibers were used as the ink for 3D printing to prepare 3D cartilage scaffolds with controllable nanofiber structures, which were successfully applied to rabbit articular cartilage repair [666,667].

3.2.3.6. Tendon-to-bone interface. The tendon-to-bone interface is a special migratory area from soft tissue to bone transformation,

consisting of tendon, uncalcified fibrocartilage, calcified fibrocartilage, and bone [668,669]. The main surgical procedure for treating tendon or ligament injuries is to suture tendon and ligament to the bone surface or the bone marrow tract [670]. The reconstruction of the normal composite structure of the tendon-to-bone interface will largely affect the recovery of joint kinematics and dynamics. However, after tendon and ligament injury repair, patients often experience scar healing, resulting in poor treatment outcomes [671]. Currently, more and more studies are devoted to exploring therapeutic approaches that can significantly restore the normal tendon-to-bone interface complex structure and promote regeneration [672,673].

Electrospun nanofibers are increasingly being interested as tissue engineering scaffolds to promote tendon-bone healing by manipulating cell adhesion, proliferation, migration, and differentiation, as well as mimicking the native structure [674]. On this basis, modifying electrospun nanofibers with hierarchical structure to mimic the physiological structure of the tendon-to-bone interface is an important way to promote the repair of the tendon-bone interface [10,675,676]. In one study, microfiber yarns of aligned PCL/gelatin and random PCL/gelatin/HAP were fabricated by wet spinning and then constructed into 3D scaffolds to control mineral distribution and cell alignment, mimicking the characteristics of the tendon-bone interface (Fig. 14A–E) [677]. Considering that collagen type II and type X were significant components in the nonmineralized and mineralized fibrocartilage regions of the tendon-to-bone interface, the presence of these collagens was important. As demonstrated in Fig. 14F–G, a high positive of collagen type II and type X was observed in the interface section of the scaffolds.

Scaffold structures with different gradients also allow cells to differentiate along the gradients to repair the damaged tendon-bone interface. In one study, 3D HAP gradient scaffolds with spatial mineral distribution had good mechanical properties and structural anisotropy through the combination of electrospinning technology and traditional textile crafts [678]. These scaffolds could guide rat-derived BMSCs-oriented differentiation and have great potential for tendon-to-bone regeneration. In another study, scaffolds consisting of three functionally distinct regions were generated, including a gradation in mineral content that scales to match the native tissue, uniaxial channels aligned similarly to tendon fascicles, and a highly porous HAP/PLGA inverse opal structure that replicates the characteristics of trabecular bone, respectively [679]. The scaffolds with different gradients enabled cells to differentiate directionally along the mineral gradient, enhancing the formation of the tendon-to-bone interface. The insertion of the gradient composite membrane in the tendon-to-bone interface was beneficial to the healing and regeneration process. PCL/calcium phosphate silicate composite nanofibrous films were constructed with the gradient distribution of calcium phosphate silicate content using the magnetic tape casting technique [680]. In another study, a PU electrospun membrane with a gradient distribution of mineral content was prepared [681]. Along with specific directions, the photothermal effect was adopted to regulate the orientation of the nanofibers from the aligned array to random deposition in the membrane. Zinc and copper-based MOFs were dispersed in PLA solution for the further fabrication of bipolar membrane, which could accelerate tendon and bone regeneration [682].

The effects of gradient on the direction of stem cell proliferation and differentiation can be explored by loading growth factors with density gradients on scaffolds. Platelet-derived growth factor-BB (PDGF-BB) was immobilized on nanofibers in a gradient profile, indicating that the tenogenic proliferation and differentiation of adipose-derived stem cells (ADSCs) were affected by the PDGF-BB gradient rather than the arrangement of nanofibers [683]. Based on this, the tendon differentiation of ADSCs was controlled by the gradient, resulting in the controlled mineralization at the bone-tendon interface.

For tissue engineering, there are still some distances to the goal of restoring a normal tissue structure and function. The electrospun nanofibrous scaffolds promote tissue regeneration, while also acting as a linkage or carrier of bioactive substances for enhancing the functional reconstruction of different tissues. These substances, together with scaffold structures, successfully improve the survival environment of the target tissues. In the future, greater investment is required to fabricate electrospun fiber products on a larger scale. Clinical applications require more in-depth research, as well as the need to come up with designs that contain multiple signals to guide tissue regeneration.

3.2.4. Tumor diagnosis, monitoring, and treatment

For tumor diagnosis, monitoring and treatment, drug delivery systems based on nanomaterials (especially nanoparticles) can passively target the tumor site through enhanced permeability and retention, but their delivery efficiencies are rather low (less than 1 %), resulting in the majority of therapeutic drugs being distributed throughout the body rather than to the tumor site [684,685]. In addition, it is difficult for drugs to reach their targets efficiently since most of them are released before they are administered. Therefore, it is highly desirable to develop new delivery systems to increase the efficiency of drug delivery and reduce systemic toxicity.

Electrospun nanofibers can also be utilized as local drug delivery systems for the treatment of cancer [686,687], which exhibit unique advantages in comparison to other nanomaterials. The core is the ability to achieve locally directed, long-term controlled release of active ingredients or drugs, dramatically increasing the therapeutic efficiency. Electrospun nanofibers offer promising options due to their diverse composition, surface modifiability, ECM-like structure, porosity, and high surface area [688]. A variety of electrospun nanofibers based on various natural polymers (e.g., collagen, albumin, silk proteins, chitosan, cellulose, DNA, and their derivatives) and synthetic polymers (e.g., PEO, PCL, PLA, polydioxanone, and their copolymers) have been reported as localized drug delivery system [568,689]. Bioactive molecules, such as drugs, RNA, and photothermal/photodynamic agents, can be incorporated into the electrospun nanofibers during the electrospinning process or nanofiber modification [256,690–695]. Furthermore, other functions can be integrated into the electrospun nanofibers by surface modification of the inorganic and polymer layers, resulting in composite electrospun nanofibers with fluorescent, magnetic, and targeting capabilities for imaging-guided targeted tumor therapy [696].

A variety of electrospun nanofibers with designable functions have been reported recently, including stimuli-responsive drug delivery, gene delivery, magnetic hyperthermia, photothermal therapy, and photodynamic therapy, which can be applied to various

therapeutic applications [697–701]. For example, the introduction of Er-doped strontium titanate into electrospun nanofibers enabled fluorescence imaging, while the doping of NaGdF₄:Yb/Er@NaGdF₄:Yb enabled dual-modality imaging with fluorescence and MRI [702,703]. For stimulus-responsive drug delivery, the drugs can be triggered and released from electrospun nanofibers in the presence of endogenous stimuli (e.g., pH, temperature, and redox reactions) and exogenous stimuli (e.g., light, ultrasound, electric, and magnetic fields) [704–708]. For example, a pH- or ROS-responsive system can be constructed to respond to the microenvironments enriched with acidic and ROS at tumor sites. In one study, a ROS-sensitive polymer was used to co-encapsulate elesclomol and Cu to form nanoparticles [709]. Elesclomol and Cu were triggered to be released by excess intracellular ROS after entry into cancer cells, which worked in a concerted way to not only kill cancer cells by cuproptosis but also induce immune responses. A 3D nanofibrous scaffold was fabricated by combining the liquid-assisted electrospinning, gas foaming, and metal-polyphenol coordination interactions to achieve efficient trapping and controlled release of circulating tumor cells [710]. Compared with traditional 2D nanofibrous mat, the 3D nanofibrous scaffold could achieve a higher capture efficiency (90.4 % v.s. 78.5 %) toward cancer cells in a shorter time (30 min v.s. 90 min) and exhibited superior capture performance toward heterogeneous cancer cells (HepG2, HCT116, HeLa, and A549) in an epithelial cell adhesion molecule (EpCAM)-independent manner.

Among the many treatments available, immunotherapy is a revolutionary cancer treatment that uses the immune system of the body to recognize, attack, and destroy tumor cells. Traditional cancer treatments, such as radiotherapy and chemotherapy, can kill cancer cells to a certain extent, but they also cause great damage to normal cells. Tumor immunotherapy, on the other hand, enables more precise and effective treatment by activating the immune system so that immune cells can recognize and attack tumor cells. For example, antibody-mediated immunotherapy, which is characterized by high efficiency, high specificity, and low side effects, has good efficacy in cancer treatment by driving immune cells and cytokines to kill tumor cells or interacting with tumor-specific receptors to induce apoptosis [711–713]. However, tumor immunotherapy also faces some challenges. One of them is how to deliver immunotherapeutic drugs accurately to the tumor site to maximize the therapeutic effect while reducing the impact on normal tissues. Antibody therapy, for example, is limited by the short half-life and burst release of antibodies, resulting in low local therapeutic concentrations and causing some systemic toxicity [714,715].

Electrospun nanofiber-based localized drug delivery systems can effectively solve this problem and achieve precise antibody delivery locally to the tumor. For example, agonistic rat anti-human CD40 antibody was grafted onto the surface of electrospun PLLA nanofibers through PDA mediated crosslinking reaction (Fig. 15A) [716]. The scaffold showed multifunctional anti-tumor effects and promoted regeneration of healthy tissues, as well as retaining antibody activity and local release of CD40mAb, making it a potential platform for localized tumor treatment without causing damage to normal tissues. In another study, a transcutaneous tumor vaccine patch was prepared by electrospinning [717]. The nanofiber patch was loaded with tyrosinase-related protein-2 (TRP2) and CpG, serving as antigen and adjuvant, respectively, and showed significant inhibitory effects for melanoma growth. Moreover, the good transdermal delivery, the combination of the patch and aPD-1 achieved a synergistic in tumor immunotherapy, which was associated with the increased targeting of DC cells and the infiltration of CD4 + and CD8 + T cells at the tumor site (Fig. 15B, C). Combining other novel therapies with immunotherapy via electrospun nanofibers allows for synergistic therapies. For example, a composite Janus electrospun fibrous scaffold was loaded with lyophilized inactivated cancer cells, imiquimod (the immune adjuvant), and 5-fluorouracil, for postoperative immuno-chemotherapy of tumors, which could initiate an effective immune response and assist immunotherapy by directly killing cancer cells and remodeling the tumor microenvironment [718].

Overall, the electrospun nanofibers-based local therapy system provides strong support for tumor therapy and is expected to further promote the development of the field of tumor therapy. For future development, more complex therapeutic needs can be met by taking advantage of the unique local delivery, stage delivery, and long-lasting delivery functions of electrospun fibrous scaffolds. For example, bone and nerve-related tumors have the dual needs of tumor removal and tissue repair and regeneration. There are already some studies focusing on these two disease models [719,720]. It is believed that by giving full play to the advantages of electrospun nanofibers, more innovative local therapeutic solutions can be realized in the future, which will truly bring better treatment options for cancer patients in the clinic.

3.3. Electrospun nanofibers for energy storage and conversion

Energy shortage has always been one of the major development issues of greatest concern to mankind. Specifically, energy storage and conversion play an important role in the stability, sustainability, and reliability of the energy system, and are of great significance in promoting the development of clean energy, improving the efficiency of energy utilization and addressing global energy challenges [721,722]. In this section, the application of electrospun nanofibers for energy storage and conversion is discussed.

3.3.1. Energy storage devices

Energy storage devices have been widely applied in specific fields, such as electric vehicles, renewable energy storage, and smart grids, and flexible, foldable, and wearable electronic devices are also of great interest. Energy storage devices mainly consist of supercapacitors and batteries, which often require elastic and lightweight properties with excellent long-term stability and high energy density [23,24]. Supercapacitors and batteries have similar functions, and both include separators, electrolytes, and electrodes.

Supercapacitors, known as electric double-layer capacitors, are effective power sources in energy storage devices because of their long cycle life and fast charge and discharge capacity [723–728]. Especially, asymmetric supercapacitors with high-performance and flexibility have emerged as a competitive candidate for energy storage systems in wearable electronic devices. Supercapacitors utilize charge separation to store energy, and they have faster charge and discharge rates and longer cycle life than conventional batteries. However, the energy density of supercapacitors is low relative to that of conventional batteries, so in applications that require high-

capacity energy storage, there is a need to further increase the energy density of supercapacitors to meet a wider range of needs.

Lithium-oxygen (Li-O₂) and lithium-sulfur batteries developing at a high rate but are still not commercialized, are selected as specific representatives of batteries. Li-O₂ batteries, also known as Li-air batteries, show ultra-high energy density (ca. 3500 Wh/kg), which is much higher than other similar batteries such as LIBs and are expected to be the next generation of batteries [729]. A typical Li-O₂ battery consists of a porous cathode, an organic electrolyte, and a metal Li anode, where the oxygen reduction reaction (ORR) and oxygen evolution reaction (OER) occur to form and decompose Li₂O₂ ($\text{Li}^+ + \text{O}_2 \leftrightarrow \text{Li}_2\text{O}_2$) on the cathode surface. Theoretically, continuous power generation is possible if oxygen is supplied from the air. However, the actual process is very complicated, and the system faces several challenging issues, including electrochemical sluggish reactions and side reactions in the cathode, electrolyte decomposition, and anode corrosion and pulverization [730,731]. Li-S battery is currently considered another one of the most promising battery systems due to its high specific energy capacity of 1675 mAh g⁻¹ and superior energy density of about 2670 Wh kg⁻¹ [732–734]. Cell cathode materials mainly including elemental sulfur can offer several admirable advantages, such as cost-effectiveness, environmental friendliness, abundance, and non-toxicity. All of these merits make high-performance Li-S batteries have been highly attractive [735–738]. However, the practical application of Li-S batteries still faces some challenges, mainly including the inherently low electron conductivities of elemental sulfur of cell cathode and its discharge products (Li₂S or Li₂S₂), huge volume expansion of cell electrode, serious “shuttle effect” of lithium polysulfide (Li_xS_y) and notorious growth of lithium dendrites during charge–discharge processes.

Electrospun nanofibers have attracted much attention in the development of energy storage devices because of their versatile material sources (organic/inorganic), controllable secondary and tertiary structures, high specific surface area, large surface-to-volume ratios, short diffusion distances, lightweight and flexible properties [739,740]. For example, in Li-O₂ batteries, the interconnected electrospun nanofibrous membrane with high porosity and specific surface area plays a crucial role in the mass transport of oxygen, providing more active sites for product storage and enhancing electron and charge transfer [741]. Additionally, the interpenetrating networks ensure high strength and mechanical flexibility, facilitating the utilization of flexible substrates, self-supported electrodes, and efficient electrical current. In the following, the application of electrospun nanofibers for separators and electrolytes will be firstly discussed. Due to the complexity of the electrode structure and its versatile functions, the applications of electrospun nanofibers as electrodes in supercapacitors and batteries will be discussed separately. In both supercapacitors and batteries, a separator is a thin film or layer of material located between the positive and negative electrodes to serve as a physical barrier for preventing them from coming into direct contact and short-circuiting, avoiding hazardous situations such as overheating, fire, or explosion of the memory. At the same time, ions (e.g., lithium ions, nickel ions, etc.) are allowed to pass through.

Separator for batteries. In the case of batteries, separator preparation technology has advanced over the decades, and conventional separators made of porous polymer membranes or glass fiber membranes are gradually failing to meet their high-performance requirements [742]. To produce separators in batteries, such as sodium-ion batteries (SIBs) and lithium-ion batteries (LIBs), electrospinning has become the mainstream approach [743]. Electrospun nanofibers possess a large specific surface area, which increases the contact area between the active materials and the electrolyte, shortening the diffusion path of ions during the electrochemical reaction and enhancing transmission efficiency [744]. Electrospun nanofibrous membrane has a tunable pore size and distribution, facilitating the penetration of active substances into the separator. Additionally, the electrospun nanofibers can disperse a large number of Li⁺ insertion sites in an ordered manner, reducing the charge transfer resistance at the interface between the electrolyte and active materials [56].

Nowadays, electrospun nanofiber membranes based on a large number of polymers, such as PAN, PVA, Polyvinylidene fluoride (PVDF), PI, poly(isophthaloyl metaphenylene diamine (PMIA), PAA, PMMA, and their modified materials also have been developed to form separator materials for enhancing the electrochemical performances of Li-S batteries [745–752]. For example, the octa(aminophenyl) silsesquioxane modified poly-m-phenylene isophthalamide separators have been developed and applied for high-performance Li-S batteries based on their merits such as strong physical confinement, chemical adsorption, and high mechanical properties with relatively uniform pore size distribution of the electrospun nanofiber membrane itself [753]. Moreover, enhancing the performance of nanofibers can be achieved by regulating the interfacial interactions between polar functional groups (e.g., C≡N, C=O, NH, C-F) and the electrolyte in LIBs and SIBs separators. For example, by changing some acetyl groups to hydroxyl groups in cellulose acetate nanofibers, the chemical stability and wettability of separator could be improved [754]. In another study, PAN nanofibrous membrane was modified by hydrolyzing the nitrile groups and then growing silica aerogel *in-situ*, enhancing the chemical and thermal stability [755]. As known, functional nanocomposites containing inorganic nanoparticles like silicon dioxide (SiO₂), titanium dioxide (TiO₂), zirconium oxide (ZrO₂), zinc oxide (ZnO), and calcium carbonate (CaCO₃) also have been prepared and applied to cell separators for further enhancing the electrochemical performances of cell to a certain extent [756–758]. Electrospun CNF-coated separators are also widely utilized to effectively enhance cell performances of high-performance Li-S batteries, which can effectively suppress the “shuttle effect” of Li_xS_y, accommodate the significant volume change of electrodes and suppress the growth of lithium dendrites during cell cycle.

By regulating the polymer components and fiber structure, functional separators can be achieved. For instance, phase-change temperature-regulating fibers adopt a phase-change material paraffin wax with a melting point of about 45 °C as the core to sense thermal changes, while a high decomposition temperature polymer serves as the shell to maintain the polymer skeleton [759]. In case of the battery fails, the separator can effectively suppress the temperature rise through the melting of phase change materials and ensure battery safety. Looking toward the future, it is important to monitor the physical and chemical changes during battery operation. Therefore, intelligently designed nanofibers-based sensing separators and computing devices should be developed to detect battery operating status in suitable environments [760].

Electrolytes. Electrolytes play a key role in both supercapacitors and batteries, where they are responsible for transporting ions

between the electrodes for charge storage and release. Conventional electrolytes are conductive solutions. Polymer electrolytes, such as all-solid-state polymer electrolytes, gel polymer electrolytes, porous polymer electrolytes, and composite polymer electrolytes, replace the conductive solution with a conductive solid, exhibiting superior properties. These advantages include enhanced thermal and chemical stability, higher energy density, faster charging speeds, longer cycle life, and a broader operating temperature range. These properties make them highly beneficial for various applications, especially in advanced energy storage systems [761,762].

To produce advanced solid-state batteries, the fabrication of solid-state electrolytes is of great importance. Electrospinning is widely employed to fabricate solid-state electrolytes because of its advantages in preparing nanofibers with good mechanical performance [763]. The conductivity and stability of solid electrolytes based on electrospun nanofibers are progressively improving by regulating the structure and composition. In one typical study, $\text{Li}_{0.33}\text{La}_{0.55}\text{TiO}_3$ (LLTO) nanowires were prepared by electrospinning and then dispersed into PAN/ LiClO_4 polymer electrolyte to obtain a novel composite solid-state electrolyte [764]. The nanowire filler showed a higher aspect ratio than the traditional LLTO nanoparticles to form a continuous ion transport path over a longer distance, reducing the number of connections along the ion path between the LLTO particles (Fig. 16A). The PAN/ LiClO_4 electrolyte incorporated with 15 wt% LLTO nanowires exhibited an ionic conductivity of 2.4×10^{-4} S/cm at room temperature, which was three orders of magnitude higher than that of LLTO nanoparticles with the same content (Fig. 16B). Furthermore, replacing randomly oriented nanowires in the polymer electrolyte with nanowires aligned along the average direction of the electrolyte resulted in the shortest ionic conduction paths and the smallest particle junctions, which further improved the ionic conductivity from 5.40×10^{-6} S/cm to 6.05×10^{-5} S/cm (Fig. 16C) [765]. In one study, garnet-type porous $\text{Li}_{6.4}\text{La}_3\text{Zr}_2\text{Al}_{0.2}\text{O}_{12}$ (LLZO) nanowires were prepared by electrospinning followed by high-temperature calcination and then directly soaked into a PEO/bis(trifluoromethane)sulfonimide lithium salt (LiTFSI) solution [766]. The obtained electrolyte film showed outstanding mechanical performance with a high ionic conductivity of 2.5×10^{-4} S/cm at room temperature (Fig. 16D, E). The electrochemical and thermal instability of PEO-based electrolytes needs to be further improved.

A series of solid-state electrolytes have been fabricated through a simultaneous electrospinning and electrospray method, which allows for the incorporation of up to > 70 wt% of inorganic materials into the resulting flexible composite film [767]. The composite films with PAN as the polymer phase and cubic garnet-type oxide $\text{Li}_{6.75}\text{La}_3\text{Zr}_{1.75}\text{Ta}_{0.25}\text{O}_{12}$ as the inorganic fillers exhibited a high ionic conductivity of 1.18 mS/cm and areal conductance of 472 mS/cm² at room temperature [768]. The high conductivity originated from a large amount of continuous and fast ions conducting interfaces throughout the bulk of the film, called the film bulk interface superionic conductor, which may also yield Na^+ and Mg^{2+} conductors [768]. Bulk interface superionic conductors can also create entirely new ionic conductors using inexpensive materials and scalable processes. All these results demonstrate the overwhelming advantage of electrospinning technology in preparing high-performance solid-state electrolytes.

Electrodes for supercapacitors. It is a critical challenge to design and fabricate electrodes with high capacity, cycling stability, and high flexibility simultaneously. Electrospun nanofibers have been developed as a new type of electrodes to provide large surface area, efficient charge transfer, and a stable structure to substantially improve the performance of supercapacitors [768,769]. Electrospun nanofibers composed of carbon materials are often applied to improve the stability of structured electrodes during cycling. The strategies to optimize electrode performance mainly include the graphitization regulation of carbon-based components, the design of surface and internal hole structure, and the hybridization of high-volume substances. For example, generating hierarchically porous structures, such as core/shell and hollow tubular structures, in the carbon-based electrospun nanofibers is one standard optimization approach to improve the electrode surface area and electrolyte immiscibility (Fig. 17A, B) [770]. In addition, the conductivity of the electrodes can be enhanced by hybridization with conductive additives, such as different elements (e.g., N, P, S, etc.), active materials (e.g., metals, metal oxides, and metal sulfides), and conductive polymers. Many pseudocapacitive transition metal oxides, including MnO_2 , RuO_2 , and NiO , have been used as cathode materials to improve the capacities of asymmetric supercapacitors [771–773]. In particular, Co_3O_4 has been widely used as a cathode material because of its high theoretical capacity of up to 3560F g⁻¹, highly reversible redox reactions, and environmental friendliness [774,775]. Transition metal sulfides, including binary and ternary sulfides (e.g., nickel sulfide, FeCo_2S_4), exhibit smaller band gaps and more oxidation states and thus richer oxidation reactions and higher conductivity than the corresponding metal oxides. Therefore, transition metal sulfides are suitable for hybridization with CNF to improve the electrical conductivity and are applied as electrode materials in supercapacitors [776–778].

Anodes of asymmetric supercapacitors are mainly composed of graphitized carbon materials or hybrids. For example, Fe_2O_3 has been extensively studied as anode owing to its excellent capacitive performance at negative potentials, environmental friendliness, natural abundance, and low cost [780,781]. Practically, the actual capacity of pure Fe_2O_3 is much lower because of the low electrical conductivity and ionic diffusion rate of doping metal oxide. Therefore, synthesizing nanostructures with carbon or conductive polymers is an effective strategy to enhance the electrochemical performance of Fe_2O_3 [782–784].

The mechanical brittleness of electrospun CNF is a critical factor limiting their development as electrode materials for supercapacitors. Biomimetic structural design is an ingenious strategy to improve the structural stability of CNF under different mechanical deformations [357,785,786]. Reed-like electrospun CNF with hierarchical macropores were carbonized and etched to obtain products with mechanical flexibility and foldability, which could maintain high electronic conductivity and chemical stability despite bending and twisting (Fig. 17C–E) [357].

Notably, electrospun CNF-based 3D aerogels have promoted the development of all-solid-state wearable supercapacitors. The 3D network with many pores and compressible elasticity significantly promotes the penetration and diffusion of ions [787–789]. In one study, a hierarchical aerogel composed of graphene/carbon nanofibers was fabricated by surface-induced co-assembly, which exhibited high elasticity, great structural robustness, and a high specific capacitance of 180F g⁻¹ at 1 A g⁻¹ [790]. In another study, an elastic aerogel was fabricated by welding adjacent CNF with PVP as solder, followed by freeze-drying and carbonization [786]. The aerogel exhibited remarkable electrical conductivity, excellent reversible compressibility, and a high specific capacitance of 300F g⁻¹

at 0.3 A g^{-1} . Furthermore, CNTs and Co_3O_4 nanoparticles were uniformly grown on the CNF surface of the aerogels, showing a high specific capacitance of 2376 F g^{-1} at 1 A g^{-1} .

Although the above strategies have brought great progress in the development of electrode materials in supercapacitors, it is still a challenge in practical applications to acquire excellent performance while using simple methods [791]. Some issues are awaiting more facial, efficient, and easy industrialized solutions. The first is the optimization of microstructures and properties of electrospun CNF to be applied as the electrodes. The microstructures of electrospun CNF have great importance for electrochemical performance. The pore size should match the ion size of the supercapacitors. Generally, amorphous carbon allows all ions to access, but relatively low electrical conductivity is one of the constraints. Graphitic carbons can improve the electric conductivity but reduce the ion access. Heteroatoms doping, such as N, S, and P, etc., and the d-spacing of graphene layers in electrospun CNF are promising methods for better capacity performance. The combined process of oxidation and partial reduction is the main method to expand the interlayer spacing of graphitic carbon. Then comes the issue of long-term durability of electrospun CNF-based electrodes. In practical applications, durability is an important indicator of energy storage systems. However, the stable cycling of active materials in electrospun CNF is a key challenge, and it is difficult to achieve the desired stability and lifetime. It is a promising method to load active materials with hollow carbon nanospheres or nanofibers, or to optimize the size of hollow structures to adapt to volume change of active materials to improve the long-term durability of electrode materials. In addition, the prepared electrospun CNF should have the characteristics of high conductivity, large specific surface area, and porous structure. The non-polar surface of freestanding CNF is not conducive to attracting electrolyte immersion. One solution is to functionalize the surface of CNF, such as hydrophilic treatment using functional groups (e.g., $-\text{COOH}$ and $-\text{OH}$), metal oxides, metal sulfides, and metal hydroxides. Industrial production of electrospun electrode material is the ultimate problem to be faced. The large-scale nanofiber production has been largely overcome, and further efforts should be made to explore more facile preparation processes of composite electrode materials. Such as post-treatments by the hydrothermal method and chemical vapor deposition technique have been already used to form secondary structures on electrospun nanofibers, but the stability of the membrane during the preparation process is difficult for large-scale production.

Electrodes for Li-O₂ battery. Various electrocatalysts and membranes based on electrospun nanofibers, including metal oxides, carbon composites, and polymers, have been developed as electrodes for cathode improvement and anode protection to improve the stability and efficiency of Li-O₂ batteries [771,792,793].

Catalyst cathodes based on metal nanofibers. Typically, for cathode improvement, one efficient strategy is to develop bifunctional catalysts for alleviating the sluggish kinetics during the ORR and OER in the cathode. The catalyst in the cathode should possess equipped porous structure, good catalytic behavior and stability, and excellent electron conductivity. Metal oxides are vital in enhancing electrocatalytic activity due to their surface oxygen valence, ionic conductivity, and various oxidation states [794]. For example, $\text{La}_{0.75}\text{Sr}_{0.25}\text{MnO}_3$ nanofibers were employed in Li-O₂ batteries because of their unique porous structure and surface oxygen valence, which could maximize the contact of catalytic sites and promote the transfer of electrons and reactants [795]. The assembled Li-O₂ battery exhibited enhanced durability and reduced voltage gap. Moreover, hollow and hierarchical porous architectures can be regulated by adjusting the concentration of precursors for electrospinning [796]. However, bulk metal oxide usually suffers from poor electrical conductivity. To address this issue, various carbon-based catalysts have been explored, such as metal nitride functionalized CNF, metal oxide combined with nitrogen-doped carbon nanofibers, and precious metals [797,798]. These carbon-based materials serve as both current collectors and catalysts due to their good strength, superior conductivity, and interpenetrating pores. For example, brush-like Co_4N nanorods were incorporated into CNF and then acted as a current collector catalyst for the air-cathode [741]. This nitrogen-doped metal composite with high electrical conductivity helped reduce band gap or overlap the valence bands, facilitating the formation of the film-type Li_2O_2 and achieving a good long-term cyclability battery for over 177 cycles (Fig. 17F-H). However, carbon is susceptible to oxidation by intermediates (O^{2-}) and final products Li_2O_2 , leading to the production of irreversible side products like Li_2CO_3 [779,799,800]. To this end, carbon-free and binder-free electrodes have also been explored. All-metal and metal oxide deposited on polymer nanofibers, such as IrO_x deposited on PI nanofiber and Ag nanowires combined with chitin, have been developed as cathodes, exhibiting chemical stability without parasitic side reactions and providing a novel strategy for flexible metal-air batteries [801,802]. Despite the promising potential of carbon-free electrodes, the volume change resulting from the formation and decomposition of Li_2O_2 may lead to performance degradation. Thus, the design of the cathode structure plays a crucial role in the performance of Li-O₂ batteries. More work is needed to develop high catalytic activity, carbon surface protection, and mechanically stable carbon-free cathodes to further enhance the stability of the batteries.

Lithium metal-hosted anodes based on nanofibers. To achieve the potential high energy density of Li-O₂ batteries, a Li metal anode is necessary. However, Li anodes encounter corrosion, pulverization, and cracking due to side reactions with H_2O , CO_2 , O_2 , and the intermediates during cycling. Many strategies based on electrospun nanofibers have been explored to suppress these parasitic reactions, including the use of a protection nanofibrous membrane, modification of separator, and 3D architecture hosts [799,803–805]. For example, a polymer fiber with functional groups was designed to regulate the deposition of Li^+ homogeneously on the current collector, achieving dendrite-free Li plating [803]. The engineering of nucleation seeds offers a new approach to regulate Li deposition into 3D substrates, thereby restricting the growth of Li dendrites. Similarly, CNF embedded with ultrafine silver nanoparticles (Ag NPs) demonstrated the ability to have a practical solubility in Li, facilitating Li deposition on Ag NPs with zero overpotential [806]. Additionally, the use of considerably ordered angstrom-level pores in MOF on PI nanofibers showed promising results in controlling the migration of large-sized anions, leading to selective Li-ion transport and homogeneous Li electrodeposition [807].

Electrodes for Lithium-sulfur (Li-S) battery. Electrospun nanofibers have been prepared and employed for high-performance Li-S cells, owing to their enviable advantages such as large specific surface area, high porosity, and controllable pore size, which effectively suppress the “shuttle effect” of Li_xS_y , greatly facilitate the transmission of lithium ions, and significantly improve the wettability for liquid electrolytes if suitable precursor nanofiber materials or nanofiber membranes are selected [808]. The application of electrospun

nanofibers in Li-S batteries can mainly be categorized into three aspects: cell cathode host, separators, and interlayers. The various applications of Li-S cell separators have been introduced and discussed above.

Cathodes host. To solve the above problems, the main strategy is to design and prepare cathode materials with good conductivity, high pore volume, and strong adsorption to dissolved Li_xS_y for high-performance Li-S cells. The commonly used cathode host materials are mainly composed of various carbon materials, some elements or compounds of doped-carbon materials, inorganic materials, and polymer materials with some special structures. As everyone knows, carbon materials have great advantages as the main component of high-performance Li-S battery cathode materials [809]. Especially, CNF has some merits such as high specific surface area, ensuring high sulfur load for the cathode of Li-S battery even under good electronic conductivity [810]. Moreover, the small diameter of CNF is also conducive to fast ions and electrons transport, thus providing a convenient 1D channel for the axial transport of ions and electrons. Finally, the conductivity and activities of assembled Li-S cells can be greatly improved [811]. In addition, there are many lattice defects to effectively modify the surface of CNF, which can provide more reaction sites between Li_xS_y and Li ions. Some carbon fibers can be designed with a multi-level pore structure, which also can store more active substances, facilitate liquid electrolyte infiltration, and weaken the diffusion of Li_xS_y [812]. At present, the common raw materials for preparing CNF through electrospinning and subsequent carbonization processes mainly include PVA, PVP, PAN, PMMA, PLA, and other polymers with different decomposition temperatures [813–818]. However, pure carbon fibers are mostly non-polar materials, which makes it difficult to inhibit polar Li_xS_y effectively. To this end, a large number of CNF can be modified with heteroatoms, such as metal elements (Fe, Co, Ni, Cu, etc.) [819–822], or fabricated to various compounds by doping with carbon spheres, CNTs, graphene, rGO, metal oxide, metal nitride, metal sulfide, metal carbide and other functional materials [805,823–829]. The physical adsorption of high-performance Li-S cells can be achieved by physical confinement, and the chemical adsorption of Li_xS_y by forming strong chemical bonds with dissolved Li_xS_y . In addition, some electrospun nanofibers based on polymers have been prepared and applied as cathodes of Li-S batteries, such as CoSe_2 -C Nanofibers [830], Carbon-based nanofibers [831], microporous carbon polyhedrons-PAN nanofibers [832], S-PAN/ketjen black nanofibers [833], composite fiber based on PAN with conductive backbone of CNTs [834]. When these materials act as cathodes for Li-S cells, the electrochemical performances of assembled batteries can be significantly enhanced.

Interlayers. To further enhance Li-S battery performance by effectively suppressing the “shuttle effect” and greatly reducing lithium dendrite growth, a functional interlayer based on electrospun nanofibers with good conductivity and high surface area including some special structural design can be introduced between cell cathodes/anodes and separators [835]. Meanwhile, a large number of freestanding electrospun carbon nanofiber fabrics, boasting tunable porous structures and outstanding electrical conductivity, also have become the prevailing choice for interlayers in high-performance Li-S batteries [836,837]. These fabrics are primarily derived from raw materials such as PAN, cellulose diacetate, PAA, and oxidized poly(acrylonitrile-co-vinylpyrrolidone) (PANVP) and so on [838–840]. Furthermore, some modifications with elements or compounds, mainly including N, B, TiO_2 , manganese oxide (MnO), ZrO_2 , ZnO , vanadium pentoxide (V_2O_5), titanium suboxide (Ti_4O_7), molybdenum dioxide (MoO_2), cementite (Fe_3C) and so on, have been introduced to the electrospun CNF membranes to further enhance their utilities in Li-S battery interlayers [808,841–846]. Some functional interlayers based on various polymers and composite with polymers, such as Nafion polymer layer or PAN-nitrogen-doped carbon black interlayer, have also been employed in interlayers of assembled Li-S batteries, which can be served to adjust structural changes, facilitate Li-ion transportation, and exhibit exceptional absorption properties for Li_xS_y during cell discharge-charge processes [847]. For anodic interlayers, the Li dendrites also can be inhibited by modifying the CNF with silver nanoparticles (AgNPs) [806], electrospun modified PAA nanofibers [848], lotus leaf electrospun CNF [849], and 3D porous carbon fibers loaded with Ag NPs [850]. These anodic interlayers also can contribute significantly to the overall safety and performance improvement of Li-S batteries.

3.3.2. Energy conversion

The growing demand for energy and the need for renewable energy sources and efficient energy conversion have driven the rapid development of nanotechnology. In the field of energy conversion, nanogenerators have attracted widespread attention as a novel technology [851]. Nanogenerators utilize mechanical vibration or pressure in the environment to convert into electrical energy, providing a sustainable energy solution for self-powered and wearable devices. In the research of nanogenerators, harvesting energy from mechanical vibration and pressure by using nanomaterials has become an important research direction [852].

From 2006 to 2010, the electrical output of piezoelectric nanogenerators had already reached the volt and nano-ampere level, and further enhancements using ZnO nanowire arrays were challenging at that time [426,853,854]. Researchers then explored alternative approaches to improve nanogenerator output by i) designing new devices based on different ZnO morphologies, which later led to the successful development of ZnO textured thin films [855], and ii) focusing on developing new materials with higher piezoelectric coefficient. Ferroelectric materials such as lead zirconate titanate (PZT), barium titanate (BTO), lead magnesium niobate-lead titanate (PMN-PT), and potassium sodium niobate (KNN) showed promise with piezoelectric coefficients reaching hundreds of pC/N compared to the 17 pC/N for ZnO. However, minimal research progress was made in this direction before 2010 due to the difficulty in synthesizing ferroelectric nanowire arrays [856]. In addition, nanowires synthesized by hydrothermal and vapor deposition approaches faced limitations in wire length and precise control over stoichiometric ratio, respectively.

Electrospun nanofibers offer unique advantages in piezoelectric nanogenerators compared to nanowires, nanorods, and nanofibers produced through other synthesis methods such as hydrothermal, chemical vapor deposition, and physical vapor deposition. First, the ultra-high length-to-width ratio of electrospun nanofibers provides a superior surface area for energy conversion, thereby increasing the opportunity for energy capture. Second, electrospun nanofibers endow the material with unique flexibility, which enables the nanogenerator to better adapt to ambient vibration and pressure changes and thus convert mechanical energy into electrical energy more efficiently. Meanwhile, the preparation process of electrospun nanofibers can easily enable the construction of multi-element materials, further enhancing the flexibility and diversity of energy conversion. This provides the possibility of energy conversion

by different mechanisms, thus broadening the application fields of nanogenerators [857]. In addition, the diameter of electrospun nanofibers can be precisely controlled, which is very important in the preparation of nanogenerators. A precisely controlled diameter optimizes the energy conversion efficiency and ensures consistent performance. Finally, the external electrode polarization during the preparation of electrospun nanofibers provides an additional means of control for the preparation of piezoelectric nanofibers, further enhancing the piezoelectric effect of the material [858].

As a typical example, a PVDF nanofiber-based nanogenerator was developed by NFES, where the long ferroelectric β -PVDF was obtained by in-situ mechanical stretching and electrical poling (Fig. 18A) [859]. This nanogenerator demonstrated moderate output due to the relatively low piezoelectric coefficient of the nanofibers. Afterward, a nanogenerator with an output of 1.6 V was fabricated by PZT nanofibers on a rigid substrate (Fig. 18B), which laid the groundwork for the subsequent development of nanogenerator based on ferroelectric ceramic nanofiber [423]. However, issues persisted with rigid substrates and fragmentary nanofibers during high-temperature sintering. Furthermore, based on PZT nanofibers, an “aligned electrospun fiber peeling off-free sintering” technique was developed, and the resultant nanogenerator achieved a 6 V voltage output (Fig. 18C) [428]. This approach also solved the fragmentation problems by using fragile PZT ceramic nanofibers to fabricate flexible wearable nanogenerators, which have been widely used since then [429,431,860,861]. In 2013, BTO nanofibers with different arrangement structures were fabricated, and it was demonstrated that the alignment state of the nanofibers between the two electrodes had a significant effect on the output of the nanogenerator (Fig. 18D) [424]. Vertically aligned $\text{Pb}(\text{Zr}_{0.52}\text{Ti}_{0.48})\text{O}_3$ nanofiber arrays, with millimeter-level nanofiber lengths and a large number of nanofibers in parallel between electrodes, generated much higher output for both voltage and current output, reaching a value of 209 V and 53 μA , respectively (Fig. 18E) [429]. Another lamination integration method (Fig. 18F) has been developed, achieving 320 μA with 12 layers of integration [425]. Besides the large integration, the electrospinning technology is suitable for the preparation of multi-element lead-free piezoelectric nanofibers, such as $0.5\text{Ba}(\text{Zr}_{0.2}\text{Ti}_{0.8})\text{O}_3$ – $0.5(\text{Ba}_{0.7}\text{Ca}_{0.3})\text{TiO}_3$ (BZT-BCT) [431], Mn-doped $(\text{Na}_{0.5}\text{K}_{0.5})\text{NbO}_3$ (NKN) [862], $(\text{Na}_{0.5}\text{Bi}_{0.5})\text{TiO}_3$ – BaTiO_3 (BNT-BTO) [863], $\text{Bi}_{5-x}\text{La}_x\text{Ti}_3\text{FeO}_{15}$ (BLTF) [864], etc. Furthermore, it is also suitable to produce piezoelectric polymer-ceramic nanoparticle composite nanofibers [865,866], as shown in Fig. 18G, leading to an output of 6 V and 1.5 μA . In summary, nanogenerators based on electrospun nanofibers show great promise due to their low cost, high output, and flexibility. However, it is crucial to carefully distinguish between piezoelectricity, triboelectricity, and flexoelectricity source of output, especially when using soft polymer materials for piezoelectric and package components.

As another effective energy conversion technology, TENGs based on friction electrification effect and electrostatic induction effect can convert many environmental energies (such as biomechanical energy, wind energy, blue energy, etc.) into electrical energy, and they also have self-powered sensing functions in some specific applications [867–871]. To enhance the energy harvest/conversion efficiencies of TENGs, increasing the contact area or surface roughness of the triboelectric layer of TENGs is considered one of the most ideal optimized schemes [871,872]. The micro/nanostructured electrospun nanofibrous membrane/mat has the features of high specific surface area, high surface roughness, good flexibility and gas permeability, etc., which can endow triboelectric materials with higher surface charge density. For instance, single-spun Nylon nanofibrous membrane and single-spun PVDF nanofibrous membrane were used as the triboelectric positive layer and negative layer of TENG, respectively (Fig. 19A) [873]. The working principle of corresponding TENG is shown in Fig. 19B. In the same case, the output performance of the TENG ($I_{sc} = 81 \mu\text{A}$) was increased by about 3 times compared with the smooth flat film (Fig. 19C). While modifying the surface morphology of the material, the blending electrospun process can further adjust the triboelectric polarity of the material itself through multi-element compounding [874–876]. MXene is a 2D nanomaterial characterized by high tribonegativity and conductivity. PVA/MXene composite nanofibrous membrane was obtained by incorporating MXene into the PVA by blending electrospinning, which was used as the tribonegative layer and paired with the tribopositive electrospun silk nanofibrous membrane to assemble TENG (Fig. 19D) [877]. Through the improvement of dual strategies, this all-electrospun-based TENG exhibited excellent stability, durability and power generation performance, and its maximum power density reached 1087.6 mW/m^2 (Fig. 19E). Coaxial electrospinning is a unique form of blending electrospun process, which can produce triboelectric fibrous materials with core-sheath structures [878–880]. Through in-situ curing in the coaxial electrospinning process, PDMS compounded with barium titanate (BT) nanoparticles served as the core of the coaxial nanofiber, and PVDF served as the corresponding shell layer to replace the traditional composite membrane (Fig. 19F) [880]. Benefiting from the core material with high dielectric constant, PDMS/BT@PVDF nanofibrous membrane exhibited higher tribonegativity. It was paired with the electrospun PHBV nanofibrous membrane to construct TENG. The output voltage, current, and maximum power density of the assembled TENG could reach 1020 V, 29 μA , and 2.2 W/m^2 , respectively. The various components of TENG (including triboelectric layers, electrodes, and substrates) can also be constructed simultaneously through an integrated electrospinning-electrospraying process [881–883]. These components combined with electrospinning process often own better stretchability, which will improve the deformability of TENGs greatly. For instance, a self-interlocked stretchable nanofibrous membrane was designed by simultaneous electrospinning of PVDF-HFP and electrospaying of SEBS (Fig. 19G) [881]. The electrospayed Styrene-Ethylene-Butylene-Styrene (SEBS) microspheres served as the elastic binders and hydrophobic modifiers to enhance the stretchability (ultimate strain of $\sim 490\%$) and waterproofness of electrospun PVDF-HFP fibers networks. This nanofibrous membrane was used as the triboelectric layer of TENG in single-electrode mode, which could produce a maximum output power density of 219.66 mW/m^2 when contacting the skin. It is worth noting that the electricity generated by TENGs can also be used to drive electrospinning equipment [884–886]. These studies enhance the relationship between the electrospinning process and nanogenerator devices, thereby advancing the development of electrospinning techniques in the field of flexible electronics.

Nanogenerators based on electrospun nanofibers show great promise due to their low cost, high output, and flexibility. However, it is crucial to carefully distinguish between piezoelectricity, triboelectricity, and flexoelectricity source of output, especially when using soft polymer materials for piezoelectric and package components. Although significant progress has been made in utilizing electrospun nanofibers for energy conversion and storage devices, there are still challenges for further development. First, there is no uniform

standard for the performance evaluation of nanofibers, so it is necessary to clarify the relationship between the chemical structure, physical parameters, and properties of electrospun nanofiber materials through systematic experiments. Second, the cumbersome preparation process and cost limit its large-scale production and application [887]. These are urgent future issues for energy conversion and storage devices based on electrospun nanofibers.

3.4. Electrospun nanofibers for catalysis

Electrospun nanofibers composed of polymers, carbon or ceramics with high specific surface area, rich spatial structure, and high stability are naturally good supports for a variety of catalytic systems. For example, metal nanoparticles, enzyme-like and even microorganisms, have shown unique potential for thermal, photocatalytic, electrocatalytic, enzyme-like and microbial catalysis [888,889]. In this section, we will discuss the great importance and advantages of electrospun nanofibers for catalysis by presenting some recent applications.

3.4.1. Thermal catalysis

In thermal catalysis, metal nanoparticles with catalytic activity have been extensively used for a large number of reactions. However, the instability of nanoparticles in aqueous solution makes them very susceptible to aggregation and oxidation under heated conditions. To address these challenges, metal nanoparticles are immobilized or synthesized *in-situ* on various supports, such as nanofibers [890], dendrimers [891], zeolites [892], metal oxide [893], microspheres, and mesoporous silica [894,895]. Among these supports, electrospun nanofibers have garnered increasing attention owing to their adjustable morphology, high porosity, specific surface area, abundant functional groups, and excellent mechanical stability. The researchers have achieved breakthroughs in thermal catalysis by introducing polymers or CNF and adjusting the composition and spatial structure.

Active metals can be effectively dispersed on electrospun polymer nanofibers through the strong metal-nanofiber interaction, significantly enhancing the catalytic activity and cyclic stability in the thermocatalytic reaction. For example, Pt@MIL-101(Cr) (MIL stands for Material Institute Lavoisier) was highly dispersed in electrospun PCL nanofibers to obtain a “catalytic carpet”, which was extremely efficient in the hydrogenation of cyclohexene, while retaining the nanofiber structure for full recycling with zero weight loss [896]. Catalytically active Pd nanoparticles were immobilized on electrospun PEI/PVA nanofibers, indicating outstanding catalytic activity and reusability in reducing Cr(VI) to Cr(III) [897]. This approach of preparing metal nanoparticles immobilized polymer nanofibers with high surface area-to-volume ratio enhanced mechanical durability, and uniform nanoparticle distribution can be extended to prepare different fiber systems for sensing, environmental science, and biomedical science in addition to catalysis. MOFs can be combined with electrospinning to ensure their excellent stability of the massively exposed catalytic sites. For instance, lanthanide-based MOF nanofibers were prepared using MOF BIT-58 (BIT stands for Beijing Institute of Technology) in the Knoevenagel condensation reaction, showing high catalytic efficiency [754].

Electrospun CNF prepared by carbonization and other methods can also support metal nanoparticles with catalytic activity. For example, ruthenium nanoparticles supported on electrospun CNF demonstrated excellent catalytic activity and stability in the hydrolytic dehydrogenation of methylamine borane [898]. Porous and hollow nanofibers can be applied as the support of metal nanoparticles to endow the hybrid system with novel properties. The metal nanoparticles are encapsulated within the porous structure of the nanofiber framework due to the confinement effect, preserving all exposed catalytic sites accessible to the reactants. Simultaneously, the embedded catalysts are protected from harsh external environments with low mass transfer resistance, thereby improving catalytic performance. For example, porous CNF was prepared through electrospinning and high-temperature pyrolysis technology using PMMA as pore-forming agents, Ni salts and PAN as precursors [899]. The porous structure exposed more Ni active sites on the CNF, resulting in higher catalytic activity in the Heck reactions. Electrospun core-sheath nanofibers, with PMMA/manganese acetate as the core and PAN as the shell, were carbonized and CO₂-activated to produce Mn₃O₄ nanoparticles embedded in hollow-activated CNF (Fig. 20A) [900]. The hollow nanofibers exhibited a remarkable ability to adsorb toluene, with a longer breakthrough time of toluene adsorption than conventional activated CNF (Fig. 20B). The hollow nanofibers showed a catalytic oxidation of toluene to CO₂ with a conversion of 99 % ± 0.5 % at 280 °C, and no catalytic activity degradation after four hours of testing at alternating temperatures (260 and 280 °C).

Electrospun nanofibers can be applied as templates to produce porous hollow structures composed of metal nanoparticle-metal oxide nanotube composite catalysts. The structure can enhance the interfacial contact between metal nanoparticles and metal oxide carriers, promote interfacial electron transfer, and accelerate the catalytic reaction process. For example, PdO_x/NiO nanofibers catalyst consisting of porous NiO nanofibers and *in-situ* anchored PdO_x species were prepared by electrospinning-pyrolysis strategy [905]. The porous NiO nanofibers serving as catalyst support could provide a larger specific surface area and more accessible active sites for further improving the catalytic performance. Core-sheath Pd/CeO₂ nanotube was prepared by electrospinning and high-temperature calcination, which fully improved the interface contact between doped Pd and CeO₂ and strengthened the interaction between Pd and CeO₂ [906]. Then, Ni dopants were introduced into the nanotubes, which facilitated the exposure of more Pd active sites and thus promoted sufficient contact between the reactants and the active center, leading to higher catalytic activity in the Suzuki reaction.

3.4.2. Photocatalysis

Electrospun nanofibers are widely used in photocatalytic reactions due to their strong electronic transmission, high mechanical strength, flexibility, and easy recycling [907,908]. Nanofibers made of semiconductor oxide materials are used for photodegrading organic molecules into nontoxic products (e.g., CO₂ and H₂O) or photocatalytic reducing toxic heavy metal ions to nontoxic products in

water [909,910]. For instance, TiO_2/GO composite nanofibers exhibited higher charge carrier mobility and stronger photocatalytic activity under visible light irradiation compared with bare TiO_2 nanofibers [911]. A highly hydrophilic chitosan/PAN@ $\text{FeOOH}/\text{g-C}_3\text{N}_4$ nanofibrous membrane showed remarkable mechanical strength, excellent surface hydrophilicity, and visible light response for photodegradation methylene blue and erythromycin [912].

Electrospun nanofibers have also been used in photocatalytic water splitting for hydrogen production, CO_2 reduction, and photocatalytic nitrogen fixation. For example, composite hierarchically branched TiO_2 (HBT)/ $\text{g-C}_3\text{N}_4$ (CN)/ SnSe_2 nanofibers (Fig. 20C, D) exhibited excellent photocatalytic performance by producing hydrogen about $2375 \mu\text{mol}\cdot\text{g}^{-1}\cdot\text{h}^{-1}$ under the visible light irradiation ($\lambda = 420 \text{ nm}$), which was attributed to SnSe_2 reducing charge recombination by increasing electron transfer and providing active sites for hydrogen production as a co-catalyst (Fig. 20E) [901]. $\text{BiOBr}_{x-1}\text{I}_x/\text{CNF}$ photocatalysts significantly improved the photocatalytic nitrogen fixation [913]. The high electrical conductivity of CNF enabled efficient capture and transfer of electrons, leading to the effective separation of photoinduced charges. In another study, Bi-metal and oxygen vacancies (OVs) co-modified $\text{Bi}_{12}\text{TiO}_{20}$ (Bi/BTO) composite photocatalyst exhibited significantly higher photocatalytic NO removal activity than the original BTO under visible light irradiation because of the combined effect of the surface plasmon resonance effect of OVs and Bi particles [914].

The photocatalytic efficiency of electrospun composite nanofibers can be further improved by designing and constructing special microstructures. For example, mesoporous carbonate-doped phase-junction TiO_2 nanotubes were fabricated by electrospinning and calcination, in which the refined porous structure could increase the optical path by multiple reflection effect, enhancing the light harvesting [915]. TiO_2/NiS core-sheath direct Z-type nanostructure was obtained by vertically growing NiS nanosheets on electrospun TiO_2 nanofibers [916]. The closely-contact layered structure and natural Z-type mechanism significantly promoted the separation of useful electron-hole pairs and efficient hydrogen production of photocatalysis. In another work, graphitic carbon nitride/PLA fibers were constructed with a large number of pores on the surface and in the core, which had excellent photocatalytic activity, repeatability, and stability to degrade various emerging pollutants in wastewater [917]. Other semiconductors or semiconductor composites, such as BiVO_4 nanotubes [918], $\text{C-ZnIn}_2\text{S}_4$ hollow nanotubes [919], $\text{Ni}_{0.33}\text{Co}_{0.67}\text{Te}$ [729], rGO@TiO_2 [920], $\text{TiO}_2/\text{SrTiO}_3/\text{g-C}_3\text{N}_4$ [921] also exhibited excellent photocatalytic performance.

3.4.3. Electrocatalysis

Electrospun nanofibers represented by inorganic nanofibers as active components or scaffold materials have attracted significant attention in electrocatalysis, including water splitting, carbon dioxide reduction reaction, and nitrogen reduction reaction (NRR). The large length-to-diameter ratio of electrospun nanofibers can provide direct pathways for electron/mass transfer, and the high specific surface area can facilitate the exposure of active sites. The tunable morphology, size, and surface chemistry of electrospun nanofibers enable the optimization of electrocatalytic activity, while the excellent flexibility is beneficial for the assembly of freestanding electrodes [922,923]. At present, noble metal-based electrocatalysts incorporating Pt, RuO_2 , IrO_2 , and Au, etc. are still representing the most advanced materials in various similar products, with excellent catalytic performance [921,924]. However, their exorbitant price, scarce resources, and poor durability are challenging to be used for large-scale commercial applications. Therefore, most researchers in this field have been working on developing new electrocatalysts to reduce the consumption of noble metals by partially or even wholly replacing them with low-cost alternatives that are abundant on earth. Heteroatoms-doped carbons, transition metal oxides, hydroxides, chalcogenides, phosphides, nitrides, carbides, MOFs, functional hybrids, etc. have been confirmed as potential candidates for high-efficiency noble metal-free electrocatalysts. In the past few years, significant progress has been made in introducing these materials into electrospun nanofibers for applications in electrocatalytic water splitting, CO_2RR , and NRR.

Electrocatalytic water splitting. Water electrolysis without any toxic by-products throughout the process is considered the most promising method to produce clean hydrogen fuels. It is driven by two characteristic half-reactions of the cathode and anode: hydrogen evolution reaction (HER) and OER [922]. Generally, a voltage higher than the theoretical value (1.23 V) is needed for the overall water splitting under practical conditions. Therefore, exploring advanced bifunctional electrocatalysts for both HER and OER has always been a research hotspot. Electrospun nanofibers based on heteroatom-doped CNF and their hybrids with transition metals, alloys, or metal compounds have been demonstrated as desirable HER electrocatalysts. Complex OER with a 4-electron transfer process often requires higher energy and higher overpotential than simple 2-electron HER [925]. Transition metal alloys, oxides, and carbon-based composite nanofibers obtained by electrospinning combined with heat treatments are typical OER electrocatalysts. Nevertheless, the catalysts for HER usually exhibit excellent activity in acidic media, while most OER catalysts are only suitable for alkaline electrolytes [922]. Even so, properties of bifunctional catalysts based on electrospun nanofibers have been reported to exhibit good electrocatalytic performance at high pH, such as Co nanoparticles-embedded porous CNF, CNF-supported PdNi, PtNi, or RuNi alloys, $\text{WS}_2/\text{Co}_9\text{S}_8$ nanocrystals grown on hollow CNF, core-sheath $\text{CoS}_2\text{-C@MoS}_2$ nanofibers, MoS_2 nanosheets-immobilized Co-N-C flakes on CNF, and Ni/ Mo_2C nanoparticles-anchored nitrogen-doped carbon nanofibers (Ni/ $\text{Mo}_2\text{C}/\text{NCNF}$), etc. [902,926–932]. Taking Ni/ $\text{Mo}_2\text{C}/\text{NCNF}$ as an example, the optimized hybrid achieved a current density of 10 mA cm^{-2} at small overpotentials for HER (143 mV) and OER (288 mV) [902]. The alkaline electrolyzer with Ni/ $\text{Mo}_2\text{C}/\text{NCNF}$ as anode and cathode catalysts just required a low voltage of 1.64 V to reach 10 mA cm^{-2} , and it also presented good stability during the long-term testing of 100 h (Fig. 20F, G). In addition, electrospun porous NCNF may be an alternative support matrix for single-atom catalysts, which could maximize the utilization of metal atoms, fully expose active centers with unique electronic structure and coordination environment and accelerate the electrochemical reaction kinetics.

Electrocatalytic CO_2RR . CO_2 recycling based on electrochemical reduction is one of the fundamental strategies for alleviating global warming caused by excessive consumption of fossil fuels [929]. The cathodic reaction in electrocatalytic CO_2 reduction is: $x\text{CO}_2 + n\text{H}^+ + n\text{e}^- \rightarrow \text{product} + y\text{H}_2\text{O}$. Various products, including CO, hydrocarbons, aldehydes, and alcohols, can be formed due to their similar thermodynamic equilibrium potentials, resulting in poor selectivity toward different products [933]. It has been proved that Cu

is the only metal to reduce CO_2 to a sequence of products requiring $> 2e^-$ transfers with considerable Faradaic efficiencies [933]. The Faradaic efficiency of electrospun Cu-embedded NCNF at -0.57 V (vs. reversible hydrogen electrode (RHE)) was 62 %, which has great potential for applications in ethylene production [934].

To improve the selectivity of specific products, a wide spectrum of nanofibers-based CO_2 RR electrocatalysts have been designed and constructed by electrospinning and high-temperature calcination. Typically, $\text{Cu}_{1.96}\text{S}/\text{Cu}$ -encapsulated NCNF possessed a high selectivity of > 80 % for the electrochemical reduction of CO_2 to CO at -0.68 V vs. RHE [935]. This outstanding performance was attributed to the unique $\text{Cu}_{1.96}\text{S}/\text{Cu}$ tandem configuration, where Cu served as a $\ast\text{CO}$ -generating site enabling the dissociation of $\text{C}=\text{O}$ bonds and the adjacent $\text{Cu}_{1.96}\text{S}$ promoted the subsequent $\ast\text{CO}$ desorption. Sn-based catalysts with excellent selectivity to C_1 products (i. e., HCOOH and CO) have drawn increasing attention in electrochemical CO_2 RR [936]. The wire-in-tube structured SnO_2 fabricated by electrospinning provided an extremely high Faradaic efficiency of > 90 % for the CO_2 conversion to C_1 products within the potential range of -0.89 – -1.29 V vs. RHE, suggesting that large specific surface area and massive grain boundaries significantly contributed to the enhancement of electrocatalytic activity toward CO_2 RR [936]. Overall, it remains one of the mainstream research directions to elevate the selectivity of CO_2 RR electrocatalysts to specific products by tailoring their electronic structures.

Electrocatalytic NRR. Electrocatalytic NRR at room temperature is a simple, energy-saving, and sustainable technology for synthesizing NH_3 from green and abundant H_2O and N_2 . However, the low NH_3 yield rate and poor Faradaic efficiency limit the commercial application of this process, so it is of great importance to develop high-efficiency NRR electrocatalysts. Electrospun nanofibers/nanotubes, such as ZrO_2 , Nb_2O_5 , $\text{Bi}_4\text{V}_2\text{O}_{11}/\text{CeO}_2$, $\text{In}_2\text{O}_{3-x}/\text{CeO}_{2-y}$, Pd/CNF , and $\text{Cr}_3\text{C}_2/\text{CNF}$, etc., have been demonstrated as NRR catalysts [937–941]. Among them, the optimized $\text{In}_2\text{O}_{3-x}/\text{CeO}_{2-y}$ nanotubes with abundant OV s exhibited superior electrocatalytic stability and activity, in terms of Faradaic efficiency (16.1 % at -0.3 V vs. RHE) and average NH_3 production rate ($26.1 \mu\text{g h}^{-1} \text{mg}_{\text{cat}}^{-1}$) [938]. The NRR mechanism on $\text{In}_2\text{O}_{3-x}/\text{CeO}_{2-y}$ was the typical dissociative pathway, where the ample localized electrons around the OV s critically impacted the polarization and activation of N_2 molecules and conducted to the subsequent hydrogenation process.

3.4.4. Enzyme-like catalysis

In recent years, nanomaterials-based enzyme-like catalysts, also known as nanozymes, have gained significant attention due to their easy preparation and exceptional environmental stability [942,943]. These nanozymes showcase a wide array of natural enzyme-mimicking activities, including peroxidase, oxidase, catalase, and superoxide dismutase-like activities [942,943]. These properties have paved the way for promising applications in biosensing, medical science, environmental technology, and food testing. The catalytic activity of nanozymes is heavily influenced by their morphology and chemical structure. The integration of electrospinning technique has further expanded the compositional diversity and structural morphological control of nanozymes [10,944]. In this section, we will delve into the fabrication of electrospun nanofibers for enzyme-like catalysis, examine typical materials and strategies to enhance enzyme-like activity, and explore the diverse applications of electrospun nanofibers-based nanozymes.

A variety of electrospun metal oxide nanofibers have emerged as promising enzyme mimics, thanks to their excellent enzyme-like catalytic properties. For example, electrospun magnetite (Fe_3O_4) nanofibers with hollow fiber-like morphology and wall thicknesses of 15–25 nm exhibited peroxidase-like catalytic activity, outperforming commercial Fe_3O_4 nanoparticles in terms of efficiency [945]. Similarly, electrospun Co_3O_4 nanotubes demonstrated promising potential as mimics of peroxidase, oxidase, and catalase, highlighting multiple enzyme-like functionalities [946]. Recently, ABX₃-type perovskites have been reported for their outstanding enzyme-like efficiency, with electrospun $\text{LaMnO}_{3+\delta}$ nanofibers exhibiting excellent oxidase-like activity, which is highly correlated with the calcination temperature [946]. Remarkably, the optimized $\text{LaMnO}_{3+\delta}$ nanofibers displayed exceptional flexibility, making them suitable for on-demand colorimetric sensing applications. Despite their enzyme-like activity, some electrospun nanofibers still exhibit lower efficiency compared to natural enzymes.

Numerous strategies have been developed to enhance the catalytic activity of nanozymes, such as compositional regulation, interfacial engineering, confinement effect, and single-atom construction. Bimetallic oxides, achieved through compositional manipulation, frequently demonstrate enhanced enzyme-like activity when compared to their single-component metal oxide counterparts due to the proliferation of active sites [947]. Interfacial engineering offers another avenue for improving the enzyme-like properties of nanozymes. For example, ternary $\text{TiO}_2/\text{MoS}_2/\text{CoFe}_2\text{O}_4$ nanofibers were prepared, featuring two distinct interfaces between TiO_2 and MoS_2 , and another between MoS_2 and CoFe_2O_4 components [948]. These nanofibers exhibited significantly higher peroxidase-like activity when compared to single or dual-component catalysts. Similar to compositional manipulation, interfacial engineering facilitates electron transfer from substrates to nanozymes, thereby enhancing peroxidase-like activity. The confinement effect and single-atom design have also been successfully utilized in boosting the catalytic activity for enzyme-mimicking. For example, a wrapping-pyrolysis route has been developed to prepare N-doped carbon nanotubes confined Fe nanoparticles for peroxidase mimicking [949]. The optimized catalyst exhibited exceptional peroxidase-like activity due to excellent interactions between the catalyst and the peroxidase substrate, synergistic effects from confinement, and efficient electron transfer. In addition, recent studies have shown that single-atom iron confined within carbon nanotubes derived from PPy nanotubes displayed outstanding catalytic activity for peroxidase mimicking, with a turnover frequency over 2900 times higher than that of commercial Fe_3O_4 catalysts (Fig. 20H), underscoring the high efficiency of single-atom catalysts for enzyme mimicking [903].

Nanozyme is frequently employed in sensing detection, with electrospun enzyme-like nanofibers showcasing superior detection capabilities. H_2O_2 , as a participant in the peroxidase-like reaction, can be accurately detected by sensitively measuring its concentration through an enzyme-like reaction mediated by electrospun nanofiber-based nanozymes. For example, Cu^{2+} -doped PPy nanotubes, prepared through an electrospinning-template polymerization-*in-situ* doping route, have been employed as peroxidase mimics for the detection of H_2O_2 , boasting a limit of detection of $1.62 \mu\text{M}$ [950]. Moreover, nanozyme reaction systems are capable of detecting various molecules and ions by monitoring their impact on the oxidation of peroxidase and oxidase substrates. Hierarchical

sheet-on-tube PPy@CoO/NiO nanotubes, synthesized through an electrospinning-template polymerization-wet chemical synthesis route, were utilized as peroxidase-like catalysts for the detection of ascorbic acid, exhibiting a limit of detection of 0.183 μM [951]. Additionally, total antioxidant capacity sensors were constructed using peroxidase-like nanozyme systems for the assessment of antioxidant parameters in commercial beverages and fruits, further demonstrating the practical applications of electrospun nanofibers-based nanozymes [903].

3.4.5. Microbial catalysis

Microbial catalysis plays a crucial role in microbial fuel cells (MFCs), also known as bioelectrochemical systems. In these systems, viable microorganisms, also called electroactive bacteria, convert organic waste in wastewater or soil into electricity, facilitating waste recycling and addressing climate change concerns [952,953]. Natural MFCs offer several advantages, such as ambient operating conditions, neutral pH working conditions, and a wide range of abundant biodegradable substrates, making them a promising avenue for sustainable energy supply. However, certain limitations hinder the full development of MFCs, including low power density, high cost, and the absence of full-scale MFCs in natural environments [954,955]. To overcome these challenges, the use of novel advanced anodic materials has been recognized as an effective approach [956–958]. The promising electrode materials possess an accessible surface area for accommodating a large number of bacteria, a conductive network for electron transfer, and excellent corrosion resistance and biocompatibility, thus promoting practical applications of MFCs for domestic and industrial waste treatment.

Nanofiber networks offer unique advantages due to their 3D structure, providing enhanced convenience for electroactive bacteria adhesion and mass diffusion through significant specific surface area and hierarchically macroporous structures. Among them, CNFs stand out for their excellent conductivity, compatibility, and mechanical strength, making them suitable as binder-free electrodes without the need to add additional conductive materials. Leveraging these superiorities, many carbon-based composite anodes have been developed to improve the loading of bacteria and power production in MFCs.

Early reports explored the use of 3D carbon fiber electrodes produced by gas-assisted electrospinning and solution electrospinning [959]. Through this fiber-assembled MFC, bioelectrocatalytic current density of up to 30 A m^{-2} was achieved, indicating favorable formation of electroactive microbial biofilms. The open macroporous structure in these carbon fibers provided ideal growth sites for electroactive bacteria, and the interconnected individual fibers of the nonwoven structure contributed to the formation of cross-linked biofilms, facilitating optimal conduction and electron transfer. Building on this success, various carbon-based composites have been developed, such as LBL carbon fiber membranes [960], nitrogen-doping carbon nanofiber membranes [961,962], and conductive nanofibers [963], as well as metal oxides and carbon composites [964]. These materials could increase the active pore structure and the attachment of electroactive bacteria. The electron transfer rate to the anode remains a critical intrinsic factor limiting the power generation of MFCs. Further strategies should focus on improving biofilm-electrode interactions and the electron transfer rate. In addition, CNF may fracture due to the low Young's modulus after the carbonization process. Therefore, it is crucial to fabricate CNF-based electrodes with conductive biofilm, high mechanical strength, and appropriate flexibility.

One innovative approach is to add carbon nanotubes to create a conductive biofilm where electroactive bacteria can form a composite biofilm in the anode chamber [965]. Another design is the interpenetrated carbon nanotubes/carbon nanofibers (CNTs/CNF) electrode, which can be created through electrospinning and heat pressing, promoting improved inter-junction of fiber aggregates, mechanical strength, and reduced contact resistance [966]. This self-standing electrode enhances the capability of attaching and reproducing electroactive bacteria, ensuring optimal colonization and effective electron transfer between the electrode and microorganisms, thereby facilitating extracellular electron transfer between microbe cells and the anode. Additionally, electrospun Fe_2O_3 nanofibers coupled with CNTs with high porosity and a 3D interpenetrated network allowed efficient nutrient and metabolite diffusion, further promoting effective extracellular electron transfer rates [964].

Despite these advancements, it remains a challenge to fully utilize the interior surface and pores for microorganism colonization because bacteria are generally larger than the pore distribution. Enlarging the pores can enhance substrate transport but may limit the loading of bacteria due to reduced total surface area. To address this issue, bacteria-encapsulated nanofibers were developed as bioelectrodes through coaxial electrospinning (Fig. 20I), offering advantages such as enhanced bacteria loading and biofilm growth through the construction of cell division in the core-sheath structure, while the conductive shell facilitates extracellular electron transfer throughout the electrodes [904]. However, the complicated manufacturing process and poor polymer conductivity present some limitations. To overcome these challenges, future research should explore functional group mediator metal oxides with porous structures on single fibers and proper encapsulation into the interpenetrated interior surface of CNF, along with other relevant manipulations.

3.5. Flexible electronic devices

Flexible electronic devices have become the focus of cutting-edge scientific research. Unlike traditional rigid devices, flexible devices offer advantages such as flexibility, mobility, and bendability, leading to breakthrough applications across various sectors, such as medical, health monitoring, and smart wearable devices [967–969]. To promote the commercialization of manufactured flexible devices, several key points should be considered: (i) the material utilized should be flexible and/or stretchable [970]; (ii) devices should be comfortable to use with good compatibility [971,972]; (iii) the device should be as thin as possible while maintaining the favorable performance [973,974]. These challenges indicate the choice of materials and manufacturing processes for flexible electronic devices.

Electrospun nanofibers/membranes offer several appealing properties in the realm of flexible electronic devices: i) electrospinning has the advantages of simple operation, good continuity, and strong controllability; ii) a wide variety of spinnable materials (e.g., PU,

PS, PVA, etc.) are available; *iii*) the morphology of electrospun nanofibers can be well regulated (e.g., wrinkles, waves, etc.); *iv*) electrospun nanofibers possess high specific surface area, high porosity, good mechanical strength, flexibility and/or stretchability, and air permeability; *v*) the surfaces of electrospun nanofibers contain many easily modifiable functional groups, enabling the achievement of desired properties through further modifications. These advantages have made electrospun nanofibers increasingly popular in the development of flexible electronic device products [975–978]. In this section, we will discuss the applications and development direction of electrospun nanofibers in flexible electronic devices, including sensors, energy storage and conversion, field effect transistors, and organic light-emitting diodes (OLEDs) from the needs of practical applications.

3.5.1. Sensors

Sensors play a critical role in detecting and converting measured information into electrical signals or other required forms for practical applications. Among them, flexible sensors are commonly used for strain, pressure, humidity, temperature, and multimodal sensing applications [979–982]. They have been widely used in human health monitoring, human–computer interaction, intelligent control, and other fields [983]. However, to meet practical needs and applications, these sensors require further enhancements in several properties: *i*) high sensitivity over a wide detection range, *ii*) flexibility, biocompatibility, and stability, *iii*) excellent sensing performance while being environmentally friendly [984–988].

Considering the demand for improved sensor performance, electrospun nanofibers offer distinct advantages. The large specific surface area and porous characteristics of electrospun nanofibers improve the sensitivity and stability of flexible sensors, ensuring a wide detection range. The electrospun fibers are lightweight, highly flexible/stretchable, and breathable, making the fabricated sensors more comfortable to wear. The electrospun nanofibers can be modified to possess specific functions, such as hydrophobicity, antibacterial properties, electrical conductivity, anti-wrinkle properties, antistatic properties, biocompatibility, degradability, etc [989–993]. Therefore, electrospinning technology is critical for addressing practical application issues with flexible sensors. Furthermore, electrospun nanofibers are essential for improving various sensor evaluation parameters, including sensitivity, detection limit, and response time.

Flexible piezocapacitive sensors utilizing nanomaterial-polymer composite-based nanofibrous membranes offer an attractive alternative to more traditional piezoelectric and piezoresistive wearable sensors owing to their ultralow-powered nature, fast response, low hysteresis, and insensitivity to temperature change. For example, a red light-emitting flexible pressure sensor was constructed using electrospun Eu^{3+} -doped P(VDF-HFP)/GO composite nanofibers through the LBL spinning method [994]. The high β -phase concentration (96.3 %) was achieved, leading to a high piezoelectricity of the composite nanofibers. Moreover, the sandwich structure sensor had a sensitivity of 0.72 kPa^{-1} , an ultrahigh output, good hydrophobicity and even certain fluorescence properties. These excellent properties give it great potential for applications not only in flexible sensors, but also in photoluminescent fabrics, soft actuators, and energy storage devices. In another study, a piezoelectric sensor based on electrospun PVAc/graphene nanofibers was prepared, which could be applied to wearable Internet of Things devices and human physiological function monitoring [995]. The sensors showed superior pressure sensing performance, robustness, and reliability. A series of tests involving human physiological parameter monitoring were conducted to underscore the applicability of sensors for IoT-enabled personalized health care, soft robotics, and next-generation prosthetic devices. The future development direction should focus on further improving the desired properties mentioned above.

3.5.2. Energy storage and conversion devices

Energy storage and conversion components are the energy source of flexible electronic devices and play an indispensable role. In addition to meeting the basic high energy density, high power, high conversion efficiency, and high stability and safety of the power supply, the special requirement of flexible electronics about “flexibility” is necessary [996,997]. In Section 3.4, we have described in detail the use of electrospun nanofibers for energy storage and conversion, including supercapacitors and batteries that can provide energy directly, and nanogenerators that can convert other energies into electricity. These are important energy sources in flexible electronic devices. In this section, we will focus on discussing the needs and corresponding applications of these electrospun nanofiber-based energy devices in flexible electronics.

Supercapacitors and batteries. Compared to conventional rigid electronic devices, flexible energy storage devices maintain electrochemical properties even be deformed, and the performance and reliability of the devices in different environments and usage scenarios should be ensured [998]. From these perspectives, the design of supercapacitors based on electrospun nanofiber for flexible electronic devices is guided by the following requirements: *i*) excellent electrode materials to prepare supercapacitors with high-power, high-energy density, and desirable capacitance; *ii*) excellent separator materials that directly impact supercapacitor electrochemical performance and safety; *iii*) long cycle stability and fast charge–discharge rate for the fabricated device; *iv*) good electrochemical performance and excellent mechanical properties under dynamic deformation [999].

Regarding the electrode materials, in one study, free-standing electrodes composed of $\text{Ti}_3\text{C}_2\text{Tx}$ MXene/CNF were prepared by electrospinning for use in flexible supercapacitors [1000]. The electrodes demonstrated good gravimetric capacitance up to 120 F/g at 2 mV/s and maintained a higher capacitance value of 90 F/g at 300 mV/s in comparison to pure CNF electrodes. Due to the high degree of mechanical flexibility of CNF, the resultant flexible supercapacitors also demonstrated long-term cycling stability (98 % retention after 10 K charge–discharge cycles) with improved capacitance, conductivity, and mechanical properties. In another study, highly flexible nitrogen-doped porous MXene electrospun nanofibers were applied as self-supporting electrode materials and assembled into structural supercapacitor composites [1001]. Benefitting from the abundant mesopores structure and uniform nitrogen atom doping, the assembled structural supercapacitors exhibited excellent electrochemical properties and robust long-term durability, achieving an energy density of 12.78 Wh kg^{-1} at a power density of 1080 W kg^{-1} and long-term cycling stability up to 5000 cycles. Similarly, a core-

triple-shelled hierarchical nanostructure was fabricated by the sequential growth of conductive polyaniline (PANI) layers and $\text{Ni}_2(\text{CO}_3)(\text{OH})_2$ nanosheets on the graphene-coated electrospun CNF [1002]. The optimal electrode exhibited a high specific capacitance of 1565 F g^{-1} at 1 A/g , exceeding most nickel hydroxide-based nickel carbonate electrodes reported in the literature. The resultant hybrid supercapacitor delivered a high energy density of 35.4 Wh kg^{-1} @ 750 W kg^{-1} and a long cycle lifespan. These electrode materials improve the limitation of flexible supercapacitors in flexible electronic applications because of their low energy density, making them have broad application prospects in flexible electronic energy storage devices, especially in the next generation of wearable devices.

Flexible batteries based on electrospun nanofibers have also made great strides [1003,1004]. For example, a porous membrane composed of electrospun $\text{Sb}_2\text{S}_3/\text{TiO}_2/\text{C}$ nanofibers was prepared using titanium (IV) isopropyl alcohol as a coupling agent and then assembled into a lithium-ion half-cell or a full-cell without a slurry coating process [975]. In a lithium-ion half-cell, the porous $\text{Sb}_2\text{S}_3/\text{TiO}_2/\text{C}$ nanofibrous membrane could be cycled 800 times at high current density of 2000 mA g^{-1} . The battery showed improved mechanical properties, electrochemical performance, and heat resistance, indicating the practical value in flexible LIBs. In another study, the inner and outer walls of hollow CNF were separately integrated with OER-active O, N co-coordinated Ni single atoms and ORR-active $\text{Co}_3\text{O}_4/\text{Co}_{1-x}\text{S}$ nanosheet arrays by coaxial electrospinning combined with pyrolysis and solvothermal process [1004]. The fabricated Janus-structured nanofibers served as the flexible free-standing bifunctional oxygen electrocatalyst, exhibiting a high open-circuit potential (1.45 V), high capacity ($808 \text{ mAh g}^{-1} \text{ Zn}$), and extremely long life (over 200 h at 10 mA cm^{-2}). Furthermore, the assembled flexible all-solid-state zinc–air batteries showed excellent cycle stability (over 80 h).

Electrospun nanofibers-based flexible power supply has special and irreplaceable advantages in flexible electronic devices, representing one of the important development directions in the future. However, there are still some challenges that require the joint efforts of researchers before practical industrialization and commercialization: i) improving the energy density to increase the applying range of wearable devices; ii) improving the mechanical durability of power devices to guarantee stable performance under various deformation states; iii) improving the cycling life in practice.

Nanogenerators. Health monitoring and wearable electronic devices require overcoming the limitations of traditional battery-powered methods, such as environmental pollution, large size, and short lifetime. Therefore, there is an urgent need for a lightweight, flexible, and sustainable power source to build wearable electronic devices [95]. Nanogenerators, based on piezoelectric or triboelectric effects, are able to achieve self-sufficiency in electrical energy, showing great potential for wearable devices, which not only reduces the dependence on external power sources but also makes the devices more convenient and flexible in daily use [427,877,1005].

The introduction of electrospun nanofibers can further improve the performance of nanogenerators and make them suitable for the needs of flexible electronics. In one study, waterproof, breathable and wearable electronic was fabricated based on nanofibers-TENGs, in which electrospun PA66/MWCNTs nanofibers were used as the tribo-positive layer and electrospun PVDF nanofibers as the tribo-negative layer, respectively [978]. Owing to the coupling effect between the nano-network structure and porous structure, the effective contact area was effectively enhanced. The nanofibrous TENG demonstrated the peak voltage, current and maximum power density up to 142 V , $15.5 \mu\text{A}$ and 1.30 W/m^2 , respectively, with excellent durability and stability under $10,000$ pressure cycles. In addition, the as-obtained nanofibers-TENG had a high gas permeability of 11.5 mm s^{-1} and exhibited good washable characteristics. For the nanogenerators based on electrospun nanofibers, the future development direction should focus on improving the energy conversion efficiency, obtaining higher power output, as well as maintaining good power conversion efficiency and stability under dynamic deformation conditions.

3.5.2.1. Dye-sensitized solar cells (DSSCs). Solar cells also play a huge role in flexible electronics by realizing energy self-sufficiency through light-to-electricity conversion. Flexible DSSCs offer new opportunities to harvest and convert solar energy into electrical energy, primarily utilizing wide-bandgap semiconductor porous films like TiO_2 and ZnO along with photosensitizing dyes [1006]. Compared to traditional solar cells, DSSCs have advantages such as simple process, non-toxicity, green production, low cost, and long life [1007]. However, the conversion efficiency remains a concern. Given the large specific surface area and porous characteristics, electrospun nanofibers often show a high dye sensitizer adsorption and excellent charge transport capacity, making them ideal candidates for flexible DSSCs electrodes with improved conversion efficiency [1008].

The prerequisite for obtaining high-performance DSSCs is possessing excellent catalytic performance for the counter electrodes. Electrolyte is an indispensable component in DSSCs, playing a key role in the faster regeneration of dyes and the transport of internal charge carriers between electrodes. In one study, electrospun $\text{NiCo}_2\text{S}_4/\text{CNF}$ composite fibers were applied in the counter electrode of DSSCs. Good power conversion efficiency (9.0%) and stability have been realized owing to a synergistic effect of the high catalysis of NiCo_2S_4 and the conductivity of CNF [817]. In another study, NiMoO_4 nanoparticles were loaded onto carbon nanofibers ($\text{NiMoO}_4/\text{CNF}$) to enhance the diffusion of the electrolyte and provide more active sites for redox reactions [1009]. The as-prepared DSSCs displayed higher PCE of 7.67% v.s. Pt of 7.17% and CNF of 5.65% , providing a new choice for high-efficiency and low-cost DSSCs Pt-free counter electrode. Functional electrolytes based on polymer nanofibers have also been developed. For example, polymeric ionic liquid was synthesized by covalently grafting vinyl imidazolium iodide and methyl methacrylate onto PEO [1010]. By electrospinning, tungsten oxide nanoparticles incorporated in polymeric ionic liquid nanofibrous membrane were fabricated and applied as a functional electrolyte for quasi-solid state DSSC, which showed a power conversion efficiency (η) of 7.2% and a stability of 94.4% after 500 h .

3.5.3. Flexible stretchable field-effect transistors

Flexible stretchable field-effect transistors (FETs), with the unique advantage of being able to bend and stretch, often serve as crucial signal modulation and electronic switching elements by controlling the charge transport behavior using an external electric

field [1011]. In this case, transistor devices are widely used in the biomedical field, such as wearable devices like smart bracelets and watches to monitor physiological parameters like blood pressure, blood oxygen, and heart rate [1012], and in the foldable electronic displays, photovoltaic cells, and other innovative applications [1013]. Although significant progress has been made in the practical application of transistor devices, there is still a need for the development of new active layer materials to improve the mobility, switching ratio, flexibility, and stability of the transistor devices for better commercialization.

The introduction of electrospun nanofibers to construct flexible stretchable FET has the following advantages: (i) the thickness of the nanofibers can be adjusted to achieve the desired flexibility; (ii) nanofibers, being one-dimensional (1D), minimize the grain boundary effect in thin-film materials, resulting in higher carrier mobility than traditional thin-film materials [1014]; (iii) Electrospinning can enhance charge carrier transport and limited flexibility through organic semiconductor nanofibers [1015].

For example, electrospun Yb^{3+} -doped In_2O_3 nanofibers were applied in FET, and with a doping concentration of 4 mol%, the FETs showed a better electrical performance, with a high mobility of $6.67 \text{ cm}^2/\text{Vs}$, an acceptable threshold voltage of 3.27 V, and a suitable on/off current ratio of 107, especially the enhanced bias stress stability [1016]. When applied to ethanol gas sensors, the stability was enhanced while the sensitivity was improved with a high response of 40 to 10 ppm. The FET sensor also showed a low detection limit of 1 ppm and improved the sensing performance from sensitivity to selectivity. Similarly, FETs based on Nd-doped aligned In_2O_3 nanofibers exhibited a high mobility of $5.5 \text{ cm}^2\text{V}^{-1}\text{s}^{-1}$ and a switching current ratio of 10^7 [1017]. When applied to acetone gas sensors, excellent performance was obtained at room temperature, such as high response (88) at 4 ppm, fast response and recovery time (31/53 s), relatively low detection limit (69 ppb), and acceptable acetone gas selectivity. In addition, a plasticity-tunable electrospun ZnO nanofiber-based FET was developed to simulate the changes in synaptic function [1018]. With the increase of electrospinning time (fiber coverage), the number of fibers could increase the carrier transport channel to improve the FET performance. The optimized electrospinning time, annealing temperature, perovskite doping, and other parameters were selected to regulate the device's plasticity and enhance the synaptic transistor's performance. Perovskite-doped devices with ultralow energy consumption down to ca. 0.2554 fJ and the handwritten recognition application showed the great potential of synaptic transistors based on a 1D nanostructure active layer for building next-generation neuromorphic networks.

3.5.4. Organic light-emitting diodes

OLEDs have attracted huge attention over decades for enhanced human visual data processing driven by their thinness, lightness, less power consumption, fast response, high definition, flexibility, and ultrahigh luminous efficiency, thus [1019]. However, OLEDs still suffer commercialized challenges such as short lifetimes, high costs, and size constraints [1020]. Currently, researchers are exploring the potential of using electrospun nanofibers to enhance OLEDs performance for these raw materials used in the electrospinning process are compatible with organic materials of OLEDs [1021]. In one study, white LEDs were fabricated based on electrospun PVA nanofibers doped with Ag nanoparticles and Piromex dye [1022]. Compared to conventional films, the threshold of PVA/Ag nanofibers was reduced by 35 %. In another study, multicolor circularly polarized luminescence active electrospun polyacetylene/achiral fluorescent dyes/PAN composite nanofibers were fabricated to construct low-cost, flexible light-emitting devices [1023]. The highest luminescence dissymmetry factor (g_{lum}) of the obtained nanofibers could reach 10^{-2} accompanied with excellent adjustability and low energy transfer efficiency.

Electrospinning also provides a simple and effective way to construct intelligent optical structures and advanced optoelectronic devices. For example, brightly luminescent CsPbBr_3 nanocrystals were encapsulated in superhydrophobic poly(vinylidene fluoride-co-hexafluoropropylene)/polystyrene (PVDF-HFP)/PS electrospun nanofibers [1024]. The as-prepared nanofibers showed high photoluminescence quantum yield of 87.9 % and improved fluorescence intensity retention. Furthermore, the composite membrane-based white light-emitting diode exhibited wide color gamut covering 117 % of national television system committee standard, indicating the prospect in solid-state lighting and display applications. Despite these advantages, electrospun nanofibrous membranes are still in their early stages for OLED devices and further in-depth research is required.

Electrospinning technology provides an effective route for flexible electronic devices. In addition to these applications, electrospun nanofibers and membranes can be used in a wide range of applications such as flexible/stretchable electrochemical sensors [1025], heaters [1026], brain-computer interfaces [1027], actuators [1028], and other flexible devices. Electrospun nanofibers have significantly contributed to portability, multi-functional integration, wearing comfort, performance optimization, and other aspects, making these devices more practical in daily life. However, some challenges remain: (i) the mechanical tensile/flexibility strength of electrospun nanofibers decreases noticeably after doping or calcination; (ii) the electrochemical properties of electrospun nanofibers still lag metals, carbon-based polymers, and conductive polymers; (iii) achieving high-precision positioning of electrospun fibers is difficult, resulting in performance discrepancies among flexible devices. Effectively addressing these challenges will be crucial in maximizing the advantages of electrospun nanofibers and advancing their commercial applications.

3.5.5. Soft robotics

Soft robotics have gained huge attention in diverse new fields, where conventional rigid robots are limited, including industrial processing, healthcare, agriculture, automation, marine, and engineering for their high flexibility/stretchability, robust mechanical compliance and easy deformation.[1029,1030] Compared with rigid robots depend on simple control of joints and limbs, soft robot requires more complicated functions to accurately control/monitor the shape/position of different parts of the soft robots and be aware of external stimuli (e.g., heat, pressure, light, and sound, etc.) [1031–1033], making the integration of sensors into soft robots are inevitable. In Section 3.5.1, we have described in detail the use of electrospun nanofibers for flexible strain, pressure, humidity, temperature sensors. In this section, we focus on discussing the electrospun nanofibers-based artificial muscles in soft robots.

As for soft robotics, artificial muscles play an important role in replacing various biological or mechanical components to generate

reproducible mechanical processes without deterioration. Given the flexibility and unique anisotropic properties of electrospun nanofibers, electrospinning offers an innovative technique in fabricating artificial muscles [1034,1035]. Furthermore, prompted by the conventional textile processing techniques (twisting, weaving, and knitting), electrospun nanofibers can be also assembled into the intrinsic architecture of biological muscles [1036,1037]. For example, electrospun skeletal muscle-like PU assembly has been developed. Interestingly, the muscle-like PU assembly exhibits slightly higher strength and stiffness compared to the skeletal muscle ones. To enable the electrospun nanofibers-based muscle with remote actuating function, polydopamine-coated electrospun liquid crystal elastomer microfiber actuators have been developed, which could generate 60 % actuation strain within 0.2 s with high 400 W Kg⁻¹ power density by controlling remote near-infrared laser [1038]. Additionally, ultra-high durability was achieved with 10⁶ cycles of loading and unloading at 20 % strain and 90 °C, without any degradation. To expand the remotely controlled geometry alteration, bi-layer hydrogel actuator with p(4-acryloylbenzophenone-co-N-isopropylacrylamide) layer and Fe₃O₄/PAN layer has been fabricated by electrospinning. The as-prepared product showed complex higher-level programmable movements for its programmable complex remote photothermal-responsiveness with rapid response (178°/s) and high tensile strength (4.59 MPa) [1039].

3.5.6. Bioelectronics

Bioelectronics [1040,1041], which can record physiological signals by transducing signals from the biological system to electrical signals at the bio-electronics interface, play a vital role in many biological fields such as blood glucose sensors, cardiac pacemakers, health monitoring, and deep-brain stimulators. Because of their small diameter, high surface area, and tunable conductivity/flexibility/compatibility, electrospun nanofibers have been widely investigated in fabricating high-efficient bioelectronics [1042,1043]. In one study, topologically optimized electrospun piezoelectric PVDF nanofiber mats were developed as acoustic sensors to enhance electromechanical conversion across a wide bandwidth. Compared to traditional electrospun nanofiber mat-based sensors, the new design achieved a 300 % increase in electric output and a 478 % improvement in frequency response range. Furthermore, 100 % classification accuracy in human voice speech recognition was achieved with the assistance of deep learning [1044].

Electrospun nanofiber membrane-based soft electronics in epidermal bioelectronics has also been widely investigated for their conformal compatibility with the human body and associated performance improvements. For example, filtration-based direct local nanowire patterning method on the electrospun nanofiber membrane using dispenser systems has been developed in fabricating stretchable, breathable, and highly conductive epidermal bioelectronics harnessing various types of metal nanowires, including Ag, Ag@Au core-sheath, and Ag@(Au-Pt) core-sheath nanowires. Construction of support bed under nanofiber membrane, fluid flow can be realized. The composite membrane can be spontaneously replicated according to diverse human body geometries *in-situ*. The as-prepared epidermal bioelectronics could record *in vivo* epicardial signals, epidermal electrochemical behaviors, and customized epidermal electromyography-based human-machine interfaces.

Electrospinning also offers special applications in constructing ideal interfaces that directly bridge thin-film electronics with soft tissues. For example, an ultrasoft microfiber composite ultrathin (< 5 μm) hydrogel film has been developed by embedding an electrospun PU microfiber network into the poly(vinyl alcohol) hydrogel. The tunable Young's Modulus at wide range of microfiber composite hydrogels imparts a prominent mechanical match with human living organs and tissues. Furthermore, the incorporation of sodium chloride and glycerol provides the composite hydrogel with high ionic conductivity, anti-freeze, and anti-dehydration properties. The hydrogel can monitor electromyography in high quality for 48 h in ambient air with lower background noise.

<!--MANI-->.

3.6. 3.6. Electrospun nanofibers for special engineering materials

Electrospinning technology is an efficient method for fabricating flexible and continuous non-oxide ceramic fibers from polymer precursors with diameters over a scale from nano- to micro-meters by managing the processing parameters. Benefiting from the high porosity and high surface area of electrospun nanofibers, functional customization is expected to be achieved through reasonable multi-component design and fiber structure construction. Therefore, they have great application prospects in some special engineering materials, such as high-temperature insulating materials, wave-absorbing materials, sound-absorbing materials, and impact-resistant materials. In this section, we will discuss the latest achievements in the applications of electrospun nanofibers in special engineering materials.

3.6.1. High-temperature insulating materials

Electrospinning technology is instrumental in creating heat-resistant fiber membranes used in various applications, including batteries, supercapacitors, and air filtrations. On the one hand, because of the high porosity of electrospun fibers, these tiny pores can form an air barrier between the fibers. Air is a poor conductor of heat, so these pores can slow down the conduction of heat, thus realizing the heat insulation effect. On the other hand, by compounding and processing the electrospun fibers, the fiber membrane can be further endowed with the ability to insulate heat. According to their chemical composition, they can be divided into polymer-based (amides, imines, imidazoles, etc.) and inorganic-based (ceramics, metals, etc.) fibers. For example, polyacrylic acid (PAA) was employed as a precursor to produce a PI film by amidation for Li battery separators [1045]. The PI separator exhibited excellent thermal stability, even at 500 °C, with no significant shrinkage or color change after being exposed to 150 °C for 1 h. Similarly, PAN/poly(m-phenylene isophthalamide) composite fiber membrane with excellent mechanical properties and high-temperature resistance was prepared for filtering high-temperature gas [1003]. The composite membrane could be treated at 140–220 °C for 30 min without volume change with a filtration efficiency of 99 %, indicating its excellent high-temperature resistance.

Inorganic-based electrospun fiber membranes surpass their polymer-based counterparts in resistance to high temperatures

(>1000 °C) and corrosion. For example, heat-resistant fibers were prepared by combining ZrO_2 with low thermal conductivity and SiC with infrared thermal radiation shielding [1046]. These composite fibers retained their original morphology when heated in air at 1800 °C for 1 h or after being immersed in 1 M NaOH solution for 30 min. Similarly, N-doped hollow SiC fibers were prepared by coaxial electrospinning followed by thermal or electron beam irradiation curing [1047]. The composite fibers exhibited an ultra-low thermal conductivity ($0.026 \pm 0.013 \text{ W m}^{-1} \text{ K}^{-1}$) at room temperature due to the multilayer scattering mechanism. Even when heated to 1000 °C, their weight remained almost unchanged. In another study, lamellar multi-arch structured ceramic nanofibrous aerogels were prepared by immersing electrospun $\text{ZrO}_2\text{-Al}_2\text{O}_3$ nanofibers in $\text{Al}(\text{H}_2\text{PO}_4)_3$ solution followed by freeze-drying and calcination (Fig. 21A) [1048]. The obtained ceramic nanofibrous aerogels exhibited high-temperature resistance up to 1300 °C and thermal insulation performance with low thermal conductivity ($0.0322 \text{ W m}^{-1} \text{ K}^{-1}$). Furthermore, electrospinning allows the preparation of other high-temperature and heat-resistant fibers, such as mullite fibers [1049] and Cu nanowires/carbon black composite fibers [1050]. These materials exhibited remarkable thermal stability and heat resistance, making them suitable for various high-temperature applications.

3.6.2. Wave-absorbing materials

Electrospun nanofibers are widely utilized in the field of microwave absorption due to their high anisotropy and multiple scattering effects. However, a single component may have poor impedance matching and dielectric loss. In this case, dielectric materials can be added to improve impedance matching and promote dielectric loss. Additionally, introducing heterogeneous interfaces between multiple components can enhance interface polarization and dipole polarization, further improving microwave absorption performance [1054,1055]. In microwave absorbing materials, SiC nanofibers and CNF often act as substrates and are combined with other materials (e.g., graphene [992], MWCNTs [1056], hafnium carbide [1057], and vanadium nitride [168]) or doped with elements (N, P) [1058]. In addition, the incorporation of magnetic nanoparticles, including magnetic metal elements, magnetic metal oxides, and magnetic alloys, in the nanofibers can further optimize impedance matching and coordinate dielectric loss and magnetic loss mechanisms, effectively enhancing microwave absorption [1059].

Apart from optimizing the chemical composition, the design of hierarchical gradient and porous structure plays a crucial role in enhancing the multiple reflections of microwaves within the material to achieve effective attenuation. For example, coaxial electrospinning and solvothermal methods were applied to prepare electromagnetic-gradient hierarchical $\text{TiO}_2\text{@Co/C@Co/Ni}$ carbon microtube composites [1051]. Its maximum reflection loss value reached -53.99 dB at 2.0 mm and the effective absorption bandwidths ($\text{RL} \leq -10 \text{ dB}$) were as wide as 6.0 GHz, covering most of the Ku band (Fig. 21B). The scalable fabrication of microwave-absorbing functional aerogel spheres was achieved by the combination of multiaxial electrospinning and freeze-drying on the multiscale. For example, Fe_3O_4 aerogel microspheres [1060] and graphene aerogel spheres [1061] were obtained by coaxial and triaxial electrospinning technologies, respectively, followed by freeze-drying. The porous aerogel structures facilitated internal multiple scattering and geometric configuration effects, enhancing microwave absorption and attenuation. Typically, the as-obtained hollow graphene aerogels showed a minimum reflection loss of -52.7 dB , and a broad effective absorption bandwidth (f_E) of 7.0 GHz with thickness of 2.3 mm. Furthermore, it is essential to endow microwave-absorbing materials with the versatility to adapt to complex use environments. In one study, magnetic nanoparticles $\text{FeNi/NiFe}_2\text{O}_4/\text{NiO}$ were embedded onto the surface of CNF to form rough nanostructures, which showed an effective absorption bandwidth of 8 GHz [1062]. In another study, self-healing superhydrophobic core-sheath PVDF/ Fe_3O_4 @PPy fibers were obtained through electrospinning a PVDF/ Fe_3O_4 mixture and *in-situ* chemical oxidative polymerization of PPy, followed by chemical vapor deposition with fluoroalkylsilane, which showed promise for further advancing microwave-absorbing materials [1063].

3.6.3. Sound-absorbing materials

Traditional sound-absorbing materials are effective in the high-frequency region (> 2500 Hz) but often lack sound absorption capacity in the medium and low-frequency region (< 500 Hz, 500–2500 Hz) [1064]. Electrospun nanofibers can increase the contact area between the internal pores and sound waves to facilitate energy dissipation. The excellent flexibility of electrospun fibers also enables the construction of resonant structures. When sound waves act on these structures, sound energy can be converted into heat energy or kinetic energy, enhancing the sound absorption capacity at medium and low frequencies [1065]. In one study, a bilayer composite membrane was prepared by placing electrospun nanofibers made of collagen hydrolysate/PVA on coir, and the maximum sound absorption peak of the composite membrane could be reduced to 200–1000 Hz, effectively promoting sound absorption in the lower frequency [1066]. Furthermore, a tri-layer membrane was constructed with the porous PAN fibers used as the external layer, which facilitated sound absorption and further enhanced low-frequency sound absorption capability [1067].

Piezoelectric materials can be further introduced in electrospun nanofiber membranes to achieve acoustic-electric conversion. Such materials usually have a large dipole moment and can change the degree of polarization when subjected to an external force, generating an electrical signal [978]. For example, piezoelectric material PVDF was combined with carbon nanotubes and graphene to prepare nanofiber membranes for absorbing sound waves and converting them into electric energy [1068,1069]. Through piezoelectric shunt damping, the membranes reduced the sound transmission under medium and low-frequency resonance, resulting in a high absorption coefficient of up to 0.9 and noise reduction coefficient of up to 0.56 in the mid-frequency region, demonstrating excellent sound absorption performance in both low and medium frequencies.

The 2D electrospun nanofiber membranes also face low thickness and dense structure, resulting in a narrow sound absorption band. To solve this problem, a fibrous sponge was prepared by humidity-assisted multistep electrospinning followed by physical/chemical dual cross-linking (Fig. 21C) [1052]. The resulting sponge material, with a gradient variation of porosity and pore sizes in the Z direction, exhibited high-efficiency broadband acoustic wave absorption, achieving a noise reduction coefficient up to 0.53. The design

of this gradient-structured fiber sponge opens a new way for the development of ideal sound-absorbing materials.

3.6.4. Impact-resistant materials

Common strategies for preparing strong polymer thin films with impact-resistant functions include adding inorganic materials such as carbon tubes, carbon fibers, 2D materials such as GO and metallic/metal oxide particles to the thin polymer film. However, these methods may lead to an increase in the specific gravity, incompatibility between organic and inorganic materials, anisotropy of mechanical properties caused by uneven distribution of filler material, pore formation, and/or high cost, reducing their strength. Electrospinning allows the production of submicron to nanoscale fibers composed of various types of constituent materials (polymers, metal particles, CNTs, CNCs, ceramics, metal powders and nanoparticles). By adjusting the electrospinning parameters (e.g. voltage, solution viscosity, fiber size and nozzle-to-collector distance) and the electrospinning process (uniaxial, coaxial, etc.), it is possible to precisely control the structure and thus improve the above-mentioned defects. The nano/sub-micron fibers prepared by electrospinning have a high specific surface area.

Electrospun nanofibers can be incorporated into and surrounded by polymer matrix to prepare composites with excellent mechanical properties by preventing the formation of voids or stress concentration areas. For example, helicoidally arranged nylon electrospun nanofibers were embedded in an epoxy resin matrix to prepare composite membrane with a tensile strength of 39 MPa and excellent impact energy absorption performance (absorption energy 1.4 kJ m^{-2}) in the pendulum impact test (Fig. 21D) [1053]. In the falling ball test, the 1 mm thick films were subjected to the impact of a 0.25 kg ball falling from 8 cm. In another study, 13 layers of uniaxially aligned arrays of PAN electrospun fibers at 45° angular offsets were embedded in PVA matrix to prepare the fiber-reinforced strong polymer thin films, which showed a specific tensile strength of $5 \text{ MPa cm}^3 \text{ g}^{-1}$ and could sustain specific impact energy $8 \pm 0.9 \text{ mJ cm}^3 \text{ g}^{-1}$ [1070]. This novel fabrication method enables further production of smaller fibers (sub-micron or even nanoscale) and further tuning of the fiber-substrate material interface and fiber-to-fiber adhesion through LBL processing (using additive manufacturing methods). These parameters allow greater control and tunability of impact performances of the synthetic materials for various applications from army combat wear to sports and biomedical/wearable applications.

3.7. Electrospun nanofibers for clothing textile and health

3.7.1. Clothing textile

In the realm of functional clothing, it is vital to meet different function requirements such as oil resistance and hydrophobicity while focusing on design aesthetics, wear comfort, recyclability and sustainability. Humans adapt to hot summers or cold winters, or some extreme environments, through clothing. However, the performance of current textile materials still needs to be improved. In addition to traditional textile materials, various innovative materials like aerogels, ceramic fibers, nanofibers, silica, graphene, acetate fibers, recycled fibers, and fibers with ecological carbonization functions have been explored for cooling or thermal insulation. In high temperatures or some special environments, clothing often cannot dissipate heat in time utilizing heat radiation and breathability, which can cause an imbalance in body temperature. For example, medical protective clothing ensures safety, so the seal is extremely strong. This can cause poor internal air permeability, poor moisture permeability, radiation and poor heat dissipation greatly affect the wearing comfort of healthcare workers and may even cause physiological injury. The versatility of electrospun fibers provides a very good solution. For example, a nanofiber membrane-based moisture-wicking passive cooling hierarchical metafabric could couple selective optical cooling and wick-evaporation cooling to achieve efficient temperature and moisture management [1071]. The hierarchical metafabric showed high sunlight reflectivity (99.16 % in the $0.3\text{--}0.76 \text{ }\mu\text{m}$ wavelength range and 88.60 % in the $0.76\text{--}2.5 \text{ }\mu\text{m}$ wavelength range), selective infrared emissivity (78.13 % in the $8\text{--}13 \text{ }\mu\text{m}$ wavelength range), and good moisture permeability owing to the optical properties of the material and hierarchical morphology design. Cooling performance experiments revealed that covering simulated skin with the hierarchical metafabric could prevent overheating by 16.6°C compared with traditional textiles, including a contribution from management of the humidity (ca. 8.2°C). In addition to the personal thermal management ability, the hierarchical metafabric also showed good wearability.

In addition to being used for cooling, winter clothing to protect against the cold is indispensable, but traditional winter clothing for warmth is often single-style and bulky, lacking a certain sense of design and fashion. Due to the very small diameter of electrospun fibers, extremely low infrared heat radiation emission can be achieved, enabling efficient cold protection. For example, silica composite nanofibers with closed cell structure and excellent thermal insulation performance were prepared by electrospinning using hollow $\text{SiO}_2/\text{TiO}_2$ spheres as pore-forming agents and infrared shielding agents [1072]. The addition of hollow $\text{SiO}_2/\text{TiO}_2$ spheres broke the continuity of heat transfer pathways inside the nanofibers and enhanced the infrared thermal radiation shielding performance of the nanofibers, endowing the nanofibers with ultra-low thermal conductivity and low infrared transmittance. In another study, an electrospun SiZrNOC nanofiber membrane showed a high tensile strength ($1.98 \pm 0.09 \text{ MPa}$), excellent thermal stability (1100°C in air), and superior thermal insulation performance with a thermal conductivity of $0.112 \text{ W}\cdot\text{m}^{-1}\cdot\text{K}^{-1}$ at 1000°C [1073]. In addition, the prepared SiZrNOC nanofiber membrane-reinforced SiO_2 aerogel composites exhibited ultralow thermal conductivity of $0.044 \text{ W}\cdot\text{m}^{-1}\cdot\text{K}^{-1}$ at 1000°C .

To keep warm/cool, some clothing tries to go about maintaining body temperature through active energy-consuming heating/cooling while insulating/cooling. However, certain challenges still exist in the application of these materials in electrospinning processes and large-scale production. Radiant heat management realizes “passive” heating or cooling by regulating the heat radiation relationship of the body surface. This “passive” process does not consume energy; thus, it surpasses most of the traditional energy-consuming cooling or heating methods. For example, electrospinning could reduce the diameter of PAN nanofibers to $0.77 \text{ }\mu\text{m}$, which was much lower than that of $19.5 \text{ }\mu\text{m}$ for commercial PAN fabrics, resulting in the dramatically reduced heat loss due to the

emission of infrared radiation with a low mid-infrared emissivity (15 %) [1074]. Notably, by further coating the surface of the PAN nanofibers with dye molecules and silver, the obtained colored fabrics showed a solar energy utilization of up to 50 %, achieving excellent infrared heating performance while maintaining the aesthetics of the clothing at the same time (Fig. 22). At a low ambient temperature of 14 °C, the fabric could maintain the body temperature at 33–35 °C. In addition, the nanofibers had excellent water vapor transmission rate, water evaporation rate, air permeability, and mechanical stability, and thus showed great potential for practical applications in infrared heat management textiles.

The breathability and moisture conductivity of clothing also play a vital role in ensuring the comfort of the wearer. The main principle of designing breathable and moisture-conducting materials lies in setting the micropore diameter of the material between that of gas molecules and water molecules, enabling the entry of gas molecules while preventing water molecules from permeating. In one study, a bilayer porous membrane composed of one layer of electrospun cellulose acetate nanofibers and another layer of electrospun PVA/PAA nanofibers was laminated onto polyester fabrics to examine their practical applications in the textile area [1075]. The composite laminated fabric exhibited a value for one-way moisture transport capability of 960.76 % with an overall moisture management capacity performance of 0.84 % and the moisture absorption and perspiration could reach level 5. In another study, a hydrophobic electrospun AgNPs-PS nanofiber membrane with a contact angle > 90° was bonded to a hydrophilic PET membrane, and the obtained hydrophobic-hydrophilic composite structure achieved unidirectional water permeation function [1024].

A robust strategy was presented for the construction of durable superhydrophobic waterproof and breathable nanofibrous membranes by the combination of humidity-induced electrospinning and dip-coating technology [1076]. The hierarchical rough surface of the nanofibers was in-situ generated by tailoring the phase separation behaviors of the charge jets. Then, the waterborne acrylic resins with low surface energy were linked onto PVDF/ blocked isocyanate nanofibers via the bridging effect to construct a stable superhydrophobic coating. As a result, the developed PVDF@waterborne acrylic resins nanofibrous membranes exhibited durable superhydrophobicity offering a great level of protection and thermalwet comfort. Considering the scalable synthesis procedure and comprehensive properties, we envision that the developed superhydrophobic waterproof and breathable membranes are promising applications in protective garments, medical hygiene, and electronics.

3.7.2. Cosmetic materials

Electrospun nanofibers also have a place in beauty products, such as cosmetics and skincare products. When incorporated into skin care products, nanofibers enhance the adaptability of skin tissue to the external environment. Their distinctive characteristics facilitate excellent interactions with the skin and damaged tissue, while also enabling increased loading capacity for agents, high liquid absorption capacities, and high oxygen and water vapor permeability [1077]. Additionally, nanofibers possess excellent antibacterial, antioxidant, and anti-inflammatory functions, making them valuable components in cosmetic masks, therapeutics, skin care wipes, and renewal products. The emergence of fiber-based medicinal cosmetics signifies the dawn of a more environmentally friendly and sustainable green cosmetics market [1078]. For example, a dissolvable adhesive mask with moisturizing properties was prepared by electrospinning collagen peptides, silk cellulose and PVP in formic acid solution [1079]. As another typical example, active components, pomegranate and sea buckthorn were encapsulated in electrospun PLA/PVP nanofibers, in which the antioxidant activity of the active compounds could be well maintained [1080]. Moreover, an anti-wrinkle nanofiber face mask containing ascorbic acid, retinoic acid, gold nanoparticles, and collagen was fabricated by electrospinning [1081]. The face mask could only be wetted when applied to the skin, enhancing the product stability, and the high surface area-to-volume ratio of the nanofiber mask ensured maximum contact with the skin surface and enhanced skin permeation to restore a healthier appearance. At the same time, it is important to ensure the safety of skin care and cosmetic products, so that possible toxic substances and heavy metals need to be detected accurately. Versatile electrospun nanofibers can also play an important role. For example, electrospun PVA/citric acid/Au NPs nanofibers with non-toxic, cost-effective, and biodegradable sorbents were used for the determination of Pb²⁺ and Cu²⁺ in cosmetic samples [1082].

Electrospun nanofibers have great application potential in the cosmetics industry to design and develop non-toxic, anti-aging, green cosmetics and care products. As skincare and cosmetic products are closely linked to human health and fashion, advances in fiber production technologies allow the design of new products with versatile applications in cosmetic and skin care products. The development of nanofiber-based and bio-based cosmetics is expected to attract increasing attention and recognition.

4. Advanced characterization technologies for electrospun nanofibers and their derivations

The development of advanced characterization methods always leads to breakthroughs in one field. In the field of research on electrospun nanofibers and their derivatives, the application of advanced characterization tools is gaining widespread attention. These characterization tools provide insights into the structure, properties, and performance of electrospun nanofibers, revealing their intrinsic characteristics at the nanoscale. Specific characterization methods, such as *in-situ* spectroscopy and microscopy characterization, can analyze individual nanofibers, 2D fiber films, and 3D nanofiber assemblies. In this case, the relationship between the microstructures and macroscopic properties can be observed *in-situ*, enabling the researchers to gain a more in-depth understanding of electrospun nanofibers and their derivatives, revealing their potential applications [1083]. The application of these characterization methods will promote the development of the electrospun fiber field and provide more accurate guidance for material design and engineering.

4.1. Specific characterizations of electrospun nanofibers

Advances in instrumentation science and technology have driven the application of different characterization methods to better

study electrospun nanofibers, including 1D individual nanofiber, 2D nanofiber membranes, and 3D nanofiber assemblies. In this section, we aim to discuss advanced characterization techniques at the macroscopic and microscopic levels in 1D, 2D, and 3D levels, with a focus on representative examples.

4.1.1. Advanced characterizations of individual nanofiber

To gain a deeper understanding of electrospun nanofibers, it is necessary to start with the most basic characterization study on an individual nanofiber. One such method is the *in-situ* single-nanowire device, which allows for the investigation of intrinsic properties of materials at the nanoscale. Unlike many conventional material characterization techniques that provide average signals from relatively large domains, the *in-situ* single-nanowire device can offer a more detailed understanding of mesoscale features, establishing a direct link between the structure and the obtained results. In one study, a single-nanowire electrode device was designed, in which only one nanowire was applied as the cathode or anode while classical materials as the counter electrode and electrolyte (Fig 23A–C) [1084]. No binders or conducting carbon additives were introduced into the system. Typically, a Si/a-Si nanowire/LiCoO₂ electrode device provided a direct relationship between the electrical transport, structure, and electrochemical properties of a single nanowire electrode through electrochemical performance tests. Based on this, the same group proposed a more advanced device five years later (Fig 23D, E). This device provided a unique platform for *in-situ* electrochemical and electrical probing by masking the nanowires with photoresist to set up multiple contacts on a single nanowire electrode, allowing for a more precise recording of the current-carrier transport process over time on a single nanowire platform [1085].

The above single-nanowire platform usually detects the current and voltage of single nanowires. Besides, it is also convenient to combine the platform with many other characterization methods (Fig. 24), such as photoluminescence spectrum [1086], Bragg coherent x-ray diffractive imaging [1087], nano-angle-resolved photoemission spectroscopy [1088], nanofocusing X-ray [1089], Raman thermography [1090], cathodoluminescence (CL) spectra [1091], Kelvin probe force microscopy [1092], conductive atomic force microscopy (AFM) [1093], atom probe tomography [1094], and tip-enhanced Raman spectroscopy [1095].

In general, the single-nanowire platform shows the possibility to combine kinds of probe-related technologies and spectra with nanometer resolution, significantly enhancing spatial resolution capabilities to enable basic and practical research in various fields, especially in energy storage applications. Even though the current *in-situ* single-nanowire devices can only apply to the nanowire materials with a diameter of less than 150 nm, fortunately, with the development of electrospinning, it is convenient to prepare ultra-fine nanowires, no matter what the components of the material are.

4.1.2. Advanced characterizations of 2D fibrous membranes

Pore size is one of the most essential factors that determine the performance of 2D nanofibrous membranes in various applications. For the electrospun nanofiber membrane, the geometric pore size is decreased with the reduction of nanofiber diameters [1096]. Therefore, the controllable pore size can provide instructions on the fabrication of nanofiber membranes in desired applications, such as air filtration, hydrogen storage, tissue engineering, etc.

Macroscopically, the size and distribution of pores of electrospun nanofiber membranes can be examined using a capillary flow porometer, while the pore structure and specific surface area can be characterized by performing the N₂ adsorption and desorption test. Flexibility holds paramount importance in assessing the compliance of nanofiber membranes under stretching conditions. Specifically, for 2D electrospun nanofiber membranes, possessing a lower modulus signifies heightened flexibility. These membranes can readily undergo substantial deformation without fracturing, denoting their capacity for both a small elastic modulus and a high yield strength. In contrast, alternative forms of 2D membranes tend to exhibit greater stiffness, rendering them comparatively weaker [1097]. The softness of the membrane can be measured using tissue softness analyzer under the guidance of ASTM standard D 2923–01 [1097,1098]. Additionally, the thermal analysis of the membrane can be evaluated by synchronous thermal analysis (STA) technology.

Microscopically, the morphology and the nanofiber diameters can also be observed by SEM, transmission electron microscopy (TEM), and AFM. The structural evaluation and phase formation can be characterized by X-ray diffraction (XRD) technique. X-ray photoelectron spectroscopy (XPS) and energy-dispersive X-ray spectroscopy (EDS) can also be employed to detect the surface element types or their chemical species.

4.1.3. Advanced characterizations for 3D nanofibrous assembly

With the development of the 3D nanofibrous structure, versatile high-performance fibrous sponges and nanofiber-composite hydrogels have been prepared. To reveal their morphology and properties, advanced characterizations have been employed. For microscopic characterization of the 3D electrospun nanofiber assembly, SEM gives a direct view of the porosity and surface morphology [1099]. Moreover, using *in-situ* SEM can provide *in-situ* observation of the microstructure evolution of the 3D fibrous sponge under the action of external force [1100]. Additionally, spectroscopy is also used to detect the components or structures. For example, the chemical structure of silica nanofibers-reinforced hydrogels was investigated by XPS [1100]. At the macroscopic level, the mechanical property is a key requirement for the evaluation of the 3D electrospun nanofiber assembly. Generally, compression tests including stress-strain and fatigue tests are carried out for the characterization of mechanical properties [1101]. These measurements are sometimes conducted under extreme conditions. In one study, SiO₂ nanofibrous aerogels were conducted 500 cycles of compression test at –100 and 500 °C to demonstrate the highly elastic properties under extreme temperature conditions [779].

4.2. In-situ spectroscopy

Compared with traditional spectroscopy, *in-situ* spectroscopy is a real-time analysis method that offers the advantage of analyzing

changes in sample composition, structure, etc. as environmental conditions change. *In-situ* spectroscopic analysis helps to understand the specific reaction mechanisms involved in electrospun fibers, which is an important guide for optimizing and expanding their applications. Nowadays, there are many *in-situ* spectroscopy technologies applied in electrospun nanofibers, such as *in-situ* XRD, *in-situ* XPS, *in-situ* Fourier transform infrared spectroscopy (FTIR), *in-situ* Raman spectroscopy, *in-situ* X-ray absorption fine structure (XAFS), and so on.

4.2.1. *In-situ* XRD

XRD is widely used to study crystal structures, as it is based on the X-ray scattering from regularly arranged atoms within crystal cells. This scattering interference produces diffraction patterns with different orientations and intensities, particularly in crystalline or partially crystalline structured materials [1102]. *In-situ* XRD can monitor the structural changes of phase transition during a reaction or temperature changes (heating/cooling). For the inorganic electrospun nanofibers, the high-temperature sintering process removes the polymer matrix from the precursor nanofibers and leads to the crystallization of the inorganic component. In this process, *in-situ* high-temperature XRD can monitor the structural changes at elevated temperatures, verify the effect of high-temperature sintering on the nanofibers, and then analyze their dynamic structural evolution. For example, pure tungsten oxide nanofibers of about 100 nm were obtained by electrospinning a mixture of isopropanol tungsten sol-gel precursor and poly(vinyl acetate) (PVAc) followed by calcination [1103]. During the calcination process, the continuous transition of electrospun tungsten oxide nanofibers from the amorphous nanocomplex phase to the crystalline tungsten oxide phase was recorded using a synchrotron-based *in-situ* XRD method, which is crucial for optimizing the heat treatment temperature to obtain a specific tungsten oxide phase. Moreover, a tunnel-structured $K_{1.28}Ti_8O_{16}@N$ -doped CNF anode was prepared via simple electrospinning and subsequent thermal treatment with urea acted as the additional convenient nitrogen source [1104]. *In-situ* XRD measurement confirmed the intercalation reaction mechanism and robust structure during Na^+ insertion/extraction, providing a facile strategy to synthesize stable, reversible, and long-cycle anode for SIBs.

In addition to changing the temperature, chemical reactions are accompanied by changes in the crystal structure, such as in a typical lithium-ion battery electrochemical reaction. With increasing interest in research on LIBs in recent years, what happens to LIBs materials during the charging and discharging process has attracted more attention. However, due to the sensitivity of working electrodes to the external environment, the results from *ex-situ* measurements of electrochemical processes may not fully reflect what is truly taking place. Therefore, understanding information under realistic battery operating conditions is of vital importance. Thus, *in-situ* electrochemical XRD is developed to monitor the structural changes of LIBs materials during lithiation/delithiation cycling. Using this approach, the lithium storage mechanism of many different LIBs materials has been extensively investigated, such as electrospun nanowires and nanotubes of KNb_3O_8 [1060], $LiY(WO_4)_2$ [1105], $GaNb_{11}O_{29}$ [1106], $K_2Nb_8O_{21}$ [1107], $CuFeS_2$ [1108], $W_9Nb_8O_{47}$ [1109], $Li_2-xNa_xTiSiO_5/C$ [1110], $LiY(MoO_4)_2$ [1111], $WNB_{60}O_{153}$ [1112], and $BaNb_{3.6}O_{10}$ [1113]. Similarly, the understanding of Na-ion storage mechanism could also be obtained using *in-situ* XRD techniques [1086,1114].

4.2.2. *In-situ* XPS

XPS is a method to analyze the chemical composition or valence state on the surface of materials within 10 nm by using the kinetic energy or binding energy of photoelectrons [1115]. Compared to *ex-situ* XPS, *in-situ* XPS can monitor the material changes in structure and composition under conditional influence. With its internal Ar ion sputtering function, *in-situ* XPS can track changes in the layered or core-sheath structure materials as environmental temperature increases. For example, Ar gas cluster ion beam sputtering in combination with *in-situ* XPS (GCIB-XPS) was applied to analyze buried GaP/Si (001) heterointerfaces [1116]. By digging a crater into the 20 nm thick GaP(001) film, they observed the formation of metallic Ga on the GaP surface.

In-situ XPS can also be applied to study changes and the mechanism behind them induced by photostimulation. In one study, a TiO_2/NiS core-sheath photocatalyst for photocatalytic H_2 production was fabricated by hydrothermally growing NiS nanoplates onto TiO_2 electrospun nanofibers [916]. With the help of *in-situ* XPS analysis, the photoexcited electrons in TiO_2 migrated to NiS under UV-visible light irradiation, suggesting that a direct Z-scheme heterojunction was formed in the NiS/ TiO_2 hybrid. Similarly, from *in-situ* XPS, it was verified that the electron immigration in the synthesized sulfur-doped g- C_3N_4 (SCN)/ TiO_2 photocatalyst followed the S-scheme heterojunction mechanism [1117]. In addition, an *in-situ* electrochemical XPS apparatus was constructed to explore the solid/liquid interfaces under potential control [1118]. In another study, an internal argon ion sputter gun was used in a standard lab-scale photoelectron spectrometer to deposit thin metal films (e.g. lithium) on the sample surface [1119]. This could straightforwardly investigate the formation of an interfacial reaction zone (interphase) at the surface of a solid electrolyte by photoelectron spectroscopy after direct deposition. These methods may also provide different research strategies for the analysis of electrospun nanofibers.

4.2.3. *In-situ* FTIR

FTIR, a spectroscopic technique, is used to detect the molecular vibrational and rotational energy level transitions caused by the selective absorption of certain wavelengths of infrared light by molecules. This provides information about chemical bonds or functional groups in the sample, allowing the identification of its chemical constitution [1120]. *In-situ* FTIR allows for continuous monitoring of structural changes of electrospun nanofibers under different conditions, such as atmosphere, temperature, light, etc., facilitating comprehensive and thorough studies of reaction mechanisms [1121]. *In-situ* variable-temperature FTIR has been used in the investigation of the structural changes of material for a long time. As for electrospun nanofibers, the *in-situ* FTIR was performed on electrospun nylon-6 fibers heated to various temperatures until melting and their specific brill transition was elucidated [1122]. Different types of electrospun nanofibers, such as 1, 4-polyisoprene [1123], silica-cellulose diacetate [154], PAN [1124], etc., have been investigated by this method.

Different solvent vapors can also be used for *in-situ* FTIR. For example, a micro-FTIR spectrometer was applied to collect *in-situ*

spectra of a cellulose nanofiber membrane over a wide range of relative humidity levels, with the aid of a specially designed sample chamber [1125]. This study provided valuable insights into the mechanism of water adsorption on cellulose nanofiber membranes and contributed to the search for optimal strategies to reduce water adsorption. It was also traced by FTIR measurements that the microstructure of syndiotactic PS chains transformed from amorphous as-spun fibers to form δ -crystallites, which was induced by the saturated solvent vapors [1126].

In the field of catalysis, *in-situ* FTIR is also widely used. In one study, [1127] electrospun amorphous carbon/reduced GO wrapped- Co_3O_4 ternary nanofibers were fabricated for an advanced ammonia sensor, and the underlying chemical sensing process was detected in detail by *in-situ* FTIR, indicating a water-mediated catalytic oxidation transducing mechanism. Under different light conditions, *in-situ* FTIR can be used to monitor the reaction process of photocatalysts and help researchers understand the corresponding photocatalytic mechanism [914]. In the aspect of electrocatalysis, *in-situ* FTIR coupled with voltammetry was performed to reveal ORR mechanism of carbon nitride-PAN nanofibers [1124].

4.2.4. *In-situ* Raman spectroscopy

Raman spectroscopy is a powerful technique for characterizing the vibration modes of molecules, offering high selectivity and availability [1128–1130]. This technique can provide rotational and vibrational modes of samples by measuring the inelastic scattering caused by changes in polarizability [1131,1132]. Recently, *in-situ* Raman measurements were utilized to understand electrocatalytic processes, elucidate the structure evolution of catalysts, and establish relationships between structure and performance [925,1133–1135]. As electrochemical measurements were usually performed in liquid electrolytes, the low Raman scattering cross-section of water makes Raman spectroscopy more viable for *in-situ* characterizations without any notable interference to the surface signal [1136–1139].

One application of *in-situ* Raman is to identify the active site of multiphase catalysts during the electrocatalytic water-splitting process. The interfacial active phases of $\text{Ni}_2\text{W}_4\text{C}-\text{W}_3\text{C}$ Janus structures for the hydrogen evolution reaction/oxygen evolution reaction (HER/OER) were investigated via *in-situ* Raman [1140]. During the OER operation with potentials from 0.5–1.1 V, the detected Raman peaks at 337 and 909 cm^{-1} for $\nu_{\text{W-OH}}$ and $\nu_{\text{W-OOH}}$ peaks of $\text{Ni}_2\text{W}_4\text{C}-\text{W}_3\text{C}$ enhanced gradually, suggesting the strong absorption of OH^- on W atoms and the continuous formation of OOH^* intermediates. For the HER process, there were no $\nu_{\text{W-OOH}}$ peaks observed with the increased potentials in the range of -1.2 – -1.5 V vs. hydrogen electrode. At -1.5 V vs. hydrogen electrode, the peak for $\nu_{\text{W-OH}}$ emerged at 909 cm^{-1} , demonstrating that the adsorbed water molecules dissociated into H_{ads} species and OH^- ions during cathodic polarization. In another study, the *in-situ* Raman was applied to investigate the real active sites in substituted Co_3C supported on CNF [1141]. The changes in Raman peak intensity for Co-OH bonds indicated that HER process generated the OH^- while the OER process consumed OH^- . The Raman peak intensity suggested the changes in the local concentration of OH^- , further demonstrating that the Co atoms in $\text{V}_{0.28}\text{Co}_{2.72}\text{C}$ were the absorption sites for the OH^- .

In-situ Raman is also used to explore the mechanism of gas catalysis. In one study, the reaction intermediates on AuNi alloy/CNF during electrochemical CO_2 reduction was monitored by *in-situ* Raman spectroscopy [1142]. Electrochemical N_2 reduction reaction recently became a hot spot in the electrocatalysis field, however, unveiling the reaction pathway remains a huge challenge [1143]. The time-dependent *in-situ* Raman spectroscopy was applied to capture the electrochemical N_2 reduction reaction (eNRR) intermediates [92]. The Raman peak emerged at 1525 cm^{-1} , ascribed to the $-\text{NH}$, gradually emerged and enhanced as the eNRR progressed, demonstrating the formation of $-\text{NH}$ intermediates on the surfaces of $\text{B}_{11}\text{-VC/CNF}$. In summary, the development of *in-situ* Raman characterization techniques accelerates the discovery and design of new catalytic materials for sustainable energy technologies.

4.2.5. *In-situ* XAFS

X-ray absorption spectroscopy (XAS) using synchrotron radiation sources provides atom-specific structural and elemental information in local environments, supplementing the limitations of vibrational analytical techniques [1144–1146]. Two typical regions of XAS are X-ray absorption near edge structure (XANES) and EXAFS [1146]. XANES is sensitive to oxidation states and electronic structures, while the EXAFS provides information on the coordination environments, including the coordination numbers and the bond distances [1147,1148]. Due to the high-energy synchrotron and strong penetrating ability, hard XAS makes it easy to perform operando measurements under ambient conditions [1149,1150].

Recently, synchrotron-based *in-situ* XAS was employed to probe the electronic structures and coordination environments of the electrocatalysts for photoelectrochemical water splitting [1151]. The *in-situ* XAS uncovered the chemical and structural changes that took place on both NiFeOOH and $\alpha\text{-Fe}_2\text{O}_3$ and suggested the spontaneous formation of FeOOH species at the hematite/ Ni(Fe)OOH interface. These findings possibly play an important role in dictating the charge carrier transfer across the interface. *In-situ* XAS has also been extensively utilized to probe the changes in electrocatalysts for the ORR, oxygen evolution, electrochemical CO_2 reduction (ECR), and CO oxidation [1152–1154]. For example, the *in-situ* XAS was used to investigate the synergistic catalytic effects of Co-Mn spinel oxide catalyst for ORR, suggesting the oxidation state changes of Co and Mn under both steady-state and non-steady-state conditions [1155]. Therefore, the Co-Mn spinel oxide catalyst exhibited a higher ORR activity than the individual $\text{Co}_3\text{O}_4/\text{C}$ and $\text{Mn}_3\text{O}_4/\text{C}$ and commercial Pt/C catalysts in alkaline fuel cells. Another study also focuses on the understanding of ORR. Nitrogen-doped carbon-supported Mn single atoms in the form of an Mn-N₄ structure were designed [1156]. The *in-situ* XAS revealed that the Mn active site changed with applied potential ($\text{OH}_{\text{ads}}\text{-Mn}^{\text{H}^+}\text{-N}_4 + \text{e}^- \leftrightarrow \text{Mn}^{\text{L}^+}\text{-N}_4 + \text{OH}^-$) during the alkaline ORR, suggesting that the $\text{Mn}^{\text{L}^+}\text{-N}_4$ without coverage of OH_{ads} was the catalytic center. The combined density functional theory calculations further demonstrated that the ORR performance was ascribed to much easier electron transfer from the $\text{Mn}^{\text{L}^+}\text{-N}_4$ site to the adsorbed $^*\text{OH}$ species, giving a high-power density and extraordinary durability. The fast *in-situ* XAS could also be applied to probe the evolving electronic and crystal structures under ECR conditions [1157]. In another study, high-pressure *in-situ* XAS was applied to correlate the structure,

composition, and catalytic performance of well-defined Cu and $\text{Cu}_{0.7}\text{Zn}_{0.3}$ nanoparticles supported on $\text{ZnO}/\text{Al}_2\text{O}_3$ for methanol synthesis reaction [1158]. The addition of Zn promoted the methanol formation selectivity for the $\text{CuZn}/\text{Al}_2\text{O}_3$ and the CuZn/SiO_2 catalysts, highlighting the importance of the intimate CuZn interaction for the $\text{CO}_2 + \text{CO}$ hydrogenation reaction. *In-situ* characterization techniques make the real-time monitoring of the structures of catalysts, the consumption and/or generation of intermediate species, and reaction processes at the catalyst/electrolyte interface [1147].

These above *in-situ* spectroscopic characterizations are based on different mechanisms and allow material analysis at the molecular and atomic levels. This has an irreplaceable great advantage for exploring the changes and related mechanisms of the composition and structure of electrospun fiber samples when physical or chemical changes occur. Looking forward to the future, by combining different characterization methods to conduct multi-angle and all-round *in-situ* analysis of electrospun nanofibers, it is believed that it will help to understand the formation and reaction mechanisms of various electrospun nanofibers more comprehensively.

4.3. *In-situ* microscopy characterization

Versatile physical/chemical changes (including fracture, failure, and crystal growth) always occur during the fabrication and utilization of nanofibers. *In-situ* microscopy techniques can dynamically observe the change in microstructure and even on the atomic scale. Among these methods, *in-situ* TEM, SEM, and fluorescence microscopy provide important means for understanding the properties of electrospun fibers.

4.3.1. *In-situ* TEM characterization

Recently, *in-situ* TEM has played an important role in exploring the formation of nanofibers and revealing the molecular or atomic mechanism involving structural evolution and property changes due to its high resolution, attracting considerable attention from researchers. TEM allows direct observation of dynamic changes under different conditions. At the same time, it is superior and comprehensive. It can also present many aspects of information including morphology, structure, and composition with the help of other attachments such as selected area electron diffraction, energy dispersive spectroscopy, electron energy loss spectroscopy, *etc.* The combined techniques give a direct observation under different external stimuli to explore micromechanical properties among atoms, the atomic behavior of high-temperature reactions, the migration and morphology change of substances during the reaction process, *etc.*

In-situ TEM provides an important theoretical basis for studying the mechanism of nanofiber formation behavior, structural evolution, and property change. In terms of the nanofiber formation process and involved structural evolution, *in-situ* TEM directly helps us understand the active state, structure, chemical distribution of elements, and diffusion mode of carbon atoms during the formation of nanomaterials at the atomic level. For example, to deepen the in-depth understanding of the active state and active structure of alloy catalysts, Huang's team [1159] used *in-situ* TEM technology to study the dynamic changes of Ni-Co bimetallic catalysts in the growth of carbon nanofibers. They prepared *in-situ* TEM samples by injecting suspended liquid of catalyst precursor onto a micro-electro-mechanical system heating chip. After plasma cleaning, the loaded chip was installed in a fixator, subsequently, it was inserted into the TEM chamber where the growth of carbon nanofibers was studied in a reaction atmosphere of a mixture of C_2H_4 , H_2 , and He (volume ratio 1:1:2) at 300 kV and 550 °C. Real-time TEM imaging showed that the prepared alloy catalyst was highly dynamic, showing periodic deformation (elongation/contraction cycles) during the growth of the carbon nanofibers. Fragmentation of catalyst nanoparticles was observed associated with catalyst deactivation and termination of carbon nanofiber growth. High-resolution atomic scale imaging combined with *in-situ* electron energy loss spectroscopy further determined the active structure as a face-centered cubic Ni-Co bimetallic alloy.

Similarly, Yassar et al. [1160] studied the formation and stability of metal nanoparticles on carbon nanofiber carriers using an electrical-biasing *in-situ* TEM device and simulated high-temperature impact method. They first did this by impregnating carbon nanofibers in a solution of metal salt precursors, followed by Joule heating in a TEM. *In-situ* observation results showed that the formation of metal nanoparticles was closely related to the synchronous crystallization of carbon nanofibers. The phase transition from amorphous carbon nanofibers to disordered turbostratic graphite was accompanied by the formation of defect edge planes and volume expansion, which provided an ideal site for the nucleation and stabilization of nanoparticles. Through the intercalation of metal atoms, strong bonding was formed to enhance its thermal stability. In summary, *in-situ* TEM can provide an intuitive view of the formation mechanisms of nanomaterials at the atomic scale.

In view of nanofiber structural evolution and property change characterization, it is intriguing to explore the impact of mechanical strength on the structural integration of nanofibers using *in-situ* TEM, which can provide a direct and quantitative way to investigate the micromechanical properties and the tensile stress- and strain-induced structural transformation. In one study, a device was set up in combination with the *in-situ* TEM to clarify the bond nature in the Pt monatomic chain, indicating the string tension between the Pt atoms [1161] (Fig. 25A). Furthermore, microelectromechanical system (MEMS) device at the nanoscale, tensile stress at a value of up to about 5 GPa was applied to individual gallium arsenide (GaAs) nanowires (Fig. 25B–F) [1162]. The local strain within the nanowire along the length and the perpendicular directions were measured, respectively, by *in-situ* scanning TEM-nanobeam electron diffraction. To explore the mechanical stress- and strain-induced modification in the charge transport properties, an electrical measurement device within *in-situ* TEM was set up. The conductivity of the nanowires was reduced under tensile strains. Such a phenomenon in GaAs nanowires was derived from the modification of the valence band structure during the straining. Through *in-situ* TEM, the intriguing correlation among lattice deformation, band structure, and charge transport in electrospun nanofibers can be better investigated.

Currently, liquid-cell electron microscopy attracts much attention because of its ability to *in-situ* image liquid-phase dynamics at nano or even atomic-scale resolution. Many studies have explored dynamical events in liquids by focusing on only one cell. Versatile

and substantial liquid cells were fabricated by coaxial electrospinning to demonstrate the bubble dynamics and the bubble-driven Au nanoparticle motions statistically using *in-situ* TEM [1163]. Additionally, the *in-situ* TEM systems can be combined with the optical *in-situ* studies. For example, an *in-situ* photon delivery system was developed by Waviks Inc. and could be mounted on any scanning TEM system as an assist [820].

In-situ TEM has been used to observe and understand the chemical reaction phenomenon of nanofibers with *in-situ* heating as well. For instance, it can be applied to the research of making high-quality contacts on semiconductors by exploring the axial metal–semiconductor interface. In one study, the Cu-Ge nanowire solid-state reaction in the nanometer spatial resolution was observed by using *in-situ* heating in TEM [1164]. The thermal stability of inorganic nanomaterials is crucial for their catalytic performance. *In-situ* heating TEM under an O₂ environment revealed sintering and structural decomposition of CeO₂ [1165].

The structural performance of nanowire electrode materials in batteries can be observed in real-time at the atomic scale through *in-situ* TEM, which is the key to the design and improvement of electrode materials. For example, the *in-situ* cycling rate performance of vanadium oxide-coated tin dioxide nanowire electrode was observed under the *in-situ* open-cell TEM while tuning the lithiation/delithiation current (Fig. 26) [1166]. The layered vanadium oxide coating strategy led to the good rate performance of such a high-capacity compositional material. Besides, the *in-situ* high-resolution TEM was applied to observe the lithiation/delithiation of LiFePO₄ nanowires in real-time at the atomic level [1167]. Li-sublattice disordered solid-solution zone was preferentially formed at the surface of the nanowires during electrochemical delithiation. In another study, *in-situ* TEM was applied to study suitable electrode materials for potassium-ion batteries, the robust structural integrity of the red P encapsulated nitrogen-doped porous hollow carbon nanofibers matrix electrode with small volume expansion during potassiation [1168]. Additionally, the evolution of nanofiber in the field emission process can also be observed by *in-situ* TEM. The change of structure and electrical property of Fe-included carbon nanofibers was observed under *in-situ* TEM [1169]. The fibrous amorphous and/or very fine crystallites changed into the graphitic hollow structure, and thus the electrical property was improved. This kind of *in-situ* TEM research of carbon nanofibers can offer significant information to benefit the application of electron-emitter sources in the future.

4.3.2. *In-situ* SEM characterization

In-situ SEM enables the identification of element distribution and content in nanofibers, as well as the measurement of their mechanical properties. Its advantages lie in the large sample space, low damage, and minimal requirement for environmental vacuum, allowing for the analysis of material deformation, fracture micro-zones, and chemical reactions in the specimen storehouse. There are some reports on the experimental methods of studying the structural changes of fibrous materials by *in-situ* SEM.

First, *in-situ* SEM can be used to test the mechanical properties of nanofibers. For example, to uncover the relationship between the cycle life of electrode materials and their mechanical properties, the tensile strength of Si nanowires was measured, and Young's modulus was calculated by the *in-situ* SEM strategy with a microelectromechanical force sensor and piezo-driven actuator [1170]. Additionally, real-time observation of the cracking process of nanofibrous materials by *in-situ* SEM plays an important role in the study of their failure mechanism. To reveal the super-elasticity and fatigue resistance characteristics of hard carbon aerogel composed of carbon fiber network, the stress and strain process of CNF network structural materials were monitored in real-time through *in-situ* SEM (Fig. 27) [1171]. The results showed that the overall structure of the hard carbon aerogels was restored to its virgin shape even after 50% compression, and there was no obvious structural damage or irreversible deformation. *In-situ* SEM observation further confirmed that the excellent mechanical properties of hard carbon aerogels were ascribed to the hard carbon welds between fibers in the nanofiber network.

Recently, *in-situ* SEM has also been widely used to solve the problem of correlation and coupling between electrochemical and mechanical properties of sensing materials, which deepens the comprehension of the functional mechanism of electrode materials. *In-situ* SEM was employed to reveal the conductivity and sensing pathways of CNT fibers in the bionic flexible double-sided electronic skin (Fig. 28) [1172]. In detail, mechanical components were used in a SEM to apply forces to the carbon nanotube sponge. The deformation of the microfibers in the carbon nanotube sponge under external forces and the successive contact process of the deformed fibers were also monitored in real time. The carbon nanotube fibers passed through each other to establish contact points, forming new conductive paths. This also explained the sensing principle of piezoresistive sensors and realized the detection of force direction, which would be of great significance for the application of the future human–computer interaction field.

In addition to testing the mechanical properties of materials, *in-situ* SEM can also be applied to evaluate the effect of molding and modification of nanofibers. The electrochemical deposition and dissolution behavior of sodium metal on CNF current collector was observed in real-time at the nanoscale using the *in-situ* SEM technique (Fig. 29) [1173]. These findings provided a possible solution for uniform deposition of sodium metal on the negative electrode structure of fibrous form, inhibition of dendrite growth, and full utilization of the internal space of the collector, which is an important guideline for the development of high-efficiency all-solid-state sodium metal battery systems (e.g., NaO₂, NaS).

4.3.3. *In-situ* fluorescence microscopy characterization

Fluorescence microscopy can characterize fluorescent substances for element tracking, morphology observation, and physical performance analysis, raising continual interest in the characterization of electrospun nanofibers. The normal fluorescence techniques required complicated sample preparation. One specific property tended to be confirmed by a combination of two or more types of equipment. Moreover, it could only gain results for a single point in time. The exploration of the reaction process and the local variations is always a great challenge.

With the advent of super-resolution and single-molecule fluorescence techniques, the real-time monitoring of single-molecular diffusion and orientation, as well as morphology and dynamic interactions in nanoscale materials has been realized. Confocal

fluorescence microscopy has become popular in the field of nanofibers because of its high resolution and real-time dynamic monitoring of microstructures. The fibers can be viewed from any perspective without physical cutting, which is convenient for measurements of fiber dimensions, microfibril angle, and 3D structure. Real-time analysis of process parameters helps to get more accurate conclusions and a better understanding of the mechanism. In the 1990 s, Jang *et al.* [1174] successfully developed an image analysis procedure, in which the fiber cross-sectional area and wall thickness could be indirectly defined with a maximum-gradient edge-finding technique. They measured the transverse dimensions of wood pulp fibers under the monitor of confocal laser scanning microscopy. In the following years, the Jang research group still strived in the confocal detection of fibers and obtained the evolvement rule of fibril angle, collapse behavior, fiber coarseness, and structural analysis.

Recently, significant efforts have focused on *in-situ* fluorescence microscopy characterization of nanofibers, particularly their adsorption properties. Li *et al.* [1175] reported a quantitative measurement, which could study the dynamic adsorption of ciprofloxacin on CNF. In virtue of fluorescence spectrometer, they converted the fluorescence intensity into the concentration of ciprofloxacin *in-situ*, which exhibited excellent correspondence with the pseudo-second-order model and the Langmuir model, respectively. Nanofibers doped with fluorescent agents were also used as an acid indicator. Electrospun nano-porous luminescence PET nanofibers showed extremely excellent adsorption of acid gases [1176]. The superior property made it a preference as a rapid indicator for acid gases as there was a linear relationship between acid gas concentration and fluorescence intensity. The process could be accomplished within 10 s and all the fibers could be recycled for further use.

Nowadays, *in-situ* fluorescence microscopy has been applied to medical, material, chemical and physical fields, *etc.* Although confocal fluorescence microscopy is well-known as high-resolution and easy to operate, it is limited to such specific excitation wavelengths, resulting in the limitation of its application scope. Furthermore, according to the site testing, experimental results are often subjected to the surrounding environment, the laser-induced fluorescence systems, and the fluorescence reagents. As a result, external interference may be a great challenge for relevant experiments.

To observe the microstructure and internal structure of nanofibers, it is inevitable to use *in-situ* TEM and SEM techniques. In addition, *in-situ* observation based on fluorescence microscopy can characterize the structure as well as the function of the nanofibers and ensure that the material can be recycled for further use. Therefore, *in-situ* fluorescence microscopy may play an important role in the development and service process detection of nanofibers and their derivations. *In-situ* tools may be used more and more widely in the characterization of materials by the further combination of these techniques. Moreover, with the development of technology, the characterizations are expected to be easier to operate, and the new *in-situ* methods are expected greatly. The advantages and disadvantages of the different methods are displayed in Table 4.

Although these advanced characterization techniques have made breakthrough progress in the field of basic scientific research, at present, the transition from fundamental research to industrial quality control poses significant challenges for advanced *in-situ* characterization techniques. The key challenges and potential solutions are as follows:

(1) Cost and Complexity: The high cost and technical complexity of *in-situ* characterization equipment, along with the need for skilled operators, hinder its integration into large-scale production lines. Future efforts should focus on developing cost-effective, user-friendly instruments with simplified interfaces and increased automation. Miniaturized and modular designs for portable *in-situ* devices suited to industrial environments are also needed.

(2) Characterization Speed and Data Processing: High temporal and spatial resolution *in-situ* techniques require substantial time for data acquisition and processing, while industrial lines demand real-time or rapid detection. Fast-scanning and automated data processing algorithms are essential for enhancing efficiency. Integrating machine learning and artificial intelligence will enable automated analysis and defect identification.

(3) Sample Preparation Complexity: Many *in-situ* techniques, particularly TEM, involve complex sample preparation, which limits large-scale application. Simplifying preparation procedures and developing fast, minimal-treatment methods are critical. Research on non-destructive or in-line characterization techniques will further reduce preprocessing requirements.

(4) Environmental and Operational Conditions: Industrial settings often present vibrations, temperature fluctuations, and other adverse conditions compromising stability and accuracy. More robust and adaptable equipment designs, combined with vibration isolation and temperature control systems, are necessary to ensure reliable performance in challenging environments.

(5) Data Standardization and Reliability: *In-situ* characterization techniques generate complex data, with potential inconsistencies across different methods and instruments, complicating quality control standardization. Therefore, we should establish industry standards and guidelines to ensure data comparability, along with unified databases and reference samples for calibration and validation, is imperative.

In summary, *in-situ* characterization holds great promise for industrial quality control, but overcoming current barriers requires advances in cost reduction, automation, rapid detection, and standardization. Multidisciplinary collaboration and technological innovation are key drivers for this transformation.

5. Electrospun nanofibers in industry

Over the past decades, electrospun nanofiber technology has made tremendous progress in the laboratory, with its ability to enable the preparation of highly efficient, versatile, and controllable nanofibers by controlling the charge, electric field and rheological properties as well as the choice of materials. How to migrate these laboratory results to industry remains a challenging task. Industrialization requires higher manufacturing efficiency, more stable process control, and flexibility to adapt to different industrial needs. This chapter will delve into the breakthrough applications of electrospun nanofibers in industry, covering a wide range of aspects from industrial equipment, manufacturing technology, and product structure to marketing, as well as the problems, challenges, and

possibilities.

5.1. Industrial equipment and manufacturing technology

The high-value end-product opportunities of electrospun nanofibers have promoted the rapid development of electrospinning industrial equipment. The main challenge lies in improving the production efficiency and operational stability of industrial systems. In the past two decades, experts from academia and industry have proposed new principles and methods to launch industrial electrospinning systems. Currently, needle-array systems and needleless systems of electrospinning devices for mass production have been developed and gradually applied in the industry [1177]. Additionally, the combination of 3D printing and straight line of electrospinning jet, so-called electro-hydrodynamic direct-writing [1178], has aroused great attention because fine fiber diameter and constructability of 3D topology can be obtained. As the demand for nanofiber-based products continues to grow, ongoing research and technological advancements in electrospinning will further drive the progress of industrial-scale production. By addressing the challenges of production efficiency and system stability, electrospinning technology has the potential to revolutionize various industries and pave the way for new applications and breakthroughs.

5.1.1. Needle-arrays systems

Conventional single-needle electrospinning systems have very low nanofiber production efficiency and can only achieve a flow rate of 0.1–5 mL/h, with a final fiber yield of only 0.1–1.0 g/h [1179–1181]. Multi-needle or needle-array systems are a replication of the single-needle laboratory system, which can substantially increase production and have been widely used in industrial electrospinning machines (Table 5). However, it still presents several challenges: (i) inhibition and maldistribution of the jet caused by the superposition principle of electric field [1182], (ii) significant evaporation of solvent in solution electrospinning, and (iii) running interruption due to blockage at needle-tips [1183].

Theoretically, the higher the density of the needle array, the higher the efficiency of electrospinning. However, the superposition principle of electric fields may result in lower electric field intensity for the needles in the central region, while those in the exterior zone experience higher electric field intensity [1184]. In the central region, some of the needles may not undergo jetting, whereas needles in the exterior zone demonstrate a noticeable whipping effect and result in a larger deposition area. Therefore, controlling the strength of the electric field at the location of each needle so that it remains consistent is central to optimizing the needle array system.

Introducing electrodes is an efficient way to scale up multi-needle electrospinning processes. A variety of auxiliary electrodes can be employed to generate secondary electric fields in the needle arrays to ensure overall electric field uniformity. For example, Kim *et al.* [1185] added a cylindrical electrode around the five-needle system in 2006 and revealed that the initial streamlines and jets of nanofibers from the nozzles could maintain stable jet motion without any interruption near charged jets. Therefore, this method significantly enhanced the productivity of nanofibers to its maximum potential. In 2010, a shield ring was utilized on multiple needles, and the uniform electric field near the tips of the needles produced the same effect [1186]. In 2012, an auxiliary plate was connected to a three-needle system to improve the electrospinning efficiency and achieve uniform fiber distribution [1187]. In 2019, a needle-assisted electrode was introduced into a multi-needle system, and the electrospinning efficiency was seven times higher and resulted in thinner and more evenly distributed nanofibers [1188]. In 2022, a laterally charged plate was applied as an auxiliary electrode in a linear array of 20 needles, achieving electric field homogenization [1189]. Incorporating a parallel side plate as an auxiliary electrode in the multi-needle electrospinning process facilitates the homogenization of the electric field, semi-vertical angle of the electrospinning jet, and fiber deposition area.

Adjusting the needle arrangement pattern, including the arrangement of needles and their spacing, is another efficient way to achieve electric field uniformity under the combined effect of the external electric field and the repulsive force between the jets. In 2005, three types of multi-jet electrospinning heads: series, elliptic and concentric were developed, and the concentric electrospinning head was determined to be the most efficient type, with a high productivity of 1 mg PVA per minute [1190]. In 2014, various arrangements of 1–7 nozzles were designed, and the degrees of nanofibers and breaking stress of filaments decreased as the average offsets increased for the same number of needles [1191]. In 2015, the mass production of electrospun nanofibers was achieved by a modified upward cylindrical-type multi-nozzles system in both laboratory and industrial settings [1192]. In 2018, three types of needle distribution with higher needle density were designed, the trapezoidal arrangement at a distance of 15 mm produced a homogeneous electric field, while other arrangements required a distance of over 30 mm [1193]. The height of the needles or their distance from each other can also be adjusted to create a uniform electric field with multiple needles. By adjusting the needle length to create a convex arc at the tip of the needles, the homogeneous field intensity was achieved [1194]. This method was also applied by other researchers to eliminate the “end effect” [1195]. In 2020, needles arranged in an arc array could result in a uniform field intensity [1196,1197].

Besides the induction of needle arrays, another way to improve the efficiency of needle electrospinning is to utilize air assist to increase the jet flow rate and improve jet stability. In 2014, a modified air-jet electrospinning technology was developed to achieve a 40-fold increase compared to the single-needle electrospinning setup [1198]. In 2020, an air cover was designed to assist airflow on the basis of an arc array needle, and the critical voltage of the jet was reduced, and the electrospinning efficiency and stability were improved with the addition of the auxiliary airflow [1196]. In the same year, coaxial gas-assisted needle was designed with an intermediate shaft supplying gas and the outer shaft supplying solution, and 4.7 times higher productivity was achieved than that without gas assistance [23].

Unsuitable electric field strength, flow rate, and solvent volatility may lead to clogging of the needle tip, causing interruption of fluid flow. To solve this problem, using a large-diameter needle and high flow rates could effectively avoid blocking the needle tip

[1199]. The stability of multi-needle electrospinning technology can be effectively enhanced through the methods. At the same time, these methods can be combined to further enhance the stability of multi-needle electrospinning. It is believed that through continuous research and technical advancements, the stability and fiber quality of this technology can be further enhanced, enabling it to play a more significant role in practical applications.

5.1.2. Needleless electrospinning

Needleless electrospinning involves creating multiple jets of polymer solution or melts on a free surface under high electric field intensity, eliminating the need for conventional needle-like structures. The concept of needleless electrospinning was first introduced in a patent back in 1979, which proposed the use of a ringlike nozzle [1200]. Subsequently, the Czech Republic made significant advancements in 2004 by developing needleless electrospinning equipment that utilized a rotating roller and wire electrode [1201]. This breakthrough not only facilitated the industrialization of the technology but also gave rise to the establishment of the well-known national brand “Nanospider”. The structural differences allow needleless electrospinning to avoid the problems associated with traditional multi-needle electrospinning methods and offer improved efficiency, reduced clogging, and enhanced practicality. With continuous research and development, it holds promising potential for various applications in the field of nanofiber production and beyond.

As shown in Table 6, different types of needleless electrospinning equipment have been developed to reduce the required voltage and increase production yield. The shape of the nozzle surface in these devices ranges from flat to curved, from 2D to 3D, to maximize the nozzle output while ensuring uniform electric field strength. The simplest linear spinning system, for example, can be categorized into wire electrospinning (Fig. 30A) [1202], linear laser electrospinning [1203], linear melt differential electrospinning (Fig. 30B) [1204], moving conventional yarn (Fig. 30C) [1205], and linear flume nozzle (Fig. 30D) [1206]. These systems are relatively easier to operate compared to needle-array systems. On the other hand, curved structures encompass spiral coils (Fig. 30E) [1207], rotary cones [1208], parallel ring arrays [1209], wheel nozzle [1210], umbrella-like melt differential nozzle (Fig. 30F) [1211], string electrospinning [1212], and annular nozzle [1213]. These curved structures lead to a more uniform distribution of jets due to the homogenization effect caused by repulsion between adjacent jets. Additionally, multiple jets can be categorized from cylinder [1214], splashing [1215], bubbles [1216], and magnetic fluid as curved surface systems, which eliminate the need for complicated flow rate control but may require higher voltage. Systems based on 3D structure, such as pyramid (Fig. 30G) [1217], conical wire coil (Fig. 30H) [1218], threaded rod nozzle [1219], and two-level coil [1220], exhibit higher efficiency in converting polymer solutions into nanofibers.

A major challenge faced by the industry is the solidification of the solution remaining on the surface of the needleless nozzle, due to the large free liquid surface of the open vessel which is susceptible to solvent evaporation, water vapor absorption, etc. To address this issue, researchers often employ a screening board in needleless electrospinning with a bathing or dipping system. This board covers the solution tank to slow down solvent volatilization and maintain the solution concentration. Elmarco’s “Nanospider” technology introduces a moving case attached to a wire electrode which clears and coats the solution during each cycle, thereby enhancing efficiency. This concept has also been applied to the online self-cleaning threaded rod nozzle to further improve efficiency [1243].

Apart from the advancements in nozzle design, efforts are being made to optimize the process parameters and improve overall system efficiency [1244]. Optimizing parameters such as electric field intensity, solution concentration, flow rate, and nozzle rotation speed can significantly impact the electrospinning process and resultant nanofiber characteristics. Additionally, from an industrialization perspective, ongoing research is focused on improving the scalability and reproducibility of needleless electrospinning technology, which is crucial for successful integration into various industries. It is essential to scale up the process for large-scale production without compromising the quality and uniformity of nanofibers.

In conclusion, needleless electrospinning has witnessed significant progress and presents a promising alternative to traditional needle-based electrospinning. The diversification of nozzle designs, continuous optimization of process parameters, and exploration of new materials are driving the technology forward. As researchers and industries collaborate to address challenges and discover new opportunities, needleless electrospinning is poised to play an increasingly vital role in the nanofiber manufacturing landscape.

5.1.3. 3D printed electrospinning

Direct-writing electrospinning (DWE) technology can combine the advantages of traditional electrospinning and 3D printing while mitigating their disadvantages, enabling the accurate regulation of both deposition points and the number of layers for achieving a 3D structure with electrospun fibers [977,1245]. In DWE, the electrospinning head (or spinning nozzle) can follow a program-controlled path, so that programmed 3D fiber structures with excellent orientation can be obtained in DWE. In contrast to additive manufacturing technology, DWE provides the optimal balance between high resolution and production speed through electrically induced stretching. DWE can be classified into solution and melt DWE based on the employed material state. The former is often called NFES because of the short spinning distance [45], while the latter is named melt electrowriting (MEW) [1246]. Although the materials applied are different, the critical concern in the DWE process remains controlling the pathway of a single jet and its precise deposition. In general, there are three ways to realize the precise deposition of fibers during the DWE: *i*) using a stable straight jet trajectory to limit the collection distance to a few millimeters to centimeters; *ii*) reducing the applied voltage to reduce the jet whip during electrospinning; *iii*) using a moving stage as a collector paired with precise relative motion between it and the polymer source, which exerts a drag force on the jet to force its flight along a straight path. Nowadays, using the above three strategies ultimately results in precisely programmed geometries.

The development of DWE has undergone several stages. In 2003, Kameoka *et al.* [1247] proposed a method of preparing ordered patterned fibers by electrospinning. A silicon scanning tip was used as a nozzle immersed in a polymer solution, and the collection

distance and applied voltage were reduced to 0.5–1 cm and 4–6 kV, respectively. This was the first report of obtaining the electrospun fibers orderly using the DWE technique. Although this research provided a foundation for further exploration of DWE, the alignment degree of the deposited fiber is relatively low. To enhance the alignment of the single fiber, a method of direct-writing nanofibers using a tungsten tip nozzle and a controllable x-y stage was proposed [1208]. By further reducing both the spinning distance and voltage to 500 μm and 600 V, respectively, this approach achieved significant improvements in order degree. The concept of NFES is illustrated in Fig. 31 [1248]. This study provided a one-step method for preparing pre-designed fibers. Furthermore, 3D PEO fibers were made under an extremely low spinning voltage of 200 V [1249].

To meet the demands of various applications, researchers have begun developing melt DWE. In 2011, the MEW technique using melt polymer as a spinning source was applied to produce ordered fibers for bioengineering applications [1178]. The viscosity of the polymer source was higher than that of NFES in this process, which suppressed the whipping of the jet and resulted in a long, straight, and stable path for the jet. In brief, the DWE technology has undergone rapid development in less than 20 years, progressing from initial orderly fiber deposition to complex 3D structure construction. In terms of precise deposition, high resolution, and eco-friendliness, the DWE technique would become one of the main manners of manufacturing complicated 3D models in the future.

Nowadays, the research of DWE mainly focuses on the following aspects [1245,1250]. Firstly, the success of constructing a pre-designed model by DWE primarily depends on the relative motion between the jet speed and the collector translation speed [1245]. Increasing the translation speed of the collector causes the jet path to deviate from its straight-line trajectory due to the strong drag force induced by the motion of the collector (Fig. 32A–C). Only when the translational speed of the fiber collector exceeds the jet velocity can the jet channel remain straight and orderly for fiber deposition. This collector translation speed is called critical translation speed. Furthermore, as the jet speed remains constant, the deposited fibers transition from a coiled state to a straight state with an increasing translation speed of the collector (Fig. 32D–G). Although critical translation speed plays a significant role in the DWE process, other processing parameters such as voltage, needle-to-collector distance, raw materials, temperature, and humidity are equally important for ensuring high-quality output. Specifically, increasing the electrospinning voltage can cause disordered fiber deposition by increasing the speed and whipping of the jet. It should be noted that DWE fibers are usually coarser than those obtained from traditional electrospinning, which may limit its application.

Secondly, the improvement of DWE apparatus can be categorized into three main aspects. One is realizing the manipulation of processing parameters by creating DWE setup. For example, the use of print omics has been demonstrated to inspect processing parameters through the digital loop of inputs/outputs, enabling real-time automated parameter control [1251]. The second method involves scaling up systems to meet industry output requirements, with the most commonly used approach being the implementation of multiple nozzles [1252–1254]. The final approach involves integrating other technologies, such as traditional electrospinning [1255,1256], coaxial electrospinning [1257,1258], and 3D printing [1259], to make structures with special functions. Furthermore, commonly employed materials include various polymers, and researchers are also investigating the materials utilized in DWE to enhance the versatility of this technique [1260,1261]. Finally, it is about finding the potential applications of the DWE technique, which is mostly used in electronic components, flexible devices, and biomedical scaffolds.

In conclusion, DWE is a technique that evolved from the combination of traditional electrospinning and 3D printing. It exhibits clear advantages over both methods. Compared to traditional electrospinning, DWE can achieve ordered patterns, while compared to 3D printing, it offers higher resolution capabilities. Over time, DWE has made significant progress in terms of process, setup, materials, and applications. However, several weaknesses need to be overcome: (i) the thicker fibers compared to traditional electrospinning; (ii) the effect of processing parameters matching on the fiber path; (iii) the influence of residual charge on the accuracy of deposition and height of the 3D structure; (iv) low production efficiency. To solve the above problems and broaden the applications of the DWE approach, the prospects of this technique will be driven by the following aspects: (i) optimizing the parameters and processing techniques, selecting suitable materials and reducing fiber diameter; (ii) developing economical DWE equipment with a well-programmed system; (iii) exploring alternative methods for scale-up production, apart from multiple nozzles; (iv) employing coating or additives to expand the ranges of materials; (v) exploring the principle of DWE technique based on theoretical simulation and path planning. By addressing these challenges and exploring the potential improvements, the application of DWE is expected to expand further, enabling its adoption in a wider range of fields and opening new opportunities for precise and scalable nanofiber fabrication.

5.2. Structure of nanofibrous products for various applications

The fibrous structure of electrospun products is highly influenced by the specific application. In general, nanofibrous structures can be classified into four main types: supported nanofiber membrane, self-supported nanofiber membrane, nanofiber yarn, and composite nanofiber yarn. Understanding the unique characteristics and properties of these nanofibrous structures is crucial in customizing electrospun products to meet diverse application requirements. By leveraging the advantages offered by these structures and optimizing their fabrication techniques, researchers and industry can further unlock the potential of electrospun products in various fields.

5.2.1. Supported nanofiber membrane

This type of structure involves depositing nanofibers onto a solid substrate or support material. The presence of a supporting layer enhances mechanical strength and stability, making it ideal for applications requiring robust filtration, separation, and protective barriers. To improve the mechanical durability of electrospun nanofibers, they are usually supported on a substrate consisting of microfibrillar materials whose intrinsic mechanical behavior is different from that of electrospun nanofibers. This ensures their ability to withstand mechanical impact when used in various applications such as air filters, water treatment membranes, and waterproof and

moisture-permeable fabrics.

For example, nanofiber-based air filters with high efficiency have been available on the market for over 30 years (Fig. 33A) [165]. Electrospun nanofiber membranes can significantly improve air filtration efficiency for blocking particulate dust while maintaining a low-pressure drop with a thin layer. Similarly, the COVID-19 outbreak has spurred significant advancements in the development of advanced facemasks and protective clothing that offer superior protection while maintaining wear comfort [1262]. Within the past several years, numerous commercial facemasks featuring a nanofibrous layer have been introduced to the market. In these products, a thin layer of nanofibers is directly electrospun onto a conventional melt-blown or spun-bond nonwoven fabric [1263,1264]. By utilizing nonwoven fabric for mechanical stability and processability, the addition of a thin layer of nanofibers can significantly enhance filtration efficiency while having a minimal impact on breathing resistance.

These examples illustrate the practical benefits of using supported nanofiber structures in real-world applications. The combination of electrospun nanofibers and a suitable substrate material allows for the simultaneous customization of mechanical properties and functionality, enabling their successful integration into a wide range of advanced products and technologies. Continued research and innovation in this area hold great promise for further enhancing the performance and versatility of supported nanofiber membranes in diverse industrial and healthcare applications.

5.2.2. Self-supported nanofiber membrane

Self-supported nanofiber membranes are freestanding and do not rely on additional support, which possess distinct advantages in applications independently requiring high mechanical integrity and performance [1267]. For example, PI is a high-performance polymer that yields electrospun nanofibers with outstanding mechanical properties. Based on their porosity and thickness, self-supported PI nanofiber membranes could serve as advanced separators in various types of batteries, which exhibited excellent thermal stability, significantly enhancing operational safety and reducing charging time (Fig. 33B) [1265]. Through designing nanofibrous membranes for enhanced functionality, further research and optimization of self-supported nanofibrous membranes are critical to unlocking their full potential in driving the next generation of innovative and efficient devices. It also holds great promise for advancing various fields such as sustainable energy technologies.

5.2.3. Nanofiber yarn

Nanofiber yarn is formed by collecting and twisting electrospun nanofibers into continuous and thread-like flexible structures, which have been applied in various fields, including textiles, wearable electronics, and biomedical applications [1268,1269]. Various techniques have been developed to produce nanofiber yarns, including the auxiliary electrode method [1270], water bath method [1271], and rotating collector method [1207]. For example, it is possible to continuously manufacture nanofiber yarn by employing a rotating funnel as an intermediate collector to create a cone-shaped fibrous structure prior to being drawn into a nanofibrous yarn structure (Fig. 33C) [1207]. The twist level of the nanofiber yarn can be effectively controlled by adjusting the rotating speed of the device (Fig. 33D). Various polymeric materials have been successfully transformed into nanofiber yarns, which can be utilized independently [1272] or further processed to create woven or knitted textile structures for various applications, such as tissue scaffolds [1273] and strain sensors [1274]. With the production of nanofiber yarns by these innovative technologies, the application potential of electrospinning can be extended beyond fiber membranes. In addition, the versatility of nanofiber yarns offers new opportunities for integrating nanofiber structures into traditional textile processing, allowing for the creation of functional fabrics with enhanced properties. The continued advancement of nanofiber yarn production and its integration into textiles hold promise for driving innovation in various industries.

5.2.4. Composite nanofiber yarn

Composite nanofiber yarn is a textile material that consists of a combination of two or more different types of nanofibers, which gives extensive potential applications in various fields [1274–1276]. By utilizing the manufacturing techniques for nanofiber yarn, it is possible to produce composite nanofiber yarns that exhibit improved application performance or additional functionalities. For example, by wrapping electrospun PAN nanofiber threads onto commercial cotton yarn and carbonizing the composite structure, a highly sensitive yarn-structured strain sensor was created for wearable electronic applications [1277]. Electrospinning can be further integrated with the fiber web processing of traditional textile engineering to achieve large-scale production of composite nanofiber yarns [1278]. In this method, nanofibers are electrospun onto a regular fiber web before undergoing drawing, roving, and spinning processes. As a result, the produced composite yarn contains nanofibers that are distributed and composed in a controlled manner (Fig. 33E) [1266]. By combining electrospun nanofibers with conventional textile fibers, composite nanofiber yarns not only increase surface area but also offer additional functions, such as moisture release/transfer [1266] and antibacterial properties [1279]. This innovative approach opens up more possibilities for the emerging application of nanofibers while expanding the functionalities of traditional textile materials. The prospects for the application of composite nanofiber yarns are highly promising in various fields, including smart textiles, sensors, and medical materials.

5.3. 5.3 Major manufacturers and batch-produced products of electrospun nanofibers

5.3.1. Market demand and major manufacturers

Electrospinning is currently experiencing steady growth in market demand. The significant attention garnered across various industries can be attributed to its high efficiency, low cost, diverse applications, and wide-ranging applicability. At present, its main market demand is as follows. (i) Biomedical and healthcare applications: electrospinning technology is extensively utilized in the

medical field to produce medical-grade nanofiber materials, such as medical masks, band-aids, wound dressings, and tissue engineering scaffolds, and the demand for high-efficiency filtration and protective performance has significantly increased, especially in response to the COVID-19 outbreak. (ii) Environmental protection and filtration: electrospun fiber products have been applied in air filtration, water treatment, and pollutant capture, particularly in automotive, industrial, and household applications. (iii) New energy and electronics: electrospun fibers have been applied to electrode materials to enhance the energy density, conductivity and flexibility of batteries and supercapacitors for a variety of electronic products. (iv) Textile and clothing industry: electrospun fibers can be used for functional modification of textiles, such as enhancing the waterproof, antibacterial, moisture-regulating, and flame-retardant properties of the fabrics. There are many electrospinning equipment manufacturers around the world, such as Elmarco/Nanospider, Electrospinning Company, Inovenso, Linari Engineering and Beijing Beijing Ruili Analytical Instrument (China) Co., Ltd., which constantly promote the innovation and development of electrospinning technology. With the continuous expansion of the application of electrospinning in many industries, more and more companies devote themselves to this field and are committed to meeting the needs and challenges of different industries. With the continuous development of nanotechnology and the expansion of its applications, the electrospinning market is expected to continue growing, which may lead to the emergence of more manufacturers, providing innovative and high-performance nanofiber materials for various industries.

5.3.2. Batch-produced products

Electrospinning equipment mainly includes laboratory-level equipment, large-scale equipment, and electrospinning accessories. Product applications encompass a wide range of fields, including biomedical, air and water filtration, batteries, sensors, cosmetics, clothing, and food packaging. Numerous foreign companies have emerged as pioneers in the industrialization of electrospinning and the electrospinning equipment developed has been industrialized. The industrialization of electrospinning technology has overcome its technical bottleneck, particularly in recent years. The advancement of needleless electrospinning technology has been instrumental in driving the industrialization of electrospinning equipment.

The global nanofibers market is poised for growth and is projected to increase from USD 1383 million in 2023 to USD 6940 million by 2030 [134]. This trajectory indicates a compound annual growth rate of 25.92 % from 2023 to 2030. Specifically, North America accounted for the largest share of the global nanofibers market with a share of about 35 % and a market size of about US\$ 484.91 Mn. This is mainly due to advanced R&D infrastructure and high demand. Asia Pacific is the fastest-growing market with a share of about 25 % and a market size of about US\$ 345.65 Mn. Especially in China and India, it mainly benefits from government investments and technological advancements.

Key growth drivers include the expansion of application areas, such as the increasing use of nanofibers in medical, filtration, energy storage, and electronics. In the field of biomedical engineering, electrospinning is used to fabricate scaffolds. It can produce synthetic polymer ultrafine fibers with diameters ranging from several micrometers to tens of nanometers. These ultrafine fibers possess high specific surface area, flexible surface functionality, and excellent mechanical properties, which enable them to physically simulate the extracellular matrix structure of natural tissues. They can be used to manufacture wound dressings, medical prostheses, drug delivery systems, DNA release systems, and tissue engineering scaffolds. For instance, fiber membranes prepared by electrospinning can serve as effective drug carriers for transdermal drug delivery. A fiber membrane containing tandospirone, prepared by meltblown electrospinning, can be used for related biomedical purposes. Compared with coatings, electrospun fiber membranes have the advantages of breathability and high drug-loading rate. However, the use of organic solvents in solution electrospinning poses pollution and safety risks, limiting its industrialization and direct application in the biomedical field. Meltblown electrospinning can mitigate this issue to a certain extent.

In the textile field, it can be used to manufacture textile products such as windproof, waterproof, and breathable fabrics for clothing. Foshan MBRT Nanofiberlabs Technology Co., Ltd. [<https://www.nanofiberlabs.com/>] produces nano-fiber new material products including windproof, waterproof, and breathable fabrics for clothing. Its R&D team owns more than 200 patents, cooperates with more than 10,000 customers, and has more than 100 industrial cooperation cases worldwide. It is committed to the technological innovation and customer service of nano-fibers in multiple fields such as textiles, striving to create more valuable products and provide high-quality services.

In the filtration field, it is used to manufacture air filtration media. The products of Foshan MBRT Nanofiberlabs Technology Co., Ltd. include nano-fiber new material products such as air filtration media. Nanometer or micrometer fibers prepared by electrospinning technology can effectively intercept particulate impurities in the air due to their small fiber diameter, thereby achieving the purpose of air filtration and purification.

In the battery field, it can be used to manufacture battery separators. Jiangxi Advanced Materials Nanofiber Technology Co., Ltd. [<https://www.hinanofiber.com/>] uses polyimide to produce lithium-ion power battery separators for automobiles. The nano-fiber separators formed by electrospinning have good high and low-temperature properties, which can effectively improve the safety characteristics of lithium-ion batteries and effectively improve the rate discharge characteristics of lithium-ion batteries.

Table 7 shows the global companies that provide electrospun nanofiber products. Technological advancements, such as advances in production technology have improved the efficiency and quality of nanofiber production and reduced costs, as well as increased environmental demand. This is because the use of nanofibers in renewable energy and eco-friendly products helps to reduce environmental impact and meet the growing demand for environmental protection.

5.4. Current challenges, possibilities and comparisons with other nanofiber-producing technologies

Electrospinning technology presents immense opportunities for producing nanofiber materials with extensive applications in

various fields [10]. Despite the potential benefits, several challenges must be addressed to scale up and industrialize the electrospun nanofiber production. These challenges include improving production rates, implementing effective quality control measures, developing solvent recycling methods, and enhancing mechanical strength (Fig. 34). The limited productivity of electrospun nanofibers poses a significant challenge, impeding their widespread application. Currently, manufacturing equipment for electrospinning nanofiber membranes can now be equipped with up to 1200 nozzles for multi-jet electrospinning. These membranes have a thickness ranging from 40 to 50 μm , and the production rate reaches approximately 12–15 m^2/h [1280]. To increase production rates, the approach can be expanded by utilizing multiple modules, like conventional fiber manufacturing processes, to further increase the number of nozzles. This has a direct impact on productivity and provides an opportunity to industrialize electrospinning technology. Certainly, the superior properties of electrospun nanofibers compared to conventional fiber membranes also make them relatively less demanding in terms of actual throughput. For example, electrospun nanofibers were successfully utilized to enhance melt-blown PP face masks to N-95 levels during the COVID-19 pandemic [27]. The PP face mask, when covered by an electrospun nanofiber thin layer (ca. 3 μm), can achieve an air filtration efficiency of up to 99.1 % against 300 nm NaCl aerogels with a low-pressure drop of only 72 Pa. The production rate of manufacturing face masks is satisfactory due to the minimal number of nanofibers required, which is the key factor in achieving success.

Ensuring quality control of electrospun nanofibers in the manufacturing process is another critical challenge. Critical concerns such as thickness uniformity, fiber diameter, distribution, and the elimination of beads and dripping must be addressed to achieve electrospun nanofiber products with high efficiency and quality [10]. Thickness uniformity issues are caused by the multi-nozzle approach and can be improved by assigning specific movement patterns to the multi-nozzles or exploring other electrospinning methods. Additionally, fiber diameter and distribution equally affect the uniformity of nanofibers, which can influence their morphology and properties. Thus, in the pursuit of large-scale production, optimizing the multiple-nozzle electrospinning process should focus on improving the delivery system of the electrospinning solution, enhancing electrical field distribution, and ensuring stability to achieve uniform fiber diameter [1281]. Defects like drippings and beads significantly reduce the mechanical properties and porosity of electrospun nanofibrous membranes, but a general quality criterion for large-scale production has not yet been established.

The use of large quantities of organic solvents in the electrospinning process raises health and safety concerns, as well as environmental issues related to solvent evaporation. The concentration of the electrospinning solution is typically 10–20 wt%, with the remaining 80–90 wt% being solvent which, if not recycled, will be released into the atmosphere. In addition, most of the solvents used are volatile, environmentally harmful organic compounds. Therefore, effective solvent recovery or reprocessing methods must be used when scaling up production. Water can be used as a solvent for dissolving polymers and manufacturing electrospun nanofibers, but this method is only applicable to water-soluble polymers [1282]. Other solvent-free options, such as melt electrospinning [1283] and emulsion electrospinning [1273], have been recently developed. A typical electrospinning process requires post-treatment of the evaporated solvent. If pure solvents are used, solvent condensation can be conducted, but if solvent mixtures are employed, solvent burning may be adopted. In order to achieve carbon emission reduction and neutralization, alternative methods such as absorption, condensation, and collection have been explored. The potential hazards of electrospun nanofibers on human beings and other living species are mainly related to the residual solvent from the electrospinning process and the inhalation safety, as they belong to a class of 1D nanomaterials similar to asbestos, which may be more susceptible to inhalation due to their size, triggering respiratory and lung health problems.

Lastly, the mechanical strength of electrospun nanofibrous membranes imposes limitations on their overall applications [1284]. In addition to attachment to a mechanically supported substrate, the mechanical enhancement of the nanofibers themselves can be achieved by aligning the fibers through specific collection methods and thermal stretching, or by incorporating inorganic nanoparticles. However, the limited number of contact points and different material properties of electrospun nanofibers randomly deposited on a substrate can lead to relatively weak adhesion between nonwoven structured nanofibers, especially between different layers of the membrane. There are several pathways available to enhance the adhesion between nanofibers and the substrate, as well as between different layers of the membrane, such as pre-treating the substrate, utilizing solvent vapor welding [1285], employing dilute solvent vapor welding [1286], or applying hot-press crosslinking. These methods effectively improve the mechanical strength of the nanofibrous membrane, even during scaling-up processes.

It is worth mentioning that a two-nozzle electrospinning setup can be utilized to engineer an interpenetrating nanofibrous network, where two types of nanofiber components are intertwined to form a composite membrane [1287]. In this case, one nanofiber component functions as the mechanical support (*i.e.*, substrate), while another serves as the functional component, providing various functionalities such as adsorption capacity to the composite membrane. The adhesion problem between the nanofibers and the substrate can be effectively solved by creating an interpenetrating nanofibrous structure that integrates the substrate component with the barrier layer.

Conventional fiber manufacturing processes have also faced these problems and have been successfully solved, providing valuable insights and solutions to the challenges that arise in the electrospinning process. For example, productivity can be increased using multiple modules, while mechanical strength can be improved via melt-blown techniques. In addition, the fiber uniformity can be controlled for quality assurance, and solvents can be recycled to reduce waste. In addition to electrospinning, various other techniques have been developed for the generation of nanofibers, including bicomponent extrusion, phase separation, template synthesis, and drawing. Bicomponent extrusion refers to the process of extruding two different polymers together through a single nozzle, resulting in a fiber with distinct properties from each polymer [1288]. Examples of bicomponent fibers include core-sheath, eccentric, islands-in-the-sea and segmented pie fibers. In the process of phase separation, a polymer is initially mixed with a solvent and then separated into different phases due to physical inconsistency. The extraction of the solvent phase results in obtaining polymer nanofibers [1289]. Template synthesis is a commonly employed method for the production of inorganic nanofibers, such as carbon nanotubes and

nanofibers [1290]. The drawing process can be characterized as dry spinning at a molecular level, but this process is not continuous. Only viscoelastic materials can remain sufficiently solid to hold up the developed stress during pulling. Although various techniques can produce nanofibers, electrospinning is considered the most promising due to its simple process, controllable fiber size, repeatability, and scalability of production.

In conclusion, the industrialization of electrospinning technology presents both opportunities and challenges, indicating that there is still ample room for improvement. The exceptional properties and diverse applications of electrospun nanofibers facilitate their production scaling up.

6. . Future perspectives of electrospinning and electrospun nanofibers

Although significant progress has been achieved in the field of electrospinning technology, there still exist numerous opportunities for further development and improvement concerning engineering challenges, industrialization, and standardization of electrospun fibrous products (Fig. 35).

6.1. Fabrication, properties and functions of electrospun nanofibers

The field of electrospun nanofibers has witnessed remarkable advancements, and several challenges still need to be addressed to fully unleash their potential. These key challenges include producing high-performance nanofibers with comprehensive properties, achieving precise structures, and integrating multiple functions. At present, researchers are diligently working to tackle these challenges, pushing the boundaries of electrospinning technology and exploring new practical applications and industrial scalability for this promising field.

6.1.1. High-performance electrospun nanofibers

Electrospinning has proven its capability to produce a diverse range of nanofibers with distinct properties, and achieving comprehensive, high-performance characteristics in electrospun fibers remains an ongoing challenge. Taking the thermal resistance function as an example, electrospun polymeric fibers exhibit good toughness but lack sufficient thermal resistance [1291], while electrospun ceramic fibers demonstrate excellent thermal properties but suffer from mechanical defects such as brittleness [1097,1292,1293]. A solution to this challenge lies in preparing composites using a combination of polymers and inorganic materials through electrospinning. By harnessing the individual strengths of each component, electrospun nanofibers with a balanced combination of thermal resistance and mechanical performance can be created. Various electrospinning techniques can be explored to achieve this, such as the application of composite solutions using coaxial electrospinning [1294], triaxial electrospinning [1295], or side-by-side electrospinning [1296]. These techniques allow for precise adjustments to the components and structures of the resulting electrospun composite fibers. Another promising avenue is the development of electrospun carbon fibers, as the natural electrical conductivity lends itself to applications such as in the energy and electronics sectors [1297,1298]. While traditional carbon fibers have demonstrated exceptional mechanical performance and widespread commercial applications, the mechanical properties of electrospun carbon fibers still fall short of their commercial counterparts. Consequently, the pursuit of high mechanical performance electrospun fibers that can rival conventional carbon fibers remains a significant challenge.

6.1.2. Ordering of electrospun nanofibers

Electrospun nanofibers with various morphologies can have great potential for different applications. In addition to the construction of individual nanofiber with specific structure and assembling the nanofibers into a construct with typical architecture, it is also a challenge to precisely weave them into knitted fabrics on a large scale. Knitted fabrics can be categorized into two approaches: textile warp knitted fabric and weft knitting fabric [1299,1300]. The unique characteristics of knitted fabrics are determined by their own structures, which depend on the arrangement of yarn within each stitch. The utilization of technology further defines the implementation of specialized knitting stitches. In weft knitting fabric, yarn is arranged horizontally (parallel) to form a circular pattern, while in warp knitting, yarn is arranged longitudinally to create a circular pattern. These different knitting technologies greatly influence the fabric style, allowing for the creation of new knitted fabric styles using the same material by combining the two methods. When designing knitting products, meticulous attention must be paid to the fabric's physical and mechanical properties, particularly tensile strength, elongation, and elasticity in various directions [1301]. These factors are critical for ensuring the fabric's durability and usability in diverse applications. Therefore, the development of suitable devices or equipment for fabricating fabrics from electrospun nanofibers will be crucial for their wider commercial applications in the future. Such advancements would enable the integration of electrospun fibers into a broader range of textile products, benefiting industries that require specialized fabrics with enhanced properties.

6.1.3. Multi-functional electrospun nanofibers

Electrospinning stands as one of the most promising methods for multi-functional applications. Looking ahead, electrospinning technology and electrospun nanofibers hold tremendous potential across various fields, including stimuli-responsive nanofibers, smart fibers and textiles, and intelligent biomedical fibrous materials.

Stimuli-responsive electrospun nanofibers. Stimuli-responsive polymers represent intelligent materials capable of sensing and interacting with their surrounding environment. The combination of electrospinning with such materials forms smart fibers that are capable of changing their physical and chemical properties in response to external stimuli and are therefore known as stimulus-

responsive electrospun nanofibers. The successful construction of such electrospun nanofibers paves the way for the innovative development of various smart fibers [1302,1303]. Notably, their smaller size enables a much faster response to external stimuli compared to bulk stimuli-responsive hydrogels, as the inverse relationship between size and responsiveness allows for efficient diffusion of external stimuli throughout the material [1304].

External stimuli responses encompass factors such as temperature, pH, light, electricity, and magnetic fields, significantly influenced by material properties [1305–1308]. The potential development directions for stimuli-responsive electrospun nanofibers are as follows: (i) tailoring stimulation-responsive electrospun nanofibers with smaller diameters and new morphologies or specific functions, (ii) exploring stimulation-responsive electrospun nanofibers with hollow or multi-channel structures to offer larger specific surface areas for loading functional or bioactive components, (iii) enhancing intelligence by designing multiple stimuli-responsive electrospun nanofibers rather than single-stimulus responsive ones, and (iv) scaling up production and reducing preparation costs to facilitate their industrialization and practical applications. By addressing these research directions, the full potential of stimulus-responsive electrospun nanofibers can be unleashed, paving the way for innovative applications in different industries. The utilization of these intelligent materials holds the promise of revolutionizing fields such as medicine, sensors, and wearable technology, contributing to a smarter and more interconnected world.

Smart electrospun nanofibers. Smart electrospun nanofibers stand at the forefront of the functional fiber revolution, encompassing various cutting-edge applications such as optical fiber [1309], grating fiber [1310], light scattering fiber [1311], conductive fiber [1312], piezoelectric fiber [1313], thermo-sensitive fiber [1314] and photochromic fiber [1284]. Additionally, they have facilitated the emergence of thin, flexible power supplies for microelectronic component chip calculators [1315]. The rapid development of advanced technologies, including sound and image recognition, smart fibers and smart textiles are spurred by the increasing popularity of microsensors, mobile phones, and mobile networks. These technologies find widespread applications in diverse fields such as communications, electronics and power, medical care, health care, protective clothing, and smart city construction [1300,1316–1318]. The advancement of smart textiles is currently hindered by the weight of numerous electrical wires and battery stacks, thereby impeding their seamless integration into the luxury fashion industry. To overcome this limitation, future fashion designers must gain access to innovative wearable technology and smart products that are lightweight, thin, and washable. Embedding conductive fibers and yarn into very small devices still requires extensive research and development, necessitating cross-border collaboration among experts from different disciplines. By addressing these challenges and exploring novel avenues for innovation, smart electrospun nanofibers will undoubtedly continue to revolutionize various industries and drive the development of intelligent textiles with enhanced functionality and practical applications. As researchers and engineers work together to overcome current limitations, the future of intelligent textiles promises to be even more remarkable and transformative.

Intelligent electrospun biomedical nanofibers. Intelligent electrospun nanofibers have emerged as versatile platforms, exhibiting high surface area, tunable mechanical properties, and tailored functionalities. Personalized medicine is set to benefit immensely from these fibers, as they enable the design and production of nanofibers with precise properties to cater to individual patient needs. This avenue opens doors for targeted drug delivery, facilitating improved therapeutic outcomes and minimizing side effects [1319]. Furthermore, the integration of biosensing capabilities into these nanofibers offers the prospect of real-time health monitoring and early disease detection, pushing the boundaries of preventive medicine [1320]. Even so, this exciting journey is always accompanied by challenges. The future trends of smart electrospun biomedical nanofibers can be outlined as follows. (i) Optimizing the electrospinning process to ensure consistent and reproducible results becomes critical for ensuring precision and efficiency, and thus the complex interactions among the parameters require a deeper understanding [1321]. (ii) Biocompatibility remains a cornerstone concern as these nanofibers find their way into the human body, and rigorous testing and validation are essential to ensure that promising innovations do not compromise patient safety. (iii) The translation from laboratory-scale production to large-scale manufacturing presents economic and technological hurdles that must be overcome for these advancements to benefit a broader population. In conclusion, the trajectory of intelligent electrospun nanofibers in biomedicine is poised for continued growth and transformative impact. The synergy of cutting-edge technology and medical innovation holds the potential to revolutionize diagnostics, treatments, and patient outcomes. Through interdisciplinary collaboration and dedication, the era of intelligent electrospun nanofibers in biomedicine is not only on the horizon but promises to reshape the future of healthcare.

Smart stealth electrospun nanofibrous materials. Modern electronic reconnaissance equipment now covers nearly all valuable electromagnetic wavebands, and detection technology is advancing toward sophisticated intelligence. Among various detection methods, radar and infrared detection stand out as the most effective and common ones [1292,1322]. As a result, enhancing stealth performance has become a key research focus in the field of current stealth technology. In particular, the development of infrared/radar-compatible stealth materials has garnered significant attention [1323]. Electrospun nanofibers exhibit new absorption channels due to their small size effect and low-frequency oscillation properties, which have been considered to be one of the best candidates for wave-absorbing materials [1324]. The powerful wave-absorbing ability allows the use of nanofibers in stealth applications to increase the efficacy of stealth technology. By leveraging the unique properties of nanofibers, researchers can explore novel approaches to enhance the absorption and attenuation of electromagnetic waves to improve the stealth performance of equipment.

6.2. Industrial production of electrospun nanofibers

6.2.1. New principles and equipment designs for nanofiber manufacturing

Over the years, electrospinning as an emerging technique has gradually matured and achieved industrial breakthroughs. However, there are still some challenges to overcome the industrial production issues of electrospun nanofibers. New principles and equipment designs are further required to promote sustainable development of electrospinning and electrospun nanofiber manufacturing. High-

speed centrifugal electrospinning is a promising improved process for nanofiber manufacturing, which combines the principles of centrifugal spinning and electrospinning, and its core components are centrifuge and reservoir [1325]. Centrifugal electrospinning equipment uses a rotating body with holes or meshes that rotate at high speed to eject the spinning fluid by centrifugal force, which enters the electrostatic field and forms a large number of jets to produce a large number of fibers. The centrifugal needleless electrospinning device invented by Liu's team (Patent: CN103255485B) not only achieved the process of large-scale and continuous production of nanofibers but also overcame the problem of uneven fiber diameter. Therefore, compared to traditional electrospinning, high-speed centrifugal spinning appears more suitable for industrial-scale production, as evidenced by the successful preparation of ethyl cellulose (EC)/PVP fibers with microporous and nano-porous structures [1326]. However, centrifugal electrospinning mostly uses polymer solutions as spinning raw materials, where most of the used solvents are toxic and can cause environmental pollution if not handled properly, and solvent volatilization in the process of nanofibers preparation reduces the production efficiency [1181].

In the quest for green polymer nanofiber manufacturing, "zero solvent" melt electrospinning has emerged as a significant development direction [1283,1327]. Breakthroughs in principle exploration, method innovation, process equipment development, and industrial application have propelled this technique forward. The establishment of a physical model and analysis of melt differential electrospinning have led to a better, theoretical understanding of jet spacing and fiber diameter correlation [1328]. The electrospinning efficiency has been significantly improved compared to the capillary method. Innovative approaches, such as electric field homogenization methods and equipment, have been devised [1329]. Moreover, modular design concepts and multi-field coupling melt differential electrospinning techniques have paved the way for industrialized production processes and equipment, culminating in the world's first set of melt electrospinning nanofiber production lines [1330,1331]. For example, Chen's group has innovated the development of polymer melt differential electrospinning (PMDES) method [1211], which utilizes particular flow channel to uniformly disperse the polymer melt over the cone of a differential nozzle, so that tens of thousands of fiber jets are generated from a single nozzle under the effect of an electric field. Moreover, this breakthrough makes it possible to produce polymer fibers without the use of any solvents, thus truly demonstrating a zero-pollution process. This breakthrough solves the challenges of nozzle clogging and low single-nozzle productivity that are common in conventional electrospinning and opens a new path to industrial-scale manufacturing. Simultaneously, Yang's group used needle-free melt electrospinning technology to prepare oriented PP fibers [1332]. Using this technology, the effect of oriented fiber membrane arrangement on filtration efficiency was studied. ANSYS software was used to conduct electric field simulation as a guide, the optimal distance from the nozzle to the electrode and the influence of electric field strength on fiber diameter were studied by experiments. It was determined that due to the short duration of the electric field action, the stretching effect is not significant, and therefore the fiber diameter remains larger even if the conditions are of higher electric field strength. Besides, the oriented fiber film has higher retention efficiency for particles of 0.5 μm and maintains the same permeation flux as the native membrane. This set of theoretical calculations to design to practical testing and optimization paves the way for subsequent industrial production. However, melt electrospinning tends to produce larger fibers due to the higher viscosity and lower conductivity of the polymer melt [1283]. Therefore, Chen's group proposed a new dual-electrode structure melt differential electrospinning [1333]. This investigation has revealed the impact of different dual-electrode structures on the quantity, diameter, and distribution range of fibers. When the sum of the upper and lower electrode voltages is kept constant and varied over a range, the low voltage in the two-electrode structure increases the number of fibers and reduces the fiber diameter. On this basis, Chen *et al.* reported a melt electrospinning writing technique by combining melt electrospinning with 3D printing technology [1334]. Therefore, melt electrospinning writing technology is an emerging method combining melt electrospinning and 3D printing stage [1178]. This research has combined micromolding and turning processes to successfully mass-produce tadpole-like magnetic polycaprolactone/ Fe_3O_4 (PCL/ Fe_3O_4) microrobot. On the one hand, melt electrospinning writing enables programmable electrospinning that exhibits a high level of controllability in terms of fiber deposition position, fiber diameter and fiber shape in series production. On the other hand, complex shapes or geometries can also be designed under automatic computer control by melt electrospinning writing. This research also provides a theoretical reference for subsequent industrial mass production of complex structures, advanced shape design and multifunctional micro-robots.

Besides, with the promotion of sustainability strategies, the development of biodegradable and environmentally friendly electrospun fiber products has also become an important development direction. The global problem of waste disposal has also prompted the search for solutions with biodegradable polymers that have properties comparable to those of petroleum-based materials. Xu *et al.* used the "electrostatic spinning-electrospray" strategy to obtain biodegradable and renewable PLA fiber membranes without sacrificing the biodegradability of PLA nanofiber membranes [1335,1336]. The surface roughness and electret properties are improved to provide excellent PM capture performance. These PLA fiber membranes are not only expected to replace traditional polymer air filters, masks, protective clothing, etc. but also provide a new way to subsequently solve the plastic/microplastic pollution caused by discarded masks based on traditional polymer fibers. In addition to PLA, Polyhydroxyalkanoate (PHA) polymers are commonly used in the production of every day and biomedical materials as an all-bio-based, fully degradable natural polyester. However, the preparation of pure PHA fibers is still a challenge at present. With the development of biorefinery technology, the cost of PHA production will continue to decrease; and the optimization of modification technology will further enhance the performance of PHA and expand its applications, thus promoting the green and sustainable development of human society as an emerging bio-based biodegradable material [1337,1338]. PHBV/PLA composite fiber with the trade name of 'Hoso®' is now available in the market, and the fabrics made from it are soft and smooth, with good drape, dyeing rate and color fastness, and at the same time, it has high antibacterial and mite repellent properties. In addition, companies such as Blue Crystal Microbial and Microstructure Factory have also made many efforts and advancements in the mass production and application of PHA [<https://www.bluepha.com/blog/pha-phbh>] [<https://www.phabuilder.com/>]. It is believed that in the near future, electrospun PHA fibers will be applied in more fields, injecting new vitality into the cause of environmental protection.

In conclusion, the pursuit of new principles and equipment designs for green nanofiber manufacturing has yielded remarkable advancements. Researchers are driving innovations represented by high-speed centrifugal spinning and “zero-solvent” melt electrospinning, pushing the boundaries of sustainable and efficient nanofiber production. These developments have far-reaching implications for various industries, including fashion, electronics, and environmental protection. As scientists continue to explore and optimize these technologies, the path toward a greener and more sustainable future becomes increasingly tangible.

6.2.2. Advancing upstream and downstream markets for electrospun nanofibers

Electrospun nanofibers have been turned into a variety of upstream and downstream products. For example, ultra-strong, durable and function-oriented nanofiber fabrics developed by electrospinning nanotechnology have been used in many consumer applications, such as filtration [1339], defensive and protective clothing, and medical dressings [1340], household items, food packaging, cosmetics [1341]. For example, Jiangxi Xiancai nanofiber Technology Co., Ltd. in China has developed nanometer-breathable protective clothing using electrospun PI fibrous aerogel [<https://www.hinano.com/productinfo/666790.html>]. The clothing features a nano-sized superfine fiber “textile” with high porosity and small aperture, ensuring waterproof breathability, effective filtration of fine particles and warming requirements. Lime Co., Ltd. also offers technical textiles for the sports and leisure market, utilizing nanofiber membrane lamination material that provides waterproof and windproof properties while maintaining high air permeability [<https://www.limenano.com/media/media.php?type=view&idx=5290>]. E-Spin Technologies has developed textile fabric laminates with nanofiber layers, delivering exceptional breathability and comfort for wearers in outdoor and sportswear applications [<https://espintechologies.com/air-filtration-media>].

In addition to clothing, filter paper is also an application for electrospun nanofibers. Compared with the traditional wood pulp fiber filter paper, the filtering efficiency of nanofiber filter paper is greatly improved [1342]. Nanofiber filter papers, with diameters typically below 200 nm, achieve filtration efficiencies of more than 99.999 %, allowing for high dust tolerance and extended service life. The development of nanofiber industrial filter papers addresses the increasingly serious issue of PM_{2.5} and escalating environmental air pollution, demanding higher filtration efficiency and improved air permeability for industrial equipment air filters. Nanofiber industrial filter papers offer a solution to enhance air filter performance, prolong equipment life, reduce particulate contamination in equipment systems, and reduce maintenance frequency and operating energy consumption. For instance, Shijiazhuang Chentai Filter Paper Co., Ltd. produces automotive filter papers, including electrospun nano-filter papers, breaking international monopolies and filling domestic gaps in the industry [<https://www.chentai.net>].

The integration of electrospinning technology with nanotechnology has propelled nonwoven nanofibers into modern high-efficiency products. This trend is expected to extend further into various functional textile industry sectors, fostering innovation in product applications. Future research will focus on producing environmentally friendly and multifunctional electrospun nanofibers, streamlining manufacturing processes, and reducing costs. The ultimate objective is to transition electrospun nanofibers of various types and functions from laboratory-scale research to industrial-scale production. As these advancements continue, nanotechnology through electrospinning is poised to revolutionize multiple industries, promising a future of enhanced and innovative product applications.

6.3. Standardization of electrospun nanofiber products

Standardization of electrospun nanofibrous products is of paramount importance for the development and commercialization of this technology. Standardization ensures that products meet specific quality and performance requirements, promoting consistency, safety, and reliability in their applications.

6.3.1. The significance of standardization

Standardization plays a crucial role in trust and confidence among consumers, researchers, and industries alike. By defining uniform specifications and testing methods, standardization ensures that electrospun nanofibrous products meet the expected performance criteria across different manufacturing processes and applications. It enables seamless integration and compatibility with existing products and systems, facilitating the broader adoption of electrospun nanofibers in various fields such as textiles, medical devices, filtration, and electronics. Moreover, standardization provides a basis for regulatory compliance and quality assurance. As electrospun nanofibrous products find their way into critical applications like biomedical materials and protective clothing, adherence to recognized standards becomes essential for ensuring safety and efficacy. Standardized testing methods enable the assessment of product performance, durability, and other crucial attributes, making it easier to evaluate their suitability for specific use cases. Furthermore, standardization supports research and innovation by creating a common language and framework for knowledge exchange. Scientists and engineers can rely on established standards to compare results, share data, and build upon existing research. This collaborative approach drives advancements in electrospinning technology, fostering a more efficient and productive research environment.

6.3.2. The establishment and upgrading of standards

The establishment and continuous upgrading of standards require the collective efforts of experts, industry stakeholders, and regulatory bodies. In the early stages of electrospinning technology development, creating foundational standards is essential. These standards may encompass parameters such as fiber diameter, mechanical properties, safety, and environmental impact. As the technology matures and finds broader applications, more specialized standards can be introduced, addressing specific sectors and applications. To ensure the effectiveness and relevance of standards, they must be periodically reviewed and updated. As technology

advances, new insights and innovations may require adjustments to existing standards or the development of new ones. Additionally, international harmonization of standards is crucial for promoting global trade and cooperation in the field of electrospinning. The standardization process should be transparent and inclusive. Collaboration between academia, industry, government agencies, and standardization organizations fosters a comprehensive and well-rounded approach to standard development. In conclusion, standardization is a vital aspect of advancing electrospun fibrous products from the laboratory to widespread commercial applications. Meanwhile, artificial intelligence can be used to monitor the key parameters in the electrospinning process in real time, such as voltage, flow rate, receiving distance, etc., and intelligently adjust according to preset standards or models. By promoting consistency, safety, and quality, standardized electrospun nanofibers can unlock their full potential, revolutionizing various industries and enhancing the overall quality of life.

6.3.3. Existing standards related to electrospun nanofibers

The properties of electrospun nanofibers make them ideally suited for a variety of applications, especially in the fields of face masks and protective clothing [1343,1344], and the national standards related to electrospun nanofibers already exist for these two areas. Regarding protective face masks, electrospun nanofibers have the characteristics of high porosity and low airflow resistance, which mainly play the role of filtration and are especially suitable for medical-grade protective masks. In China, medical protective masks are subjected to specific standards, as summarized in Table 8. These standards define essential performance criteria, including filtration efficiency, bacterial filtration efficiency, and breathing resistance, ensuring the efficacy and safety of medical protective masks that incorporate electrospun nanofiber-based filters. These masks play a crucial role in safeguarding public health by effectively filtering out particles, pathogens, and pollutants.

Regarding protective clothing, the application of nanotechnology in clothing treatment requires compliance with relevant national safety indicators and standards, as shown in Table 9. Table 10. Table 11.. By adhering to these national standards, clothing manufacturers can ensure the safety and reliability of nanotechnology-treated clothing. Electrospun nanofibers integrated into textiles can confer various functional properties, such as antibacterial effects, stain resistance, and enhanced durability. Proper regulation and adherence to these standards are essential to guaranteeing the quality and consumer acceptance of nanotechnology-enhanced clothing products.

In conclusion, the existence of well-defined standards related to electrospun nanofibers in face masks and nanotechnology-treated clothing is crucial in promoting public health, enhancing protection, and ensuring the safe and responsible use of these innovative materials in various applications. As technology evolves and our understanding of nanomaterials improves, continuous research and refinement of these standards will be essential to address emerging challenges and ensure the sustainable development of nanofiber-based products.

6.4. Artificial intelligence for electrospinning

With the rapid advancement of the Internet of Things (IoT), intelligent products are gradually becoming part of everyday life. Similarly, the electrospinning industry must integrate artificial intelligence (AI) to align with the developments of Industry 4.0. The role of AI in electrospinning will primarily focus on parameter regulation and industrial production optimization.

Firstly, the integration of electrospinning and AI will allow machines to predict the characteristics of the spinning fluid jet—such as diameter, morphology, and surface properties—and adjust spinning parameters to improve the consistency and quality of the nanofibers. This combination will facilitate full automation of the electrospinning process. Currently, large-scale production machines (whether multi-needle or needleless) produce nanofibers with varying diameters. However, AI, through big data analytics and machine learning algorithms, can accurately predict and adjust key parameters like polymer solution concentration, spinning voltage, current, distance, and nozzle rate. For example, Zhu et al. employed AI technology to determine optimal manufacturing parameters for electrospun PVDF/PU nanofibers [1345]. Additionally, AI is expected to deeply analyze and mine data (such as fiber diameter, morphology, and distribution) during the electrospinning process. This analysis can uncover the relationships between fiber properties and spinning parameters, offering a scientific basis for further optimization.

Secondly, AI can significantly optimize the production process by quickly identifying bottlenecks and detecting operational faults—such as voltage instability or abnormal flow rates—in real time. Using predictive algorithms, AI can monitor equipment performance, provide early warnings of potential issues, and ensure stable operations, ultimately enabling process automation and reducing the need for manual intervention. Additionally, AI can enhance production scheduling and efficiency by integrating data acquisition, processing, and control systems into a fully automated setup. This system would enable remote monitoring and control of high-voltage power supplies, as well as real-time data collection and analysis, streamlining the entire production process. In the future, these systems will become more intelligent, adapting to changes in production plans, environmental conditions, and equipment performance, ensuring smooth, continuous production through automatic adjustments.

In conclusion, AI offers tremendous potential for optimizing electrospun nanofibers design and improving production efficiency. Although research on the direct integration of AI with electrospinning is still in its early stages, the continuous evolution of AI technology is expected to drive its broader application in electrospinning, leading to transformative advancements in both material science and the manufacturing industry.

CRediT authorship contribution statement

Ce Wang: Writing – review & editing. **Wei Wang:** Writing – original draft. **Hongxu Qi:** Writing – original draft. **Yunqian Dai:**

Conceptualization. **Shaohua Jiang**: Writing – original draft. **Bin Ding**: Writing – original draft. **Xianfeng Wang**: Writing – original draft. **Congju Li**: Writing – original draft. **Jinfeng Zeng**: Writing – original draft. **Tong Wu**: Writing – original draft. **Haoyi Li**: Writing – original draft. **Yuanfei Wang**: Writing – original draft. **Yong Zhao**: Writing – review & editing. **Wenli Wang**: Writing – original draft. **Zhenyu Li**: Writing – original draft. **Xiumei Mo**: Writing – original draft. **Haoqing Hou**: Writing – original draft. **Lijie Dong**: Writing – original draft. **Hongyang Ma**: Writing – original draft. **Yong Liu**: Writing – original draft. **Chunlei Su**: Writing – original draft. **Jie Bai**: Writing – original draft. **Weiwei Wu**: Writing – original draft. **Gang Guo**: Writing – original draft. **Guangdi Nie**: Writing – original draft. **Nü Wang**: Writing – original draft. **Han Zhu**: Writing – original draft. **Jing Bai**: Writing – original draft. **Jian Fang**: Writing – original draft. **Daxin Liang**: Writing – original draft. **Zhichen Ba**: Writing – original draft. **Guangping Han**: Writing – original draft. **Xiaofeng Lu**: Writing – original draft. **Kaizhong Wang**: Writing – original draft. **Xiaoyong Zhang**: Writing – original draft. **Weimin Kang**: Writing – original draft. **Nanping Deng**: Writing – original draft. **Wei Hu**: Writing – original draft. **Weihua Chen**: Writing – original draft. **Xiuling Zhang**: Writing – original draft. **Dongzhi Yang**: Writing – original draft. **Fengyun Wang**: Writing – original draft. **Ye Bian**: Writing – original draft. **Zi'ang Liu**: Writing – original draft. **Liang Zhang**: Writing – original draft. **Xiang Li**: Writing – original draft. **Lei Li**: Writing – original draft. **Yongxin Li**: Writing – original draft. **Hui Huang**: Writing – original draft. **Xiaoteng Jia**: Writing – original draft. **Xiaofeng Li**: Writing – original draft. **Daxiang Yang**: Writing – original draft. **Xianchang Jin**: Writing – review & editing, Writing – original draft. **Shiyang Li**: Writing – original draft. **Xindan Zhang**: Writing – original draft. **Nan Tang**: Writing – original draft. **Ruinan Hao**: Writing – original draft. **Feng Tian**: Writing – review & editing. **Liqiang Mai**: Writing – review & editing. **Yen Wei**: Writing – review & editing. **Jiajia Xue**: Writing – review & editing.

Declaration of competing interest

The authors declare that they have no known competing financial interests or personal relationships that could have appeared to influence the work reported in this paper.

Acknowledgements

This work is supported by the National Natural Science Foundation of China (Grant No. 52221006, 21875084, 52273055, 22475044, 51925302, 52073052, 52073238, 51773163, 51673011, 21374008, 51772158, 31971308, 52103057, 52273058, 52173059, 31400497, 21865016, 51973157, 52203066, 52073044, 21771164, 51972015, 51773082, 51773082, and U1804129), the 2021 International Training Project of High-level Talents in Henan Province, the Zhongyuan Youth Talent Support Program of Henan Province, the Natural Science Foundation of the Jiangsu Higher Education Institutions of China (21KJA540002), the Open Funds of State Key Laboratory of Oil and Gas Reservoir Geology and Exploitation (PLN2022_38, SWPU), the Youth Innovation S&T Support Program in Higher Education Institutions of Shandong Province (2023KJ358), the National Key R&D Program Sub-project 2022YFC3203801, and the Fundamental Research Funds for the Central Universities (buctrc202312).

Data availability

No data was used for the research described in the article.

References

- [1] Ding Y, Onyilagha O, Zhu Z. Electrospun nanofibers for tactile sensors. In: Zhou Y, Chou H-H, editors. *Functional tactile sensors*. Cambridge: Woodhead Publishing; 2021. p. 159–96.
- [2] Babar AA, Iqbal N, Wang X, Yu J, Ding B. Introduction and historical overview. In: Ding B, Wang X, Yu J, editors. *Electrospinning: Nanofabrication and applications*. Norwich: William Andrew; 2019. p. 3–20.
- [3] Xu T, Ding Y, Wang Z, Zhao Y, Wu W, Fong H, et al. Three-dimensional and ultralight sponges with tunable conductivity assembled from electrospun nanofibers for a highly sensitive tactile pressure sensor. *J Mater Chem C* 2017;5:10288–94. <https://doi.org/10.1039/c7tc03456c>.
- [4] Abolhasani MM, Naebe M, Amiri MH, Shirvanimoghaddam K, Anwar S, Michels JJ, et al. Hierarchically structured porous piezoelectric polymer nanofibers for energy harvesting. *Adv Sci* 2020;7:2000517. <https://doi.org/10.1002/advs.202000517>.
- [5] Sehaqui H, Mushi NE, Morimune S, Salajkova M, Nishino T, Berglund LA. Cellulose nanofiber orientation in nanopaper and nanocomposites by cold drawing. *ACS Appl Mater Interfaces* 2012;4:1043–9. <https://doi.org/10.1021/am2016766>.
- [6] Ma ML, Kuang Y, Gao Y, Zhang Y, Gao P, Xu B. Aromatic-aromatic interactions induce the self-assembly of pentapeptidic derivatives in water to form nanofibers and supramolecular hydrogels. *J Am Chem Soc* 2010;132:2719–28. <https://doi.org/10.1021/ja9088764>.
- [7] Yan C, Chen G, Zhou X, Sun J, Lv C. Template-based engineering of carbon-doped Co₃O₄ hollow nanofibers as anode materials for lithium-ion batteries. *Adv Funct Mater* 2016;26:1428–36. <https://doi.org/10.1002/adfm.201504695>.
- [8] Zhao J, Han W, Tu M, Huan S, Zeng R, Wu H, et al. Preparation and properties of biomimetic porous nanofibrous poly(L-lactide) scaffold with chitosan nanofiber network by a dual thermally induced phase separation technique. *Mater Sci Eng C* 2012;32:1496–502. <https://doi.org/10.1016/j.msec.2012.04.031>.
- [9] Chen YJ, Shafiq M, Liu MY, Morsi Y, Mo XM. Advanced fabrication for electrospun three-dimensional nanofiber aerogels and scaffolds. *Bioact Mater* 2020;5: 963–79. <https://doi.org/10.1016/j.bioactmat.2020.06.023>.
- [10] Xue JJ, Wu T, Dai YQ, Xia YN. Electrospinning and electrospun nanofibers: Methods, materials, and applications. *Chem Rev* 2019;119:5298–415. <https://doi.org/10.1021/acs.chemrev.8b00593>.
- [11] Taylor GI. Disintegration of water drops in an electric field. *Proc R Soc Lond A Math Phys Sci* 1964;280:383–97. <https://doi.org/10.1098/rspa.1964.0151>.
- [12] Wang G, Zhang H, Qian B, Wang J, Jian X, Qiu J. Preparation and characterization of electrospun poly(phthalazinone ether nitrile ketone) membrane with novel thermally stable properties. *Appl Surf Sci* 2015;351:169–74. <https://doi.org/10.1016/j.apsusc.2015.05.124>.
- [13] Huang Y, Bu N, Duan Y, Pan Y, Liu H, Yin Z, et al. Electrohydrodynamic direct-writing. *Nanoscale* 2017;5(2013):12007. <https://doi.org/10.1039/c3nr04329k>.
- [14] Reneker DH, Yarin AL. Electrospinning jets and polymer nanofibers. *Polymer* 2008;49:2387–425. <https://doi.org/10.1016/j.polymer.2008.02.002>.
- [15] Han T, Reneker DH, Yarin AL. Buckling of jets in electrospinning. *Polymer* 2007;48:6064–76. <https://doi.org/10.1016/j.polymer.2007.08.002>.

- [16] Park YS, Kim J, Oh JM, Park S, Cho S, Ko H, et al. Near-field electrospinning for three-dimensional stacked nanoarchitectures with high aspect ratios. *Nano Lett* 2020;20:441–8. <https://doi.org/10.1021/acs.nanolett.9b04162>.
- [17] Yin Z, Huang Y, Duan Y, Zhang H. Mechano-electrospinning (MES). In: Yin Z, Huang Y, Duan Y, Zhang H, editors. *Electrohydrodynamic direct-writing for flexible electronic manufacturing*. Singapore: Springer Singapore; 2018. p. 31–65.
- [18] Yue YP, Gong XB, Jiao WL, Li Y, Yin X, Si Y, et al. In-situ electrospinning of thymol-loaded PU fibrous membranes for waterproof, breathable, and antibacterial wound dressing application. *J Colloid Interface Sci* 2021;592:310–8. <https://doi.org/10.1016/j.jcis.2021.02.048>.
- [19] Qin M, Mou XJ, Dong WH, Liu JX, Liu H, Dai Z, et al. In-situ electrospinning wound healing films composed of zein and clove essential oil. *Macromol Mater Eng* 2020;305:1900790. <https://doi.org/10.1002/mame.201900790>.
- [20] Mouthuy PA, Groszkowski L, Ye H. Performances of a portable electrospinning apparatus. *Biotechnol Lett* 2015;37:1107–16. <https://doi.org/10.1007/s10529-014-1760-6>.
- [21] Liu Y, Liu H, Xiong J, Li A, Wang R, Wang L, et al. Bioinspired design of electrospun nanofiber based aerogel for efficient and cost-effective solar vapor generation. *Chem Eng J* 2022;427:131539. <https://doi.org/10.1016/j.cej.2021.131539>.
- [22] Chavoshnejad P, Razavi MJ. Effect of the interfiber bonding on the mechanical behavior of electrospun fibrous mats. *Sci Rep* 2020;10:7709. <https://doi.org/10.1038/s41598-020-64735-5>.
- [23] Zhang Z, Liang X, Li J, Qian J, Liu Y, Yang S, et al. Interfacial engineering of NiO/NiCo₂O₄ porous nanofibers as efficient bifunctional catalysts for rechargeable zinc-air batteries. *ACS Appl Mater Interfaces* 2020;12:21661–9. <https://doi.org/10.1021/acsami.0c03672>.
- [24] Cheng G, Yin CC, Tu H, Jiang S, Wang Q, Zhou X, et al. Controlled co-delivery of growth factors through layer-by-layer assembly of core-shell nanofibers for improving bone regeneration. *ACS Nano* 2019;13:6372–82. <https://doi.org/10.1021/acsnano.8b06032>.
- [25] Zhang S, Liu H, Yin X, Li Z, Yu J, Ding B. Tailoring mechanically robust poly (m-phenylene isophthalamide) nanofiber/nets for ultrathin high-efficiency air filter. *Sci Rep* 2017;7:40550. <https://doi.org/10.1038/srep40550>.
- [26] Pant HR, Kim HJ, Joshi MK, Pant B, Park CH, Kim JI, et al. One-step fabrication of multifunctional composite polyurethane spider-web-like nanofibrous membrane for water purification. *J Hazard Mater* 2014;264:25–33. <https://doi.org/10.1016/j.jhazmat.2013.10.066>.
- [27] Lu T, Cui J, Qu Q, Wang Y, Zhang J, Xiong R, et al. Multistructured electrospun nanofibers for air filtration: A review. *ACS Appl Mater Interfaces* 2021;13:23293–313. <https://doi.org/10.1021/acsami.1c06520>.
- [28] Tran HD, D'Arcy JM, Wang Y, Beltramo PJ, Strong VA, Kaner RB. The oxidation of aniline to produce “polyaniline”: A process yielding many different nanoscale structures. *J Mater Chem* 2011;21:3534–50. <https://doi.org/10.1039/c0jm02699a>.
- [29] Rayleigh L. On the instability of jets. *Proc Lond Math Soc* 1878;1:4–13. <https://doi.org/10.1112/plms/s1-10.1.4>.
- [30] Formhals A. United States: Patent Application Publication. US patent 1934;1:504.
- [31] Norton CL. Method of and apparatus for producing fibrous or filamentary material. US 2048651 A, 1936.
- [32] Fong H, Reneker DH. Elastomeric nanofibers of styrene-butadiene-styrene triblock copolymer. *J Polym Sci Part B: Polym Phys* 1999;37:3488–93. [https://doi.org/10.1002/\(SICI\)1099-0488\(19991215\)37:24<3488::AID-POLB9>3.0.CO;2-M](https://doi.org/10.1002/(SICI)1099-0488(19991215)37:24<3488::AID-POLB9>3.0.CO;2-M).
- [33] Doshi J, Reneker DH. Electrospinning process and applications of electrospun fibers. *J Electrostat* 1995;35:151–60. [https://doi.org/10.1016/0304-3886\(95\)00041-8](https://doi.org/10.1016/0304-3886(95)00041-8).
- [34] Bognitzki M, Czado W, Frese T, Schaper A, Hellwig M, Steinhart M, et al. Nanostructured fibers via electrospinning. *Adv Mater* 2001;13:70–2. [https://doi.org/10.1002/1521-4095\(200101\)13:1<70::AID-ADMA70>3.0.CO;2-H](https://doi.org/10.1002/1521-4095(200101)13:1<70::AID-ADMA70>3.0.CO;2-H).
- [35] Ko F, Gogotsi Y, Ali A, Naguib N, Ye H, Yang GL, et al. Electrospinning of continuous carbon nanotube-filled nanofiber yarns. *Adv Mater* 2003;15:1161–5. <https://doi.org/10.1002/adma.200304955>.
- [36] Sun Z, Zussman E, Yarin AL, Wendorff JH, Greiner A. Compound core-shell polymer nanofibers by co-electrospinning. *Adv Mater* 2003;15:1929–32. <https://doi.org/10.1002/adma.200305136>.
- [37] Li D, Xia YN. Direct fabrication of composite and ceramic hollow nanofibers by electrospinning. *Nano Lett* 2004;4:933–8. <https://doi.org/10.1021/nl049590f>.
- [38] Yarin AL, Zussman E. Upward needleless electrospinning of multiple nanofibers. *Polymer* 2004;45:2977–80. <https://doi.org/10.1016/j.polymer.2004.02.066>.
- [39] Li D, Wang YL, Xia YN. Electrospinning of polymeric and ceramic nanofibers as uniaxially aligned arrays. *Nano Lett* 2003;3:1167–71. <https://doi.org/10.1021/nl0344256>.
- [40] Xu CY, Inai R, Kotaki M, Ramakrishna S. Aligned biodegradable nanofibrous structure: a potential scaffold for blood vessel engineering. *Biomaterials* 2004;25:877–86. [https://doi.org/10.1016/S0142-9612\(03\)00593-3](https://doi.org/10.1016/S0142-9612(03)00593-3).
- [41] Katta P, Alessandro M, Ramsier RD, Chase GG. Continuous electrospinning of aligned polymer nanofibers onto a wire drum collector. *Nano Lett* 2004;4:2215–8. <https://doi.org/10.1021/nl0486158>.
- [42] Yang D, Lu B, Zhao Y, Jiang X. Fabrication of aligned fibrous arrays by magnetic electrospinning. *Adv Mater* 2007;19:3702. <https://doi.org/10.1002/adma.200700171>.
- [43] Lin T, Wang H, Wang X. Self-crimping bicomponent nanofibers electrospun from polyacrylonitrile and elastomeric polyurethane. *Adv Mater* 2005;17:2699–703. <https://doi.org/10.1002/adma.200500901>.
- [44] Gupta P, Wilkes GL. Some investigations on the fiber formation by utilizing a side-by-side bicomponent electrospinning approach. *Polymer* 2003;44:6353–9. [https://doi.org/10.1016/S0032-3861\(03\)00616-5](https://doi.org/10.1016/S0032-3861(03)00616-5).
- [45] Sun D, Chang C, Li S, Lin L. Near-field electrospinning. *Nano Lett* 2006;6:839–42. <https://doi.org/10.1021/nl0602701>.
- [46] Ding B, Li C, Miyauchi Y, Kuwaki O, Shiratori S. Formation of novel 2D polymer nanowebs via electrospinning. *Nanotechnology* 2006;17:3685–91. <https://doi.org/10.1088/0957-4484/17/15/011>.
- [47] Zhao Y, Cao X, Jiang L. Bio-mimic multichannel microtubes by a facile method. *J Am Chem Soc* 2007;129:764–5. <https://doi.org/10.1021/ja068165g>.
- [48] Si Y, Yu J, Tang X, Ge J, Ding B. Ultralight nanofibre-assembled cellular aerogels with superelasticity and multifunctionality. *Nat Commun* 2014;5:5802. <https://doi.org/10.1038/ncomms5802>.
- [49] Niu CJ, Meng JS, Wang XP, Han CH, Yan MY, Zhao KN, et al. General synthesis of complex nanotubes by gradient electrospinning and controlled pyrolysis. *Nat Commun* 2015;6:7402. <https://doi.org/10.1038/ncomms8402>.
- [50] Xue JJ, Xie JW, Liu WY, Xia YN. Electrospun nanofibers: new concepts, materials, and applications. *Acc Chem Res* 2017;50:1976–87. <https://doi.org/10.1021/acs.accounts.7b00218>.
- [51] Shin YM, Hohman MM, Brenner MP, Rutledge GC. Experimental characterization of electrospinning: The electrically forced jet and instabilities. *Polymer* 2001;42:9955–67. [https://doi.org/10.1016/S0032-3861\(01\)00540-7](https://doi.org/10.1016/S0032-3861(01)00540-7).
- [52] Morikawa K, Vashisth A, Grimme CJ, Green MJ, Naraghi M. Wire melt electrospinning of thin polymeric fibers via strong electrostatic field gradients. *Macromol Mater Eng* 2018;304:1800417. <https://doi.org/10.1002/mame.201800417>.
- [53] Fridrikh SV, Yu JH, Brenner MP, Rutledge GC. Controlling the fiber diameter during electrospinning. *Phys Rev Lett* 2003;90:144502. <https://doi.org/10.1103/PhysRevLett.90.144502>.
- [54] Hu J, Wang X, Ding B, Lin J, Yu J, Sun G. One-step electro-spinning/netting technique for controllably preparing polyurethane nano-fiber/net. *Macromol Rapid Commun* 2011;32:1729–34. <https://doi.org/10.1002/marc.201100343>.
- [55] He JH, Wu Y, Zuo WW. Critical length of straight jet in electrospinning. *Polymer* 2005;46:12637–40. <https://doi.org/10.1016/j.polymer.2005.10.130>.
- [56] Chen X, Zhang Y, He X, Li H, Wei B, Yang W. Electrospinning on a plucked string. *J Mater Sci* 2018;54:901–10. <https://doi.org/10.1007/s10853-018-2870-7>.
- [57] Ding W, Wei S, Zhu J, Chen X, Rutman D, Guo Z. Manipulated electrospun PVA nanofibers with inexpensive salts. *Macromol Mater Eng* 2010;295:958–65. <https://doi.org/10.1002/mame.201000188>.
- [58] Mazoochi T, Hamadani M, Ahmadi M, Jabbari V. Investigation on the morphological characteristics of nanofibrous membrane as electrospun in the different processing parameters. *Int J Ind Chem* 2012;3:1–8. <https://doi.org/10.1186/2228-5547-3-2>.
- [59] Yang GZ, Li HP, Yang JH, Wan J, Yu DG. Influence of working temperature on the formation of electrospun polymer nanofibers. *Nanoscale Res Lett* 2017;12:55. <https://doi.org/10.1186/s11671-016-1824-8>.

- [60] Wang X, Ding B, Yu J, Yang J. Large-scale fabrication of two-dimensional spider-web-like gelatin nano-nets via electro-netting. *Colloids Surf B Biointerfaces* 2011;86:345–52. <https://doi.org/10.1016/j.colsurfb.2011.04.018>.
- [61] Sheoran N, Boland B, Thornton S, Bochinski JR, Clarke LI. Increasing ionic conductivity within thermoplastics via commercial additives results in a dramatic decrease in fiber diameter from melt electrospinning. *Soft Matter* 2021;17:9264–79. <https://doi.org/10.1039/d1sm01101d>.
- [62] Singh YP, Dasgupta S, Nayar S, Bhaskar R. Optimization of electrospinning process & parameters for producing defect-free chitosan/polyethylene oxide nanofibers for bone tissue engineering. *J Biomater Sci Polym Ed* 2020;31:781–803. <https://doi.org/10.1080/09205063.2020.1718824>.
- [63] Bosworth LA, Downes S. Acetone, a sustainable solvent for electrospinning poly(ϵ -caprolactone) fibres: Effect of varying parameters and solution concentrations on fibre diameter. *J Polym Environ* 2012;20:879–86. <https://doi.org/10.1007/s10924-012-0436-3>.
- [64] Luo CJ, Stride E, Edirisinghe M. Mapping the influence of solubility and dielectric constant on electrospinning polycaprolactone solutions. *Macromolecules* 2012;45:4669–80. <https://doi.org/10.1021/ma300656u>.
- [65] Angammana CJ, Jayaram SH. Analysis of the effects of solution conductivity on electrospinning process and fiber morphology. *IEEE Trans Ind Appl* 2011;47:1109–17. <https://doi.org/10.1109/Tia.2011.2127431>.
- [66] Haider A, Haider S, Kang IK. A comprehensive review summarizing the effect of electrospinning parameters and potential applications of nanofibers in biomedical and biotechnology. *Arab J Chem* 2018;11:1165–88. <https://doi.org/10.1016/j.arabjc.2015.11.015>.
- [67] Barakat NAM, Kanjwal MA, Sheikh FA, Kim HY. Spider-net within the N6, PVA and PU electrospun nanofiber mats using salt addition: Novel strategy in the electrospinning process. *Polymer* 2009;50:4389–96. <https://doi.org/10.1016/j.polymer.2009.07.005>.
- [68] Choi JS, Lee SW, Jeong L, Bae S-H, Min BC, Youk JH, et al. Effect of organosoluble salts on the nanofibrous structure of electrospun poly(3-hydroxybutyrate-co-3-hydroxyvalerate). *Int J Biol Macromol* 2004;34:249–56. <https://doi.org/10.1016/j.ijbiomac.2004.06.001>.
- [69] Fong H, Chun I, Reneker DH. Beaded nanofibers formed during electrospinning. *Polymer* 1999;40:4585–92. [https://doi.org/10.1016/s0032-3861\(99\)00068-3](https://doi.org/10.1016/s0032-3861(99)00068-3).
- [70] Zheng JY, Zhuang MF, Yu ZJ, Zheng GF, Zhao Y, Wang H, et al. The effect of surfactants on the diameter and morphology of electrospun ultrafine nanofiber. *J Nanomater* 2014;2014:1–9. <https://doi.org/10.1155/2014/689298>.
- [71] Termonia Y, Smith P. Kinetic model for tensile deformation of polymers. 2. Effect of entanglement spacing. *Macromolecules* 1988;21:2184–9. <https://doi.org/10.1021/ma00185a051>.
- [72] Conte AA, Hu X, Beachley V. Role of draw rate and molecular weight when electrospun nanofibers are post-drawn with residual solvent. *Macromol Mater Eng* 2022;308:2200475. <https://doi.org/10.1002/mame.202200475>.
- [73] Liu Y, Ma GP, Fang DW, Xu JA, Zhang HW, Nie J. Effects of solution properties and electric field on the electrospinning of hyaluronic acid. *Carbohydr Polym* 2011;83:1011–5. <https://doi.org/10.1016/j.carbpol.2010.08.061>.
- [74] Zhang Q, Wang X, Fu J, Liu R, He H, Ma J, et al. Electrospinning of ultrafine conducting polymer composite nanofibers with diameter less than 70 nm as high sensitive gas sensor. *Materials* 2018;11:1744. <https://doi.org/10.3390/ma11091744>.
- [75] Gilbert M. Relation of structure to thermal and mechanical properties. *Brydson's plastics materials* 2017:59–73. <https://doi.org/10.1016/b978-0-323-35824-8.00004-9>.
- [76] Dalton PD, Klinkhammer K, Salber J, Klee D, Möller M. Direct in vitro electrospinning with polymer melts. *Biomacromolecules* 2006;7:686–90. <https://doi.org/10.1021/bm050777q>.
- [77] Hutmacher DW, Dalton PD. Melt electrospinning. *Chem Asian J* 2011;6:44–56. <https://doi.org/10.1002/asia.201000436>.
- [78] Dalton PD, Grafahrend D, Klinkhammer K, Klee D, Möller M. Electrospinning of polymer melts: Phenomenological observations. *Polymer* 2007;48:6823–33. <https://doi.org/10.1016/j.polymer.2007.09.037>.
- [79] Nayak R, Kyrtatzis IL, Truong YB, Padhye R, Arnold L. Melt-electrospinning of polypropylene with conductive additives. *J Mater Sci* 2012;47:6387–96. <https://doi.org/10.1007/s10853-012-6563-3>.
- [80] Daeniche J, Lämmlein M, Steinhübel F, Schubert DW. Revealing key parameters to minimize the diameter of polypropylene fibers produced in the melt electrospinning process. *E-Polymers* 2019;19:330–40. <https://doi.org/10.1515/epoly-2019-0034>.
- [81] Wu JE, Xu SS, Han CC, Yuan GC. Controlled drug release: On the evolution of physically entrapped drug inside the electrospun poly(lactic-co-glycolic acid) matrix. *J Control Release* 2021;331:472–9. <https://doi.org/10.1016/j.jconrel.2021.01.038>.
- [82] Hou L, Wang N, Man X, Cui Z, Wu J, Liu J, et al. Interpenetrating Janus membrane for high rectification ratio liquid unidirectional penetration. *ACS Nano* 2019;13:4124–32. <https://doi.org/10.1021/acsnano.8b08753>.
- [83] Hsu MH, Chang CJ. Ag-doped ZnO nanorods coated metal wire meshes as hierarchical photocatalysts with high visible-light driven photoactivity and photostability. *J Hazard Mater* 2014;278:444–53. <https://doi.org/10.1016/j.jhazmat.2014.06.038>.
- [84] Ramalingam R, Dhand C, Mayandi V, Leung CM, Ezhilarasu H, Karuppannan SK, et al. Core-shell structured antimicrobial nanofiber dressings containing herbal extract and antibiotics combination for the prevention of biofilms and promotion of cutaneous wound healing. *ACS Appl Mater Interfaces* 2021;13:24356–69. <https://doi.org/10.1021/acsami.0c20642>.
- [85] Pham QP, Sharma U, Mikos AG. Electrospun poly(ϵ -caprolactone) microfiber and multilayer nanofiber/microfiber scaffolds: Characterization of scaffolds and measurement of cellular infiltration. *Biomacromolecules* 2006;7:2796–805. <https://doi.org/10.1021/bm060680j>.
- [86] Zdarta J, Jankowska K, Wyszowska M, Kijenska-Gawronska E, Zgola-Grzeskowiak A, Pinelo M, et al. Robust biodegradation of naproxen and diclofenac by laccase immobilized using electrospun nanofibers with enhanced stability and reusability. *Mater Sci Eng C* 2019;103:109789. <https://doi.org/10.1016/j.msec.2019.109789>.
- [87] Kchaou M, Alquraish M, Abuhasel K, Abdullah A, Ali A. Electrospun nanofibrous scaffolds: review of current progress in the properties and manufacturing process, and possible applications for COVID-19. *Polymers* 2021;13:916. <https://doi.org/10.3390/polym13060916>.
- [88] Szewczyk PK, Gradyas A, Kim SK, Persano L, Marzec M, Krysztal A, et al. Enhanced piezoelectricity of electrospun polyvinylidene fluoride fibers for energy harvesting. *ACS Appl Mater Interfaces* 2020;12:13575–83. <https://doi.org/10.1021/acsami.0c02578>.
- [89] Jiang H, Fang D, Hsiao BS, Chu B, Chen W. Optimization and characterization of dextran membranes prepared by electrospinning. *Biomacromolecules* 2004;5:326–33. <https://doi.org/10.1021/bm034345w>.
- [90] Ueki T, Yoshihara A, Teramura Y, Takai M. Fast and selective cell isolation from blood sample by microfiber fabric system with vacuum aspiration. *Sci Technol Adv Mater* 2016;17:807–15. <https://doi.org/10.1080/14686996.2016.1243006>.
- [91] Celebioglu A, Uyar T. Hydrocortisone/cyclodextrin complex electrospun nanofibers for a fast-dissolving oral drug delivery system. *RSC Med Chem* 2020;11:245–58. <https://doi.org/10.1039/c9md00390h>.
- [92] Cai J, Zhang D, Zhou R, Zhu RY, Fei P, Zhu ZZ, et al. Hydrophobic interface starch nanofibrous film for food packaging: From bioinspired design to self-cleaning action. *J Agric Food Chem* 2021;69:5067–75. <https://doi.org/10.1021/acs.jafc.1c00230>.
- [93] Diep E, Schiffman JD. Encapsulating bacteria in alginate-based electrospun nanofibers. *Biomater Sci* 2021;9:4364–73. <https://doi.org/10.1039/d0bm02205e>.
- [94] Hu X, Wang X, Li S, Zhou W, Song W. Antibacterial electrospun polyvinyl alcohol nanofibers encapsulating berberine-hydroxypropyl- β -cyclodextrin inclusion complex. *J Drug Deliv Sci Technol* 2021;64:102649. <https://doi.org/10.1016/j.jddst.2021.102649>.
- [95] Zhou Y, Shen M, Cui X, Shao Y, Li L, Zhang Y. Triboelectric nanogenerator based self-powered sensor for artificial intelligence. *Nano Energy* 2021;84:105887. <https://doi.org/10.1016/j.nanoen.2021.105887>.
- [96] Lai YM, Zhao Y, Cai WP, Song J, Jia YT, Ding B, et al. Constructing ionic gradient and lithophilic interphase for high-rate Li-metal anode. *Small* 2019;15:e1905171. <https://doi.org/10.1002/sml.201905171>.
- [97] Leong MF, Chian KS, Mhaisalkar PS, Ong WF, Ratner BD. Effect of electrospun poly(D,L-lactide) fibrous scaffold with nanoporous surface on attachment of porcine esophageal epithelial cells and protein adsorption. *J Biomed Mater Res A* 2009;89a:1040–8. <https://doi.org/10.1002/jbm.a.32061>.
- [98] Ma ML, Gupta M, Li Z, Zhai L, Gleason KK, Cohen RE, et al. Decorated electrospun fibers exhibiting superhydrophobicity. *Adv Mater* 2007;19:255–9. <https://doi.org/10.1002/adma.200601449>.

- [99] Zheng JF, Zhang HY, Zhao ZG, Han CC. Construction of hierarchical structures by electrospinning or electrospraying. *Polymer* 2012;53:546–54. <https://doi.org/10.1016/j.polymer.2011.12.018>.
- [100] Lu P, Xia Y. Maneuvering the internal porosity and surface morphology of electrospun polystyrene yarns by controlling the solvent and relative humidity. *Langmuir* 2013;29:7070–8. <https://doi.org/10.1021/la400747y>.
- [101] Wang Z, He HY, Liu S, Wang H, Zeng QS, Liu Z, et al. Air stable organic-inorganic perovskite nanocrystals@polymer nanofibers and waveguide lasing. *Small* 2020;16:e2004409. <https://doi.org/10.1002/sml.202004409>.
- [102] Ura DP, Knapczyk-Korczak J, Szewczyk PK, Sroczyk EA, Busolo T, Marzec MM, et al. Surface potential driven water harvesting from fog. *ACS Nano* 2021;15:8848–59. <https://doi.org/10.1021/acsnano.1c01437>.
- [103] Cheng J, Li H, Zhou J, Lin Z, Wu D, Liu C, et al. Laser induced porous electrospun fibers for enhanced filtration of xylene gas. *J Hazard Mater* 2020;399:122976. <https://doi.org/10.1016/j.jhazmat.2020.122976>.
- [104] Zhang X, Guo M, Guo Q, Liu N, Wang Y, Wu T. Modulating axonal growth and neural stem cell migration with the use of uniaxially aligned nanofiber yarns welded with NGF-loaded microparticles. *Mater Today Adv* 2023;17:100343. <https://doi.org/10.1016/j.mtadv.2023.100343>.
- [105] Li Z, Tian C, Jiao D, Li J, Li Y, Zhou X, et al. Synergistic effects of silver nanoparticles and cisplatin in combating inflammation and hyperplasia of airway stents. *Bioact Mater* 2022;9:266–80. <https://doi.org/10.1016/j.bioactmat.2021.07.029>.
- [106] Meng ZJ, Mu XD, He JK, Zhang JL, Ling R, Li DC. Embedding aligned nanofiber architectures within 3D-printed polycaprolactone scaffolds for directed cellular infiltration and tissue regeneration. *Int J Extrem Manuf* 2023;5:025001. <https://doi.org/10.1088/2631-7990/acbd6c>.
- [107] Liu N, Zhou Z, Ning X, Zhang X, Guo Q, Guo M, et al. Enhancing the paracrine effects of adipose stem cells using nanofiber-based meshes prepared by light-welding for accelerating wound healing. *Mater Design* 2023;225:111582. <https://doi.org/10.1016/j.matdes.2022.111582>.
- [108] Chen P, Xu C, Wu P, Liu K, Chen F, Chen Y, et al. Wirelessly powered electrical-stimulation based on biodegradable 3D piezoelectric scaffolds promotes the spinal cord injury repair. *ACS Nano* 2022;16:16513–28. <https://doi.org/10.1021/acsnano.2c05818>.
- [109] Liu M, Shafiq M, Sun B, Wu J, Wang W, El-Newehy M, et al. Composite superelastic aerogel scaffolds containing flexible SiO₂ nanofibers promote bone regeneration. *Adv Healthc Mater* 2022;11:e2200499. <https://doi.org/10.1002/adhm.202200499>.
- [110] Shi C, Zhou A, Fang D, Lu T, Wang J, Song Y, et al. Oregon essential oil/ β -cyclodextrin inclusion compound polylactic acid/polycaprolactone electrospun nanofibers for active food packaging. *Chem Eng J* 2022;445:136746. <https://doi.org/10.1016/j.cej.2022.136746>.
- [111] Yu H, Li Y, Pan Y, Wang H, Wang W, Ren X, et al. Multifunctional porous poly (l-lactic acid) nanofiber membranes with enhanced anti-inflammation, angiogenesis and antibacterial properties for diabetic wound healing. *J Nanobiotechnology* 2023;21:110. <https://doi.org/10.1186/s12951-023-01847-w>.
- [112] Weng CJ, Lee D, Ho J, Liu SJ. Doxycycline-embedded nanofibrous membranes help promote healing of tendon rupture. *Int J Nanomedicine* 2020;15:125–36. <https://doi.org/10.2147/ijn.s217697>.
- [113] Jin S, Xia X, Huang J, Yuan C, Zuo Y, Li Y, et al. Recent advances in PLGA-based biomaterials for bone tissue regeneration. *Acta Biomater* 2021;127:56–79. <https://doi.org/10.1016/j.actbio.2021.03.067>.
- [114] Ghitman J, Biru EI, Stan R, Iovu H. Review of hybrid PLGA nanoparticles: Future of smart drug delivery and theranostics medicine. *Mater Design* 2020;193:108805. <https://doi.org/10.1016/j.matdes.2020.108805>.
- [115] Zhou J, Yi T, Zhang Z, Yu DG, Liu P, Wang L, et al. Electrospun janus core (ethyl cellulose/polyethylene oxide) @ shell (hydroxypropyl methyl cellulose acetate succinate) hybrids for an enhanced colon-targeted prolonged drug absorbance. *Adv Compos Hybrid Mater* 2023;6:189. <https://doi.org/10.1007/s42114-023-00766-6>.
- [116] Feng K, Huang RM, Wu RQ, Wei YS, Zong MH, Linhardt RJ, et al. A novel route for double-layered encapsulation of probiotics with improved viability under adverse conditions. *Food Chem* 2020;310:125977. <https://doi.org/10.1016/j.foodchem.2019.125977>.
- [117] Li T, Qi H, Dong X, Li G, Zhai W. Highly robust conductive organo-hydrogels with powerful sensing capabilities under large mechanical stress. *Adv Mater* 2023;36:e2304145. <https://doi.org/10.1002/adma.202304145>.
- [118] Zhao P, Zhou KC, Xia YR, Qian C, Yu DG, Xie YF, et al. Electrospun trilayer eccentric Janus nanofibers for a combined treatment of periodontitis. *Adv Fiber Mater* 2024;6. <https://doi.org/10.1007/s42765-024-00397-6>.
- [119] Rahman SU, Oh JH, Cho YD, Chung SH, Lee G, Baek JH, et al. Fibrous topography-potentiated canonical Wnt signaling directs the odontoblastic differentiation of dental pulp-derived stem cells. *ACS Appl Mater Interfaces* 2018;10:17526–41. <https://doi.org/10.1021/acsmi.7b19782>.
- [120] Wu K, Yang W, Jiao Y, Zhou C. A surface molecularly imprinted electrospun polyethersulfone (PES) fiber mat for selective removal of bilirubin. *J Mater Chem B* 2017;5:5763–73. <https://doi.org/10.1039/c7tb00643h>.
- [121] Bae J, Baek I, Choi H. Mechanically enhanced PES electrospun nanofiber membranes (ENMs) for microfiltration: The effects of ENM properties on membrane performance. *Water Res* 2016;105:406–12. <https://doi.org/10.1016/j.watres.2016.09.020>.
- [122] Liu H, Yuan XL, Liu T, Zhang W, Dong H, Chu ZY. Freestanding nanofiber-assembled aptasensor for precisely and ultrafast electrochemical detection of alzheimer's disease biomarkers. *Adv Healthc Mater* 2024;13:e2304355. <https://doi.org/10.1002/adhm.202304355>.
- [123] Li T, Qu M, Carlos C, Gu L, Jin F, Yuan T, et al. High-performance poly(vinylidene difluoride)/dopamine core/shell piezoelectric nanofiber and its application for biomedical sensors. *Adv Mater* 2020;33:e2006093. <https://doi.org/10.1002/adma.202006093>.
- [124] Cheng Y, Wang J, Lu XF, Wang C. An all-nanofibrous Janus textile with directional perspiration for triboelectric nanogenerator and self-powered e-skin sensor. *Nano Energy* 2023;117:108852. <https://doi.org/10.1016/j.nanoen.2023.108852>.
- [125] Le TT, Curry EJ, Vinikoor T, Das R, Liu Y, Sheets D, et al. Piezoelectric nanofiber membrane for reusable, stable, and highly functional face mask filter with long-term biodegradability. *Adv Funct Mater* 2022;32:2113040. <https://doi.org/10.1002/adfm.202113040>.
- [126] Du WW, Li ZK, Zhao YL, Zhang X, Pang LL, Wang W, et al. Biocompatible and breathable all-fiber-based piezoresistive sensor with high sensitivity for human physiological movements monitoring. *Chem Eng J* 2022;446:137268. <https://doi.org/10.1016/j.cej.2022.137268>.
- [127] Fan W, Lei R, Dou H, Wu Z, Lu L, Wang S, et al. Sweat permeable and ultrahigh strength 3D PVDF piezoelectric nanoyarn fabric strain sensor. *Nat Commun* 2024;15:3509. <https://doi.org/10.1038/s41467-024-47810-7>.
- [128] Wang J, Teng C, Yan L. Applications of deep eutectic solvents in the extraction, dissolution, and functional materials of chitin: Research progress and prospects. *Green Chem* 2022;24:552–64. <https://doi.org/10.1039/d1gc04340d>.
- [129] Shi L, Li Z, Zhang Y, Ren Z, Zhang Y, Li S, et al. Electrospun starch-based nanofiber mats for odor adsorption of oyster peptides: Recyclability and structural characterization. *Food Hydrocoll* 2024;147:109408. <https://doi.org/10.1016/j.foodhyd.2023.109408>.
- [130] Cao LT, Liu Q, Ren J, Chen WS, Pei Y, Kaplan DL, et al. Electro-blown spun silk/graphene nanoionotronic skin for multifunctional fire protection and alarm. *Adv Mater* 2021;33:e2102500. <https://doi.org/10.1002/adma.202102500>.
- [131] Xiong J, Hu Q, Wu J, Jia Z, Ge S, Cao Y, et al. Structurally stable electrospun nanofibrous cellulose acetate/chitosan biocomposite membranes for the removal of chromium ions from the polluted water. *Adv Compos Hybrid Mater* 2023;6:99. <https://doi.org/10.1007/s42114-023-00680-x>.
- [132] Rokade KA, Kumbhar DD, Patil SL, Sutar SS, More KV, Dandge PB, et al. Cognifiber: Harnessing biocompatible and biodegradable 1D collagen nanofibers for sustainable nonvolatile memory and synaptic learning applications. *Adv Mater* 2024;36:e2312484. <https://doi.org/10.1002/adma.202312484>.
- [133] Mu JX, Meng ZX, Liu XR, Guan P, Lian H. Implantable nanofiber membranes with synergistic photothermal and autophagy inhibition effects for enhanced tumor therapy efficacy. *Adv Fiber Mater* 2023;5:1810–25. <https://doi.org/10.1007/s42765-023-00311-6>.
- [134] Angel N, Li S, Yan F, Kong L. Recent advances in electrospinning of nanofibers from bio-based carbohydrate polymers and their applications. *Trends Food Sci Technol* 2022;120:308–24. <https://doi.org/10.1016/j.tifs.2022.01.003>.
- [135] Zou YP, Zhou C, Li ZL, Han XW, Tong L, Liu TJH, et al. Hydrophobic tetracycline immobilized in fibrous hyaluronan regulates adhesive collagen-based hydrogel stability for infected wound healing. *Small* 2023;19:e2303414. <https://doi.org/10.1002/sml.202303414>.
- [136] Wang M, Tan Y, Li D, Xu G, Yin D, Xiao Y, et al. Negative isolation of circulating tumor cells using a microfluidic platform integrated with streptavidin-functionalized PLGA nanofibers. *Adv Fiber Mater* 2021;3:192–202. <https://doi.org/10.1007/s42765-021-00075-x>.
- [137] Ewaldz E, Brettmann B. Molecular interactions in electrospinning: From polymer mixtures to supramolecular assemblies. *ACS Appl Polym Mater* 2019;1:298–308. <https://doi.org/10.1021/acsapm.8b00073>.

- [138] Shekarforoush E, Mendes AC, Baj V, Beeren SR, Chronakis IS. Electrospun phospholipid fibers as micro-encapsulation and antioxidant matrices. *Molecules* 2017;22:1708. <https://doi.org/10.3390/molecules22101708>.
- [139] Wang Y, Chou J, Sun Y, Wen S, Vasilescu S, Zhang H. Supramolecular-based nanofibers *Mater Sci Eng C* 2019;101:650–9. <https://doi.org/10.1016/j.msec.2019.04.021>.
- [140] Dodero A, Schlatter G, Hebraud A, Vicini S, Castellano M. Polymer-free cyclodextrin and natural polymer-cyclodextrin electrospun nanofibers: A comprehensive review on current applications and future perspectives. *Carbohydr Polym* 2021;264:118042. <https://doi.org/10.1016/j.carbpol.2021.118042>.
- [141] Qin Z, Jiang Q, Zou Y, Chen M, Li J, Li Y, et al. Synthesis of nanosized gamma-cyclodextrin metal-organic frameworks as carriers of limonene for fresh-cut fruit preservation based on polycaprolactone nanofibers. *Small* 2024;20:e2400399. <https://doi.org/10.1002/sml.202400399>.
- [142] Celebioglu A, Uyar T. Fast dissolving oral drug delivery system based on electrospun nanofibrous webs of cyclodextrin/ibuprofen inclusion complex nanofibers. *Mol Pharm* 2019;16:4387–98. <https://doi.org/10.1021/acs.molpharmaceut.9b00798>.
- [143] Meng Z, Zhu L, Wang X, Zhu M. Electrospun nanofibrous composite membranes for separations. *Acc Mater Res* 2023;4:180–92. <https://doi.org/10.1021/accountsmr.2c00219>.
- [144] Muthukrishnan L. An overview on electrospinning and its advancement toward hard and soft tissue engineering applications. *Colloid Polym Sci* 2022;300:875–901. <https://doi.org/10.1007/s00396-022-04997-9>.
- [145] Wu Y, Wu J, Zhu C, Zhang L, Yan J. Mxene-intercalation induced ordered brick-mortar structures of allomorph junctions for enhanced flexibility in TiO₂ nanofibers and photocatalytic efficiency. *Chem Eng J* 2023;465:142798. <https://doi.org/10.1016/j.cej.2023.142798>.
- [146] Dou T, Zhu Y, Chu Z, Sun L, Li Z, Jing L. Controlled synthesis of Au@TiO₂ mesoporous hollow nanofibers by one-step polyethylenimine-regulated electrospinning method for efficiently photocatalytic oxidation of CO. *Appl Catal B-Environ Energy* 2024;354:124112. <https://doi.org/10.1016/j.apcatb.2024.124112>.
- [147] Dong SL, Maciejewska B, Millar R, Grobert N. 3D electrospinning of Al₂O₃/ZrO₂ fibrous aerogels for multipurpose thermal insulation. *Adv Compos Hybrid Mater* 2023;6:186. <https://doi.org/10.1007/s42114-023-00760-y>.
- [148] Zhang XX, Cheng XT, Si Y, Yu JY, Ding B. All-ceramic and elastic aerogels with nanofibrous-granular binary synergistic structure for thermal superinsulation. *ACS Nano* 2022;16:5487–95. <https://doi.org/10.1021/acsnano.1c09668>.
- [149] Cui J, Cai YC, Yu X, Shen YH, Zhou TY, Sun BB, et al. Flexible copper-doped silica fibers promote infected conjunctival tissue repair through antibacterial and anti-inflammatory effects. *Adv Fiber Mater* 2024;6:278–96. <https://doi.org/10.1007/s42765-023-00358-5>.
- [150] Wang F, Dai JW, Huang LQ, Si Y, Yu JY, Ding B. Biomimetic and superelastic silica nanofibrous aerogels with rechargeable bactericidal function for antifouling water disinfection. *ACS Nano* 2020;14:8975–84. <https://doi.org/10.1021/acsnano.0c03793>.
- [151] Loccufer E, Watson G, Zhao Y, Meledina M, Denis R, Derakhshandeh PG, et al. CO₂ methanation with Ru@MIL-101 nanoparticles fixated on silica nanofibrous veils as stand-alone structured catalytic carrier. *Appl Catal B* 2023;320:121972. <https://doi.org/10.1016/j.apcatb.2022.121972>.
- [152] Wen X, Xiong J, Sun Z, Wang L, Yu J, Qin X. A general strategy to electrospin nanofibers with ultrahigh molecular chain orientation. *Engineering* 2023;29:179–87. <https://doi.org/10.1016/j.eng.2022.09.008>.
- [153] Liu C, Liao YL, Jiao WL, Zhang XH, Wang N, Yu JY, et al. High toughness combined with high strength in oxide ceramic nanofibers. *Adv Mater* 2023;35:e2304401. <https://doi.org/10.1002/adma.202304401>.
- [154] Pirzada T, Ashrafi Z, Xie W, Khan SA. Cellulose silica hybrid nanofiber aerogels: From sol–gel electrospun nanofibers to multifunctional aerogels. *Adv Funct Mater* 2019;30:1907359. <https://doi.org/10.1002/adfm.201907359>.
- [155] Lim SK, Hwang S-H, Chang D, Kim S. Preparation of mesoporous In₂O₃ nanofibers by electrospinning and their application as a CO gas sensor. *Sensors Actuators B: Chem* 2010;149:28–33. <https://doi.org/10.1016/j.snb.2010.06.039>.
- [156] Guo X, Wang X, Li X, Jiang Y-C, Han S, Ma L, et al. Endothelial cell migration on poly (ε-caprolactone) nanofibers coated with a nanohybrid shish-kebab structure mimicking collagen fibrils. *Biomacromolecules* 2020;21:1202–13. <https://doi.org/10.1021/acs.biomac.9b01638>.
- [157] Yao S, Ramakrishna S, Chen G. Recent advances in metal–organic frameworks based on electrospinning for energy storage. *Adv Fiber Mater* 2023;5:1592–617. <https://doi.org/10.1007/s42765-023-00287-3>.
- [158] Wang Y, Cao R, Wang C, Song X, Wang R, Liu J, et al. In-situ embedding hydrogen-bonded organic frameworks nanocrystals in electrospinning nanofibers for ultrastable broad-spectrum antibacterial activity. *Adv Funct Mater* 2023;33:2214388. <https://doi.org/10.1002/adfm.202214388>.
- [159] Wang Z, Xiang L, Lin F, Tang YK, Deng LF, Cui WG. A biomaterial-based hedging immune strategy for scarless tendon healing. *Adv Mater* 2023;35:e2305201. <https://doi.org/10.1002/adma.202305201>.
- [160] Perez-Puyana V, Wieringa P, Guerrero A, Romero A, Moroni L. (Macro)molecular imprinting of proteins on PCL electrospun scaffolds. *ACS Appl Mater Interfaces* 2021;13:29293–302. <https://doi.org/10.1021/acsami.1c04022>.
- [161] Wu SY, Wan ZY, Kamal S, Zabihi F, Hu ML, Bahi A, et al. Intense-light sensing yarns achieved by interfused inorganic halide perovskite nanofiber network. *Adv Fiber Mater* 2024;6:865–82. <https://doi.org/10.1007/s42765-023-00366-5>.
- [162] Qi L, Huang Y, Sun D, Liu Z, Jiang Y, Liu J, et al. Guiding the path to healing: CuO₂-laden nanocomposite membrane for diabetic wound treatment. *Small* 2023;20:e2305100. <https://doi.org/10.1002/sml.202305100>.
- [163] Smok W, Zaborowska M, Tański T, Radoń A. Novel In₂O₃/SnO₂ heterojunction 1D nanostructure photocatalyst for mb degradation. *Opt Mater* 2023;139:113757. <https://doi.org/10.1016/j.optmat.2023.113757>.
- [164] Park KR, Cho HB, Lee J, Song Y, Kim WB, Choa YH. Design of highly porous SnO₂-CuO nanotubes for enhancing H₂S gas sensor performance. *Sens Actuators B: Chem* 2020;302:127179. <https://doi.org/10.1016/j.snb.2019.127179>.
- [165] Yang DH, Kong L, Zhong M, Zhu J, Bu XH. Metal-organic gel-derived Fe_xO_y/nitrogen-doped carbon films for enhanced lithium storage. *Small* 2019;15:e1804058. <https://doi.org/10.1002/sml.201804058>.
- [166] Tian LD, Ji DX, Zhang S, He XW, Ramakrishna S, Zhang QY. A humidity-induced nontemplating route toward hierarchical porous carbon fiber hybrid for efficient bifunctional oxygen catalysis. *Small* 2020;16:e2001743. <https://doi.org/10.1002/sml.202001743>.
- [167] Li T, Li S, Liu Q, Yin J, Sun D, Zhang M, et al. Immobilization of Ni₃CO nanoparticles into N-doped carbon nanotube/nanofiber integrated hierarchically branched architectures toward efficient overall water splitting. *Adv Sci* 2019;7:1902371. <https://doi.org/10.1002/advs.201902371>.
- [168] Yuan X, Wang R, Huang W, Kong L, Guo S, Cheng L. Morphology design of Co-electrospinning MnO-VN/C nanofibers for enhancing the microwave absorption performances. *ACS Appl Mater Interfaces* 2020;12:13208–16. <https://doi.org/10.1021/acsami.9b23310>.
- [169] Wang Y, Wang S, Lou XW. Dispersed nickel cobalt oxyphosphide nanoparticles confined in multichannel hollow carbon fibers for photocatalytic CO₂ reduction. *Angew Chem Int Ed* 2019;58:17236–40. <https://doi.org/10.1002/anie.201909707>.
- [170] Virijević K, Zivanović MN, Nikolić D, Milivojević N, Pavić J, Morić I, et al. AI-driven optimization of PCL/PEG electrospun scaffolds for enhanced in vivo wound healing. *ACS Appl Mater Interfaces* 2024;18:22989–3002. <https://doi.org/10.1021/acsami.4c03266>.
- [171] Yao ZX, Qian Y, Jin Y, Wang SK, Li JH, Yuan WE, et al. Biomimetic multilayer polycaprolactone/sodium alginate hydrogel scaffolds loaded with melatonin facilitate tendon regeneration. *Carbohydr Polym* 2022;277:118865. <https://doi.org/10.1016/j.carbpol.2021.118865>.
- [172] Quilez-Molina AI, Barroso-Solares S, Hurtado-García V, Heredia-Guerrero JA, Rodríguez-Mendez ML, Rodríguez-Pérez MA, et al. Encapsulation of copper nanoparticles in electrospun nanofibers for sustainable removal of pesticides. *ACS Appl Mater Interfaces* 2023;15:20385–97. <https://doi.org/10.1021/acsami.3c00849>.
- [173] Liu Y, Li S, Lan W, Hossen MA, Qin W, Lee K. Electrospun antibacterial and antiviral poly(ε-caprolactone)/zein/ag bead-on-string membranes and its application in air filtration. *Mater Today Adv* 2021;12:100173. <https://doi.org/10.1016/j.mtadv.2021.100173>.
- [174] Deng R, Luo Z, Rao Z, Lin Z, Chen S, Zhou J, et al. Decellularized extracellular matrix containing electrospun fibers for nerve regeneration: A comparison between core–shell structured and preblended composites. *Adv Fiber Mater* 2022;4:503–19. <https://doi.org/10.1007/s42765-021-00124-5>.
- [175] Ojha AK, Rajasekaran R, Hansda AK, Singh A, Dutta A, Seesala VS, et al. Biodegradable multi-layered silk fibroin-PCL stent for the management of cervical atresia: In vitro cytocompatibility and extracellular matrix remodeling in vivo. *ACS Appl Mater Interfaces* 2023;15:39099–116. <https://doi.org/10.1021/acsami.3c06585>.

- [176] Hwang C, Park S, Kang IG, Kim HE, Han CM. Tantalum-coated polylactic acid fibrous membranes for guided bone regeneration. *Mater Sci Eng C* 2020;115: 111112. <https://doi.org/10.1016/j.msec.2020.111112>.
- [177] Chen J, Zhang G, Zhao Y, Zhou M, Zhong A, Sun J. Promotion of skin regeneration through co-axial electrospun fibers loaded with basic fibroblast growth factor. *Adv Compos Hybrid Mater* 2022;5:1111–25. <https://doi.org/10.1007/s42114-022-00439-w>.
- [178] Yin J, Xu L, Ahmed A. Batch preparation and characterization of electrospun porous polylactic acid-based nanofiber membranes for antibacterial wound dressing. *Adv Fiber Mater* 2022;4:832–44. <https://doi.org/10.1007/s42765-022-00141-y>.
- [179] Xu L, Li QS, Wang HB, Liu H, Yu DG, Bligh SWA, et al. Electrospun multi-functional medicated tri-section Janus nanofibers for an improved anti-adhesion tendon repair. *Chem Eng J* 2024;492:152359. <https://doi.org/10.1016/j.cej.2024.152359>.
- [180] Tai Y, Yang S, Yu S, Banerjee A, Myung NV, Nam J. Modulation of piezoelectric properties in electrospun PLLA nanofibers for application-specific self-powered stem cell culture platforms. *Nano Energy* 2021;89:106444. <https://doi.org/10.1016/j.nanoen.2021.106444>.
- [181] Lv YR, Sang XY, Tian Z, Jiang SP, Li CX, Guo QY, et al. Electrospun hydroxyapatite loaded L-poly(lactic acid) aligned nanofibrous membrane patch for rotator cuff repair. *Int J Biol Macromol* 2022;217:180–7. <https://doi.org/10.1016/j.ijbiomac.2022.07.061>.
- [182] Yao YT, Jia XS, Chen SM, Zhong J, Wang XD, Gong QM, et al. Extensive cell seeding densities adaptable SF/PGA electrospinning scaffolds for bone tissue engineering. *Biomater Adv* 2022;137:212834. <https://doi.org/10.1016/j.bioadv.2022.212834>.
- [183] Ajallouean F, Guerra PR, Bahl MI, Torp AM, Hwu ET, Licht TR, et al. Multi-layer PLGA-pullulan-PLGA electrospun nanofibers for probiotic delivery. *Food Hydrocoll* 2022;123:107112. <https://doi.org/10.1016/j.foodhyd.2021.107112>.
- [184] Shang LL, Liu ZQ, Ma BJ, Shao JL, Wang B, Ma CX, et al. Dimethylallyl glycine/nanosilicates-loaded osteogenic/angiogenic difunctional fibrous structure for functional periodontal tissue regeneration. *Bioact Mater* 2021;6:1175–88. <https://doi.org/10.1016/j.bioactmat.2020.10.010>.
- [185] Chen Y, Xu W, Shafiq M, Tang J, Hao J, Xie X, et al. Three-dimensional porous gas-foamed electrospun nanofiber scaffold for cartilage regeneration. *J Colloid Interface Sci* 2021;603:94–109. <https://doi.org/10.1016/j.jcis.2021.06.067>.
- [186] Lee SH, Jeon S, Qu X, Kang MS, Lee JH, Han DW, et al. Ternary MXene-loaded PLCL/collagen nanofibrous scaffolds that promote spontaneous osteogenic differentiation. *Nano Converg* 2022;9:38. <https://doi.org/10.1186/s40580-022-00329-3>.
- [187] Luo G, Xie J, Liu J, Zhang Q, Luo Y, Li M, et al. Highly conductive, stretchable, durable, breathable electrodes based on electrospun polyurethane mats superficially decorated with carbon nanotubes for multifunctional wearable electronics. *Chem Eng J* 2023;451:138549. <https://doi.org/10.1016/j.cej.2022.138549>.
- [188] Zhong TH, Liu WC, Liu H. Green electrospinning of chitin propionate to manufacture nanofiber mats. *Carbohydr Polym* 2021;273:118593. <https://doi.org/10.1016/j.carbpol.2021.118593>.
- [189] El Fawal G, Abu-Serie MM, Mo X, Wang H. Diethyldithiocarbamate/silk fibroin/polyethylene oxide nanofibrous for cancer therapy: Fabrication, characterization and in vitro evaluation. *Int J Biol Macromol* 2021;193:293–9. <https://doi.org/10.1016/j.ijbiomac.2021.10.039>.
- [190] Wu Z, Li Q, Wang L, Zhang Y, Liu W, Zhao S, et al. A novel biomimetic nanofibrous cardiac tissue engineering scaffold with adjustable mechanical and electrical properties based on poly (glycerol sebacate) and polyaniline. *Mater Today Bio* 2023;23:100798. <https://doi.org/10.1016/j.mtbio.2023.100798>.
- [191] Chen H-Y, Khumsupan D, Patel AK, Kee PE, Ng H-S, Hsu H-Y, et al. Immobilization of *Kluyveromyces marxianus* K21 via coaxial electrospinning of PVA and sugarcane bagasse composite for bioethanol production. *Appl Energy* 2024;356:122405. <https://doi.org/10.1016/j.apenergy.2023.122405>.
- [192] Yan G, Yang Z, Li J, Li H, Wei J, Shi L, et al. Multi-unit needleless electrospinning for one-step construction of 3D waterproof MF-PVA nanofibrous membranes as high-performance air filters. *Small* 2023;19:e2206403. <https://doi.org/10.1002/smll.202206403>.
- [193] Bayrakci M, Keskinates M, Karamanoglu BY. Antibacterial, thermal decomposition and in vitro time release studies of chloramphenicol from novel PLA and PVA nanofiber mats. *Mater Sci Eng C* 2021;122:111895. <https://doi.org/10.1016/j.msec.2021.111895>.
- [194] Amer AM, El-Dek SI, Farghali AA, Shehata N. Management of ibuprofen in wastewater using electrospun nanofibers developed from PET and PS wastes. *Chemosphere* 2024;359:142313. <https://doi.org/10.1016/j.chemosphere.2024.142313>.
- [195] Hussain A, Mohamed MM, Aijaz MO, Karim MR, Aziz MA. Electrospun PEI/PAN membrane for advanced Zn ion hybrid supercapacitors. *J Energy Storage* 2024;84:110974. <https://doi.org/10.1016/j.est.2024.110974>.
- [196] Niu LY, Zhang BC, Sun J, Wang JJ, Qin CX, Dai LX. Fabrication of photocatalytic PAN nanofiber membrane loading with TiO₂@rGO by electro-spinning & electro-spraying. *Compos B Eng* 2023;266:111046. <https://doi.org/10.1016/j.compositesb.2023.111046>.
- [197] Qi Q, Wang W, Wang Y, Yu D. Robust light-driven interfacial water evaporator by electrospinning SiO₂/MWCNTs-COOH/PAN photothermal fiber membrane. *Sep Purif Technol* 2020;239:116595. <https://doi.org/10.1016/j.seppur.2020.116595>.
- [198] Guo Y, Zhang H, Zhong Y, Shi S, Wang Z, Wang P, et al. Triboelectric nanogenerator-based near-field electrospinning system for optimizing PVDF fibers with high piezoelectric performance. *ACS Appl Mater Interfaces* 2023;15:5242–52. <https://doi.org/10.1021/acsami.2c19568>.
- [199] Shao Z, Zhang X, Song Z, Liu J, Liu X, Zhang C. Simulation guided coaxial electrospinning of polyvinylidene fluoride hollow fibers with tailored piezoelectric performance. *Small* 2023;19:e2303285. <https://doi.org/10.1002/smll.202303285>.
- [200] Yu Y, Zhao X, Ge H, Ye L. A self-powered piezoelectric poly (vinyl alcohol)/polyvinylidene fluoride fiber membrane with alternating multilayer porous structure for energy harvesting and wearable sensors. *Composites Sci Technol* 2024;247:110429. <https://doi.org/10.1016/j.compscitech.2023.110429>.
- [201] Wang S, Tong W, Li Y, Zhang P, Liu Y, Chen Y, et al. Contributions of piezoelectricity and triboelectricity to a hydroxyapatite/PVDF-HFP fiber-film nanogenerator. *Nano Energy* 2023;105:108026. <https://doi.org/10.1016/j.nanoen.2022.108026>.
- [202] Cui W, Fan T, Li Y, Wang X, Liu X, Lu C, et al. Robust functional Janus nanofibrous membranes for efficient harsh environmental air filtration and oil/water separation. *J Membr Sci* 2022;663:121018. <https://doi.org/10.1016/j.memsci.2022.121018>.
- [203] Xiao YN, Xie FW, Luo H, Tang RX, Hou JZ. Electrospinning SA@PVDF-HFP core-shell nanofibers based on a visual light transmission response to alcohol for intelligent packaging. *ACS Appl Mater Interfaces* 2022;14:8437–47. <https://doi.org/10.1021/acsami.1c23055>.
- [204] Chen J-P, Chen S-C, Wu X-Q, Ke X-X, Wu R-X, Zheng Y-M. Multilevel structured TPU/PS/PA-6 composite membrane for high-efficiency airborne particles capture: Preparation, performance evaluation and mechanism insights. *J Membr Sci* 2021;633:119392. <https://doi.org/10.1016/j.memsci.2021.119392>.
- [205] Korkut I, Aydin ES. Electrospun PAN-PS membranes with improved hydrophobic properties for high-performance oil/water separation. *Sep Purif Technol* 2024;331:125590. <https://doi.org/10.1016/j.seppur.2023.125590>.
- [206] Xiong CD, Wang LM, Yu JL, Qin XH, Wang RW, Yu JY. Continuous self-crimped micro-nanofiber via one-step electrospinning. *Compos Part A Appl Sci Manuf* 2022;158:106959. <https://doi.org/10.1016/j.compositesa.2022.106959>.
- [207] Kallem P, Banat F, Yejin L, Choi H. High performance nanofiber-supported thin film composite forward osmosis membranes based on continuous thermal-rolling pretreated electrospun PES/PAN blend substrates. *Chemosphere* 2020;261:127687. <https://doi.org/10.1016/j.chemosphere.2020.127687>.
- [208] Eskitoros-Togay SM, Bulbul YE, Cinar ZK, Sahin A, Dilsiz N. Fabrication of PVP/sulfonated PES electrospun membranes decorated by sulfonated halloysite nanotubes via electrospinning method and enhanced performance of proton exchange membrane fuel cells. *Int J Hydrogen Energy* 2023;48:280–90. <https://doi.org/10.1016/j.ijhydene.2022.09.214>.
- [209] Zhou W, Zhang X, Gong X, Ding M, Yu J, Zhang S, et al. Environmentally friendly polyamide nanofiber membranes with interconnective amphiphobic channels for seawater desalination. *ACS Appl Mater Interfaces* 2022;14:35287–96. <https://doi.org/10.1021/acsami.2c12061>.
- [210] Wang J, Xu J, He Y. Novel smart textile with ultraviolet shielding and thermo-regulation fabricated via electrospinning. *J Energy Storage* 2021;42:103094. <https://doi.org/10.1016/j.est.2021.103094>.
- [211] Zhao J, Wang X, Xu Y, He P, Si Y, Liu L, et al. Multifunctional, waterproof, and breathable nanofibrous textiles based on fluorine-free, all-water-based coatings. *ACS Appl Mater Interfaces* 2020;12:15911–8. <https://doi.org/10.1021/acsami.0c00846>.
- [212] Shao Z, Chen Y, Jiang J, Xiao Y, Kang G, Wang X, et al. Multistage-split ultrafine fluffy nanofibrous membrane for high-efficiency antibacterial air filtration. *ACS Appl Mater Interfaces* 2022;14:18989–9001. <https://doi.org/10.1021/acsami.2c04700>.
- [213] Goher SS, Aly SH, Abu-Serie MM, El-Moslami SH, Allam AA, Diab NH, et al. Electrospun tamarindus indica-loaded antimicrobial PMMA/cellulose acetate/PEO nanofibrous scaffolds for accelerated wound healing: In-vitro and in-vivo assessments. *Int J Biol Macromol* 2024;258:128793. <https://doi.org/10.1016/j.ijbiomac.2023.128793>.

- [214] Tsai YT, Maggay IV, Venault A, Lin YF. Fluorine-free and hydrophobic/oleophilic PMMA/PDMS electrospun nanofibrous membranes for gravity-driven removal of water from oil-rich emulsions. *Sep Purif Technol* 2021;279:119720. <https://doi.org/10.1016/j.seppur.2021.119720>.
- [215] Xia J, Zheng Z, Guo Y. Mechanically and electrically robust, electro-spun PVDF/PMMA blend films for durable triboelectric nanogenerators. *Compos Part A Appl Sci Manuf* 2022;157:106914. <https://doi.org/10.1016/j.compositesa.2022.106914>.
- [216] Zhou M, Wu B, Zhang X, Cao S, Ma P, Wang K, et al. Preparation and UV photoelectric properties of aligned ZnO-TiO₂ and TiO₂-ZnO core-shell structured heterojunction nanotubes. *ACS Appl Mater Interfaces* 2020;12:38490–8. <https://doi.org/10.1021/acsami.0c03550>.
- [217] Wu T, Xue JJ, Xia YN. Engraving the surface of electrospun microfibers with nanoscale grooves promotes the outgrowth of neurites and the migration of schwann cells. *Angew Chem Int Ed* 2020;59:15626–32. <https://doi.org/10.1002/anie.202002593>.
- [218] Liao XL, Sun DX, Cao S, Zhang N, Huang T, Lei YZ, et al. Freely switchable super-hydrophobicity and super-hydrophilicity of sponge-like poly (vinylidene fluoride) porous fibers for highly efficient oil/ water separation. *J Hazard Mater* 2021;416:125926. <https://doi.org/10.1016/j.jhazmat.2021.125926>.
- [219] Huang J, Liu Y, Lin J, Su J, Redshaw C, Feng X, et al. Novel pyrene-based aggregation-induced emission luminogen (AIEgen) composite phase change fibers with satisfactory fluorescence anti-counterfeiting, temperature sensing, and high-temperature warning functions for solar-thermal energy storage. *Adv Compos Hybrid Mater* 2023;6:126. <https://doi.org/10.1007/s42114-023-00706-4>.
- [220] Wu Z, Bao C, Zhou S, Yang T, Wang L, Li M, et al. The synergetic effect of bioactive molecule-loaded electrospun core-shell fibres for reconstruction of critical-sized calvarial bone defect-the effect of synergetic release on bone formation. *Cell Prolif* 2020;53:e12796. <https://doi.org/10.1111/cpr.12796>.
- [221] Bhattacharya S, Roy I, Tice A, Chapman C, Udangawa R, Chakrapani V, et al. High-conductivity and high-capacitance electrospun fibers for supercapacitor applications. *ACS Appl Mater Interfaces* 2020;12:19369–76. <https://doi.org/10.1021/acsami.9b21696>.
- [222] Daraeinejad Z, Shabani I. Enhancing cellular infiltration on fluffy polyaniline-based electrospun nanofibers. *Front Bioeng Biotechnol* 2021;9:641371. <https://doi.org/10.3389/fbioe.2021.641371>.
- [223] Santiago-Morales J, Amariei G, Letón P, Rosal R. Antimicrobial activity of poly (vinyl alcohol)-poly (acrylic acid) electrospun nanofibers. *Colloids Surf B Biointerfaces* 2016;146:144–51. <https://doi.org/10.1016/j.colsurfb.2016.04.052>.
- [224] Rao SS, Jayapal SG, Rajiv S. Biodegradable electrospun nanocomposite fibers based on Poly (2-hydroxy ethyl methacrylate) and bamboo cellulose. *Compos B Eng* 2014;60:43–8. <https://doi.org/10.1016/j.compositesb.2013.12.068>.
- [225] Zhang B, Lalani R, Cheng F, Liu QS, Liu LY. Dual-functional electrospun Poly (2-hydroxyethyl methacrylate). *J Biomed Mater Res A* 2011;99a:455–66. <https://doi.org/10.1002/jbm.a.33205>.
- [226] Séon-Lutz M, Couffin AC, Vignoud S, Schlatter G, Hébraud A. Electrospinning in water and in-situ crosslinking of hyaluronic acid/cyclodextrin nanofibers: Towards wound dressing with controlled drug release. *Carbohydr Polym* 2019;207:276–87. <https://doi.org/10.1016/j.carbpol.2018.11.085>.
- [227] Agrahari V, Meng J, Ezoulin MJ, Youm I, Dim DC, Molteni A, et al. Stimuli-sensitive thiolated hyaluronic acid based nanofibers: Synthesis, preclinical safety and in vitro anti-HIV activity. *Nanomedicine (Lond)* 2016;11:2935–58. <https://doi.org/10.2217/nnm-2016-0103>.
- [228] Martin AR, Patel JM, Locke RC, Eby MR, Saleh KS, Davidson MD, et al. Nanofibrous hyaluronic acid scaffolds delivering TGF-β3 and SDF-1α for articular cartilage repair in a large animal model. *Acta Biomater* 2021;126:170–82. <https://doi.org/10.1016/j.actbio.2021.03.013>.
- [229] Song KH, Heo SJ, Peredo AP, Davidson MD, Mauck RL, Burdick JA. Influence of fiber stiffness on meniscal cell migration into dense fibrous networks. *Adv Healthc Mater* 2019;9:e1901228. <https://doi.org/10.1002/adhm.201901228>.
- [230] Zhao Q, Jiang Y, Duan Z, Yuan Z, Zha J, Wu Z, et al. A Nb₂CT_x/sodium alginate-based composite film with neuron-like network for self-powered humidity sensing. *Chem Eng J* 2022;438:135588. <https://doi.org/10.1016/j.cej.2022.135588>.
- [231] Yang X, Yang D, Zhu X, Nie J, Ma G. Electrospun and photocrosslinked gelatin/dextran-maleic anhydride composite fibers for tissue engineering. *Eur Polym J* 2019;113:142–7. <https://doi.org/10.1016/j.eurpolymj.2019.01.059>.
- [232] Street RM, Huseynova T, Xu X, Chandrasekaran P, Han L, Shih WY, et al. Variable piezoelectricity of electrospun chitin. *Carbohydr Polym* 2018;195:218–24. <https://doi.org/10.1016/j.carbpol.2018.04.086>.
- [233] Nisar N, Tsuzuki T, Lowe A, Rossiter JT, Javadi A, Powell G, et al. Chitin nanofibers trigger membrane bound defense signaling and induce elicitor activity in plants. *Int J Biol Macromol* 2021;178:253–62. <https://doi.org/10.1016/j.ijbiomac.2021.02.164>.
- [234] Wang N, Wang XF, Jia YT, Li XQ, Yu JY, Ding B. Electrospun nanofibrous chitosan membranes modified with polyethyleneimine for formaldehyde detection. *Carbohydr Polym* 2014;108:192–9. <https://doi.org/10.1016/j.carbpol.2014.02.088>.
- [235] Fonseca LM, Cruxen CED, Brun GP, Fiorentini AM, Zavareze ED, Lim LT, et al. Development of antimicrobial and antioxidant electrospun soluble potato starch nanofibers loaded with carvacrol. *Int J Biol Macromol* 2019;139:1182–90. <https://doi.org/10.1016/j.ijbiomac.2019.08.096>.
- [236] Vasilyev G, Vilensky R, Zussman E. The ternary system amylose-amylopectin-formic acid as precursor for electrospun fibers with tunable mechanical properties. *Carbohydr Polym* 2019;214:186–94. <https://doi.org/10.1016/j.carbpol.2019.03.047>.
- [237] Fonseca LM, de Oliveira JP, de Oliveira PD, Zavareze ED, Dias ARG, Lim LT. Electrospinning of native and anionic corn starch fibers with different amylose contents. *Food Res Int* 2019;116:1318–26. <https://doi.org/10.1016/j.foodres.2018.10.021>.
- [238] Dai JM, Bai M, Li CZ, Cui HY, Lin L. The improvement of sodium dodecyl sulfate on the electrospinning of gelatin O/W emulsions for production of core-shell nanofibers. *Food Hydrocolloid* 2023;145:109092. <https://doi.org/10.1016/j.foodhyd.2023.109092>.
- [239] Buttafoco L, Kolkman NG, Engbers-Buijtenhuijs P, Poot AA, Dijkstra PJ, Vermes I, et al. Electrospinning of collagen and elastin for tissue engineering applications. *Biomaterials* 2006;27:724–34. <https://doi.org/10.1016/j.biomaterials.2005.06.024>.
- [240] Carlisle CR, Coulais C, Namboothiry M, Carroll DL, Hantgan RR, Guthold M. The mechanical properties of individual, electrospun fibrinogen fibers. *Biomaterials* 2009;30:1205–13. <https://doi.org/10.1016/j.biomaterials.2008.11.006>.
- [241] McManus MC, Boland ED, Koo HP, Barnes CP, Pawlowski KJ, Wnek GE, et al. Mechanical properties of electrospun fibrinogen structures. *Acta Biomater* 2006;2:19–28. <https://doi.org/10.1016/j.actbio.2005.09.008>.
- [242] Park BK, Um IC. Effect of molecular weight on electro-spinning performance of regenerated silk. *Int J Biol Macromol* 2018;106:1166–72. <https://doi.org/10.1016/j.ijbiomac.2017.08.115>.
- [243] Pignatelli C, Perotto G, Nardini M, Cancedda R, Mastrogiacomio M, Athanassiou A. Electrospun silk fibroin fibers for storage and controlled release of human platelet lysate. *Acta Biomater* 2018;73:365–76. <https://doi.org/10.1016/j.actbio.2018.04.025>.
- [244] Wang S, Zhu J, Shen M, Zhu M, Shi X. Poly(amidoamine) dendrimer-enabled simultaneous stabilization and functionalization of electrospun Poly (gamma-glutamic acid) nanofibers. *ACS Appl Mater Interfaces* 2014;6:2153–61. <https://doi.org/10.1021/am405273v>.
- [245] Melendez-Rodriguez B, Reis MAM, Carvalho M, Sammon C, Cabedo L, Torres-Giner S, et al. Development and characterization of electrospun biopapers of Poly(3-hydroxybutyrate-co-3-hydroxyvalerate) derived from cheese whey with varying 3-hydroxyvalerate contents. *Biomacromolecules* 2021;22:2935–53. <https://doi.org/10.1021/acs.biomac.1c00353>.
- [246] Cacciotti I, Pallotto F, Scognamiglio V, Moscone D, Arduini F. Reusable optical multi-plate sensing system for pesticide detection by using electrospun membranes as smart support for acetylcholinesterase immobilisation. *Mater Sci Eng C* 2020;111:110744. <https://doi.org/10.1016/j.msec.2020.110744>.
- [247] Kuntzler SG, Almeida ACA, Costa JAV, Morais MG. Polyhydroxybutyrate and phenolic compounds microalgae electrospun nanofibers: A novel nanomaterial with antibacterial activity. *Int J Biol Macromol* 2018;113:1008–14. <https://doi.org/10.1016/j.ijbiomac.2018.03.002>.
- [248] Hosseini FS, Soleimanifar F, Aidun A, Enderami SE, Saburi E, Marzouni HZ, et al. Poly (3-hydroxybutyrate-co-3-hydroxyvalerate) improved osteogenic differentiation of the human induced pluripotent stem cells while considered as an artificial extracellular matrix. *J Cell Physiol* 2019;234:11537–44. <https://doi.org/10.1002/jcp.27807>.
- [249] Arampatzis AS, Giannakoula K, Kontogiannopoulos KN, Theodoridis K, Aggelidou E, Rat A, et al. Novel electrospun poly-hydroxybutyrate scaffolds as carriers for the wound healing agents alkaninins and shikonins. *Regen Biomater* 2021;8. <https://doi.org/10.1093/rb/rbab011>. pp. rbab011.
- [250] Xie Y, Zhang Q, Zheng W, Jiang X. Small molecule-capped gold nanoclusters for curing skin infections. *ACS Appl Mater Interfaces* 2021;13:35306–14. <https://doi.org/10.1021/acsami.1c04944>.
- [251] Lv Y, Ma J, Liu K, Jiang Y, Yang G, Liu Y, et al. Rapid elimination of trace bisphenol pollutants with porous beta-cyclodextrin modified cellulose nanofibrous membrane in water: Adsorption behavior and mechanism. *J Hazard Mater* 2021;403:123666. <https://doi.org/10.1016/j.jhazmat.2020.123666>.

- [252] Celebioglu A, Uyar T. Fast-dissolving antioxidant curcumin/cyclodextrin inclusion complex electrospun nanofibrous webs. *Food Chem* 2020;317:126397. <https://doi.org/10.1016/j.foodchem.2020.126397>.
- [253] Celebioglu A, Uyar T. Development of ferulic acid/cyclodextrin inclusion complex nanofibers for fast-dissolving drug delivery system. *Int J Pharm* 2020;584:119395. <https://doi.org/10.1016/j.ijpharm.2020.119395>.
- [254] Mao Y, Guidoin R, Brochu G, Li Y, Zhang Z, Wang FJ, et al. Facile fabrication of phospholipid-functionalized nanofiber-based barriers with enhanced anti-adhesion efficiency. *Colloids Surf B Biointerfaces* 2021;203:111728. <https://doi.org/10.1016/j.colsurfb.2021.111728>.
- [255] Li Z, Fang Y, Zhang J, Lou XWD. Necklace-like structures composed of Fe₃N@C yolk-shell particles as an advanced anode for sodium-ion batteries. *Adv Mater* 2018;30:e1800525. <https://doi.org/10.1002/adma.201800525>.
- [256] Radmansouri M, Bahmani E, Sarikhani E, Rahmani K, Sharifianjazi F, Irani M. Doxorubicin hydrochloride-loaded electrospun chitosan/cobalt ferrite/titanium oxide nanofibers for hyperthermic tumor cell treatment and controlled drug release. *Int J Biol Macromol* 2018;116:378–84. <https://doi.org/10.1016/j.ijbiomac.2018.04.161>.
- [257] Zhao W, Hu X, Ci S, Chen J, Wang G, Xu Q, et al. N-doped carbon nanofibers with interweaved nanochannels for high-performance sodium-ion storage. *Small* 2019;15:e1904054. <https://doi.org/10.1002/sml.201904054>.
- [258] Zhang M, Cui J, Lu T, Tang G, Wu S, Ma W, et al. Robust, functionalized reduced graphene-based nanofibrous membrane for contaminated water purification. *Chem Eng J* 2021;404:126347. <https://doi.org/10.1016/j.cej.2020.126347>.
- [259] Wang L, Yang G, Wang J, Peng S, Yan W, Ramakrishna S. Controllable design of MoS₂ nanosheets grown on nitrogen-doped branched TiO₂/C nanofibers: Toward enhanced sodium storage performance induced by pseudocapacitance behavior. *Small* 2019;16:e1904589. <https://doi.org/10.1002/sml.201904589>.
- [260] Ahmed R, Tariq M, Ali I, Asghar R, Noorunnisa Khanam P, Augustine R, et al. Novel electrospun chitosan/polyvinyl alcohol/zinc oxide nanofibrous mats with antibacterial and antioxidant properties for diabetic wound healing. *Int J Biol Macromol* 2018;120:385–93. <https://doi.org/10.1016/j.ijbiomac.2018.08.057>.
- [261] Gao S, Wang N, Li S, Li D, Cui Z, Yue G, et al. A multi-wall Sn/SnO₂@carbon hollow nanofiber anode material for high-rate and long-life lithium-ion batteries. *Angew Chem Int Ed* 2020;59:2465–72. <https://doi.org/10.1002/anie.201913170>.
- [262] Zhang C, Shen L, Shen JQ, Liu F, Chen G, Tao R, et al. Anion-sorbent composite separator for high-rate lithium-ion batteries. *Adv Mater* 2019;31:e1808338. <https://doi.org/10.1002/adma.201808338>.
- [263] Wu TY, Wu XJ, Li LH, Hao MM, Wu G, Zhang T, et al. Anisotropic boron-carbon hetero-nanosheets for ultrahigh energy density supercapacitors. *Angew Chem Int Ed* 2020;59:23800–9. <https://doi.org/10.1002/anie.202011523>.
- [264] Li ZS, Xue KH, Wang JS, Li JG, Ao X, Sun HC, et al. Cation and anion Co-doped perovskite nanofibers for highly efficient electrocatalytic oxygen evolution. *ACS Appl Mater Interfaces* 2020;12:41259–68. <https://doi.org/10.1021/acsami.0c10045>.
- [265] Cui JX, Lu T, Li FH, Wang YL, Lei JD, Ma WJ, et al. Flexible and transparent composite nanofibre membrane that was fabricated via a “green” electrospinning method for efficient particulate matter 2.5 capture. *J Colloid Interface Sci* 2021;582:506–14. <https://doi.org/10.1016/j.jcis.2020.08.075>.
- [266] Liu Y, Gao X, Wang ZP, Wang K, Dou XY, Zhu HG, et al. Controlled synthesis of bismuth oxychloride-carbon nanofiber hybrid materials as highly efficient electrodes for rocking-chair capacitive deionization. *Chem Eng J* 2021;403:126326. <https://doi.org/10.1016/j.cej.2020.126326>.
- [267] Li S, Liu J, Ma L, Yu L-J, Hou L, Li D, et al. Okra-like multichannel TiO₂@NC fibers membrane with spatial and chemical restriction on shuttle-effect for lithium-sulfur batteries. *Adv Fiber Mater* 2022;5:252–65. <https://doi.org/10.1007/s42765-022-00217-9>.
- [268] Shen QY, Zhao XD, Liu YC, Li YP, Zhang J, Zhang N, et al. Dual-strategy of cation-doping and nanoengineering enables fast and stable sodium-ion storage in a novel Fe/Mn-based layered oxide cathode. *Adv Sci* 2020;7:2002199. <https://doi.org/10.1002/advs.202002199>.
- [269] Kang YT, Chen JH, Feng SS, Zhou HX, Zhou FQ, Low ZX, et al. Efficient removal of high-temperature particulate matters via a heat resistant and flame retardant thermally-oxidized PAN/PVP/SnO₂ nanofiber membrane. *J Membr Sci* 2022;662:120985. <https://doi.org/10.1016/j.memsci.2022.120985>.
- [270] Shao S, Zhou S, Li L, Li J, Luo C, Wang J, et al. Osteoblast function on electrically conductive electrospun PLA/MWCNTs nanofibers. *Biomaterials* 2011;32:2821–33. <https://doi.org/10.1016/j.biomaterials.2011.01.051>.
- [271] Tan HL, Kai D, Pasbakhsh P, Teow SY, Lim YY, Pushpamalar J. Electrospun cellulose acetate butyrate/polyethylene glycol (CAB/PEG) composite nanofibers: A potential scaffold for tissue engineering. *Colloids Surf B Biointerfaces* 2020;188:110713. <https://doi.org/10.1016/j.colsurfb.2019.110713>.
- [272] Saha NR, Roy I, Sarkar G, Bhattacharyya A, Das R, Rana D, et al. Development of active packaging material based on cellulose acetate butyrate/polyethylene glycol/aryl ammonium cation modified clay. *Carbohydr Polym* 2018;187:8–18. <https://doi.org/10.1016/j.carbpol.2018.01.065>.
- [273] Cheng XQ, Jiao Y, Sun ZK, Yang XB, Cheng ZJ, Bai Q, et al. Constructing scalable superhydrophobic membranes for ultrafast water-oil separation. *ACS Nano* 2021;15:3500–8. <https://doi.org/10.1021/acsnano.1c00158>.
- [274] Xu Y, Ruan J, Pang Y, Sun H, Liang C, Li H, et al. Homologous strategy to construct high-performance coupling electrodes for advanced potassium-ion hybrid capacitors. *Nanomicro Lett* 2020;13:14. <https://doi.org/10.1007/s40820-020-00524-z>.
- [275] Han N, Johnson J, Lannutti JJ, Winter JO. Hydrogel-electrospun fiber composite materials for hydrophilic protein release. *J Control Release* 2012;158:165–70. <https://doi.org/10.1016/j.jconrel.2011.09.094>.
- [276] Song JQ, Zhu GL, Wang L, An G, Shi XT, Wang YJ. Assembling of electrospun meshes into three-dimensional porous scaffolds for bone repair. *Biofabrication* 2017;9:015018. <https://doi.org/10.1088/1758-5090/aa5c99>.
- [277] Liverani L, Lacina J, Roether JA, Boccardi E, Killian MS, Schmuki P, et al. Incorporation of bioactive glass nanoparticles in electrospun PCL/chitosan fibers by using benign solvents. *Bioact Mater* 2018;3:55–63. <https://doi.org/10.1016/j.bioactmat.2017.05.003>.
- [278] Yang J, Xu L, Ding Y, Liu C, Wang B, Yu Y, et al. NIR-LL-triggered composite nanofibers to simultaneously achieve intracranial hemostasis, killing superbug and residual cancer cells in brain tumor resection surgery. *Adv Fiber Mater* 2022;5:209–22. <https://doi.org/10.1007/s42765-022-00210-2>.
- [279] Monteiro AP, Rocha CM, Oliveira MF, Gontijo SM, Agudelo RR, Sinisterra RD, et al. Nanofibers containing tetracycline/beta-cyclodextrin: Physico-chemical characterization and antimicrobial evaluation. *Carbohydr Polym* 2017;156:417–26. <https://doi.org/10.1016/j.carbpol.2016.09.059>.
- [280] Xu ZH, Liu P, Li HY, Zhang MK, Wu QY. In vitro study on electrospun lecithin-based poly (L-lactic acid) scaffolds and their biocompatibility. *J Biomater Sci Polym Ed* 2020;31:2285–98. <https://doi.org/10.1080/09205063.2020.1802837>.
- [281] Feng B, Wang SB, Hu DJ, Fu W, Wu JL, Hong HF, et al. Bioresorbable electrospun gelatin/polycaprolactone nanofibrous membrane as a barrier to prevent cardiac postoperative adhesion. *Acta Biomater* 2019;83:211–20. <https://doi.org/10.1016/j.actbio.2018.10.022>.
- [282] Wang L, Yang J, Ran B, Yang X, Zheng W, Long Y, et al. Small molecular TGF-β1-inhibitor-loaded electrospun fibrous scaffolds for preventing hypertrophic scars. *ACS Appl Mater Interfaces* 2017;9:32545–53. <https://doi.org/10.1021/acsami.7b09796>.
- [283] Zahran SME, Abdel-Halim AH, Nassar K, Nada AA. Fabrication of nanofiltration membrane based on non-biofouling PVP/lecithin nanofibers reinforced with microcrystalline cellulose via needle and needle-less electrospinning techniques. *Int J Biol Macromol* 2020;157:530–43. <https://doi.org/10.1016/j.ijbiomac.2020.04.152>.
- [284] Jiang C, Ling Z, Xu Y, Bao J, Feng L, Cheng H, et al. Long-term, synergistic and high-efficient antibacterial polyacrylonitrile nanofibrous membrane prepared by “one-pot” electrospinning process. *J Colloid Interface Sci* 2022;609:718–33. <https://doi.org/10.1016/j.jcis.2021.11.075>.
- [285] Jin G, Prabhakaran M, Kai D, Ramakrishna S. Controlled release of multiple epidermal induction factors through core-shell nanofibers for skin regeneration. *Eur J Pharm Biopharm* 2013;85:689–98. <https://doi.org/10.1016/j.ejpb.2013.06.002>.
- [286] Wen S, Hu Y, Zhang Y, Huang S, Zuo Y, Y. J Min Dual-functional core-shell electrospun mats with precisely controlled release of anti-inflammatory and antibacterial agents Mater Sci and Eng C 2019;100:514–22. <https://doi.org/10.1016/j.msec.2019.02.076>.
- [287] J. Zhang, K. Qiu, B. Sun, J. Fang, K. Zhang, H. El-Hamshary, et al. The aligned core-sheath nanofibers with electrical conductivity for neural tissue engineering. *J Mater Chem B*, 2 (2014), pp. 7945-7954, 10.1039/c4tb01185f.
- [288] Lan B, Zhong C, Wang S, Ao Y, Liu Y, Sun Y, et al. A highly sensitive coaxial nanofiber mask for respiratory monitoring assisted with machine learning. *Adv Fiber Mater* 2024. <https://doi.org/10.1007/s42765-024-00420-w>.
- [289] Fang S, Shen L, Tong Z, Zheng H, Zhang F, Zhang X. Si nanoparticles encapsulated in elastic hollow carbon fibres for Li-ion battery anodes with high structural stability. *Nanoscale* 2015;7:7409–14. <https://doi.org/10.1039/c5nr00132c>.

- [290] Zhang X, Thavasi V, Mhaisalkar S, Ramakrishna S. Novel hollow mesoporous 1D TiO₂ nanofibers as photovoltaic and photocatalytic materials. *Nanoscale* 2012;4:1707–16. <https://doi.org/10.1039/c2nr11251e>.
- [291] Hwang S, Kim Y, Hong S, Lim S. Cu/CuO@ZnO hollow nanofiber gas sensor: effect of hollow nanofiber structure and P–N junction on operating temperature and sensitivity. *Sensors* 2019;19:3151. <https://doi.org/10.3390/s19143151>.
- [292] Liu Y, Liu Q, Lin W, Yang X, Yang W, Zheng J, et al. Advanced supercapacitors based on porous hollow carbon nanofiber electrodes with high specific capacitance and large energy density. *ACS Appl Mater Interfaces* 2020;12:4777–86. <https://doi.org/10.1021/acsami.9b19977>.
- [293] McCann J, Marquez M, Xia Y. Highly porous fibers by electrospinning into a cryogenic liquid. *J Am Chem Soc* 2006;128:1436–7. <https://doi.org/10.1021/ja056810y>.
- [294] Song K, Wu Q, Zhang Z, Ren S, Lei T, Negulescu II, et al. Porous carbon nanofibers from electrospun biomass tar/polyacrylonitrile/silver hybrids as antimicrobial materials. *ACS Appl Mater Interfaces* 2015;7:15108–16. <https://doi.org/10.1021/acsami.5b04479>.
- [295] Rezaeibei E, Wood-Adams PM, Demarquette NR. Complex morphology formation in electrospinning of binary and ternary poly (lactic acid) solutions. *Macromolecules* 2018;51:4094–107. <https://doi.org/10.1021/acs.macromol.8b00083>.
- [296] Nguyen T, Ghosh C, Hwang S, Chanunpanich N, J Park Porous core/sheath composite nanofibers fabricated by coaxial electrospinning as a potential mat for drug release system *Int J Pharm* 2012;439:296–306. <https://doi.org/10.1016/j.ijpharm.2012.09.019>.
- [297] Chen S, John J, McCarthy A, Carlson M, Li X, Xie J. Fast transformation of 2D nanofiber membranes into pre-molded 3D scaffolds with biomimetic and oriented porous structure for biomedical applications. *Appl Phys Rev* 2020;7:021406. <https://doi.org/10.1063/1.5144808>.
- [298] Wang HK, Yang XM, Wu QZ, Zhang QB, Chen HX, Jing HM, et al. Encapsulating silica/antimony into porous electrospun carbon nanofibers with robust structure stability for high-efficiency lithium storage. *ACS Nano* 2018;12:3406–16. <https://doi.org/10.1021/acsnano.7b09092>.
- [299] Lou Z, Li F, Deng J, Wang L, Zhang T. Branch-like hierarchical heterostructure (α -Fe₂O₃/TiO₂): a novel sensing material for trimethylamine gas sensor. *ACS Appl Mater Interfaces* 2013;5:12310–6. <https://doi.org/10.1021/am402532v>.
- [300] Lencova S, Stindlova M, Havlickova K, Jencova V, Peroutka V, Navratilova K, et al. Influence of fiber diameter of polycaprolactone nanofibrous materials on biofilm formation and retention of bacterial cells. *ACS Appl Mater Interfaces* 2024;16:25813–24. <https://doi.org/10.1021/acsami.4c03642>.
- [301] Wei Y, Liu Z, Zhu X, Jiang L, Shi W, Wang Y, et al. Dual directions to address the problem of aseptic loosening via electrospun PLGA@aspirin nanofiber coatings on titanium. *Biomaterials* 2020;257:120237. <https://doi.org/10.1016/j.biomaterials.2020.120237>.
- [302] Huang Q, He F, Yu J, Zhang J, Du X, Li Q, et al. Microfluidic spinning-induced heterotypic bead-on-string fibers for dual-cargo release and wound healing. *J Mater Chem B* 2021;9:2727–35. <https://doi.org/10.1039/d0tb02305a>.
- [303] Esmailian S, Irani S, Bakhshi H, Zandi M. Biodegradable bead-on-spring nanofibers releasing β -carotene for bone tissue engineering. *Mater Sci Eng C* 2018;92: 800–6. <https://doi.org/10.1016/j.msec.2018.07.030>.
- [304] Yu T, Petrovic M, Attia A, Galindo D, Staub MC, Kim S, et al. MC3T3 E1 cell response to mineralized nanofiber shish kebab structures. *J Biomed Mater Res B Appl Biomater* 2021;109:1601–10. <https://doi.org/10.1002/jbm.b.34818>.
- [305] Wang X, Salick MR, Wang X, Cordie T, Han W, Peng Y, et al. Poly(epsilon-caprolactone) nanofibers with a self-induced nanohybrid shish-kebab structure mimicking collagen fibrils. *Biomaterials* 2013;34:3557–69. <https://doi.org/10.1021/bm400928b>.
- [306] Jing X, Mi H-Y, Wang X-C, Peng X-F, Turng L-S. Shish-kebab-structured poly(ϵ -caprolactone) nanofibers hierarchically decorated with chitosan–poly (ϵ -caprolactone) copolymers for bone tissue engineering. *ACS Appl Mater Interfaces* 2015;7:6955–65. <https://doi.org/10.1021/acsami.5b00900>.
- [307] Zhu G, Wang C, Yang T, Gao N, Zhang Y, Zhu J, et al. Bio-inspired gradient poly(lactic acid) nanofibers for active capturing of PM_{0.3} and real-time respiratory monitoring. *J Hazard Mater* 2024;474:134781. <https://doi.org/10.1016/j.jhazmat.2024.134781>.
- [308] Xu Y, Zhang X, Li Y, Zhang Y, Zhao T, Zeng Y. Radiative cooling face mask based on mixed micro- and nanofibrous fabric. *Chem Eng J* 2024;481:148722. <https://doi.org/10.1016/j.cej.2024.148722>.
- [309] Yu T, Gleeson SE, Li CY, Marcolongo M. Electrospun poly (ϵ -caprolactone) nanofiber shish kebabs mimic mineralized bony surface features. *J Biomed Mater Res B* 2019;107:1141–9. <https://doi.org/10.1002/jbm.b.34207>.
- [310] Karbowiczek JE, Ura DP, Stachewicz U. Nanoparticles distribution and agglomeration analysis in electrospun fiber based composites for desired mechanical performance of poly(3-hydroxybutyrate-co-3-hydroxyvalerate (PHBV) scaffolds with hydroxyapatite (HA) and titanium dioxide (TiO₂) towards medical applications. *Compos Part B-eng* 2022;241:110011. <https://doi.org/10.1016/j.compositesb.2022.110011>.
- [311] Yang R, Zhu Y, Chen F, Qin D, Xiong Z. Bioinspired macroscopic ribbon fibers with a nacre-mimetic architecture based on highly ordered alignment of ultralong hydroxyapatite nanowires. *ACS Nano* 2018;12:12284–95. <https://doi.org/10.1021/acsnano.8b06096>.
- [312] Topuz F, Uyar T. Electrospinning of gelatin with tunable fiber morphology from round to flat/ribbon. *Mater Sci Eng C* 2017;80:371–8. <https://doi.org/10.1016/j.msec.2017.06.001>.
- [313] Li Y, Guo F, Hao Y, Gupta S, Hu J, Wang Y, et al. Helical nanofiber yarn enabling highly stretchable engineered microtissue. *Proc Natl Acad Sci USA* 2019;116: 9245–50. <https://doi.org/10.1073/pnas.1821617116>.
- [314] Lou Z, Wang L, Yu K, Wei Q, Hussain T, Xia X, et al. Electrospun PVB/AVE NMs as mask filter layer for win-win effects of filtration and antibacterial activity. *J Membr Sci* 2023;672:121473. <https://doi.org/10.1016/j.memsci.2023.121473>.
- [315] Dai Y, Lu T, Li L, Zhang F, Xu H, Li H, et al. Electrospun composite PLLA-PPSB nanofiber nerve conduits for peripheral nerve defects repair and regeneration. *Adv Healthc Mater* 2024;13:e2303539. <https://doi.org/10.1002/adhm.202303539>.
- [316] Xing W, Ma Z, Wang C, Lu J, Gao J, Yu C, et al. Novel molecular organic framework composite molecularly imprinted nanofibrous membranes with a bioinspired viscid bead structure for selective recognition and separation of atrazine. *ACS Appl Mater Interfaces* 2021;13:28749–63. <https://doi.org/10.1021/acsami.1c02829>.
- [317] Gulzar S, Tagrida M, Nilsuwan K, Prodpran T, Benjakul S. Electrospinning of gelatin/chitosan nanofibers incorporated with tannic acid and chitooligosaccharides on polylactic acid film: characteristics and bioactivities. *Food Hydrocoll* 2022;133:107916. <https://doi.org/10.1016/j.foodhyd.2022.107916>.
- [318] Chen S, Ge L, Wang H, Cheng Y, Gorantla S, Poluektova LY, et al. Eluted 25-hydroxyvitamin D3 from radially aligned nanofiber scaffolds enhances cathelicidin production while reducing inflammatory response in human immune system-engrafted mice. *Acta Biomater* 2019;97:187–99. <https://doi.org/10.1016/j.actbio.2019.08.005>.
- [319] Li P, Ruan L, Jiang G, Sun Y, Wang R, Gao X, et al. Design of 3D polycaprolactone/ ϵ -polylysine-modified chitosan fibrous scaffolds with incorporation of bioactive factors for accelerating wound healing. *Acta Biomater* 2022;152:197–209. <https://doi.org/10.1016/j.actbio.2022.08.075>.
- [320] John J, McCarthy A, Wang H, Chen S, Su Y, Davis E, et al. Engineering biomimetic nanofiber microspheres with tailored size, predesigned structure, and desired composition via gas bubble-mediated coaxial electrospray. *Small* 2020;16:e1907393. <https://doi.org/10.1002/smll.201907393>.
- [321] Cao L, Yu X, Yin X, Si Y, Yu J, Ding B. Hierarchically maze-like structured nanofiber aerogels for effective low-frequency sound absorption. *J Colloid Interface Sci* 2021;597:21–8. <https://doi.org/10.1016/j.jcis.2021.03.172>.
- [322] Qin Z, Zhao S, Fang X, Zhao B, Deng J, Pan K. Flexible, ultra-light, and 3D designed white-light-emitting nanofiber aerogel. *Adv Funct Mater* 2021;32:2109240. <https://doi.org/10.1002/adfm.202109240>.
- [323] Cheesbrough A, Sciscione F, Riccio F, Harley P, R'Bibo L, Ziakas G, et al. Biobased elastomer nanofibers guide light-controlled human-iPSC-derived skeletal myofibers. *Adv Mater* 2022;34:e2110441. <https://doi.org/10.1002/adma.202110441>.
- [324] Jia J, Peng Y, Zha X, Ke K, Bao R, Liu Z, et al. Janus and heteromodulus elastomeric fiber mats feature regulable stress redistribution for boosted strain sensing performance. *ACS Nano* 2022;16:16806–15. <https://doi.org/10.1021/acsnano.2c06482>.
- [325] Liu L, Li R, Liu F, Huang L, Liu W, Wang J, et al. Highly elastic and strain sensing corn protein electrospun fibers for monitoring of wound healing. *ACS Nano* 2023;17:9600–10. <https://doi.org/10.1021/acsnano.3c03087>.
- [326] Qiao ZG, Lian MF, Han Y, Sun BB, Zhang X, Jiang WB, et al. Bioinspired stratified electrowritten fiber-reinforced hydrogel constructs with layer-specific induction capacity for functional osteochondral regeneration. *Biomaterials* 2021;266:120385. <https://doi.org/10.1016/j.biomaterials.2020.120385>.

- [327] Rao F, Wang Y, Zhang D, Lu C, Cao Z, Sui J, et al. Aligned chitosan nanofiber hydrogel grafted with peptides mimicking bioactive brain-derived neurotrophic factor and vascular endothelial growth factor repair long-distance sciatic nerve defects in rats. *Theranostics* 2020;10:1590–603. <https://doi.org/10.7150/thno.36272>.
- [328] Liu S, Ma J, Xu L, Lin W, Xue W, Huang M, et al. An electrospun polyurethane scaffold-reinforced zwitterionic hydrogel as a biocompatible device. *J Mater Chem B* 2020;8:2443–53. <https://doi.org/10.1039/c9tb02870f>.
- [329] John J, Choksi M, Chen S, Boda S, Su Y, McCarthy A, et al. Tethering peptides onto biomimetic and injectable nanofiber microspheres to direct cellular response. *Nanomedicine* 2019;22:102081. <https://doi.org/10.1016/j.nano.2019.102081>.
- [330] Chen R, Wang M. Synthesis of hierarchical TiO₂ micro/nanostructure and its application in hybrid solar cell. *Mater Lett* 2012;69:41–4. <https://doi.org/10.1016/j.matlet.2011.11.070>.
- [331] Rampichová M, Kuzelová EK, Filová E, Chvojka J, Safka J, Pelcl M, et al. Composite 3D printed scaffold with structured electrospun nanofibers promotes chondrocyte adhesion and infiltration. *Cell Adhes Migr* 2018;12:271–85. <https://doi.org/10.1080/19336918.2017.1385713>.
- [332] Xuan H, Li B, Xiong F, Wu S, Zhang Z, Yang Y, et al. Tailoring nano-porous surface of aligned electrospun poly (L-Lactic Acid) fibers for nerve tissue engineering. *Int J Mol Sci* 2021;22:3536. <https://doi.org/10.3390/ijms22073536>.
- [333] Shahabipour F, Tavafoghi M, Aninwene GE, Bonakdar S, Oskuee RK, Shokrgozar MA, et al. Coaxial 3D bioprinting of tri-polymer scaffolds to improve the osteogenic and vasculogenic potential of cells in co-culture models. *J Biomed Mater Res A* 2022;110:1077–89. <https://doi.org/10.1002/jbm.a.37354>.
- [334] Fang Y, Wang C, Liu Z, Ko J, Chen L, Zhang T, et al. 3D printed conductive multiscale nerve guidance conduit with hierarchical fibers for peripheral nerve regeneration. *Adv Sci* 2023;10:e2205744. <https://doi.org/10.1002/adv.202205744>.
- [335] Wang ML, Wang K, Yang YY, Liu YN, Yu DG. Electrospun environment remediation nanofibers using unspinnable liquids as the sheath fluids: A review. *Polymers* 2020;12:103. <https://doi.org/10.3390/polym12010103>.
- [336] Reyes CG, Lagerwall JPF. Disruption of electrospinning due to water condensation into the Taylor cone. *ACS Appl Mater Interfaces* 2020;12:26566–76. <https://doi.org/10.1021/acsami.0c03338>.
- [337] Lian SJ, Lamprou D, Zhao M. Electrospinning technologies for the delivery of biopharmaceuticals: Current status and future trends. *Int J Pharm* 2024;651:123641. <https://doi.org/10.1016/j.ijpharm.2023.123641>.
- [338] Patel D, Wei WY, Singh H, Xu K, Beck C, Wildy M, et al. Efficient and secure encapsulation of a natural phase change material in nanofibers using coaxial electrospinning for sustainable thermal energy storage. *ACS Sustainable Chem Eng* 2023;11:11570–9. <https://doi.org/10.1021/acssuschemeng.3c02094>.
- [339] Gu JC, Yagi S, Meng J, Dong YB, Qian C, Zhao DF, et al. High-efficiency production of core-sheath nanofiber membrane via co-axial electro-centrifugal spinning for controlled drug release. *J Membr Sci* 2022;654:120571. <https://doi.org/10.1016/j.memsci.2022.120571>.
- [340] Zhao D, Yang N, Xu L, Du J, Yang Y, Wang D. Hollow structures as drug carriers: Recognition, response, and release. *Nano Res* 2021;15:739–57. <https://doi.org/10.1007/s12274-021-3595-5>.
- [341] Zhang Y, Zhu C, Xiong Y, Gao Z, Hu W, Shi J, et al. Multi-channel hollow carbon nanofibers with graphene-like shell-structure and ultrahigh surface area for high-performance Zn-ion hybrid capacitors. *Small Methods* 2023;7:e2300714. <https://doi.org/10.1002/smt.202300714>.
- [342] Li L, Peng S, Lee JKY, Ji D, Srinivasan M, Ramakrishna S. Electrospun hollow nanofibers for advanced secondary batteries. *Nano Energy* 2017;39:111–39. <https://doi.org/10.1016/j.nanoen.2017.06.050>.
- [343] Rathore P, Schiffman JD. Beyond the single-nozzle: Coaxial electrospinning enables innovative nanofiber chemistries, geometries, and applications. *ACS Appl Mater Interfaces* 2021;13:48–66. <https://doi.org/10.1021/acsami.0c17706>.
- [344] Dror Y, Salalha W, Avrahami R, Zussman E, Yarin AL, Dersch R, et al. One-step production of polymeric microtubes by co-electrospinning. *Small* 2007;3:1064–73. <https://doi.org/10.1002/sml.200600536>.
- [345] Na HN, Chen P, Wong SC, Hague S, Li Q. Fabrication of PVDF/PVA microtubules by coaxial electrospinning. *Polymer* 2012;53:2736–43. <https://doi.org/10.1016/j.polymer.2012.04.021>.
- [346] Pan C-T, Yen C-K, Wang S-Y, Lai Y-C, Lin L, Huang JC, et al. Near-field electrospinning enhances the energy harvesting of hollow PVDF piezoelectric fibers. *RSC Adv* 2015;5:85073–81. <https://doi.org/10.1039/c5ra16604g>.
- [347] Chang WK, Xu FJ, Mu XY, Ji LL, Ma GP, Nie J. Fabrication of nanostructured hollow TiO₂ nanofibers with enhanced photocatalytic activity by coaxial electrospinning. *Mater Res Bull* 2013;48:2661. <https://doi.org/10.1016/j.materresbull.2013.03.035>.
- [348] Yoon J, Yang HS, Lee BS, Yu WR. Recent progress in coaxial electrospinning: New parameters, various structures, and wide applications. *Adv Mater* 2018;30:e1704765. <https://doi.org/10.1002/adma.201704765>.
- [349] Homaeigohar S, Davoudpour Y, Habibi Y, Elbahri M. The electrospun ceramic hollow nanofibers. *Nanomaterials* 2017;7:383. <https://doi.org/10.3390/nano7110383>.
- [350] Bazilevsky AV, Yarin AL, Megaridis CM. Co-electrospinning of core-shell fibers using a single-nozzle technique. *Langmuir* 2007;23:2311–4. <https://doi.org/10.1021/la063194q>.
- [351] Yu Y, Gu L, Zhu C, van Aken PA, Maier J. Tin nanoparticles encapsulated in porous multichannel carbon microtubes: Preparation by single-nozzle electrospinning and application as anode material for high-performance Li-based batteries. *J Am Chem Soc* 2009;131:15984–5. <https://doi.org/10.1021/ja906261c>.
- [352] Gao K, Shen M, Duan C, Xiong C, Dai L, Zhao W, et al. Co-N-doped directional multichannel PAN/CA-based electrospun carbon nanofibers as high-efficiency bifunctional oxygen electrocatalysts for Zn-air batteries. *ACS Sustainable Chem Eng* 2021;9:17068–77. <https://doi.org/10.1021/acssuschemeng.1c06040>.
- [353] Zhang LF, Hsieh YL. Carbon nanofibers with nanoporosity and hollow channels from binary polyacrylonitrile systems. *Eur Polym J* 2009;45:47–56. <https://doi.org/10.1016/j.eurpolymj.2008.09.035>.
- [354] Cheng YL, Zou BL, Wang CJ, Liu YJ, Fan XZ, Zhu L, et al. Formation mechanism of Fe₂O₃ hollow fibers by direct annealing of the electrospun composite fibers and their magnetic, electrochemical properties. *CrystEngComm* 2011;13:2863–70. <https://doi.org/10.1039/c0ce00379d>.
- [355] Peng SJ, Li LL, Hu YX, Srinivasan M, Cheng FY, Chen J, et al. Fabrication of spinel one-dimensional architectures by single-spinneret electrospinning for energy storage applications. *ACS Nano* 2015;9:1945–54. <https://doi.org/10.1021/nn506851x>.
- [356] Yin YB, Xu JJ, Liu QC, Zhang XB. Macroporous interconnected hollow carbon nanofibers inspired by golden-toad eggs toward a binder-free, high-rate, and flexible electrode. *Adv Mater* 2016;28:7494–500. <https://doi.org/10.1002/adma.201600012>.
- [357] Sun YM, Sills RB, Hu XL, Seh ZW, Xiao X, Xui HH, et al. A bamboo-inspired nanostructure design for flexible, foldable, and twistable energy storage devices. *Nano Lett* 2015;15:3899–906. <https://doi.org/10.1021/acs.nanolett.5b00738>.
- [358] Zhao X, Wang Y, Chen H, Xu Y. Revisiting the calcination-induced multi-layer hollowing of electrospun solid fibers. *CrystEngComm* 2016;18:8637–44. <https://doi.org/10.1039/c6ce01863g>.
- [359] Zhang F, Si Y, Yu J, Ding B. Electrospun porous engineered nanofiber materials: A versatile medium for energy and environmental applications. *Chem Eng J* 2023;456:140989. <https://doi.org/10.1016/j.cej.2022.140989>.
- [360] Liu R, Hou L, Yue G, Li H, Zhang J, Liu J, et al. Progress of fabrication and applications of electrospun hierarchically porous nanofibers. *Adv Fiber Mater* 2022;4:604–30. <https://doi.org/10.1007/s42765-022-00132-z>.
- [361] Min TT, Zhou LP, Sun XL, Du HY, Zhu Z, Wen YQ. Electrospun functional polymeric nanofibers for active food packaging: A review. *Food Chem* 2022;391:133239. <https://doi.org/10.1016/j.foodchem.2022.133239>.
- [362] Shahrousvand M, Haddadi-Asl V, Shahrousvand M. Step-by-step design of poly (epsilon-caprolactone) /chitosan/melilotus officinalis extract electrospun nanofibers for wound dressing applications. *Int J Biol Macromol* 2021;180:36–50. <https://doi.org/10.1016/j.ijbiomac.2021.03.046>.
- [363] McKenna E, Futrega K, Klein TJ, Altalhi TA, Popat A, Kumeria T, et al. Spray nebulization enables polycaprolactone nanofiber production in a manner suitable for generation of scaffolds or direct deposition of nanofibers onto cells. *Biofabrication* 2023;15:025003. <https://doi.org/10.1088/1758-5090/aca5b7>.
- [364] Sanhueza C, Hermosilla J, Bugallo-Casal A, Da Silva-Candal A, Taboada C, Millan R, et al. One-step electrospun scaffold of dual-sized gelatin/poly-3-hydroxybutyrate nano/microfibers for skin regeneration in diabetic wound. *Mater Sci Eng C* 2021;119:111602. <https://doi.org/10.1016/j.msec.2020.111602>.

- [365] Alvarez-Ortega O, Ruiz-Ramirez LR, Garibay-Alvarado JA, Donohue-Cornejo A, Espinosa-Cristobal LF, Cuevas-Gonzalez JC, et al. Preliminary biocompatibility tests of poly-epsilon-caprolactone/silver nanofibers in wistar rats. *Polymers* 2021;13:1135. <https://doi.org/10.3390/polym13071135>.
- [366] Borrego M, Martín-Alfonso JE, Sánchez MC, Valencia C, Franco JM. Electrospun lignin-PVP nanofibers and their ability for structuring oil. *Int J Biol Macromol* 2021;180:212–21. <https://doi.org/10.1016/j.ijbiomac.2021.03.069>.
- [367] Szewczyk PK, Stachewicz U. The impact of relative humidity on electrospun polymer fibers: From structural changes to fiber morphology. *Adv Colloid Interface Sci* 2020;286:102315. <https://doi.org/10.1016/j.cis.2020.102315>.
- [368] Wang P, Lv H, Cao X, Liu Y, Yu DG. Recent progress of the preparation and application of electrospun porous nanofibers. *Polymers* 2023;15:921. <https://doi.org/10.3390/polym15040921>.
- [369] Rezabeigi E, Demarquette NR. Ultraporos membranes electrospun from nonsolvent-induced phase-separated ternary systems. *Macromol Rapid Commun* 2019;40:e1800880. <https://doi.org/10.1002/marc.201800880>.
- [370] Wei WY, Wildy M, Xu K, Schossig J, Hu X, Hyun DC, et al. Advancing nanofiber research: Assessing nonsolvent contributions to structure using coaxial electrospinning. *Langmuir* 2023;39:10881–91. <https://doi.org/10.1021/acs.langmuir.3c01038>.
- [371] Nayani K, Katepalli H, Sharma CS, Sharma A, Patil S, Venkataraghavan R. Electrospinning combined with nonsolvent-induced phase separation to fabricate highly porous and hollow submicrometer polymer fibers. *Ind Eng Chem Res* 2012;51:1761–6. <https://doi.org/10.1021/ie2009229>.
- [372] Wei XB, Wang L, Duan CM, Chen K, Li X, Guo XM, et al. Cardiac patches made of brown adipose-derived stem cell sheets and conductive electrospun nanofibers restore infarcted heart for ischemic myocardial infarction. *Bioact Mater* 2023;27:271–87. <https://doi.org/10.1016/j.bioactmat.2023.03.023>.
- [373] Zheng X, Liu Y, Liu X, Li Q, Zheng Y. A novel PVDF-TiO₂@g-C₃N₄ composite electrospun fiber for efficient photocatalytic degradation of tetracycline under visible light irradiation. *Ecotoxicol Environ Saf* 2021;210:111866. <https://doi.org/10.1016/j.ecoenv.2020.111866>.
- [374] M. Mehraban, A. Zadhoush, S. Abdolkarim Hosseini Ravandi, R. Bagheri, A. Heidarkhan Tehrani. Preparation of porous nanofibers from electrospun polyacrylonitrile/calcium carbonate composite nanofibers using porogen leaching technique. *J Appl Polym Sci*, 128 (2013), pp. 926–933, 10.1002/app.38091.
- [375] Mokhtari-Shourijeh Z, Montazerghaem L, Olya M. Preparation of porous nanofibers from electrospun polyacrylonitrile/polyvinylidene fluoride composite nanofibers by inexpensive salt using for dye adsorption. *J Polym Environ* 2018;26:3550–63. <https://doi.org/10.1007/s10924-018-1238-z>.
- [376] Zhou G, Xu Z, Chen GS, Liu RL, Wang YM. Hydrophobic/oleophobic nanofibrous filter media with bead-on-string structure for efficient personal protection of dust in mines. *Environ Res* 2023;226:115699. <https://doi.org/10.1016/j.envres.2023.115699>.
- [377] Ner Y, Stuart JA, Whited G, Sotzing GA. Electrospinning nanoribbons of a bioengineered silk-elastin-like protein (SELP) from water. *Polymer* 2009;50:5828–36. <https://doi.org/10.1016/j.polymer.2009.09.017>.
- [378] Liu WJ, Huang C, Jin XY. Electrospinning of grooved polystyrene fibers: Effect of solvent systems. *Nanoscale Res Lett* 2015;10:949. <https://doi.org/10.1186/s11671-015-0949-5>.
- [379] Liu W, Huang C, Jin X. Tailoring the grooved texture of electrospun polystyrene nanofibers by controlling the solvent system and relative humidity. *Nanoscale Res Lett* 2014;9:350. <https://doi.org/10.1186/1556-276X-9-350>.
- [380] Liang MM, Chen X, Xu Y, Zhu L, Jin XY, Huang C. Double-grooved nanofibre surfaces with enhanced anisotropic hydrophobicity. *Nanoscale* 2017;9:16214–22. <https://doi.org/10.1039/c7nr05188c>.
- [381] Xu T, Yang H, Yang D, Yu ZZ. Polylactic acid nanofiber scaffold decorated with chitosan islandlike topography for bone tissue engineering. *ACS Appl Mater Interfaces* 2017;9:21094–210104. <https://doi.org/10.1021/acsami.7b01176>.
- [382] Yao YG, Huang ZN, Xie PF, Lacey SD, Jacob RJ, Xie H, et al. Carbothermal shock synthesis of high-entropy-alloy nanoparticles. *Science* 2018;359:1489–94. <https://doi.org/10.1126/science.aan5412>.
- [383] Sarker M, Dobner C, Zahl P, Fiankor C, Zhang J, Saxena A, et al. Porous nanographenes, graphene nanoribbons, and nanoporous graphene selectively synthesized from the same molecular precursor. *J Am Chem Soc* 2024;146:14453–67. <https://doi.org/10.1021/jacs.3c10842>.
- [384] Koombhongse S, Liu WX, Reneker DH. Flat polymer ribbons and other shapes by electrospinning. *J Polym Sci B Polym Phys* 2001;39:2598–606. <https://doi.org/10.1002/polb.10015>.
- [385] Fan X, Wang Y, Zheng M, Dunne F, Liu T, Fu X, et al. Morphology engineering of protein fabrics for advanced and sustainable filtration. *J Mater Chem A Mater* 2018;6:21585–95. <https://doi.org/10.1039/c8ta08717b>.
- [386] Guo M, Wang XF, Liu YJ, Yu HC, Dong JH, Cui ZX, et al. Hierarchical shish-kebab structures functionalizing nanofibers for controlled drug release and improved antithrombogenicity. *Biomacromolecules* 2022;23:1337–49. <https://doi.org/10.1021/acs.biomac.1c01572>.
- [387] Jiang N, He JK, Zhang W, Li D, Lv Y. Directed differentiation of BMSCs on structural/compositional gradient nanofibrous scaffolds for ligament-bone osteointegration. *Mater Sci Eng C* 2020;110:110711. <https://doi.org/10.1016/j.msec.2020.110711>.
- [388] Chen X, Gleeson SE, Yu T, Khan N, Yucha RW, Marcolongo M, et al. Hierarchically ordered polymer nanofiber shish kebabs as a bone scaffold material. *J Biomed Mater Res A* 2017;105:1786–98. <https://doi.org/10.1002/jbm.a.36039>.
- [389] Dong B, Guo Y, Sun S, Mi H, He P, Antwi-Afari M, et al. Shish-kebab-structured uhmwpe coating for efficient and cost-effective oil-water separation. *ACS Appl Mater Interfaces* 2020;12:58252–62. <https://doi.org/10.1021/acsami.0c17900>.
- [390] Ji H, Zhou X, Chen X, Zhao H, Wang Y, Zhu H, et al. Deformation-induced crystallization behavior of isotactic polypropylene sheets containing a β -nucleating agent under solid-state stretching. *Polymers* 2020;12. <https://doi.org/10.3390/polym12061258>.
- [391] Rickel A, Deng X, Engbertson D, Hong Z. Electrospun nanofiber scaffold for vascular tissue engineering. *Mater Sci Eng C* 2021;129:112373. <https://doi.org/10.1016/j.msec.2021.112373>.
- [392] Ikegami Y, Shafiq M, Aishima S, Ijima H. Heparin/growth factors-immobilized aligned electrospun nanofibers promote nerve regeneration in polycaprolactone/gelatin-based nerve guidance conduits. *Adv Fiber Mater* 2023;5:696. <https://doi.org/10.1007/s42765-023-00261-z>.
- [393] Yu CC, Chen YW, Yeh PY, Hsiao YS, Lin WT, Kuo CW, et al. Random and aligned electrospun PLGA nanofibers embedded in microfluidic chips for cancer cell isolation and integration with air foam technology for cell release. *J Nanobiotechnology* 2019;17:31. <https://doi.org/10.1186/s12951-019-0466-2>.
- [394] Wang X, Lv F, Li T, Han Y, Yi Z, Liu M, et al. Electrospun micropatterned nanocomposites incorporated with Cu₂S nanoflowers for skin tumor therapy and wound healing. *ACS Nano* 2017;11:11337–49. <https://doi.org/10.1021/acs.nano.7b05858>.
- [395] Chen W, Chen S, Morsi Y, El-Hamshary H, El-Newhy M, Fan C, et al. Superabsorbent 3D scaffold based on electrospun nanofibers for cartilage tissue engineering. *ACS Appl Mater Interfaces* 2016;8:24415–25. <https://doi.org/10.1021/acsami.6b06825>.
- [396] Shirole A, Sapkota J, Foster E, Weder C. Shape memory composites based on electrospun poly(vinyl alcohol) fibers and a thermoplastic polyether block amide elastomer. *ACS Appl Mater Interfaces* 2016;8:6701–8. <https://doi.org/10.1021/acsami.6b00834>.
- [397] Xue J, Wu T, Qiu J, Xia Y. Accelerating cell migration along radially aligned nanofibers through the addition of electrosprayed nanoparticles in a radial density gradient. *Part Part Syst Charact* 2022;39:2100280. <https://doi.org/10.1002/ppsc.202100280>.
- [398] Daghrery A, Ferreira J, Xu J, Golafshan N, Kaigler D, Bhaduri SB, et al. Tissue-specific melt electrowritten polymeric scaffolds for coordinated regeneration of soft and hard periodontal tissues. *Bioact Mater* 2023;19:268–81. <https://doi.org/10.1016/j.bioactmat.2022.04.013>.
- [399] Li D, Tao L, Shen Y, Sun B, Xie X, Ke Q, et al. Fabrication of multilayered nanofiber scaffolds with a highly aligned nanofiber yarn for anisotropic tissue regeneration. *ACS Omega* 2020;5:24340–50. <https://doi.org/10.1021/acsomega.0c02554>.
- [400] Chen L, Mei S, Fu K, Zhou J. Spinning the future: the convergence of nanofiber technologies and yarn fabrication. *ACS Nano* 2024;18:15358–86. <https://doi.org/10.1021/acsnano.4c02399>.
- [401] Jin X, Al-Qatatsheh A, Subhani K, Salim N. An ultralight, elastic carbon nanofiber aerogel with efficient energy storage and sorption properties. *Nanoscale* 2022;14:6854–65. <https://doi.org/10.1039/d2nr00083k>.
- [402] Kharaghani D, Kaffashaei E, Haider M, Kim I. The effect of polymeric nanofibers used for 3D-printed scaffolds on cellular activity in tissue engineering: a review. *Int J Mol Sci* 2023;24. <https://doi.org/10.3390/ijms24119464>.
- [403] Keirouz A, Chung M, Kwon J, Fortunato G, Radacsi N. 2D and 3D electrospinning technologies for the fabrication of nanofibrous scaffolds for skin tissue engineering: a review. *Wires Nano Nanobi* 2020;12:e1626.

- [404] Park J, Sharma J, Monaghan KW, Meyer 3rd HM, Cullen DA, Rossy AM, et al. Styrene-based elastomer composites with functionalized graphene oxide and silica nanofiber fillers: mechanical and thermal conductivity properties. *Nanomaterials* 2020;10. <https://doi.org/10.3390/nano10091682>.
- [405] Ribeiro JS, Daghery A, Dubey N, Li C, Mei L, Fenno JC, et al. Hybrid antimicrobial hydrogel as injectable therapeutics for oral infection ablation. *Biomacromolecules* 2020;21:3945–56. <https://doi.org/10.1021/acs.biomac.0c01131>.
- [406] Yang L, Zhang Y, Xiao Z, Zhang W, Li L, Fan Y. Electrospun polymeric fibers decorated with silk microcapsules via encapsulation and surface immobilization for drug delivery. *Macromol Biosci* 2023;23:e2300190. <https://doi.org/10.1002/mabi.202300190>.
- [407] Baniasadi H, Ajdary R, Trifol J, Rojas O, Seppälä J. Direct ink writing of aloe vera/cellulose nanofibrils bio-hydrogels. *Carbohydr Polym* 2021;266:118114. <https://doi.org/10.1016/j.carbpol.2021.118114>.
- [408] Liu J, Sun L, Xu W, Wang Q, Yu S, Sun J. Current advances and future perspectives of 3D printing natural-derived biopolymers. *Carbohydr Polym* 2019;207:297–316. <https://doi.org/10.1016/j.carbpol.2018.11.077>.
- [409] Yang J, An X, Liu L, Tang S, Cao H, Xu Q, et al. Cellulose, hemicellulose, lignin, and their derivatives as multi-components of bio-based feedstocks for 3D printing. *Carbohydr Polym* 2020;250:116881. <https://doi.org/10.1016/j.carbpol.2020.116881>.
- [410] Chimene D, Kaunas R, Gaharwar AK. Hydrogel bioink reinforcement for additive manufacturing: a focused review of emerging strategies. *Adv Mater* 2020;32:e1902026. <https://doi.org/10.1002/adma.201902026>.
- [411] Cheng F, Cao X, Li H, Liu T, Xie X, Huang D, et al. Generation of cost-effective paper-based tissue models through matrix-assisted sacrificial 3D printing. *Nano Lett* 2019;19:3603–11. <https://doi.org/10.1021/acs.nanolett.9b00583>.
- [412] Sakai S, Yoshii A, Sakurai S, Horii K, Nagasuna O. Silk fibroin nanofibers: a promising ink additive for extrusion three-dimensional bioprinting. *Mater Today Bio* 2020;8:100078. <https://doi.org/10.1016/j.mtbio.2020.100078>.
- [413] Huang L, Yuan W, Hong Y, Fan S, Yao X, Ren T, et al. 3D printed hydrogels with oxidized cellulose nanofibers and silk fibroin for the proliferation of lung epithelial stem cells. *Cellu* 2020;28:241–57. <https://doi.org/10.1007/s10570-020-03526-7>.
- [414] Heid S, Boccaccini AR. Advancing bioinks for 3D bioprinting using reactive fillers: a review. *Acta Biomater* 2020;113:1–22. <https://doi.org/10.1016/j.actbio.2020.06.040>.
- [415] Zhou X, Dai Z, Liu S, Bao J, Guo Y. Ultra-uniform SnOx/carbon nanohybrids toward advanced lithium-ion battery anodes. *Adv Mater* 2014;26:3943–9. <https://doi.org/10.1002/adma.201400173>.
- [416] Yoo J, Park J, Kwon Y, Chung J, Choi IC, Nam J, et al. Augmented peripheral nerve regeneration through elastic nerve guidance conduits prepared using a porous PLLC membrane with a 3D printed collagen hydrogel. *Biomater Sci* 2020;8:6261–71. <https://doi.org/10.1039/d0bm00847h>.
- [417] Hernández-Rivera D, Rodríguez-Roldán G, Mora-Martínez R, Suaste-Gómez E. A capacitive humidity sensor based on an electrospun PVDF/Graphene membrane. *Sensors* 2017;5:1009. <https://doi.org/10.3390/s17051009>.
- [418] Shao H, Fang J, Wang H, Lin T. Effect of electrospinning parameters and polymer concentrations on mechanical-to-electrical energy conversion of randomly-oriented electrospun poly(vinylidene fluoride) nanofiber mats. *Rsc Adv* 2015;5:14345–50. <https://doi.org/10.1039/c4ra16360e>.
- [419] Mercante LA, Scagion VP, Migliorini FL, Mattoso LHC, Correa DS. Electrospinning-based (bio)sensors for food and agricultural applications: A review. *Trac-Trends Anal Chem* 2017;91:91–103. <https://doi.org/10.1016/j.trac.2017.04.004>.
- [420] Ramesh B, Cherian K, Fakoya A. Fabrication and electrospinning of 3D biodegradable Poly-L-Lactic Acid (PLLA) nanofibers for clinical application. *Methods Mol Biol* 2020;2125:119–28. <https://doi.org/10.1007/9781071019213>.
- [421] Kim I, Khetan S, Baker B, Chen C, Burdick J. Fibrous hyaluronic acid hydrogels that direct MSC chondrogenesis through mechanical and adhesive cues. *Biomaterials* 2013;34:5571–80. <https://doi.org/10.1016/j.biomaterials.2013.04.004>.
- [422] C. Chang, V.H. Tran, J. Wang, Y.K. Fuh, L. Lin. Direct-write piezoelectric polymeric nanogenerator with high energy conversion efficiency. *Nano Lett*, 10 (2010), pp. 726–731.
- [423] Chen X, Xu S, Yao N, Shi Y. 1.6 V nanogenerator for mechanical energy harvesting using PZT nanofibers. *Nano Lett* 2010;10:2133–7. <https://doi.org/10.1021/nl100812k>.
- [424] Yan J, Jeong Y. High performance flexible piezoelectric nanogenerators based on BaTiO₃ nanofibers in different alignment modes. *ACS Appl Mater Interfaces* 2016;8:15700–9. <https://doi.org/10.1021/acsami.6b02177>.
- [425] Gu L, Liu JM, Cui N, Xu Q, Du T, Zhang L, et al. Enhancing the current density of a piezoelectric nanogenerator using a three-dimensional intercalation electrode. *Nat Commun* 2020;11:1030. <https://doi.org/10.1038/s41467-020-14846-4>.
- [426] Yang R, Qin Y, Dai L, Wang Z. Power generation with laterally packaged piezoelectric fine wires. *Nat Nanotechnol* 2009;4:34–9. <https://doi.org/10.1038/nnano.2008.314>.
- [427] Wang Z, Song J. Piezoelectric nanogenerators based on zinc oxide nanowire arrays. *Science* 2006;312:242–6. <https://doi.org/10.1126/science.1124005>.
- [428] Wu W, Bai S, Yuan M, Qin Y, Wang Z, Jing T. Lead zirconate titanate nanowire textile nanogenerator for wearable energy-harvesting and self-powered devices. *ACS Nano* 2012;6:6231–5. <https://doi.org/10.1021/nn3016585>.
- [429] Gu L, Cui N, Cheng L, Xu Q, Bai S, Yuan M, et al. Flexible fiber nanogenerator with 209 V output voltage directly powers a light-emitting diode. *Nano Lett* 2013;13:91–4. <https://doi.org/10.1021/nl303539c>.
- [430] Rorvik PM, Grande T, Einarsrud MA. One-dimensional nanostructures of ferroelectric perovskites. *Adv Mater* 2011;23:4007–34. <https://doi.org/10.1002/adma.201004676>.
- [431] Wu W, Cheng L, Bai S, Dou W, Xu Q, Wei Z, et al. Electrospinning lead-free 0.5Ba(Zr_{0.2}Ti_{0.8})O₃–0.5(Ba_{0.7}Ca_{0.3})TiO₃ nanowires and their application in energy harvesting. *J Mater Chem A* 2013;1:7332–8. <https://doi.org/10.1039/c3ta10792b>.
- [432] Bai S, Xu Q, Gu L, Ma F, Qin Y, Wang ZL. Single crystalline lead zirconate titanate (PZT) nano/micro-wire based self-powered UV sensor. *Nano Energy* 2012;1:789–95. <https://doi.org/10.1016/j.nanoen.2012.09.001>.
- [433] Gopal R, Kaur S, Ma ZW, Chan C, Ramakrishna S, Matsuura T. Electrospun nanofibrous filtration membrane. *J Membr Sci* 2006;281:581–6. <https://doi.org/10.1016/j.memsci.2006.04.026>.
- [434] Wang R, Liu Y, Li B, Hsiao B, Chu B. Electrospun nanofibrous membranes for high flux microfiltration. *J Membr Sci* 2012;392:167–74. <https://doi.org/10.1016/j.memsci.2011.12.019>.
- [435] Barhate R, Loong C, Ramakrishna S. Preparation and characterization of nanofibrous filtering media. *J Membr Sci* 2006;283:209–18. <https://doi.org/10.1016/j.memsci.2006.06.030>.
- [436] Wang B, Liang WX, Guo ZG, Liu WM. Biomimetic super-lyophobic and super-lyophilic materials applied for oil/water separation: a new strategy beyond nature. *Chem Soc Rev* 2015;44:336–61. <https://doi.org/10.1039/c4cs00220b>.
- [437] Obaid M, Mohamed H, Yassin M, Fadali O, Kim H, et al. Under-oil superhydrophilic wetted PVDF electrospun modified membrane for continuous gravitational oil/water separation with outstanding flux. *Water Res* 2017;123:524–35. <https://doi.org/10.1016/j.watres.2017.06.079>.
- [438] Qing W, Shi X, Deng Y, Zhang W, Wang J, Tang CY. Robust superhydrophobic-superoleophilic polytetrafluoroethylene nanofibrous membrane for oil/water separation. *J Membr Sci* 2017;540:354–61. <https://doi.org/10.1016/j.memsci.2017.06.060>.
- [439] Ge J, Zong D, Jin Q, Yu J, Ding B. Biomimetic and superwetttable nanofibrous skins for highly efficient separation of oil-in-water emulsions. *Adv Funct Mater* 2018;28:1705051. <https://doi.org/10.1002/adfm.201705051>.
- [440] Wang Y, Di J, Wang L, Li X, Wang N, Wang B, et al. Infused-liquid-switchable porous nanofibrous membranes for multiphase liquid separation. *Nat Commun* 2017;8:575. <https://doi.org/10.1038/s41467-017-00474-y>.
- [441] Zhu Z, Wang W, Qi D, Luo Y, Liu Y, Xu Y, et al. Calcinable polymer membrane with revivability for efficient oily-water remediation. *Adv Mater* 2018;30:e1801870. <https://doi.org/10.1002/adma.201801870>.
- [442] Zhao Y, Gu Y, Liu B, Yan Y, Shan C, Guo J, et al. Pulsed hydraulic-pressure-responsive self-cleaning membrane. *Nature* 2022;608:69–73. <https://doi.org/10.1038/s41586-022-04942-4>.
- [443] Yoon K, Hsiao B, Chu B. High flux nanofiltration membranes based on interfacially polymerized polyamide barrier layer on polyacrylonitrile nanofibrous scaffolds. *J Membr Sci* 2009;326:484–92. <https://doi.org/10.1016/j.memsci.2008.10.023>.

- [444] Kaur S, Sundarrajan S, Rana D, Matsuura T, Ramakrishna S. Influence of electrospun fiber size on the separation efficiency of thin film nanofiltration composite membrane. *J Membr Sci* 2012;392:101–11. <https://doi.org/10.1016/j.memsci.2011.12.005>.
- [445] Zhao Z, Zheng J, Wang M, Zhang H, Han C. High performance ultrafiltration membrane based on modified chitosan coating and electrospun nanofibrous PVDF scaffolds. *J Membr Sci* 2012;394:209–17. <https://doi.org/10.1016/j.memsci.2011.12.043>.
- [446] Subramanian S, Seeram R. New directions in nanofiltration applications — are nanofibers the right materials as membranes in desalination? *Desalination* 2013;308:198–208. <https://doi.org/10.1016/j.desal.2012.08.014>.
- [447] Kim S, Heath DE, Kentish SE. Composite membranes with nanofibrous cross-hatched supports for reverse osmosis desalination. *ACS Appl Mater Interfaces* 2020;12:44720–30. <https://doi.org/10.1021/acsami.0c12588>.
- [448] Song X, Liu Z, Sun D. Nano gives the answer: breaking the bottleneck of internal concentration polarization with a nanofiber composite forward osmosis membrane for a high water production rate. *Adv Mater* 2011;23:3256–60. <https://doi.org/10.1002/adma.201100510>.
- [449] Bui N, Lind M, Hoek E, McCutcheon J. Electrospun nanofiber supported thin film composite membranes for engineered osmosis. *J Membr Sci* 2011;385:10–9. <https://doi.org/10.1016/j.memsci.2011.08.002>.
- [450] Deshmukh A, Boo C, Karanikola V, Lin S, Straub AP, Tong T, et al. Membrane distillation at the water-energy nexus: limits, opportunities, and challenges. *Energy Environ Sci* 2018;11:1177–96. <https://doi.org/10.1039/c8ee00291f>.
- [451] Liao Y, Wang R, Fane A. Fabrication of bioinspired composite nanofiber membranes with robust superhydrophobicity for direct contact membrane distillation. *Environ Sci Technol* 2014;48:6335–41. <https://doi.org/10.1021/es405795s>.
- [452] Li M, Cao Y, Zhang X. Hierarchically structured nanoparticle-free omniphobic membrane for high-performance membrane distillation. *Environ Sci Technol* 2023;57:5841–51. <https://doi.org/10.1021/acs.est.2c07880>.
- [453] Chew N, Zhao S, Wang R. Recent advances in membrane development for treating surfactant- and oil-containing feed streams via membrane distillation. *Adv Colloid Interface Sci* 2019;273:102022. <https://doi.org/10.1016/j.cis.2019.102022>.
- [454] Zhu Z, Liu Y, Hou H, Shi W, Qu F, Cui F, et al. Dual-bioinspired design for constructing membranes with superhydrophobicity for direct contact membrane distillation. *Environ Sci Technol* 2018;52:3027–36. <https://doi.org/10.1021/acs.est.7b06227>.
- [455] Deka B, Lee E, Guo J, Kharraz J, An A. Electrospun nanofiber membranes incorporating PDMS-aerogel superhydrophobic coating with enhanced flux and improved antiwettability in membrane distillation. *Environ Sci Technol* 2019;53:4948–58. <https://doi.org/10.1021/acs.est.8b07254>.
- [456] Huang Y, Wang Z, Jin J, Lin S. Novel Janus membrane for membrane distillation with simultaneous fouling and wetting resistance. *Environ Sci Technol* 2017;51:13304–10. <https://doi.org/10.1021/acs.est.7b02848>.
- [457] Wang Z, Hou D, Lin S. Composite membrane with underwater-oleophobic surface for anti-oil-fouling membrane distillation. *Environ Sci Technol* 2016;50:3866–74. <https://doi.org/10.1021/acs.est.5b05976>.
- [458] Lu D, Zhou Z, Wang Z, Ho DT, Sheng G, Chen L, et al. An Ultrahigh-flux nanoporous graphene membrane for sustainable seawater desalination using low-grade heat. *Adv Mater* 2022;34:e2109718. <https://doi.org/10.1002/adma.202109718>.
- [459] He A, Jiang Z, Wu Y, Hussain H, Rawle J, Briggs ME, et al. A smart and responsive crystalline porous organic cage membrane with switchable pore apertures for graded molecular sieving. *Nat Mater* 2022;21:463–70. <https://doi.org/10.1038/s41563-021-01168-z>.
- [460] Su C, Horseman T, Cao H, Christie K, Li Y, Lin S. Robust superhydrophobic membrane for membrane distillation with excellent scaling resistance. *Environ Sci Technol* 2019;53:11801–9. <https://doi.org/10.1021/acs.est.9b04362>.
- [461] Zhu Z, Zhong L, Horseman T, Liu Z, Zeng G, Li Z, et al. Superhydrophobic-omniphobic membrane with anti-deformable pores for membrane distillation with excellent wetting resistance. *J Membr Sci* 2021;620:118768. <https://doi.org/10.1016/j.memsci.2020.118768>.
- [462] Zhong L, An L, Han Y, Zhu Z, Liu D, Liu D, et al. In-situ three-dimensional welded nanofibrous membranes for robust membrane distillation of concentrated seawater. *Environ Sci Technol* 2021;55:11308–17. <https://doi.org/10.1021/acs.est.1c02687>.
- [463] Wang X, Hsiao B. Electrospun nanofiber membranes. *Curr Opin Chem Eng* 2016;12:62–81. <https://doi.org/10.1016/j.coche.2016.03.001>.
- [464] Chen H, Huang M, Liu Y, Meng L, Ma M. Functionalized electrospun nanofiber membranes for water treatment: a review. *Sci Total Environ* 2020;739:139944. <https://doi.org/10.1016/j.scitotenv.2020.139944>.
- [465] Zhao R, Lu X, Wang C. Electrospinning based all-nano composite materials: recent achievements and perspectives. *Compos Commun* 2018;10:140–50. <https://doi.org/10.1016/j.coco.2018.09.005>.
- [466] Liu X, Deng Q, Zheng Y, Wang D, Ni B. Microplastics aging in wastewater treatment plants: Focusing on physicochemical characteristics changes and corresponding environmental risks. *Water Res* 2022;221:118780. <https://doi.org/10.1016/j.watres.2022.118780>.
- [467] Lv Y, Ma J, Yu Z, Liu S, Yang G, Liu Y, et al. Fabrication of covalent organic frameworks modified nanofibrous membrane for efficiently enriching and detecting the trace polychlorinated biphenyls in water. *Water Res* 2023;235:119892. <https://doi.org/10.1016/j.watres.2023.119892>.
- [468] Herath A, Salehi M, Jansone-Popova S. Production of polyacrylonitrile/ionic covalent organic framework hybrid nanofibers for effective removal of chromium (VI) from water. *J Hazard Mater* 2022;427:128167. <https://doi.org/10.1016/j.jhazmat.2021.128167>.
- [469] Li X, Zhang C, Zhao R, Lu X, Xu X, Jia X, et al. Efficient adsorption of gold ions from aqueous systems with thioamide-group chelating nanofiber membranes. *Chem Eng J* 2013;229:420–8. <https://doi.org/10.1016/j.cej.2013.06.022>.
- [470] Zhao R, Li X, Sun B, Shen M, Tan X, Ding Y, et al. Preparation of phosphorylated polyacrylonitrile-based nanofiber mat and its application for heavy metal ion removal. *Chem Eng J* 2015;268:290–9. <https://doi.org/10.1016/j.cej.2015.01.061>.
- [471] Zhao R, Li X, Sun BL, Li YZ, Li YM, Yang R, et al. Branched polyethylenimine grafted electrospun polyacrylonitrile fiber membrane: a novel and effective adsorbent for Cr(VI) remediation in wastewater. *J Mater Chem A* 2017;5:1133–44. <https://doi.org/10.1039/c6ta09784g>.
- [472] Li Y, Zhao R, Chao S, Sun B, Wang C, Li X. Polydopamine coating assisted synthesis of MnO₂ loaded inorganic/organic composite electrospun fiber adsorbent for efficient removal of Pb²⁺ from water. *Chem Eng J* 2018;344:277–89. <https://doi.org/10.1016/j.cej.2018.03.044>.
- [473] Zhao R, Ma T, Zhao S, Rong H, Tian Y, Zhu G. Uniform and stable immobilization of metal-organic frameworks into chitosan matrix for enhanced tetracycline removal from water. *Chem Eng J* 2020;382:122893. <https://doi.org/10.1016/j.cej.2019.122893>.
- [474] Zhao R, Tian Y, Li S, Ma T, Lei H, Zhu G. An electrospun fiber based metal-organic framework composite membrane for fast, continuous, and simultaneous removal of insoluble and soluble contaminants from water. *J Mater Chem A* 2019;7:22559–70. <https://doi.org/10.1039/c9ta04664j>.
- [475] Chao S, Li X, Li Y, Wang Y, Wang C. Preparation of polydopamine-modified zeolitic imidazolate framework-8 functionalized electrospun fibers for efficient removal of tetracycline. *J Colloid Interface Sci* 2019;552:506–16. <https://doi.org/10.1016/j.jcis.2019.05.078>.
- [476] Jia S, Lin P, Li Y, Teng Y, Wang J, Yang T, et al. Flexible UiO-67(Zr)/cyclodextrin-based nanofiber membrane for efficient removal of ibuprofen. *Sep Purif Technol* 2024;333:125850. <https://doi.org/10.1016/j.seppur.2023.125850>.
- [477] Zhao R, Li Y, Sun B, Chao S, Li X, Wang C, et al. Highly flexible magnesium silicate nanofibrous membranes for effective removal of methylene blue from aqueous solution. *Chem Eng J* 2019;359:1603–16. <https://doi.org/10.1016/j.cej.2018.11.011>.
- [478] Horzum N, Shahwan T, Parlak O, Demir M. Synthesis of amidoximated polyacrylonitrile fibers and its application for sorption of aqueous uranyl ions under continuous flow. *Chem Eng J* 2012;213:41–9. <https://doi.org/10.1016/j.cej.2012.09.114>.
- [479] Zhao R, Chen D, Gao N, Yuan L, Hu W, Cui F, et al. Porous cationic electrospun fibers with sufficient adsorption sites for effective and continuous 99TcO₄⁻ uptake. *Adv Funct Mater* 2022;32:2200618. <https://doi.org/10.1002/adfm.202200618>.
- [480] Kim H, Kim M, Lee W, Kim S. Rapid removal of radioactive cesium by polyacrylonitrile nanofibers containing prussian blue. *J Hazard Mater* 2018;347:106–13. <https://doi.org/10.1016/j.jhazmat.2017.12.050>.
- [481] Vivas E, Lee S, Cho K. Brushite-infused polyacrylonitrile nanofiber adsorbent for strontium removal from water. *J Environ Manage* 2020;270:110837. <https://doi.org/10.1016/j.jenvman.2020.110837>.
- [482] Yang C. Aerosol filtration application using fibrous media—an industrial perspective. *Chin J Chem Eng* 2012;20:1–9. [https://doi.org/10.1016/S1004-9541\(12\)60356-5](https://doi.org/10.1016/S1004-9541(12)60356-5).
- [483] Li Y, Yin X, Yu J, Ding B. Electrospun nanofibers for high-performance air filtration. *Compos Commun* 2019;15:6–19. <https://doi.org/10.1016/j.coco.2019.06.003>.

- [484] Song J, Zhang B, Lu Z, Xing Z, Liu T, Wei W, et al. Hierarchical porous poly(L-lactic acid) nanofibrous membrane for ultrafine particulate aerosol filtration. *ACS Appl Mater Interfaces* 2019;11:46261–8. <https://doi.org/10.1021/acsami.9b18083>.
- [485] Li J, Zhang D, Yang T, Yang S, Yang X, Zhu H. Nanofibrous membrane of graphene oxide-in-polyacrylonitrile composite with low filtration resistance for the effective capture of PM_{2.5}. *J Membrane Sci* 2018;551:85–92. <https://doi.org/10.1016/j.memsci.2018.01.025>.
- [486] Wang S, Zhao X, Yin X, Yu J, Ding B. Electret polyvinylidene fluoride nanofibers hybridized by polytetrafluoroethylene nanoparticles for high-efficiency air filtration. *ACS Appl Mater Interfaces* 2016;8:23985–94. <https://doi.org/10.1021/acsami.6b08262>.
- [487] Gu G, Han C, Lu C, He C, Jiang T, Gao Z, et al. Triboelectric nanogenerator enhanced nanofiber air filters for efficient particulate matter removal. *ACS Nano* 2017;11:6211–7. <https://doi.org/10.1021/acsnano.7b02321>.
- [488] Zhu D, Hou J, Qian M, Jin D, Hao T, Pan Y, et al. Nitrate-functionalized patch confers cardioprotection and improves heart repair after myocardial infarction via local nitric oxide delivery. *Nat Commun* 2021;12:4501. <https://doi.org/10.1038/s41467-021-24804-3>.
- [489] Matulevicius J, Kliucininkas L, Martuzevicius D, Krugly E, Tichonovas M, Baltrusaitis J. Design and characterization of electrospun polyamide nanofiber media for air filtration applications. *J Nanomater* 2014;2014:1–13. <https://doi.org/10.1155/2014/859656>.
- [490] Zhang Q, Young T, Harper D, Liles T, Wang S. Optimization of electrospun poly(vinyl alcohol)/cellulose nanocrystals composite nanofibrous filter fabrication using response surface methodology. *Carbohydr Polym Technol Appl* 2021;2:100120. <https://doi.org/10.1016/j.carpta.2021.100120>.
- [491] Zuo F, Zhang S, Liu H, Fong H, Yin X, Yu J, et al. Free-standing polyurethane nanofiber/nets air filters for effective PM capture. *Small* 2017;13:1702139. <https://doi.org/10.1002/smll.201702139>.
- [492] Zhang S, Liu H, Tang N, Ge J, Yu J, Ding B. Direct electronetting of high-performance membranes based on self-assembled 2D nanoarchitected networks. *Nat Commun* 2019;10:1458. <https://doi.org/10.1038/s41467-019-09444-y>.
- [493] Zhao X, Wang S, Yin X, Yu J, Ding B. Slip-effect functional air filter for efficient purification of PM_{2.5}. *Sci Rep* 2016;6:35472. <https://doi.org/10.1038/srep35472>.
- [494] Liu S, Zhang F, Zheng G, Dai K, Liu C, Shen C, et al. Direct microscopic observation of shish-kebab structure in high-temperature electrospun iPP fibers. *Mater Lett* 2016;172:149–52. <https://doi.org/10.1016/j.matlet.2016.02.111>.
- [495] Tien C, Chen J, Li S, Li Z, Zheng Y, Peng A, et al. Experimental and theoretical analysis of loading characteristics of different electret media with various properties toward the design of ideal depth filtration for nanoparticles and fine particles. *Sep Purif Technol* 2020;233:116002. <https://doi.org/10.1016/j.seppur.2019.116002>.
- [496] Cheng Y, Wang C, Zhong J, Lin S, Xiao Y, Zhong Q, et al. Electrospun polyetherimide electret nonwoven for bi-functional smart face mask. *Nano Energy* 2017;34:562–9. <https://doi.org/10.1016/j.nanoen.2017.03.011>.
- [497] Yang X, Pu Y, Li S, Liu X, Wang Z, Yuan D, et al. Electrospun polymer composite membrane with superior thermal stability and excellent chemical resistance for high-efficiency PM_{2.5} capture. *ACS Appl Mater Interfaces* 2019;11:43188–99. <https://doi.org/10.1021/acsami.9b15219>.
- [498] Sun Q, Leung WWF. Charged PVDF multi-layer filters with enhanced filtration performance for filtering nano-aerosols. *Sep Purif Technol* 2019;212:854–76. <https://doi.org/10.1016/j.seppur.2018.11.063>.
- [499] Liu C, Hsu PC, Lee HW, Ye M, Zheng G, Liu N, et al. Transparent air filter for high-efficiency PM_{2.5} capture. *Nat Commun* 2015;6:6205. <https://doi.org/10.1038/ncomms7205>.
- [500] Zhang Y, Yuan S, Feng X, Li H, Zhou J, Wang B. Preparation of nanofibrous metal-organic framework filters for efficient air pollution control. *J Am Chem Soc* 2016;138:5785–8. <https://doi.org/10.1021/jacs.6b02553>.
- [501] Liu G, Nie J, Han C, Jiang T, Yang Z, Pang Y, et al. Self-powered electrostatic adsorption face mask based on a triboelectric nanogenerator. *ACS Appl Mater Interfaces* 2018;10:7126–33. <https://doi.org/10.1021/acsami.7b18732>.
- [502] Fu X, Liu J, Ding C, Lin S, Zhong W. Building bimodal structures by a wettability difference-driven strategy for high-performance protein air-filters. *J Hazard Mater* 2021;415:125742. <https://doi.org/10.1016/j.jhazmat.2021.125742>.
- [503] Liu J, Ding C, Dunne F, Guo Y, Fu X, Zhong W. A bimodal protein fabric enabled via in-situ diffusion for high-performance air filtration. *Environ Sci Technol* 2020;54:12042–50. <https://doi.org/10.1021/acs.est.0c02828>.
- [504] Zhang Q, Li Q, Young TM, Harper DP, Wang S. A novel method for fabricating an electrospun poly (vinyl alcohol)/cellulose nanocrystals composite nanofibrous filter with low air resistance for high-efficiency filtration of particulate matter. *ACS Sustain Chem Eng* 2019;7:8706–14. <https://doi.org/10.1021/acssuschemeng.9b00605>.
- [505] Lv D, Wang R, Tang G, Mou Z, Lei J, Han J, et al. Ecofriendly electrospun membranes loaded with visible-light-responding nanoparticles for multifunctional usages: highly efficient air filtration, dye scavenging, and bactericidal activity. *ACS Appl Mater Interfaces* 2019;11:12880–9. <https://doi.org/10.1021/acsami.9b01508>.
- [506] Zhang Q, Li Q, Zhang L, Wang S, Harper DP, Wu Q, et al. Preparation of electrospun nanofibrous poly(vinyl alcohol)/cellulose nanocrystals air filter for efficient particulate matter removal with repetitive usage capability via facile heat treatment. *Chem Eng J* 2020;399:125768. <https://doi.org/10.1016/j.cej.2020.125768>.
- [507] Liu YB, Du XY, Wang JN, Yin Y, Wang B, Zhao S, et al. High efficient detoxification of mustard gas surrogate based on nanofibrous fabric. *J Hazard Mater* 2018;347:25–30. <https://doi.org/10.1016/j.jhazmat.2017.12.041>.
- [508] Wang P, Cheng L, Zhang L. Lightweight, flexible SiCN ceramic nanowires applied as effective microwave absorbers in high frequency. *Chem Eng J* 2018;338:248–60. <https://doi.org/10.1016/j.cej.2017.12.008>.
- [509] Huang L, Li J, Li Y, He X, Yuan Y. Lightweight and flexible hybrid film based on delicate design of electrospun nanofibers for high-performance electromagnetic interference shielding. *Nanoscale* 2019;11:8616–25. <https://doi.org/10.1039/c9nr02102g>.
- [510] Shahzad F, Alhabeb M, Hatter CB, Anasori B, Hong SM, Koo CM, et al. Electromagnetic interference shielding with 2D transition metal carbides (MXenes). *Science* 2016;353:1137–40. <https://doi.org/10.1126/science.aag2421>.
- [511] Jamil M, Hazlan MH, Ramli RM, Noor Azman NZ. Study of electrospun PVA-based concentrations nanofibre filled with Bi₂O₃ or WO₃ as potential X-ray shielding material. *Radiat Phys Chem* 2019;156:272–82. <https://doi.org/10.1016/j.radphyschem.2018.11.018>.
- [512] Rashidi M, Rezaei A, Bijari S, Jaymand M, Samadian H, Arkan E, et al. Microfibers nanocomposite based on polyacrylonitrile fibers/bismuth oxide nanoparticles as X-ray shielding material. *J Appl Polym Sci* 2021;138:50755. <https://doi.org/10.1002/app.50755>.
- [513] Jacobsen C, Garcia-Moreno PJ, Mendes AC, Mateiu RV, Chronakis IS. Use of electrohydrodynamic processing for encapsulation of sensitive bioactive compounds and applications in food. *Annu Rev Food Sci Technol* 2018;9:525–49. <https://doi.org/10.1146/annurev-food-030117-012348>.
- [514] Echeogoyen Y, Fabra MJ, Castro-Mayorga JL, Cherpinski A, Lagaron JM. High throughput electrohydrodynamic processing in food encapsulation and food packaging applications: Viewpoint. *Trends Food Sci Technol* 2017;60:71–9. <https://doi.org/10.1016/j.tifs.2016.10.019>.
- [515] Xu C, Cao Y, Lei C, Li Z, Kumeria T, Meka AK, et al. Polymer-mesoporous silica nanoparticle core-shell nanofibers as a dual-drug-delivery system for guided tissue regeneration. *ACS Appl Nano Mater* 2020;3:1457–67. <https://doi.org/10.1021/acsnm.9b02298>.
- [516] Wen P, Wen Y, Zong M, Linhardt R, Wu H. Encapsulation of bioactive compound in electrospun fibers and its potential application. *J Agric Food Chem* 2017;65:9161–79. <https://doi.org/10.1021/acs.jafc.7b02956>.
- [517] Yu B, Zhang X, Yan J, Liu D, Li L, Pei R, et al. Improved stability, antitumor effect, and controlled release of recombinant soluble TRAIL by combining genetic engineering with coaxial electrospinning. *ACS Appl Bio Mater* 2019;2:2414–20. <https://doi.org/10.1021/acsbm.9b00119>.
- [518] Zhan FC, Yan XX, Li J, Sheng F, Li B. Encapsulation of tangeretin in PVA/PAA crosslinking electrospun fibers by emulsion-electrospinning: morphology characterization, slow-release, and antioxidant activity assessment. *Food Chem* 2021;337:127763. <https://doi.org/10.1016/j.foodchem.2020.127763>.
- [519] Guo M, Wang H, Wang Q, Chen M, Li L, Li X, et al. Intelligent double-layer fiber mats with high colorimetric response sensitivity for food freshness monitoring and preservation. *Food Hydrocoll* 2020;101:105468. <https://doi.org/10.1016/j.foodhyd.2019.105468>.
- [520] Jia R, Tian W, Bai H, Zhang J, Wang S, Zhang J. Amine-responsive cellulose-based ratiometric fluorescent materials for real-time and visual detection of shrimp and crab freshness. *Nat Commun* 2019;10:795. <https://doi.org/10.1038/s41467-019-08675-3>.

- [521] van der Vlies AJ, Xu J, Ghasemi M, Bator C, Bell A, Rosoff-Verbit B, et al. Thioether-based polymeric micelles with fine-tuned oxidation sensitivities for chemotherapeutic drug delivery. *Biomacromolecules* 2022;23:77–88. <https://doi.org/10.1021/acs.biomac.1c01010>.
- [522] Li W, Chen J, Zhao S, Huang T, Ying H, Trujillo C, et al. High drug-loaded microspheres enabled by controlled in-droplet precipitation promote functional recovery after spinal cord injury. *Nat Commun* 2022;13:1262. <https://doi.org/10.1038/s41467-022-28787-7>.
- [523] Lai W, Wong W, Rogach A. Molecular design of layer-by-layer functionalized liposomes for oral drug delivery. *ACS Appl Mater Interfaces* 2020;12:43341–51. <https://doi.org/10.1021/acsami.0c13504>.
- [524] Krysiak ZJ, Stachewicz U. Electrospun fibers as carriers for topical drug delivery and release in skin bandages and patches for atopic dermatitis treatment. *WIREs Nanomed Nanobiotechnol* 2022;15:e1829.
- [525] Zhao P, Zhou K, Xia Y, Qian C, Yu DG, Xie Y, et al. Electrospun trilayer eccentric Janus nanofibers for a combined treatment of periodontitis. *Adv Fiber Mater* 2024;6:1053–73. <https://doi.org/10.1007/s42765-024-00397-6>.
- [526] Xue JJ, Shi R, Niu YZ, Gong M, Coates P, Crawford A, et al. Fabrication of drug-loaded anti-infective guided tissue regeneration membrane with adjustable biodegradation property. *Colloid Surface B* 2015;135:846–54. <https://doi.org/10.1016/j.colsurfb.2015.03.031>.
- [527] Zakaria M, Shibahara K, Nakane K. Melt-electrospun polyethylene nanofiber obtained from polyethylene/polyvinyl butyral blend film. *Polymers* 2020;12:pp. <https://doi.org/10.3390/polym12020457>.
- [528] Xue J, He M, Niu Y, Liu H, Crawford A, Coates P, et al. Preparation and in vivo efficient anti-infection property of GTR/GBR implant made by metronidazole loaded electrospun polycaprolactone nanofiber membrane. *Int J Pharm* 2014;475:566–77. <https://doi.org/10.1016/j.ijpharm.2014.09.026>.
- [529] Lode D, Iline S, Ella S, Camille G, Hubert R, Karen DC. Nanostructured hydrogels by blend electrospinning of polycaprolactone/gelatin nanofibers. *Nanomaterials* 2018;8:551. <https://doi.org/10.3390/nano8070551>.
- [530] Jirofti N, Golandi M, Movaffagh J, Ahmadi FS, Kalalinia F. Improvement of the wound-healing process by curcumin-loaded chitosan/collagen blend electrospun nanofibers: in vitro and in vivo studies. *ACS Biomater Sci Eng* 2021;7:3886–97. <https://doi.org/10.1021/acsbiomaterials.1c00131>.
- [531] Man Z, Yin L, Shao Z, Zhang X, Hu X, Zhu J, et al. The effects of co-delivery of BMSC-affinity peptide and rhTGF- β 1 from coaxial electrospun scaffolds on chondrogenic differentiation. *Biomaterials* 2014;35:5250–60. <https://doi.org/10.1016/j.biomaterials.2014.03.031>.
- [532] Yu DG, Wang M, Ge R. Strategies for sustained drug release from electrospun multi-layer nanostructures. *WIREs Nanomed Nanobiotechnol* 2022;14:e1772.
- [533] He Z, Liu S, Li ZM, Xu JZ, Liu Y, Luo E. Coaxial TP/APR electrospun nanofibers for programmed controlling inflammation and promoting bone regeneration in periodontitis-related alveolar bone defect models. *Mater Today Bio* 2022;16:100438. <https://doi.org/10.1016/j.mtbio.2022.100438>.
- [534] Kyuchyuk S, Paneva D, Manolova N, Rashkov IB, Karashanova D, Markova N, et al. Composite core-double sheath fibers based on some biodegradable polyesters obtained by self-organization during electrospinning. *J Appl Polym Sci* 2024;141:e55179. <https://doi.org/10.1002/app.55179>.
- [535] Zandi N, Lotfi R, Tamjid E, Shokrgozar MA, Simchi A. Core-sheath gelatin based electrospun nanofibers for dual delivery release of biomolecules and therapeutics. *Mater Sci Eng C* 2020;108:110432. <https://doi.org/10.1016/j.msec.2019.110432>.
- [536] Ghosal K, Augustine R, Zaszczynska A, Barman M, Jain A, Hasan A, et al. Novel drug delivery systems based on triaxial electrospinning based nanofibers. *React Funct Polym* 2021;163:104895. <https://doi.org/10.1016/j.reactfunctpolym.2021.104895>.
- [537] Yang Y, Chang S, Bai Y, Du Y, Yu DG. Electrospun triaxial nanofibers with middle blank cellulose acetate layers for accurate dual-stage drug release. *Carbohydr polym* 2020;243:116477. <https://doi.org/10.1016/j.carbpol.2020.116477>.
- [538] Zhang X, Chi C, Chen J, Zhang X, Gong M, Wang X, et al. Electrospun quad-axial nanofibers for controlled and sustained drug delivery. *Mater Des* 2021;206. <https://doi.org/10.1016/j.matdes.2021.109732>.
- [539] Jiannan Li, Weiguo Xu, Di Li, et al. Locally deployable nanofiber patch for sequential drug delivery in treatment of primary and advanced orthotopic hepatomas. *ACS Nano* 2018;12:6685–99. <https://doi.org/10.1021/acsnano.8b01729>.
- [540] Negahdari N, Alizadeh S, Majidi J, Saeed M, Ghadimi T, Tahermanesh K, et al. Heat-treated alginate-polycaprolactone core-shell nanofibers by emulsion electrospinning process for biomedical applications. *Int J Biol Macromol* 2024;275:133709. <https://doi.org/10.1016/j.ijbiomac.2024.133709>.
- [541] Zhao C, Huang L, Tang J, Lv L, Wang X, Dong X, et al. Multifunctional nanofibrous scaffolds for enhancing full-thickness wound healing loaded with Bletilla striata polysaccharides. *Int J Biol Macromol* 2024;278:134597. <https://doi.org/10.1016/j.ijbiomac.2024.134597>.
- [542] Li Q, Chen R, Cui T, Bai Y, Hu J, Yu J, et al. Robust gradient hydrogel-loaded nanofiber fleshy artificial skin via a coupled microfluidic electrospinning-reactive coating strategy. *Adv Healthc Mater* 2024;13:2304321. <https://doi.org/10.1002/adhm.202304321>.
- [543] Pimentel E, Brito-Pereira R, Marques-Almeida T, Ribeiro C, Cardoso V. Tailoring electrospun poly(L-lactic acid) nanofibers as substrates for microfluidic applications. *ACS Appl Mater Interfaces* 2018;10:9. <https://doi.org/10.1021/acsami.9b12461>.
- [544] Hou Y, Xu X, Zhou Y, Li Q, Zhu L, Liu C, et al. Versatile bioactive glass/zeolitic imidazolate framework-8-based skin scaffolds toward high-performance wound healing. *ACS Appl Mater Interfaces* 2024;16:8228–37. <https://doi.org/10.1021/acsami.3c14529>.
- [545] He Y, Li X, Ma J, Ni G, Yang G, Zhou S. Programmable codelivery of doxorubicin and apatinib using an implantable hierarchical-structured fiber device for overcoming cancer multidrug resistance. *Small* 2019;15:e1804397. <https://doi.org/10.1002/smll.201804397>.
- [546] Yao Y, Ding J, Wang Z, Zhang H, Xie J, Wang Y, et al. ROS-responsive polyurethane fibrous patches loaded with methylprednisolone (MP) for restoring structures and functions of infarcted myocardium in vivo. *Biomaterials* 2020;232:119726. <https://doi.org/10.1016/j.biomaterials.2019.119726>.
- [547] Puiggali-Jou A, Cejudo A, Del Valle LJ, Aleman C. Smart drug delivery from electrospun fibers through electroresponsive polymeric nanoparticles. *ACS Appl Bio Mater* 2018;1:1594–605. <https://doi.org/10.1021/acsbam.8b00459>.
- [548] Luzhansky I, Sudlow L, Brogan D, Wood M, Berezin MY. Imaging in the repair of peripheral nerve injury. *Nanomedicine* 2019;14:2659–77. <https://doi.org/10.2217/nmm-2019-0115>.
- [549] Liu G, Zhu J, Guo H, Sun A, Chen P, Xi L, et al. Mo₂C-derived polyoxometalate for NIR-II photoacoustic imaging-guided chemodynamic/photothermal synergistic therapy. *Angew Chem Int Ed* 2019;58:18641–6. <https://doi.org/10.1002/anie.201910815>.
- [550] Chen Z, Peng Y, Li Y, Xie X, Wei X, Yang G, et al. Aptamer-dendrimer functionalized magnetic nano-octahedrons: theranostic drug/gene delivery platform for near-infrared/magnetic resonance imaging-guided magnetochemotherapy. *ACS Nano* 2021;15:16683–96. <https://doi.org/10.1021/acsnano.1c06667>.
- [551] Yu M, Xu X, Cai Y, Zou L, Shuai X. Perfluorohexane-cored nanodroplets for stimulations-responsive ultrasonography and O₂-potentiated photodynamic therapy. *Biomaterials* 2018;175:61–71. <https://doi.org/10.1016/j.biomaterials.2018.05.019>.
- [552] Das S, Bharadwaj P, Bilal M, Barani M, Rahdar A, Taboada P, et al. Stimuli-responsive polymeric nanocarriers for drug delivery, imaging, and theragnosis. *Polymers* 2020;12:1397. <https://doi.org/10.3390/polym12061397>.
- [553] Fu Q, Zhu R, Song J, Yang H, Chen X. Photoacoustic imaging: contrast agents and their biomedical applications. *Adv Mater* 2019;31:e1805875. <https://doi.org/10.1002/adma.201805875>.
- [554] Nguyen V, Fan W, Zhu T, Qian W, Li Y, Liu B, et al. Long-term, noninvasive in vivo tracking of progenitor cells using multimodality photoacoustic, optical coherence tomography, and fluorescence imaging. *ACS Nano* 2021;15:13289–306. <https://doi.org/10.1021/acsnano.1c03035>.
- [555] Rabiee N, Yarak M, Garakani S, Garakani S, Ahmadi S, Lajevardi A, et al. Recent advances in porphyrin-based nanocomposites for effective targeted imaging and therapy. *Biomaterials* 2020;232:119707. <https://doi.org/10.1016/j.biomaterials.2019.119707>.
- [556] Steinberg I, Huland D, Vermesh O, Frostig H, Tummers W, Gambhir S. Photoacoustic clinical imaging Photoacoustics 2019;14:77–98. <https://doi.org/10.1016/j.pacs.2019.05.001>.
- [557] Li C, Xia J, Wei X, Yan H, Si Z, Ju S. pH-activated near-infrared fluorescence nanoprobe imaging tumors by sensing the acidic microenvironment. *Adv Funct Mater* 2010;20:2222–30. <https://doi.org/10.1002/adfm.201000038>.
- [558] Chen S, Chen M, Yang J, Zeng XQ, Zhou YB, Yang S, et al. Design and engineering of hypoxia and acidic pH dual-stimuli-responsive intelligent fluorescent nanoprobe for precise tumor imaging. *Small* 2021;17:e2100243. <https://doi.org/10.1002/smll.202100243>.
- [559] Voskuil F, Steinkamp P, Zhao T, van der Vegt B, Koller M, Doff J, et al. Exploiting metabolic acidosis in solid cancers using a tumor-agnostic pH-activatable nanoprobe for fluorescence-guided surgery. *Nat Commun* 2020;11:3257. <https://doi.org/10.1038/s41467-020-16814-4>.
- [560] Zhao X, Yang CX, Chen LG, Yan XP. Dual-stimuli responsive and reversibly activatable theranostic nanoprobe for precision tumor-targeting and fluorescence-guided photothermal therapy. *Nat Commun* 2017;8:14998. <https://doi.org/10.1038/ncomms14998>.

- [561] Lei K, Chen Y, Wang J, Peng X, Yu L, Ding J. Non-invasive monitoring of in vivo degradation of a radiopaque thermoreversible hydrogel and its efficacy in preventing post-operative adhesions. *Acta Biomater* 2017;55:396–409. <https://doi.org/10.1016/j.actbio.2017.03.042>.
- [562] Li Y, Shan S, Zhang R, Sun C, Hu X, Fan J, et al. Imaging and downstaging bladder cancer with the ¹⁷⁷Lu-labeled bioorthogonal nanoprobe. *ACS Nano* 2024;18:17209–17. <https://doi.org/10.1021/acsnano.4c04303>.
- [563] Lei L, Yang F, Meng X, Xu L, Liang P, Ma Y, et al. Noninvasive imaging of tumor glycolysis and chemotherapeutic resistance via de novo design of molecular afterglow scaffold. *J Am Chem Soc* 2023;145:24386–400. <https://doi.org/10.1021/jacs.3c09473>.
- [564] Zhao S, Li G, Tong C, Chen W, Wang P, Dai J, et al. Full activation pattern mapping by simultaneous deep brain stimulation and fMRI with graphene fiber electrodes. *Nat Commun* 2020;11:1788. <https://doi.org/10.1038/s41467-020-15570-9>.
- [565] Wang L, Li B, Xu F, Li Y, Xu Z, Wei D, et al. Visual in vivo degradation of injectable hydrogel by real-time and non-invasive tracking using carbon nanodots as fluorescent indicator. *Biomaterials* 2017;145:192–206. <https://doi.org/10.1016/j.biomaterials.2017.08.039>.
- [566] Yun BJ, Kwon JE, Lee K, Koh WG. Highly sensitive metal-enhanced fluorescence biosensor prepared on electrospun fibers decorated with silica-coated silver nanoparticles. *Sensor Actuat B-Chem* 2019;284:140–7. <https://doi.org/10.1016/j.snb.2018.12.096>.
- [567] Grasso G, Onesto V, Forciniti S, D'Amone E, Colella F, Pierantoni L, et al. Highly sensitive ratiometric fluorescent fiber matrices for oxygen sensing with micrometer spatial resolution. *Bio-Des Manuf* 2024;7:292–306. <https://doi.org/10.1007/s42242-024-00277-3>.
- [568] Zhao J, Cui W. Functional electrospun fibers for local therapy of cancer. *Adv Fiber Mater* 2020;2:229–45. <https://doi.org/10.1007/s42765-020-00053-9>.
- [569] Jin M, Yu D, Galdes C, Williams G, Bligh S. Theranostic fibers for simultaneous imaging and drug delivery. *Mol Pharm* 2016;13:2457–65. <https://doi.org/10.1021/acs.molpharmaceut.6b00197>.
- [570] Zhao WX, Hu CX, Xu T. In vivo bioprinting: Broadening the therapeutic horizon for tissue injuries. *Bioact Mater* 2023;25:201–22. <https://doi.org/10.1016/j.bioactmat.2023.01>.
- [571] Gao, X. Yu, X. Wang, Y. He, J. Ding. Biomaterial-related cell microenvironment in tissue engineering and regenerative medicine. *Engineering*, 13(2022), pp. 31–45. <https://doi.org/10.1016/j.eng.2021.11.025>.
- [572] Liu S, Yu J, Gan Y, Qiu X, Gao Z, Wang H, et al. Biomimetic natural biomaterials for tissue engineering and regenerative medicine: new biosynthesis methods, recent advances, and emerging applications. *Mil Med Res* 2023;10:16. <https://doi.org/10.1186/s40779-023-00448-w>.
- [573] Lu Y, Zhao M, Peng Y, He S, Zhu X, Hu C, et al. A physicochemical double-cross-linked gelatin hydrogel with enhanced antibacterial and anti-inflammatory capabilities for improving wound healing. *J Nanobiotechnology* 2022;20:426. <https://doi.org/10.1186/s12951-022-01634-z>.
- [574] Cochran C, Rippon MG, Rogers A, Walmsley R, Knottenbelt D, Bowler P. Application of an in vitro model to evaluate bioadhesion of fibroblasts and epithelial cells to two different dressings. *Biomaterials* 1999;20:1237–44. [https://doi.org/10.1016/s0142-9612\(99\)00025-3](https://doi.org/10.1016/s0142-9612(99)00025-3).
- [575] Liu L, Zhu Y, Tao Z, Chen Y, Zhang L, Dong A. Black phosphorus-based conductive hydrogels assisted by electrical stimulus for skin tissue engineering. *Adv Healthc Mater* 2023;12:e2301817. <https://doi.org/10.1002/adhm.202301817>.
- [576] Hong Y, Wang M, Hu D, Wang Y, Ji S, Xiang J, et al. NIR-responsive multifunctional artificial skin for regenerative wound healing. *Adv Funct Mater* 2024;2405876. <https://doi.org/10.1002/adfm.202405876>.
- [577] Ailincăi D, Cibotaru S, Anisiei A, Coman CG, Pasca AS, Rosca I, et al. Mesoporous chitosan nanofibers loaded with norfloxacin and coated with phenylboronic acid perform as bioabsorbable active dressings to accelerate the healing of burn wounds. *Carbohydr Polym* 2023;318:121135. <https://doi.org/10.1016/j.carbpol.2023.121135>.
- [578] Yu P, Guo J, Li J, Shi X, Wang L, Chen W, et al. Repair of skin defects with electrospun collagen/chitosan and fibroin/chitosan compound nanofiber scaffolds compared with gauze dressing. *J Biomater Tiss Eng* 2017;7:386–92. <https://doi.org/10.1166/jbt.2017.1580>.
- [579] Zhang D, Fan L, Ma L, Liu J, Zhou K, Song X, et al. Helicobacter pylori ribosomal protein-A2 peptide/silk fibroin nanofibrous composites as potential wound dressing. *J Biomed Nanotechnol* 2019;15:507–17. <https://doi.org/10.1166/jbn.2019.2707>.
- [580] Khan AUR, Huang K, Khalaji M, Yu F, Xie X, Zhu T, et al. Multifunctional bioactive core-shell electrospun membrane capable to terminate inflammatory cycle and promote angiogenesis in diabetic wound. *Bioact Mater* 2021;6:2783–800. <https://doi.org/10.1016/j.bioactmat.2021.01.040>.
- [581] Li D, Gao Y, Wang Y, Yang X, He C, Zhu M, et al. Evaluation of biocompatibility and immunogenicity of micro/nanofiber materials based on tilapia skin collagen. *J Biomater Appl* 2019;33:1118–27. <https://doi.org/10.1177/0885328218820180>.
- [582] Tian Z, Sui B, Mo X, Jiao S. Multifunctional and biomimetic fish collagen/bioactive glass nanofibers: fabrication, antibacterial activity and inducing skin regeneration in vitro and in vivo. *Int J Nanomed* 2017;12:3495–507. <https://doi.org/10.2147/ijn.s132459>.
- [583] Ma L, Zhang D, Yang X, Zhang L, Chu J, Kai G, et al. Cirsium Japonicum DC ingredients-loaded silk fibroin nanofibrous matrices with excellent hemostatic activity. *Biomed Phys Eng Expr* 2018;4:025035. <https://doi.org/10.1088/2057-1976/aaabf0>.
- [584] Zhang K, Bai X, Yuan Z, Cao X, Jiao X, Li Y, et al. Layered nanofiber sponge with an improved capacity for promoting blood coagulation and wound healing. *Biomaterials* 2019;204:70–9. <https://doi.org/10.1016/j.biomaterials.2019.03.008>.
- [585] Wang CB, Chu CY, Zhao XW, Yang Y, Hu C, Liu L, et al. The diameter factor of aligned membranes facilitates wound healing by promoting epithelialization in an immune way. *Bioact Mater* 2022;11:206–17. <https://doi.org/10.1016/j.bioactmat.2021.09.022>.
- [586] Wen Z, Chen Y, Liao P, Wang F, Zeng W, Liu S, et al. In-situ precision cell electrospinning as an efficient stem cell delivery approach for cutaneous wound healing. *Adv Healthc Mater* 2023;12:e2300970. <https://doi.org/10.1002/adhm.202300970>.
- [587] Tao R, Mi B, Hu Y, Lin S, Xiong Y, Lu X, et al. Hallmarks of peripheral nerve function in bone regeneration. *Bone Res* 2023;11:6. <https://doi.org/10.1038/s41413-022-00240-x>.
- [588] Scott-Solomon E, Neurobiology Y. Stem cell biology, and immunology: an emerging triad for understanding tissue homeostasis and repair. *Annu Rev Cell Dev Biol* 2022;38:419–46. <https://doi.org/10.1146/annurev-cellbio-120320-032429>.
- [589] Schmidt C, Leach JB. Neural tissue engineering: strategies for repair and regeneration. *Annu Rev Biomed Eng* 2003;5:293–347. <https://doi.org/10.1146/annurev.bioeng.5.011303.120731>.
- [590] Zheng C, Yang Z, Chen S, Zhang F, Rao Z, Zhao C, et al. Nanofibrous nerve guidance conduits decorated with decellularized matrix hydrogel facilitate peripheral nerve injury repair. *Theranostics* 2021;11:2917–31. <https://doi.org/10.7150/thno.50825>.
- [591] Jin F, Li T, Yuan T, Du L, Lai C, Wu Q, et al. Physiologically self-regulated, fully implantable, battery-free system for peripheral nerve restoration. *Adv Mater* 2021;33:e2104175. <https://doi.org/10.1002/adma.202104175>.
- [592] Sarker M, Naghieh S, McInnes A, Schreyer D, Chen X. Regeneration of peripheral nerves by nerve guidance conduits: influence of design, biopolymers, cells, growth factors, and physical stimuli. *Prog Neurobiol* 2018;171:125–50. <https://doi.org/10.1016/j.pneurobio.2018.07.002>.
- [593] Jin B, Yu Y, Lou C, Zhang X, Gong B, Chen J, et al. Combining a density gradient of biomacromolecular nanoparticles with biological effectors in an electrospun fiber-based nerve guidance conduit to promote peripheral nerve repair. *Adv Sci* 2022;10:e2203296. <https://doi.org/10.1002/adv.202203296>.
- [594] Wu S, Qi Y, Shi W, Kuss M, Chen S, Duan B. Electrospun conductive nanofiber yarns for accelerating mesenchymal stem cells differentiation and maturation into Schwann cell-like cells under a combination of electrical stimulation and chemical induction. *Acta Biomater* 2022;139:91–104. <https://doi.org/10.1016/j.actbio.2020.11.042>.
- [595] Sun B, Zhou Z, Li D, Wu T, Zheng H, Liu J, et al. Polypyrrole-coated poly(l-lactic acid-co-ε-caprolactone)/silk fibroin nanofibrous nerve guidance conduit induced nerve regeneration in rat. *Mater Sci Eng C* 2019;94:190–9. <https://doi.org/10.1016/j.msec.2018.09.021>.
- [596] Wang J, Xiong H, Zhu T, Liu Y, Pan H, Fan C, et al. Bioinspired multichannel nerve guidance conduit based on shape memory nanofibers for potential application in peripheral nerve repair. *ACS Nano* 2020;14:12579–95. <https://doi.org/10.1021/acsnano.0c03570>.
- [597] Huang C, Ouyang Y, Niu H, He N, Ke Q, Jin X, et al. Nerve guidance conduits from aligned nanofibers: improvement of nerve regeneration through longitudinal nanogrooves on a fiber surface. *ACS Appl Mater Interfaces* 2015;7:7189–96. <https://doi.org/10.1021/am509227t>.
- [598] Jeon J, Lee MS, Lim J, Park S, Kim SM, Kim D-I, et al. Micro-grooved nerve guidance conduits combined with microfiber for rat sciatic nerve regeneration. *J Ind Eng Chem* 2020;90:214–23. <https://doi.org/10.1016/j.jiec.2020.07.014>.
- [599] Li D, Pan X, Sun B, Wu T, Chen W, Huang C, et al. Nerve conduits constructed by electrospun P(LLA-CL) nanofibers and PLLA nanofiber yarns. *J Mater Chem B* 2015;3:8823–31. <https://doi.org/10.1039/c5tb01402f>.

- [600] Sun B, Zhou Z, Wu T, Chen W, Li D, Zheng H, et al. Development of nanofiber sponges-containing nerve guidance conduit for peripheral nerve regeneration in vivo. *ACS Appl Mater Interfaces* 2017;9:26684–96. <https://doi.org/10.1021/acsami.7b06707>.
- [601] Li X, Zhang T, Li C, Xu W, Guan Y, Li X, et al. Electrical stimulation accelerates Wallerian degeneration and promotes nerve regeneration after sciatic nerve injury. *Glia* 2022;71:758–74. <https://doi.org/10.1002/glia.24309>.
- [602] Liu K, Yan S, Liu Y, Liu J, Li R, Zhao L, et al. Conductive and alignment-optimized porous fiber conduits with electrical stimulation for peripheral nerve regeneration. *Mater Today Bio* 2024;26:101064. <https://doi.org/10.1016/j.mtbio.2024.101064>.
- [603] Zhang J, Zhang X, Wang C, Li F, Qiao Z, Zeng L, et al. Conductive composite fiber with optimized alignment guides neural regeneration under electrical stimulation. *Adv Healthc Mater* 2020;10:e2000604. <https://doi.org/10.1002/adhm.202000604>.
- [604] Li X, Zhang C, Haggerty A, Yan J, Lan M, Seu M, et al. The effect of a nanofiber-hydrogel composite on neural tissue repair and regeneration in the contused spinal cord. *Biomaterials* 2020;245:119978. <https://doi.org/10.1016/j.biomaterials.2020.119978>.
- [605] Milbreta U, Nguyen L, Diao H, Lin J, Wu W, Sun C, et al. Three-dimensional nanofiber hybrid scaffold directs and enhances axonal regeneration after spinal cord injury. *ACS Biomater Sci Eng* 2016;2:1319–29. <https://doi.org/10.1021/acsbiomaterials.6b00248>.
- [606] Zhang S, Wang X, Li W, Xu X, Hu J, Kang X, et al. Polycaprolactone/polysialic acid hybrid, multifunctional nanofiber scaffolds for treatment of spinal cord injury. *Acta Biomater* 2018;77:15–27. <https://doi.org/10.1016/j.actbio.2018.06.038>.
- [607] Rahimi B, Behroozi Z, Motamednezhad A, Jafarpour M, Hamblin M, Moshiri A, et al. Study of nerve cell regeneration on nanofibers containing cerium oxide nanoparticles in a spinal cord injury model in rats. *J Mater Sci Mater Med* 2023;34:9. <https://doi.org/10.1007/s10856-023-06711-9>.
- [608] Browning MB, Dempsey D, Guiza V, Becerra S, Rivera J, Russell B, et al. Multilayer vascular grafts based on collagen-mimetic proteins. *Acta Biomater* 2012;8:1010–21. <https://doi.org/10.1016/j.actbio.2011.11.015>.
- [609] Weekes A, Bartnikowski N, Pinto N, Jenkins J, Meinert C, Klein TJ. Biofabrication of small diameter tissue-engineered vascular grafts. *Acta Biomater* 2022;138:92–111. <https://doi.org/10.1016/j.actbio.2021.11.012>.
- [610] Durán-Rey D, Crisóstomo V, Sánchez-Margallo JA, Sánchez-Margallo FM. Systematic review of tissue-engineered vascular grafts. *Front Bioeng Biotechnol* 2021;9:771400. <https://doi.org/10.3389/fbioe.2021.771400>.
- [611] Niu Y, Galluzzi M, Fu M, Hu J, Xia H. In vivo performance of electrospun tubular hyaluronic acid/collagen nanofibrous scaffolds for vascular reconstruction in the rabbit model. *J Nanobiotechnology* 2021;19:349. <https://doi.org/10.1186/s12951-021-01091-0>.
- [612] Kuang H, Wang Y, Shi Y, Yao W, He X, Liu X, et al. Construction and performance evaluation of Hep/silk-PLCL composite nanofiber small-caliber artificial blood vessel graft. *Biomaterials* 2020;259:120288. <https://doi.org/10.1016/j.biomaterials.2020.120288>.
- [613] Fahad MAA, Lee HY, Park S, Choi M, Shanto PC, Park M, et al. Small-diameter vascular graft composing of core-shell structured micro-nanofibers loaded with heparin and VEGF for endothelialization and prevention of neointimal hyperplasia. *Biomaterials* 2024;306:122507. <https://doi.org/10.1016/j.biomaterials.2024.122507>.
- [614] Kuang H, Wang Y, Hu J, Wang C, Lu S, Mo X. A method for preparation of an internal layer of artificial vascular graft co-modified with salivianolic acid b and heparin. *ACS Appl Mater Interfaces* 2018;10:19365–72. <https://doi.org/10.1021/acsami.8b02602>.
- [615] He G, Chen G, Liu W, Ye D, Liu X, Liang X, et al. Salivianolic acid B: a review of pharmacological effects, safety, combination therapy, new dosage forms, and novel drug delivery routes. *Pharmaceutics* 2023;15:2235. <https://doi.org/10.3390/pharmaceutics15092235>.
- [616] Zhang Y, Li X, Guex A, Liu S, Müller E, Malini R, et al. A compliant and biomimetic three-layered vascular graft for small blood vessels. *Biofabrication* 2017;9:025010. <https://doi.org/10.1088/1758-5090/aa6bae>.
- [617] Tong W, Zhang J, Wang Y, Li D, Sun B, El-Hamshary H, et al. Fabrication and preliminary study of a biomimetic tri-layer tubular graft based on fibers and fiber yarns for vascular tissue engineering. *Mater Sci Eng C* 2018;82:121–9. <https://doi.org/10.1016/j.msec.2017.08.072>.
- [618] Wu Y, Ranjan VD, Zhang Y. A Living 3D In Vitro Neuronal Network Cultured inside Hollow Electrospun Microfibers. *Adv Biosyst* 2018;2:e1700218. <https://doi.org/10.1002/adbi.201700218>.
- [619] Cuenca JP, Kang HJ, Fahad MAA, Park M, Choi M, Lee HY, et al. Physico-mechanical and biological evaluation of heparin/VEGF-loaded electrospun polycaprolactone/decellularized rat aorta extracellular matrix for small-diameter vascular grafts. *J Biomater Sci Polym Ed* 2022;33:1664–84. <https://doi.org/10.1080/09205063.2022.2069398>.
- [620] Virani S, Alonso A, Benjamin E, Bittencourt M, Callaway C, Carson A, et al. Heart disease and stroke statistics-2020 update: a report from the american heart association. *Circulation* 2020;141:E139–596. <https://doi.org/10.1161/Cir.0000000000000757>.
- [621] Zhang J, Guo Y, Bai Y, Wei Y. Application of biomedical materials in the diagnosis and treatment of myocardial infarction. *J Nanobiotechnology* 2023;21:298. <https://doi.org/10.1186/s12951-023-02063-2>.
- [622] Hilgendorf I, Frantz S, Frangogiannis NG. Repair of the infarcted heart: cellular effectors, molecular mechanisms and therapeutic opportunities. *Circ Res* 2024;134:1718–51. <https://doi.org/10.1161/circresaha.124.323658>.
- [623] Alam P, Maliken BD, Jones SM, Ivey MJ, Wu Z, Wang Y, et al. Cardiac remodeling and repair: recent approaches, advancements, and future perspective. *Int J Mol Sci* 2021;22:13104. <https://doi.org/10.3390/ijms222313104>.
- [624] Bergmann O, Bhardwaj RD, Bernard S, Zdunek S, Barnabé-Heider F, Walsh S, et al. Evidence for cardiomyocyte renewal in humans. *Science* 2009;324:98–102. <https://doi.org/10.1126/science.1164680>.
- [625] Duelen R, Sampaioles M. Stem cell technology in cardiac regeneration: a pluripotent stem cell promise. *EBioMedicine* 2017;16:30–40. <https://doi.org/10.1016/j.ebiom.2017.01.029>.
- [626] Choudhury D, Tun HW, Wang T, Naing MW. Organ-derived decellularized extracellular matrix: a game changer for bioink manufacturing? *Trends Biotechnol* 2018;36:787–805. <https://doi.org/10.1016/j.tibtech.2018.03.003>.
- [627] Silva A, Rodrigues S, Caldeira J, Nunes A, Sampaio-Pinto V, Resende T, et al. Three-dimensional scaffolds of fetal decellularized hearts exhibit enhanced potential to support cardiac cells in comparison to the adult. *Biomaterials* 2016;104:52–64. <https://doi.org/10.1016/j.biomaterials.2016.06.062>.
- [628] Wang Z, Zhang F, Wang Z, Liu Y, Fu X, Jin A, et al. Hierarchical assembly of bioactive amphiphilic molecule pairs into supramolecular nanofibril self-supportive scaffolds for stem cell differentiation. *J Am Chem Soc* 2016;138:15027–34. <https://doi.org/10.1021/jacs.6b09014>.
- [629] Meng J, Xiao B, Wu F, Sun L, Li B, Guo W, et al. Co-axial fibrous scaffolds integrating with carbon fiber promote cardiac tissue regeneration post myocardial infarction. *Mater Today Bio* 2022;16:100415. <https://doi.org/10.1016/j.mtbio.2022.100415>.
- [630] Motta S, Peters M, Chantre C, Chang H, Cera L, Liu Q, et al. On-demand heart valve manufacturing using focused rotary jet spinning. *Matter* 2023;6:1860–79. <https://doi.org/10.1016/j.matt.2023.05.025>.
- [631] Zhang G, Li W, Yu M, Huang H, Wang Y, Han Z, et al. Electric-field-driven printed 3D highly ordered microstructure with cell feature size promotes the maturation of engineered cardiac tissues. *Adv Sci* 2023;10:e2206264. <https://doi.org/10.1002/advs.202206264>.
- [632] Qiu Z, Zhao J, Huang F, Bao L, Chen Y, Yang K, et al. Myocardial fibrosis reversion via rhACE2-electrospun fibrous patch for ventricular remodeling prevention. *NPJ Regen Med* 2021;6:44. <https://doi.org/10.1038/s41536-021-00154-y>.
- [633] Gil-Cabrerizo P, Scacchetti I, Garbayo E, Blanco-Prieto MJ. Cardiac tissue engineering for myocardial infarction treatment. *Eur J Pharm Sci* 2023;185:106439. <https://doi.org/10.1016/j.ejps.2023.106439>.
- [634] Razeghian-Jahromi I, Matta AG, Canitrot R, Zibaeenezhad MJ, Razmkhah M, Safari A, et al. Surfing the clinical trials of mesenchymal stem cell therapy in ischemic cardiomyopathy. *Stem Cell Res Ther* 2021;12:361. <https://doi.org/10.1186/s13287-021-02443-1>.
- [635] Wu Q, Wang J, Tan WL, Jiang Y, Wang S, Li Q, et al. Extracellular vesicles from human embryonic stem cell-derived cardiovascular progenitor cells promote cardiac infarct healing through reducing cardiomyocyte death and promoting angiogenesis. *Cell Death Dis* 2020;11:354. <https://doi.org/10.1038/s41419-020-2508-y>.
- [636] Kanda P, Alarcon E, Yeuchyk T, Parent S, de Kemp RA, Variola F, et al. Deterministic encapsulation of human cardiac stem cells in variable composition nanoporous gel cocoons to enhance therapeutic repair of injured myocardium. *ACS Nano* 2018;12:4338–50. <https://doi.org/10.1021/acsnano.7b08881>.
- [637] Chen J, Zhan Y, Wang Y, Han D, Tao B, Luo Z, et al. Chitosan/silk fibroin modified nanofibrous patches with mesenchymal stem cells prevent heart remodeling post-myocardial infarction in rats. *Acta Biomater* 2018;80:154–68. <https://doi.org/10.1016/j.actbio.2018.09.013>.

- [638] Streeter B, Xue J, Xia Y, Davis M. Electrospun nanofiber-based patches for the delivery of cardiac progenitor cells. *ACS Appl Mater Interfaces* 2019;11:18242–53. <https://doi.org/10.1021/acsami.9b04473>.
- [639] Pennisi E. Tending tender tendons. *Science* 2002;295:1011. <https://doi.org/10.1126/science.295.5557.1011>.
- [640] Butler D, Juncosa N, Dressler M. Functional efficacy of tendon repair processes. *Annu Rev Biomed Eng* 2004;6:303–29. <https://doi.org/10.1146/annurev.bioeng.6.040803.140240>.
- [641] Duquin T, Buyea C, Bisson L. Which method of rotator cuff repair leads to the highest rate of structural healing? A systematic review. *Am J Sports Med* 2010;38:835–41. <https://doi.org/10.1177/0363546509359679>.
- [642] Rinoldi C, Kijenska-Gawronska E, Khademhosseini A, Tamayol A, Swieszkowski W. Fibrous systems as potential solutions for tendon and ligament repair, healing, and regeneration. *Adv Healthc Mater* 2021;10:e2001305. <https://doi.org/10.1002/adhm.202001305>.
- [643] Staples R, Ivanovski S, Vaquette C. Fibre-guiding biphasic scaffold for perpendicular periodontal ligament attachment. *Acta Biomater* 2022;150:221–37. <https://doi.org/10.1016/j.actbio.2022.07.023>.
- [644] Zhu C, Qiu J, Thomopoulos S, Xia Y. Augmenting tendon-to-bone repair with functionally graded scaffolds. *Adv Healthc Mater* 2021;10:e2002269. <https://doi.org/10.1002/adhm.202002269>.
- [645] Pien N, Peeters I, Deconinck L, Van Damme L, De Wilde L, Martens A, et al. Design and development of a reinforced tubular electrospun construct for the repair of ruptures of deep flexor tendons. *Mater Sci Eng C* 2021;119:11504. <https://doi.org/10.1016/j.msec.2020.111504>.
- [646] Wang L, Zhu T, Kang Y, Zhang J, Du J, Gao H, et al. Crimped nanofiber scaffold mimicking tendon-to-bone interface for fatty-infiltrated massive rotator cuff repair. *Bioact Mater* 2022;16:149–61. <https://doi.org/10.1016/j.bioactmat.2022.01.031>.
- [647] Dong L, Li L, Song Y, Fang Y, Liu J, Chen P, et al. MSC-derived immunomodulatory extracellular matrix functionalized electrospun fibers for mitigating foreign-body reaction and tendon adhesion. *Acta Biomater* 2021;133:280–96. <https://doi.org/10.1016/j.actbio.2021.04.035>.
- [648] Chen W, Chen Y, Ren Y, Gao C, Ning C, Deng H, et al. Lipid nanoparticle-assisted miR29a delivery based on core-shell nanofibers improves tendon healing by cross-regulation of the immune response and matrix remodeling. *Biomaterials* 2022;291:121888. <https://doi.org/10.1016/j.biomaterials.2022.121888>.
- [649] Yuan Z, Sheng D, Jiang L, Shafiq M, Khan AUR, Hashim R, et al. Vascular endothelial growth factor-capturing aligned electrospun polycaprolactone/gelatin nanofibers promote patellar ligament regeneration. *Acta Biomater* 2022;140:233–46. <https://doi.org/10.1016/j.actbio.2021.11.040>.
- [650] Wang H, Yu R, Wang M, Wang S, Ouyang X, Yan Z, et al. Insulin-like growth factor binding protein 4 loaded electrospun membrane ameliorating tendon injury by promoting retention of IGF-1. *J Control Release* 2023;356:162–74. <https://doi.org/10.1016/j.jconrel.2023.02.039>.
- [651] Abdulmalik S, Gallo J, Nip J, Katebifar S, Arul M, Lebaschi A, et al. Nanofiber matrix formulations for the delivery of Exendin-4 for tendon regeneration: in vitro and in vivo assessment. *Bioact Mater* 2023;25:42–60. <https://doi.org/10.1016/j.bioactmat.2023.01.013>.
- [652] Song Y, Li L, Zhao W, Qian Y, Dong L, Fang Y, et al. Surface modification of electrospun fibers with mechano-growth factor for mitigating the foreign-body reaction. *Bioact Mater* 2021;6:2983–98. <https://doi.org/10.1016/j.bioactmat.2021.02.020>.
- [653] Berner A, Reichert J, Muller M, Zellner J, Pfeifer C, Dienstknecht T, et al. Treatment of long bone defects and non-unions: from research to clinical practice. *Cell Tissue Res* 2012;347:501–19. <https://doi.org/10.1007/s00441-011-1184-8>.
- [654] Zhang J, Liu W, Schnitzler V, Tancret F, Boulter J. Calcium phosphate cements for bone substitution: chemistry, handling and mechanical properties. *Acta Biomater* 2014;10:1035–49. <https://doi.org/10.1016/j.actbio.2013.11.001>.
- [655] Moore W, Graves S, Bain G. Synthetic bone graft substitutes. *ANZ J Surg* 2015;71:354–61. <https://doi.org/10.1046/j.1440-1622.2001.02128.x>.
- [656] Bose S, Roy M, Bandopadhyay A. Recent advances in bone tissue engineering scaffolds. *Trends Biotechnol* 2012;30:546–54. <https://doi.org/10.1016/j.tibtech.2012.07.005>.
- [657] Roberts T, Rosenbaum A. Bone grafts, bone substitutes and orthobiologics the bridge between basic science and clinical advancements in fracture healing. *Organogenesis* 2012;8:114–24. <https://doi.org/10.4161/org.23306>.
- [658] Weiner S, Wagner HD. The material bone: structure-mechanical function relations. *Annu Rev Mater Sci* 1998;28:271–98. <https://doi.org/10.1146/annurev.matsci.28.1.271>.
- [659] Xie X, Chen Y, Wang X, Xu X, Shen Y, Khan A, et al. Electrospinning nanofiber scaffolds for soft and hard tissue regeneration. *J Mater Sci Technol* 2020;59:243–61. <https://doi.org/10.1016/j.jmst.2020.04.037>.
- [660] N. Marins, B. Lee, E. RM, A. Raghavan, N. Villarreal Carreno, K. Grandfield. Niobium pentoxide and hydroxyapatite particle loaded electrospun polycaprolactone/gelatin membranes for bone tissue engineering. *Colloids Surf B Biointerfaces*, 182 (2019), pp. 110386, 10.1016/j.colsurfb.2019.110386.
- [661] Ko E, Lee J, Kim H, Yang S, Yang D, Yang K, et al. Electrospun silk fibroin nanofibrous scaffolds with two-stage hydroxyapatite functionalization for enhancing the osteogenic differentiation of human adipose-derived mesenchymal stem cells. *ACS Appl Mater Interfaces* 2018;10:7614–25. <https://doi.org/10.1021/acsami.7b03328>.
- [662] Ye K, Liu D, Kuang H, Cai J, Chen W, Sun B, et al. Three-dimensional electrospun nanofibrous scaffolds displaying bone morphogenetic protein-2-derived peptides for the promotion of osteogenic differentiation of stem cells and bone regeneration. *J Colloid Interface Sci* 2019;534:625–36. <https://doi.org/10.1016/j.jcis.2018.09.071>.
- [663] Yi W, Wenguo C, Xin Z, et al. Bone remodeling-inspired dual delivery electrospun nanofibers for promoting bone regeneration. *Nanoscale* 2019;11:60–71. <https://doi.org/10.1039/C8NR07329E>.
- [664] Nukavarapu S, Dorcemus D. Osteochondral tissue engineering: current strategies and challenges. *Biotechnol Adv* 2013;31:706–21. <https://doi.org/10.1016/j.biotechadv.2012.11.004>.
- [665] Moran C, Pascual-Garrido C, Chubinskaya S, Potter H, Warren R, Cole B, et al. Restoration of articular cartilage. *J Bone Joint Surg Am* 2014;96:336–44. <https://doi.org/10.2106/JBJS.L.01329>.
- [666] Chen W, Xu Y, Liu Y, Wang Z, Li Y, Jiang G, et al. Three-dimensional printed electrospun fiber-based scaffold for cartilage regeneration. *Mater Des* 2019;179:107886. <https://doi.org/10.1016/j.matdes.2019.107886>.
- [667] Chen W, Xu Y, Li Y, Jia L, Zhou G. 3D printing electrospinning fiber-reinforced decellularized extracellular matrix for cartilage regeneration. *Chem Eng J* 2019;382:122986. <https://doi.org/10.1016/j.cej.2019.122986>.
- [668] Zhou Y, Zhang J, Yang J, Narava M, Zhao G, Yuan T, et al. Kartogenin with PRP promotes the formation of fibrocartilage zone in the tendon-bone interface. *J Tissue Eng Regen Med* 2017;11:3445–56. <https://doi.org/10.1002/term.2258>.
- [669] Lei T, Zhang T, Ju W, Chen X, Heng BC, Shen W, et al. Biomimetic strategies for tendon/ligament-to-bone interface regeneration. *Bioact Mater* 2021;6:2491–510. <https://doi.org/10.1016/j.bioactmat.2021.01.022>.
- [670] Takahashi H, Tamaki H, Oyama M, Yamamoto N, Onishi H. Time-dependent changes in the structure of calcified fibrocartilage in the rat Achilles tendon-bone interface with sciatic denervation. *Anat Rec (Hoboken)* 2017;300:2166–74. <https://doi.org/10.1002/ar.23684>.
- [671] Lu H, Li S, Zhang T, Wang Z, Chen C, Chen H, et al. Treadmill running initiation times and bone-tendon interface repair in a murine rotator cuff repair model. *J Orthop Res* 2021;39:2017–27. <https://doi.org/10.1002/jor.24863>.
- [672] Lee K, Lee J, Jang J, Shim Y, Lee K. Tendon-bone interface healing using an injectable rhBMP-2-containing collagen gel in a rabbit extra-articular bone tunnel model. *J Tissue Eng Regen Med* 2017;11:1435–41. <https://doi.org/10.1002/term.2041>.
- [673] Loeffler B, Scannell B, Peindl R, Connor P, Davis D, Hoelscher G, et al. Cell-based tissue engineering augments tendon-to-bone healing in a rat supraspinatus model. *J Orthop Res* 2013;31:407–12. <https://doi.org/10.1002/jor.22234>.
- [674] Xue J, Pignano D, Xia Y. Maneuvering the migration and differentiation of stem cells with electrospun nanofibers. *Adv Sci* 2020;7:2000735. <https://doi.org/10.1002/advs.202000735>.
- [675] Gao H, Wang L, Lin Z, Jin H, Lyu Y, Kang Y, et al. Bi-lineage inducible and immunoregulatory electrospun fibers scaffolds for synchronous regeneration of tendon-to-bone interface. *Mater Today Bio* 2023;22:100749. <https://doi.org/10.1016/j.mtbio.2023.100749>.
- [676] Xu X, Si Y, Zhao Y, Ke Q, Hu J. Electrospun textile strategies in tendon to bone junction reconstruction. *Adv Fiber Mater* 2023;5:764–90. <https://doi.org/10.1007/s42765-022-00233-9>.

- [677] Calejo I, Costa-Almeida R, Reis R, Gomes M. A textile platform using continuous aligned and textured composite microfibers to engineer tendon-to-bone interface gradient scaffolds. *Adv Healthc Mater* 2019;8:e1900200. <https://doi.org/10.1002/adhm.201900200>.
- [678] Xie X, Cai J, Yao Y, Chen Y, Khan A, Wu J, et al. A woven scaffold with continuous mineral gradients for tendon-to-bone tissue engineering. *Compos B Eng* 2021;212:108679. <https://doi.org/10.1016/j.compositesb.2021.108679>.
- [679] Zhu C, Pongkitwitton S, Qiu J, Thomopoulos S, Xia Y. Design and fabrication of a hierarchically structured scaffold for tendon-to-bone repair. *Adv Mater* 2018;30:e1707306. <https://doi.org/10.1002/adma.201707306>.
- [680] Zhu GS, Sun ZC, Hui P, Chen WW, Jiang XY. Composite film with antibacterial gold nanoparticles and silk fibroin for treating multidrug-resistant *E. coli*-infected wounds. *ACS Biomater Sci Eng* 2021;7:1827–35. <https://doi.org/10.1021/acsbomaterials.0c01271>.
- [681] Yu C, Wang T, Diao H, Liu N, Zhang Y, Jiang H, et al. Photothermal-triggered structural change of nanofiber scaffold integrating with graded mineralization to promote tendon-to-bone interface regeneration. *Adv Fiber Mater* 2022;4:908–22. <https://doi.org/10.1007/s42765-022-00154-7>.
- [682] Yang R, Zheng Y, Zhang Y, Li G, Xu Y, Zhang Y, et al. Bipolar metal flexible electrospun fibrous membrane based on metal-organic framework for gradient healing of tendon-to-bone interface regeneration. *Adv Healthc Mater* 2022;11:e2200072. <https://doi.org/10.1002/adhm.202200072>.
- [683] Madhurakkat Perikamana S, Lee J, Ahmad T, Kim E, Byun H, Lee S, et al. Harnessing biochemical and structural cues for tenogenic differentiation of adipose derived stem cells (ADSCs) and development of an in vitro tissue interface mimicking tendon-bone insertion graft. *Biomaterials* 2018;165:79–93. <https://doi.org/10.1016/j.biomaterials.2018.02.046>.
- [684] Sun Q, Zhou Z, Qiu N, Shen Y. Rational design of cancer nanomedicine: Nanoproperty integration and synchronization. *Adv Mater* 2017;29:1606628. <https://doi.org/10.1002/adma.201606628>.
- [685] Rosenblum D, Joshi N, Tao W, Karp J, Peer D. Progress and challenges towards targeted delivery of cancer therapeutics. *Nat Commun* 2018;9:1410. <https://doi.org/10.1038/s41467-018-03705-y>.
- [686] Li X, Pan J, Li Y, Xu F, Hou J, Yang G, et al. Development of a localized drug delivery system with a step-by-step cell internalization capacity for cancer immunotherapy. *ACS Nano* 2022;16:5778. <https://doi.org/10.1021/acsnano.1c10892>.
- [687] Li Y, Yuan R, Luo Y, Guo X, Yang G, Li X, et al. A hierarchical structured fiber device remodeling the acidic tumor microenvironment for enhanced cancer immunotherapy. *Adv Mater* 2023;35:e2300216. <https://doi.org/10.1002/adma.202300216>.
- [688] Fu Y, Li X, Ren Z, Mao C, Han G. Multifunctional electrospun nanofibers for enhancing localized cancer treatment. *Small* 2018;14:e1801183. <https://doi.org/10.1002/smll.201801183>.
- [689] Khoshnevisan K, Maleki H, Samadian H, Shahsavari S, Sarrafzadeh M, Larijani B, et al. Cellulose acetate electrospun nanofibers for drug delivery systems: Applications and recent advances. *Carbohydr Polym* 2018;198:131–41. <https://doi.org/10.1016/j.carbpol.2018.06.072>.
- [690] Akpan U, Pellegrini M, Obayemi J, Ezenwafor T, Browl D, Ani C, et al. Prodigiosin-loaded electrospun nanofibers scaffold for localized treatment of triple negative breast cancer. *Mater Sci Eng C* 2020;114:110976. <https://doi.org/10.1016/j.msec.2020.110976>.
- [691] Samadzadeh S, Mousazadeh H, Ghareghomi S, Dadashpour M, Babazadeh M, Zarghami N. Anticancer efficacy of metformin-loaded plga nanofibers towards the post-surgical therapy of lung cancer. *J Drug Deliv Sci Technol* 2021;61:102318. <https://doi.org/10.1016/j.jddst.2020.102318>.
- [692] Rasouli S, Montazeri M, Mashayekhi S, Sadeghi-Soureh S, Dadashpour M, Mousazadeh H, et al. Synergistic anticancer effects of electrospun nanofiber-mediated codelivery of curcumin and chrysin: Possible application in prevention of breast cancer local recurrence. *J Drug Deliv Sci Technol* 2020;55:101402. <https://doi.org/10.1016/j.jddst.2019.101402>.
- [693] Arumugam M, Murugesan B, Pandiyan N, Chinnalagu D, Rangasamy G, Mahalingam S. Electrospinning cellulose acetate/silk fibroin/au-ag hybrid composite nanofiber for enhanced biocidal activity against mcf-7 breast cancer cell. *Mater Sci Eng C* 2021;123:112019. <https://doi.org/10.1016/j.msec.2021.112019>.
- [694] Jin J, Saiding Q, Wang X, Qin M, Xiang Y, Cheng R, et al. Rapid extracellular matrix remodeling via gene-electrospun fibers as a “patch” for tissue regeneration. *Adv Funct Mater* 2021;31:2009879. <https://doi.org/10.1002/adfm.202009879>.
- [695] Wu L, Gu Y, Liu L, Tang J, Mao J, Xi K, et al. Hierarchical micro/nanofibrous membranes of sustained releasing VEGF for periosteal regeneration. *Biomaterials* 2020;227:119555. <https://doi.org/10.1016/j.biomaterials.2019.119555>.
- [696] Ding Y, Li W, Zhang F, Liu Z, Zanjanzadeh Ezazi N, Liu D, et al. Electrospun fibrous architectures for drug delivery, tissue engineering and cancer therapy. *Adv Funct Mater* 2018;29:1802852. <https://doi.org/10.1002/adfm.201802852>.
- [697] Samadzadeh S, Babazadeh M, Zarghami N, Pilehvar-Soltanahmadi Y, Mousazadeh H. An implantable smart hyperthermia nanofiber with switchable, controlled and sustained drug release: Possible application in prevention of cancer local recurrence. *Mater Sci Eng C* 2021;118:111384. <https://doi.org/10.1016/j.msec.2020.111384>.
- [698] Hu P, Zhao Y, Zhang J, Yu S, Yan J, Wang X, et al. In-situ melt electrospun polycaprolactone/fe3o4 nanofibers for magnetic hyperthermia. *Mater Sci Eng C* 2020;110:110708. <https://doi.org/10.1016/j.msec.2020.110708>.
- [699] Nakielski P, Pawlowska S, Rinoldi C, Ziai Y, De Sio L, Urbanek O, et al. Multifunctional platform based on electrospun nanofibers and plasmonic hydrogel: A smart nanostructured pillow for near-infrared light-driven biomedical applications. *ACS Appl Mater Interfaces* 2020;12:54328–42. <https://doi.org/10.1021/acsami.0c13266>.
- [700] Zhang Y, Wang J, Xiao J, Fang T, Hu N, Li M, et al. An electrospun fiber-covered stent with programmable dual drug release for endothelialization acceleration and lumen stenosis prevention. *Acta Biomater* 2019;94:295–305. <https://doi.org/10.1016/j.actbio.2019.06.008>.
- [701] Xiao J, Cheng L, Fang T, Zhang Y, Zhou J, Cheng R, et al. Nanoparticle-embedded electrospun fiber-covered stent to assist intraluminal photodynamic treatment of oesophageal cancer. *Small* 2019;15:e1904979. <https://doi.org/10.1002/smll.201904979>.
- [702] Fu Y, Li X, Sun C, Ren Z, Weng W, Mao C, et al. pH-Triggered SrTiO₃:Er Nanofibers with Optically Monitored and Controlled Drug Delivery Functionality. *ACS Appl Mater Interfaces* 2015;7:25514–21. <https://doi.org/10.1021/acsami.5b08953>.
- [703] Chen Y, Liu S, Hou Z, Ma P, Yang D, Li C, et al. Multifunctional electrospinning composite fibers for orthotopic cancer treatment in vivo. *Nano Res* 2015;8:1917–31. <https://doi.org/10.1007/s12274-014-0701-y>.
- [704] Ghafoor B, Aleem A, Najabat Ali M, Mir M. Review of the fabrication techniques and applications of polymeric electrospun nanofibers for drug delivery systems. *J Drug Deliv Sci Technol* 2018;48:82–7. <https://doi.org/10.1016/j.jddst.2018.09.005>.
- [705] Xiao J, Zhang Y, Fang T, Yuan T, Tian Q, Liu J, et al. Mineralized manganese dioxide channel as the stent coating for in-situ precise tumor navigation. *Nano Res* 2021;14:2464–6. <https://doi.org/10.1007/s12274-021-3299-x>.
- [706] Xi K, Gu Y, Tang J, Chen H, Xu Y, Wu L, et al. Microenvironment-responsive immunoregulatory electrospun fibers for promoting nerve function recovery. *Nat Commun* 2020;11:4504. <https://doi.org/10.1038/s41467-020-18265-3>.
- [707] Wang G, Gao J, Fu Y, Ren Z, Huang J, Li X, et al. Implantable composite fibres with self-supplied H₂O₂ for localized chemodynamic therapy. *Chem Eng J* 2020;388:124211. <https://doi.org/10.1016/j.cej.2020.124211>.
- [708] Chen K, Li Y, Li Y, Tan Y, Liu Y, Pan W, et al. Stimuli-responsive electrospun nanofibers for drug delivery, cancer therapy, wound dressing, and tissue engineering. *J Nanobiotechnology* 2023;21:237. <https://doi.org/10.1186/s12951-023-01987-z>.
- [709] Guo B, Yang F, Zhang L, Zhao Q, Wang W, Yin L, et al. Cuproptosis induced by ROS responsive nanoparticles with elesclamol and copper combined with αPD-L1 for enhanced cancer immunotherapy. *Adv Mater* 2023;35:e2212267. <https://doi.org/10.1002/adma.202212267>.
- [710] Luo Z, He Y, Li M, Ge Y, Huang Y, Liu X, et al. Tumor microenvironment-inspired glutathione-responsive three-dimensional fibrous network for efficient trapping and gentle release of circulating tumor cells. *ACS Appl Mater Interfaces* 2023;15:24013–22. <https://doi.org/10.1021/acsami.3c00307>.
- [711] Zhang Y, Zhang Z. The history and advances in cancer immunotherapy: Understanding the characteristics of tumor-infiltrating immune cells and their therapeutic implications. *Cell Mol Immunol* 2020;17:807–21. <https://doi.org/10.1038/s41423-020-0488-6>.
- [712] Alex D, Jill M, Michael J. A guide to cancer immunotherapy: from T cell basic science to clinical practice. *Nat Rev Immunol* 2020;20:651–68. <https://doi.org/10.1038/s41577-020-0306-5>.
- [713] Van Wagoner C, Rivera-Escalera F, Jaimes-Delgadillo N, Chu C, Zent C, Elliott M. Antibody-mediated phagocytosis in cancer immunotherapy. *Immunol Rev* 2023;319:128–41. <https://doi.org/10.1111/imr.13265>.
- [714] Wu A, Senter P. Arming antibodies: prospects and challenges for immunoconjugates. *Nat Biotechnol* 2005;23:1137–46. <https://doi.org/10.1038/nbt1141>.

- [715] Sgouros G, Bodei L, McDevitt M, Nedrow J. Radiopharmaceutical therapy in cancer: Clinical advances and challenges. *Nat Rev Drug Discov* 2020;19:589–608. <https://doi.org/10.1038/s41573-020-0073-9>.
- [716] Liu X, Zhang H, Cheng R, Gu Y, Yin Y, Sun Z, et al. An immunological electrospun scaffold for tumor cell killing and healthy tissue regeneration. *Mater Horiz* 2018;5:1082–91. <https://doi.org/10.1039/c8mh00704g>.
- [717] Song X, Jiang Y, Zhang W, Elfawal G, Wang K, Jiang D, et al. Transcutaneous tumor vaccination combined with anti-programmed death-1 monoclonal antibody treatment produces a synergistic antitumor effect. *Acta Biomater* 2022;140:247–60. <https://doi.org/10.1016/j.actbio.2021.11.033>.
- [718] Kuang G, Zhang Q, Yu Y, Ding X, Sun W, Shen X, et al. Lyophilization-inactivated cancer cells composited Janus scaffold for tumor postoperative immunotherapy. *Chem Eng J* 2023;455:140619. <https://doi.org/10.1016/j.cej.2022.140619>.
- [719] Rezk AI, Lee J, Kim BS, Chun S. Strategically designed bifunctional polydopamine enwrapping polycaprolactone-hydroxyapatite-doxorubicin composite nanofibers for osteosarcoma treatment and bone regeneration. *ACS Appl Mater Interfaces* 2024;16:22946–57. <https://doi.org/10.1021/acsami.4c03015>.
- [720] Hu Y, Zhou L, Wang Z, Ye Z, Liu H, Lu Y, et al. Assembled embedded 3d hydrogel system for asynchronous drug delivery to inhibit postoperative recurrence of malignant glioma and promote neurological recovery. *Adv Funct Mater* 2024;34:2401383. <https://doi.org/10.1002/adfm.202401383>.
- [721] Teixeira J, Costa R, Pires A, Pereira A, Pereira C. Hybrid dual-function thermal energy harvesting and storage technologies: Towards self-chargeable flexible/wearable devices. *Dalton Trans* 2021;50:9983–10013. <https://doi.org/10.1039/d1dt01568k>.
- [722] Shin H, Yoo J, Sung Y, Chung D. Dynamic electrochemical interfaces for energy conversion and storage. *JACS Au* 2022;2:2222–34. <https://doi.org/10.1021/jacsau.2c00385>.
- [723] Xu X, Shi W, Li P, Ye S, Ye C, Ye H, et al. Facile fabrication of three-dimensional graphene and metal–organic framework composites and their derivatives for flexible all-solid-state supercapacitors. *Chem Mater* 2017;29:6058–65. <https://doi.org/10.1021/acs.chemmater.7b01947>.
- [724] Yuan K, Xu Y, Uihlein J, Brunklaus G, Shi L, Heiderhoff R, et al. Straightforward generation of pillared, microporous graphene frameworks for use in supercapacitors. *Adv Mater* 2015;27:6714–21. <https://doi.org/10.1002/adma.201503390>.
- [725] Zhao J, Jiang Y, Fan H, Liu M, Zhuo O, Wang X, et al. Porous 3D few-layer graphene-like carbon for ultrahigh-power supercapacitors with well-defined structure-performance relationship. *Adv Mater* 2017;29:1604569. <https://doi.org/10.1002/adma.201604569>.
- [726] Xu T, Yang D, Fan Z, Li X, Liu Y, Guo C, et al. Reduced graphene oxide/carbon nanotube hybrid fibers with narrowly distributed mesopores for flexible supercapacitors with high volumetric capacitances and satisfactory durability. *Carbon* 2019;152:134–43. <https://doi.org/10.1016/j.carbon.2019.06.005>.
- [727] Yu Z, Tetard L, Zhai L, Thomas J. Supercapacitor electrode materials: Nanostructures from 0 to 3 dimensions. *Energy Environ Sci* 2015;8:702–30. <https://doi.org/10.1039/c4ee03229b>.
- [728] Zhang S, Yang D, Zhang M, Liu Y, Xu T, Yang J, et al. Synthesis of novel bimetallic nickel cobalt telluride nanotubes on nickel foam for high-performance hybrid supercapacitors. *Inorg Chem Front* 2020;7:477–86. <https://doi.org/10.1039/c9qi01395d>.
- [729] Guo D, Wu J, Liu Z, Liu X, Xu Z, Gu Z, et al. High-performance, long-life lithium-oxygen batteries based on solid and liquid dual catalysts. *ACS Appl Energy Mater* 2024;7:275–84. <https://doi.org/10.1021/acsaelm.3c02592>.
- [730] Chen K, Huang G, Zhang X. Efforts towards practical and sustainable Li/N-air batteries. *Chin J Chem* 2020;39:32–42. <https://doi.org/10.1002/cjoc.202000408>.
- [731] Li Z, Gao R, Feng M, Deng Y, Xiao D, Zheng Y, et al. Modulating metal–organic frameworks as advanced oxygen electrocatalysts. *Adv Energy Mater* 2021;11:2003291. <https://doi.org/10.1002/aenm.202003291>.
- [732] Manthiram A, Fu Y, Chung S, Zu C, Su Y. Rechargeable lithium-sulfur batteries. *Chem Rev* 2014;114:11751–87. <https://doi.org/10.1021/cr500062v>.
- [733] Bruce P, Freunberger S, Hardwick L, Tarascon J. Li–O₂ and Li–S batteries with high energy storage. *Nat Mater* 2011;11:19–29. <https://doi.org/10.1038/nmat3191>.
- [734] Xing HY, Zhang K, Chang R, Wen ZQ, Xu YL. Integrating CoP/Co heterojunction into nitrogen-doped carbon polyhedrons as electrocatalysts to promote polysulfides conversion in lithium-sulfur batteries. *J Colloid Interface Sci* 2025;677:181–93. <https://doi.org/10.1016/j.jcis.2024.08.011>.
- [735] Avinash R, Golareh J. Advances in fibrous materials for high-capacity lithium sulfur batteries. *Nano Energy* 2024;122:109265. <https://doi.org/10.1016/j.nanoen.2024.109265>.
- [736] Liu D, Wang ZC, Guo ZC, Tian Y, Wang C. Electrospun CuCoNi0.6 coating necklace-like N-doped carbon nanofibers for high performance lithium-sulfur batteries. *J Colloid Interface Sci* 2023;645:705–14. <https://doi.org/10.1016/j.jcis.2023.04.183>.
- [737] Fan HR, Si YB, Zhang YM, Zhu FL, Wang X, Fu YZ. Grapevine-like high entropy oxide composites boost high-performance lithium sulfur batteries as bifunctional interlayers. *Green Energy Environ* 2024;9:565–72. <https://doi.org/10.1016/j.gee.2022.11.001>.
- [738] Luo J, Liu XF, Wen L, Jia QL, Zhang SW, Zhang HJ. Self-standing lotus root-like host materials for high-performance lithium-sulfur batteries. *Adv Fiber Mater* 2022;4:1656–68. <https://doi.org/10.1007/s42765-022-00206-y>.
- [739] Baghali M, Jayathilaka W, Ramakrishna S. The role of electrospun nanomaterials in the future of energy and environment. *Materials (Basel)* 2021;14:pp. <https://doi.org/10.3390/ma14030558>.
- [740] Pasquini L. Nanostructured materials for energy storage and conversion. *Nanomaterials (Basel)* 2022;12:pp. <https://doi.org/10.3390/nano12091583>.
- [741] Yoon K, Shin K, Park J, Cho S, Kim C, Jung J, et al. Brush-like cobalt nitride anchored carbon nanofiber membrane: Current collector-catalyst integrated cathode for long cycle Li–O₂ batteries. *ACS Nano* 2017;12:128–39. <https://doi.org/10.1021/acs.nano.7b03794>.
- [742] Lee S, Franklin S, Hassani F, Yokota T, Nayeem M, Wang Y, et al. Nanomesh pressure sensor for monitoring finger manipulation without sensory interference. *Science* 2020;370:966–70. <https://doi.org/10.1126/science.abc9735>.
- [743] Zhang L, Li X, Yang M, Chen W. High-safety separators for lithium-ion batteries and sodium-ion batteries: Advances and perspective. *Energy Storage Mater* 2021;41:522–45. <https://doi.org/10.1016/j.ensm.2021.06.033>.
- [744] Wei Q, Xiong F, Tan S, Huang L, Lan E, Dunn B, et al. Porous one-dimensional nanomaterials: Design, fabrication and applications in electrochemical energy storage. *Adv Mater* 2017;29:1602300. <https://doi.org/10.1002/adma.201602300>.
- [745] Rao M, Geng X, Li X, Hu S, Li W. Lithium-sulfur cell with combining carbon nanofibers–sulfur cathode and gel polymer electrolyte. *J Power Sources* 2012;212:179–85. <https://doi.org/10.1016/j.jpowsour.2012.03.111>.
- [746] Jiang K, Gao S, Wang R, Jiang M, Han J, Gu T, et al. Lithium sulfonate/carboxylate-anchored polyvinyl alcohol separators for lithium sulfur batteries. *ACS Appl Mater Interfaces* 2018;10:18310–5. <https://doi.org/10.1021/acsami.8b03290>.
- [747] Wei H, Ma J, Li BA, Zuo YX, Xia DG. Enhanced cycle performance of lithium-sulfur batteries using a separator modified with a pvdf-c layer. *ACS Appl Mater Interfaces* 2014;6:20276–81. <https://doi.org/10.1021/am505807k>.
- [748] Wang L, Deng N, Fan L, Wang L, Wang G, Kang W, et al. A novel hot-pressed electrospun polyimide separator for lithium-sulfur batteries. *Mater Lett* 2018;233:224–7. <https://doi.org/10.1016/j.matlet.2018.09.011>.
- [749] Deng NP, Wang LY, Feng Y, Liu M, Li QX, Wang G, et al. Co-based and Cu-based MOFs modified separators to strengthen the kinetics of redox reaction and inhibit lithium-dendrite for long-life lithium-sulfur batteries. *Chem Eng J* 2020;388:124241. <https://doi.org/10.1016/j.cej.2020.124241>.
- [750] Zhou CY, Wang J, Zhu XB, Chen K, Ouyang Y, Wu Y, et al. A dual-functional poly(vinyl alcohol)/poly(lithium acrylate) composite nanofiber separator for ionic shielding of polysulfides enables high-rate and ultra-stable Li-S batteries. *Nano Res* 2021;14:1541–50. <https://doi.org/10.1007/s12274-020-3213-y>.
- [751] Liu M, Jiang HR, Ren YX, Zhou D, Kang FY, Zhao TS. In-situ fabrication of a freestanding acrylate-based hierarchical electrolyte for lithium-sulfur batteries. *Electrochim Acta* 2016;213:871–8. <https://doi.org/10.1016/j.electacta.2016.08.015>.
- [752] Zhu P, Zhu J, Zang J, Chen C, Lu Y, Jiang M, et al. A novel bi-functional double-layer rGO–PVDF/PVDF composite nanofiber membrane separator with enhanced thermal stability and effective polysulfide inhibition for high-performance lithium–sulfur batteries. *J Mater Chem A* 2017;5:15096–104. <https://doi.org/10.1039/c7ta03301j>.
- [753] Zhao H, Deng N, Yan J, Kang W, Ju J, Wang L, et al. Effect of OctaphenylPolyhedral oligomeric silsesquioxane on the electrospun Poly-m-phenylene isophthalamid separators for lithium-ion batteries with high safety and excellent electrochemical performance. *Chem Eng J* 2019;356:11–21. <https://doi.org/10.1016/j.cej.2018.09.010>.

- [754] Chen W, Zhang L, Liu C, Feng X, Zhang J, Guan L, et al. Electrospun flexible cellulose acetate-based separators for sodium-ion batteries with ultralong cycle stability and excellent wettability: The role of interface chemical groups. *ACS Appl Mater Interfaces* 2018;10:23883–90. <https://doi.org/10.1021/acsami.8b06706>.
- [755] Zhang L, Feng G, Li X, Cui S, Ying S, Feng X, et al. Synergism of surface group transfer and in-situ growth of silica-aerogel induced high-performance modified polyacrylonitrile separator for lithium/sodium-ion batteries. *J Membr Sci* 2019;577:137–44. <https://doi.org/10.1016/j.memsci.2019.02.002>.
- [756] Deng N, Kang W, Liu Y, Ju J, Wu D, Li L, et al. A review on separators for lithium sulfur battery: Progress and prospects. *J Power Sources* 2016;331:132–55. <https://doi.org/10.1016/j.jpowsour.2016.09.044>.
- [757] Li S, Zhang W, Zheng J, Lv M, Song H, Du L. Inhibition of polysulfide shuttles in Li-S batteries: Modified separators and solid-state electrolytes. *Adv Energy Mater* 2020;11:2000779. <https://doi.org/10.1002/aenm.202000779>.
- [758] Feng Y, Wang G, Ju J, Zhao Y, Kang W, Deng N, et al. Towards high energy density Li-S batteries with high sulfur loading: From key issues to advanced strategies. *Energy Storage Mater* 2020;32:320–55. <https://doi.org/10.1016/j.ensm.2020.06.043>.
- [759] Liu Z, Hu Q, Guo S, Yu L, Hu X. Thermoregulating separators based on phase-change materials for safe lithium-ion batteries. *Adv Mater* 2021;33:e2008088. <https://doi.org/10.1002/adma.202008088>.
- [760] Ma W, Zhang Y, Pan S, Cheng Y, Shao Z, Xiang H, et al. Smart fibers for energy conversion and storage. *Chem Soc Rev* 2021;50:7009–61. <https://doi.org/10.1039/d0cs01603a>.
- [761] Ray A, Saruhan B. Application of ionic liquids for batteries and supercapacitors. *Materials* 2021;14:2942. <https://doi.org/10.3390/ma14112942>.
- [762] Fan X, Zhong C, Liu J, Ding J, Deng Y, Han X, et al. Opportunities of flexible and portable electrochemical devices for energy storage: Expanding the spotlight onto semi-solid/solid electrolytes. *Chem Rev* 2022;122:17155–239. <https://doi.org/10.1021/acs.chemrev.2c00196>.
- [763] Wang M, Wu Y, Qiu M, Li X, Li C, Li R, et al. Research progress in electrospinning engineering for all-solid-state electrolytes of lithium metal batteries. *J Energy Chem* 2021;61:253–68. <https://doi.org/10.1016/j.jechem.2021.02.023>.
- [764] Liu W, Liu N, Sun J, Hsu P, Li Y, Lee H, et al. Ionic conductivity enhancement of polymer electrolytes with ceramic nanowire fillers. *Nano Lett* 2015;15:2740–5. <https://doi.org/10.1021/acs.nanolett.5b00600>.
- [765] Liu W, Lee S, Lin D, Shi F, Wang S, Sendek A, et al. Enhancing ionic conductivity in composite polymer electrolytes with well-aligned ceramic nanowires. *Nat Energy* 2017;2:17035. <https://doi.org/10.1038/energy.2017.35>.
- [766] Fu K, Gong Y, Dai J, Gong A, Han X, Yao Y, et al. Flexible, solid-state, ion-conducting membrane with 3D garnet nanofiber networks for lithium batteries. *Proc Natl Acad Sci USA* 2016;113:7094–9. <https://doi.org/10.1073/pnas.1600422113>.
- [767] Hu C, Qi J, Zhang Y, Xie S, Liu B, Xue G, et al. Room-temperature all-solid-state sodium battery based on bulk interfacial superionic conductor. *Nano Lett* 2021;21:10354–60. <https://doi.org/10.1021/acs.nanolett.1c03605>.
- [768] Hu C, Shen Y, Shen M, Liu X, Chen H, Liu C, et al. Superionic conductors via bulk interfacial conduction. *J Am Chem Soc* 2020;142:18035–41. <https://doi.org/10.1021/jacs.0c07060>.
- [769] Wang Y, Wu X, Han Y, Li T. Flexible supercapacitor: Overview and outlooks. *J Energy Storage* 2021;42:103053. <https://doi.org/10.1016/j.est.2021.103053>.
- [770] Chen L, Lu Y, Yu L, Lou X. Designed formation of hollow particle-based nitrogen-doped carbon nanofibers for high-performance supercapacitors. *Energy Environ Sci* 2017;10:1777–83. <https://doi.org/10.1039/c7ee00488e>.
- [771] Lv Z, Luo Y, Tang Y, Wei J, Zhu Z, Zhou X, et al. Editable supercapacitors with customizable stretchability based on mechanically strengthened ultralong MnO₂ nanowire composite. *Adv Mater* 2017;30:pp. <https://doi.org/10.1002/adma.201704531>.
- [772] Zhai S, Wang C, Karahan H, Wang Y, Chen X, Sui X, et al. Nano-RuO₂-decorated holey graphene composite fibers for micro-supercapacitors with ultrahigh energy density. *Small* 2018;14:e1800582. <https://doi.org/10.1002/smll.201800582>.
- [773] Li Q, Guo J, Xu D, Guo J, Ou X, Hu Y, et al. Electrospun N-doped porous carbon nanofibers incorporated with NiO nanoparticles as free-standing film electrodes for high-performance supercapacitors and CO₂ capture. *Small* 2018;14:e1704203. <https://doi.org/10.1002/smll.201704203>.
- [774] M. Dadaso D, C. Sachin S, L. P. E., D. Sumit, K. Vishal, J. Chaitali, et al. Electrochemical characterization of electrospun Co₃O₄/PAN-based carbon nanofiber composites for supercapacitor applications. *J Mater Sci*, 59 (2024), pp. 11440–11453, 10.1007/s10853-024-09852-6.
- [775] U. Ahmad, A. M. Shaheer, I. Ahmed A., A. Hassan, A. Mohsen A. M., et al. Electrospun Co₃O₄ nanofibers as potential material for enhanced supercapacitors and chemo-sensor applications. *J Mater Res Technol*, 21 (2022), pp. 5018–5031, 10.1016/j.jmrt.2022.11.094.
- [776] Rama Raju G, Pavitra E, Nagaraju G, Sekhar S, Ghoreishian S, Kwak C, et al. Rational design of forest-like nickel sulfide hierarchical architectures with ultrahigh areal capacity as a binder-free cathode material for hybrid supercapacitors. *J Mater Chem A* 2018;6:13178–90. <https://doi.org/10.1039/c8ta02597e>.
- [777] Liu Q, Hong X, You X, Zhang X, Zhao X, Chen X, et al. Designing heterostructured metal sulfide core-shell nanoneedle films as battery-type electrodes for hybrid supercapacitors. *Energy Storage Mater* 2020;24:541–9. <https://doi.org/10.1016/j.ensm.2019.07.001>.
- [778] Tang S, Zhu B, Shi X, Wu J, Meng X. General controlled sulfidation toward achieving novel nanosheet-built porous square-FeCo₂S₄-tube arrays for high-performance asymmetric all-solid-state pseudocapacitors. *Adv Energy Mater* 2016;7:1601985. <https://doi.org/10.1002/aenm.201601985>.
- [779] Zhang X, Liu C, Zhang X, Si Y, Yu J, Ding B. Super strong, shear resistant, and highly elastic lamellar structured ceramic nanofibrous aerogels for thermal insulation. *J Mater Chem A* 2021;9:27415–23. <https://doi.org/10.1039/d1ta08879c>.
- [780] Song Y, Liu T, Li M, Yao B, Kou T, Feng D, et al. Engineering of mesoscale pores in balancing mass loading and rate capability of hematite films for electrochemical capacitors. *Adv Energy Mater* 2018;8. <https://doi.org/10.1002/aenm.201801784>.
- [781] Zhou Z, Zhang Q, Sun J, He B, Guo J, Li Q, et al. Metal-organic framework derived spindle-like carbon incorporated alpha-Fe₂O₃ grown on carbon nanotube fiber as anodes for high-performance wearable asymmetric supercapacitors. *ACS Nano* 2018;12:9333–41. <https://doi.org/10.1021/acsnano.8b04336>.
- [782] Kumar S, Saeed G, Kim N, Lee J. Hierarchical nanohoneycomb-like CoMoO₄-MnO₂ core-shell and Fe₂O₃ nanosheet arrays on 3D graphene foam with excellent supercapacitive performance. *J Mater Chem A* 2018;6:7182–93. <https://doi.org/10.1039/c8ta00889b>.
- [783] Zeng Y, Han Y, Zhao Y, Zeng Y, Yu M, Liu Y, et al. Advanced Ti-doped Fe₂O₃@PEDOT core/shell anode for high-energy asymmetric supercapacitors. *Adv Energy Mater* 2015;5:1402176. <https://doi.org/10.1002/aenm.201402176>.
- [784] Wang S, Geng J, Zhao X, Xing Y. Elevated sintering capability and electrical conductivity of Fe₂O₃-doped Ce_{0.8}Sm_{0.1}Nd_{0.1}O_{2.8} as an electrolyte in IT-SOFCs. *Mater Chem Phys B* 2023;309:128345. <https://doi.org/10.1016/j.matchemphys.2023.128345>.
- [785] Yu R, Shi Y, Yang D, Liu Y, Qu J, Yu Z. Graphene oxide/chitosan aerogel microspheres with honeycomb-cobweb and radially oriented microchannel structures for broad-spectrum and rapid adsorption of water contaminants. *ACS Appl Mater Interfaces* 2017;9:21809–19. <https://doi.org/10.1021/acsami.7b04655>.
- [786] Zhang M, Yang D, Zhang S, Xu T, Shi Y, Liu Y, et al. Elastic and hierarchical carbon nanofiber aerogels and their hybrids with carbon nanotubes and cobalt oxide nanoparticles for high-performance asymmetric supercapacitors. *Carbon* 2020;158:873–84. <https://doi.org/10.1016/j.carbon.2019.11.071>.
- [787] Si Y, Fu Q, Wang X, Zhu J, Yu J, Sun G, et al. Superelastic and superhydrophobic nanofiber-assembled cellular aerogels for effective separation of oil/water emulsions. *ACS Nano* 2015;9:3791–9. <https://doi.org/10.1021/nn506633b>.
- [788] Si Y, Wang X, Yan C, Yang L, Yu J, Ding B. Ultralight biomass-derived carbonaceous nanofibrous aerogels with superelasticity and high pressure-sensitivity. *Adv Mater* 2016;28:9512–8. <https://doi.org/10.1002/adma.201603143>.
- [789] Xu T, Miszuk J, Zhao Y, Sun H, Fong H. Electrospun polycaprolactone 3D nanofibrous scaffold with interconnected and hierarchically structured pores for bone tissue engineering. *Adv Healthc Mater* 2015;4:2238–46. <https://doi.org/10.1002/adhm.201500345>.
- [790] Huang Y, Lai F, Zhang L, Lu H, Miao Y, Liu T. Elastic carbon aerogels reconstructed from electrospun nanofibers and graphene as three-dimensional networked matrix for efficient energy storage/conversion. *Sci Rep* 2016;6:31541. <https://doi.org/10.1038/srep31541>.
- [791] Zhu Q, Zhao D, Cheng M, Zhou J, Owusu K, Mai L, et al. A new view of supercapacitors: Integrated supercapacitors. *Adv Energy Mater* 2019;9:pp. <https://doi.org/10.1002/aenm.201901081>.
- [792] Zhang X, Gong Y, Li S, Sun C. Porous perovskite La_{0.6}Sr_{0.4}Co_{0.8}Mn_{0.2}O₃ nanofibers Loaded with RuO₂ nanosheets as an efficient and durable bifunctional catalyst for rechargeable Li-O₂ batteries. *ACS Catal* 2017;7:7737–47. <https://doi.org/10.1021/acscatal.7b02153>.
- [793] Ryu W, Gittleton F, Schwab M, Goh T, Taylor A. A mesoporous catalytic membrane architecture for lithium-oxygen battery systems. *Nano Lett* 2015;15:434–41. <https://doi.org/10.1021/nl503760n>.

- [794] Sung M, Lee G, Kim D. Kinetic insight into perovskite $\text{La}_{0.8}\text{Sr}_{0.2}\text{VO}_3$ nanofibers as an efficient electrocatalytic cathode for high-rate Li-O₂ batteries. *InfoMat* 2021;3:1295–12310. <https://doi.org/10.1002/inf2.12243>.
- [795] Xu J, Xu D, Wang Z, Wang H, Zhang L, Zhang X. Synthesis of perovskite-based porous $\text{La}_{0.75}\text{Sr}_{0.25}\text{MnO}_3$ nanotubes as a highly efficient electrocatalyst for rechargeable lithium-oxygen batteries. *Angew Chem Int Ed* 2013;125:3979–82. <https://doi.org/10.1002/ange.201210057>.
- [796] Wu H, Sun W, Shen J, Lu C, Wang Y, Wang Z, et al. Improved structural design of single- and double-wall MnCo_2O_4 nanotube cathodes for long-life Li-O₂ batteries. *Nanoscale* 2018;10:13149–58. <https://doi.org/10.1039/c8nr02795a>.
- [797] Xue H, Mu X, Tang J, Fan X, Gong H, Wang T, et al. A nickel cobaltate nanoparticle-decorated hierarchical porous N-doped carbon nanofiber film as a binder-free self-supported cathode for nonaqueous Li-O₂ batteries. *J Mater Chem A* 2016;4:9106–12. <https://doi.org/10.1039/c6ta01712f>.
- [798] Nam J, Jung J, Youn D, Cho S, Cheong J, Kim M, et al. Free-standing carbon nanofibers protected by a thin metallic iridium layer for extended life-cycle Li-oxygen batteries. *ACS Appl Mater Interfaces* 2020;12:55756–65. <https://doi.org/10.1021/acsami.0c13325>.
- [799] Chen K, Huang G, Ma J, Wang J, Yang D, Yang X, et al. The stabilization effect of CO₂ in lithium-oxygen/CO₂ Batteries. *Angew Chem Int Ed* 2020;59:16661–7. <https://doi.org/10.1002/ange.202006303>.
- [800] Ottakam Thotiyil M, Freunberger S, Peng Z, Bruce P. The carbon electrode in nonaqueous Li-O₂ cells. *J Am Chem Soc* 2012;135:494–500. <https://doi.org/10.1021/ja310258x>.
- [801] Jung J, Nam J, Klyukin K, Youn D, Kim I. Straightforward strategy toward a shape-deformable carbon-free cathode for flexible Li-air batteries in ambient air. *Nano Energy* 2021;83:105821. <https://doi.org/10.1016/j.nanoen.2021.105821>.
- [802] Jung J, Im H, Lee D, Yu S, Jang J, Yoon K, et al. Conducting nanopaper: A carbon-free cathode platform for Li-O₂ batteries. *ACS Energy Lett* 2017;2:673–80. <https://doi.org/10.1021/acseenergylett.7b00045>.
- [803] Liang Z, Zheng G, Liu C, Liu N, Li W, Yan K, et al. Polymer nanofiber-guided uniform lithium deposition for battery electrodes. *Nano Lett* 2015;15:2910–6. <https://doi.org/10.1021/nl5046318>.
- [804] Zhao C, Xiong S, Li H, Li Z, Qi C, Yang H, et al. A dendrite-free composite Li metal anode enabled by lithiophilic Co, N codoped porous carbon nanofibers. *J Power Sources* 2021;483. <https://doi.org/10.1016/j.jpowsour.2020.229188>.
- [805] Wang G, Xiong X, Lin Z, Zheng J, Fenghua Z, Li Y, et al. Uniform Li deposition regulated via three-dimensional polyvinyl alcohol nanofiber networks for effective Li metal anodes. *Nanoscale* 2018;10:10018–24. <https://doi.org/10.1039/c8nr01995a>.
- [806] Yang C, Yao Y, He S, Xie H, Hitz E, Hu L. Ultrafine silver nanoparticles for seeded lithium deposition toward stable lithium metal anode. *Adv Mater* 2017;29:1702714. <https://doi.org/10.1002/adma.201702714>.
- [807] Du L, Zhang B, Yang C, Cui L, Xu L. Leaf-inspired quasi-solid electrolyte enables uniform lithium deposition and suppressed lithium-electrolyte reactions for lithium metal batteries. *Energy Storage Mater* 2023;61:102914. <https://doi.org/10.1016/j.ensm.2023.102914>.
- [808] Lee J, Jun J, Jang J, Manthiram A. Sulfur-immobilized, activated porous carbon nanotube composite based cathodes for lithium-sulfur batteries. *Small* 2017;13:1602984. <https://doi.org/10.1002/smll.201602984>.
- [809] Fu A, Wang C, Pei F, Cui J, Fang X, Zheng N. Recent advances in hollow porous carbon materials for lithium-sulfur batteries. *Small* 2019;15:e1804786. <https://doi.org/10.1002/smll.201804786>.
- [810] Zhang S, Zheng M, Lin Z, Li N, Liu Y, Zhao B, et al. Activated carbon with ultrahigh specific surface area synthesized from natural plant material for lithium-sulfur batteries. *J Mater Chem A* 2014;2:15889–96. <https://doi.org/10.1039/c4ta03503h>.
- [811] Ruan R, Wang Y, Hu C, Gao A, Xu L. Electrode potential regulation of carbon fiber based on galvanic coupling and its application in electrochemical grafting. *ACS Appl Mater Interfaces* 2021;13:17013–21. <https://doi.org/10.1021/acsami.1c00292>.
- [812] Shih H, Chang J, Cho C, Li C. Nano-carbon-fiber-penetrated sulfur crystals as potential cathode active material for high-performance lithium-sulfur batteries. *Carbon* 2020;159:401–11. <https://doi.org/10.1016/j.carbon.2019.12.055>.
- [813] Deng N, Kang W, Ju J, Fan L, Zhuang X, Ma X, et al. Polyvinyl alcohol-derived carbon nanofibers/carbon nanotubes/sulfur electrode with honeycomb-like hierarchical porous structure for the stable-capacity lithium/sulfur batteries. *J Power Sources* 2017;346:1–12. <https://doi.org/10.1016/j.jpowsour.2017.02.022>.
- [814] Liang Y, Kang W, Zhong C, Deng N, Cheng B. Multifunctional LaF_3 doped pomegranate-like porous carbon nanofibers with high-speed transfer channel and strong polar interface for high stability lithium sulfur battery. *Chem Eng J* 2021;403:126449. <https://doi.org/10.1016/j.cej.2020.126449>.
- [815] Ji L, Rao M, Aloni S, Wang L, Cairns E, Zhang Y. Porous carbon nanofiber-sulfur composite electrodes for lithium/sulfur cells. *Energy Environ Sci* 2011;4:5053–9. <https://doi.org/10.1039/c1ee02256c>.
- [816] Zeng L, Pan F, Li W, Jiang Y, Zhong X, Yu Y. Free-standing porous carbon nanofibers-sulfur composite for flexible Li-S battery cathode. *Nanoscale* 2014;6:9579–87. <https://doi.org/10.1039/c4nr02498b>.
- [817] Li L, Zhang X, Liang B, Zhang Y, Zhang W. One-step hydrothermal synthesis of NiCo_2S_4 loaded on electrospun carbon nanofibers as an efficient counter electrode for dye-sensitized solar cells. *Sol Energy* 2020;202:358–64. <https://doi.org/10.1016/j.solener.2020.03.110>.
- [818] Liu P, Wang Y, Liu J. Biomass-derived porous carbon materials for advanced lithium sulfur batteries. *J Energy Chem* 2019;34:171–85. <https://doi.org/10.1016/j.jechem.2018.10.005>.
- [819] Yang H, Yang Y, Zhang X, Li Y, Qaisrani N, Zhang F, et al. Nitrogen-doped porous carbon networks with active Fe-N_x sites to enhance catalytic conversion of polysulfides in lithium-sulfur batteries. *ACS Appl Mater Interfaces* 2019;11:31860–8. <https://doi.org/10.1021/acsami.9b08962>.
- [820] Wu Y, Liu C, Moore T, Magel G, Garfinkel D, Camden J, et al. Exploring photothermal pathways via in-situ laser heating in the transmission electron microscope: Recrystallization, grain growth, phase separation, and dewetting in $\text{Ag}_{0.5}\text{Ni}_{0.5}$ thin films. *Microsc Microanal* 2018;24:647–56. <https://doi.org/10.1017/S1431927618015465>.
- [821] Zhang Y, Zhao Y, Yermukhambetova A, Bakenov Z, Chen P. Ternary sulfur/polyacrylonitrile/ $\text{Mg}_0.6\text{Ni}_0.4\text{O}$ composite cathodes for high performance lithium/sulfur batteries. *J Mater Chem A* 2013;1:295–301. <https://doi.org/10.1039/c2ta00105e>.
- [822] Gao X, Wang Y, Ma Z, Jiang W, Zou Y, Lu C. A ternary sulfonium composite $\text{Cu}_3\text{BiS}_3/\text{S}$ as cathode materials for lithium-sulfur batteries. *J Mater Sci* 2016;51:5139–45. <https://doi.org/10.1007/s10853-016-9816-8>.
- [823] Zhang C, Wu H, Yuan C, Guo Z, Lou X. Confining sulfur in double-shelled hollow carbon spheres for lithium-sulfur batteries. *Angew Chem Int Ed* 2013;44:9592–5. <https://doi.org/10.1002/chem.201302013>.
- [824] Zuo X, Zhen M, Wang C. Ni@ N-doped graphene nanosheets and CNTs hybrids modified separator as efficient polysulfide barrier for high-performance lithium sulfur batteries. *Nano Res* 2019;12:829–36. <https://doi.org/10.1007/s12274-019-2298-7>.
- [825] Yu M, Ma J, Song H, Wang A, Tian F, Wang Y, et al. Atomic layer deposited TiO_2 on a nitrogen-doped graphene/sulfur electrode for high performance lithium-sulfur batteries. *Energy Environ Sci* 2016;9:1495–503. <https://doi.org/10.1039/c5ee03902a>.
- [826] Zheng Y, Yi Y, Fan M, Liu H, Li X, Zhang R, et al. A high-entropy metal oxide as chemical anchor of polysulfide for lithium-sulfur batteries. *Energy Storage Mater* 2019;23:678–83. <https://doi.org/10.1016/j.ensm.2019.02.030>.
- [827] Jiang G, Xu F, Yang S, Wu J, Wei B, Wang H. Mesoporous, conductive molybdenum nitride as efficient sulfur hosts for high-performance lithium-sulfur batteries. *J Power Sources* 2018;395:77–84. <https://doi.org/10.1016/j.jpowsour.2018.05.061>.
- [828] Wei CB, Shao XD, Wang T, Gan RH, Liu H, Wang GX, et al. Advanced Lithium-sulfur batteries enabled by a flexible electrocatalytic membrane of TiO_2 and SiO_2 co-decorated necklace-like carbon nanofibers. *Appl Surf Sci* 2024;659:159923. <https://doi.org/10.1016/j.apsusc.2024.159923>.
- [829] Wang ZP, Liu CX, Wang YY, Zhang SQ, Huang M, Bai JB, et al. Nitrogen-doped carbon nanofiber loaded MOF-derived NiCo bimetallic nanoparticles accelerate the redox transformation of polysulfide for lithium-sulfur batteries. *J Electroanal Chem* 2024;959:118185. <https://doi.org/10.1016/j.jelechem.2024.118185>.
- [830] Xu J, Ao J, Juan YH, Xie YM, Zhou XHW. Beaded $\text{CoSe}_2\text{-C}$ nanofibers for high-performance lithium-sulfur batteries. *Nanomaterials* 2023;13:2492. <https://doi.org/10.3390/nano13172492>.
- [831] Wei CB, Shao XD, Lin F, Liu XY, Ding W, Wang GX, et al. A review of electrospun carbon-based nanofibers materials used in lithium-sulfur batteries. *Chem* 2024;e202401442. <https://doi.org/10.1002/chem.202401442>.

- [832] Zhang Y, Wu Z, Pan G, Liu S, Gao X. Microporous carbon polyhedrons encapsulated polyacrylonitrile nanofibers as sulfur immobilizer for lithium-sulfur battery. *ACS Appl Mater Interfaces* 2017;9:12436–44. <https://doi.org/10.1021/acsami.7b00389>.
- [833] Kalybekkyzy S, Mentbayeva A, Kahraman M, Zhang Y, Bakonov Z. Flexible S/D/PAN/KB nanofiber composite as binder-free cathodes for Li-S batteries. *J Electrochem Soc* 2019;166:A5396–53402. <https://doi.org/10.1149/2.0571903jes>.
- [834] Razzaq A, Yao Y, Shah R, Qi P, Miao L, Chen M, et al. High-performance lithium sulfur batteries enabled by a synergy between sulfur and carbon nanotubes. *Energy Storage Mater* 2019;16:194–202. <https://doi.org/10.1016/j.ensm.2018.05.006>.
- [835] Deng N, Liu Y, Li Q, Yan J, Lei W, Wang G, et al. Functional mechanism analysis and customized structure design of interlayers for high performance Li-S battery. *Energy Storage Mater* 2019;23:314–49. <https://doi.org/10.1016/j.ensm.2019.04.042>.
- [836] Junho L, Sang Yeop H, Byeong Il O, Young Gyu J, Nae Yeon J, Wook A, et al. Dual chemifunctional tin(IV) oxide/nanoperforated graphene interlayer as a polysulfide adsorbent for use in high-performance lithium-sulfur batteries. *Chem Eng J* 2024;480:147996. <https://doi.org/10.1016/j.cej.2023.147996>.
- [837] Gao LT, Wang XY, Cao Q, Jing B. Geometric design of carbon-based interlayer for advanced lithium-sulfur batteries. *J Energy Storage* 2024;96:112661. <https://doi.org/10.1016/j.est.2024.112661>.
- [838] Leng XL, Zeng J, Yang MD, Li CP, Prabhakar VSV, Chen JL, et al. Bimetallic Ni-Co MOF@PAN modified electrospun separator enhances high-performance lithium-sulfur batteries. *J Energy Chem* 2023;82:484–96. <https://doi.org/10.1016/j.jechem.2023.03.017>.
- [839] Elif Ceylan C, Osman O, Serap Hayat S, Rezan D. Freestanding oxidized poly(acrylonitrile-co-vinylpyrrolidone)/SnCl₂ nanofibers as interlayer for Lithium-Sulfur batteries. *J Power Sources* 2019;412:472–9. <https://doi.org/10.1016/j.jpowsour.2018.11.082>.
- [840] Wang Y, Chen HX, Yu FD, Wei SY, Song JH, He QF, et al. Oxygen self-doping pyrolyzed polyacrylic acid as sulfur host with physical/chemical adsorption dual function for lithium-sulfur batteries. *Chin Chem Lett* 2024;35:109001. <https://doi.org/10.1016/j.ccl.2023.109001>.
- [841] Li Y, Zhu J, Shi R, Dirican M, Zhu P, Yan C, et al. Ultrafine and polar ZnO-inlaid porous nitrogen-doped carbon nanofiber as efficient polysulfide adsorbent for high-performance lithium-sulfur batteries with long lifespan. *Chem Eng J* 2018;349:376–87. <https://doi.org/10.1016/j.cej.2018.05.074>.
- [842] Zhao T, Ye Y, Peng X, Divitini G, Kim H, Lao C, et al. Advanced lithium-sulfur batteries enabled by a bio-inspired polysulfide adsorptive brush. *Adv Funct Mater* 2016;26:8418–26. <https://doi.org/10.1002/adfm.201604069>.
- [843] Guo Y, Li J, Pitcheri R, Zhu J, Wen P, Qiu Y. Electrospun Ti₄O₇/C conductive nanofibers as interlayer for lithium-sulfur batteries with ultra long cycle life and high-rate capability. *Chem Eng J* 2019;355:390–8. <https://doi.org/10.1016/j.cej.2018.08.143>.
- [844] Zhuang R, Yao S, Shen X, Li T. A freestanding MoO₂-decorated carbon nanofibers interlayer for rechargeable lithium sulfur battery. *Int J Energy Res* 2019;43:1111–20. <https://doi.org/10.1002/er.4334>.
- [845] Huang J, Zhang B, Xu Z, Abouali S, Akbari Garakani M, Huang J, et al. Novel interlayer made from Fe₃C/carbon nanofiber webs for high performance lithium-sulfur batteries. *J Power Sources* 2015;285:43–50. <https://doi.org/10.1016/j.jpowsour.2015.02.140>.
- [846] Zhu J, Pitcheri R, Kang T, Guo Y, Li J, Qiu Y. Electrospun carbon nanofibers decorated with MnO nanoparticles as a sulfur-adsorbent for lithium-sulfur batteries. *Ceram Int* 2018;44:16837–43. <https://doi.org/10.1016/j.ceramint.2018.06.119>.
- [847] Peng Y, Zhang Y, Wang Y, Shen X, Wang F, Li H, et al. Directly coating a multifunctional interlayer on the cathode via electrospinning for advanced lithium-sulfur batteries. *ACS Appl Mater Interfaces* 2017;9:29804–11. <https://doi.org/10.1021/acsami.7b08804>.
- [848] Gao T, Le T, Yang Y, Yu Z, Huang Z, Kang F. Effects of electrospun carbon nanofibers' interlayers on high-performance lithium-sulfur batteries. *Materials* 2017;10:376. <https://doi.org/10.3390/ma10040376>.
- [849] Xiang J, Zhao Y, Yuan L, Chen C, Shen Y, Hu F, et al. A strategy of selective and dendrite-free lithium deposition for lithium batteries. *Nano Energy* 2017;42:262–8. <https://doi.org/10.1016/j.nanoen.2017.10.065>.
- [850] Liu M, Deng N, Ju J, Wang L, Wang G, Ma Y, et al. Silver nanoparticle-doped 3D porous carbon nanofibers as separator coating for stable lithium metal anodes. *ACS Appl Mater Interfaces* 2019;11:17843–52. <https://doi.org/10.1021/acsami.9b04122>.
- [851] Zhao H, Lei Y. 3D nanostructures for the next generation of high-performance nanodevices for electrochemical energy conversion and storage. *Adv Energy Mater* 2020;10. pp. 2001460. <https://doi.org/10.1002/aenm.202001460>.
- [852] Kang S, Kim S, Lee H, Mhin S, Ryu J, Kim Y, et al. High-power energy harvesting and imperceptible pulse sensing through peapod-inspired hierarchically designed piezoelectric nanofibers. *Nano Energy* 2022;100:107386. <https://doi.org/10.1016/j.nanoen.2022.107386>.
- [853] Xu S, Qin Y, Xu C, Wei Y, Yang R, Wang Z. Self-powered nanowire devices. *Nat Nanotechnol* 2010;5:366–873. <https://doi.org/10.1038/nnano.2010.46>.
- [854] Zhu G, Yang R, Wang S, Wang Z. Flexible high-output nanogenerator based on lateral ZnO nanowire array. *Nano Lett* 2010;10:3151–5. <https://doi.org/10.1021/nl101973h>.
- [855] Hu Y, Lin L, Zhang Y, Wang Z. Replacing a battery by a nanogenerator with 20 V output. *Adv Mater* 2012;24:110–4. <https://doi.org/10.1002/adma.201103727>.
- [856] Xu S, Hansen B, Wang Z. Piezoelectric-nanowire-enabled power source for driving wireless microelectronics. *Nat Commun* 2010;1:93. <https://doi.org/10.1038/ncomms1098>.
- [857] Chang J, Lin M. Piezoelectric nanofibers for energy scavenging applications. *Nano Energy* 2012;356–71. <https://doi.org/10.1016/j.nanoen.2012.02.003>.
- [858] Yu S, Tai Y, Milam-Guerrero J, Nam J, Myung N. Electrospun organic piezoelectric nanofibers and their energy and bio applications. *Nano Energy* 2022;97:107174. <https://doi.org/10.1016/j.nanoen.2022.107174>.
- [859] Chang C, Tran V, Wang J, Fuh Y, Lin L. Direct-write piezoelectric polymeric nanogenerator with high energy conversion efficiency. *Nano Lett* 2010;10:726–31. <https://doi.org/10.1021/nl9040719>.
- [860] Yuan M, Cheng L, Xu Q, Wu W, Bai S, Gu L, et al. Biocompatible nanogenerators through high piezoelectric coefficient 0.5Ba(Zr_{0.2}Ti_{0.8})O₃-0.5(Ba_{0.7}Ca_{0.3})TiO₃ nanowires for in-vivo applications. *Adv Mater* 2014;26:7432–7. <https://doi.org/10.1002/adma.201402868>.
- [861] Cui N, Wu W, Zhao Y, Bai S, Meng L, Qin Y, et al. Magnetic force driven nanogenerators as a noncontact energy harvester and sensor. *Nano Lett* 2012;12:3701–5. <https://doi.org/10.1021/nl301490q>.
- [862] Kang H, Chang J, Koh K, Lin L, Cho Y. High quality Mn-Doped (Na,K)NbO₃ nanofibers for flexible piezoelectric nanogenerators. *ACS Appl Mater Interfaces* 2014;6:10576–82. <https://doi.org/10.1021/am502234q>.
- [863] Liu B, Lu B, Chen X, Wu X, Shi S, Xu L, et al. A high-performance flexible piezoelectric energy harvester based on lead-free (Na_{0.5}Bi_{0.5})TiO₃-BaTiO₃ piezoelectric nanofibers. *J Mater Chem A* 2017;5:23634–40. <https://doi.org/10.1039/c7ta07570g>.
- [864] Zhao Y, Fan H, Ren X, Long C, Liu G, Liu Z. Lead-free Bi_{5-x}La_xTi₃FeO₁₅ (x = 0, 1) nanofibers toward wool keratin-based biocompatible piezoelectric nanogenerators. *J Mater Chem C* 2016;4:7324–31. <https://doi.org/10.1039/c6tc01828a>.
- [865] Guan X, Xu B, Gong J. Hierarchically architected polydopamine modified BaTiO₃@P (VDF-TrFE) nanocomposite fiber mats for flexible piezoelectric nanogenerators and self-powered sensors. *Nano Energy* 2020;70:104516. <https://doi.org/10.1016/j.nanoen.2020.104516>.
- [866] An S, Jo H, Li G, Samuel E, Yoon S, Yarin A. Sustainable nanotextured wave energy harvester based on ferroelectric fatigue-free and flexoelectricity-enhanced piezoelectric p(VDF-TrFE) nanofibers with BaSrTiO₃ nanoparticles. *Adv Funct Mater* 2020;30:2001150. <https://doi.org/10.1002/adfm.202001150>.
- [867] Wang Z, Chen J, Lin L. Progress in triboelectric nanogenerators as a new energy technology and self-powered sensors. *Energy Environ Sci* 2015;8:2250–82. <https://doi.org/10.1039/c5ee01532d>.
- [868] Gajula P, Yoon JU, Woo I, Oh S-J, Bae JW. Triboelectric touch sensor array system for energy generation and self-powered human-machine interfaces based on chemically functionalized, electrospun rGO/nylon-12 and micro-patterned Ecoflex/MoS₂ films. *Nano Energy* 2024;121:109278. <https://doi.org/10.1016/j.nanoen.2024.109278>.
- [869] Chen B, Yang Y, Wang Z. Scavenging wind energy by triboelectric nanogenerators. *Adv Energy Mater* 2018;8:1702649. <https://doi.org/10.1002/aenm.201702649>.
- [870] Dong K, Peng X, Wang Z. Fiber/fabric-based piezoelectric and triboelectric nanogenerators for flexible/stretchable and wearable electronics and artificial intelligence. *Adv Mater* 2019;32:e1902549. <https://doi.org/10.1002/adma.201902549>.
- [871] Yu A, Zhu Y, Wang W, Zhai J. Progress in triboelectric materials: Toward high performance and widespread applications. *Adv Funct Mater* 2019;29:1900098. <https://doi.org/10.1002/adfm.201900098>.

- [872] Niu Z, Cheng W, Cao M, Wang D, Wang Q, Han J, et al. Recent advances in cellulose-based flexible triboelectric nanogenerators. *Nano Energy* 2021;87:106175. <https://doi.org/10.1016/j.nanoen.2021.106175>.
- [873] Zheng YB, Cheng L, Yuan MM, Wang Z, Zhang L, Qin Y, et al. An electrospun nanowire-based triboelectric nanogenerator and its application in a fully self-powered UV detector. *Nanoscale* 2014;6:7842–6. <https://doi.org/10.1039/c4nr01934b>.
- [874] Im JS, Park IK. Mechanically robust magnetic Fe₃O₄ nanoparticle/polyvinylidene fluoride composite nanofiber and its application in a triboelectric nanogenerator. *ACS Appl Mater Interfaces* 2018;10:25660–5. <https://doi.org/10.1021/acsami.8b07621>.
- [875] Pu X, Zha JW, Zhao CL, Gong SB, Gao JF, Li RKY. Flexible PVDF/nylon-11 electrospun fibrous membranes with aligned ZnO nanowires as potential triboelectric nanogenerators. *Chem Eng J* 2020;398:125526. <https://doi.org/10.1016/j.cej.2020.125526>.
- [876] Lan LY, Xiong JQ, Gao DC, Li Y, Chen J, Lv J, et al. Breathable nanogenerators for an on-plant self-powered sustainable agriculture system. *ACS Nano* 2021;15:5307–15. <https://doi.org/10.1021/acsnano.0c10817>.
- [877] Jiang CM, Wu C, Li XJ, Yao Y, Lan LY, Zhao FN, et al. All-electrospun flexible triboelectric nanogenerator based on metallic mxene nanosheets. *Nano Energy* 2019;59:268–76. <https://doi.org/10.1016/j.nanoen.2019.02.052>.
- [878] Lin MF, Xiong JQ, Wang JX, Parida K, Lee PS. Core-shell nanofiber mats for tactile pressure sensor and nanogenerator applications. *Nano Energy* 2018;44:248–55. <https://doi.org/10.1016/j.nanoen.2017.12.004>.
- [879] Yu B, Yu H, Huang T, Wang HZ, Zhu MF. A biomimetic nanofiber-based triboelectric nanogenerator with an ultrahigh transfer charge density. *Nano Energy* 2018;48:464–70. <https://doi.org/10.1016/j.nanoen.2018.03.064>.
- [880] Zhang X, Lv S, Lu X, Yu H, Huang T, Zhang Q, et al. Synergistic enhancement of coaxial nanofiber-based triboelectric nanogenerator through dielectric and dispersity modulation. *Nano Energy* 2020;75:104894. <https://doi.org/10.1016/j.nanoen.2020.104894>.
- [881] Li Y, Xiong J, Lv J, Chen J, Gao D, Zhang X, et al. Mechanically interlocked stretchable nanofibers for multifunctional wearable triboelectric nanogenerator. *Nano Energy* 2020;78:105358. <https://doi.org/10.1016/j.nanoen.2020.105358>.
- [882] Su M, Kim B. Silk fibroin-carbon nanotube composites based fiber substrated wearable triboelectric nanogenerator. *ACS Appl Nano Mater* 2020;3:9759–70. <https://doi.org/10.1021/acsnano.0c01854>.
- [883] Jiang Y, Dong K, Li X, An J, Wu D, Peng X, et al. Stretchable, washable, and ultrathin triboelectric nanogenerators as skin-like highly sensitive self-powered haptic sensors. *Adv Funct Mater* 2020;31:200558. <https://doi.org/10.1002/adfm.202005584>.
- [884] Li C, Yin Y, Wang B, Zhou T, Wang J, Luo J, et al. Self-powered electrospinning system driven by a triboelectric nanogenerator. *ACS Nano* 2017;11:10439–45. <https://doi.org/10.1021/acsnano.7b05626>.
- [885] Han Y, Zou J, Li Z, Wang W, Jie Y, Ma J, et al. Si@void@C nanofibers fabricated using a self-powered electrospinning system for lithium-ion batteries. *ACS Nano* 2018;12:4835–43. <https://doi.org/10.1021/acsnano.8b01558>.
- [886] Lei R, Shi Y, Ding Y, Nie J, Li S, Wang F, et al. Sustainable high-voltage source based on triboelectric nanogenerator with a charge accumulation strategy. *Energy Environ Sci* 2020;13:2178–90. <https://doi.org/10.1039/d0ee01236j>.
- [887] Shi F, Chen C, Xu Z-L. Recent advances on electrospun nanofiber materials for post-lithium ion batteries. *Adv Fiber Mater* 2021;3:275–301. <https://doi.org/10.1007/s42765-021-00070-2>.
- [888] Sarkodie B, Amesimeku J, Frimpong C, Howard EK, Feng Q, Xu Z. Photocatalytic degradation of dyes by novel electrospun nanofibers: A review. *Chemosphere* 2023;313:137654. <https://doi.org/10.1016/j.chemosphere.2022.137654>.
- [889] Wang TT, Chen Z, Gong WB, Xu F, Song X, He X, et al. Electrospun carbon nanofibers and their applications in several areas. *ACS Omega* 2023;8:22316–30. <https://doi.org/10.1021/acsomega.3c01114>.
- [890] Dong H, Fey E, Gandelman A, Jones WE. Synthesis and assembly of metal nanoparticles on electrospun poly(4-vinylpyridine) fibers and poly(4-vinylpyridine) composite fibers. *Chem Mater* 2006;18:2008–11. <https://doi.org/10.1021/cm052436p>.
- [891] Koga H, Tokunaga E, Hidaka M, Umemura Y, Saito T, Isogai A, et al. Topochemical synthesis and catalysis of metal nanoparticles exposed on crystalline cellulose nanofibers. *Chem Commun* 2010;46:8567–9. <https://doi.org/10.1039/c0cc02754e>.
- [892] Mandal S, Roy D, Chaudhari RV, Sastry M. Pt and Pd nanoparticles immobilized on amine-functionalized zeolite: Excellent catalysts for hydrogenation and heck reactions. *Chem Mater* 2004;16:3714–24. <https://doi.org/10.1021/cm0352504>.
- [893] Afsar J, Zolfigol MA, Khazaei A. [Fe₃O₄@SiO₂(CH₂)₃im]C₆F₅O as a new hydrophilic and task-specific nanomagnetic catalyst: Application for synthesis of β -azido alcohols and thiuranes under mild and green conditions. *ChemistrySelect* 2018;3:11134–40. <https://doi.org/10.1002/slct.201802118>.
- [894] K. Paskalis Sahaya Murpin, A. Subramanian, K. Hyoun-il, R. Deepthi Koolath, P. Vinoth Kumar, P. Umappa, et al. An efficient and durable electrocatalyst based on strongly coupled Pt nanoparticles on CeO₂ microspheres for co-resilient methanol oxidation. *J Phys Chem C*, 126 (2022), pp. 18670-18682, 10.1021/acsc.jpcc.2c05069.
- [895] Harikrishnan V, Aarthi K, Abinaya M, Aishwarya D, Sakthivel G. Metal nanoparticle ornatd mesoporous silica: A potential nano-interface for uric acid detection. *Microporous Mesoporous Mater* 2021;324:111313. <https://doi.org/10.1016/j.micromeso.2021.111313>.
- [896] Leus K, Krishnaraj C, Verhoeven L, Cremers V, Dendooven J, Ramachandran RK, et al. Catalytic carpets: Pt@MIL-101@electrospun PCL, a surprisingly active and robust hydrogenation catalyst. *J Catal* 2018;360:81–8. <https://doi.org/10.1016/j.jcat.2018.01.018>.
- [897] Huang YP, Ma H, Wang SG, Shen MW, Guo R, Cao XY, et al. Efficient catalytic reduction of hexavalent chromium using palladium nanoparticle-immobilized electrospun polymer nanofibers. *ACS Appl Mater Interfaces* 2012;4:3054–61. <https://doi.org/10.1021/am300417s>.
- [898] Khalily MA, Yurderi M, Haider A, Bulut A, Patil B, Zahmakiran M, et al. Atomic layer deposition of ruthenium nanoparticles on electrospun carbon nanofibers: A highly efficient nanocatalyst for the hydrolytic dehydrogenation of methylamine borane. *ACS Appl Mater Interfaces* 2018;10:26162–9. <https://doi.org/10.1021/acsami.8b04822>.
- [899] Zhu Y, Bai J, Li C, Wang J. Controllable preparation of one-dimensional hybrid catalytic materials of nickel nanoparticles/porous carbon fibers and study of their performance as catalyst for heck reaction. *J Porous Mater* 2016;24:21–7. <https://doi.org/10.1007/s10934-016-0232-x>.
- [900] Kang S, Hwang J. Fabrication of hollow activated carbon nanofibers (HACNFs) containing manganese oxide catalyst for toluene removal via two-step process of electrospinning and thermal treatment. *Chem Eng J* 2020;379:122315. <https://doi.org/10.1016/j.cej.2019.122315>.
- [901] Nasir MS, Yang G, Ayub I, Wang S, Yan W. Tin diselenide a stable co-catalyst coupled with branched TiO₂ fiber and g-C₃N₄ quantum dots for photocatalytic hydrogen evolution. *Appl Catal B Environ* 2020;270:118900. <https://doi.org/10.1016/j.apcatb.2020.118900>.
- [902] Li M, Zhu Y, Wang H, Wang C, Pinna N, Lu X. Ni strongly coupled with Mo₂C encapsulated in nitrogen-doped carbon nanofibers as robust bifunctional catalyst for overall water splitting. *Adv Energy Mater* 2019;9:1803185. <https://doi.org/10.1002/aenm.201803185>.
- [903] Song N, Zhong M, Xu J, Wang C, Lu X. Single-atom iron confined within polypyrrole-derived carbon nanotubes with exceptional peroxidase-like activity for total antioxidant capacity. *Sens Actuators B: Chem* 2022;351:130969. <https://doi.org/10.1016/j.snb.2021.130969>.
- [904] Sanchez JL, Laberty-Robert C. A novel microbial fuel cell electrode design: Prototyping a self-standing one-step bacteria-encapsulating bioanode with electrospinning. *J Mater Chem B* 2021;9:4309–18. <https://doi.org/10.1039/d1tb00680k>.
- [905] Wang T, Tao X, Wu D, Lu X, Yu Q, Liu S, et al. High activity and stability of PdO_x anchored in porous NiO nanofibers for catalyzing Suzuki coupling reactions. *J Phys Chem C* 2020;124:22539–49. <https://doi.org/10.1021/acs.jpcc.0c06979>.
- [906] Liu B, Xu T, Li C, Bai J. Activating Pd nanoparticles via the Mott-Schottky effect in Ni doped CeO₂ nanotubes for enhanced catalytic Suzuki reaction. *Mol Catal* 2022;528:112452. <https://doi.org/10.1016/j.mcat.2022.112452>.
- [907] He C-H, Gong J. The preparation of PVA-Pt/TiO₂ composite nanofiber aggregate and the photocatalytic degradation of solid-phase polyvinyl alcohol. *Polym Degrad Stab* 2003;81:117–24. [https://doi.org/10.1016/s0141-3910\(03\)00080-6](https://doi.org/10.1016/s0141-3910(03)00080-6).
- [908] Li B, Zhang B, Nie S, Shao L, Hu L. Optimization of plasmon-induced photocatalysis in electrospun Au/CeO₂ hybrid nanofibers for selective oxidation of benzyl alcohol. *J Catal* 2017;348:256–64. <https://doi.org/10.1016/j.jcat.2016.12.025>.
- [909] Gao H, Zhang P, Zhao J, Zhang Y, Hu J, Shao G. Plasmon enhancement on photocatalytic hydrogen production over the Z-scheme photosynthetic heterojunction system. *Appl Catal B Environ* 2017;210:297–305. <https://doi.org/10.1016/j.apcatb.2017.03.050>.

- [910] Sonawane AV, Murthy ZVP. Synthesis, characterization, and application of ZIF-8/Ag₃PO₄, MoS₂/Ag₃PO₄, and h-BN/Ag₃PO₄ based photocatalytic nanocomposite polyvinylidene fluoride mixed matrix membranes for effective removal of drimaren orange P2R. *J Membr Sci* 2022;641:119939. <https://doi.org/10.1016/j.memsci.2021.119939>.
- [911] Zhang L, Zhang Q, Xie H, Guo J, Lyu H, Li Y, et al. Electrospun titania nanofibers segregated by graphene oxide for improved visible light photocatalysis. *Appl Catal B Environ* 2017;201:470–8. <https://doi.org/10.1016/j.apcatb.2016.08.056>.
- [912] Zheng SY, Chen HS, Tong X, Wang ZW, Crittenden JC, Huang MH. Integration of a photo-Fenton reaction and a membrane filtration using CS/PAN@FeOOH/g-C₃N₄ Electrospun nanofibers: Synthesis, characterization, self-cleaning performance and mechanism. *Appl Catal B Environ* 2021;281:119519. <https://doi.org/10.1016/j.apcatb.2020.119519>.
- [913] Hua C, Dong X, Zheng N, Zhang X, Xue M. In-situ fabrication of self-assembled BiOBr_x1–x coated on carbon nanofibers for efficient solar light-driven photocatalytic nitrogen fixation. *Sustain Energy Fuels* 2020;4:6196–202. <https://doi.org/10.1039/d0se01274b>.
- [914] Liu H, Mei H, Miao N, Pan L, Jin Z, Zhu G, et al. Synergistic photocatalytic NO removal of oxygen vacancies and metallic bismuth on Bi12TiO₂₀ nanofibers under visible light irradiation. *Chem Eng J* 2021;414:128748. <https://doi.org/10.1016/j.cej.2021.128748>.
- [915] Wang P, Zhou Q, Xia Y, Zhan S, Li Y. Understanding the charge separation and transfer in mesoporous carbonate-doped phase-junction TiO₂ nanotubes for photocatalytic hydrogen production. *Appl Catal B Environ* 2018;225:433–44. <https://doi.org/10.1016/j.apcatb.2017.11.069>.
- [916] Xu F, Zhang L, Cheng B, Jiaguo JY. Engineering. Direct Z-Scheme TiO₂/NiS core-shell hybrid nanofibers with enhanced photocatalytic H₂-production activity. *ACS Sustainable Chem Eng* 2018;6:12291–8. <https://doi.org/10.1021/acssuschemeng.8b02710>.
- [917] Qian M, Yang F, Li N, Gao J, Chen X, Xu T, et al. A novel biodegradable porous graphitic carbon nitride/poly(lactic acid) fiber photocatalyst for efficient elimination of carbamazepine under solar irradiation. *Chem Eng J* 2021;414:128845. <https://doi.org/10.1016/j.cej.2021.128845>.
- [918] Lv C, Sun J, Chen G, Zhou Y, Li D, Wang Z, et al. Organic salt induced electrospinning gradient effect: Achievement of BiVO₄ nanotubes with promoted photocatalytic performance. *Appl Catal B Environ* 2017;208:14–21. <https://doi.org/10.1016/j.apcatb.2017.02.058>.
- [919] Li GQ, Liang HO, Yu HY, Xu T, Bai J. Interstitial carbon doped of setaria viridis-like ZnIn₂S₄ hollow tubes for efficient the performance of photocatalytic hydrogen production. *Int J Hydrogen Energy* 2021;46:29951–9. <https://doi.org/10.1016/j.ijhydene.2021.06.150>.
- [920] Gao Y, Yan N, Jiang C, Xu C, Yu S, Liang P, et al. Filtration-enhanced highly efficient photocatalytic degradation with a novel electrospun rGO@TiO₂ nanofibrous membrane: Implication for improving photocatalytic efficiency. *Appl Catal B Environ* 2020;268:118737. <https://doi.org/10.1016/j.apcatb.2020.118737>.
- [921] Tao R, Li XH, Li XW, Shao CL, Liu YC. TiO₂/SrTiO₃/g-C₃N₄ ternary heterojunction nanofibers: gradient energy band, cascade charge transfer, enhanced photocatalytic hydrogen evolution, and nitrogen fixation. *Nanoscale* 2020;12:8320–9. <https://doi.org/10.1039/D0NR00219D>.
- [922] Zhang Z, Wu X, Kou Z, Song N, Nie G, Wang C, et al. Rational design of electrospun nanofiber-typed electrocatalysts for water splitting: A review. *Chem Eng J* 2022;428:131133. <https://doi.org/10.1016/j.cej.2021.131133>.
- [923] Nie G, Zhang Z, Wang T, Wang C, Kou Z. Electrospun one-dimensional electrocatalysts for oxygen reduction reaction: Insights into structure-activity relationship. *ACS Appl Mater Interfaces* 2021;13:37961–78. <https://doi.org/10.1021/acsaami.1c08798>.
- [924] Dou S, Wang X, Wang S. Rational design of transition metal-based materials for highly efficient electrocatalysis. *Small Methods* 2018;3:1800211. <https://doi.org/10.1002/smt.201800211>.
- [925] Guo S, Li Y, Tang S, Zhang Y, Li X, Sobrido AJ, et al. Monitoring hydrogen evolution reaction intermediates of transition metal dichalcogenides via operando Raman spectroscopy. *Adv Funct Mater* 2020;30:2003035. <https://doi.org/10.1002/adfm.202003035>.
- [926] Zhao Y, Zhang J, Li K, Ao Z, Wang C, Liu H, et al. Electrospun cobalt embedded porous nitrogen doped carbon nanofibers as an efficient catalyst for water splitting. *J Mater Chem A* 2016;4:12818–24. <https://doi.org/10.1039/c6ta04244a>.
- [927] Chen JW, Wang J, Chen JD, Wang LN. A bifunctional electrocatalyst of PtNi nanoparticles immobilized on three-dimensional carbon nanofiber mats for efficient and stable water splitting in both acid and basic media. *J Mater Sci* 2017;52:13064–77. <https://doi.org/10.1007/s10853-017-1410-1>.
- [928] Li M, Wang H, Zhu W, Li W, Wang C, Lu X. RuNi nanoparticles embedded in N-doped carbon nanofibers as a robust bifunctional catalyst for efficient overall water splitting. *Adv Sci* 2020;7:1901833. <https://doi.org/10.1002/advs.201901833>.
- [929] Zhu Y, Song L, Song N, Li M, Wang C, Lu X. Bifunctional and efficient CoS₂-C@MoS₂ core-shell nanofiber electrocatalyst for water splitting. *ACS Sustainable Chem Eng* 2019;7:2899–905. <https://doi.org/10.1021/acssuschemeng.8b05462>.
- [930] Ji D, Peng S, Fan L, Li L, Qin X, Ramakrishna S. Thin MoS₂ nanosheets grafted MOFs-derived porous Co–N–C flakes grown on electrospun carbon nanofibers as self-supported bifunctional catalysts for overall water splitting. *J Mater Chem A* 2017;5:23898–908. <https://doi.org/10.1039/c7ta08166a>.
- [931] Chen J, Chen J, Yu D, Zhang M, Zhu H, Du M. Carbon nanofiber-supported PdNi alloy nanoparticles as highly efficient bifunctional catalysts for hydrogen and oxygen evolution reactions. *Electrochim Acta* 2017;246:17–26. <https://doi.org/10.1016/j.electacta.2017.06.047>.
- [932] Wang F-F, Xu L, Wang P, Zhang Y. W_xCo_yS core-shell grown on hollow-porous carbon fiber (HCF) as synergistic electrocatalysts for efficient water splitting. *Electrochim Acta* 2019;306:437–45. <https://doi.org/10.1016/j.electacta.2019.03.091>.
- [933] Nitopi S, Bertheussen E, Scott SB, Liu X, Engstfeld AK, Horch S, et al. Progress and perspectives of electrochemical CO₂ reduction on copper in aqueous electrolyte. *Chem Rev* 2019;119:7610–72. <https://doi.org/10.1021/acs.chemrev.8b00705>.
- [934] Lee J-C, Kim J-Y, Joo W-H, Hong D, Oh S-H, Kim B, et al. Thermodynamically driven self-formation of copper-embedded nitrogen-doped carbon nanofiber catalysts for a cascade electroreduction of carbon dioxide to ethylene. *J Mater Chem A* 2020;8:11632–41. <https://doi.org/10.1039/d0ta03322g>.
- [935] Liu S, Cao Y, Liu H, Wang H, Zhang B, Zhang Y, et al. Efficient electrochemical reduction of CO₂ promoted by the electrospun Cu_{1.96}S/Cu tandem catalyst. *Nanoscale* 2021;13:16986–94. <https://doi.org/10.1039/d1nr04802c>.
- [936] Fan L, Xia Z, Xu M, Lu Y, Li Z. 1D SnO₂ with wire-in-tube architectures for highly selective electrochemical reduction of CO₂ to C1 products. *Adv Funct Mater* 2018;28:1706289. <https://doi.org/10.1002/adfm.201706289>.
- [937] Xia J, Guo H, Cheng M, Chen C, Wang M, Xiang Y, et al. Electrospun zirconia nanofibers for enhancing the electrochemical synthesis of ammonia by artificial nitrogen fixation. *J Mater Chem A* 2021;9:2145–51. <https://doi.org/10.1039/d0ta08089f>.
- [938] Wang Z, Shen J, Fu W, Liao J, Dong J, Zhuang P, et al. Controlled oxygen vacancy engineering on In₂O_{3-x}/CeO_(2-y) nanotubes for highly selective and efficient electrocatalytic nitrogen reduction. *Inorg Chem Front* 2020;7:3609–19. <https://doi.org/10.1039/D0QI00749H>.
- [939] Lv C, Yan C, Chen G, Ding Y, Sun J, Zhou Y, et al. An amorphous noble-metal-free electrocatalyst that enables nitrogen fixation under ambient conditions. *Angew Chem Int Ed* 2018;57:6073–6. <https://doi.org/10.1002/anie.201801538>.
- [940] Wang Y, Ma Z, Liu K, Yang X, Wang J, Wang X. Rigid anchoring of highly crystallized and uniformly dispersed Pd nanocrystals on carbon fibers for ambient electrocatalytic reduction of nitrogen to ammonia. *Dalton Trans* 2021;50:6975–81. <https://doi.org/10.1039/d1dt00682g>.
- [941] Yu G, Guo H, Liu S, Chen L, Alshehri AA, Alzahrani KA, et al. Cr₃C₂ nanoparticle-embedded carbon nanofiber for artificial synthesis of NH₃ through N₂ fixation under ambient conditions. *ACS Appl Mater Interfaces* 2019;11:35764–9. <https://doi.org/10.1021/acsaami.9b12675>.
- [942] Huang Y, Ren J, Qu X. Nanozymes: Classification, catalytic mechanisms, activity regulation, and applications. *Chem Rev* 2019;119:4357–412. <https://doi.org/10.1021/acs.chemrev.8b00672>.
- [943] Song W, Zhao B, Wang C, Ozaki Y, Lu XF. Functional nanomaterials with unique enzyme-like characteristics for sensing applications. *J Mater Chem B* 2019;7:850–75. <https://doi.org/10.1039/c8tb02878h>.
- [944] Song W, Zhao B, Wang C, Lu X. Electrospun nanofibrous materials: A versatile platform for enzyme mimicking and their sensing applications. *Compos Commun* 2019;12:1–13. <https://doi.org/10.1016/j.coco.2018.12.005>.
- [945] Chen S, Chi M, Zhu Y, Gao M, Wang C, Lu X. A facile synthesis of superparamagnetic Fe₃O₄ nanofibers with superior peroxidase-like catalytic activity for sensitive colorimetric detection of l-cysteine. *Appl Surf Sci* 2018;440:237–44. <https://doi.org/10.1016/j.apsusc.2018.01.152>.
- [946] Song L, Zhu Y, Yang Z, Wang C, Lu X. Oxidase-mimicking activity of perovskite LaMnO_{3-δ} nanofibers and their application for colorimetric sensing. *J Mater Chem B* 2018;6:5931–9. <https://doi.org/10.1039/c8tb01706a>.
- [947] Gao M, Lu X, Chi M, Chen S, Wang C. Fabrication of oxidase-like hollow MnCo₂O₄ nanofibers and their sensitive colorimetric detection of sulfite and L-cysteine. *Inorg Chem Front* 2017;4:1862–9. <https://doi.org/10.1039/c7qi00458c>.

- [948] Zhu WD, Li M, Chen S, Wang C, Lu X. Interfacial engineering regulating the peroxidase-like property of ternary composite nanofibers and their sensing applications. *Appl Surf Sci* 2019;491:138–46. <https://doi.org/10.1016/j.apsusc.2019.06.163>.
- [949] Song N, Zhang Y, Ren S, Wang C, Lu X. Rational design of conducting polymer-derived tubular carbon nanoreactors for enhanced enzyme-like catalysis and total antioxidant capacity bioassay application. *Anal Chem* 2022;94:11695–702. <https://doi.org/10.1021/acs.analchem.2c02511>.
- [950] Song N, Chen S, Tian D, Li Y, Wang C, Lu X. Cu-doped polypyrrole nanotubes with promoted efficiency for peroxidase mimicking and electrochemical biosensing. *Mater Today Chem* 2020;18:100374. <https://doi.org/10.1016/j.mtchem.2020.100374>.
- [951] Song N, Wang C, Lu X. Rational design of hierarchical CoO/NiO nanosheets on conductive polypyrrole nanotubes for peroxidase mimicking and sensing application. *ACS Sustainable Chem Eng* 2020;8:11069–78. <https://doi.org/10.1021/acssuschemeng.0c00249>.
- [952] Wu S, Li H, Zhou X, Liang P, Zhang X, Jiang Y, et al. A novel pilot-scale stacked microbial fuel cell for efficient electricity generation and wastewater treatment. *Water Res* 2016;98:396–403. <https://doi.org/10.1016/j.watres.2016.04.043>.
- [953] Zuo K, Wang K, DuChanois RM, Fang Q, Deemer EM, Huang X, et al. Selective membranes in water and wastewater treatment: Role of advanced materials. *Mater Today* 2021;50:516–32. <https://doi.org/10.1016/j.mattod.2021.06.013>.
- [954] Slate AJ, Whitehead KA, Brownson DAC, Banks CE. Microbial fuel cells: An overview of current technology. *Renew Sust Energ Rev* 2019;101:60–81. <https://doi.org/10.1016/j.rser.2018.09.044>.
- [955] Santoro C, Arbizzani C, Erable B, Ieropoulos I. Microbial fuel cells: From fundamentals to applications. A review *J Power Sources* 2017;356:225–44. <https://doi.org/10.1016/j.jpowsour.2017.03.109>.
- [956] Zhang Q, Liu L. A microbial fuel cell system with manganese dioxide/titanium dioxide/graphitic carbon nitride coated granular activated carbon cathode successfully treated organic acids industrial wastewater with residual nitric acid. *Bioresour Technol* 2020;304:122992. <https://doi.org/10.1016/j.biortech.2020.122992>.
- [957] Dong Z, Zhang Q, Chen B-Y, Hong J. Oxidation of bisphenol A by persulfate via Fe_3O_4 - α - MnO_2 nanoflower-like catalyst: Mechanism and efficiency. *Chem Eng J* 2019;357:337–47. <https://doi.org/10.1016/j.cej.2018.09.179>.
- [958] Xu H, Quan X, Xiao Z, Chen L. Effect of anodes decoration with metal and metal oxides nanoparticles on pharmaceutically active compounds removal and power generation in microbial fuel cells. *Chem Eng J* 2018;335:539–47. <https://doi.org/10.1016/j.cej.2017.10.159>.
- [959] Chen SL, Hou HQ, Harnisch F, Patil SA, Carmona-Martinez AA, Agarwal S, et al. Electrospun and solution blown three-dimensional carbon fiber nonwovens for application as electrodes in microbial fuel cells. *Energy Environ Sci* 2011;4:1417–21. <https://doi.org/10.1039/c0ee00446d>.
- [960] Chen SL, He GH, Carmona-Martinez AA, Agarwal S, Greiner A, Hou HQ, et al. Electrospun carbon fiber mat with layered architecture for anode in microbial fuel cells. *Electrochem Commun* 2011;13:1026–9. <https://doi.org/10.1016/j.elecom.2011.06.009>.
- [961] Massaglia G, Margaria V, Fiorentin MR, Pasha K, Sacco A, Castellino M, et al. Nonwoven mats of N-doped carbon nanofibers as high-performing anodes in microbial fuel cells. *Mater Today Energy* 2020;16:100385. <https://doi.org/10.1016/j.mtener.2020.100385>.
- [962] Sanchez JL, Pinto D, Laberty-Robert C. Electrospun carbon fibers for microbial fuel cells: A novel bioanode design applied to wastewater treatment. *Electrochim Acta* 2021;373:137864. <https://doi.org/10.1016/j.electacta.2021.137864>.
- [963] Ghasemi B, Yaghmaei S, Ghaderi S, Bayat A, Mardanpour MM. Effects of chemical, electrochemical, and electrospun deposition of polyaniline coatings on surface of anode electrodes for evaluation of MFCs' performance. *J Environ Chem Eng* 2020;8:104039. <https://doi.org/10.1016/j.jece.2020.104039>.
- [964] Liu Y, Zhang X, Li H, Peng L, Qin Y, Lin X, et al. Porous α - Fe_2O_3 nanofiber combined with carbon nanotube as anode to enhance the bioelectricity generation for microbial fuel cell. *Electrochim Acta* 2021;391:138984. <https://doi.org/10.1016/j.electacta.2021.138984>.
- [965] Liang P, Wang H, Xia X, Huang X, Mo Y, Cao X, et al. Carbon nanotube powders as electrode modifier to enhance the activity of anodic biofilm in microbial fuel cells. *Biosens Bioelectron* 2011;26:3000–4. <https://doi.org/10.1016/j.bios.2010.12.002>.
- [966] Cai T, Huang M, Huang Y, Zheng W. Enhanced performance of microbial fuel cells by electrospinning carbon nanofibers hybrid carbon nanotubes composite anode. *Int J Hydrogen Energy* 2019;44:3088–98. <https://doi.org/10.1016/j.ijhydene.2018.11.205>.
- [967] Wang JL, Hassan M, Liu JW, Yu SH. Nanowire assemblies for flexible electronic devices: Recent advances and perspectives. *Adv Mater* 2018;30:e1803430. <https://doi.org/10.1002/adma.201803430>.
- [968] Qi D, Zhang K, Tian G, Jiang B, Huang Y. Stretchable electronics based on PDMS substrates. *Adv Mater* 2021;33:e2003155. <https://doi.org/10.1002/adma.202003155>.
- [969] Zhang Y, Zhang T, Huang Z, Yang J. A new class of electronic devices based on flexible porous substrates. *Adv Sci* 2022;9:e2105084. <https://doi.org/10.1002/advs.202105084>.
- [970] Cheng T, Zhang Y, Lai WY, Huang W. Stretchable thin-film electrodes for flexible electronics with high deformability and stretchability. *Adv Mater* 2015;27:3349–76. <https://doi.org/10.1002/adma.201405864>.
- [971] Ye G, Wan Y, Wu J, Zhuang W, Zhou Z, Jin T, et al. Multifunctional device integrating dual-temperature regulator for outdoor personal thermal comfort and triboelectric nanogenerator for self-powered human-machine interaction. *Nano Energy* 2022;97:107148. <https://doi.org/10.1016/j.nanoen.2022.107148>.
- [972] Tian G, Liu Y, Yu M, Liang C, Yang D, Huang J, et al. Electrostatic interaction-based high tissue adhesive, stretchable microelectrode arrays for the electrophysiological interface. *ACS Appl Mater Interfaces* 2022;14:4852–61. <https://doi.org/10.1021/acsami.1c18983>.
- [973] Das S, Gulotty R, Sumant AV, Roelofs A. All two-dimensional, flexible, transparent, and thinnest thin film transistor. *Nano Lett* 2014;14:2861–6. <https://doi.org/10.1021/nl5009037>.
- [974] Eda G, Fanchini G, Chhowalla M. Large-area ultrathin films of reduced graphene oxide as a transparent and flexible electronic material. *Nat Nanotechnol* 2008;3:270–4. <https://doi.org/10.1038/nnano.2008.83>.
- [975] Xia J, Zhang X, Yang Y, Wang X, Yao J. Electrospinning fabrication of flexible, foldable, and twistable $\text{Sb}_2\text{S}_3/\text{TiO}_2/\text{C}$ nanofiber anode for lithium ion batteries. *Chem Eng J* 2021;413:127400. <https://doi.org/10.1016/j.cej.2020.127400>.
- [976] Sun B, Long Y-Z, Chen Z-J, Liu S-L, Zhang H-D, Zhang J-C, et al. Recent advances in flexible and stretchable electronic devices via electrospinning. *J Mater Chem C* 2014;2:1209–19. <https://doi.org/10.1039/c3tc31680g>.
- [977] He X-X, Zheng J, Yu G-F, You M-H, Yu M, Ning X, et al. Near-field electrospinning: Progress and applications. *J Phys Chem C* 2017;121:8663–78. <https://doi.org/10.1021/acs.jpcc.6b12783>.
- [978] Sun N, Wang G-G, Zhao H-X, Cai Y-W, Li J-Z, Li G-Z, et al. Waterproof, breathable and washable triboelectric nanogenerator based on electrospun nanofiber films for wearable electronics. *Nano Energy* 2021;90:106639. <https://doi.org/10.1016/j.nanoen.2021.106639>.
- [979] Gao J, Fan Y, Zhang Q, Luo L, Hu X, Li Y, et al. Ultra-robust and extensible fibrous mechanical sensors for wearable smart healthcare. *Adv Mater* 2022;34:2107511. <https://doi.org/10.1002/adma.202107511>.
- [980] Persano L, Dagdeviren C, Su YW, Zhang YH, Girardo S, Pisignano D, et al. High performance piezoelectric devices based on aligned arrays of nanofibers of poly(vinylidene fluoride-co-trifluoroethylene). *Nat Commun* 2013;4:1–10. <https://doi.org/10.1038/ncomms2639>.
- [981] Park M, Im J, Shin M, Min Y, Park J, Cho H, et al. Highly stretchable electric circuits from a composite material of silver nanoparticles and elastomeric fibres. *Nat Nanotechnol* 2012;7:803–9. <https://doi.org/10.1038/nnano.2012.206>.
- [982] Cheng H, Wang B, Yang K, Yang Y, Wang C. A high-performance piezoresistive sensor based on poly(styrene-co-methacrylic acid)/polypyrrole microspheres/graphene-decorated TPU electrospun membrane for human motion detection. *Chem Eng J* 2021;426:131152. <https://doi.org/10.1016/j.cej.2021.131152>.
- [983] Guo Y, Wei X, Gao S, Yue W, Li Y, Shen G. Recent advances in carbon material-based multifunctional sensors and their applications in electronic skin systems. *Adv Funct Mater* 2021;31:2104288. <https://doi.org/10.1002/adfm.202104288>.
- [984] Tkachev S, Monteiro M, Santos J, Placidi E, Ben Hassine M, Marques P, et al. Environmentally friendly graphene inks for touch screen sensors. *Adv Funct Mater* 2021;31:2103287. <https://doi.org/10.1002/adfm.202103287>.
- [985] Xu W, Huang L, Wong M, Chen L, Bai G, Hao J. Environmentally friendly hydrogel-based triboelectric nanogenerators for versatile energy harvesting and self-powered sensors. *Adv Energy Mater* 2016;7:1601529. <https://doi.org/10.1002/aenm.201601529>.
- [986] Wang S, Ning H, Hu N, Liu Y, Liu F, Zou R, et al. Environmentally-friendly and multifunctional graphene-silk fabric strain sensor for human-motion detection. *Adv Mater Interfaces* 2019;7:1901507. <https://doi.org/10.1002/admi.201901507>.

- [987] Ayissi Eyebé G, Bideau B, Boubekeur N, Loranger É, Domingue F. Environmentally-friendly cellulose nanofibre sheets for humidity sensing in microwave frequencies. *Sens Actuators B: Chem* 2017;245:484–92. <https://doi.org/10.1016/j.snb.2017.01.130>.
- [988] Ren JS, Wang CX, Zhang X, Carey T, Chen KL, Yin YJ, et al. Environmentally-friendly conductive cotton fabric as flexible strain sensor based on hot press reduced graphene oxide. *Carbon* 2017;111:622–30. <https://doi.org/10.1016/j.carbon.2016.10.045>.
- [989] Huang C, Xiao M, Li Z, Fu Z, Shi R. Bioinspired breathable biodegradable bioelastomer-based flexible wearable electronics for high-sensitivity human-interactive sensing. *Chem Eng J* 2024;486:150013. <https://doi.org/10.1016/j.cej.2024.150013>.
- [990] Qiu H, Song W, Wang X, Zhang J, Fan Z, Yu M, et al. A calibration-free self-powered sensor for vital sign monitoring and finger tap communication based on wearable triboelectric nanogenerator. *Nano Energy* 2019;58:536–42. <https://doi.org/10.1016/j.nanoen.2019.01.069>.
- [991] Ma C, Hao S, Yu W, Liu X, Wang Y, Wang Y, et al. Compliant and breathable electrospun epidermal electrode towards artifact-free electrophysiological monitoring. *Chem Eng J* 2024;490:151118. <https://doi.org/10.1016/j.cej.2024.151118>.
- [992] Su X, Han M, Liu Y, Wang J, Liang C, Liu Y. In-situ construction of nitrogen-doped reduced graphene oxide@carbon nanofibers towards the synergetic enhancement of their microwave absorption properties via integrating point defects and structure engineering. *J Colloid Interface Sci* 2022;628:984–94. <https://doi.org/10.1016/j.jcis.2022.08.094>.
- [993] Fuh Y, Ye J, Chen P, Huang Z. A highly flexible and substrate-independent self-powered deformation sensor based on massively aligned piezoelectric nano-/microfibers. *J Mater Chem A* 2014;2:16101–6. <https://doi.org/10.1039/c4ta01720j>.
- [994] Fu G, Shi Q, Liang Y, He Y, Xue R, He S, et al. Eu3+-doped electrospun polyvinylidene fluoride-hexafluoropropylene/graphene oxide multilayer composite nanofiber for the fabrication of flexible pressure sensors. *ACS Omega* 2022;7:23521–31. <https://doi.org/10.1021/acsomega.2c02024>.
- [995] Sengupta D, Lu L, Gomes DR, Jayawardhana B, Pei Y, Kottapalli AGP. Fabric-like electrospun PVAc-graphene nanofiber webs as wearable and degradable piezocapacitive sensors. *ACS Appl Mater Interfaces* 2023;15:22351–66. <https://doi.org/10.1021/acsami.3c03113>.
- [996] Liang J, Zhao H, Yue L, Fan G, Li T, Lu S, et al. Recent advances in electrospun nanofibers for supercapacitors. *J Mater Chem A* 2020;8:16747–89. <https://doi.org/10.1039/d0ta05100d>.
- [997] Li X, Chen W, Qian Q, Huang H, Chen Y, Wang Z, et al. Electrospinning-based strategies for battery materials. *Adv Energy Mater* 2021;11:2000845. <https://doi.org/10.1002/aenm.202000845>.
- [998] Li X, Wang G, Wang X, Li X, Ji J. Flexible supercapacitor based on MnO₂ nanoparticles via electrospinning. *J Mater Chem A* 2013;1:10103–6. <https://doi.org/10.1039/C3TA11172TH>.
- [999] Sayak R, Prajnashree P, Sudip B. Electrospun highly porous carbon nitride-carbon nanofibers for high performance supercapacitor application. *J Energy Storage* 2024;91:112007. <https://doi.org/10.1016/j.est.2024.112007>.
- [1000] Hwang H, Byun S, Yuk S, Kim S, Song SH, Lee D. High-rate electrospun Ti₃C₂Tx MXene/carbon nanofiber electrodes for flexible supercapacitors. *Appl Surf Sci* 2021;556:149710. <https://doi.org/10.1016/j.apsusc.2021.149710>.
- [1001] Tao X, Zhang L, He X, Fang L, Wang H, Zhang L, et al. Nitrogen-Doped Porous MXene (Ti₃C₂) for flexible supercapacitors with enhanced storage performance. *Molecules* 2022;27:4890. <https://doi.org/10.3390/molecules27154890>.
- [1002] Zhao Y, Wang Y, Huang Y, Liu W, Hu J, Zheng J, et al. Nickel carbonate hydroxide-based core-triple-shelled nanofibers with ultrahigh specific capacity for flexible hybrid supercapacitors. *J Colloid Interface Sci* 2023;630:444–51. <https://doi.org/10.1016/j.jcis.2022.10.128>.
- [1003] Zhang H, Xie Y, Song Y, Qin X. Preparation of high-temperature resistant poly (m-phenylene isophthalamide)/polyacrylonitrile composite nanofibers membrane for air filtration. *Colloids Surf Physicochem Eng Aspects* 2021;624:126831. <https://doi.org/10.1016/j.colsurfa.2021.126831>.
- [1004] Chen Y, Qiao S, Tang Y, Du Y, Zhang D, Wang W, et al. Double-faced atomic-level engineering of hollow carbon nanofibers as free-standing bifunctional oxygen electrocatalysts for flexible Zn–air battery. *ACS Nano* 2022;16:15273–85. <https://doi.org/10.1021/acsnano.2c06700>.
- [1005] Zi Y, Wang ZL. Nanogenerators: An emerging technology towards nanoenergy. *APL Mater* 2017;5:074103. <https://doi.org/10.1063/1.4977208>.
- [1006] Devadiga D, Selvakumar M, Shetty P, Santosh MS. The integration of flexible dye-sensitized solar cells and storage devices towards wearable self-charging power systems: A review. *Renew Sust Energ Rev* 2022;159:112252. <https://doi.org/10.1016/j.rser.2022.112252>.
- [1007] Choudhury BD, Lin C, Shawon SMAZ, Soliz-Martinez J, Gutierrez J, Huda MN, et al. Carbon fibers coated with ternary Ni–Co–Se alloy particles as a low-cost counter electrode for flexible dye sensitized solar cells. *ACS Appl Energy Mater* 2021;4:870–8. <https://doi.org/10.1021/acsaeam.0c02764>.
- [1008] Huang X, Shen P, Zhao B, Feng X, Jiang S, Chen H, et al. Stainless steel mesh-based flexible quasi-solid dye-sensitized solar cells. *Sol Energy Mater Sol Cells* 2010;94:1005–10. <https://doi.org/10.1016/j.solmat.2010.02.005>.
- [1009] Wang S, Wang Z, Qi W, Guo H, Liu Y, Luo Y, et al. Synthesis of carbon nanofibers supported NiMoO₄ nanoparticles composites used for liquid thin film solar cells counter electrode. *Int J Hydrogen Energy* 2023;48:31187–96. <https://doi.org/10.1016/j.ijhydene.2023.04.094>.
- [1010] Thomas M, Rajiv S. Grafted PEO polymeric ionic liquid nanocomposite electrospun membrane for efficient and stable dye sensitized solar cell. *Electrochim Acta* 2020;341:136040. <https://doi.org/10.1016/j.electacta.2020.136040>.
- [1011] Wang X, Liu Y, Chen Q, Yan Y, Rao Z, Lin Z, et al. Recent advances in stretchable field-effect transistors. *J Mater Chem C* 2021;9:7796–828. <https://doi.org/10.1039/d1tc01082d>.
- [1012] Li M-Z, Han S-T, Zhou Y. Recent advances in flexible field-effect transistors toward wearable sensors. *Adv Intell Syst* 2020;2:2000113. <https://doi.org/10.1002/aisy.202000113>.
- [1013] Liu K, Ouyang B, Guo XJ, Guo YL, Liu YQ. Advances in flexible organic field-effect transistors and their applications for flexible electronics. *Npj Flex Electron* 2022;6:1–19. <https://doi.org/10.1038/s41528-022-00133-3>.
- [1014] Briseno AL, Mannsfeld SCB, Lu XM, Xiong YJ, Jenekhe SA, Bao ZN, et al. Fabrication of field-effect transistors from hexathiapentacene single-crystal nanowires. *Nano Lett* 2007;7:668–75. <https://doi.org/10.1021/nl0627036>.
- [1015] Wang Y, Yokota T, Someya T. Electrospun nanofiber-based soft electronics. *NPG Asia Mater* 2021;13:22. <https://doi.org/10.1038/s41427-020-00267-8>.
- [1016] Jun L, Chen Q, Fu W, Wang Y, Zhu W, Zhang J. Electrospun Yb-doped In₂O₃ nanofiber field-effect transistors for highly sensitive ethanol sensors. *ACS Appl Mater Interfaces* 2020;12:38425–34. <https://doi.org/10.1021/acsami.0c12259>.
- [1017] Jun L, Li L, Chen Q, Zhu W, Zhang J. Ultrasensitive room-temperature acetone gas sensors employing green-solvent-processed aligned In₂O₃ nanofiber field-effect transistors. *J Mater Chem C* 2022;10:860–9. <https://doi.org/10.1039/D1TC04618G>.
- [1018] Guo Y, Wu F, Dun GH, Cui T, Liu Y, Tan X, et al. Electrospun nanofiber-based synaptic transistor with tunable plasticity for neuromorphic computing. *Adv Funct Mater* 2023;33:2208055. <https://doi.org/10.1002/adfm.202208055>.
- [1019] Jeong SY, Shim HR, Na Y, Kang KS, Jeon Y, Choi S, et al. Foldable and washable textile-based OLEDs with a multi-functional near-room-temperature encapsulation layer for smart e-textiles. *Npj Flex Electron* 2021;5:15. <https://doi.org/10.1038/s41528-021-00112-0>.
- [1020] R. Mina, Y. Kou, S. Ifor D. W. Improving the air stability of flexible top-emitting organic light-emitting diodes. *Npj Flex. Electron*, 8 (2024), pp. 51,10.1038/s41528-024-00338-8.
- [1021] Iulia Corina C, Monica E, Silviu P, Ionut E, Constantin Claudiu C. Organic Light-Emitting Diodes with Electrospun Electrodes for Double-Side Emissions. *Micromachines* 2023;14:543. <https://doi.org/10.3390/mi14030543>.
- [1022] Chen W-C, Shiao J-H, Tsai T-L, Jiang D-H, Chen L-C, Chang C-H, et al. Multiple scattering from electrospun nanofibers with embedded silver nanoparticles of tunable shape for random lasers and white-light-emitting diodes. *ACS Appl Mater Interfaces* 2020;12:2783–92. <https://doi.org/10.1021/acsami.9b16059>.
- [1023] Li P, Gao X, Zhao B, Pan K, Deng J. Multi-color tunable and white circularly polarized luminescent composite nanofibers electrospun from chiral helical polymer. *Adv Fiber Mater* 2022;4:1632–44. <https://doi.org/10.1007/s42765-022-00196-x>.
- [1024] Li C, Wang H, Zhao X, Yang K, Meng Q, Zhang L. Fabrication of unidirectional water permeable PS/PET composite nanofibers modified with silver nanoparticles via electrospinning. *Membranes* 2023;13:257. <https://doi.org/10.3390/membranes13030257>.
- [1025] Chinnappan A, Baskar C, Baskar S, Ratheesh G, Ramakrishna S. An overview of electrospun nanofibers and their application in energy storage, sensors and wearable/flexible electronics. *J Mater Chem C* 2017;5:12657–73. <https://doi.org/10.1039/c7tc03058d>.
- [1026] Woo H, Kim S, Yoon S, Kim K, Kim GH, An T, et al. Highly flexible and transparent film heater with electrospun copper conductive network via junction-free structure. *J Alloys Compd* 2021;886:161191. <https://doi.org/10.1016/j.jallcom.2021.161191>.

- [1027] Liang C, Liu Y, Lu W, Tian G, Zhao Q, Yang D, et al. Strategies for interface issues and challenges of neural electrodes. *Nanoscale* 2022;14:3346–66. <https://doi.org/10.1039/d1nr07226a>.
- [1028] Sharafkhani S, Kokabi M. High performance flexible actuator: PVDF nanofibers incorporated with axially aligned carbon nanotubes. *Compos B Eng* 2021;222: 109060. <https://doi.org/10.1016/j.compositesb.2021.109060>.
- [1029] Laschi C, Mazzolai B, Cianchetti M. Soft robotics: Technologies and systems pushing the boundaries of robot abilities. *Sci Robot* 2016;1. <https://doi.org/10.1126/scirobotics.aah3690>. p. eah3690.
- [1030] Xin Y, Zhou X, Tan M, Chen S, Huang P, Jiang Y, et al. 3D-printed electrohydrodynamic pump and development of anti-swelling organohydrogel for soft robotics. *Adv Mater* 2025;2415210. <https://doi.org/10.1002/adma.202415210>.
- [1031] Hegde C, Su J, Tan JMR, He K, Chen X, Magdassi S. Sensing in soft robotics. *ACS Nano* 2023;17:15277–307. <https://doi.org/10.1021/acsnano.3c04089>.
- [1032] Jeon SH, Hwang GW, Kim J, Lim D, Son Y, Yang TH, et al. Super-adaptive electroactive programmable adhesive materials to challenging surfaces: From intelligent soft robotics to XR haptic interfaces. *InfoMat* 2024:e12640. <https://doi.org/10.1002/inf2.12640>.
- [1033] Jung Y, Kwon K, Lee J, Ko SH. Untethered soft actuators for soft standalone robotics. *Nat Commun* 2024;15:3510. <https://doi.org/10.1038/s41467-024-47639-0>.
- [1034] Su Y, Chen C, Pan H, Yang Y, Chen G, Zhao X, et al. Muscle fibers inspired high-performance piezoelectric textiles for wearable physiological monitoring. *Adv Funct Mater* 2021;31:2010962. <https://doi.org/10.1002/adfm.202010962>.
- [1035] Wang L, Wu Y, Guo B, Ma PX. Nanofiber yarn/hydrogel core-shell scaffolds mimicking native skeletal muscle tissue for guiding 3D myoblast alignment, elongation, and differentiation. *ACS Nano* 2015;9:9167–79. <https://doi.org/10.1021/acsnano.5b03644>.
- [1036] Gotti C, Sensini A, Fornaia G, Gualandi C, Zucchelli A, Focarete ML. Biomimetic hierarchically arranged nanofibrous structures resembling the architecture and the passive mechanical properties of skeletal muscles: a step forward toward artificial muscle. *Front Bioeng Biotechnol* 2020;8:767. <https://doi.org/10.3389/fbioe.2020.00767>.
- [1037] Sensini A, Gotti C, Belcarì J, Zucchelli A, Focarete ML, Gualandi C, et al. Morphologically bioinspired hierarchical nylon 6,6 electrospun assembly recreating the structure and performance of tendons and ligaments. *Med Eng Phys* 2019;71:79–90. <https://doi.org/10.1016/j.medengphy.2019.06.019>.
- [1038] He QG, Wang ZJ, Wang Y, Wang ZJ, Li CH, Annappooranan R, et al. Electrospun liquid crystal elastomer microfiber actuator. *Sci Robot*, 2021;6. Article eabi9704. <https://doi.org/10.1126/scirobotics.abi9704>.
- [1039] Wei X, Chen L, Wang Y, Sun Y, Ma C, Yang X, et al. An electrospinning anisotropic hydrogel with remotely-controlled photo-responsive deformation and long-range navigation for synergist actuation. *Chem Eng J* 2022;433:134258. <https://doi.org/10.1016/j.cej.2021.134258>.
- [1040] Deng J, Yuk H, Wu JJ, Varela CE, Chen XY, Roche ET, et al. Electrical bioadhesive interface for bioelectronics. *Nat Mater* 2020;20:229–36. <https://doi.org/10.1038/s41563-020-00814-2>.
- [1041] Z.K. Li, J.J. Lu, T. Ji, Y.M. Xue, L.B. Zhao, K. Zhao, et al. Self-healing hydrogel bioelectronics *Adv Mater*, 36 (2024), Article 2306350, [10.1002/adma.202306350](https://doi.org/10.1002/adma.202306350).
- [1042] Wu S, Dong T, Li Y, Sun M, Qi Y, Liu J, et al. State-of-the-art review of advanced electrospun nanofiber yarn-based textiles for biomedical applications. *Appl Mater Today* 2022;27:101473. <https://doi.org/10.1016/j.apmt.2022.101473>.
- [1043] Ma Z, Huang Q, Xu Q, Zhuang Q, Zhao X, Yang Y, et al. Permeable superelastic liquid-metal fibre mat enables biocompatible and monolithic stretchable electronics. *Nat Mater* 2021;20:859–68. <https://doi.org/10.1038/s41563-020-00902-3>.
- [1044] B. Lan, X. Xiao, A.D. Carlo, W. Deng, T. Yang, L. Jin, et al. Topological nanofibers enhanced piezoelectric membranes for soft bioelectronics. *Adv Funct Mater*, 32 (2022), Article 2207393, [10.1002/adfm.202207393](https://doi.org/10.1002/adfm.202207393).
- [1045] Miao Y, Zhu G, Hou H, Xia Y, Liu T. Electrospun polyimide nanofiber-based nonwoven separators for lithium-ion batteries. *J Power Sources* 2013;226:82–6. <https://doi.org/10.1016/j.jpowsour.2012.10.027>.
- [1046] Wang Y, Han C, Zheng D, Lei Y. Large-scale, flexible and high-temperature resistant ZrO₂/SiC ultrafine fibers with a radial gradient composition. *J Mater Chem A* 2014;2:9607–12. <https://doi.org/10.1039/c4ta00347k>.
- [1047] Liu Y, Liu Y, Choi WC, Chae S, Lee J, Kim BS, et al. Highly flexible, erosion resistant and nitrogen doped hollow SiC fibrous mats for high temperature thermal insulators. *J Mater Chem A* 2017;5:2664–72. <https://doi.org/10.1039/c6ta09475a>.
- [1048] Zhang X, Wang F, Dou L, Cheng X, Si Y, Yu J, et al. Ultrastrong, superelastic, and lamellar multiarch structured ZrO₂-Al₂O₃ nanofibrous aerogels with high-temperature resistance over 1300 °C. *ACS Nano* 2020;14:15616–25. <https://doi.org/10.1021/acsnano.0c06423>.
- [1049] Wei H-Y, Li H, Cui Y, Sang R-L, Wang H-Y, Wang P, et al. Synthesis of flexible mullite nanofibers by electrospinning based on nonhydrolytic sol-gel method. *J Sol-Gel Sci Technol* 2017;82:718–27. <https://doi.org/10.1007/s10971-017-4354-7>.
- [1050] Ji S, Park J, Jo Y, Kim YB, Jang J, Kim SK, et al. Haze-free transparent electrodes using metal nanofibers with carbon shells for high-temperature stability. *Appl Surf Sci* 2019;483:1101–9. <https://doi.org/10.1016/j.apsusc.2019.04.052>.
- [1051] Jin C, Wu Z, Zhang R, Qian X, Xu H, Che R. 1D electromagnetic-gradient hierarchical carbon microtube via coaxial electrospinning design for enhanced microwave absorption. *ACS Appl Mater Interfaces* 2021;13:15939–49. <https://doi.org/10.1021/acsmi.1c03129>.
- [1052] Feng Y, Zong D, Hou Y, Yin X, Zhang S, Duan L, et al. Gradient structured micro/nanofibrous sponges with superior compressibility and stretchability for broadband sound absorption. *J Colloid Interface Sci* 2021;593:59–66. <https://doi.org/10.1016/j.jcis.2021.03.013>.
- [1053] Chen R, Liu J, Yang C, Weitz DA, He H, Li D, et al. Transparent impact-resistant composite films with bioinspired hierarchical structure. *ACS Appl Mater Interfaces* 2019;11:23616–22. <https://doi.org/10.1021/acsmi.9b06500>.
- [1054] Qin M, Zhang L, Wu H. Dielectric loss mechanism in electromagnetic wave absorbing materials. *Adv Sci* 2022;9:e2105553. <https://doi.org/10.1002/advs.202105553>.
- [1055] Li L, Chen Z, Pan F, Guo H, Wang X, Cheng J, et al. Electrospinning technology on one dimensional microwave absorbers: Fundamentals, current progress, and perspectives. *Chem Eng J* 2023;470:144236. <https://doi.org/10.1016/j.cej.2023.144236>.
- [1056] Zhang Y, Zhao Y, Chen Q, Hou Y, Zhang Q, Cheng L, et al. Flexible SiC-CNTs hybrid fiber mats for tunable and broadband microwave absorption. *Ceram Int* 2021;47:8123–32. <https://doi.org/10.1016/j.ceramint.2020.11.167>.
- [1057] Hou Y, Cheng L, Zhang Y, Yang Y, Deng C, Yang Z, et al. Enhanced flexibility and microwave absorption properties of HfC/SiC nanofiber mats. *ACS Appl Mater Interfaces* 2018;10:29876–83. <https://doi.org/10.1021/acsmi.8b07980>.
- [1058] Tian S, Li A, Cui J, Sun Z, Liu H, Yan Z, et al. Order effect of nitrogen and phosphorus co-doping carbon nanofibers for enhancing electromagnetic wave absorption. *Carbon* 2023;203:580–9. <https://doi.org/10.1016/j.carbon.2022.12.018>.
- [1059] Xiang J, Li J, Zhang X, Ye Q, Xu J, Shen X. Magnetic carbon nanofibers containing uniformly dispersed Fe/Co/Ni nanoparticles as stable and high-performance electromagnetic wave absorbers. *J Mater Chem A* 2014;2:16905–14. <https://doi.org/10.1039/c4ta03732d>.
- [1060] Meng F, Wang H, Wei Z, Chen T, Li CL, et al. Generation of graphene-based aerogel microspheres for broadband and tunable high-performance microwave absorption by electrospinning-freeze drying process. *Nano Res* 2018;11:2847–61. <https://doi.org/10.1007/s12274-017-1915-6>.
- [1061] Li T, Zhi D, Chen Y, Li B, Zhou Z, Meng F. Multiaxial electrospun generation of hollow graphene aerogel spheres for broadband high-performance microwave absorption. *Nano Res* 2020;13:477–84. <https://doi.org/10.1007/s12274-020-2632-0>.
- [1062] Shen Y, Wei Y, Ma J, Zhang Y, Ji B, Tang J, et al. Self-cleaning functionalized FeNi/NiFe₂O₄/NiO/C nanofibers with enhanced microwave absorption performance. *Ceram Int* 2020;46:13397–406. <https://doi.org/10.1016/j.ceramint.2020.02.121>.
- [1063] Li Y, Zhao Y, Lu X, Zhu Y, Jiang L. Self-healing superhydrophobic polyvinylidene fluoride/Fe₃O₄@polypyrrole fiber with core-sheath structures for superior microwave absorption. *Nano Res* 2016;9:2034–45. <https://doi.org/10.1007/s12274-016-1094-x>.
- [1064] Hassan T, Jamshaid H, Mishra R, Khan MQ, Petru M, Tichy M, et al. Factors affecting acoustic properties of natural-fiber-based materials and composites: A review. *Textiles* 2021;1:55–85. <https://doi.org/10.3390/textiles1010005>.
- [1065] Kalinová K. Nanofibrous resonant membrane for acoustic applications. *J Nanomater* 2011;2011:1–6. <https://doi.org/10.1155/2011/265720>.
- [1066] Selvaraj S, Jeevan V, Rao JR, Fathima NN. Conversion of tannery solid waste to sound absorbing nanofibrous materials: A road to sustainability. *J Clean Prod* 2019;213:375–83. <https://doi.org/10.1016/j.jclepro.2018.12.144>.

- [1067] Selvaraj S, Ramalingam S, Parida S, Rao JR, Nishter NF. Chromium containing leather trimmings valorization: Sustainable sound absorber from collagen hydrolysate intercalated electrospun nanofibers. *J Hazard Mater* 2021;405:124231. <https://doi.org/10.1016/j.jhazmat.2020.124231>.
- [1068] Wu CM, Chou MH. Sound absorption of electrospun polyvinylidene fluoride/graphene membranes. *Eur Polym J* 2016;82:35–45. <https://doi.org/10.1016/j.eurpolymj.2016.07.001>.
- [1069] Wu C, Chou M. Polymorphism, piezoelectricity and sound absorption of electrospun PVDF membranes with and without carbon nanotubes. *Composites Sci Technol* 2016;127:127–33. <https://doi.org/10.1016/j.compscitech.2016.03.001>.
- [1070] Sahay R, Agarwal K, Subramani K, Raghavan N, Budiman AS, Bajji A. Helicoidally arranged polyacrylonitrile fiber-reinforced strong and impact-resistant thin polyvinyl alcohol film enabled by electrospinning-based additive manufacturing. *Polymers* 2020;12:2102376. <https://doi.org/10.3390/polym12102376>.
- [1071] Zhang X, Yang W, Shao Z, Li Y, Su Y, Zhang Q, et al. A moisture-wicking passive radiative cooling hierarchical metafabric. *ACS Nano* 2022;16:2188–97. <https://doi.org/10.1021/acsnano.1c08227>.
- [1072] Zhang B, Tong Z, Pang Y, Xu H, Li X, Ji H. Design and electrospun closed cell structured sio2 nanocomposite fiber by hollow SiO₂/TiO₂ spheres for thermal insulation. *Composites Sci Technol* 2022;218:109152. <https://doi.org/10.1016/j.compscitech.2021.109152>.
- [1073] 6] X. Zhang, N. Xu, Y. Jiang, H. Liu, H. Xu, C. Han, et al. Robust, fire-resistant, and thermal-stable SiZrNOC nanofiber membranes with amorphous microstructure for high-temperature thermal superinsulation. *J Adv Cerami*, 12 (2023), pp. 36–48, 10.26599/JAC.2023.9220664.
- [1074] Li X, Yang Y, Quan Z, Wang L, Ji D, Li F, et al. Tailoring body surface infrared radiation behavior through colored nanofibers for efficient passive radiative heating textiles. *Chem Eng J* 2022;430:133093. <https://doi.org/10.1016/j.cej.2021.133093>.
- [1075] Zou FW, Dong YQ, Wang MH, Sliman H, Wang XF, Zhao T. Designing unidirectional moisture transport fabric based on PA/CA membrane fabricated by electrospinning. *Fiber Polym* 2021;22:2404–12. <https://doi.org/10.1007/s12221-021-1121-8>.
- [1076] Gong X, Ji Y, Liu X, Yu J, Zhang S, Ding B. Biomimetic and durably superhydrophobic nanofibrous membranes for high-performance waterproof and breathable textiles. *Adv Funct Mater* 2024;34:2316030. <https://doi.org/10.1002/adfm.202316030>.
- [1077] Fulya Y, Gizem C, Gamze T. Nanofibers in cosmetics. In: Rahman M, Asiri A, editors. *Nanofiber research-reaching new heights*. Rijeka: InTech; 2016. p. 127–45.
- [1078] Meftahi A, Samyn P, Geravand SA, Khajavi R, Alibkhshi S, Bechelany M, et al. Nanocelluloses as skin biocompatible materials for skincare, cosmetics, and healthcare: Formulations, regulations, and emerging applications. *Carbohydr Polym* 2022;278:118956. <https://doi.org/10.1016/j.carbpol.2021.118956>.
- [1079] 2] N. Gao, J. Wu, Y. Liu. Preparation of a dissolved collagen peptide-silk fibroin composite fiber mask by electrospinning. *Journal of Beijing University of Chemical Technology*, 45 (2018), pp. 21–28, 10.13543/j.bhxbzr.2018.06.004.
- [1080] Miletić A, Pavlič B, Ristić I, Zeković Z, Pilić B. Encapsulation of fatty oils into electrospun nanofibers for cosmetic products with antioxidant activity. *Appl Sci* 2019;9:2955. <https://doi.org/10.3390/app9152955>.
- [1081] Fathi-Azarbayjani A, Qun L, Chan YW, Chan SY. Novel vitamin and gold-loaded nanofiber facial mask for topical delivery. *AAPS Pharm Sci Tech* 2010;11:1164–70. <https://doi.org/10.1208/s12249-010-9475-z>.
- [1082] Mehrani Z, Karimpour Z, Ebrahimzadeh H. Using PVA/CA/Au NPs electrospun nanofibers as a green nanosorbent to preconcentrate and determine Pb²⁺ and Cu²⁺ in rice samples, water sources and cosmetics. *New J Chem* 2020;44:15000–9. <https://doi.org/10.1039/d0nj03352a>.
- [1083] Odularu AT. Basic principles of electrospinning, mechanisms, nanofibre production, and anticancer drug delivery. *J Chem* 2022;2022:1–15. <https://doi.org/10.1155/2022/9283325>.
- [1084] Mai L, Dong Y, Xu L, Han C. Single nanowire electrochemical devices. *Nano Lett* 2010;10:4273–8. <https://doi.org/10.1021/nl102845r>.
- [1085] Xu X, Yan M, Tian X, Yang C, Shi M, Wei Q, et al. In-situ investigation of Li and Na ion transport with single nanowire electrochemical devices. *Nano Lett* 2015;15:3879–84. <https://doi.org/10.1021/acs.nanolett.5b00705>.
- [1086] Liu Y, Shen Q, Zhao X, Zhang J, Liu X, Wang T, et al. Hierarchical engineering of porous P2-Na₂/3Ni₁/3Mn₂/3O₂ nanofibers assembled by nanoparticles enables superior sodium-ion storage cathodes. *Adv Funct Mater* 2020;30:1907837. <https://doi.org/10.1002/adfm.201907837>.
- [1087] Hill MO, Schmiedekne P, Huang CY, Maddali S, Hu XB, Hruszkewycz SO, et al. 3D Bragg coherent diffraction imaging of extended nanowires: defect formation in highly strained InGaAs quantum wells. *ACS Nano* 2022;16:20281–93. <https://doi.org/10.1021/acsnano.2c06071>.
- [1088] Krieg J, Chen CY, Avila J, Zhang ZY, Sigle W, Zhang HB, et al. Exploring the electronic structure and chemical homogeneity of individual Bi₂Te₃ nanowires by nano-angle-resolved photoemission spectroscopy. *Nano Lett* 2016;16:4001–7. <https://doi.org/10.1021/acs.nanolett.6b00400>.
- [1089] Marçal LAB, Benter S, Irish A, Dzhibaev D, Oksenberg E, Rothman A, et al. Inducing ferroelastic domains in single-crystal CsPbBr₃ perovskite nanowires using atomic force microscopy. *Phys Rev Mater* 2021;5:L063001. <https://doi.org/10.1103/PhysRevMaterials.5.L063001>.
- [1090] Anaya J, Rossi S, Alomari M, Kohn E, Toth L, Pecz B, et al. Thermal conductivity of ultrathin nano-crystalline diamond films determined by Raman thermography assisted by silicon nanowires. *Appl Phys Lett* 2015;106:223101. <https://doi.org/10.1063/1.4922035>.
- [1091] Chen H-L, De Lépinar R, Scaccabarozzi A, Oehler F, Harmand J-C, Cattoni A, et al. Quantitative assessment of carrier density by cathodoluminescence. *II GaAs nanowires Phys Rev Appl* 2021;15:024007. <https://doi.org/10.1103/PhysRevApplied.15.024007>.
- [1092] Sarkar R, Bhunia S, Jana D, Nag D, Chatterjee S, Laha A. Growth of uniform Mg-doped p-AlGaIn nanowires using plasma-assisted molecular beam epitaxy technique for UV-A emitters. *Nanotechnology* 2022;33:384001. <https://doi.org/10.1088/1361-6528/ac7472>.
- [1093] Alekseev PA, Sharov VA, Borodin BR, Dunaevskiy MS, Reznik RR. Effect of the lattice mismatch on the efficiency of the GaAs nanowire/Si substrate solar cell. *J Phys Conf Ser* 2015;2021:012004. <https://doi.org/10.1088/1742-6596/2015/1/012004>.
- [1094] Tang S, Tang J, Chiu TW, Uzuhashi J, Tang DM, Ohkubo T, et al. A controllable and efficient method for the fabrication of a single HfC nanowire field-emission point electron source aided by low keV FIB milling. *Nanoscale* 2020;12:16770–4. <https://doi.org/10.1039/d0nr03406a>.
- [1095] S. Parida, A. Patsha, K.K. Madapu, S.J.J.o.A.P. Dhara. Nano-spectroscopic and nanoscopic imaging of single GaN nanowires in the sub-diffraction limit. *J Appl Phys*, 127 (2020), pp. 173103, 10.1063/1.5128999.
- [1096] Jiang SH, Chen YM, Duan GG, Mei CT, Greiner A, Agarwal S. Electrospun nanofiber reinforced composites: A review. *Polym Chem* 2018;9:2685–720. <https://doi.org/10.1039/c8py00378e>.
- [1097] Zhang Y, Liu S, Yan J, Zhang X, Xia S, Zhao Y, et al. Superior flexibility in oxide ceramic crystal nanofibers. *Adv Mater* 2021;33:e2105011. <https://doi.org/10.1002/adma.202105011>.
- [1098] Mao X, Shan HR, Song J, Bai Y, Yu JY, Ding B. Brittle-flexible-brittle transition in nanocrystalline zirconia nanofibrous membranes. *CrstEngComm* 2016;18:1139–46. <https://doi.org/10.1039/c5ce02382c>.
- [1099] Chen SX, McCarthy A, John JV, Su YJ, Xie JW. Converting 2D nanofiber membranes to 3D hierarchical assemblies with structural and compositional gradients regulates cell behavior. *Adv Mater* 2020;32:e2003754. <https://doi.org/10.1002/adma.202003754>.
- [1100] Lu X, Si Y, Zhang S, Yu J, Ding B. In-situ synthesis of mechanically robust, transparent nanofiber-reinforced hydrogels for highly sensitive multiple sensing. *Adv Funct Mater* 2021;31:2103117. <https://doi.org/10.1002/adfm.202103117>.
- [1101] Wang L, Qiu Y, Lv H, Si Y, Liu L, Zhang Q, et al. 3D superelastic scaffolds constructed from flexible inorganic nanofibers with self-fitting capability and tailorable gradient for bone regeneration. *Adv Funct Mater* 2019;29:1901407. <https://doi.org/10.1002/adfm.201901407>.
- [1102] Liu D, Shadike Z, Lin R, Qian K, Li H, Li K, et al. Review of recent development of in-situ/operando characterization techniques for lithium battery research. *Adv Mater* 2019;31:e1806620. <https://doi.org/10.1002/adma.201806620>.
- [1103] Wang G, Ji Y, Huang XR, Yang XQ, Gouma PI, Dudley M. Fabrication and characterization of polycrystalline WO₃ nanofibers and their application for ammonia sensing. *J Phys Chem B* 2006;110:23777–82. <https://doi.org/10.1021/jp0635819>.
- [1104] Chen XX, Liu HQ, Zhou MZ, Fang GZ, Zhang HM, Cai ZY, et al. Constructing stable 2×2 tunnel-structured K_{1.28}Ti₈O₁₆@N-doped carbon nanofibers for ultralong cycling sodium-ion batteries. *Electrochim Acta* 2022;401:139522. <https://doi.org/10.1016/j.electacta.2021.139522>.
- [1105] Xie Z, Peng N, Liu T, Cheng X, Ye W, Zheng R, et al. In-situ characterization of LiY(WO₄) nanotubes for electrochemical energy storage. *Ceram Int* 2019;45:11812–8. <https://doi.org/10.1016/j.ceramint.2019.03.059>.
- [1106] Wang Z, Zheng R, Li Y, Yu H, Liu T, Peng N, et al. Electrochemical uptake/release of lithium in GaNb₁₁O₂₉ nanowires as anode material for rechargeable lithium ion battery. *Ceram Int* 2020;46:20537–44. <https://doi.org/10.1016/j.ceramint.2020.05.167>.

- [1107] Cheng X, Zhu H, Yu H, Ye W, Zheng R, Liu T, et al. $K_2Nb_9O_{21}$ nanotubes with superior electrochemical performance for ultrastable lithium storage. *J Mater Chem A* 2018;6:8620–32. <https://doi.org/10.1039/c8ta01411f>.
- [1108] Lan W, Li H, Lu G, Li Y, Fu D, Zhang K, et al. Hierarchical $CuFeS_2$ spheres hybridized with N-doped carbon for efficient anodic lithium storage: Synthetic optimization, electrochemical analysis and *in-situ* XRD characterization. *Electrochim Acta* 2023;463:142856. <https://doi.org/10.1016/j.electacta.2023.142856>.
- [1109] Yan L, Cheng X, Yu H, Zhu H, Liu T, Zheng R, et al. Ultrathin $W_9Nb_8O_{47}$ nanofibers modified with thermal NH_3 for superior electrochemical energy storage. *Energy Storage Mater* 2018;14:159–68. <https://doi.org/10.1016/j.ensm.2018.03.005>.
- [1110] Su D, Liu J, Pei Y, Liu L, Wang XJASS. Electrospun Na doped Li_2TiSiO_5/C nanofibers with outstanding lithium-storage performance. *Appl Surf Sci* 2020;541:148388. <https://doi.org/10.1016/j.apsusc.2020.148388>.
- [1111] Peng N, Cheng X, Yu H, Zhu H, Liu T, Zheng R, et al. $LiY(MoO_4)_2$ nanotubes: Novel zero-strain anode for electrochemical energy storage. *Energy Storage Mater* 2019;21:297–307. <https://doi.org/10.1016/j.ensm.2018.12.003>.
- [1112] Tian Q, Ye W, Yu H, Cheng X, Zhu H, Long N, et al. $WNB_{60}O_{153}$: A novel energy storage material with high rate capability. *Ceram Int* 2019;45:1893–9. <https://doi.org/10.1016/j.ceramint.2018.10.081>.
- [1113] Cheng X, Qian S, Yu H, Zhu H, Xie Y, Zheng R, et al. $BaNb_{3.6}O_{10}$ nanowires with superior electrochemical performance towards ultrafast and highly stable lithium storage. *Energy Storage Mater* 2019;16:400–10. <https://doi.org/10.1016/j.ensm.2018.06.018>.
- [1114] Yu Z-E, Lyu Y, Zou Z, Su N, He B, Wang S, et al. Understanding the structural evolution and storage mechanism of NASICON-structure $Mg_{0.5}Ti_2(PO_4)_3$ for Li-ion and Na-ion batteries. *ACS Sustainable Chem Eng* 2021;9:13414–23. <https://doi.org/10.1021/acssuschemeng.1c03519>.
- [1115] 9] M.H. Engelhard, T.C. Droubay, Y. Du, X-ray photoelectron spectroscopy application. J.C. Lindon, G.E. Tranter, D.W. Koppenaal (Eds.), *Encyclopedia of Spectroscopy and Spectrometry* (third ed.), Academic Press, Elsevier (2019), pp. 716–724, 10.1016/B978-0-12-409547-2.12102-X.
- [1116] Romanyuk O, Gordeev I, Paszuk A, Supplie O, Stoekmann JP, Houdkova J, et al. GaP/Si(001) interface study by XPS in combination with Ar gas cluster ion beam sputtering. *Appl Surf Sci* 2020;514:145903. <https://doi.org/10.1016/j.apsusc.2020.145903>.
- [1117] Wang J, Wang GH, Cheng B, Yu JG, Fan JJ. Sulfur-doped $g-C_3N_4/TiO_2$ S-scheme heterojunction photocatalyst for Congo Red photodegradation. *Chinese J Catal* 2021;42:56–68. [https://doi.org/10.1016/S1872-2067\(20\)63634-8](https://doi.org/10.1016/S1872-2067(20)63634-8).
- [1118] Masuda T, Yoshikawa H, Noguchi H, Kawasaki T, Kobata M, Kobayashi K, et al. X-ray photoelectron spectroscopy for electrochemical reactions in ordinary solvents. *Appl Phys Lett* 2013;103:317. <https://doi.org/10.1063/1.4821180>.
- [1119] Wenzel S, Randau S, Leichtweiss T, Weber DA, Sann J, Zeier WG, et al. Direct observation of the interfacial instability of the fast ionic conductor $Li_{10}GeP_2S_{12}$ at the lithium metal anode. *Chem Mater* 2016;28:2400–7. <https://doi.org/10.1021/acs.chemmater.6b00610>.
- [1120] Riaz T, Zeeshan R, Zarif F, Ilyas K, Muhammad N, Safi SZ, et al. FTIR analysis of natural and synthetic collagen. *Appl Spec Rev* 2018;53:703–46. <https://doi.org/10.1080/05704928.2018.1426595>.
- [1121] Yang Z, Yin T, Zhang F, Wu W, Lin M, Dong Z, et al. Investigation on dispersion properties of CO_2 and ester solvent mixtures using *in-situ* FTIR spectroscopy. *RSC Adv* 2020;10:18192–9. <https://doi.org/10.1039/d0ra00326c>.
- [1122] Wang C, Tsou SY, Lin HS. Brill transition of nylon-6 in electrospun nanofibers. *Colloid Polym Sci* 2012;290:1799–809. <https://doi.org/10.1007/s00396-012-2724-9>.
- [1123] Shao H, Li Z, He A, Liu C, Yao W. Fabrication of trans-1,4-polyisoprene nanofibers by electrospinning and its crystallization behavior and mechanism. *Chin J Polym Sci* 2016;34:797–804. <https://doi.org/10.1007/s10118-016-1797-1>.
- [1124] Jindal A, Gautam DK, Basu S. Electrocatalytic activity of electrospun carbon nitride-polyacrylonitrile nanofiber towards oxygen reduction reactions. *J Electroanal Chem* 2016;775:198–204. <https://doi.org/10.1016/j.jelechem.2016.05.051>.
- [1125] Guo X, Wu YQ. Characterizing molecular structure of water adsorbed by cellulose nanofiber film using *in-situ* micro-FTIR spectroscopy. *J Wood Chem Technol* 2017;37:383–92. <https://doi.org/10.1080/02773813.2017.1306078>.
- [1126] Y.W. Cheng, C.J.J.o.P.R. Wang. Solvent-induced crystallization of electrospun syndiotactic polystyrene nanofibers and its reversible desorption/sorption of volatile organic vapors. *J Polym Res*, 23 (2016), pp. 234, 10.1007/s10965-016-1130-2.
- [1127] Feng Q, Zeng Y, Xu P, Lin S, Feng C, Li X, et al. Tuning the electrical conductivity of amorphous carbon/reduced graphene oxide wrapped- Co_3O_4 ternary nanofibers for highly sensitive chemical sensors. *J Mater Chem A* 2019;7:27522–34. <https://doi.org/10.1039/c9ta11550a>.
- [1128] Kraka E, Quintano M, La Force HW, Antonio JJ, Freindorf M. The local vibrational mode theory and its place in the vibrational spectroscopy arena. *J Phys Chem A* 2022;126:8781–98. <https://doi.org/10.1021/acs.jpca.2c05962>.
- [1129] Menghrajani KS, Chen M, Dholakia K, Barnes WL. Probing vibrational strong coupling of molecules with wavelength-modulated Raman spectroscopy. *Adv Opt Mater* 2021;10:2102065. <https://doi.org/10.1002/adom.202102065>.
- [1130] Shi H, Wu T, Qiao H, Gao Z, Zhou J, Wu D, et al. Electrochemical surface-enhanced Raman spectroscopy for aniline adsorbed on silver electrodes: A DFT study of the anharmonic effects of amino wagging vibrational modes. *J Phys Chem C* 2023;127:12357–66. <https://doi.org/10.1021/acs.jpcc.3c02837>.
- [1131] Deng YL, Yeo BS. Characterization of electrocatalytic water splitting and CO_2 reduction reactions using *in-situ*/operando Raman spectroscopy. *ACS Catal* 2017;7:7873–89. <https://doi.org/10.1021/acscatal.7b02561>.
- [1132] Wen T, Li J, Zhang M, Jiao C, Pei S, Wang Z, et al. Discerning the vibrational nature of ReS_2 Raman modes using solid-angle-resolved Raman spectroscopy. *ACS Photonics* 2022;9:3557–62. <https://doi.org/10.1021/acsp Photonics.2c00865>.
- [1133] Cherevotan A, Raj J, Dheer L, Roy S, Sarkar S, Das R, et al. Operando generated ordered heterogeneous catalyst for the selective conversion of CO_2 to methanol. *ACS Energy Lett* 2021;6:509–16. <https://doi.org/10.1021/acsenrgylett.0c02614>.
- [1134] Qiu Z, Ma Y, Edvinsson T. *In operando* Raman investigation of Fe doping influence on catalytic NiO intermediates for enhanced overall water splitting. *Nano Energy* 2019;66:104118. <https://doi.org/10.1016/j.nanoen.2019.104118>.
- [1135] Zou Y, Wang S. An investigation of active sites for electrochemical CO_2 reduction reactions: From *in-situ* characterization to rational design. *Adv Sci* 2021;8:2003579. <https://doi.org/10.1002/advs.202003579>.
- [1136] Alnough W, Black R, Higgins D. Judicious selection, validation, and use of reference electrodes for *in-situ* and operando electrocatalysis studies. *Chem Catal* 2021;1:997–1013. <https://doi.org/10.1016/j.checat.2021.07.001>.
- [1137] Cao XY, Tan DX, Wulan B, Hui KS, Hui KN, Zhang JT. *In-situ* characterization for boosting electrocatalytic carbon dioxide reduction. *Small Methods* 2021;5:e2100700. <https://doi.org/10.1002/smt.202100700>.
- [1138] Cheng Q, Miao YP, Wild J, Min W, Yang Y. Emerging applications of stimulated Raman scattering microscopy in materials science. *Matter* 2021;4:1460–83. <https://doi.org/10.1016/j.matt.2021.02.013>.
- [1139] Gao J, Zhang H, Guo X, Luo J, Zakeeruddin SM, Ren D, et al. Selective C-C coupling in carbon dioxide electroreduction via efficient spillover of intermediates as supported by operando Raman spectroscopy. *J Am Chem Soc* 2019;141:18704–14. <https://doi.org/10.1021/jacs.9b07415>.
- [1140] S. Zhang, G. Gao, H. Zhu, L. Cai, X. Jiang, S. Lu, et al. *In-situ* interfacial engineering of nickel tungsten carbide Janus structures for highly efficient overall water splitting. *Sci Bull*, 65 (2020), pp. 640–650, 10.1016/j.scib.2020.02.003.
- [1141] Zhang S, Gao G, Hao J, Wang M, Zhu H, Lu S, et al. Low-electronegativity vanadium substitution in cobalt carbide induced enhanced electron transfer for efficient overall water splitting. *ACS Appl Mater Interfaces* 2019;11:43261–9. <https://doi.org/10.1021/acsaami.9b16390>.
- [1142] Hao J, Zhu H, Li Y, Liu P, Du M. Tuning the electronic structure of AuNi homogeneous solid-solution alloy with positively charged Ni center for highly selective electrochemical CO_2 reduction. *Chem Eng J* 2020;404:126523. <https://doi.org/10.1016/j.cej.2020.126523>.
- [1143] Wen Y, Zhu H, Hao J, Lu S, Du M. Metal-free boron and sulphur co-doped carbon nanofibers with optimized p-band centers for highly efficient nitrogen electroreduction to ammonia. *Appl Catal B Environ* 2021;292:120144. <https://doi.org/10.1016/j.apcatb.2021.120144>.
- [1144] Dixit MB, Park J-S, Kenesei P, Almer J, Hatzell KB. Status and prospect of *in-situ* and operando characterization of solid-state batteries. *Energy Environ Sci* 2021;14:4672–711. <https://doi.org/10.1039/d1ee00638j>.
- [1145] Li J, Gong J. Operando characterization techniques for electrocatalysis. *Energy Environ Sci* 2020;13:3748–79. <https://doi.org/10.1039/d0ee01706j>.

- [1146] Wu Z-Z, Gao F-Y, Gao M-R. Regulating the oxidation state of nanomaterials for electrocatalytic CO₂ reduction. *Energy Environ Sci* 2021;14:1121–39. <https://doi.org/10.1039/d0ee02747b>.
- [1147] Feng K, Wang YN, Guo M, Zhang JP, Li ZW, Deng TY, et al. In-situ/operando techniques to identify active sites for thermochemical conversion of CO₂ over heterogeneous catalysts. *J Energy Chem* 2021;62:153–71. <https://doi.org/10.1016/j.jchem.2021.03.054>.
- [1148] Liu X, Meng J, Zhu J, Huang M, Wen B, Guo R, et al. Comprehensive understandings into complete reconstruction of precatalysts: Synthesis, applications, and characterizations. *Adv Mater* 2021;33:e2007344. <https://doi.org/10.1002/adma.202007344>.
- [1149] Chen J, Wang L. Effects of the catalyst dynamic changes and influence of the reaction environment on the performance of electrochemical CO₂ reduction. *Adv Mater* 2021;34:e2103900. <https://doi.org/10.1002/adma.202103900>.
- [1150] Wang B, Chu S, Zheng L, Li X, Zhang J, Zhang F. Application of x-ray absorption spectroscopy in electrocatalytic water splitting and CO₂ reduction. *Small Sci* 2021;1:2100023. <https://doi.org/10.1002/smss.202100023>.
- [1151] Ismail ASM, Garcia-Torregrosa I, Vollenbroek JC, Folkertsma L, Bomer JG, Haarman T, et al. Detection of spontaneous feooh formation at the Hematite/Ni (Fe)OOH interface during photoelectrochemical water splitting by operando x-ray absorption spectroscopy. *Acs Catal* 2021;11:12324–35. <https://doi.org/10.1021/acscatal.1c02566>.
- [1152] Chen W, Wu B, Wang Y, Zhou W, Li Y, Liu T, et al. Deciphering the alternating synergy between interlayer Pt single-atom and NiFe layered double hydroxide for overall water splitting. *Energy Environ Sci* 2021;14:6428–40. <https://doi.org/10.1039/d1ee01395e>.
- [1153] Su H, Zhou W, Zhou W, Li Y, Zheng L, Zhang H, et al. In-situ spectroscopic observation of dynamic-coupling oxygen on atomically dispersed iridium electrocatalyst for acidic water oxidation. *Nat Commun* 2021;12:6118. <https://doi.org/10.1038/s41467-021-26416-3>.
- [1154] Zhang X, Truong-Phuoc L, Liao X, Tuci G, Fonda E, Papaefthymiou V, et al. An open gate for high-density metal ions in N-doped carbon networks: Powering Fe–N–C catalyst efficiency in the oxygen reduction reaction. *ACS Catal* 2021;11:8915–28. <https://doi.org/10.1021/acscatal.1c01638>.
- [1155] Yang Y, Wang Y, Xiong Y, Huang X, Shen LX, Huang R, et al. X-ray absorption spectroscopy of a synergistic Co–Mn oxide catalyst for the oxygen reduction reaction. *J Am Chem Soc* 2019;141:1463–6. <https://doi.org/10.1021/jacs.8b12243>.
- [1156] Han X, Zhang T, Chen W, Dong B, Meng G, Zheng L, et al. Mn–N4 oxygen reduction electrocatalyst: Operando investigation of active sites and high performance in Zinc–air battery. *Adv Energy Mater* 2020;11:2002753. <https://doi.org/10.1002/aenm.202002753>.
- [1157] Wu X, Guo Y, Sun Z, Xie F, Guan D, Dai J, et al. Fast operando spectroscopy tracking in-situ generation of rich defects in silver nanocrystals for highly selective electrochemical CO₂ reduction. *Nat Commun* 2021;12:660. <https://doi.org/10.1038/s41467-021-20960-8>.
- [1158] Divins NJ, Kordus D, Timoshenko J, Sinev I, Zegkinoglou I, Bergmann A, et al. Operando high-pressure investigation of size-controlled CuZn catalysts for the methanol synthesis reaction. *Nat Commun* 2021;12:1435. <https://doi.org/10.1038/s41467-021-21604-7>.
- [1159] Fan H, Qiu L, Fedorov A, Willinger M, Ding F, Huang X. Dynamic state and active structure of Ni–Co catalyst in carbon nanofiber growth revealed by in-situ transmission electron microscopy. *ACS Nano* 2021;15:17895–906. <https://doi.org/10.1021/acsnano.1c06189>.
- [1160] Huang Z, Yao Y, Pang Z, Yuan Y, Li T, He K, et al. Direct observation of the formation and stabilization of metallic nanoparticles on carbon supports. *Nat Commun* 2020;11. <https://doi.org/10.1038/s41467-020-20084-5>.
- [1161] Zhang J, Ishizuka K, Tomitori M, Arai T, Hongo K, Maezono R, et al. Peculiar atomic bond nature in platinum monatomic chains. *Nano Lett* 2021;21:3922–8. <https://doi.org/10.1021/acs.nanolett.1c00564>.
- [1162] Zeng L, Holmer J, Dhall R, Gammer C, Minor AM, Olsson E. Tuning hole mobility of individual p-doped GaAs nanowires by uniaxial tensile stress. *Nano Lett* 2021;21:3894–900. <https://doi.org/10.1021/acs.nanolett.1c00353>.
- [1163] Liu Z, Cao Z, He J, Zhang H, Ge Y, Chen B. Versatile printing of substantial liquid cells for efficiently imaging in-situ liquid-phase dynamics. *Nano Lett* 2021;21:6882–90. <https://doi.org/10.1021/acs.nanolett.1c01901>.
- [1164] K. El hajraoui, E. Robin, C. Zeiner, A. Lugstein, S. Kodjikian, J.-L. Rouvière, et al. In-situ transmission electron microscopy analysis of copper–germanium nanowire solid-state reaction. *Nano Lett*, 19 (2019), pp. 8365–8371, 10.1021/acs.nanolett.9b01797.
- [1165] Zhu M, Yin K, Wen Y, Song S, Xiong Y, Dai Y, et al. Combining in-situ TEM observations and theoretical calculation for revealing the thermal stability of CeO₂ nanoflowers. *Nano Res* 2022;15:1319–26. <https://doi.org/10.1007/s12274-021-3659-6>.
- [1166] Wang L, Yan J, Xu Z, Wang W, Wen J, Bai X. Rate mechanism of vanadium oxide coated tin dioxide nanowire electrode for lithium ion battery. *Nano Energy* 2017;42:294–9. <https://doi.org/10.1016/j.nanoen.2017.10.059>.
- [1167] Shang T, Wen Y, Xiao D, Gu L, Hu YS, Li H. Atomic-scale monitoring of electrode materials in lithium-ion batteries using in-situ transmission electron microscopy. *Adv Energy Mater* 2017;7:1700709. <https://doi.org/10.1002/aenm.201700709>.
- [1168] Wu Y, Hu S, Xu R, Wang J, Peng Z, Zhang Q, et al. Boosting potassium-ion battery performance by encapsulating red phosphorus in free-standing nitrogen-doped porous hollow carbon nanofibers. *Nano Lett* 2019;19:1351–8. <https://doi.org/10.1021/acs.nanolett.8b04957>.
- [1169] Yusop MZM, Ghosh P, Yaakob Y, Kalita G, Sasase M, Hayashi Y, et al. TEM observation of Fe-included carbon nanofiber: Evolution of structural and electrical properties in field emission process. *ACS Nano* 2012;6:9567–73. <https://doi.org/10.1021/nn302889e>.
- [1170] Boles ST, Sedlmayr A, Kraft O, Mönig R. In-situ cycling and mechanical testing of silicon nanowire anodes for lithium-ion battery applications. *Appl Phys Lett* 2012;100:243901. <https://doi.org/10.1063/1.4729145>.
- [1171] Yu Z, Qin B, Ma Z, Huang J, Li S, Zhao H, et al. Superelastic hard carbon nanofiber aerogels. *Adv Mater* 2019;31:e1900651. <https://doi.org/10.1002/adma.201900651>.
- [1172] Zhao X, Hang C, Wen X, Liu M, Zhang H, Yang F, et al. Ultrahigh-sensitive finlike double-sided e-skin for force direction detection. *ACS Appl Mater Interfaces* 2020;12:14136–44. <https://doi.org/10.1021/acsaami.9b23110>.
- [1173] Li X, Zhao L, Li P, Zhang Q, Wang M. In-situ electron microscopy observation of electrochemical sodium plating and stripping dynamics on carbon nanofiber current collectors. *Nano Energy* 2017;42:122–8. <https://doi.org/10.1016/j.nanoen.2017.10.050>.
- [1174] Jang HF, Robertson AG, Seth RS. Transverse dimensions of wood pulp fibres by confocal laser scanning microscopy and image analysis. *J Mater Sci* 1992;27:6391–400. <https://doi.org/10.1007/bf00576290>.
- [1175] Li X, Wang W, Dou J, Gao J, Chen S, Quan X, et al. Dynamic adsorption of ciprofloxacin on carbon nanofibers: Quantitative measurement by in-situ fluorescence. *J Water Process Eng* 2016;9:E14–20. <https://doi.org/10.1016/j.jwpe.2014.12.006>.
- [1176] Shu D, Xi P, Xia L, Wang X, Cheng B. Structure and properties of PET nano-porous luminescence fibers for fluorescence-indicating to acid gases. *Macromol Mater Eng* 2019;304:1900467. <https://doi.org/10.1002/mame.201900467>.
- [1177] Moon S, Lee K. Needleless and syringeless electrospinning for mass production. In: Horzum N, Demir MM, Muñoz-Espí R, Crespy D, editors. *Green electrospinning*. Berlin, Boston: De Gruyter; 2019. p. 217–38.
- [1178] Brown TD, Dalton PD, Hutmacher DW. Direct writing by way of melt electrospinning. *Adv Mater* 2011;23:5651. <https://doi.org/10.1002/adma.201103482>.
- [1179] Omer S, Forgach L, Zelko R, Sebe I. Scale-up of electrospinning: Market overview of products and devices for pharmaceutical and biomedical purposes. *Pharmaceutics* 2021;13:286. <https://doi.org/10.3390/pharmaceutics13020286>.
- [1180] Doğan YK, Demiral A, Baykara T. Single-needle electrospinning of PVA hollow nanofibers for core-shell structures. *SN Appl Sci* 2019;1:415. <https://doi.org/10.1007/s42452-019-0446-z>.
- [1181] Keirouz A, Wang Z, Reddy VS, Nagy ZK, Vass P, Buzgo M, et al. The history of electrospinning: Past, present, and future developments. *Adv Mater Technol* 2023;8:22021723. <https://doi.org/10.1002/admt.202021723>.
- [1182] Nurfaizey AH, Stanger J, Tucker N, Buunk N, Wallace A, Staiger MP. Manipulation of electrospun fibres in flight: The principle of superposition of electric fields as a control method. *J Mater Sci* 2011;47:1156–63. <https://doi.org/10.1007/s10853-011-5847-3>.
- [1183] Yu H, Li T, Chen B, Wu Y, Li Y. Preparation of aligned Eu(DBM)₃phen/PS fibers by electrospinning and their luminescence properties. *J Colloid Interface Sci* 2013;400:175–80. <https://doi.org/10.1016/j.jcis.2013.03.017>.
- [1184] Zhu Z, Wu P, Wang Z, Xu G, Wang H, Chen X, et al. Optimization of electric field uniformity of multi-needle electrospinning nozzle. *AIP Adv* 2019;9:105104. <https://doi.org/10.1063/1.5111936>.

- [1185] Kim G, Cho Y-S, Kim WD. Stability analysis for multi-jets electrospinning process modified with a cylindrical electrode. *Eur Polym J* 2006;42:2031–8. <https://doi.org/10.1016/j.eurpolymj.2006.01.026>.
- [1186] Yang Y, Jia Z, Li Q, Hou L, Liu J, Wang L, et al. A shield ring enhanced equilateral hexagon distributed multi-needle electrospinning spinneret. *IEEE T Dielect El In* 2010;17:1592–601. <https://doi.org/10.1109/tdel.2010.5595562>.
- [1187] Xie S, Zeng YC. Effects of electric field on multineedle electrospinning: Experiment and simulation study. *Ind Eng Chem Res* 2012;51:5336–45. <https://doi.org/10.1021/ie2020763>.
- [1188] Wu Y, Li Z, Fan J, Wang L, Zhang P, Liu J, et al. Improved fiber uniformity and jet number in multi-spinneret electrospinning via auxiliary electrode. *Fiber Polym* 2019;20:1172–9. <https://doi.org/10.1007/s12221-019-8859-2>.
- [1189] Beaudoin EJ, Kubaski MM, Samara M, Zednik RJ, Demarquette NR. Scaled-up multi-needle electrospinning process using parallel plate auxiliary electrodes. *Nanomaterials* (Basel) 2022;12:1356. <https://doi.org/10.3390/nano12081356>.
- [1190] Tomaszewski W, Szadkowski M. Investigation of electrospinning with the use of a multi-jet electrospinning head. *Fibres Text East Eur* 2005;13:22.
- [1191] Tian L, Zhao C, Li J, Pan Z. Multi-needle, electrospun, nanofiber filaments: Effects of the needle arrangement on the nanofiber alignment degree and electrostatic field distribution. *Text Res J* 2014;85:621–31. <https://doi.org/10.1177/0040517514549990>.
- [1192] Kim IG, Lee JH, Unnithan AR, Park CH, Kim CS. A comprehensive electric field analysis of cylinder-type multi-nozzle electrospinning system for mass production of nanofibers. *J Ind Eng Chem* 2015;31:251–6. <https://doi.org/10.1016/j.jiec.2015.06.033>.
- [1193] Zhu Z, Xu G, Chen R, Wang Z, Huang J, Chen X, et al. Uniform electric field enabled multi-needles electrospinning head based on trapezoid arrangement. *AIP Adv* 2018;8:085126. <https://doi.org/10.1063/1.5026908>.
- [1194] Liu YB, Guo LL. Homogeneous field intensity control during multi-needle electrospinning via finite element analysis and simulation. *J Nanosci Nanotechnol* 2013;13:843–7. <https://doi.org/10.1166/jnn.2013.6017>.
- [1195] Zhou F-L, Gong R-H, Porat I. Three-jet electrospinning using a flat spinneret. *J Mater Sci* 2009;44:5501–8. <https://doi.org/10.1007/s10853-009-3768-1>.
- [1196] Zheng J, Zhou C, Zhang Z, Pan Y, Kang G, Jiang J, et al. Highly efficient air-assisted multi-jet electrospinning with curved arranged spinnerets. *AIP Adv* 2020;10:025307. <https://doi.org/10.1063/1.5130531>.
- [1197] Jiang J, Zheng G, Wang X, Li W, Kang G, Chen H, et al. Arced multi-nozzle electrospinning spinneret for high-throughput production of nanofibers. *Micromachines* 2019;11:27. <https://doi.org/10.3390/mi11010027>.
- [1198] Pu C, He J, Cui S, Gao W. Fabrication of nanofibers by a modified air-jet electrospinning method. *Iran Polym J* 2013;23:13–25. <https://doi.org/10.1007/s13726-013-0195-6>.
- [1199] Phan D-N, Lee H, Huang B, Mukai Y, Kim I-S. Fabrication of electrospun chitosan/cellulose nanofibers having adsorption property with enhanced mechanical property. *Cellul* 2018;26:1781–93. <https://doi.org/10.1007/s10570-018-2169-5>.
- [1200] Islam MS, Ang BC, Andriyana A, Afifi AM. A review on fabrication of nanofibers via electrospinning and their applications. *SN Appl Sci* 2019;1:1248. <https://doi.org/10.1007/s42452-019-1288-4>.
- [1201] Dosunmu OO, Chase GG, Kataphinan W, Reneker DH. Electrospinning of polymer nanofibers from multiple jets on a porous tubular surface. *Nanotechnology* 2006;17:1123–7. <https://doi.org/10.1088/0957-4484/17/4/046>.
- [1202] Forward KM, Rutledge GC. Free surface electrospinning from a wire electrode. *Chem Eng J* 2012;183:492–503. <https://doi.org/10.1016/j.cej.2011.12.045>.
- [1203] Fujii T, Mizutani Y, Nakane K. Melt-electrospun fibers obtained from polypropylene/poly(ethylene-co-vinyl alcohol)/polypropylene three-layer films. *J Appl Polym Sci* 2018;135:46393. <https://doi.org/10.1002/app.46393>.
- [1204] Chen M, Zhang Y, Chen X, Yang W, Li H, Yousefzadeh M, et al. Polymer melt differential electrospinning from a linear slot spinneret. *J Appl Polym Sci* 2020;137:48922. <https://doi.org/10.1002/app.48922>.
- [1205] He H-J, Liu C-K, Molnar K. A novel needleless electrospinning system using a moving conventional yarn as the spinneret. *Fiber Polym* 2018;19:1472–8. <https://doi.org/10.1007/s12221-018-8183-2>.
- [1206] Wei L, Liu C, Mao X, Dong J, Fan W, Zhi C, et al. Multiple-jet needleless electrospinning approach via a linear flume spinneret. *Polymers* (Basel) 2019;11:2052. <https://doi.org/10.3390/polym11122052>.
- [1207] Ali U, Zhou Y, Wang X, Lin T. Direct electrospinning of highly twisted, continuous nanofiber yarns. *J Text Inst* 2012;103:80–8. <https://doi.org/10.1080/00405000.2011.552254>.
- [1208] Lu B, Wang Y, Liu Y, Duan H, Zhou J, Zhang Z, et al. Superhigh-throughput needleless electrospinning using a rotary cone as spinneret. *Small* 2010;6:1612–6. <https://doi.org/10.1002/sml.201000454>.
- [1209] Wang X, Lin T, Wang X. Scaling up the production rate of nanofibers by needleless electrospinning from multiple ring. *Fiber Polym* 2014;15:961–5. <https://doi.org/10.1007/s12221-014-0961-x>.
- [1210] Ali U, Niu H, Aslam S, Jabbar A, Rajput AW, Lin T. Needleless electrospinning using sprocket wheel disk spinneret. *J Mater Sci* 2017;52:7567–77. <https://doi.org/10.1007/s10853-017-0989-6>.
- [1211] Mingjun C, Youchen Z, Haoyi L, Xiangnan L, Yumei D, Bubakir MM, et al. An example of industrialization of melt electrospinning: Polymer melt differential electrospinning. *Adv Ind Eng Polym Res* 2019;2:110–5. <https://doi.org/10.1016/j.aiepr.2019.06.002>.
- [1212] Chen X, Zhang Y, Liang J, Li H, Chen M, Cheng L, et al. String electrospinning based on the standing wave vibration. *J Mater Sci* 2021;56:9518–31. <https://doi.org/10.1007/s10853-021-05845-x>.
- [1213] Wei L, Sun R, Liu C, Xiong J, Qin X. Mass production of nanofibers from needleless electrospinning by a novel annular spinneret. *Mater Design* 2019;179:107885. <https://doi.org/10.1016/j.matdes.2019.107885>.
- [1214] 8] H. Xiaoping, W. Dezhi, Z. Yongyang, S. Daoheng. Needleless electrospinning of multiple nanofibers. 7th IEEE International Conference on Nanotechnology - IEEE-NANO 2007, Proceedings, art. no. 4601311, 2007, pp. 823–826, 10.1109/NANO.2007.4601311.
- [1215] Tang S, Zeng Y, Wang X. Splashing needleless electrospinning of nanofibers. *Polym Eng Sci* 2010;50:2252–7. <https://doi.org/10.1002/pen.21767>.
- [1216] Yang R, He J, Xu L, Yu J. Bubble-electrospinning for fabricating nanofibers. *Polymer* 2009;50:5846–50. <https://doi.org/10.1016/j.polymer.2009.10.021>.
- [1217] Jiang G, Zhang S, Qin X. High throughput of quality nanofibers via one stepped pyramid-shaped spinneret. *Mater Lett* 2013;106:56–8. <https://doi.org/10.1016/j.matlet.2013.04.084>.
- [1218] Wang X, Niu H, Lin T, Wang X. Needleless electrospinning of nanofibers with a conical wire coil. *Polym Eng Sci* 2009;49:1582–6. <https://doi.org/10.1002/pen.21377>.
- [1219] Zheng G, Jiang J, Wang X, Li W, Zhong W, Guo S. Self-cleaning threaded rod spinneret for high-efficiency needleless electrospinning. *Appl Phys A* 2018;124:473. <https://doi.org/10.1007/s00339-018-1892-y>.
- [1220] Niu H, Zhou H, Yan G, Wang H, Fu S, Zhao X, et al. Enhancement of coil electrospinning using two-level coil structure. *Ind Eng Chem Res* 2018;57:15473–8. <https://doi.org/10.1021/acs.iecr.8b04145>.
- [1221] 7] Jin XZ.; Peters R.; Pearson E. Continuous wire drive system for needleless electrospinning apparatus. US Patent. 20200378033. 2020.
- [1222] Thoppay NM, Bochinski JR, Clarke LI, Gorga RE. Unconfined fluid electrospun into high quality nanofibers from a plate edge. *Polymer* 2010;51:4928–36. <https://doi.org/10.1016/j.polymer.2010.07.046>.
- [1223] Forward KM, Flores A, Rutledge GC. Production of core/shell fibers by electrospinning from a free surface. *Chem Eng Sci* 2013;104:250–9. <https://doi.org/10.1016/j.ces.2013.09.002>.
- [1224] 0] Forward, KM.; Rutledge GC. Formation of core-shell fibers and particles by free surface electrospinning. US Patent. 20150308015. 2015.
- [1225] Prahasiti G, Zulfi A, Munir MM. Needleless electrospinning system with wire spinneret: An alternative way to control morphology, size, and productivity of nanofibers. *Nano Express* 2020;1:010046. <https://doi.org/10.1088/2632-959X/ab976a>.
- [1226] J.-C. Park. Electric spinning apparatus for mass-production of nano-fiber. Finetex Ene, Inc., Seoul, KR (2011), United States Patent 7980838.
- [1227] Kim, H.; Park, J. Bottom-up electrospinning devices, and nanofibers prepared by using the same. US Patent. 20080233284. 2008.
- [1228] Kim, H. Electronic spinning apparatus, and a process of preparing nonwoven fabric using the same. US Patent. 7332050. 2008.
- [1229] Jin, X.; Peters, R.; Pearson, E. Apparatus for electrospinning liquid polymer into nanoscale or submicron scale fibers. US Patent. 20190345638. 2019.

- [1230] Li H, Chen H, Zhong X, Wu W, Ding Y, Yang W. Interjet distance in needleless melt differential electrospinning with umbellate nozzles. *J Appl Polym Sci* 2014; 131:40515. <https://doi.org/10.1002/app.40515>.
- [1231] Xiong J, Liu Y, Li A, Wei L, Wang L, Qin X, et al. Mass production of high-quality nanofibers via constructing pre-Taylor cones with high curvature on needleless electrospinning. *Mater Design* 2021;197:109247. <https://doi.org/10.1016/j.matdes.2020.109247>.
- [1232] Kara Y, He H, Molnár K. Shear-aided high-throughput electrospinning: A needleless method with enhanced jet formation. *J Appl Polym Sci* 2020;137:49104. <https://doi.org/10.1002/app.49104>.
- [1233] Yan G, Niu H, Shao H, Zhao X, Zhou H, Lin T. Curved convex slot: An effective needleless electrospinning spinneret. *J Mater Sci* 2017;52:11749–58. <https://doi.org/10.1007/s10853-017-1315-z>.
- [1234] Park, J. Method for producing nano-fiber with uniformity. US Patent. 20080277836. 2008.
- [1235] H. Niu, T. Lin, X. Wang. Needleless electrospinning. I. A comparison of cylinder and disk nozzles. *J Appl Polym Sci*, 114 (2009), pp. 3524–3530, 10.1002/app.30891.
- [1236] Chen H, Li H, Ma X, He W, Tan J, Yang W. Large scaled fabrication of microfibers by air-suction assisted needleless melt electrospinning. *Fiber Polym* 2016; 17:576–81. <https://doi.org/10.1007/s12221-016-5915-z>.
- [1237] Niu H, Wang X, Lin T. Needleless electrospinning: Influences of fibre generator geometry. *J Text* 2012;1(103):787–94. <https://doi.org/10.1080/00405000.2011.608498>.
- [1238] Liu Y, He JH. Bubble electrospinning for mass production of nanofibers. *Int J Nonlin Sci Num* 2007;8:393–6. <https://doi.org/10.1515/ijnsns.2007.8.3.393>.
- [1239] 5] Lin, T.; Wang, X.; Wang, X.; Niu, H. Electrostatic spinning assembly. 2009, US Patent. 20110311671. 2011.
- [1240] Liu Z, Chen R, He J. Active generation of multiple jets for producing nanofibres with high quality and high throughput. *Mater Design* 2016;94:496–501. <https://doi.org/10.1016/j.matdes.2016.01.075>.
- [1241] Thoppey NM, Gorga RE, Bochinski JR, Clarke LL. Effect of solution parameters on spontaneous jet formation and throughput in edge electrospinning from a fluid-filled bowl. *Macromolecules* 2012;45:6527–37. <https://doi.org/10.1021/ma301207t>.
- [1242] Thoppey NM, Bochinski JR, Clarke LL, Gorga RE. Edge electrospinning for high throughput production of quality nanofibers. *Nanotechnology* 2011;22: 345301. <https://doi.org/10.1088/0957-4484/22/34/345301>.
- [1243] Shimada N, Tsutsumi H, Nakane K, Ogihara T, Ogata N. Poly(ethylene-co-vinyl alcohol) and nylon 6/12 nanofibers produced by melt electrospinning system equipped with a line-like laser beam melting device. *J Appl Polym Sci* 2010;116:2998–3004. <https://doi.org/10.1002/app.31837>.
- [1244] Wei L, Yu H, Sun R, Liu C, Chen M, Liu H, et al. Experimental investigation of process parameters for the filtration property of nanofiber membrane fabricated by needleless electrospinning apparatus. *J Ind Text* 2021;50:1528–41. <https://doi.org/10.1177/1528083720901357>.
- [1245] Robinson TM, Hutmacher DW, Dalton PD. The next frontier in melt electrospinning: Taming the jet. *Adv Funct Mater* 2019;29:1904664. <https://doi.org/10.1002/adfm.201904664>.
- [1246] Dalton PD. Melt electrowriting with additive manufacturing principles. *Curr Opin Biomed Eng* 2017;2:49–57. <https://doi.org/10.1016/j.cobme.2017.05.007>.
- [1247] Kameoka J, Orth R, Yang Y, Czaplewski D, Mathers R, Coates GW, et al. A scanning tip electrospinning source for deposition of oriented nanofibers. *Nanotechnology* 2003;14:1124–9. <https://doi.org/10.1088/0957-4484/14/10/310>.
- [1248] Nazemi MM, Khodabandeh A, Hadjizadeh A. Near-field electrospinning: Crucial parameters, challenges, and applications. *ACS Appl Bio Mater* 2022;5: 394–412. <https://doi.org/10.1021/acsabm.1c00944>.
- [1249] Bisht GS, Canton G, Mirsepassi A, Kuinsky L, Oh S, Dunn-Rankin D, et al. Controlled continuous patterning of polymeric nanofibers on three-dimensional substrates using low-voltage near-field electrospinning. *Nano Lett* 2011;11:1831–7. <https://doi.org/10.1021/nl2006164>.
- [1250] Hochleitner G, Youssef A, Hrynevich A, Haigh JN, Jungst T, Groll J, et al. Fibre pulsing during melt electrospinning writing. *BioNanoMaterials* 2016;17: 159–71. <https://doi.org/10.1515/bnm-2015-0022>.
- [1251] Wunner FM, Mieszczynek P, Bas O, Eggert S, Maartens J, Dalton PD, et al. Printomics: The high-throughput analysis of printing parameters applied to melt electrowriting. *Biofabrication* 2019;11:025004. <https://doi.org/10.1088/1758-5090/aaf41>.
- [1252] Han W, Minhao L, Xin C, Junwei Z, Xindu C, Ziming Z. Study of deposition characteristics of multi-nozzle near-field electrospinning in electric field crossover interference conditions. *AIP Adv* 2015;5:041302. <https://doi.org/10.1063/1.4902173>.
- [1253] Huang S, Chen X, Wang Z, Zeng J, Fang F, Wang H. An investigation on multi-nozzle near field electrospinning: Experimentation and simulation. *Key Eng Mater* 2016;679:63–6. <https://doi.org/10.4028/www.scientific.net/KEM.679.63>.
- [1254] Wang Z, Chen X, Huang S, Fang F, Wang H. Research on deposition characteristics of the double-nozzle in near-field electrospinning. *Key Eng Mater* 2016; 679:59–62. <https://doi.org/10.4028/www.scientific.net/KEM.679.59>.
- [1255] Jungst T, Pennings I, Schmitz M, Rosenberg AJWP, Groll J, Gawlitta D. Heterotypic scaffold design orchestrates primary cell organization and phenotypes in cocultured small diameter vascular grafts. *Adv Funct Mater* 2019;29:1905987. <https://doi.org/10.1002/adfm.201905987>.
- [1256] Jorgensen ML, Muller C, Sikkers M, Nadzieja M, Zhang Z, Su Y, et al. A melt-electrowritten filter for capture and culture of circulating colon cancer cells. *Mater Today Bio* 2020;6:100052. <https://doi.org/10.1016/j.mtbio.2020.100052>.
- [1257] Zhou F-L, Hubbard PL, Eichhorn SJ, Parker GJM. Jet deposition in near-field electrospinning of patterned polycaprolactone and sugar-polycaprolactone core-shell fibres. *Polymer* 2011;52:3603–10. <https://doi.org/10.1016/j.polymer.2011.06.002>.
- [1258] Ahmad Z, Zhang HB, Farook U, Edirisinghe M, Stride E, Colombo P. Generation of multilayered structures for biomedical applications using a novel tri-needle coaxial device and electrohydrodynamic flow. *J R Soc Interface* 2008;5:1255–61. <https://doi.org/10.1098/rsif.2008.0247>.
- [1259] Diloksumpan P, de Ruijter M, Castilho M, Gbureck U, Vermonden T, van Weeren PR, et al. Combining multi-scale 3D printing technologies to engineer reinforced hydrogel-ceramic interfaces. *Biofabrication* 2020;12:025014. <https://doi.org/10.1088/1758-5090/ab69d9>.
- [1260] King 3rd WE, Bowlin GL. Near-field electrospinning and melt electrowriting of biomedical polymers-progress and limitations. *Polymers (Basel)* 2021;13:1097. <https://doi.org/10.3390/polym13071097>.
- [1261] Kade JC, Dalton PD. Polymers for melt electrowriting. *Adv Healthc Mater* 2021;10:e2001232. <https://doi.org/10.1002/adhm.202001232>.
- [1262] Ray SS, Soni R, Huyen DTT, Ravi S, Myung S, Lee CY, et al. Chemical engineering of electrospun nanofibrous-based three-layered nonwoven polymeric protective mask for enhanced performance. *J Appl Polym Sci* 2023;140:e53584. <https://doi.org/10.1002/app.53584>.
- [1263] Peng Z, Shi J, Xiao X, Hong Y, Li X, Zhang W, et al. Self-charging electrostatic face masks leveraging triboelectrification for prolonged air filtration. *Nat Commun* 2022;13:7835. <https://doi.org/10.1038/s41467-022-35521-w>.
- [1264] Natsathaporn P, Herwig G, Altenried S, Ren Q, Rossi RM, Crespy D, et al. Functional fiber membranes with antibacterial properties for face masks. *Adv Fiber Mater* 2023;5:1519–33. <https://doi.org/10.1007/s42765-023-00291-7>.
- [1265] China: polyimide nanofiber membranes, www.hinanofiber.com.
- [1266] Mao N, Qin X, Wang L, Yu J. Electrospun nanofiber/cotton composite yarn with enhanced moisture management ability. *Text Res J* 2021;91:1467–77. <https://doi.org/10.1177/0040517520984978>.
- [1267] Huang Y, Yang P, Yang F, Chang C. Self-supported nanoporous lysozyme/nanocellulose membranes for multifunctional wastewater purification. *J Membr Sci* 2021;635:119537. <https://doi.org/10.1016/j.memsci.2021.119537>.
- [1268] Cotrim M, Oréface R. Tailoring polycaprolactone/silk electrospun nanofiber yarns by varying compositional and processing parameters. *Polym Bull* 2023;81: 593–610. <https://doi.org/10.1007/s00289-023-04735-3>.
- [1269] Wu SY, Zabihi F, Yeap RY, Darestani MRY, Bahi A, Wan ZY, et al. Cesium lead halide perovskite decorated polyvinylidene fluoride nanofibers for wearable piezoelectric nanogenerator yarns. *ACS Nano* 2023;17:1022–35. <https://doi.org/10.1021/acsnano.2c07320>.
- [1270] Dabirian F, Hosseini Y, Ravandi SAH. Manipulation of the electric field of electrospinning system to produce polyacrylonitrile nanofiber yarn. *J Text* 2007;1 (98):237–41. <https://doi.org/10.1080/00405000701463979>.
- [1271] Teo WE, Gopal R, Ramaseshan R, Fujihara K, Ramakrishna S. A dynamic liquid support system for continuous electrospun yarn fabrication. *Polymer* 2007;48: 3400–5. <https://doi.org/10.1016/j.polymer.2007.04.044>.

- [1272] Wu SH, Liu PH, Zhang Y, Zhang HN, Qin XH. Flexible and conductive nanofiber-structured single yarn sensor for smart wearable devices. *Sensor Actuat B Chem* 2017;252:697–705. <https://doi.org/10.1016/j.snb.2017.06.062>.
- [1273] Feng Y, Xiong T, Jiang S, Liu S, Hou H. Mechanical properties and chemical resistance of electrospun polytetrafluoroethylene fibres. *RSC Adv* 2016;6:24250–6. <https://doi.org/10.1039/c5ra27676d>.
- [1274] Li Y, Zhou B, Zheng G, Liu X, Li T, Yan C, et al. Continuously prepared highly conductive and stretchable SWNT/MWNT synergistically composited electrospun thermoplastic polyurethane yarns for wearable sensing. *J Mater Chem C* 2018;6:2258–69. <https://doi.org/10.1039/c7tc04959e>.
- [1275] Wang J, Li Q, Liu D, Chen C, Chen Z, Hao J, et al. High temperature thermally conductive nanocomposite textile by “green” electrospinning. *Nanoscale* 2018;10:16868–72. <https://doi.org/10.1039/c8nr05167d>.
- [1276] Li Q, Balilonda A, Ali A, Jose R, Zabihi F, Yang S, et al. Flexible solar yarns with 15.7% power conversion efficiency, based on electrospun perovskite composite nanofibers. *Sol RRL* 2020;4:2000269. <https://doi.org/10.1002/solr.202000269>.
- [1277] Yan T, Zhou H, Niu H, Shao H, Wang H, Pan Z, et al. Highly sensitive detection of subtle movement using a flexible strain sensor from helically wrapped carbon yarns. *J Mater Chem C* 2019;7:10049–58. <https://doi.org/10.1039/c9tc03065d>.
- [1278] Yang Y, Quan Z, Zhang H, Qin X, Wang R, Yu J. Investigation on the processability, structure and properties of micro-/nano-fiber composite yarns produced by trans-scale spinning. *J Ind Text* 2022;51:5409s–s5426. <https://doi.org/10.1177/1528083720941177>.
- [1279] Qiu Q, Chen S, Li Y, Yang Y, Zhang H, Quan Z, et al. Functional nanofibers embedded into textiles for durable antibacterial properties. *Chem Eng J* 2020;384:123241. <https://doi.org/10.1016/j.cej.2019.123241>.
- [1280] Ma H, Hsiao BS. Current advances on nanofiber membranes for water purification applications. *Filtering Media by Electrospinning: Next Generation Membranes for Separation Applications* 2018:25–46. https://doi.org/10.1007/978-3-319-78163-1_2.
- [1281] Qin Z, Yan G, Zhang X, Yang Z, Li H, Wang J. Finite element method assisted design of needleless electrospinning systems for mass production of polymer nanofibers. *Chem Eng Sci* 2022;259:117817. <https://doi.org/10.1016/j.ces.2022.117817>.
- [1282] Koski A, Yim K, Shivkumar S. Effect of molecular weight on fibrous PVA produced by electrospinning. *Mater Lett* 2004;58:493–7. [https://doi.org/10.1016/S0167-577X\(03\)00532-9](https://doi.org/10.1016/S0167-577X(03)00532-9).
- [1283] Brown TD, Dalton PD, Huttmacher DW. Melt electrospinning today: An opportune time for an emerging polymer process. *Prog Polym Sci* 2016;56:116–66. <https://doi.org/10.1016/j.progpolymsci.2016.01.001>.
- [1284] Xin R, Ma HY, Venkateswaran S, Hsiao BS. Electrospun nanofibrous adsorption membranes for wastewater treatment: Mechanical strength enhancement. *Chem Res Chin Univ* 2021;37:355–65. <https://doi.org/10.1007/s40242-021-1095-5>.
- [1285] Li H, Zhu C, Xue J, Ke Q, Xia Y. Enhancing the mechanical properties of electrospun nanofiber mats through controllable welding at the cross points. *Macromol Rapid Commun* 2017;38:1600723. <https://doi.org/10.1002/marc.201600723>.
- [1286] Su CL, Lu C, Horseman T, Cao HB, Duan F, Li L, et al. Dilute solvent welding: A quick and scalable approach for enhancing the mechanical properties and narrowing the pore size distribution of electrospun nanofibrous membrane. *J Membr Sci* 2020;595:117548. <https://doi.org/10.1016/j.memsci.2019.117548>.
- [1287] Liu XX, Ma HY, Hsiao BS. Interpenetrating nanofibrous composite membranes for water purification. *ACS Appl Nano Mater* 2019;2:3606–14. <https://doi.org/10.1021/acsanm.9b00565>.
- [1288] Almetwally AA, El-Sakhawy M, Elshakankery M, Kasem MH. Technology of nano-fibers: Production techniques and properties - critical review. *J Text Assoc* 2017;78:5–14.
- [1289] Ma PX, Zhang R. Synthetic nano-scale fibrous extracellular matrix. *J Biomed Mater Res* 1999;46:60–72. [https://doi.org/10.1002/\(SICI\)1097-4636\(199907\)46:1<60::AID-JBM7>3.0.CO;2-H](https://doi.org/10.1002/(SICI)1097-4636(199907)46:1<60::AID-JBM7>3.0.CO;2-H).
- [1290] H. Yang, Yan, Y. Liu, F. Zhang, R. Zhang, Y. Yan, et al. A simple melt impregnation method to synthesize ordered mesoporous carbon and carbon nanofiber bundles with graphitized structure from pitches. *J Phys Chem B*, 108 (2004), pp. 17320–17328, 10.1021/jp046948n.
- [1291] Chen P, Cao Y, He S, Tian X, Cao Z. Improvement of mechanical and thermal properties of polylactic acid electrospun films by incorporating L-lactide functionalized cellulose nanocrystals. *Fuller Nanotub Car N* 2023;31:395–403. <https://doi.org/10.1080/1536383x.2023.2168267>.
- [1292] Guo H, Wang F, Luo H, Li Y, Lou Z, Ji Y, et al. Flexible TaC/C electrospun non-woven fabrics with multiple spatial-scale conductive frameworks for efficient electromagnetic interference shielding. *Compos Part A Appl Sci Manuf* 2021;151:106662. <https://doi.org/10.1016/j.compositesa.2021.106662>.
- [1293] Xu G, Wang K, Zhong Z, Chen C-S, Webley PA, Wang H. SiC nanofiber reinforced porous ceramic hollow fiber membranes. *J Mater Chem A* 2014;2:5841–6. <https://doi.org/10.1039/c3ta15348g>.
- [1294] Wu J, Qin X, Miao C, He Y-B, Liang G, Zhou D, et al. A honeycomb-cobweb inspired hierarchical core-shell structure design for electrospun silicon/carbon fibers as lithium-ion battery anodes. *Carbon* 2016;98:582–91. <https://doi.org/10.1016/j.carbon.2015.11.048>.
- [1295] Nagiah N, Murdock CJ, Bhattacharjee M, Nair L, Laurencin CT. Development of tripolymeric triaxial electrospun fibrous matrices for dual drug delivery applications. *Sci Rep* 2020;10:609. <https://doi.org/10.1038/s41598-020-57412-0>.
- [1296] Wang M, Li D, Li J, Li S, Chen Z, Yu D-G, et al. Electrospun janus zein-PVP nanofibers provide a two-stage controlled release of poorly water-soluble drugs. *Mater Design* 2020;196:109075. <https://doi.org/10.1016/j.matdes.2020.109075>.
- [1297] Kim BG, Kang DW, Park G, Park SH, Lee SM, Choi JW. Electrospun Li-confinable hollow carbon fibers for highly stable Li-metal batteries. *Chem Eng J* 2021;422:130017. <https://doi.org/10.1016/j.cej.2021.130017>.
- [1298] Bai Q, Shen F, Li S, Liu J, Dong L, Wang Z, et al. Cobalt@nitrogen-doped porous carbon fiber derived from the electrospun fiber of bimetal-organic framework for highly active oxygen reduction. *Small Methods* 2018;2:1800049. <https://doi.org/10.1002/smt.201800049>.
- [1299] Tokarska M. Characterization of electro-conductive textile materials by its biaxial anisotropy coefficient and resistivity. *J Mater Sci Mater Electron* 2019;30:4093–103. <https://doi.org/10.1007/s10854-019-00699-1>.
- [1300] Zhi CW, Shi S, Si YF, Fei B, Huang HT, Hu JL. Recent progress of wearable piezoelectric pressure sensors based on nanofibers, yarns, and their fabrics via electrospinning. *Adv Mater* 2023;35:2201161. <https://doi.org/10.1002/admt.202201161>.
- [1301] Dong K, Wang Y, Deng J, Dai Y, Zhang S, Zou H, et al. A highly stretchable and washable all-yarn-based self-charging knitting power textile composed of fiber triboelectric nanogenerators and supercapacitors. *ACS Nano* 2017;11:9490–9. <https://doi.org/10.1021/acs.nano.7b05317>.
- [1302] Liu L, Xu W, Ding Y, Agarwal S, Greiner A, Duan G. A review of smart electrospun fibers toward textiles. *Compos Commu* 2020;22:100506. <https://doi.org/10.1016/j.coco.2020.100506>.
- [1303] Tang JD, Mura C, Lampe KJ. Stimuli-responsive, pentapeptide, nanofiber hydrogel for tissue engineering. *J Am Chem Soc* 2019;141:4886–99. <https://doi.org/10.1021/jacs.8b13363>.
- [1304] Jin C, Song W, Liu T, Xin J, Hiscoc WC, Zhang J, et al. Temperature and pH responsive hydrogels using methacrylated lignosulfonate cross-linker: Synthesis, characterization, and properties. *ACS Sustainable Chem Eng* 2018;6:1763–71. <https://doi.org/10.1021/acsuschemeng.7b03158>.
- [1305] Jommanee N, Chanthad K, Manokruang K. Preparation of injectable hydrogels from temperature and pH responsive grafted chitosan with tuned gelation temperature suitable for tumor acidic environment. *Carbohydr Polym* 2018;198:486–94. <https://doi.org/10.1016/j.carbpol.2018.06.099>.
- [1306] Wang J, Tang F, Wang Y, Liu S, Li L. Tunable single-molecule white-light emission in stimuli-responsive hydrogel. *Adv Opt Mater* 2020;8:1901571. <https://doi.org/10.1002/adom.201901571>.
- [1307] Wang Y, Zhu Y, Wang J, Li X, Wu X, Qin Y, et al. Fe³⁺, NIR light and thermal responsive triple network composite hydrogel with multi-shape memory effect. *Composites Sci Technol* 2021;206:108653. <https://doi.org/10.1016/j.compscitech.2021.108653>.
- [1308] Zhu P, Yang W, Wang R, Gao S, Li B, Li Q. 4D printing of complex structures with a fast response time to magnetic stimulus. *ACS Appl Mater Interfaces* 2018;10:36435–42. <https://doi.org/10.1021/acsami.8b12853>.
- [1309] Yang J, Zhang X. Optical fiber delivered ultrafast plasmonic optical switch. *Adv Sci* 2021;8:2100280. <https://doi.org/10.1002/adv.202100280>.
- [1310] Lobry M, Lahem D, Loyez M, Debligny M, Chah K, David M, et al. Non-enzymatic D-glucose plasmonic optical fiber grating biosensor. *Biosens Bioelectron* 2019;142:111506. <https://doi.org/10.1016/j.bios.2019.111506>.
- [1311] Moffa M, Camposeo A, Fasano V, Fazio B, Iati MA, Maragò OM, et al. Biomineral amorphous lasers through light-scattering surfaces assembled by electrospun fiber templates. *Laser & Photonics Rev* 2017;12:1700224. <https://doi.org/10.1002/lpor.201700224>.

- [1312] Singh M, Bollella P, Gorton L, Dey ES, Dicko C. Conductive and enzyme-like silk fibers for soft sensing application. *Biosens Bioelectron* 2020;150:111859. <https://doi.org/10.1016/j.bios.2019.111859>.
- [1313] Azimi B, Milazzo M, Lazzeri A, Berrettini S, Uddin MJ, Qin Z, et al. Electrospinning piezoelectric fibers for biocompatible devices. *Adv Healthc Mater* 2019;9:e1901287. <https://doi.org/10.1002/adhm.201901287>.
- [1314] Liu W, Luo Y, Ning C, Zhang W, Zhang Q, Zou H, et al. Thermo-sensitive electroactive hydrogel combined with electrical stimulation for repair of spinal cord injury. *J Nanobiotechnology* 2021;19:286. <https://doi.org/10.1186/s12951-021-01031-y>.
- [1315] Stipelman CH, Smith ER, Diaz-Ochu M, Spackman J, Stoddard G, Kawamoto K, et al. Early-onset sepsis risk calculator integration into an electronic health record in the nursery. *Pediatrics* 2019;144:e20183464. <https://doi.org/10.1542/peds.2018-3464>.
- [1316] Wang H, Zhang Y, Liang X, Zhang Y. Smart fibers and textiles for personal health management. *ACS Nano* 2021;15:12497–508. <https://doi.org/10.1021/acsnano.1c06230>.
- [1317] Di J, Zhang X, Yong Z, Zhang Y, Li D, Li R, et al. Carbon-nanotube fibers for wearable devices and smart textiles. *Adv Mater* 2016;28:10529–38. <https://doi.org/10.1002/adma.201601186>.
- [1318] Zhang W, Ye C, Zheng K, Zhong J, Tang Y, Fan Y, et al. Tensan silk-inspired hierarchical fibers for smart textile applications. *ACS Nano* 2018;12:6968–77. <https://doi.org/10.1021/acsnano.8b02430>.
- [1319] Shafi H, Rashid R, Rather S-U, Siva Reddy DV, Azmi L, Abdal-hay A, et al. Super disintegrating oromucosal nanofiber patch of zolmitriptan for rapid delivery and efficient brain targeting. *Chem Eng J* 2023;463:142481. <https://doi.org/10.1016/j.cej.2023.142481>.
- [1320] Ji G, Chen Z, Li H, Awuye DE, Guan M, Zhu Y. Electrospinning-based biosensors for health monitoring. *Biosensors* 2022;12:876. <https://doi.org/10.3390/bios12100876>.
- [1321] Chinnappan BA, Krishnaswamy M, Xu H, Hoque ME. Electrospinning of biomedical nanofibers/nanomembranes: Effects of process parameters. *Polymers* 2022;14:3719. <https://doi.org/10.3390/polym14183719>.
- [1322] Hu R, Xi W, Liu Y, Tang K, Song J, Luo X, et al. Thermal camouflaging metamaterials *Mater Today* 2021;45:120–41. <https://doi.org/10.1016/j.mattod.2020.11.013>.
- [1323] Zhang J-K, Shi J-M, Zhao D-P, Wang Q-C, Wang C-M. Realization of compatible stealth material for infrared, laser and radar based on one-dimensional doping-structure photonic crystals. *Infrared Phys Technol* 2017;85:62–5. <https://doi.org/10.1016/j.infrared.2017.05.018>.
- [1324] Wang H, Ma Y, Qiu J, Wang J, Zhang H, Li Y, et al. Multifunctional PAN/Al–ZnO/Ag nanofibers for infrared stealth, self-cleaning, and antibacterial applications. *ACS Appl Nano Mater* 2021;5:782–90. <https://doi.org/10.1021/acsnanm.1c03518>.
- [1325] Zhang Y, Wang P, Shi Q, Ning X, Zheng J, Long Y-Z. Research progress and prospect of centrifugal electrospinning and its application. *J Alloys Compd* 2024;990:174433. <https://doi.org/10.1016/j.jallcom.2024.174433>.
- [1326] Hou T, Li XL, Lu YS, Yang B. Highly porous fibers prepared by centrifugal spinning. *Mater Design* 2017;114:303–11. <https://doi.org/10.1016/j.matdes.2016.11.019>.
- [1327] Cengiz-Çallıoğlu F, Jirsak O, Dayik M. The influence of non-solvent addition on the independent and dependent parameters in roller electrospinning of polyurethane. *J Nanosci Nanotechnol* 2013;13:4727–35. <https://doi.org/10.1166/jnn.2013.7190>.
- [1328] Sarwar Z, Krugly E, Danilovas PP, Ciuzas D, Kauneliene V, Martuzevicius D. Fabrication and characterization of peba fibers by melt and solution electrospinning. *J Mater Res Technol* 2019;8:6074–85. <https://doi.org/10.1016/j.jmrt.2019.10.001>.
- [1329] Lyu CX, Zhao P, Xie J, Dong SY, Liu JW, Rao CC, et al. Electrospinning of nanofibrous membrane and its applications in air filtration: A review. *Nanomaterials* 2021;11:1501. <https://doi.org/10.3390/nano11061501>.
- [1330] Gao J, Huang X, Wang L, Zheng N, Li W, Xue H, et al. Super-hydrophobic coatings based on non-solvent induced phase separation during electro-spraying. *J Colloid Interface Sci* 2017;506:603–12. <https://doi.org/10.1016/j.jcis.2017.07.089>.
- [1331] Akshay Kumar KP, Zare EN, Torres-Mendieta R, Wacławek S, Makvandi P, Černík M, et al. Electrospun fibers based on botanical, seaweed, microbial, and animal sourced biomacromolecules and their multidimensional applications. *Int J Biol Macromol* 2021;171:130–49. <https://doi.org/10.1016/j.ijbiomac.2020.12.205>.
- [1332] Li X, Zhang Y, Li H, Chen H, Ding Y, Yang W. Effect of oriented fiber membrane fabricated via needleless melt electrospinning on water filtration efficiency. *Desalination* 2014;344:266–73. <https://doi.org/10.1016/j.desal.2014.04.003>.
- [1333] Xia Q, Wang CM, Li WC, Han WW, Chen HB. Dual-electrode melt differential electrospinning *Fiber Polym* 2024;25:2029–42. <https://doi.org/10.1007/s12221-024-00587-4>.
- [1334] Su Y, Qiu T, Song W, Han X, Sun M, Wang Z, et al. Melt electrospinning writing of magnetic microrobots. *Adv Sci* 2021;8:2003177. <https://doi.org/10.1002/adv.202003177>.
- [1335] Wan C, He X, Zhu G, Li X, Zhu X, Chen R, et al. Extreme orientation of stereocomplexed poly (lactic acid) induced ultrafine electroactive nanofibers for respiratory healthcare and intelligent diagnosis. *ACS Sustain Chem Eng* 2024;12:9290–300. <https://doi.org/10.1021/acssuschemeng.4c02720>.
- [1336] Liang C, Li J, Chen Y, Ke L, Zhu J, Zheng L, et al. Self-Charging, breathable, and antibacterial poly(lactic acid) nanofibrous air filters by surface engineering of ultrasmall electroactive nanohybrids. *ACS Appl Mater Interf* 2023;15:57636–48. <https://doi.org/10.1021/acsnami.3c13825>.
- [1337] Kaniuk L, Stachewicz U. Development and advantages of biodegradable PHA polymers based on electrospun PHBV fibers for tissue engineering and other biomedical applications. *ACS Biomater Sci Eng* 2021;7:5339–62. <https://doi.org/10.1021/acsbmaterials.1c00757>.
- [1338] Ying TH, Ishii D, Mahara A, Murakami S, Yamaoka T, Sudesh K, et al. Scaffolds from electrospun polyhydroxyalkanoate copolymers: fabrication, characterization, bioabsorption and tissue response. *Biomaterials* 2008;29:1307–17. <https://doi.org/10.1016/j.biomaterials.2007.11.031>.
- [1339] Zhu M, Han J, Wang F, Shao W, Xiong R, Zhang Q, et al. Electrospun nanofibers membranes for effective air filtration. *Macromol Mater Eng* 2017;302:1600353. <https://doi.org/10.1002/mame.201600353>.
- [1340] Al-Enizi AM, Zagho MM, Elzatahry AA. Polymer-based electrospun nanofibers for biomedical applications. *Nanomaterials (Basel)* 2018;8:77. <https://doi.org/10.3390/nano8040259>.
- [1341] Zhang C, Li Y, Wang P, Zhang H. Electrospinning of nanofibers: Potentials and perspectives for active food packaging. *Compr Rev Food Sci Food Saf* 2020;19:479–502. <https://doi.org/10.1111/1541-4337.12536>.
- [1342] Zhou W, Yu X, Li Y, Jiao W, Si Y, Yu J, et al. Green-solvent-processed fibrous membranes with water/oil/dust-resistant and breathable performances for protective textiles. *ACS Appl Mater Interfaces* 2021;13:2081–90. <https://doi.org/10.1021/acsnami.0c20172>.
- [1343] Megelski S, Stephens JS, Chase DB, Rabolt JF. Micro- and nanostructured surface morphology on electrospun polymer fibers. *Macromolecules* 2002;35:8456–66. <https://doi.org/10.1021/ma020444a>.
- [1344] Najafi M, Frey MW. Electrospun nanofibers for chemical separation. *Nanomaterials* 2020;10:982. <https://doi.org/10.3390/nano10050982>.
- [1345] Kouchebaghi NH, Yousefzadeh M, Gharehaghaji A, Khosravi S, Khorsandi D, Haghighiaz R, et al. A machine learning-guided design and manufacturing of wearable nanofibrous acoustic energy harvester. *Nano Res* 2024;20:1–2. <https://doi.org/10.1007/s12274-024-6613-6>.